# Apport des structures cristallographiques à la compréhension du mécanisme d'inhibition des cholinestérases par les neurotoxiques organophosphorés

Florian Nachon

# UNIVERSITÉ JOSEPH FOURIER - GRENOBLE

**École doctorale Chimie et Sciences du Vivant**


**Diplôme d'Habilitation à Diriger des Recherches**

Présenté par


***Dr. Florian NACHON***


# Apport des structures cristallographiques à la compréhension du mécanisme d'inhibition des cholinestérases par les neurotoxiques organophosphorés

Soutenance le 14 mai 2014 devant le jury composé de:

Yves Bourne, Directeur de Recherche, CNRS, rapporteur
Thomas Grutter, Directeur de Recherche, CNRS, rapporteur
Dominique Bourgeois, Directeur de Recherche, CNRS, rapporteur
Juan-Carlos Fontecilla, Directeur de Recherche, CEA, président
Patrick Masson, Professeur, Service de Santé des Armées
Pierre-Yves Renard, Professeur, Université de Rouen

# Avant Propos

Les cholinestérases sont des sérines hydrolases spécialisées dans l'hydrolyse des esters de choline, en particulier, le neurotransmetteur acétylcholine. Le rôle principal de l'acétylcholinestérase humaine (hAChE) est la terminaison de la transmission de l'impulsion nerveuse au niveau des synapses cholinergiques par hydrolyse de l'acétylcholine en acide acétique et choline. Les cholinestérases sont fascinantes par leur efficacité catalytique ($10^8$-$10^9$ $M^{-1}.min^{-1}$) et par la subtilité des mécanismes catalytiques et changements conformationnels associés. Malgré des décennies de recherches, bien des aspects de leur fonctionnement restent incompris. Elles constituent un sujet d'étude riche, sans cesse renouvelé par la diversité des approches nécessaires à la compréhension de leurs différentes facettes.

Dès ma thèse, mes activités de recherche ont été centrées sur l'étude des relations structure-activité des cholinestérases et plus particulièrement de la butyrylcholinestérase humaine (hBChE). La hBChE est une enzyme très proche de l'hAChE (52% d'identité), mais diffère nettement par sa spécificité de substrat et sa sensibilité aux inhibiteurs. Elle est abondamment présente dans le plasma et dans de nombreux tissus chez les vertébrés. Mais contrairement à l'AChE, aucun rôle cholinergique ni aucun autre rôle physiologique n'a pu lui être attribué. C'est d'ailleurs une enzyme qui n'est pas vitale comme le démontre la viabilité des individus nullizygotes. Elle peut éventuellement jouer le rôle de suppléant de la hAChE en cas de déficience de cette dernière. Cependant l'importance de la hBChE est capitale d'un point de vue toxicologique et pharmacologique car elle est impliquée dans la dégradation de nombreux principes actifs, poisons ou médicaments, par exemple la cocaïne, la succinylcholine.

En raison de sa fonction essentielle dans le système nerveux, la hAChE est la cible d'un vaste répertoire de médicaments et de poisons, naturels ou synthétiques, notamment des composés organophosphorés (OP) comme les pesticides ou encore les agents neurotoxiques de guerre. L'emploi d'OP a, par le passé, entrainé des dommages importants, tant lors de conflits militaires comme dans la guerre Iran-Irak (1980-1988) ou la guerre du Golfe (1991) que dans les milieux civils comme l'attentat dans le métro de Tokyo (1995). L'usage de sarin en août 2013 dans le conflit syrien a rappelé que dans le contexte militaire et politique actuel, les armes chimiques de guerre restent une menace concrète et sérieuse, et ce malgré la Convention d'Interdiction des Armes chimiques signée en 1993 et ratifiée par 181 états.

Parallèlement, le contexte socio-économique tend vers une accélération des moyens de production, notamment dans le domaine agricole. L'utilisation de pesticides organophosphorés, bien que réglementée, provoque des intoxications accidentelles non négligeables. Surtout, l'ingestion de pesticides est le premier moyen de suicide dans le monde, en particulier en Asie rurale *(Hvistendahl 2013)*, et représente 1/3 des suicides annuels pour plus de 200 000 décès *(Eddleston 2008)*.

Comme la hAChE, la hBChE est inhibée par les carbamates et les OPs sans toutefois de symptômes associées. C'est un excellent bioépurateur des OPs, une forme injectable de hBChE étant en cours de développement pour la protection contre l'intoxication par les OPs.

Les moyens thérapeutiques actuels étant assez peu efficaces, leur développement reste une priorité et passe par la connaissance détaillée des mécanismes d'inhibition et de résistance aux traitements. C'est dans ce contexte que j'ai développé mes travaux de recherche depuis ma soutenance de thèse en 1999.

Je commencerai ce mémoire par une introduction non exhaustive sur la structure générale des cholinestérases, l'inhibition par les pesticides et neurotoxiques organophosphorés et les contre-mesures médicales des armes chimiques. Dans une seconde partie, je présenterai le cheminement ayant conduit à la résolution de la structure de la butyrylcholinestérase humaine et les principaux enseignements obtenus. Puis je montrerai l'apport des structures de cholinestérases phosphylées sur la connaissance détaillée des mécanismes d'inhibition et de vieillissement. Et enfin je présenterai mes travaux actuels et leurs perspectives sur le développement de nouvelles contremesures des toxiques de guerre organophopshorés.

# I - Introduction

## *I.1 - Rappels sur la structure des cholinestérases*

### *I.1.1 - Gène et formes moléculaires*

L'AChE des vertébrés est codée par un gène unique, distinct de celui codant pour la BChE *(Gnatt 1991)*. Chez l'Homme, le gène codant pour l'hAChE se situe sur le chromosome 7q22, et fait environ 7 kb (6 exons et 4 introns) *(Getman 1992)*. Celui de la hBChE, localisé sur le chromosome 3q26, est beaucoup plus étendu (73 kb) et contient 4 exons dont le second contient 83% de la séquence codante de la protéine mature, l'extrémité N-terminale et le site catalytique *(Arpagaus 1990)*. Les ChEs possèdent des sites de N-glycosylation (Asn-X-Ser/Thr), 3 sites pour l'hAChE, et 9 pour la hBChE *(Lockridge 1987; Soreq 1990)*. Ces glycanes contribuent à la sécrétion, la solubilité et la stabilité de l'enzyme dans son environnement, sans influencer ses propriétés catalytiques *(Velan 1993)*.

L'épissage alternatif et les modifications post-traductionnelles donnent lieu à trois formes connues pour l'AChE, différentes de par leur extrémité C-terminale. Celle-ci détermine la maturation et le devenir de l'enzyme *(Li 1993)*. La BChE, quant à elle, ne code que pour un seul transcrit, ne donnant lieu qu'à une seule forme moléculaire *(Massoulie 1993)*.

L'extrémité C-terminale, dite hydrophobe, du transcrit H (forme $AChE_H$) est capable de s'associer à un glycophosphatidylinositol (GPI), ancrant ainsi la protéine à la membrane cellulaire (**Figure 1**). Deux cystéines permettent sa dimérisation *(Coussen 2001)*. Cette forme a été identifiée uniquement dans les organes électriques et les muscles striés chez le poisson torpille *(Bon 1982)*, ainsi que dans le cerveau et à la surface des cellules sanguines des mammifères *(Haas 1986)*.

La forme $AChE_S$, soluble, monomérique, est observée dans le venin de serpent *Bungarus multicintus*. Il s'agit d'une forme dont l'extrémité C-terminale est clivée au cours de la sécrétion *(Cousin 1996)*.

La forme moléculaire majoritaire d'AChE et de BChE retrouvée chez les vertébrés possède une extrémité C-terminale amphiphile appelée peptide T ($AChE_T$ et $BChE_T$). Ce peptide T possède une série de 7 résidus aromatiques conservés, dont trois tryptophanes (domaine WAT : « Tryptophan Amphiphilic Tetramerization »), sur la même face d'une hélice $\alpha$ ainsi qu'une cystéine, permettant la formation d'un pont disulfure entre deux monomères. Les hélices $\alpha$ de quatre monomères s'associent à un peptide riche en proline appelé PRAD (Proline-Rich Attachment Domain) par le biais d'interactions noyau

aromatique/proline *(Massoulie 2002)*. Le peptide PRAD constitue l'extrémité N-terminale, soit de la protéine collagénique ColQ insérée dans la lame basale des jonctions neuromusculaires *(Cousin 1996)*, soit de la protéine PRiMA (Proline-Rich Membrane Anchor) insérée au niveau des membranes cellulaires des neurones *(Perrier 2002)*. Pour ces deux protéines, le peptide PRAD possède 2 ou 4 cystéines.

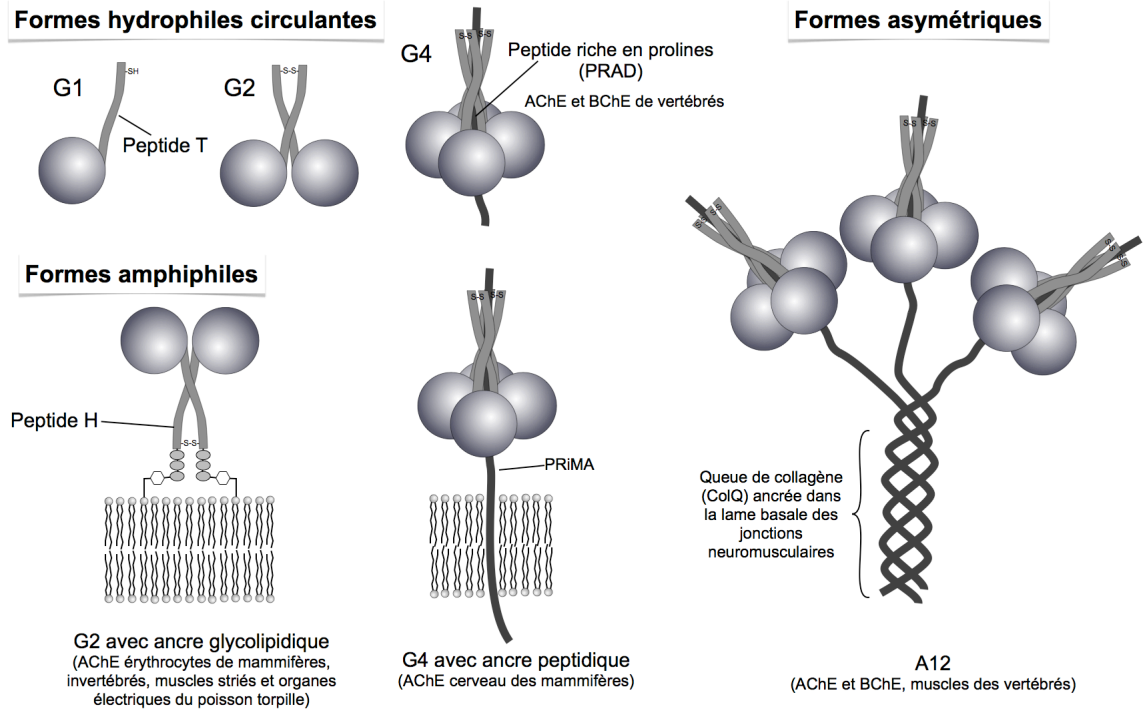


**Figure 1.** Formes moléculaires des ChEs G1, G2 et G4, respectivement formes solubles monomérique, dimérique et tétramérique ; G2-ancrée à un glycolipide ; G4-ancrées, forme tétramérique associée à la protéine PRiMA ; A12, forme tétramérique associée à la protéine ColQ via trois peptides PRAD)

Les formes $AChE_T$ et $BChE_T$ sont asymétriques et amphiphiles. ColQ possède jusqu'à trois peptides PRAD, permettant un assemblage asymétrique avec un maximum de trois tétramères (A4, A8, A12). 98 % de la BChE plasmatique, soluble, apparaît sous forme tétramérique G4, assemblée autour d'un peptide PRAD, issu de la lamellipodine *(Li 2008)*. Les formes moléculaires minoritaires hydrophiles sont la forme monomérique G1 et la forme dimérique G2 constituée de deux G1 reliées par un pont disulfure entre les Cys571 C-terminales.

### *I.1.2 - Structure tridimensionnelle et architecture du site actif*

Les ChEs font partie de la famille des α/β hydrolases à sérine, et plus particulièrement des carboxylestérases de type B *(Carr 2009)*. Elles se structurent autour d'un feuillet β flanqué d'hélices α (**Figure 2**). La triade catalytique de l'AChE est composée d'une sérine nucléophile activée par un relais de protons impliquant une histidine et un glutamate.

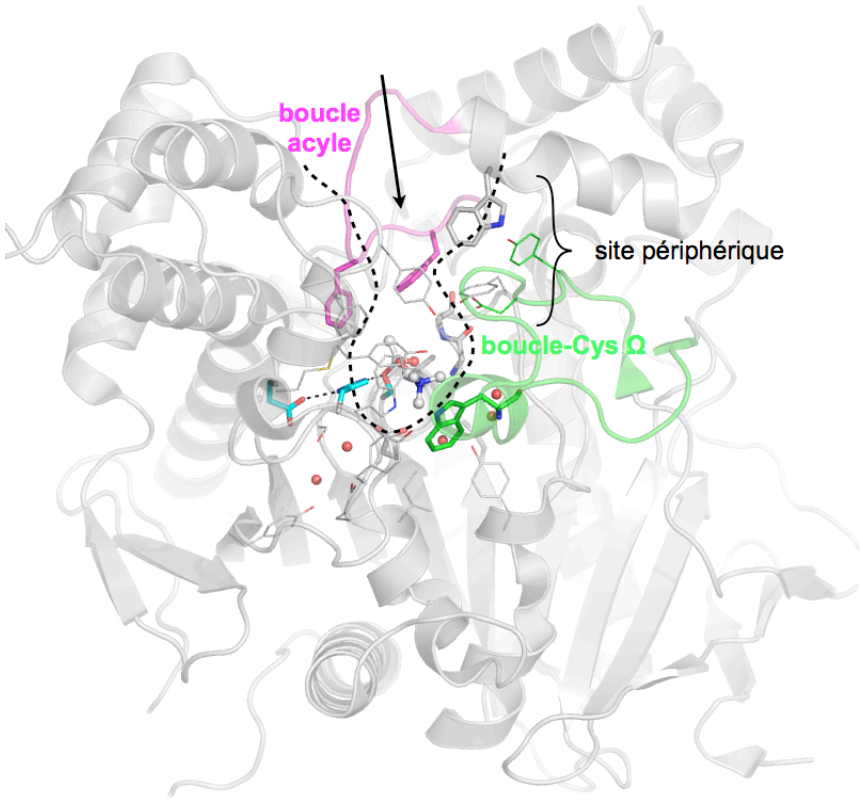


**Figure 2.** Structure tridimensionnelle de l'AChE humaine (pdb 4ey4). La forme de la gorge est esquissée par une ligne pointillée. L'entrée de la gorge est indiquée par une flèche. La triade catalytique est colorée en cyan. Une molécule d'acétylcholine dans l'état de transition est modélisée au fond de la gorge. La boucle-Cys Ω côté choline est en vert, la boucle acyle côté acétyle est en magenta.

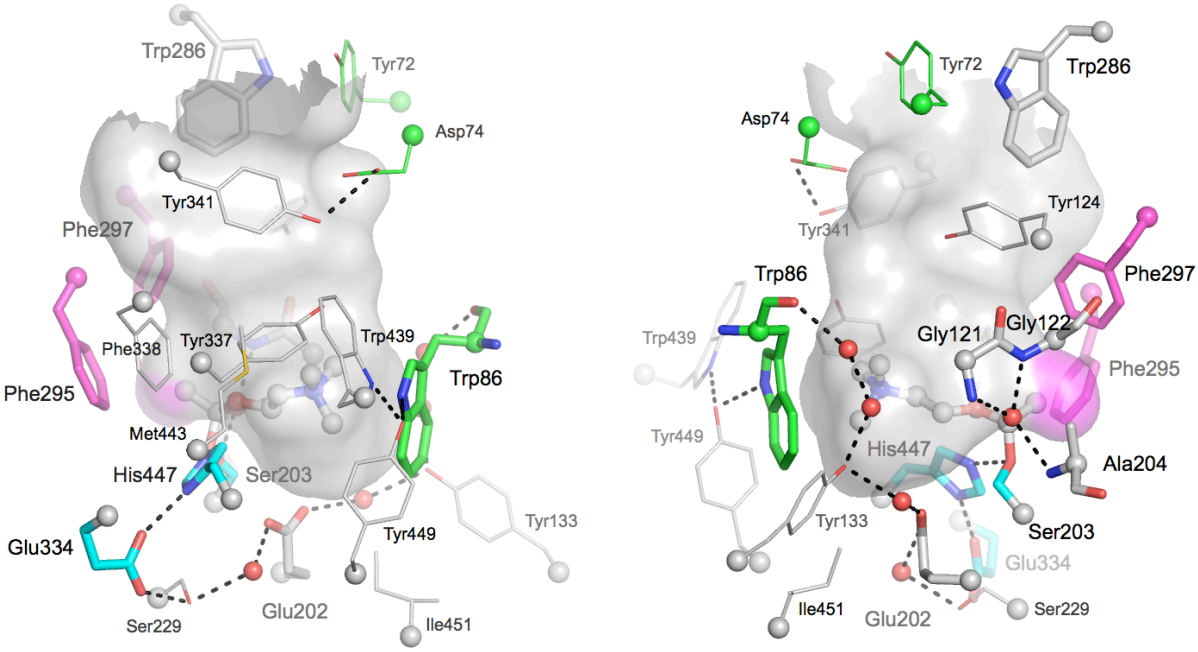


**Figure 3.** Site actif de l'hAChE. (pdb 4ey4) Le site périphérique à l'entrée de la gorge (Trp286, Tyr72 et Tyr124). Au fond de la gorge, une molécule d'acétylcholine dans l'état de transition, la triade catalytique (cyan: Ser203, His447 et Glu334), le trou oxyanion (Ala202, Gly121 et Gly122), de la poche « acyle » (magenta: Phe295 et Phe297), la poche « choline » (Trp86 et Tyr337).

Le résidu acide n'est donc pas un résidu aspartate comme chez les protéases à sérine. La triade est localisée au fond d'une gorge de 300 Å3 à environ 20 Å de la surface (**Figure 3**). Cette gorge est tapissée de 14 résidus aromatiques, avec en particulier un cluster de résidus situé à son entrée, le site périphérique. Ce site périphérique contrôle l'accès à la gorge. Deux boucles se font face de part et d'autre de la gorge: la boucle-Cys Ω forme la poche où se loge la partie choline du substrat, la boucle acyle forme la poche où se loge la partie acyle du substrat.La machinerie catalytique comprend la triade, Ser203/His447/Glu334 et le trou oxyanion composé de Gly121, Gly122, Ala202 *(Shafferman 1992)*. Le mécanisme d'hydrolyse par l'hAChE est très efficace, avec environ 2 000 molécules d'acétylthiocholine hydrolysées par seconde et par site actif *(Vellom 1993)*. Lors de la réaction catalytique, la sérine est acylée puis déacylée, grâce à un relais de protons impliquant l'imidazolium de l'histidine et le carboxylate du glutamate. Chacun des 3 NH de la chaîne principale contribue à la stabilisation de l'oxyanion de l'état de transition au cours de la réaction. La structure cristallographique de *Tc*AChE en complexe avec le 4-oxo-N,N,N-triméthylpentanaminium (OTMA), un analogue non hydrolysable de l'ACh, le met particulièrement en évidence (**Figure 4**)*(Colletier 2006)*. Un second glutamate, Glu202, intervient dans la stabilisation des états de transition par interaction électrostatique *(Ordentlich 1996)*.

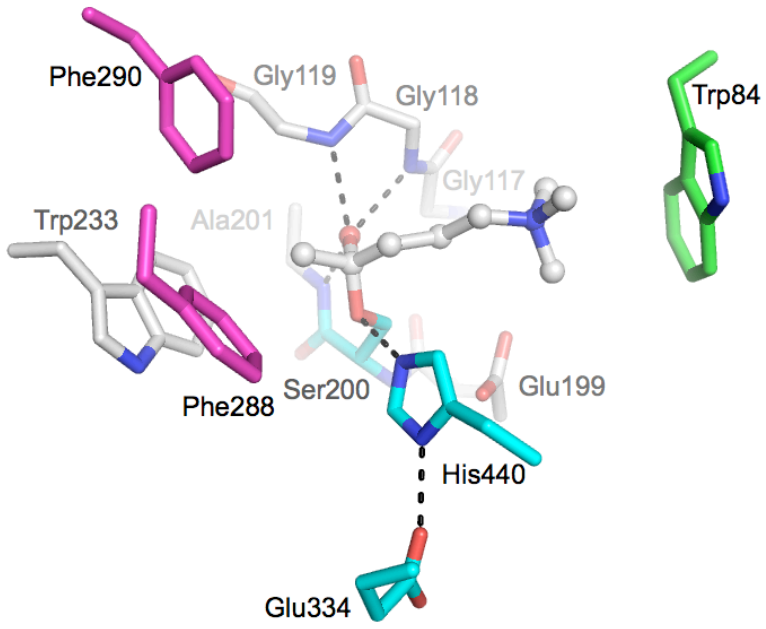


**Figure 4.** Complexe TcAChE-OTMA. (code pdb 2c5F) l'OTMA forme un hemicetal avec la sérine catalytique, stabilisé par le trou oxyanion et des interactions cation-π avec Trp84 de la poche choline.

L'ammonium quaternaire est stabilisé dans la poche choline par interaction de type cation-π avec le tryptophane de la boucle-Cys Ω *(Colletier 2006; Harel 1993; Ordentlich 1993a)*. Un second résidu aromatique renforce l'interaction cation-π avec la poche choline (Tyr337 chez l'Homme, Phe330 chez la torpille). Le méthyle de l'acétyle est confiné dans la poche acyle formée par les résidus aromatiques Phe295, Phe297 et Trp236.

### *I.1.3 - Site périphérique allostérique et trafic des substrats/produits*

Le site d'interaction des ligands périphériques à l'entrée de la gorge est constitué du cluster de résidus aromatiques Trp286/Tyr72/Tyr124, et de Asp74/Tyr341 sur la face opposée *(Barak 1994)*. Les ligands cationiques et/ou aromatiques interagissent avec les systèmes π des résidus du site (interactions cation-π et π-π) *(Bourne 2003; Harel 1993)*. Lors de son approche de l'enzyme, une molécule d'acétylcholine est captée au niveau du site périphérique, interagit en particulier avec Asp74, avant de glisser le long de la gorge pour se positionner dans le site estérasique *(Mallender 2000)*. À faible concentration, l'association d'une seconde molécule de substrat au niveau du site périphérique augmente la vitesse d'acylation *(Johnson 2003)*. En revanche, un excès de substrat *(Aldridge 1969; Radic 1991)* ou la fixation d'un ligand au site périphérique (ex : propidium) entraine un blocage du trafic du substrat et des produits dans la gorge *(Mallender 2000; Rosenberry 1999; Szegletes 1999)*. L'activité enzymatique est alors ralentie. Des études cristallographiques illustrent les détails moléculaires de ce phénomène de blocage *(Bourne 2006; Colletier 2006)*.

Le cluster Trp286/Tyr72/Tyr124 fait partie d'un réseau de résidus aromatiques incluant Phe297/Phe295 de la poche acyle, Phe398 en contact avec His447 catalytique, Tyr337 de la poche choline et Tyr341 du site périphérique (**Figure 5**).

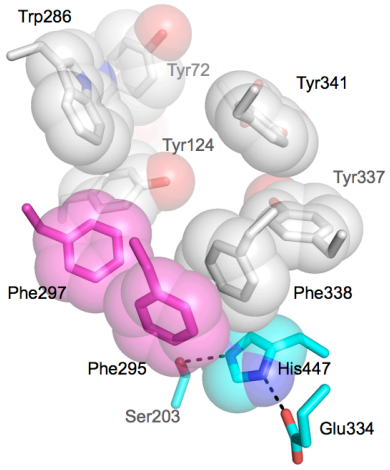


**Figure 5.** Réseau d'interactions aromatiques du site actif de l'hAChE. Ce réseau s'étend d'un versant du site périphérique (Trp286/Tyr72) à l'autre (Tyr341) via la poche acyle (magenta) et l'histidine catalytique (cyan).

Sachant que la conformation active d'His447 est stabilisée par Phe338 *(Kaplan 2004)*, l'existence de ce relai d'interactions aromatiques explique que la fixation d'un ligand au cluster puisse influencer l'activité catalytique *(Shafferman 1992)*.

La liaison H entre Asp74 et Tyr341 est un point d'ancrage de la boucle-Cys Ω. Elle joue un rôle essentiel dans le maintien de l'architecture de la poche choline. Cette liaison est à l'extrémité d'un vaste réseau de liaisons hydrogène strictement conservé chez les cholinestérases *(Koellner 2000)*. De manière remarquable, Ser203 catalytique est reliée à Tyr341 du site périphérique via 14 liaisons H, impliquant en particulier 6 molécules d'eau qui délimitent la poche choline (**Figure 6**). La mutation de résidus du réseau, comme Tyr133, perturbe l'architecture du site et réduit l'efficacité catalytique *(Barak 1995; Ordentlich 1995)*.

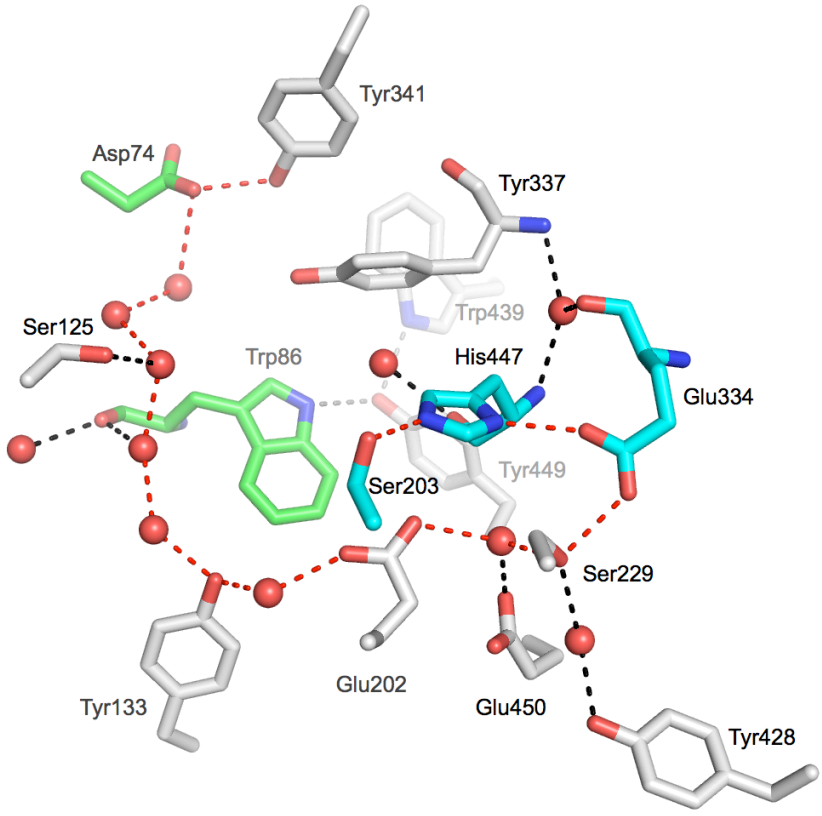


**Figure 6.** Réseau de liaisons H du site actif de l'hAChE. Ce réseau fait intervenir de nombreuses molécules d'eau (sphères en rouge) et maintient la structure de la poche choline. Il inclue la triade catalytique, un enchainement de 14 liaisons H permettant de connecter Ser203 catalytique à Tyr341 du site périphérique (pointillés en rouges). Les résidus appartenant à la boucle-Cys sont en vert, ceux de la triade en cyan.

Certains auteurs ont avancé que les dimensions restreintes de la gorge ainsi que le potentiel électrostatique pouvaient présenter un frein au trafic du substrat et des produits dans la gorge avec des conséquences sur l'efficacité catalytique *(Gilson 1994)*. Ils proposèrent une sortie alternative des produits d'hydrolyse sur la base de simulation de dynamiques moléculaire d'une centaine de ps montrant un basculement furtif du tryptophane de la boucle-

Cys Ω. La sortie des produits par cette "backdoor" permettrait un flux unidirectionnel des molécules dans la gorge qui serait un facteur important de l'efficacité catalytique. Cependant, les premières études réalisées par mutagenèse dirigée de résidus proches ou appartenant à la « backdoor » supposée (Glu84, Trp86, Asp131 et Val132), n'ont révélé aucune différence significative d'efficacité catalytique entre l'enzyme sauvage et les mutants, et donc que le passage par cette « backdoor » n'a pas d'influence sur la vitesse de catalyse *(Kronman 1994)*. Ceci paraît conforme au fait que la durée moyenne du cycle catalytique d'hydrolyse d'une molécule d'acétylthiocholine est de 500 µs, alors qu'une molécule telle que la thiocholine diffuse hors de la gorge en quelques dizaines de ns peu importe sa route *(Xu 2010)*. Cette différence d'échelle de temps de plus de 4 ordres de grandeur réfute l'hypothèse que la diffusion des molécules vers ou hors du site soit un facteur limitant pour la vitesse de catalyse.

La situation est potentiellement différente si un excès de substrat sature la gorge. L'hypothèse est que la backdoor devienne la voie de sortie principale des produits. Ceci a pu être vérifié pour l'AChE de *Drosophila melanogaster (Nachon 2008)*. Celle-ci est sujette à l'inhibition par excès de substrat et présente les particularités d'avoir une gorge plus étroite, et une absence de stabilisation du tryptophane de la backdoor (Trp83) par les résidus environnants : pas d'interaction Trp-Met et pas de liaison H indole-Tyr phénolique, Ile82 et Asp482 remplaçant respectivement des résidus Met et Tyr présents chez la plupart des AChEs. Ce tryptophane est d'ailleurs assez désordonné dans la structure de l'apo-*Dm*AChE et sa conformation laisse une ouverture d'un diamètre de 5 Å dans la poche choline *(Harel 2000)*. En cas de saturation par excès de substrat, le passage par ce canal permet de conserver 5 % d'activité résiduelle pour l'enzyme sauvage *(Nachon 2008)*. Les mutations Trp83Glu et Trp83Ala élargissent le canal à 9 Å et rendent son ouverture permanente. Dans ce cas, l'inhibition par un excès de substrat ou par des inhibiteurs périphériques (Aflatoxine, propidium) est absente : les substrats et produits peuvent aisément entrer et sortir du site actif par cette voie secondaire.

La formation d'un canal dans la poche choline a également été observé lorsque l'aflatoxine est fixée au site périphérique de la *Tc*AChE *(Sanson 2011)*. La structure cristallographique du complexe révèle une rotation à 90° de Tyr442, cette tyrosine absente chez *Dm*AChE, qui engendre une ouverture dans la poche choline.

L'occlusion de la gorge a des effets très drastiques sur l'AChE de souris (mAChE). Lorsque la fasciculine 2, une toxine peptidique, se fixe au site périphérique, l'efficacité catalytique du complexe mAChE-fas-2 est réduite de $10^6$ fois par rapport à celle de mAChE seule *(Radic 2001)*. La très faible activité résiduelle suggère que le passage par une route alternative à

l'entrée de la gorge est un évènement très rare pour ce complexe, bien que des études de dynamique moléculaire suggèrent que l'amplitude de mouvements de la boucle-Cys Ω est plus importante lorsque la fasciculine 2 est liée *(Bui 2004)*.

Quoiqu'il en soit, il apparaît que ces voies alternatives d'accès au site actif ne jouent sur l'efficacité catalytique que lorsque l'entrée de la gorge est bloquée. Or, cette situation n'est pas rencontrée dans des conditions physiologiques, où la concentration en acétylcholine ne dépasse jamais quelques mM, alors que les phénomènes d'inhibition par excès de substrat apparaissent à des concentrations supérieures d'un ordre de grandeur *(Cheng 2007)*.

### *I.2 - Les pesticides organophosphorés et neurotoxiques de guerre*

#### *I.2.1 - Caractéristiques générales et historique*

Les pesticides et neurotoxiques organophosphorés (OP) sont constitués d'un atome de phosphore pentavalent, lié à quatre substituants : un atome d'oxygène ou de soufre, un groupe partant (X), un groupement alkoxyle (O-$R_1$) et un autre groupement ($R_2$), selon la structure générale décrite dans la **figure 7** :

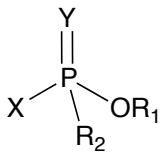


Y = O ou S
X = groupe partant, CN, F,alkoxyle, thioalkyle
R1 = alkyle
R2 = alkyle, aryle (phosphonate), alkoxyle (phosphate), thioalkyle (thiophosphate), amin (phosphoramidate)

**Figure 7.** Structure générale des OP

Les OPs sont des composés chiraux si $OR_1$ est différent de $R_2$. Ce n'est pratiquement jamais le cas des pesticides et toujours le cas pour les neurotoxiques de guerre.

Les pesticides sont des esters et amides d'acides (thio)phosphorique ou (thio)phosphonique, dont les noms sont le plus souvent identifiables par leur terminaison en "phos" ou en "thion". C'est le chimiste français P. de Clermont qui décrit en 1854, pour la première fois, la synthèse du tétraéthyl-pyrophosphate (TEPP), le premier pesticide organophosphoré commercialisé en Allemagne en 1944. La même année, le chimiste allemand G. Schrader synthétise le parathion, plus stable. Après absorption, le parathion est oxydé en paraoxon, très toxique *(Fukuto 1990)*. Du fait de cette forte toxicité tant pour les animaux que pour les insectes, de nouveaux OPs moins actifs seront synthétisées à partir des années 50. Dans les années 1970, l'interdiction de l'utilisation des pesticides organochlorés a favorisé la diffusion des OPs, plus efficaces mais moins persistants. Selon la classification

publiée en 2010 par l'Organisation Mondiale de la Santé (OMS), presque la moitié des pesticides appartenant aux deux classes les plus dangereuses (Ia et Ib) avec des $DL_{50}$ chez le rat inférieures à 50 mg/kg *per os*, sont des OPs.

Les neurotoxiques de guerre sont issus de la recherche sur les insecticides. C'est dans la deuxième moitié des années 30 que Gerhard Schrader découvrit le tabun ou GA (1936), suivi du sarin ou GB (1937) puis du soman ou GD (1944). Aux agents G pour « German » a suivi la synthèse du VX (V pour « venomous») par les Britanniques en 1953 à partir d'un insecticide, le Tétram. Les agents G sont plus volatiles mais moins persistants que les agents V. Et ces derniers sont plus toxiques, notamment par voie cutanée (**Tableau 1**).

| **Agents G** | Structure | $DL_{50}$ (mg/kg) | $LCt_{50}$ ($mg.m^{-3}$/min) |
|---|---|---|---|
| GA (tabun) | 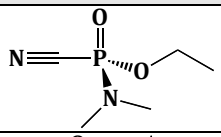 | 23 | 100-200 |
| GB (sarin) | 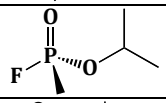 | 28 | 70-100 |
| GD (soman) | 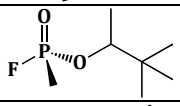 | 18 | 70 |
| GF (cyclosarin) | 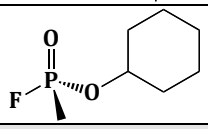 | 0.35 | n.c |
| **Agents V** | | | |
| VX | 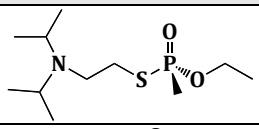 | 0.14 | 30-50 |
| VR | 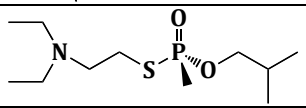 | n.c | 10-50 |
| CVX | 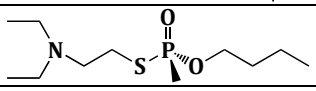 | n.c | n.c |

**Tableau 1.** Dénomination, structure et létalité des principaux neurotoxiques organophosphorés. La $DL_{50}$ estime la dose entraînant 50 % de décès après intoxication percutanée chez l'Homme. La $LCt_{50}$ estime la létalité après intoxication par inhalation chez l'Homme, en fonction du temps. (n.c : non communiqué) (Source : Federation of American Scientists et www.cbwinfo.com)

Malgré leurs caractéristiques opérationnelles qui en font des armes redoutables, la crainte des évènements du passé et des représailles à l'identique par l'ennemi a provoqué une abstention relative de leur utilisation. Cependant, le régime irakien utilisa l'ypérite, le sarin et le tabun contre les troupes iraniennes dès 1983, et contre ses populations civiles kurdes lors du massacre de Halabja, le 17 mars 1988 *(Macilwain 1993)*. Le VX fut utilisé au Japon à

Matsumoto en 1994 par la secte Aum Shinrikyo. Cette même secte perpétra un acte terroristes au sarin dans le métro de Tokyo, le 20 mars 1995. Lors de cet attentat, le bilan a fait état de 11 morts, 70 intoxiqués graves et plus de 5 000 blessés légers. Plus récemment, des analyses de prélèvements biologiques réalisés sur des victimes syriennes début 2013 ont révélés la présence de métabolites caractéristiques du sarin, prouvant l'usage de cet OP. Une attaque d'ampleur au sarin faisant plus de 1000 victimes a eu lieu le 21 Août 2013 dans la banlieue de Damas. La Syrie est l'un des 5 pays avec l'Angola, la Corée du Nord, l'Egypte, et la Somalie qui reste en dehors de la Convention sur l'Interdiction des Armes Chimiques signée le 13 janvier 1993. Israël et la Birmanie ne l'ont toutefois pas encore ratifiée.

### *I.2.2 - L'intoxication aigüe par les organophosphorés*

Les organophosphorés sont des molécules très lipophiles, qui franchissent facilement les barrières biologiques (voies transcutanée, respiratoire et digestive). Après absorption, ils réagissent avec les résidus nucléophiles des protéines, en particulier l'acétylcholinestérase et la butyrylcholinestérase, empêchant ainsi l'hydrolyse physiologique de l'acétylcholine. Ce neurotransmetteur du système nerveux est impliqué dans la mémoire et l'apprentissage au niveau central et dans l'activité musculaire et les fonctions végétatives au niveau périphérique. Une faible quantité d'OP franchit la barrière hématoencéphalique (BHE), mais suffit pour inhiber en quelques secondes toute l'activité cholinestérasique *(Vale 1998)*. L'inhibition de l'acétylcholinestérase par les OPs entraine une accumulation d'acétylcholine au niveau synaptique. Cette accumulation amplifie, d'une part, la réponse des récepteurs muscariniques au niveau des cibles du système parasympathique et, d'autre part, celle des récepteurs nicotiniques au niveau ganglionnaire des systèmes sympathique et parasympathique. On observe une stimulation puis une paralysie de la transmission de l'influx nerveux par dépolarisation persistante. Le syndrome dit « cholinergique » regroupe donc trois syndromes différents.

Le syndrome muscarinique périphérique provoque une hypersécrétion des glandes salivaires et sudorales, entre autre ; une contraction des muscles lisses (myosis, bronchoconstriction) ; une augmentation du péristaltisme (nausées, vomissements, diarrhées, crampes abdominales) ; une bradycardie et une hypotension. Le syndrome nicotinique périphérique, quant à lui, provoque la contraction des muscles striés (asthénie intense, faiblesse musculaire, fasciculations, mouvements involontaires, paralysie des muscles respiratoires) et des troubles cardiaques (tachycardie et hypertension). Au niveau du SNC, le syndrome central donne lieu à de l'agitation, de l'anxiété, des vertiges et céphalées, pouvant

aller jusqu'à un état confusionnel voire un coma convulsif avec risques de choc hémodynamique.

L'atteinte cérébrale lors d'une intoxication aux OP ne se résume pas au système cholinergique. En effet, les convulsions et les lésions cérébrales s'accompagnent d'autres symptômes comme l'œdème cellulaire ou la nécrose neuronale et mettent en jeu la perturbation d'autres systèmes de neurotransmission par effet domino (glutamate, GABA, dopamine, noradrénaline)*(Fosbraey 1990; Lallement 1993; Shih 1997)*.

### *I.2.3 - Mécanisme moléculaire de l'inhibition*

Il est généralement admis que la sérine catalytique des cholinestérases est phosphylée par un mécanisme de substitution nucléophile en ligne ($SN_2$). L'oxygène de la sérine attaque l'atome de phosphore de l'OP par la face opposée au groupe partant, ce qui conduit à un état de transition bipyramidal ou la sérine entrante et le groupe partant sont aux apex. Cet état évolue vers un adduit tétraédrique via la rupture de la liaison entre le phosphore et le groupe partant (**Figure 8**).

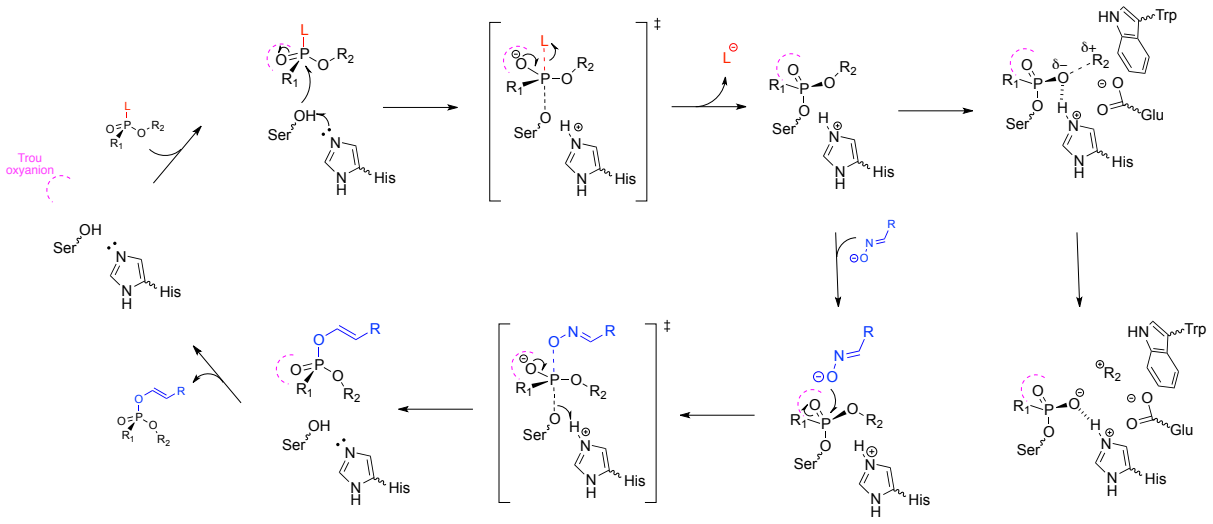


**Figure 8.** Mécanisme d'inhibition, de vieillissement et de réactivation de l'hAChE par le VX. L'inhibition par phosphylation de l'enzyme a lieu par attaque de l'oxygène de la sérine catalytique (Ser203) sur le phosphore du VX. Cette dernière peut être déphosphylée par un nucléophile fort (oxime) ou être irréversiblement modifiée par désalkylation de l'adduit.

Le conjugué formé est un analogue structural stable de l'état de transition d'acylation des esters. La déphosphylation spontanée de la sérine par l'eau, ou réactivation spontanée, est très lente *(Aldridge 1972)*. Elle est plus rapide pour les composés plus nucléophile que l'eau, tel que les oximes. C'est pourquoi les oximes sont à la base du traitement étiologique des intoxications par les OPs. Une autre réaction catalysée par l'enzyme peut suivre la phosphylation et conduire à la formation d'un conjugué beaucoup plus stable et non

réactivable : généralement, une désalkylation, appelée communément « vieillissement » *(Fleisher 1965; Ordentlich 1993b)*. La formation d'un pont salin entre l'imidazolium de l'histidine catalytique et l'oxyanion de l'adduit désalkylé est en partie à l'origine du gain de stabilité du conjugué. La vitesse de vieillissement dépend de la nature des substituants et de la stéréochimie de l'OP. Le temps de demi-vie ($t_{1/2}$) de vieillissement varie de quelques minutes pour l'hAChE inhibée par le soman à plusieurs dizaines d'heures pour la même enzyme inhibée par le VX.

| | Constante de vitesse de vieillissement ($h^{-1}$) | |
|---|---|---|
| | hAChE | hBChE |
| soman | 9,3[a,f] | 6,6[e,f] |
| sarin | 0,23[b] | 0,05[d] |
| tabun | 0,04[b] | 0,10[d] |
| VX | 0,02[b] | 0,01[d] |
| VR | 0,04[b] | n.m |
| CVX | 0,02[c] | n.m |
| DFP | 0,22[b,e] | 0,69[e] |

**Tableau 2.** Constantes de vitesse de vieillissement de l'hAChE et de la hBChE pour certains organophosphorés (sources : [a]*(Shafferman 1996)*, [b]*(Worek 2004a)*, [c]*(Aurbek 2006)*, [d]*(Aurbek 2009)*, [e]*(Masson 1997a)*, [f]*(Nachon 2005)*, n.m : valeur non mesurable).

La compréhension du mécanisme de vieillissement est un enjeu important sachant que cette étape compromet la réactivabilité de l'enzyme et donc l'efficacité du traitement. Le mécanisme de désalkylation chez l'AChE la rupture de la liaison C-O et de la formation d'un ion carbonium *(Harel 1991; Harris 1966; Michel 1967; Segall 1993; Shafferman 1996)* (**Figure 8**). Différentes études ont mis en évidence le rôle catalytique de certains résidus. Par exemple, dans le cas du soman, la désalkylation du groupement pinacolyle est catalysée par les résidus Glu199 (chez *Tc*AChE) et l'histidine catalytique (His440). Le premier stabilise électrostatiquement le développement du carbocation alors que la charge positive de l'histidine stabilise la formation de l'oxyanion, au cours de la scission de la liaison C-O *(Ordentlich 1993b; Qian 1993)*. Les résidus du site cation-π (Trp84 et Phe330) participent au mécanisme en favorisant la migration d'un méthyle vers le carbocation secondaire néoformé *(Qian 1993)*. Les structures tridimensionnelles de *Tc*AChE vieillie et non-vieillie ont confirmé l'implication de ces résidus dans le mécanisme de vieillissement et seront discutées plus en détail plus loin dans le manuscript *(Millard 1999b; Sanson 2009)*.

### *I.3 - Contremesures médicales des neurotoxiques de guerre*

#### *I.3.1 - Prétraitements*

Le principe des prétraitements est de prévenir l'inhibition de l'hAChE, soit en occupant transitoirement le site actif de l'enzyme, soit en piégeant l'OP en amont, par exemple dans la circulation sanguine.

La pyridostigmine est un carbamate utilisé dans les forces française (**Figure 9**). Il carbamyle la sérine catalytique, l'inactivant mais l'empêchant de se lier avec l'OP *(Gordon 1978)*. Comme la carbamylation de l'hAChE est transitoire, de l'hAChE active est progressivement libérée. Les personnels doivent prendre des comprimés de 30 mg toutes les 8 heures pour obtenir un taux idéal constant d'occupation de l'hAChE d'environ 30%. La pyridostigmine passe faiblement la BHE car elle est chargée. Elle ne protège donc pas les cholinestérases du système nerveux central. L'ésérine ou physostigmine est un carbamate non chargé capable de passer la BHE, mais qui possède une durée de vie courte et entraine des effets secondaires gênants *(Dirnhuber 1979)*. Elle est cependant en cours de développement au Royaume uni sous la forme d'un patch.

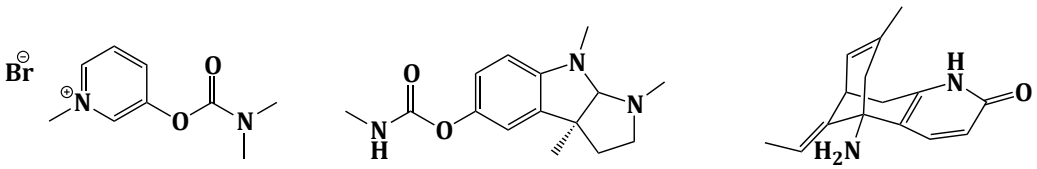


**Figure 9.** Structure chimique de la pyridostigmine, de la physostigmine et de l'huperzine A

Des inhibiteurs réversibles de l'AChE sont aussi évalués. L'(-)-huperzine A est un alkaloïde issu de la médecine traditionnelle chinoise qui a un meilleur effet protecteur que la pyridostigmine *(Grunwald 1994) (Lallement 1997)*. Elle développe des signes de toxicité aigüe aux doses prophylactiques *(Aracava 2009)*, mais donne de bons résultats en combinaison avec son isomère (+) *(Wang 2013)*. Des analogues avec une activité NMDA renforcée sont actuellement recherchés *(Gunosewoyo 2013)*.

Les enzymes bioépuratrices des OPs pourraient largement améliorer la protection et la décontamination internes et externes *(Bird 2010)*. Les recherches actuelles portent sur le développement de deux types d'enzymes : les bioépurateurs stœchiométriques, qui piègent spécifiquement et irréversiblement les OPs, et catalytiques, capable d'hydrolyser la liaison phosphoester de l'OP. Les qualités de bioépurateur stœchiométrique d'OP de butyrylcholinestérase humaine exogène ont été démontrées depuis près de 20 ans *(Raveh*

*1993; Saxena 2011)*. Environ 200 mg de hBChE sont théoriquement nécessaire chez un adulte pour protéger contre 2 $DL_{50}$ de soman *(Ashani 1998; Ashani 2004)*. Cette prophylaxie est remarquablement dépourvue d'effet secondaire *(Genovese 2010; Myers 2012)*. Les données les plus récentes sur les enzymes bioépuratrices sont détaillées dans l'article ***Nachon et al (2013) Chem. Biol. Int.*** (**Annexe B-1**).

A noter que les efforts actuels visent surtout à améliorer les méthodes de production de doses prophylactiques de hBChE, soit à partir de plasma *(Saxena 2008)*, soit d'animaux ou plantes transgéniques *(Geyer 2010; Huang 2007)*.

### *I.3.2 - Traitements*

La prise en charge d'individus intoxiqués par des pesticides ou des neurotoxiques organophosphorés associe décontamination, réanimation respiratoire et antidotes spécifiques. La réanimation respiratoire pose d'importants problèmes de logistique en cas d'afflux massif de victimes. La prise en charge de 100 blessés nécessite, sur le terrain, 120 000 litres d'oxygène pour 2 heures de ventilation, soit 200 bouteilles et 100 ventilateurs *(Bismuth 1993)*.

Les traitements antidotiques visent à contrer les effets de l'excès d'acétylcholine et à réactiver l'AChE inhibée. L'atropine, un antagoniste muscarinique, traite le bronchospasme, l'hypersécrétion bronchique et participe à l'amélioration clinique. Le traitement anticonvulsivant repose sur l'utilisation de benzodiazépines. Le diazépam (Valium®) est l'anticonvulsivant de référence. Il a un effet préventif des crises convulsives induites par les neurotoxiques mais il est sans action curative sur la crise déclarée. La kétamine (Kétalar®) présente un intérêt particulier en cas d'intoxication aux OP *(Riotte 1988)*. Elle a une action anticonvulsivante et neuroprotectrice *(Cowper 1943; Dorandeu 2003; Puu 1988)*. De plus, elle possède une AMM et est couramment utilisée en anesthésie aux doses neuroprotectrices. La réactivation de l'AChE est assurée par une oxime suffisamment nucléophile pour déplacer le groupement phosphyle de la sérine catalytique et libérer le site actif de l'AChE.

En France, l'atropine, une pro-drogue du diazépam (Avizafone) et le méthylsulfate de pralidoxime (2-pydidinium aldoxime ; 2-PAM) sont associés dans l'auto-injecteur Ineurope® bi-compartimenté fabriqué par la Pharmacie Centrale des Armées *(Rousseau 2009)*.


auto-injecteur Ineurope®

**Figure 10.** Seringues auto-injectables bi-compartimentée Ineurope®

Le 2-PAM fut découvert dans les années 50 *(Wilson 1955)* et les principales molécules développées dans les décennies qui suivirent sont des bispyridiniums qui en sont dérivées (**Figure 11**).

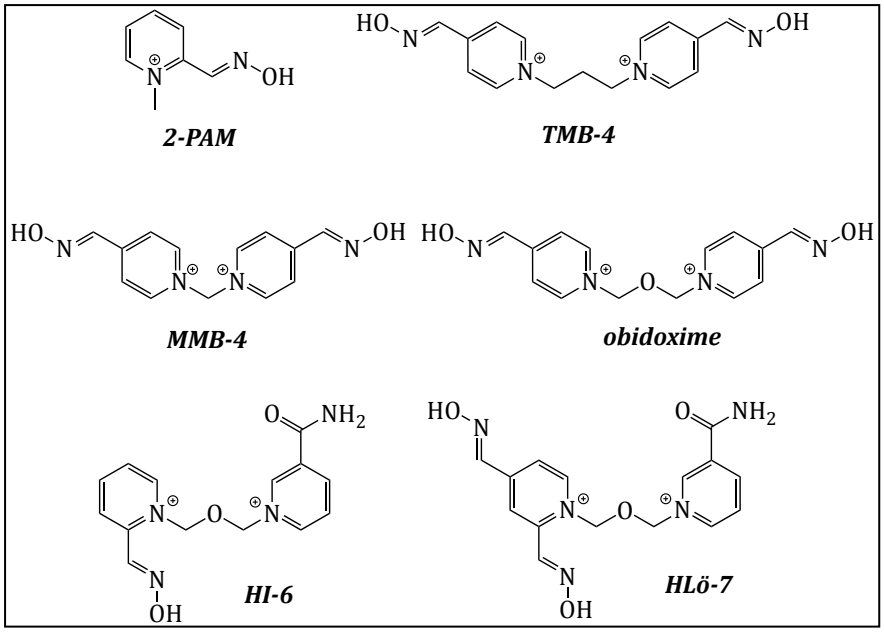


**Figure 11.** Structures chimiques des principales pyridinium aldoximes

L'efficacité d'un réactivateur peut être estimée par la constante bimoléculaire de réactivation kr2, qui est le rapport de la constante de déphosphylation, $k_r$ sur la constance de dissociation $K_D$ du complexe réactivateur/phosphyl-AChE [EP-Ox] *(Worek 2005)*:

$$[EP] + [Ox] \underset{}{\overset{K_D}{\rightleftharpoons}} [EP\text{-}Ox] \xrightarrow{k_r} [E] + [P\text{-}Ox]$$

**Figure 12.** [EP] est l'enzyme phosphylée ; [Ox] est l'oxime ; [EP-Ox] est le complexe réversible enzyme phosphylée – oxime ; [E] est l'enzyme libérée et [P-Ox] et l'oxime phosphylée.

Le **tableau 3** regroupent les constantes de la réaction de réactivation des principales oximes vis à vis de l'hAChE inhibée par différents OP. Si il apparaît que le 2-PAM est le moins efficace des réactivateurs, et qu'aucune oxime n'est efficace contre tous les OP. Le choix d'une oxime à visée thérapeutique, nécessite donc de réaliser un compromis entre son efficacité et sa toxicité selon la probabilité du risque encouru qui dépend du contexte d'emploi. Le spectre d'action d'une oxime varie selon de nombreux paramètres tels que sa concentration étroitement liée à sa toxicité et sa nature influençant son activité réactivatrice. Ces points sont exposés dans l'article de mise au point en annexe ***Vonesch et al. (2011) Médecine et Armées*** (***Annexe B-2***). Il en ressort qu'actuellement, le HI-6 semble le meilleur compromis. Même si il est inefficace vis-à-vis du tabun, le HI-6 donne de bons résultats contre le VX et le VR qui

sont des toxiques de guerre présentant une importante menace du fait de leur haute toxicité et de leur nature persistante. C'est pourquoi et il a été choisi pour très prochainement remplacer la pralidoxime dans l'autoinjecteur français.

| OP | Oxime | $K_D$ (µM) | $k_r$ ($min^{-1}$) | $k_{r2}$ ($mM^{-1}.min^{-1}$) | Références |
|---|---|---|---|---|---|
| VX | 2-PAM | 28 | 0,2 | 7,7 | |
| | obidoxime | 27 | 0,9 | 32,6 | *(Worek 2002)* |
| | HI-6 | 11 | 0,2 | 21,0 | |
| | Hlö-7 | 8 | 0,5 | 63,2 | |
| | MMB-4 | 1196 | 1, 6 | 1,3 | *(Worek 2010)* |
| | TMB-4 | | | | |
| VR | 2-PAM | 31 | 0,1 | 2,0 | |
| | obidoxime | 106 | 0,6 | 5,9 | *(Worek 2004a)* |
| | HI-6 | 9 | 0,7 | 77,2 | |
| | Hlö-7 | 5 | 0,8 | 158,5 | |
| | MMB-4 | 574 | 4,0 | 7,0 | *(Worek 2010)* |
| | TMB-4 | | | | |
| sarin | 2-PAM | 28 | 0,35 | 9,1 | |
| | obidoxime | 31 | 0,9 | 30,0 | *(Worek 2002)* |
| | HI-6 | 50 | 0,7 | 13,5 | |
| | Hlö-7 | 24 | 0,8 | 35,1 | |
| | MMB-4 | 1544 | 1,9 | 1,2 | *(Worek 2010)* |
| | TMB-4 | | | | |
| cyclosarin | 2-PAM | 3159 | 0,2 | > 0,1 | *(Worek 1998)* |
| | obidoxime | 946 | 0,4 | 0,4 | |
| | HI-6 | 47 | 1,3 | 27,5 | *(Worek 2002)* |
| | Hlö-7 | 18 | 1,7 | 92,9 | |
| | MMB-4 | 2467 | 4,5 | 1,8 | *(Worek 2010)* |
| | TMB-4 | 132 | 0,1 | 0,1 | *(Worek 1998)* |
| tabun | 2-PAM | 706 | > 0,1 | > 0,1 | |
| | obidoxime | 97 | > 0,1 | 0,4 | *(Worek 2004a)* |
| | HI-6 | *n.d* | *n.d* | *n.d* | |
| | Hlö-7 | 107 | > 0,1 | 0,2 | |
| | MMB-4 | 2418 | > 0,1 | > 0,1 | *(Worek 2010)* |
| | TMB-4 | 490 | 0,2 | 0,3 | *(Calic 2006)* |

**Tableau 3.** Constantes de réactivation de quelques oximes vis à vis l'AChE humaine érythrocytaire inhibée par différents OP. KD est la constante de dissociation du complexe [EP-Ox] ; kr est la constante de vitesse de déphosphylation du complexe [EP-Ox] et kr2 est la constante bimoléculaire de réactivation représentant l'efficacité de l'oxime. (n.d signifie qu'il n'y a pas réactivation).

Outre leur problème de spectre d'action limité et de toxicité, les oximes existantes sont doublement chargées, passent donc mal la barrière hémato-encéphalique et n'ont pas d'action sur les cholinestérases au niveau central. De nouvelles stratégies de développement d'oximes centrales ont émergées ces dernières années pour remédier à cette importante limitation. Ces stratégies sont basées sur de nouveaux nucléophiles ne portant pas de charge permanente, et/ou couplés à un ligand du site périphérique. Elles sont développées dans la revue ***Mercey et al (2012) Acc. Chem. Res.*** (**Annexe B-3**) et dans la quatrième partie de ce mémoire.

# II - Étude structurale de la butyrylcholinesterase

## *II.1 - Marquage de photoaffinité*

Le point de départ de mes travaux, au sein du laboratoire du Prof. Maurice Goeldner à la faculté de Pharmacie de Strasbourg, se situe peu après la résolution de la structure tridimensionelle de l'AChE de *Torpedo californica* en 1991 *(Sussman 1991)*. Cette structure bouleversa notre vision des cholinestérases. Contrairement à l'idée que l'on se faisait d'une enzyme très rapide dont le substrat est chargé positivement, le site actif n'est pas à la surface de l'enzyme ni de caractère anionique, mais est au contraire enfoui au fond d'une gorge étroite tapissée de résidus aromatiques. L'interaction clé entre l'enzyme et les ligands n'est donc pas de type ionique, mais de type cation-π, un type d'interaction qui avait été proposé quelques années auparavant par Dougherty *(Dougherty 1990)*. Or, dès 1980, Maurice Goeldner et Christian Hirth avaient mis au point une sonde photosensible cationique, le p-(N,N-diméthylamino)benzènediazonium (DDF), capable de se lier au site "anionique" des cholinestérases *(Goeldner 1980)*. La sonde forme une liaison covalente avec les résidus du site de liaison après activation par transfert d'énergie d'un tryptophane photoactivé. Cette particularité confère une grande spécificité à la sonde. Des photomarquages de l'AChE du poisson torpille permirent d'identifier le Trp279 comme étant l'élément essentiel du site périphérique des ligands quaternaires à l'entrée de la gorge, et les résidus Phe330 et Trp84 comme étant à la base du site de liaison des ammoniums quaternaires au fond de la gorge (poche choline) *(Harel 1993; Schalk 1994)*.

Chez la hBChE, le tryptophane du site périphérique n'est pas conservé, et sur les deux résidus phénylalanine et tryptophane de la poche choline, seul ce dernier est conservé. Les questions posées étaient: 1) le tryptophane conservé joue-t-il toujours un rôle important dans la liaison des ligands chargés chez la BChE, 2) d'autres résidus sont ils impliqués dans les interactions avec les ligands chargés, notamment au niveau d'un site périphérique? Les réponses à ces questions pouvaient être apportées en adoptant une stratégie semblable à celle utilisé avec succès sur l'AChE du poisson torpille, en utilisant le DDF tritié comme marqueur de photoaffinité. Une fois établi qu'une seule molécule de sonde photoincorporée par molécule de hBChE était suffisante pour inhiber totalement l'enzyme, et que la présence d'une concentration saturante d'un ligand connu du site actif de l'enzyme, la tacrine, permettait de protéger efficacement de l'inhibition par le photomarquage, la spécificité de la

photoincorporation était démontrée et l'essentiel du travail devenait un exercice de chimie analytique: après élimination de l'excès de sonde et trypsinolyse de l'enzyme marquée, une carte peptidique est établie par HPLC sur phase inverse, les peptides associés à la radioactivité sont séquencés et le comptage des éluats de séquençage permet de retrouver quel résidu a incorporé la sonde tritiée. Cependant, Les cartes peptidiques obtenues étaient compliquées en raison de la forte glycosylation de la hBChE (25% m/m). D'une part, les glycosylations protectrices de l'enzyme, forçait l'utilisation de conditions drastiques de trypsinolyse, favorable à des coupures aspécifiques à l'origine de peptides tronqués difficiles à séparer, d'autre part, l'hétérogénéité intrinsèque des glycosylations se retrouvait dans les temps de rétention. Une déglycosylation enzymatique totale simplifia les cartes peptidiques, et deux chromatographies consécutives (phase inverse/échangeuse de cations) permirent finalement d'obtenir des peptides suffisamment purs (**Figure 13**).

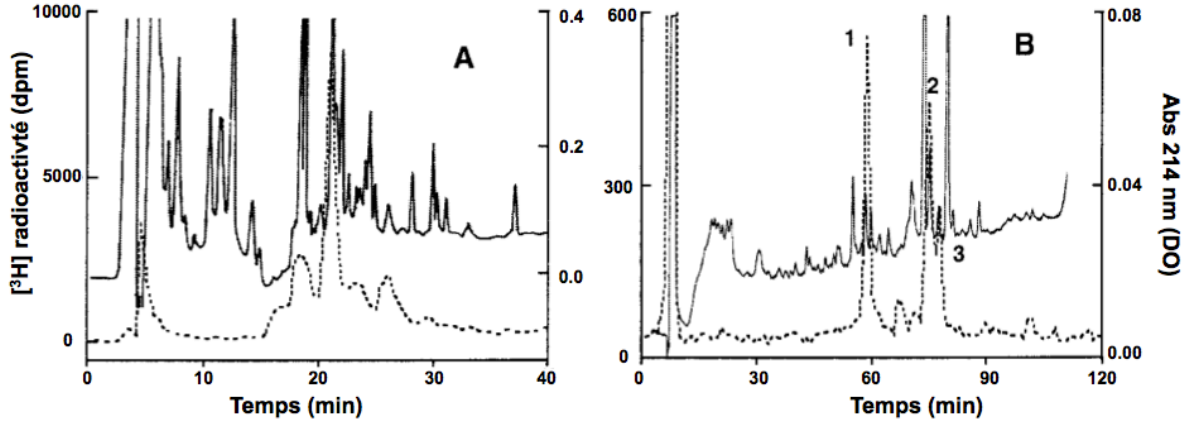


**Figure 13.** Purification des peptides photomarqués avec [$^3$H]DDF. (A) Chromotographie échangeuse de cation de type SCX. (B) Chromatographie du pic majeur de radioactivité sur phase inverse C18.

Le microséquençage du peptide 1, permis d'attribuer les signaux radioactifs à Tyr332 et ceux des pics 2 et 3 à Trp82, confirmant la prépondérance des interactions cation-π au sein de toutes les cholinestérases. La simplification des cartes issues de la déglycosylation donna également accès aux techniques de LC/MS et MALDI-TOF. Une comparaison des cartes peptidiques de l'enzyme avant et après photomarquage par le DDF non tritié, et une mesure systématique des masses des peptides élués, permis d'identifier les peptides tryptiques présentant une différence de masse correspondant à la masse de la sonde.

Les conclusions de ce travail furent que Trp82, homologue du Trp84 du poisson torpille, est le résidu essentiel du site estérasique de la hBChE et qu'il existe bien un site périphérique dont Tyr332 est un élément important (**Figure 14**).

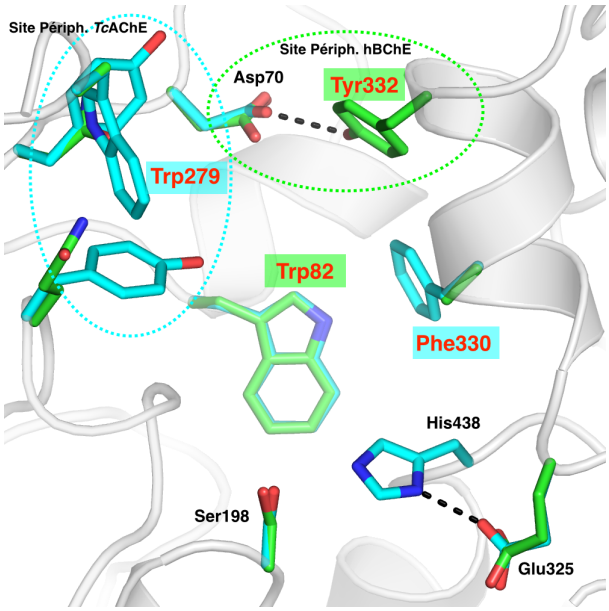


**Figure 14**. Résidus du site actif des cholinestérases photomarqués par le DDF. Les résidus de la *Tc*AChE (pdb 1ace) sont en cyan et ceux de la hBChE (modèle d'homologie de Harel basé sur *Tc*AChE ; *(Harel 1992)*) sont en vert. Les résidus photomarqués sont en annotés en rouge. Les autres résidus annotés portent la numérotation de la hBChE.

Tyr332 forme une liaison hydrogène forte avec l'autre élément important de ce site périphérique: Asp70. La mutation naturelle du résidu Asp70 en Glycine avait été à l'origine même de la découverte de l'hBChE, les porteurs de cette mutation étant victimes d'apnées prolongées après injection d'un anesthésique bisquaternaire, la succinylcholine *(Poulton 1979)*. Il avait alors été établi que cette réponse anormale était associée à une déficience d'une enzyme plasmatique responsable de l'hydrolyse de la succinylcholine: la hBChE. Ces travaux de photomarquage furent publiés dans l'article ***Nachon et al (1998) Biochemistry*** (**Annexe B-4**)

Ce travail de thèse sensibilisait sur quelques points: (i) les glycosylations sont une source de complication dont il est opportun de se débarrasser, (ii) la spectrométrie de masse est une méthode analytique puissante qui était alors souvent négligée par les biochimistes, (iii) le photomarquage est une méthode d'étude structurale fort utile pour établir la topographie d'un site actif lorsque la structure tridimensionnelle exacte d'une protéine n'est pas connue, mais est limitée. Disposer de la structure tridimensionnelle de la hBChE restait indispensable à la bonne compréhension des mécanismes d'hydrolyse et d'inhibition. L'absence de la connaissance de la structure tridimensionnelle est assez frustrante, et résoudre la structure de la butyrylcholinestérase humaine était une suite logique à ses premiers travaux.

### *II.2 - Ingénierie de la butyrylcholinestérase en vue d'améliorer sa cristallisabilité*

Ces travaux de thèse suscitèrent l'intérêt de Patrick Masson, qui me présenta à Oksana Lockridge de l'Université du Nebraska lors du *VIth Cholinesterase International Meeting* à San Diego en 1998. Le sujet de discussion tournait autour de la cristallisation de la hBChE, des problèmes rencontrés avec l'enzyme purifiée du plasma et des solutions à apporter. Travailler à partir d'une enzyme déglycosylée me semblait une solution des plus prometteuses, et très tôt Maurice Goeldner m'avait d'ailleurs encouragé à tester cette approche. Sur le conseil de Patrick Masson, Oksana Lockridge me fit une offre de stage post-doctoral de deux ans et je la rejoignis en mai 1999 peu après ma soutenance de thèse. La mise au point d'une forme cristallisable de hBChE était l'un des projets qui me furent confiés.

Ce stage post-doctoral fut l'occasion pour moi d'acquérir les techniques de biologie moléculaire et d'expression en bactérie et cellules eucaryotes. Mais la réussite au concours d'Ingénieur d'Étude et de Fabrication des Armées que Patrick Masson m'avait encouragé à passer, m'obligea à écourter mon séjour. J'intégrais donc l'unité d'enzymologie dirigée par Patrick Masson au sein du Centre de Recherche de Service de Santé des Armées à Grenoble (CRSSA), à peine 6 mois après mon arrivée aux USA. Cependant, grâce à la collaboration très active qui existait entre Oksana Lockridge et Patrick Masson je pus continuer à travailler sur le projet de cristallogénèse dès mon arrivée.

Un obstacle majeur qui s'oppose *a priori* à la cristallisation de la hBChE plasmatique est sa forte N-glycosylation. En effet, elle engendre une hétérogénéité de surface et prévient la formation de contacts intermoléculaires favorables à la cristallisation. Mes premiers essais de cristallisation de l'enzyme furent donc effectués sur de la hBChE plasmatique déglycosylée enzymatiquement, mais sans résultat. Un autre élément pouvait affecter la cristallisabilité de l'enzyme, son oligomérisation. La hBChE plasmatique est forme une structure tétramérique. de grande taille (4x85 kDa) potentiellement moins aisément cristallisable qu'un monomère. Or, Oksana Lockridge avait montré qu'il était possible d'obtenir une enzyme recombinante monomérique et stable en tronquant l'hélice C-terminale, impliquée dans la tétramérisation. Une stratégie d'ingénierie de la hBChE fut alors élaborée afin d'obtenir une protéine recombinante plus facilement cristallisable que l'enzyme plasmatique. Il s'agissait de combiner la délétion du domaine de tétramérisation, à une réduction du nombre de sites de N-glycosylation en remplaçant l'asparagine du motif N-X-S/T par une glutamine. Comme critère de sélection, l'enzyme mutée devait s'exprimer à des taux comparables ou supérieurs à l'enzyme sauvage et être stable.

Le taux d'expression de l'enzyme dépourvue de glycosylations était très faible, probablement en raison d'une mauvaise stabilité à la température d'expression dans les cellules CHO (37°C), et conformément aux observations faites sur l'enzyme plasmatique déglycosylée enzymatiquement. Le meilleur compromis taux d'expression/glycosylation était obtenu pour le mutant 4sugOff$_{17/455/481/486}$ BChE$_{\Delta 530}$, tronqué à partir du résidu Leu530 et dont 4 sites de N-glycosylation étaient supprimés sur les 10 sites potentiels. Après avoir vérifié que ce mutant possèdait les mêmes caractéristiques cinétiques que l'enzyme sauvage pour différents substrats et inhibiteurs, la production dans des bouteilles roulantes à grande échelle fut lancée (100 mg produits sur 6 mois). Conformément à nos attentes, une analyse par gel d'isoélectrofocalisation confirma que l'enzyme recombinante purifiée était beaucoup plus homogène que l'enzyme sauvage, en raison de sa plus faible glycosylation/sialylation.

Disposant d'une quantité suffisante d'enzyme recombinante purifiée, une collaboration fut entamée avec Juan-Carlos Fontecilla-Camps de l'Institut de Biologie Structurale (IBS) afin de réaliser les tests de criblage des conditions de cristallisation. Notre stratégie s'avéra très payante, vu qu'après plus d'une décennie d'essais infructueux de cristallisation de l'enzyme plasmatique, les premiers cristaux de hBChE furent obtenus en moins de 2 semaines, dès le premier test de criblage (**Figure 15**).

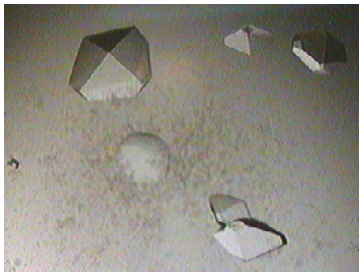

**Figure 15**. Cristaux tétragonaux de hBChE obtenues en goutte suspendue dans du tampon MES 0.1 M pH 6.5, 2.1 M $(NH_4)_2SO4$.

Ces cristaux font jusqu'à 600 µm dans leur plus grande dimension et diffractent jusqu'à 2.0 Å (données collectées à l'ESRF). Leur forme cristalline appartient au groupe d'espace tétragonal $I_{422}$. Ce travail d'ingénierie pour la cristallogenèse fit l'objet d'une publication dans l'article ***Nachon et al (2002) European Journal of Biochemistry*** (**Annexe B-5**). Dès lors, l'essentiel de mes activités de recherche fut basé sur des travaux reposant sur la cristallographie.

Un modèle initial fut rapidement trouvée par remplacement moléculaire en prenant la structure de la *Tc*AChE comme modèle de départ. La résolution de la structure de la hBChE et de certains complexes avec différents ligands fut le fruit d'un travail en binôme avec Yvain

Nicolet qui était alors dans sa dernière année de thèse à l'IBS. J'apportais mes connaissances sur les relations structure-activité des cholinestérases, et Yvain apportait son savoir-faire de cristallographe.

### *II.3 - Structure cristallographique de la butyrylcholinestérase*

Le repliement tridimensionnel de la hBChE est identique à celui de l'hAChE, on retrouve le feuillet ß central entouré d'hélices α et la triade catalytique (Ser198/His438/Glu325) localisée au fond d'une gorge (**Figure 16**). La gorge de la hBChE est d'un volume sensiblement plus important que celle de l'hAChE (500 $Å^3$ vs 300 $Å^3$), en raison du moindre nombre de résidus à chaine latérale aromatique faisant face à la cavité (**Figure 17**). En particulier, l'entrée de la gorge de la hBChE est plus spacieuse en raison de l'absence du cluster de résidus aromatiques (Trp286/Tyr72/Tyr124) présent chez l'hAChE. La poche choline est de dimension moins contrainte en raison du remplacement de Tyr337 par Ala328. La poche acyle est également nettement plus vaste car Phe295 et Phe297 sont respectivement remplacés par Leu286 et Val288. Cette différence explique en grande partie la différence de sélectivité des deux ChEs. A noter que le réseau de liaison hydrogène incluant la triade catalytique et s'étendant jusqu'au carbonyle du tryptophane de la poche choline est remarquablement conservé.

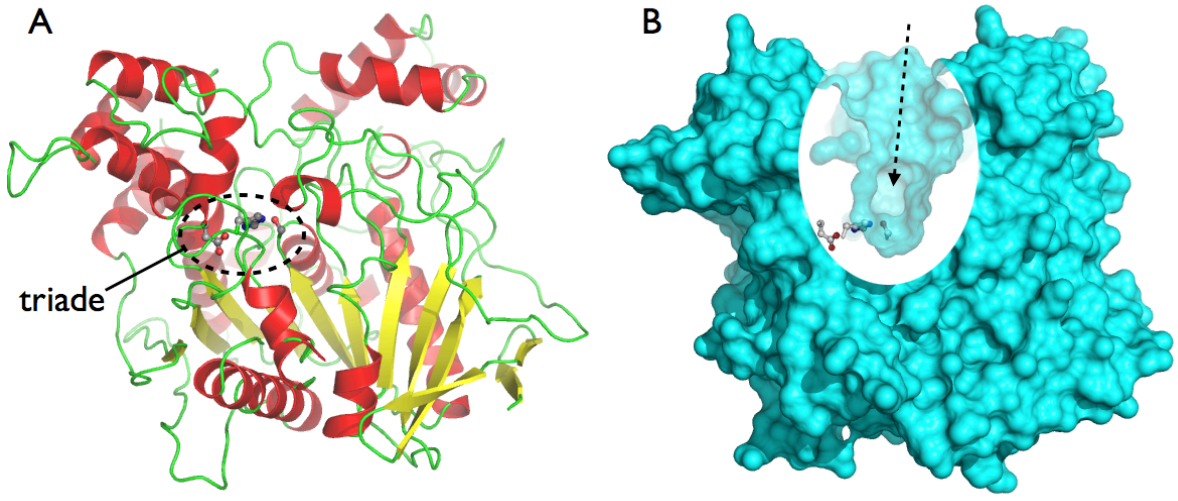


**Figure 16**. (A) Structure tridimensionnelle de la hBChE recombinante. Le feuillet β central est en jaune et les hélices α en rouges. Les régions moins structurées sont en vert. Les résidus de la triade catalytique Ser198/His438/Glu325 sont représentés en bâtonnets (oxygène en rouge; azote en bleu; carbone en gris). (B) Représentation de la surface d'accessibilité au solvant de la hBChE recombinante. La vue en coupe dans la région du site actif met en évidence la gorge menant à la triade catalytique.

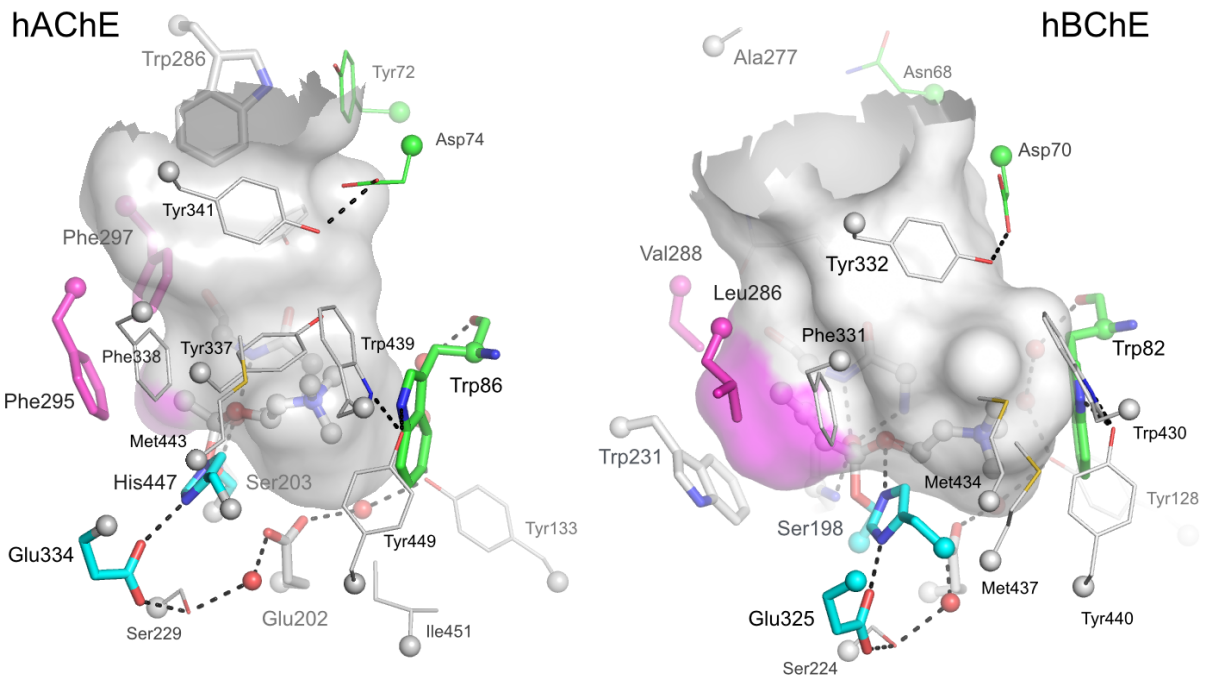


**Figure 17**. Comparaison des sites actifs de l'hAChE et hBChE. (pdb 4ey4 ; 2.16 Å et 1p0i ; 2.0 Å). Le volume de la gorge calculé à l'aide du logiciel Hollow est représenté par sa surface. Les poches acyle des deux enzymes sont en magenta, leur triade catalytique en cyan. Le résidu tryptophane essentiel de la poche choline est en vert. L'état de transition d'acylation d'une molécule d'acétylcholine (hAChE) et de butyrylcholine (hBChE) est modélisé afin d'illustrer le mode de liaison des substrats.

Il apparut au cours de la résolution de la structure qu'une molécule de nature inconnue était liée à la sérine catalytique alors qu'aucun ligand n'avait été volontairement introduit dans l'enzyme. La densité électronique de ce ligand est parfaitement modélisée par un carboxylate, éventuellement un butyrate d'après la longueur de la chaîne (**Figure 18)**.

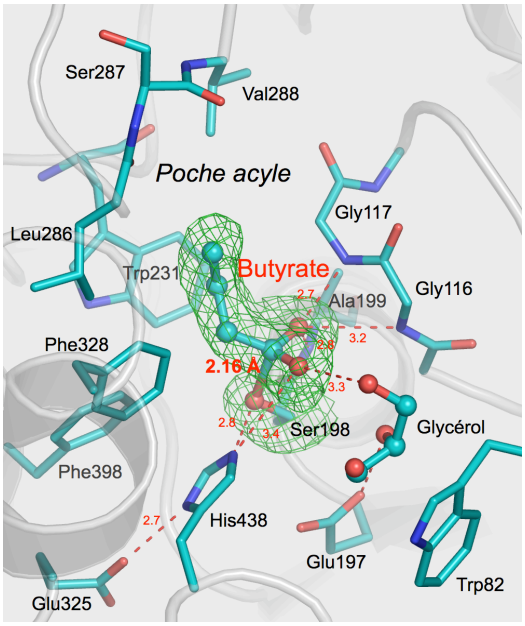


**Figure 18.** Vue du site actif avec un butyrate lié à la sérine catalytique Ser198 (pdb 1p0i ; 2.0 Å). La poche acyle est définie par les résidus Val288, Leu286 et Trp231. Le maillage vert est une carte de densité électronique calculée en omettant le carboxylate.

Le carbone carboxylique se situe à 2.16 Å de distance de Ser198-Oγ, une distance anormalement grande pour une liaison de nature covalente, suggérant une liaison dative. La chaîne du butyrate remplit la poche acyle définie par les chaînes latérales des résidus Val288, Leu286 et Trp231. Le carboxylate est stabilisé par 3 liaisons hydrogène avec les résidus Gly116, Gly117 et Ala199 qui constituent le "trou oxyanion", et une liaison hydrogène supplémentaire avec l'imidazolium de l'histidine catalytique (His438). Le carboxylate interagit également par liaison hydrogène avec une molécule qui occupe la poche choline, et ici modélisée par un glycérol (cryoprotectant utilisé). Ce complexe butyrate-sérine est un intermédiaire très proche du deuxième état de transition du cycle catalytique de l'enzyme avec la butyrylcholine comme substrat (**Figure 19**).

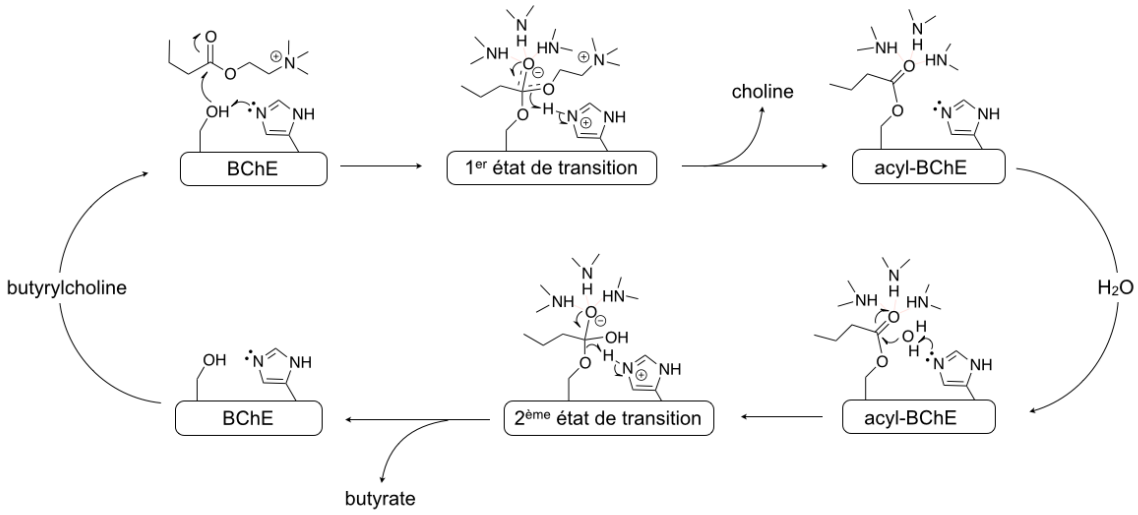


**Figure 19.** Mécanisme d'hydrolyse de la butyrylcholine par la hBChE

La présence de ce carboxylate suggère que l'état de transition de déacylation du cycle catalytique est très stabilisé lorsque la poche choline est occupée. Nous avons pu le confirmer en trempant des cristaux dans une solution contenant du bromopropionate, un analogue isostère du butyrate aisément identifiable en cristallographie grâce à la forte densité électronique du brome. Après trempage, le butyrate était effectivement déplacé par le bromopionate, leur position dans les deux structures étant virtuellement identiques. L'enzyme est donc capable de lier un carboxylate lorsque la poche choline est occupée.

En parallèle, les études cinétiques suggéraient que l'activation d'un facteur 3 en conditions d'excès de substrat était la conséquence de la liaison d'une deuxième molécule de substrat dans la gorge en faisant intervenir les résidus Tyr332 et Asp70 du site périphérique *(Masson 1997b; Masson 1999)*. Cette augmentation de l'activité pouvait donc avoir un lien avec l'occupation de la poche choline. Nous avons alors vérifié si une molécule de substrat

(butyrylthiocholine) pouvait effectivement se lier dans la poche choline dans une conformation capable de stabiliser le complexe butyrate-hBChE, modulant ainsi la catalyse.

Les essais de trempage de cristaux dans une solution contenant un large excès de butyrylthiocholine ne furent pas concluants. C'est pourquoi nous dûmes utiliser un analogue structural non-hydrolysable de l'intermédiaire tétraédrique de l'étape de déacylation, typiquement un adduit organophosphoré. Cet adduit est facilement obtenu par trempage de cristaux de hBChE dans une solution contenant un neurotoxique comme le soman. La réaction de la hBChE avec le soman conduit à la formation d'une pinacolylméthylphophonylsérine qui subit rapidement une réaction secondaire de désalkylation du groupement pinacolyle (vieillissement) (**Figure 20**).

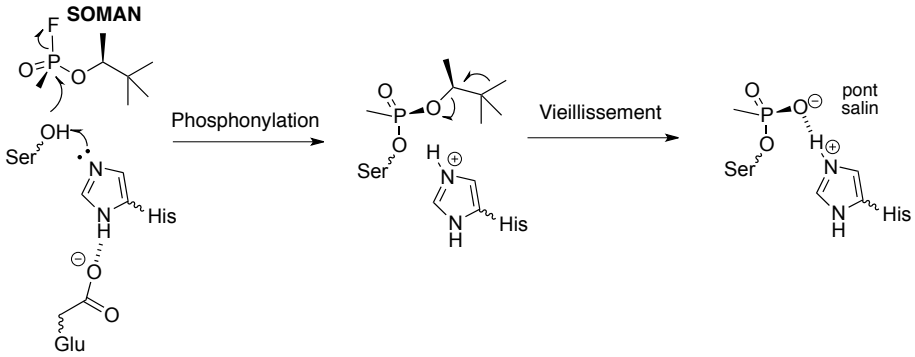


**Figure 20.** Mécanisme d'inhibition de la hBChE par le soman et vieillissement

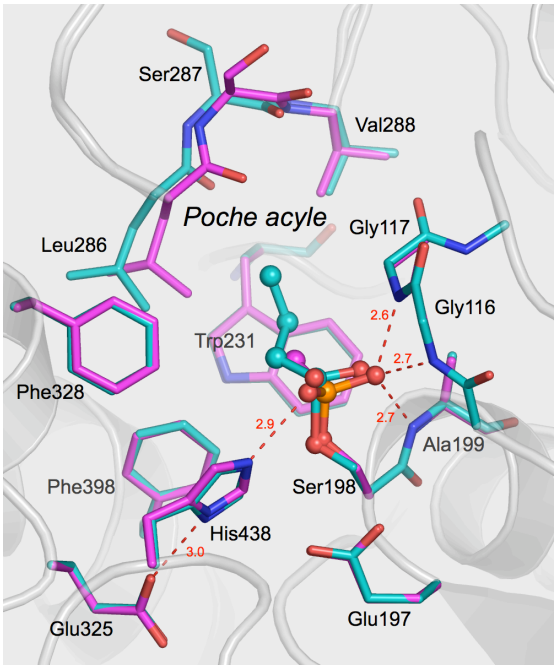


**Figure 21.** Soman-hBChE vieillie (magenta ; pdb 1p0q ; 2.4 Å) superposée au complexe butyrate-hBChE (cyan ; pdb 1p0i ; 2.0 Å).

La méthylphosphonylsérine résultant de ce vieillissement est un analogue stable structural de l'état de transition de déacylation. Nous avons tout d'abord résolu la structure de la hBChE inhibée par le soman et vieillie. La structure soman-hBChE "vieillie" est très semblable au complexe hBChE-carboxylate (**Figure 21**). La charge négative issue de la réaction de désalkylation se délocalise sur la molécule. Elle y est parfaitement stabilisée, par le trou oxyanion et ses 3 donneurs de liaison hydrogène d'une part, et par la formation d'un pont salin avec l'histidine protonée d'autre part. Cet ensemble d'interactions renforce la stabilité structurale du site actif et la stabilité globale de l'enzyme. En raison de cette stabilité accrue de l'adduit, les oximes utilisées pour réactiver les cholinestérases inhibées deviennent inefficaces sur les enzymes vieillies. La superposition de l'enzyme vieillie avec l'enzyme complexée par le carboxylate met en évidence un réarrangement de la boucle portant les résidus Leu286 et Ser287 de la poche acyle. Ce réarrangement est relatif au faible encombrement stérique que présente le méthyle du groupement méthylphosphonyl (soman) comparé à la chaîne du carboxylate. La "boucle acyle" est capable d'adapter sa conformation pour interagir de manière optimale avec les ligands. À noter que cette boucle constitue la paroi la plus fine de la gorge vis-à-vis du solvant extérieur, et au gré de ses « respirations », de petites molécules peuvent facilement diffuser de la gorge vers le solvant. En dehors de ce réarrangement, les structures des deux enzymes sont identiques ce qui conforte l'hypothèse que l'enzyme vieillie est un bon analogue structural de l'état de transition de déacylation.

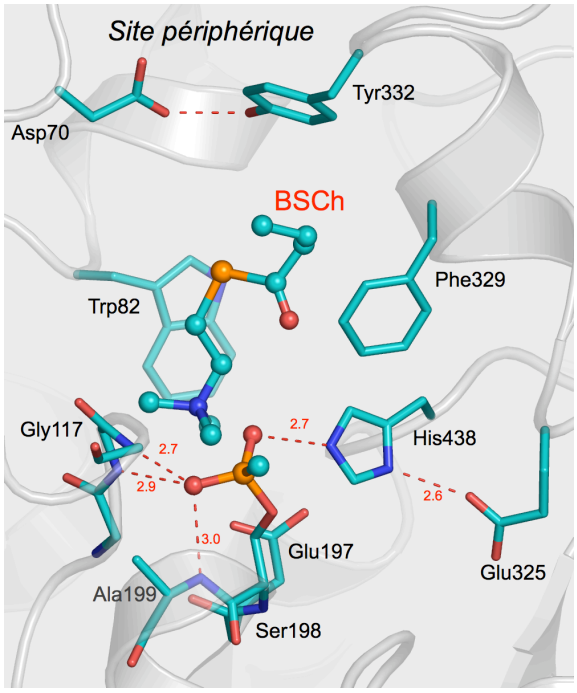


**Figure 22.** Complexe ternaire butyrylthiocholine (BSCh) et BChE/soman vieillie (pdb 1p0p ; 2.3 Å). Le résidu Trp82 est le site principal d'interaction de la tête cationique des ligands. Le site secondaire d'interaction (site périphérique) est formé par les résidus Asp70 et Tyr332.

Le complexe avec une molécule de substrat fut obtenu par trempage de cristaux de hBChE vieillie après phosphonylation par le soman dans une solution contenant de la butyrylthiocholine. La structure du complexe ternaire montre qu'une molécule de substrat est effectivement capable de se lier à la phosphonyl-enzyme et par homologie à l'acyl-enzyme (**Figure 22**). L'ammonium quaternaire et le noyau indole du résidu Trp82 forment une interaction π-cation tandis que la partie butyryle est au contact de Tyr332 du site périphérique. Dans cette position, la molécule de substrat occupe la poche choline sans encombrer L'acyl-sérine et peut potentiellement accélèrer la déacylation par stabilisation de l'état de transition. Après déacylation, le substrat peut se mettre rapidement en position favorable à l'hydrolyse par simple rotation autour de l'ammonium quaternaire fixé par Trp82. Aussi, suivant les différents substrats dérivés de la choline, on aura, soit une activation par excès de substrat pour les petites molécules (acétylcholine, butyrylcholine…) *(Masson 1993; Masson 1997b)*, soit une inhibition pour les molécules plus grosses qui vont limiter le trafic dans la gorge (benzoylcholine) *(Masson 2007)*. L'implication du résidu Tyr332 maintenu en place par liaison hydrogène avec Asp70 explique pourquoi l'affinité des substrats chargés, en particulier la succinylcholine, est altérée pour le variant naturel "atypique" Asp70Gly *(Masson 1996; Masson 1999)*. La succinylcholine, qui possèdent deux ammoniums quaternaires, l'un se fixant dans la poche choline l'autre au niveau de Tyr332, voit son hydrolyse largement ralentie du fait de cette mutation *(Masson 1997b; Mollerup 2011; Neville 1990)*.

L'ensemble de ce travail a permis de montrer les différences structurales entre l'hAChE et la BChE, clarifier le mécanisme d'hydrolyse et de donner une interprétation structurale à l'activation par excès de substrat. Il fut publié dans l'article ***Nicolet et al (2003) Journal of Biological Chemistry*** (**Annexe B-6** ; plus de 300 citations à ce jour).

### *II.4 - Stabilité des complexes carboxylates-cholinestérases*

La communauté des cholinestérasistes était particulièrement sceptique quand à la possibilité qu'un intermédiaire tétrahédrique carboxylate-hBChE avec une liaison non conventionnelle fut stable. En particulier, Daniel Quinn, un chimiste organicien spécialiste du mécanisme des sérines hydrolase, était assez hostile à notre interprétation. Cependant, il disposait d'une technique adéquate pour déterminer si il y avait bien accumulation d'un état intermédiaire dans des conditions d'activation par excès de substrat. Il s'agissait de déterminer l'effet isotopique secondaire pour un analogue deutéré de l'acétylthiocholine. La mesure de cet

effet isotopique permettait de déterminer si l'espèce réactive passe d'une hybridation sp2 à une hybridation sp3 ou vice-versa. Il nous proposa de collaborer pour mettre au point cette expérience. A sa surprise, l'observation d'un effet isotopique normal confirma que lors de l'hydrolyse de l'acétyl-hBChE, l'intermédiaire tétrahédrique est stabilisé jusqu'à s'accumuler avant d'être convertit en acétate. Ce travail fut l'object de la publication ***Tormos et al (2005) Journal of the American Chemical Society*** (**Annexe B-7**). Par la suite des calculs de mécanique quantique ont conforté que le complexe butyrate-enzyme est stabilisé lorsque le site cation-π est occupé par une molécule de substrat ou de glycérol *(Suarez 2006)*.

La présence d'un carboxylate est quasi systématique dans les structures de hBChE quand la sérine catalytique n'est pas phosphorylée mais son origine et sa nature même restent inconnues. Nous avons par exemple récemment montré qu'un carboxylate était présent dans le complexe hBChE-tacrine *(Nachon 2013)*. Cependant la densité électronique ne correspond pas à celle d'un butyrate mais est bien modélisée par une petite molécule cyclique, peut-être un dérivé de proline (**Figure 23**). Ceci suggère que la nature même du carboxylate observé dans les cristaux de hBChE est changeante et dépend de l'environnement de l'enzyme.

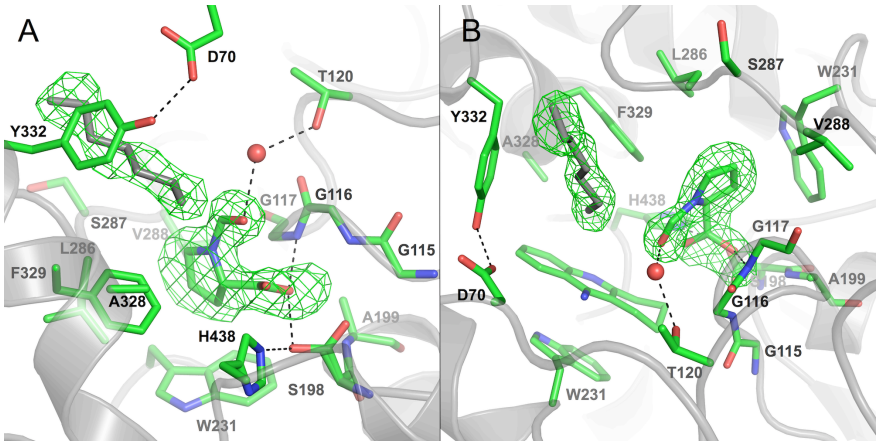


**Figure 23.** Vue latérale (A) et vue plongeante (B) de la gorge du site actif de la hBChE en complexe avec la tacrine (pdb 4bds ; 2.1 Å). Le maillage vert représente la carte de densité électronique Fo-Fc (3 σ) calculée en omettant le ligand de type carboxylate. La sérine catalytique (S198) adopte une position alternative. La densité électronique du carboxylate est interprétée par une petit molécule dérivée de la proline.

On pouvait également penser que la présence du carboxylate était propre à la forme recombinante de hBChE spécialement produite pour la cristallisation ($4sugOff_{17/455/481/486}$ $BChE_{\Delta 530}$), à son protocole de purification et aux conditions de cristallisation. Cependant, nous avons récemment eu la preuve que ce n'était pas le cas. En effet, cherchant à améliorer notre production de hBChE cristallisable, nous avons mis au point l'expression de hBChE dans des cellules S2 de drosophile *(Brazzolotto 2012)*. Le variant $4sugOff_{17/455/481/486}$ $BChE_{\Delta 530}$ n'étant pas correctement exprimé dans ce système, nous avons testé le variant $BChE_{\Delta 530}$. Celui-ci a été purifié à l'aide d'une nouvelle résine de chromatographie d'affinité à

base d'huprine plus performante et de nouvelles conditions de cristallisation ont été identifiées (0.2 M $NH_4OAc$ pH 7.4, 20% PEG 3350) dans un nouveau groupe d'espace ($P_{212121}$). A notre surprise, un carboxylate était encore présent sur la sérine catalytique malgré les changements radicaux de forme recombinante, système d'expression, protocole de purification et conditions de cristallisation (**Figure 24**).

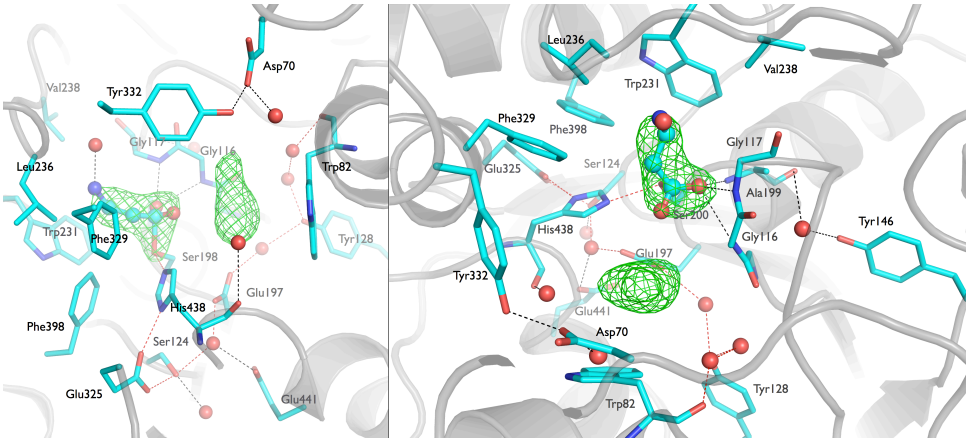


**Figure 24**. Vue latérale (à gauche) et vue plongeante (à droite) de la gorge du site actif de la hBChE exprimée en cellule S2 de drosophile (pdb 4aqd ; 2.5 Å). Le maillage vert représente la carte de densité électronique Fo-Fc (3 σ) calculée en omettant le ligand de type carboxylate. La densité électronique du carboxylate est interprétée par une ß-alanine.

Une fois encore, la nature exacte du carboxylate est incertaine, et la densité électronique fut interprétée par une ß-alanine. Un "blob" de densité non interprété témoigne de la présence d'un ligand dans la poche choline. Ce ligand participe probablement à la stabilisation du complexe sérine-carboxylate.

La hBChE est donc capable de stabiliser le complexe entre le produit acide de la réaction d'hydrolyse et la sérine catalytique dans certaines circonstances, mais qu'en est-il chez les AChEs? L'examen minutieux des données cristallographiques d'acétylcholinestérase de drosophile (*Dm*AChE), de *Tc*AChE et de souris (mAChE), le suggère fortement. Par exemple, la densité électronique proche de la sérine catalytique de l'acétylcholinestérase de drosophile complexée à un pesticide dérivé de la tacrine a été assignée à un ion sulfate (pdb 1dx4). En fait, cette densité est bien mieux modélisée par un propionate/glycinate lié à la sérine catalytique (**Figure 25**).

Encouragé par ces données, nous avons entrepris avec Daniel Quinn l'étude de l'effet isotopique secondaire sur la DmAChE. Là encore, l'accumulation d'un état intermédiaire tétrahédrique a été mis en évidence *(Tormos 2010)*.

Certaines structures de *Tc*AChE (par exemple 1ea5) montre également la présence d'une densité électronique proche de la sérine catalytique ressemblant à celle d'une molécule d'acétate. Enfin une molécule de carbonate ou acétate en contact avec la sérine catalytique et

presque systématiquement présente dans les structures de mAChE. Ces données suggèrent que toutes les cholinestérases sont capables de stabiliser un acide carboxylique dans leur site actif.

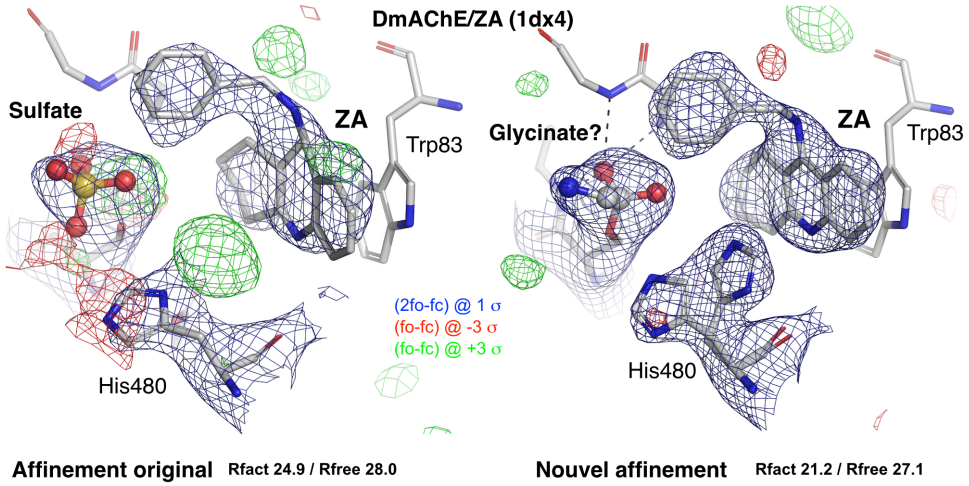


**Figure 25**. Structure du complexe DmAChE avec la N-benzyl-tacrine ZA (pdb 1dx4 ; 2.7 Å). A gauche, le modèle original déposé dans la pdb sous le code 1dx4. A droite, un nouvel affinement réaliser à partir des images de diffraction généreusement transmises par Joël Sussman. Les données sont en meilleur accord avec un carboxylate lié à la sérine catalytique plutôt qu'un sulfate non lié. L'histidine adopte deux positions alternatives.

### *II.5 - Complexes formés avec les analogues de substrat*

Les premières structures de hBChE que nous avons résolues nous ont beaucoup appris sur l'étape de déacylation du cycle catalytique. Il s'agissait de s'intéresser à l'étape d'acylation. Or, Daniel Quinn avait en sa possession une trifluoroacétophénone analogue de l'acétylcholine, le TMTFA (**Figure 26**).

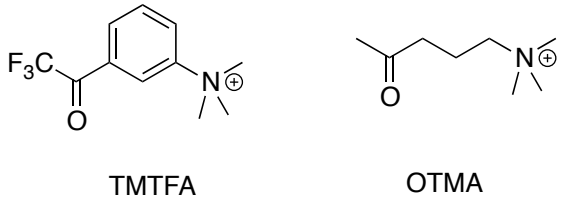


**Figure 26.** Structures chimiques du TMTFA et OTMA

La fonction cétone du TMTFA est rendue très électrophile par l'effet électroattracteur des 3 fluors en position alpha. Elle est capable de former un adduit covalent avec la sérine catalytique mimant l'état de transition de l'étape d'acylation. Nous disposions également d'un analogue non-hydrolysable de l'acétylcholine, l'OTMA, dépourvu de substituents électroattracteurs et donc moins électrophile (**Figure 26**). Comme il existait des études cristallographiques sur les complexes de la *Tc*AChE avec ces deux composés, études réalisées par les équipes de Joel Sussman du Weizmann Institute et de Martin Weik de l'IBS *(Harel*

*1996) (Colletier 2006)*, la résolution des structures des complexes avec la hBChE nous permettait une étude comparative.

Les deux structures furent obtenues par trempage de cristaux dans une solution contenant chaque ligand. La superposition des structures TMTFA-hBChE/*Tc*AChE montre que le ligand forme une liaison covalente avec la sérine catalytique dans les deux cas (1.47, 1.44 Å). L'ammonium quaternaire forme une interaction cation-π avec le Trp82/84. L'oxygène de l'hémicétal est stabilisé par liaison hydrogène avec le trou oxyanion. L'histidine de la *Tc*AChE pivote légèrement, n'étant pas contrainte par une phénylalanine adjacente comme chez la hBChE. Par contre le CF3 est beaucoup moins contraint dans la vaste poche acyle de la hBChE que dans celle de la *Tc*AChE. Cela se traduit par un décalage d'environ 0.5 Å du $CF_3$ et de Ser-Oγ (**Figure 27**).

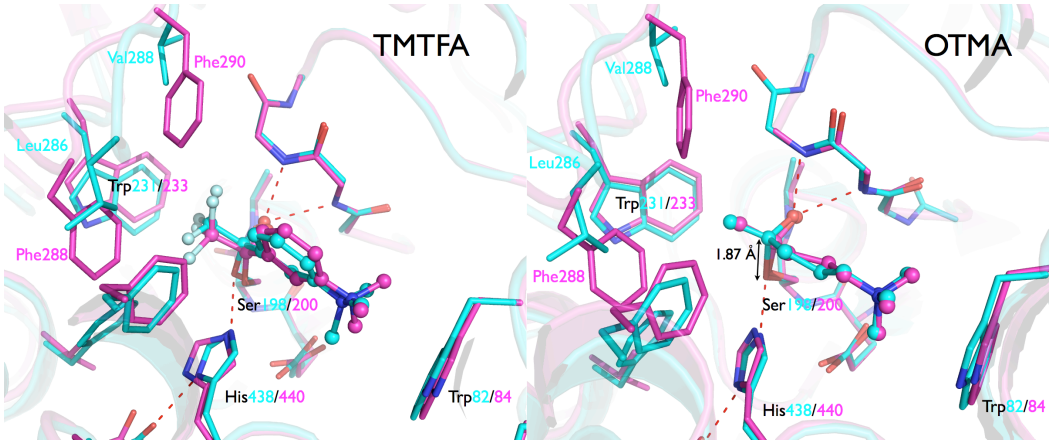


**Figure 27.** Superposition des complexes TMTFA-hBChE/TcAChE (panneau de gauche ; 2.3 Å et pdb 1amn à 2.8 Å) et OTMA-hBChE/hAChE (panneau de droite ; 2.3 Å et pdb 2vja 2.3 Å). La hBChE est couleur cyan, et la *Tc*AChE est couleur magenta. La géométrie des inhibiteurs est dictée par la topologie de la poche acyle des deux enzymes.

La superposition des structures OTMA-hBChE/*Tc*AChE suggère un rôle important pour le confinement par la poche acyle dans la stabilisation de l'état de transition d'acylation. Alors que le carbone du carbonyle et Ser-Oγ forment une liaison covalente conventionnelle chez la *Tc*AChE (1.43 Å), la liaison est nettement plus longue chez la hBChE (1.87 Å). Le faible confinement exercé par la vaste poche acyle aliphatique de la hBChE sur le méthyle de l'OTMA ne permet pas de contraindre la géométrie de l'hemicétal aussi efficacement que ne le fait la poche acyle aromatique de la *Tc*AChE. On peut faire l'hypothèse que la poche acyle exerce une contrainte similaire sur la formation de l'état de transition pour l'étape d'acylation, mais aussi pour celle de déacylation. Ces résultats sont rapportés dans un manuscript actuellement en préparation.

## III - Etude structurale des mécanismes d'inhibition et de vieillissement

### *III.1 - Rôle de la mobilité de l'histidine catalytique dans le vieillissement*

Charles Millard de l'Institute of Chemical Defense à Aberdeen aux USA avait publié un article faisant état d'un changement conformationnel radical de l'histidine catalytique lorsque la *Tc*AChE est inhibée par le VX *(Millard 1999a)*. La liaison hydrogène forte avec le glutamate de la triade (Glu327) est rompue au profit de la formation d'une liaison hydrogène avec un autre glutamate du site actif (Glu199). Le groupement éthoxy de la méthyléthoxyphosphonylsérine pointe vers l'histidine et induit un changement de conformation qui minimise les contraintes stériques. L'histidine revient d'ailleurs à sa conformation basale après vieillissement de l'adduit par déalkylation, son atome Nδ1 reformant une liaison hydrogène avec Glu327 de la triade, et Nε2 formant un pont salin avec l'oxyanion du méthylphosphonate (**Figure 28**).

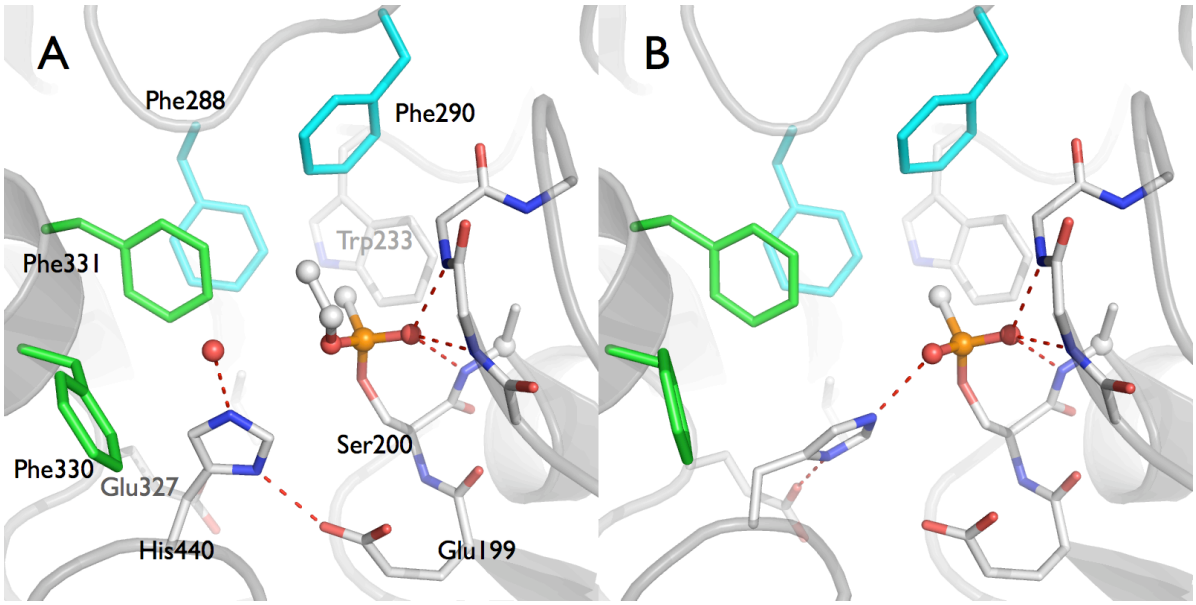


**Figure 28.** Sites actifs de la *Tc*AChE inhibée par le VX, avant (A ; 1vxr ; 2.2 Å) et après vieillissement (B ; 1vxo ; 2.4 Å). Les résidus de la poche acyle sont en cyan. Avant vieillissement, His440 forme des liaisons H avec une molécule d'eau et Glu199. Elle forme une liaison H avec Glu327 et un pont salin avec l'oxyanion du phosphonate après vieillissement.

Comme il a par ailleurs été montré que les formes ionisées de His440 et Glu199 jouent un rôle essentiel dans la désalkylation *(Masson 2010; Viragh 1997)*, Millard suggéra que l'histidine protonée ne peut efficacement catalyser la désalkylation que lorsqu'elle revient dans sa position basale, car c'est dans cette conformation qu'elle peut stabiliser le développement d'une charge négative sur l'oxygène de la liaison à rompre. Cette conformation n'est pas

favorable, Millard y vu une cause possible du temps de demi-vie de vieillissement relativement long de l'adduit (36 h).

Nous disposions de données cinétiques indiquant que l'adduit diéthylphosphoryl de hBChE vieillit près de 4 fois plus rapidement que celui de hAChE (12 vs 58 h). Suivant l'hypothèse de Millard, cette différence de vitesse pourrait traduire une différence de liberté conformationnelle de l'histidine catalytique entre l'hAChE et la hBChE, la conformation basale favorable au vieillissement serait plus stable chez la hBChE. Pour tester cette hypothèse, nous choisîmes de résoudre les structures cristallographiques de la hBChE inhibée par l'échothiophate, un OP utilisé dans le traitement du glaucome, qui forme l'adduit diéthylphosphorylsérine recherché (**Figure 29**).

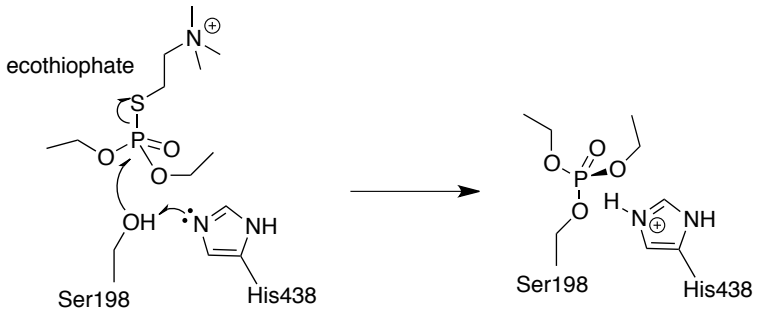


**Figure 29.** Inhibition de la hBChE par l'échothiophate avec formation d'un adduit diethylphosphoryl-sérine.

Le temps de demi-vie de vieillissement de 12 h rend possible la détermination des structures tridimensionnelles, avant et après vieillissement de l'enzyme inhibée par l'échothiophate. En effet, le temps de vieillissement est suffisamment long pour inhiber des cristaux de hBChE par trempage, et collecter des données cristallographiques avant que le vieillissement du conjugué ne soit survenu. La forme vieillie est facilement obtenue par cristallisation de l'enzyme inhibée que l'on aura laissée vieillir. Les structures des formes non vieillies et vieillies de la BChE inhibée par l'échothiophate ont respectivement été résolues à 2.1 et 2.25 Å (**Figure 30**). La structure de la forme non vieillie montre que l'oxygène non substitué est maintenu dans le trou oxyanion par 3 liaisons hydrogènes. L'un des substituants éthoxy remplie la poche acyle tandis que l'autre pointe vers His438, l'oxygène étant à 3.3 Å de Nε2. Il n'y a donc pas de changement majeur de conformation de l'histidine catalytique. Celle-ci est toujours dans une position favorable à la catalyse ce qui est en accord avec un vieillissement plus rapide que pour la hAChE. Cette stabilité conformationelle accrue pourrait résulter de l'interaction directe entre His438 et Phe398. Une interaction homologue n'existe pas chez les AChEs car cette phénylalanine est remplacée par une isoleucine.

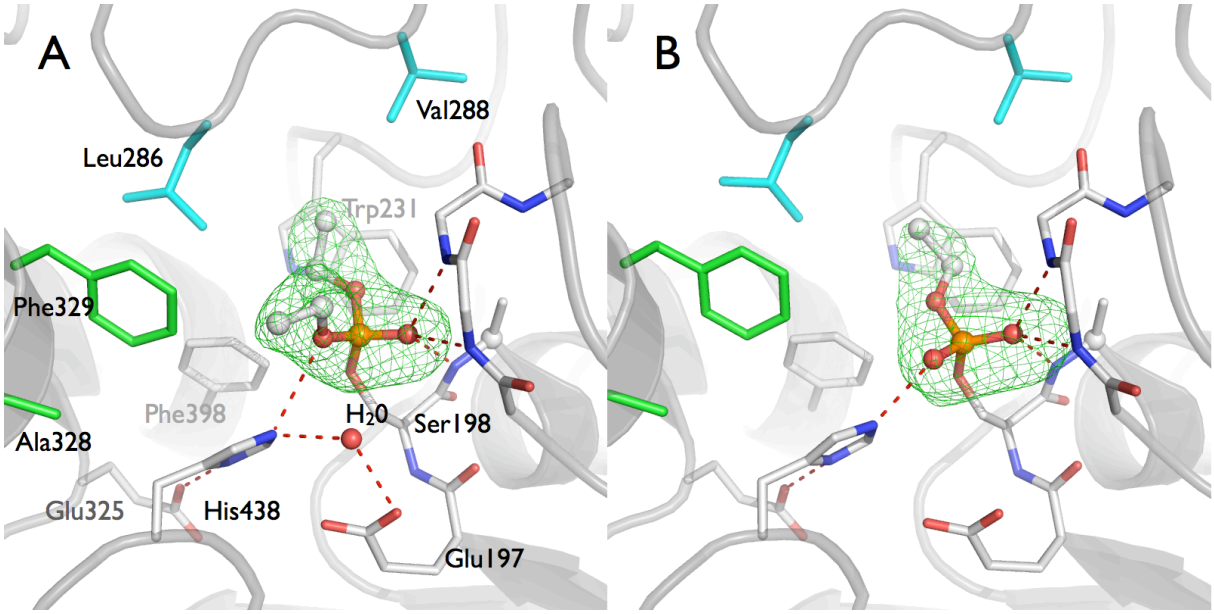


**Figure 30.** Sites actifs de la hBChE inhibée par l'échothiophate avant (A ; pdb 1xlw ; 2.25 Å) et après vieillissement (B; pdb 1xlv ; 2.10 Å). Les résidus de la poche acyle sont en cyan. Une molécule d'eau forme des liaisons H avec His438 et Glu197. Elle est en bonne position pour attaquer le phosphore. Après déalkylation, His438 forme un pont salin avec l'oxyanion du phosphate sans qu'elle ait bougée significativement. Le maillage vert représente la carte de densité électronique Fo-Fc (3 σ) calculée en omettant le ligand.

Le vieillissement est accompagné d'un léger ajustement des positions de la tête phosphoryle anionique et de l'histidine protonée conduisant à la formation du pont salin. Avant vieillissement, une molécule d'eau forme une liaison hydrogène avec His438 et Glu197 (2.9 et 2.8 Å). Elle est en position idéale pour participer au vieillissement selon 2 mécanismes possibles : soit par attaque du carbone primaire de l'éthoxy conduisant à la rupture de la liaison C-O (désalkylation), soit par attaque directe sur l'atome de phosphore via un mécanisme SN2 et rupture de la liaison P-O de l'éthoxy adjacent. Ce dernier mécanisme est analogue au mécanisme proposé pour l'isomalathion, un OP de type dithiophosphoester.

Ce travail fut effectué en collaboration avec Toyin Asojo et Gloria Borgstahl qui venaient de fonder un laboratoire de cristallographie à l'Université du Nebraska. C'est au cours de cette période que j'acquis une relative autonomie en matière de résolution des structures cristallographiques. Il fit l'objet de la publication ***Nachon et al (2005) Biochemistry*** (**Annexe B-8**).

### *III.2 - Étude du mécanisme de vieillissement par spectrométrie de masse*

Nous cherchions à déterminer lequel des deux mécanismes de vieillissement était prédominant. Comme ils se différenciaient par l'incorporation ou non d'une molécule d'eau, nous eûmes l'idée avec Larry Schopfer de l'Université du Nebraska, d'analyser le produit du vieillissement de l'adduit dans de l'eau constituée d'un isotope lourd de l'oxygène ($^{18}O$). Si le mécanisme prédominant est l'attaque nucléophile sur le phosphore, $H_2{}^{18}O$ devait être incorporée à l'adduit. Si le mécanisme dominant est la désalkylation, il ne devait pas y avoir incorporation. Il suffisait de déterminer s'il y avait incorporation d'$H_2{}^{18}O$ en spectrométrie de masse, en utilisant une méthode similaire à celle que j'avais utilisée lors de mon travail de thèse. Ce travail fut réalisé avec He Li, étudiant en thèse. Nous avons effectué une étude systématique du vieillissement des adduits de la hBChE inhibée par différentes famille d'OP conduisant à la formation de divers adduits et donc susceptible de vieillir par des mécanismes différents:

- échothiophate (adduit diéthylphosphoryl)
- dichlorvos (diméthylphosphoryl-)
- DFP (diisopropylphosphoryl-)
- isomalathion (O,S-dimethylphosphoryl-/O-methyl-S-diéthylthiosuccinylphosphoryl-)
- soman (méthylpinacolylphosphonyl-)
- sarin (méthylisopropylphosphonyl-)
- cyclohexylsarin (methylcyclohexylphosphonyl-)
- VX (méthyléthylphosphonyl-)
- VX russe (méthylisobutylphosphonyl-)

Le peptide comportant la sérine catalytique et porteur des adduits fut identifié dans chaque cas par spectrométrie de masse MALDI-TOF (**Figure 31** ; échothiophate).

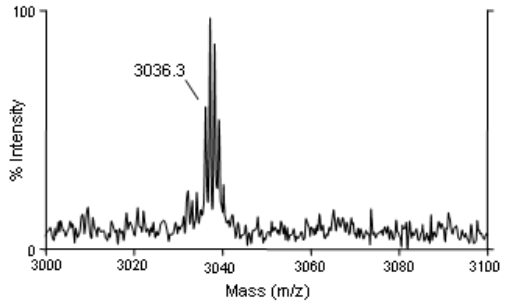


**Figure 31.** Spectre MALDI/TOF du peptide tryptique du site actif de la hBChE inhibée par l'échothiophate dans $H_2O^{18}$. Le pics à 3036.3 correspond à la masse monoisotopique attendue pour le peptide du site actif conjugué à un éthylphosphoryle après vieillissement par désalkylation (pas d'incorporation d'$O^{18}$).

La mesure de la masse des peptides avant et après vieillissement permis d'établir que le vieillissement de la BChE se fait par O-désalkylation pour l'échothiophate, le dichlorvos, le DFP, le soman, le sarin et le cyclohexylsarin. Remarquablement, nous n'avons pas observé de vieillissement pour le VX et le VR, son analogue russe. Ces cas particuliers seront étudiés plus loin dans ce mémoire. En revanche, l'isomalathion vieillit via les deux mécanismes proposés. Le produit majoritaire résulte de la cassure d'une liaison P-S suivant un mécanisme SN2 après attaque d'une molécule d'eau, et le produit minoritaire résulte de la désalkylation d'un O-méthyl ou d'un S-méthyl suivant l'énantiomère à l'origine de l'adduit. Ces travaux furent publiés dans ***He Li et al (2007) Toxicological Sciences*** (**Annexe B-9**).

### *III.3- Étude du vieillissement du tabun et de certains de ses analogues*

#### *III.3.1 - Étude du mécanisme par cristallographie et spectrométrie de masse*

Lors de cette étude mécanistique systématique par spectrométrie de masse, nous avions également analysé les produits de vieillissement de la hBChE inhibée par le tabun, éthyl-N,N-diméthylphosphoramidocyanidate. Cet organophosphoré forme un conjugué éthyl-N,N-diméthylphosphoramidylsérine qui est difficilement réactivable par les oximes connues. D'après des travaux de spectrométrie de masse réalisés sur la hAChE *(Barak 2000; Elhanany 2001)* et un travail de cristallographie réalisé sur la mAChE *(Ekstrom 2006a)*, l'adduit ne vieillit pas par désalkylation, mais via un mécanisme SN2, c'est-à-dire par attaque d'une molécule d'eau et élimination du groupement diméthylamine. Or, la masse de l'adduit vieilli de hBChE correspond à une phosphorylsérine, ce qui suggère qu'il y a à la fois désalkylation et déamination. Toutefois, il n'y a pas incorporation d'$^{18}O$ ce qui exclue que la déamination ait eu lieu quand l'enzyme était en présence d'$H_2{}^{18}O$. L'explication la plus simple était qu'il y a vieillissement par désalkylation, puis déamination "artéfactuelle" dans les conditions acides utilisées lors de l'analyse en spectrométrie de masse.

La méthode de choix pour tester cette hypothèse était de résoudre la structure de la hBChE inhibée par une solution racémique de tabun. Ce travail fut au cœur de la thèse d'Eugénie Carletti, thèse que j'ai supervisée. Nous avons résolu les structures cristallographiques du conjugué tabun-hBChE avant et après vieillissement (**Figure 32**).

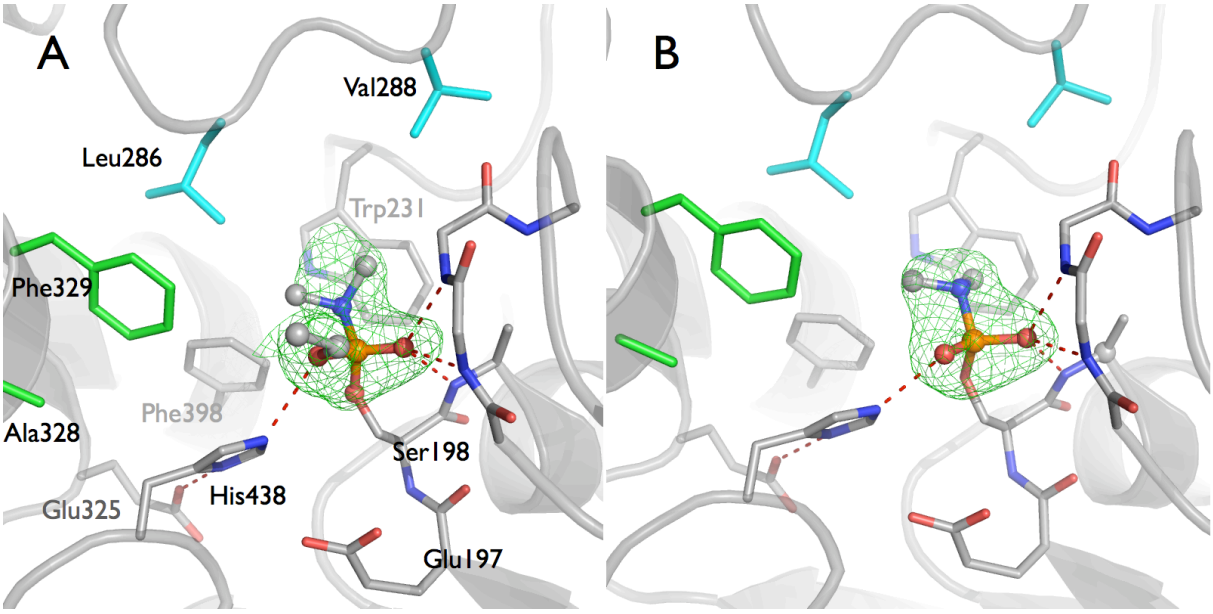


**Figure 32.** Sites actifs de la hBChE inhibée par le tabun avant (A ; pdb 3djy ; 2.1 Å) et après vieillissement (B; pdb 3dkk ; 2.3 Å). Le groupement diméthylamino est localisé dans la poche acyle (résidus en cyan). Le vieillissement résulte de la désalkylation de l'éthoxy pointant vers His438. Après désalkylation, His438 forme un pont salin avec l'oxyanion du phosphoramidate. Le maillage vert représente la carte de densité électronique Fo-Fc (3 σ) calculée en omettant le ligand.

La structure avant vieillissement montre que le tabun forme un adduit phosphoramidyl de configuration $P_R$ avec le groupement diméthylamino localisé dans la poche acyle et le groupement éthoxy pointant vers l'histidine catalytique qui reste dans sa conformation basale. Cette orientation de l'adduit est favorable à un vieillissement par désalkylation comme confirmé par la structure obtenue après vieillissement.

De plus, un examen des données cristallographiques des conjugués tabun-mAChE nous a permis de montrer que le conjugué présenté comme vieilli par déamination, était en fait partiellement désalkylé. Cette désalkylation partielle a engendré l'erreur d'interprétation des auteurs. Elle est vraisemblablement liée à la présence d'un ligand inconnu dans la poche choline. Par ailleurs, avant désalkylation, l'histidine catalytique adopte une nouvelle conformation alternative différente de celle observée dans le conjugué VX-*Tc*AChE non vieillie. Cette observation souligne une fois de plus la différence de flexibilité conformationnelle des histidines des deux familles de cholinestérases.

À la vue de ces résultats, et sachant que les résidus de la gorge de la mAChE et de la hAChE sont identiques, il semblait logique que le conjugué tabun-hAChE vieillisse également par désalkylation. D'autant plus que des résultats de cristallographies non publiés de Millard suggéraient aussi une désalkylation du conjugué tabun-*Tc*AChE. Pour conforter notre hypothèse, nous avons déterminé que 2 équivalents de tabun racémique étaient

nécessaires pour inhiber 1 équivalent de hAChE. Ceci indique que l'enzyme est énantiosélective et qu'elle forme logiquement un seul adduit, celui de configuration $P_R$ qui vieillit par désalkylation.

La conclusion de ce travail fut que les cholinestérases inhibées par le tabun vieillissent par désalkylation, et que les résultats antérieurs obtenus par spectrométrie de masse étaient artéfactuels (ce qui fut confirmé par la suite). Ce travail combinant cristallographie, spectrométrie de masse et cinétiques enzymatiques est publié dans l'article ***Carletti et al (2008) Journal of the American Chemical Society*** (**Annexe B-10**).

### *III.3.2 - Étude cristallographique du vieillissement de l'hAChE inhibée par le tabun*

Malgré le nombre d'arguments qui indiquent que le conjugué tabun-hAChE vieillit par désalkylation, je voulais obtenir une preuve plus directe de ce mécanisme en résolvant la structure du conjugué. La structure de la hAChE avait été résolue au début de la décennie par le groupe de Joël Sussman *(Kryger 2000)*. Mais c'est une protéine qui n'avait pu être cristallisée qu'en complexe avec la fasciculine, une toxine qui se fixe au niveau de son site périphérique et la stabilise. De ce fait, aucune structure de complexes avec des inhibiteurs n'avait été rapportée jusqu'à cette étude. Bien que la fasciculine couvre complètement l'entrée de la gorge, les résidus du site actif au fond de la gorge ne sont pas affectés, ce qui laisse la possibilité d'obtenir des adduits sans craindre de biais trop importants. Nous avons produit la hAChE recombinante en cellules CHO, puis avons cristallisé l'enzyme vieillie inhibée par le tabun en complexe avec la fasciculine.

La structure fut résolue à 2.8 Å de résolution, et conformément à ce que nous attendions, l'adduit vieilli est une N,N-diméthylphosphoramidylsérine résultant d'une désalkylation. Une comparaison de ce conjugué avec celui non vieilli de la mAChE montre l'ampleur de la réorganisation des résidus aromatiques du site actif qui accompagne la désalkylation (**Figure 33**). Ce travail est consigné dans l'article ***Carletti et al (2010) Journal of Medicinal Chemistry*** (**Annexe B-11**).

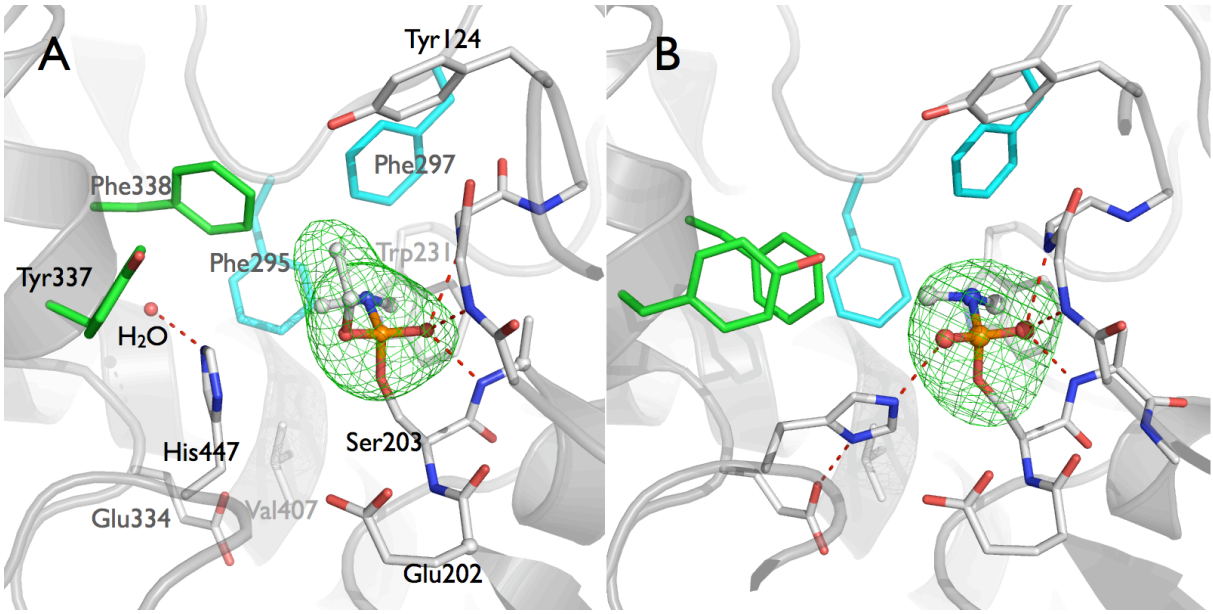


**Figure 33** : Sites actifs de la mAChE inhibée par le tabun avant vieillissement (A ; pdb 3dl4 ; 2.5 Å) et de la hAChE après vieillissement (B ; pdb 3dl7 ; 2.5 Å). Le groupement diméthylamino est localisé dans la poche acyle (résidus en cyan). Le vieillissement résulte de la désalkylation de l'éthoxy. His447 fait une liaison H avec une molécule d'eau, mais n'en fait ni avec Glu334 de la triade, ni avec Glu202. Le vieillissement est accompagné d'une importante réorganisation des résidus aromatiques du site actif (Tyr337; Phe338) et conduit à la formation du pont salin habituel. Le maillage vert représente la carte de densité électronique Fo-Fc (3 σ) calculée en omettant le ligand.

### *III.3.3 - Étude de l'inhibition de la hBChE par des analogues du tabun*

Nous avons ensuite entamé une collaboration avec Franz Worek de l'Institut de Pharmacologie et Toxicologie de la Bundeswehr à Munich, toujours dans le cadre de la thèse d'Eugénie Carletti. Il s'agissait d'une étude structure-activité sur des analogues N-monoalkyl et N,N-dialkyl du tabun (TA). L'objectif était de déterminer l'influence des substituents sur la phosphylation, la réactivation par les oximes et le vieillissement pour les OPs de la famille des phosphoramidates. L'étude cinétique réalisée par nos deux équipes est complétée par une étude cristallographique. Les résultats cinétiques indiquent que les substituants de l'azote affectent la réactivité des analogues principalement par des effets d'encombrement stérique, mais aussi par des effets électroniques. Par exemple, l'effet inductif donneur des deux substituants alkyls favorise une délocalisation du doublet libre de l'azote. Cette délocalisation peut diminuer l'électrophilie du phosphore. Ces deux effets sont moindres pour les dérivés monosubstitués ce qui explique qu'ils sont plus réactifs. L'étude cristallographique montre que malgré sa parfois grande taille, le substituant amino mono- ou disubstitué se place de préférence dans la poche acyle de la hBChE. Il est possible que cette sélectivité soit due à une interaction favorable entre le noyau indole de Trp231 et le développement de charges

partielles positives au niveau du groupement amino. Dans cette configuration, l'éthoxy des adduits pointe vers l'histidine catalytique et les conjugués vieillissent par désalkylation comme pour le tabun (**Figure 34**).

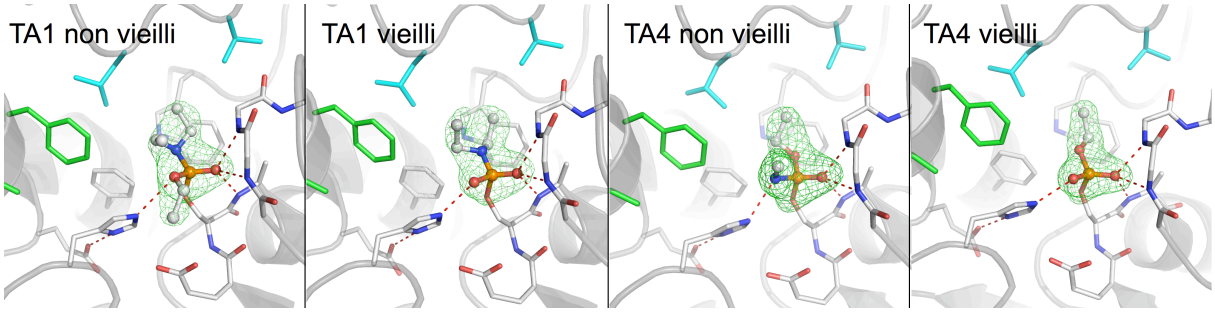


**Figure 34.** Sites actifs de la hBChE inhibée par TA1 (N,N-diéthyltabun) et TA4 (N-méthyltabun) avant et après vieillissement (pdb 2wid, 2wif, 2wig et 2wsl à respectivement 2.3, 2.25, 2.15 et 2.0 Å). Le groupement diéthylamino de TA1 est localisé dans la poche acyle (résidus en cyan). TA1 vieilli par déalkylation. Le groupement méthylamino de TA4 pointe vers His438. TA4 vieilli par substitution nucléophile sur le phosphore (SN2). Le vieillissement est accompagné de la formation du pont salin habituel. Le maillage vert représente la carte de densité électronique Fo-Fc (3 σ) calculée en omettant le ligand.

De manière inattendue, l'analogue N-méthylamino se positionne avec le groupement éthoxy dans la poche acyle et le groupement méthylamine dans la poche choline. Cette observation indique que la vaste poche acyle de la hBChE accommode mieux un substituant à 3-atomes (éthoxy) qu'un substituant à 2-atomes (méthylamine), probablement en raison d'une optimisation des interactions de van der Waals. La conséquence directe de cette orientation particulière est que l'éthoxy est éloigné de l'histidine catalytique et ne peut pas être désalkylé. Mais d'après la structure, il y a bien vieillissement par départ de la méthylamine située dans la poche choline. C'est le résultat attendu pour une attaque nucléophile par une molécule d'eau. Ce mécanisme de vieillissement est identique à celui proposé pour expliquer la formation de certains produits de vieillissement de la hBChE inhibée par l'isomalathion. Il est particulièrement important car il ne peut pas s'agir du mécanisme "en ligne" généralement postulé pour les attaques nucléophiles des adduits organophosphorés chez les cholinestérases. Dans le mécanisme "en ligne", le nucléophile attaque par la face opposée au groupe partant. Il se forme un état de transition trigonal bipyramidal dont les positions apicales sont occupées par le nucléophile et le groupe partant. Les substituants en position apicale sont les plus faiblement liés au phosphore et la rupture de la liaison entre le groupe partant et le phosphore est donc plus favorable que celles avec les substituants équatoriaux. Dans le cas du vieillissement du dérivé N-méthylé de tabun, la molécule d'eau ne peut pas attaquer par la face opposée au substituant méthylamino car elle est enfouie. Elle peut attaquer soit par la face opposée à la sérine catalytique (ce qui conduirait à une réactivation) soit plus logiquement par la face opposée à l'éthoxy, là où elle peut être activée par His438 et/ou

Glu197. Ceci implique qu'il doit y avoir réarrangement de l'état de transition bipyramidal pour que le substituant méthylamino passe d'une position équatoriale à une position apicale favorable à son départ. Cette possibilité de réarrangement a été confirmée pour cet adduit par des calculs de la densité fonctionnelle de la densité *(Kersharwani 2012)* et une étude de modélisation (Quantum Mechanics/Molecular Mechanics) suggère qu'il y a aussi un réarrangement similaire lors la phosphylation de la hAChE par le tabun *(Kwasnieski 2009)*. Ce mécanisme avec réarrangement peut être également dominant pour la réactivation des adduits OP-hAChE par les oximes, car la face des adduits opposée à la sérine est généralement moins accessible que celle côté poche choline. Or les oximes disponibles ne sont pas conçues en tenant compte de cette possibilité d'attaque latérale. Il y a donc probablement moyen de concevoir de nouvelles oximes plus efficaces basées sur cette hypothèse mécanistique.

L'ensemble du travail sur les analogues du tabun a été publié dans ***Carletti et al (2009) Biochemical Journal*** (**Annexe B-12**). Une discussion sur le mécanisme de vieillissement de l'analogue N-monométhyl de tabun et de ses implications potentielles est l'objet de la publication ***Nachon et al (2010) Chemico-Biological Interactions*** (**Annexe B-13**).

### *III.4 - Cas particulier des agents V*

Cette investigation sur les agents V découle de deux observations : (i) l'absence de détection de produits vieillis lors de l'étude par spectrométrie de masse du conjugué VX-hBChE (ii) la configuration de l'analogue N-méthylamino du tabun qui montre que l'éthoxy se place préférentiellement dans la poche acyle de la hBChE par rapport à un substituant plus petit. D'après ces deux observations il est possible que l'adduit VX (O-éthylméthylphosphonylsérine) a une configuration telle que l'éthoxy est dans la poche acyle et le méthyle pointe vers l'histidine catalytique. Selon cette hypothèse, il n'y aurait pas de désalkylation possible. Comme nous n'avions pas non plus observé de produits vieillis pour le conjugué VR-hBChE (O-isobutylméthylphosphonylsérine, VX russe), la même hypothèse est formulée. Pour la valider, nous avons entrepris de résoudre les structures de l'adduit VX-hBChE et ceux obtenus à partir des analogues russes (VR) et chinois (CVX ; adduit O-butylméthylphosphonylsérine). Ce travail a été l'objet de la première année de thèse de Marielle Wandhammer, thèse effectuée sous ma direction.

Nous avons résolu les structures cristallographiques des 3 conjugués par trempage de cristaux quelques minutes dans une solution racémique des trois agents V. Nous avons en plus

incubé des cristaux inhibés pendant 2 semaines pour observer un éventuel vieillissement *in crystallo*. Et enfin, nous avons cristallisé la hBChE préalablement inhibée et incubée pendant 2 semaines afin de vérifier que les inhibitions *in vitro* et *in crystallo* conduisent aux même adduits. Nous avons obtenu dans tous les cas une configuration dans laquelle l'alkoxy est dans la poche acyle, le méthyle pointe vers l'histidine catalytique. Dans ce cas, il ne peut donc y avoir vieillissement pas désalkylation. Encore une fois, la poche acyle de la hBChE est suffisamment spacieuse pour accommoder le plus gros groupement, ce qui la différencie de l'hAChE (**Figure 35**).

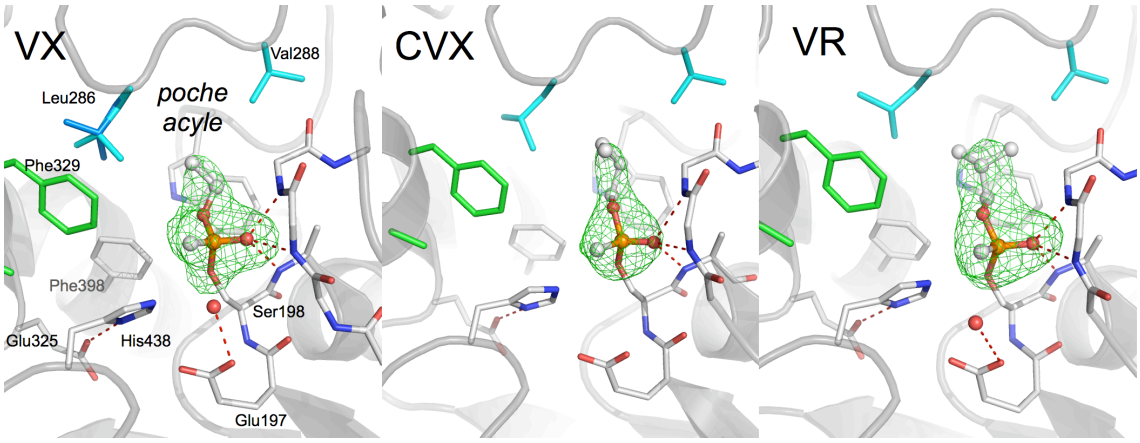


**Figure 35.** Sites actifs de la hBChE inhibée par le VX (O-éthylméthylphosphonyl- ; pdb 2xqf ; 2.1 Å), le CVX (O- butylméthylphosphonyl- ; pdb 2xqi ; 2.6 Å) et le VR (O-isobutylméthylphosphonyl- ; pdb 2xqg ; 2.3 Å). Le groupement alkoxy est systématiquement localisé dans la poche acyle tandis que le méthyle pointe vers His438. Cette configuration est défavorable au vieillissement par désalkylation. Le maillage vert représente la carte de densité électronique Fo-Fc (3 σ) calculée en omettant le ligand.

Il apparaît que les adduits des agents V racémiques sur la hBChE sont de configuration $P_S$ et ne peuvent pas désalkyler alors que les adduits sur la hAChE sont de configuration $P_R$, résultent de l'inhibition par l'isomère $P_S$ du VX et désalkylent. On pourrait penser que ces adduits étant de configuration opposée, ils sont issus des isomères opposés du VX, $P_R$ pour l'hAChE et $P_S$ pour la hBChE. Et pourtant des études cinétiques réalisées sur la hBChE et la hAChE par nos collaborateurs allemands (Franz Worek, BundesWehr) et néerlandais (Daan Noort du TNO) montrent que les deux enzymes présentent une énantiosélectivité pour le VX de configuration $P_S$ ou (-), certes plus faible pour la hBChE que pour l'hAChE (5x contre 100x). En parallèle nous avons vérifié par LC/MS que lorsqu'une solution racémique de 20 nM, 2 µM ou 200 µM de VX était incubée avec 0.5 équivalent de hBChE, c'est bien l'isomère $P_S$ qui est consommé préférentiellement. Si c'est bien essentiellement l'isomère $P_S$ qui réagit avec les deux enzymes, alors il s'ensuit que le mécanisme de phosphonylation de la hAChE par les agents V est "en ligne" avec le groupe partant opposé à la sérine catalytique, alors que le mécanisme pour la hBChE passe par un réarrangement.

Pour le confirmer nous avons étendu notre analyse cristallographique aux énantiomères purs de VX en collaboration avec nos collaborateurs du TNO (**Figure 36**).

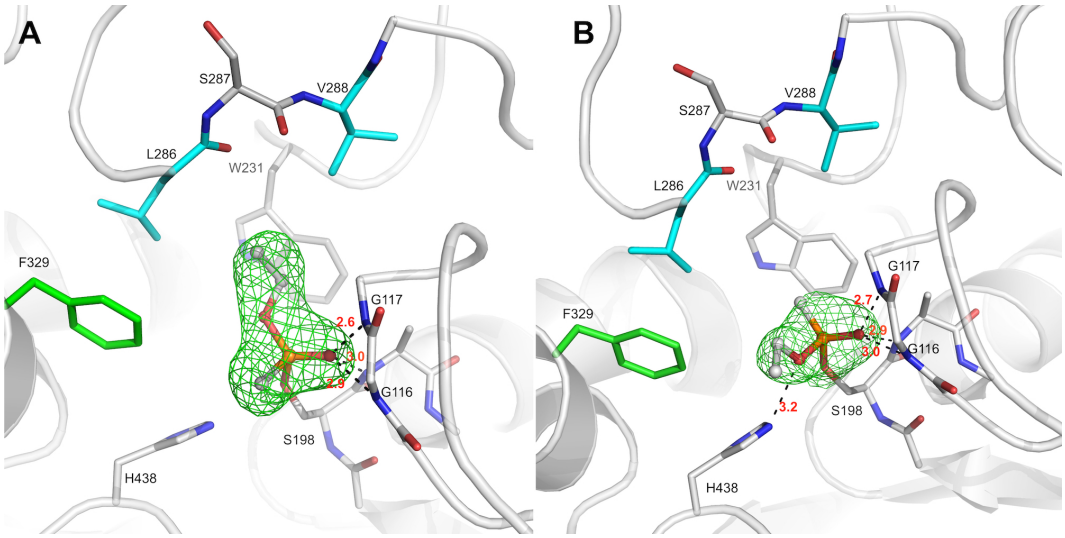


**Figure 36.** Site actif de la hBChE inhibée par le $VX_R$ (A ; pdb 2xqj ; 2.4 Å) et le $VX_S$ (B ; pdb 2xqk ; 2.4 Å). Le groupement alkoxy est localisé dans la poche acyle pour le $VX_R$ comme après inhibition par le mélange racémique. Il est orienté vers His438 pour le $VX_S$. Le maillage vert représente la carte de densité électronique Fo-Fc (3 σ) calculée en omettant le ligand.

Les structures des conjugués furent obtenues après un trempage de quelques minutes de cristaux de hBChE dans une solution contenant du $VX_R$ ou le $VX_S$. Le conjugué obtenu avec le $VX_R$ est identique à celui obtenu avec le mélange racémique: le groupement éthoxy est dans la poche choline. Le conjugué obtenu à l'aide du $VX_S$ est de configuration opposée à celle obtenue avec le mélange racémique: le groupement éthoxy pointe vers His438. Cette configuration est identique à celle obtenue pour *Tc*AChE *(Millard 1999a)* et mAChE (Ekström; pdb 2y2u). À noter que le conjugué avec le $VX_R$ a été obtenu pour chaque cristaux trempés, alors que le conjugué avec le $VX_S$ n'a pu être observé sans ambiguïté que pour un cristal trempé sur la demi-douzaine testée. Ce résultat confirme le mécanisme d'inhibition est bien "en ligne" pour les deux isomères. Le fait que le conjugué issu du $VX_S$ soit difficile à piéger et qu'il ne soit pas visible après réaction avec le mélange racémique suggère fortement qu'il s'hydrolyse spontanément très rapidement dans les cristaux alors que le conjugué issu du $VX_R$ s'accumule dans les cristaux. À ce stade, il n'est pas clair que cette surprenante réactivation spontanée du conjugués $VX_S$ soit liée à la nature cristalline de l'enzyme, ou aux conditions de cristallisation utilisée (MES 0.1 M pH 6.5, 2.1 M $(NH_4)_2SO_4$). Une mesure de la vitesse de réactivation spontanée de la hBChE inhibée par le $VX_S$ dans des conditions de cristallisation permettra de trancher. Les travaux de cristallographie ont été rapportés dans ***Wandhammer et al (2011) Journal of Biological Chemistry*** (**Annexe B-14**).

### *III.5- Vieillissement du conjugué soman-TcAChE par désalkylation*

La structure avant vieillissement de la mAChE inhibée par le tabun montre que l'histidine catalytique est mobile et adopte une conformation qui lui permet d'éviter un clash stérique avec l'éthoxy de l'adduit. La même observation avait été faite par Millard pour la *Tc*AChE inhibée par le VX, soit aussi face à un éthoxy. Il s'agissait de déterminer si l'histidine catalytique de l'AChE changeait également de conformation lorsqu'elle est face à un alkoxy très encombrant, comme le pinacolyle de l'adduit avec le soman. En fait, la désalkylation du pinacolyl en quelques minutes suggérait que non. Cependant, la rapidité de désalkylation peut aussi s'expliquer par la formation d'un carbocation secondaire relativement stable. C'est en collaboration avec Martin Weik de l'IBS que nous avons résolu la structure des adduits de soman-*Tc*AChE. Ce travail a été effectué avec Benoît Sanson alors étudiant en thèse.

Nous avons réussi à capturer l'adduit avant son vieillissement en trempant les cristaux moins de 6 minutes dans une solution légèrement basique (pH 8.2) cinétiquement défavorable à la désalkylation. La structure avant vieillissement de la *Tc*AChE inhibée par le soman montre que l'histidine catalytique ne change pas dramatiquement de conformation par rapport à sa position habituelle dans la triade. Elle reste dans une conformation favorable à la désalkylation (**Figure 37**). Toutefois, la formation du pont salin entre l'imidazolium et l'oxyanion du phosphonate se traduit par un déplacement de Nε2 de 0.8 Å au cours du vieillissement.

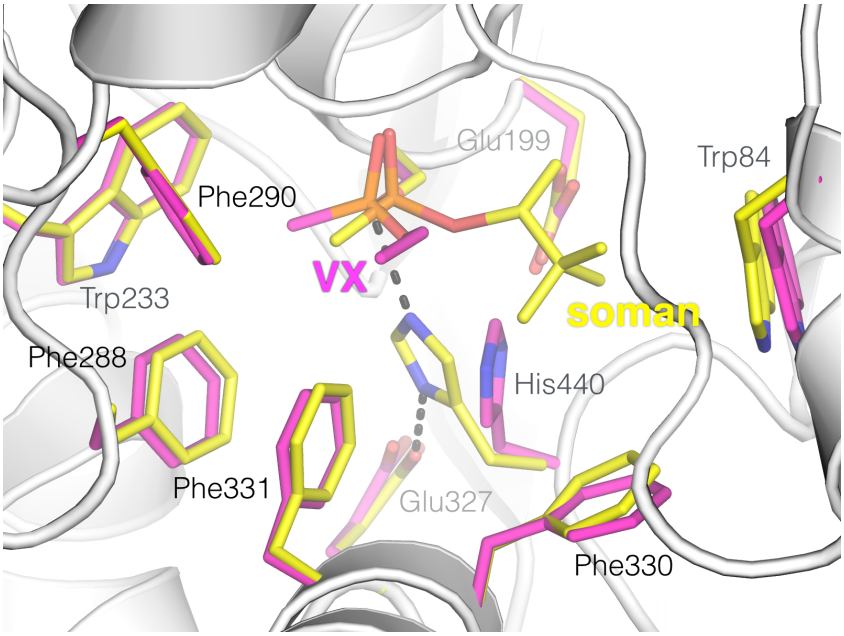


**Figure 37.** Superposition des sites actifs de la *Tc*AChE inhibée par le VX (magenta : pdb 1vxr ; 2.2 Å) et le soman (jaune : pdb 2wg2 ; 1.95 Å) avant vieillissement. His440 est restée dans sa conformation basale après inhibition par le soman.

La structure de l'adduit non vieilli permet de comprendre le mécanisme de désalkylation du pinacolyl dans ses détails. En effet, nous avons constaté une élongation de la liaison O-Cα d'environ 0.3 Å par rapport à une liaison C-O idéale. C'est une indication que la liaison est fragilisée par les interactions entre l'adduit et les résidus du site, principalement les effets électrostatiques de l'imidazolium et Glu199 et l'interaction de van der Waals avec Trp84. D'autre part, Kovach avait montré par une analyse des produits issus du pinacolyle, qu'il y a réarrangement du carbocation secondaire formé par rupture de la liaison O-Cα en un carbocation tertiaire plus stable *(Viragh 1997)*. Il y a migration d'un méthyle porté par Cβ vers Cα. Ceci suggère le scénario suivant: la liaison O-Cα est tout d'abord fragilisée et très polarisée ($O^{\delta-}$-$C\alpha^{\delta+}$). Mais elle ne se rompt pas irréversiblement tant qu'il n'y a pas eu migration d'un méthyle en provenance de Cβ vers $C\alpha^{\delta+}$. La migration du méthyle est doublement favorisée par la formation du carbocation tertiaire $C\beta^{+}$ intrinsèquement plus stable et par sa stabilisation supplémentaire par le système π de Trp84. Après migration, Cα n'est plus un centre électrophile et ne peut plus reformer la liaison par attaque de l'oxyanion. Enfin, l'imidazolium bascule légèrement pour former le pont salin avec l'oxyanion.

Ce mécanisme semble supporté par le fait que la configuration de Cα est $C_R$ dans la structure alors que les études cinétiques indiquent que l'AChE est inhibée plus rapidement par l'isomère $P_SC_S$. C'est-à-dire que Cα aurait inversé sa configuration après inhibition et serait donc passé sous forme carbocationique sans qu'il y ait rupture définitive de la liaison O-Cα. Cette étude a été publiée dans l'article ***Sanson et al (2009) Journal of Medicinal Chemistry*** (**Annexe B-15**).

### *III.6 Mécanisme d'inhibition et de vieillissement d'un dérivé du Triorthocrésylphosphate*

Le triorthocrésylphosphate (TOCP) est un additif ajouté à l'huile des moteurs d'avions soupçonné de jouer un rôle important dans le syndrome aérotoxique. Ce syndrome regroupe un ensemble de symptômes pouvant être rattachés à des troubles neurologiques *(Winder 2002)*. En effet, il arrive occasionnellement que des fumées provenant des moteurs contaminent le système de ventilation de la cabine passager. Le TOCP présent dans ces fumées est inhalé, puis métabolisé par les cytochrome p450 des microsomes du foie et l'albumine en 2-(o-cresyl)-4H-1,3,2-benzodioxaphosphoran-2-one (CBDP) (**Figure 38**).

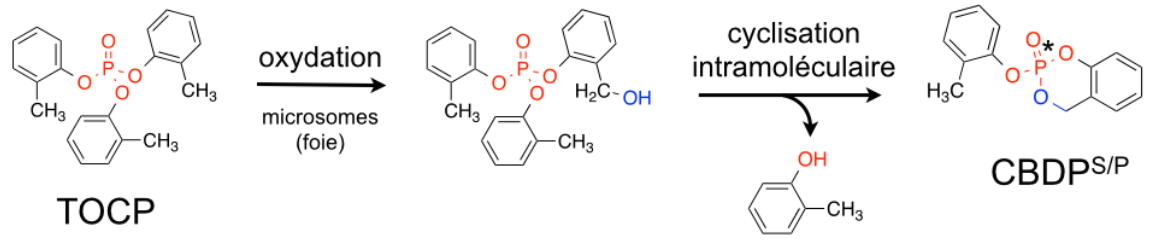


**Figure 38.** Métabolisme du Triorthocrésylphosphate (TOCP) en 2-(o-cresyl)-4H-1,3,2-benzodioxaphosphoran-2-one (CBDP).

Le CBDP est capable de phosphoryler les estérases, en particulier la neuropathy target esterase mais aussi les cholinestérases *(Aldridge 1954; Glynn 1999)*. C'est dans ce contexte que nous nous sommes intéressé au mécanisme d'inhibition des cholinestérases pour cet OP. Celui présente un intérêt particulier car d'une part, il est trop volumineux pour le site actif de l'AChE, ce qui suppose une adaptation conformationelle du site actif lors de l'inhibition, et d'autre part, les conjugués formés sont immédiatement non réactivables par les oximes, ce qui présage d'un mécanisme de vieillissement très rapide.

De la même manière que pour les autres OP, nous avons comparé la masse de l'adduit de la sérine catalytique formé au bout d'une heure par le CBDP avec la hBChE et la mAChE, dans de l'eau normale ou avec l'isotope $^{18}O$ (**Figure 39**). Cette expérience nous a montré que pour la mAChE, il y a uniquement formation de crésyl-phosphosérine. Par contre il y a formation de crésyl-phosphosérine et de phosphosérine pour la hBChE. De plus, l'expérience en $H_2{}^{18}O$ indique que la formation de phosphosérine passe par une attaque nucléophile de l'eau puisqu'il y a incorporation d'$^{18}O$ sur l'adduit. Cette étude de spectrométrie de masse a été complétée par une étude de suivie de la réaction par cristallographie.

Les structures issues de trempages de cristaux de hBChE dans une solution contenant du CBDP on été résolues pour des temps de 2 min et 12 h (**Figure 40;** A et B). La structure à 2 min de trempage montre qu'il y a rapidement formation de crésyl-phosphosérine, le crésyl étant localisé dans la poche acyle de l'enzyme. La crésyl-saligénine-phosphosérine n'a pas pu être observée malgré le temps de trempage très court. A ce stade, l'adduit est déjà une forme vieillie non réactivable, avec son oxyanion formant le classique pont salin avec l'histidine catalytique. Au bout de 12 h de trempage l'adduit a évolué en phosphosérine par déplacement du crésyl par une molécule d'eau comme déterminé précédemment en spectrométrie de masse. A noter que les liaisons de l'adduit sont très tendues car le crésyl est un peu encombrant pour la poche acyle de la hBChE pourtant spacieuse. La formation de la phosphosérine

s'accompagne d'une relaxation des liaisons, ce qui pourrait constituer une force d'entraînement pour la réaction.

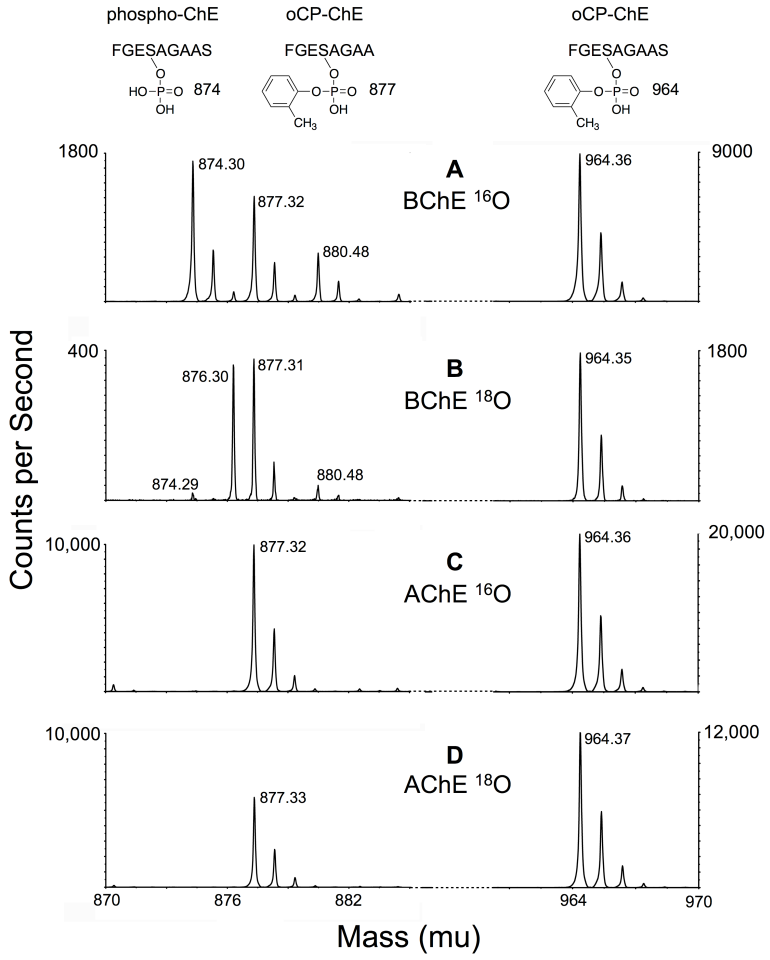


**Figure 39**. Réaction de la hBChE et mAChE avec le CBDP en présence de $H_2{}^{16}O$ (A et C) et $H_2{}^{18}O$ (B et D). Après inhibition durant 1 h et digestion à la pepsine, les peptides incluant la sérine catalytique sont analysés en MALDI/TOF (mode négatif). La séquence du peptide de masse 874 amu correspond au peptide de séquence FGES*AGAAS ou l'astérisque indique la sérine phosphorylé ($PO_4$). La masse du peptide phosphorylé est de 876 amu après réaction dans $H_2{}^{18}O$ (B), indiquant l'incorporation d'une molécule d'un oxygène provenant du solvent. Les séquences des adduits *o*-crésyl phosphate de masse 877 et 964 sont FGES*AGAA et FGES*AGAAS.

Les structures issues de trempages de cristaux de mAChE dans une solution contenant du CBDP on été résolues pour des temps de 30 min et 12 h (**Figure 40**; C et D). Pour la mAChE, l'adduit crésyl-saligénine-phosphosérine a pu être observé, avec la saligénine dans la poche acyle. Cependant, l'occupation partielle de la saligénine indique qu'environ la moitié des adduits ont déjà vieilli à ce temps. De manière remarquable, l'occupation partielle de la saligénine est corrélée à une position alternative de Phe297 qui n'a jamais été observée en dynamique moléculaire en absence de ligand. Ceci indique que c'est bien la présence de la saligénine qui induit le changement de conformation de Phe297. Cette dernière reprend d'ailleurs la conformation trouvée dans l'apoenzyme après départ de la saligénine.

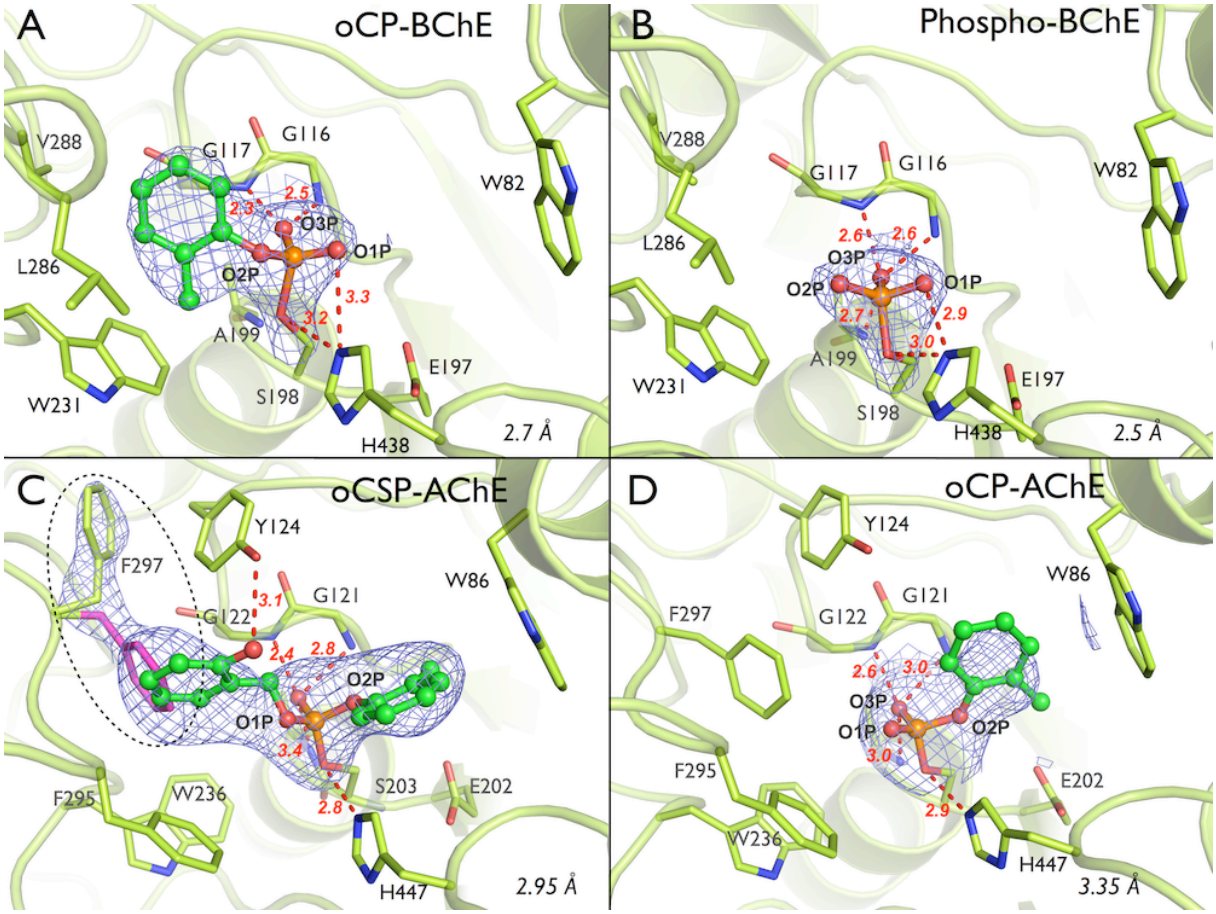


**Figure 40**. Cristallographie cinétique de l'inhibition de l'hBChE et mAChE par le CBDP. Pour la hBChE, des temps de trempage de 2 min et 12 h conduisent respectivement à la formation du conjugué *o*-crésyl-phospho-hBChE (A; pdb 4bbz ; 2.7 Å) et phospho-hBChE (B; pdb 2y1k ; 2.5 Å). Pour la mAChE, des temps de trempage de 30 min et 12 h conduisent respectivement à la formation des conjugués *o*-crésyl-saligénine-phospho-AChE (C; pdb 4bco ; 2.95 Å) et *o*-crésyl-phospho-mAChE (D; pdb 4bc1 ; 3.35 Å). La carte de densité électronique 2Fo-Fc est représentée en bleu et contourée à 1.0 σ.

Ces résultats combinés de cristallographie permettent une description détaillée de la stéréochimie de l'inhibition des deux cholinestérases par le CBDP (**Figure 41**). L'inhibition de la mAChE et hBChE implique les énantiomères opposés du CBDP, respectivement $P_R$ et $P_S$. L'isomère le plus inhibiteur de la mAChE n'est donc pas piégé par la hBChE. D'un point de vue mécanistique, il en découle deux chemins réactionnels et vieillissements différents. Pour la hBChE, la phosphorylation de la sérine catalytique conduit à la formation d'adduit crésyl-saligénine-phosphosérine très instable, dont le substituant saligénine située dans la poche choline désalkyle si rapidement qu'il ne peut être observé à l'échelle de temps des trempages de cristaux. Puis le *o*-crésyl mal accommodé dans la poche acyle est déplacée par une molécule d'eau avec au final la formation d'un conjugué phospho-hBChE non réactivable.

La phosphorylation de la mAChE est suivie par une désalkylation de la saligénine située dans la poche acyle. Cette désalkylation est inédite car l'histidine catalytique ne semble pas

impliquée vu son absence d'interaction avec l'oxyanion formé. Le conjugué *o*-crésyl-phospho-mAChE est stable, il n'y a pas formation de phospho-mAChE. Ces structures illustrent comment un inhibiteur encombrant comme le CBDP est capable d'induire un changement conformationelle et pourquoi leur vieillissement rapide rend toute réactivation vaine.

Ces travaux firent l'objet d'une publication dans les articles ***Carletti et al (2011)*** **et** ***(2013) Chemical Research in Toxicology*** *(***Annexe B-16 et B-17***)*.

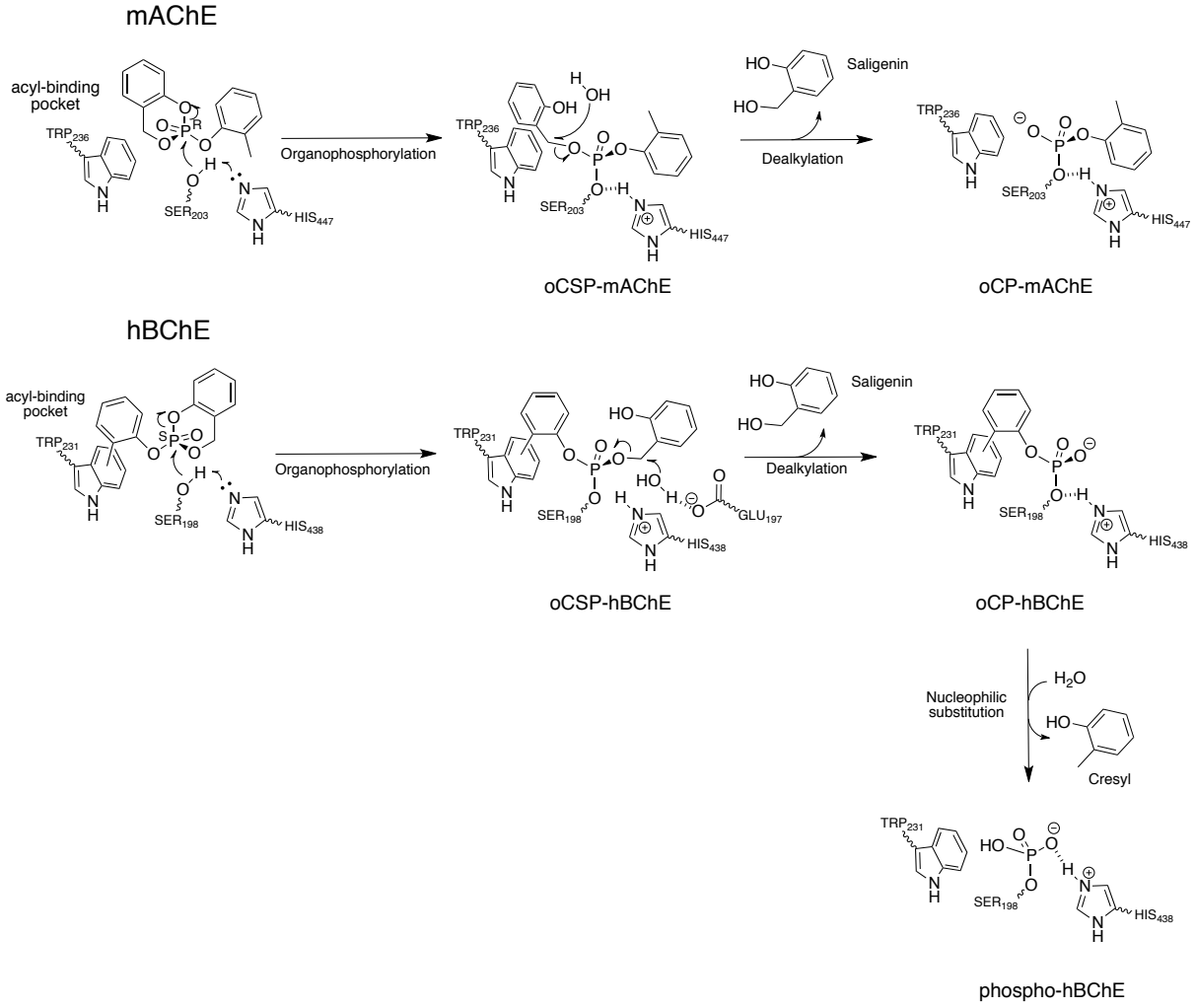


**Figure 41.** Mécanisme détaillé de l'inhibition de la mAChE et hBChE par le CBDP.

# IV - Perspectives de nouvelles contremesures médicales des toxiques de guerre organophosphorés

## IV.1 - Mutant G117H de hBChE, un bioépurateur autorégénérable

En raison de la stœchiométrie et de l'irréversibilité de la réaction de la hBChE avec les OP, la protection offerte est linéairement dépendante de la concentration plasmatique en enzyme *(Kasten 2010)*. Dès que la quantité d'OP dépasse la quantité de hBChE présente, l'OP en excès va diffuser vers les organes, y inhiber l'hAChE et les symptômes vont apparaître. La hBChE étant en quantité limitée dans le plasma (environ 5 mg/L), il est nécessaire d'augmenter la concentration plasmatique en enzyme en administrant de la hBChE exogène pour protéger contre de multiples $DL_{50}$ d'OP. En cas d'expositions multiples ou continues, les agents V ayant par exemple tendance à diffuser lentement depuis la peau sur plusieurs jours, il est nécessaire de renouveler le stock de hBChE par des administrations répétées, au fur et à mesure que celle-ci est inhibée. Comme le coût d'une dose protectrice de hBChE de 200 mg est estimé de l'ordre de plusieurs milliers voire dizaines de milliers d'euros, il apparaît économiquement très intéressant de disposer d'un variant de hBChE capable de se régénérer rapidement après inhibition, soit une enzyme capable de se réactiver spontanément en quelques minutes.

Dans les années 80, Järv a postulé que l'introduction d'un second résidu nucléophile dans le site actif des cholinestérases pourrait faciliter la déphosphylation de la sérine catalytique *(Järv 1984)*. Suivant ce principe, Millard et al ont développé en 1995, le premier mutant de hBChE ayant une activité hydrolytique vis-à-vis de certains OP *(Millard 1995)*. Pour cela, ils ont muté plusieurs résidus à proximité de la sérine catalytique en résidu histidine. L'hypothèse était que le noyau imidazole d'une l'histidine pouvait être suffisamment proche pour activer une molécule d'eau capable d'attaquer le phosphore ou même directement attaquer le phosphore. Le résultat le plus intéressant fut obtenu pour Gly117 du trou oxyanion. Ce mutant G117H est capable d'hydrolyser le paraoxon, le DFP, le sarin, l'échothiophate et le VX, mais assez lentement. Le $t_{1/2}$ de déphosphylation est de l'ordre de quelques minutes pour l'échothiophate et de l'heure pour le VX *(Lockridge 1997)*. Ce mutant n'était pas capable d'hydrolyser le soman du fait de la réaction de vieillissement très rapide en compétition avec la réaction de déphosphylation. Pour limiter la vitesse de vieillissement, Glu197, résidu connu pour catalyser la désalkylation a été muté en glutamine. Le double mutant G117H/E197Q était alors effectivement capable d'hydrolyser le soman *(Millard 1998)*. Par la suite, plus d'une soixantaine de double ou triple mutants de la hBChE ont été obtenus, tous basés sur le

même principe, mais aucun d'entre eux ne s'est révélé plus actif que le premier mutant G117H *(Masson 2008; Schopfer 2004)*. Des souris transgéniques exprimant le mutant G117H deviennent résistantes à une intoxication à l'échothiophate *(Wang 2004)*, mais le double mutant G117H/E197Q a une vitesse de phosphylation trop altérée pour offrir une protection *in vivo* par rapport à la hBChE sauvage *(Geyer 2010)*.

### *IV.2 Mutant de l'AChE de Bungarus Fasciatus*

Ce concept d'introduction d'un nouveau nucléophile a très vite été testé sur la hAChE, mais la mutation G122H, homologue à G117H, conduisait à une enzyme inactive (Shafferman, communication personnelle). Ceci pouvait facilement s'expliquer en raison des dimensions plus réduites du site actif de l'hAChE, en particulier en raison de l'encombrement de Tyr124 à proximité immédiate de la position 122. Un examen de la structure de l'hAChE montrait qu'il était nécessaire de réduire cet encombrement pour introduire une histidine sans trop perturber l'architecture du site actif. J'ai donc commencé à travailler sur des mutants de cholinestérases à réactivation spontanée accélérée en testant cette stratégie. Non pas sur l'hAChE, mais sur l'AChE de *Bungarus fasciatus* (*Bf*AChE) car elle s'exprime à des niveaux très élevés sous forme monomérique. Une comparaison du site actif de la hBChE à un modèle de *Bf*AChE suggérait que la substitution du peptide $_{122}$GFYS$_{125}$ par le peptide $_{122}$HFQT$_{125}$ permettait de retrouver une topologie homologue à celle du mutant G117H de hBChE (**Figure 42**).

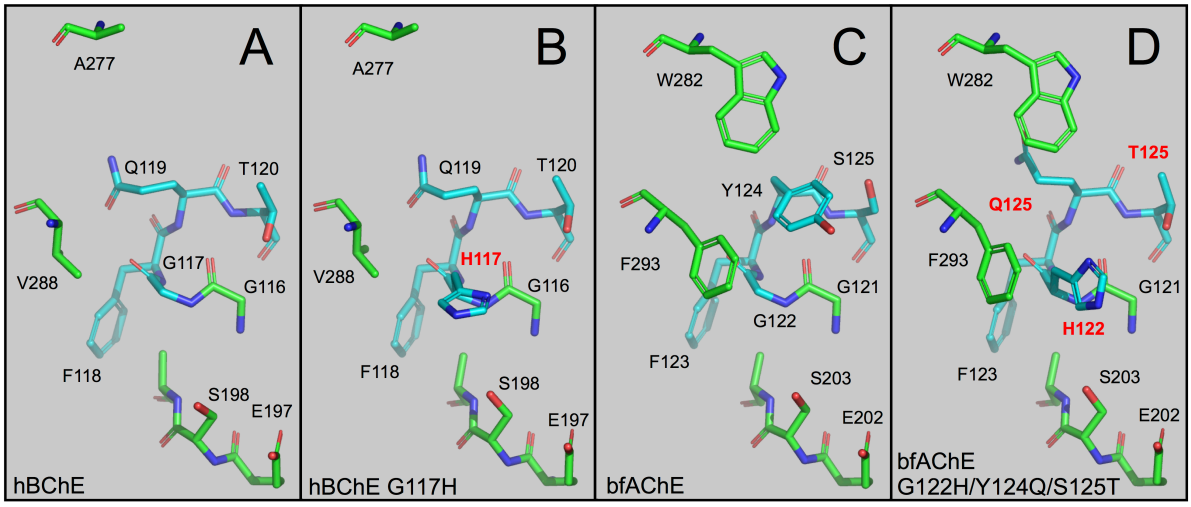


**Figure 42**. Site actif de hBChE (A), G117H hBChE (B), *Bf*AChE (C) et G122H/Y124Q/S125T (HQT) *Bf*AChE (D). Ala277 et Trp282 indiquent respectivement l'entrée du site actif de la hBChE et *Bf*AChE. Ser198 (A, B) et Ser203 (C, D) sont les sérines catalytiques. Le peptide G122H/Y124Q/S125T concerné par les mutations est en cyan. Les résidus mutés sont notés en rouge.

Malgré les modifications apportées, le site actif du triple mutant G122H/Y124Q/S125T était si altéré que son activité catalytique $k_{cat}/K_m$ sur l'acétylthiocholine était diminuée de 4 ordres de grandeur par rapport à l'enzyme sauvage. Le mutant n'était également plus inhibé par un excès de substrat et jusqu'à une concentration de 80 mM. Ce mutant est résistant à l'inhibition par des concentrations sub-millimolaires d'OP en raison d'une faible affinité, avec une activité de réactivation spontanée mesurable envers le paraoxon, l'échothiophate, et le diisopropyl phosphofluoridate (DFP). Nous avons pu éventuellement démontrer que pour ce mutant, le DFP était un substrat de type « slow-binding » de type B (isomérisation lente du complexe enzyme-DFP). Bien que son activité OP hydrolase est marginale car très inférieure à celle du mutant G117H de 1 à 3 ordres de grandeur suivant l'OP, il s'agissait tout de même du premier mutant d'AChE capable d'hydrolyser des OP. Ce travail fut publié dans l'article ***Poyot et al (2006) Biochimica et Biophysica Acta*** (**Annexe B-18**).

### *IV.3 Étude structurale du mutant G117H de hBChE*

La raison principale pour laquelle les tentatives d'amélioration des capacités hydrolytiques du mutant G117H ont échoué, était que le mécanisme de déphosphylation restait globalement incompris. Il n'était pas clair qu'il s'agissait bien d'un mécanisme acido-basique: soit l'histidine supplémentaire active une molécule d'eau qui hydrolyse la phosphylsérine, soit elle fait une attaque nucléophile directe pour former une phosphylhistidine intermédiaire, plus facilement hydrolysable. La connaissance de la structure du mutant G117H, en particulier sous sa forme phosphylée par divers OP, apparaissait comme un point critique pour comprendre le mécanisme. Le besoin pressant de cette structure était illustré par une série de publications d'étude du mécanisme reposant sur une modélisation du mutant *(Amitay 2011; Amitay 2009; Vyas 2010)*. Bien qu'intéressants, ces modèles ne pouvaient pas remplacer une structure expérimentale.

J'ai donc résolu la structure du mutant G117H, ainsi que celles avec l'intermédiaire d'hydrolyse phosphyl-Gly117His/hBChE pour l'échothiophate ainsi que pour le VX (**Figure 43**).

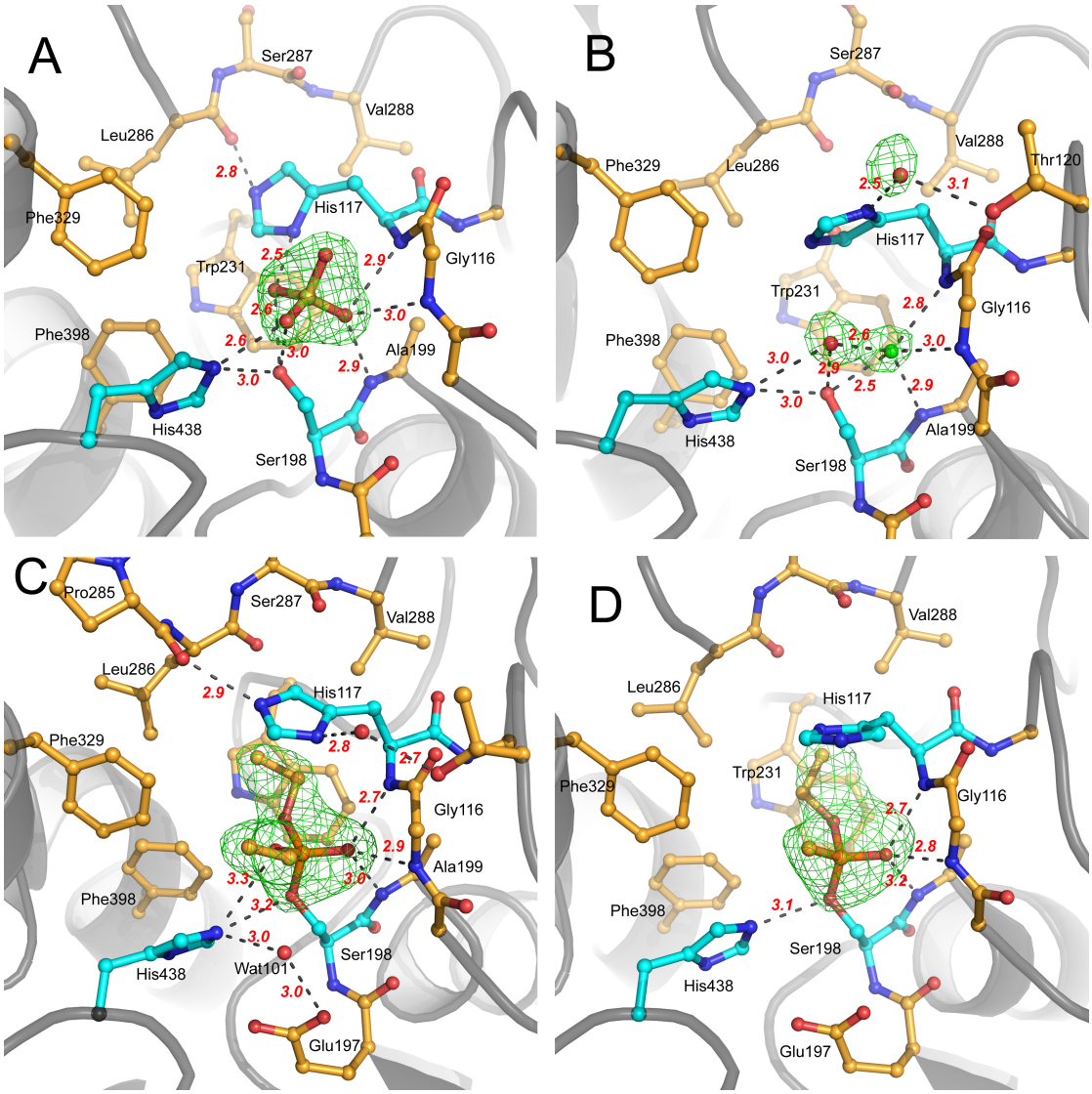


**Figure 43**. Sites actifs du mutant Gly117His de la hBChE dans les conditions habituelles de cristallisation avec 2.1 M de sulfate d'ammonium (A ; pdb 2xmb ; 2.1 Å), en présence de 10 mM de fluorure (B ; 2xmc ; 2.4 Å), inhibée par l'échothiophate (C ; pdb 2xmd; diéthylphosphorylsérine ; 2.3 Å) ou un mélange racémique de VX (D ; pdb 2xmg ; O-éthylméthylphosphonylsérine ; 2.7 Å). His117 stabilise un ion sulfate dans le sulfate actif qui est déplacé en présence de fluorure. Lorsque l'enzyme est phosphylé, His117 repose sur le groupement phosphyl.

De manière inattendue, un ion sulfate est lié au site actif dans une conformation rappelant le complexe formé avant l'attaque nucléophile de la sérine sur un OP. His117 et His438 et le trou oxyanion participent à la stabilisation de ce sulfate grâce à de nombreuses liaisons hydrogène. Cette structure montre que l'histidine est capable d'adopter une conformation pour laquelle elle ne gênerait pas stériquement un groupe partant de l'OP situé en opposition à la sérine entrante. Essayant de piéger dans le site actif des analogues $MgF_3^-$ ou $AlF_4^-$ de l'état de transition de déphosphylation, nous avons obtenu une structure dans laquelle le sulfate était déplacé par un ion fluorure (**Figure 43 ; B**). Dans ce complexe, l'imidazole de His117 adopte une conformation relaxée probablement proche de celle en absence de tout ligand.

Malgré un cycle catalytique de l'ordre de la minute, nous avons réussi à piéger l'intermédiaire diéthylphosphorylsérine formé lors de l'hydrolyse de l'échothiophate (**Figure 43 ; C**). Dans ce conjugué intermédiaire, His117 est stabilisée par deux liaisons hydrogène et coiffe l'adduit dans une conformation ne suggérant pas l'activation d'une molécule d'eau. Elle empêche même l'approche d'une molécule d'eau réactivatrice sur la face opposée à la sérine. Par contre la face adjacente à la sérine est ouverte est une molécule d'eau est prépositionnée. L'atome Nδ1 de l'imidazole est colinéaire avec le phosphore et Oγ de Ser198 ce qui semble compatible avec une attaque nucléophile directe du phosphore si il y a pivotement du noyau imidazole.

His117 adopte une conformation assez proche dans l'intermédiaire phosphonylé obtenu par trempage d'un cristal dans une solution contenant du VX. Là encore, l'activation d'une molécule d'eau en opposition à la sérine sortante semble difficile et une attaque de l'imidazole nécessite un changement de conformation qui peut présenter une barrière énergétique non négligeable. A noter que le groupement alkoxy du VX est localisé dans la poche acyle tandis que le méthyle pointe vers His438, comme observé précédemment dans l'enzyme sauvage. Cette configuration est défavorable à un vieillissement par désalkylation.

Au final ces structures ne nous ont pas permis de trancher sur le mécanisme de déphosphylation même si elles ont rendu certaines hypothèses plus réalistes que d'autres. Il en ressort qu'His117 n'agit pas comme un accepteur de proton, mais modifie le microenvironnement de la phosphylsérine de manière à rendre la déphosphorylation énergétiquement plus favorable. Cette hypothèse fut confortée par notre collaboratrice Sofya Lushchekina (Dept. de chimie de l'Université de Moscou) qui utilisa la méthode de calcul hybride mécanique quantique/mécanique moléculaire pour simuler la réaction de déphosphorylation de la diéthylphosphorylsérine (**Figure 44**).

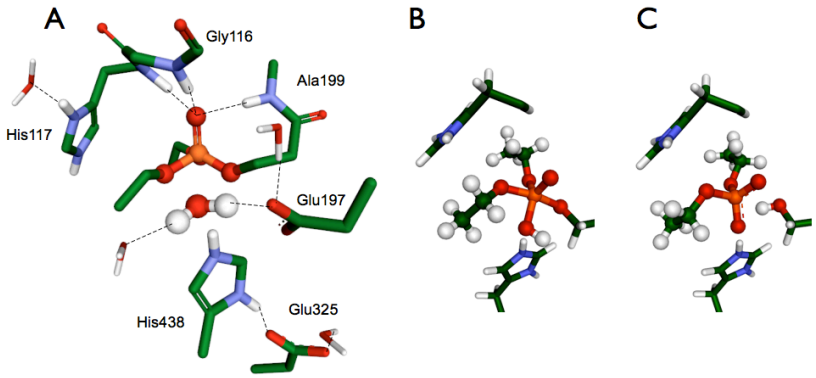


**Figure 44**. Déphosphorylation de G117H-hBChE simulée en QM/MM (B3LYP/6-31+G* et CHARMm27). (A) Une molécule d'eau présente à proximité d'une face accessible attaque le phosphore pour former un intermédiaire pentavalent (B) qui se réarrange avec libération de la sérine catalytique (C).

Les profils énergétiques de la déphosphorylation par attaque adjacente d'une molécule d'eau furent comparés pour la hBChE native et le mutant avec His117 protoné. Il s'avéra que les barrières énergétiques étaient plus élevées d'environ 10 kcal/mol pour la hBChE native, l'intermédiaire pentavalent était plus stable d'environ 5 kcal/mol et les produits de la réactions étaient bien mieux stabilisés (~20 kcal/mol). L'apport de l'histidine supplémentaire ne semble donc pas celui originellement imaginé par Millard *et al*. Surtout, il n'y a pas *a priori* de mutation évidente qui pourrait améliorer l'efficacité de ce mutant.

L'étude structurale du mécanisme d'hydrolyse fut publié dans ***Nachon et al (2011) Biochemical Journal*** (**Annexe B-19**), et l'étude QM/MM fit l'objet d'un poster à la Medical Chemica Defence Conference 2011 à Munich et d'un chapitre dans un ouvrage russe ***Lushchekina et al (2011)*** (**Annexe B-20**).

### *IV.4 - Ingénierie de l'AChE humaine*

Vu le rôle relativement passif d'His117, nous avons examiné la structure de hAChE pour vérifier si il n'était pas possible de trouver une autre position où une histidine pouvait réellement jouer le rôle de base capable d'activer une molécule d'eau capable de déphosphyler la sérine. D'après la modélisation moléculaire, Tyr124 du site périphérique semblait être une position appropriée. Le mutant Y124H peut stabiliser une molécule d'eau à la position adéquate pour un déplacement en ligne de la sérine catalytique. De plus, la modélisation suggéra qu'il était possible de reconstituer une diade en substituant la Tyr72 par un aspartate (**Figure 45**).

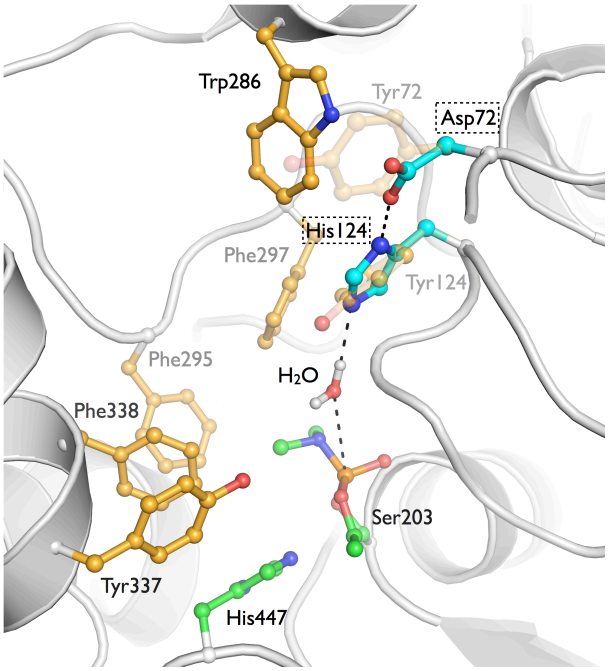


**Figure 45**. Modèle du mutant Y72D/Y124H phosphylé par le tabun. Les résidus mutés (cyan) permettraient de stabiliser une molécule d'eau dans une position propice à la déphosphoramidylation de la sérine par un mécanisme en ligne.

Les mutants Y124H et Y72D furent dont construits et testés pour leur propriété d'hydrolyse de l'acétylthiocholine et de réactivation spontanée après inhibition par les agents V. Alors que le simple mutant Y124H a un $K_M$ altéré d'1 ordre de grandeur pour l'acétylthiocholine, le double mutant Y72D/Y124H a un $K_M$ 30% inférieur à celui de l'enzyme sauvage. L'interprétation structurale de cette amélioration n'est pas claire, mais il est possible qu'Asp72 stabilise His124 dans une conformation favorable et/ou que sa charge attire à l'entrée de la gorge l'acétylthiocholine chargée positivement. Le point remarquable est qu'il n'y a pas d'altération de l'activité cholinestérasique du mutant Y72D/Y124H et qu'il pourrait donc être substitué *in vivo* à l'enzyme native sans perte fonctionnelle.

L'inhibition progressive de Y72D/Y124H en présence de 15 équivalents de VX, CVX et VR racémique est montrée **figure 46**.

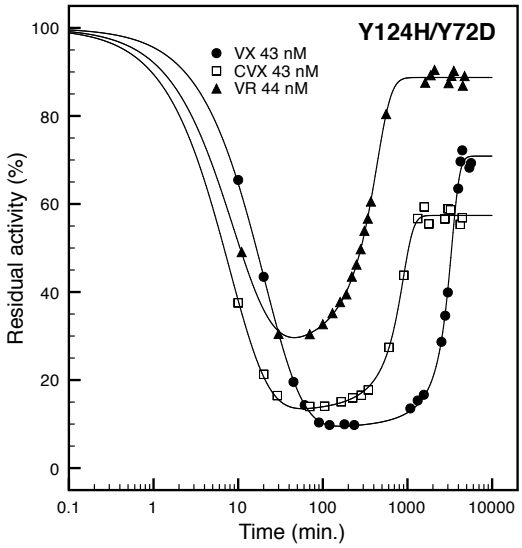


**Figure 46.** Inhibition progressive du mutant Y72D/Y124H de hAChE (~3 nM) en présence d'un large excès de VX, CVX et VR. L'activité a été suivie par prise d'échantillons d'un mélange réactionnel sur une période d'une semaine. Les courbes représentent la régression non linéaire d'un système d'équation différentiel décrivant l'inhibition concentration-dépendante du mutant avec une réactivation spontanée en compétition avec un vieillissement, les trois réactions étant décrites respectivement par des constantes de vitesse $k_i$, $k_s$ et $k_a$.

Les courbes de suivi d'activité suivent trois phase: (1) une inhibition initiale rapide suivie (2) d'un regain d'activité jusqu'à un plateau (3). Le plateau indique que la réactivation complète de l'enzyme ne peut être atteinte, probablement en raison de la réaction concurrente de vieillissement. Les constantes cinétique d'inhibition, réactivation spontanée et vieillissement obtenues à partir du modèle cinétique reproduisant les données observées mettent en évidence que $k_i$ pour le VX, CVX et VR est diminuée respectivement d'environ 30x, 100x et 60x par rapport à l'hAChE native mais reste de l'ordre de $10^6$-$10^7$ $M^{-1}min^{-1}$. La constante de vitesse de vieillissement $k_a$ est relativement inaltérée, restant moins de 2x supérieure ou inférieure à celle mesurée pour l'hAChE. La vitesse de réactivation spontanée est augmentée d'un facteur 110, 10 et 80 pour le VX, CVX et VR. A noter que $k_s$ est augmentée d'un facteur semblable pour le simple mutant Y124H.

Nous avons donc réussi à créer un mutant d'hAChE dont la vitesse de déphosphonylation est jusqu'à 2 ordres de grandeur supérieur à celle de l'enzyme sauvage, sans altération de l'activité cholinestérasique de l'enzyme. Ces vitesses restent modestes, mais on notera que par exemple dans le cas du VR et dans les conditions testées, elles permettent de garder une activité résiduelle de l'ordre de 30% malgré un net excès stœchiométrique d'agent. A ce stade le mécanisme n'est pas établi, nous n'avons pas la preuve que l'accélération de la réactivation spontanée repose bien sur un rôle d'accepteur de proton d'His124. Une étude de la réactivation

spontanée en fonction du pH pourra nous éclairer sur ce point. Cette étude fut publiée dans ***Trovaslet-Leroy et al (2011) Toxicology Letters*** (**Annexe B-21**).

### *IV.5 - Réactivation de la BChE du porc et perspectives pour la BChE humaine*

En 2008, Frédéric Dorandeu de mon département rapporta un rebond rapide de l'activité butyrylcholinestérasique plasmatique quand des porcs anesthésiés étaient intoxiqués au VX par voie *iv (Dorandeu 2008)*. Comme des essais standards d'inhibition au VX sur un échantillon de plasma de porc ne permirent pas de mettre en évidence une réactivation spontanée de la BChE de porc (pBChE), il fut conclu que le regain d'activité était plutôt lié à une libération de pBChE par un organe, comme cela a été décrit pour d'autres enzymes d'animaux empoisonnés *(Fujikawa 2005)*. Cependant, une *observation fortuite réalisée sur une cuvette oubliée une nuit dans un spectrophotomètre* nous conduisit à reconsidérer que le rebond d'activité pouvait finalement bien être lié à une réactivation spontanée de l'enzyme. Nous avons alors purifié la pBChE du plasma et pu mesurer des vitesses de réactivation spontanée importante pour les agents V (**Tableau 3**).

| agent V | $k_s$ ($min^{-1}$) | $t_{1/2}$ (min) |
|---|---|---|
| VX | 0.023 ± 0.002 | 30 |
| VR | 0.084 ± 0.006 | 8 |
| CVX | 0.088 ± 0.007 | 8 |

**Tableau 3**. constante de réactivation spontanée mesurée pour le plasma de porc et la BChE de porc purifiée du plasma.

Pour la pBChE purifiée le temps de demi-vie de réactivation spontanée est de seulement 8 min pour le VR et CVX. Ces résultats in vitro permettait de prédire un rebond très rapide de l'activité chez le porc empoisonné au VR. Pour le vérifier, nous avons conduit avec le VR une expérience *in vivo* sur le porc anesthésié, similaire à celle réalisée pour le VX, et nous avons effectivement observé le rebond rapide d'activité butyrylcholinestérasique plasmatique avec un $t_{1/2}$ de réactivation de 10 min, en accord avec les mesures *in vitro* effectuées sur la pBChE purifiée (**Figure 47**).

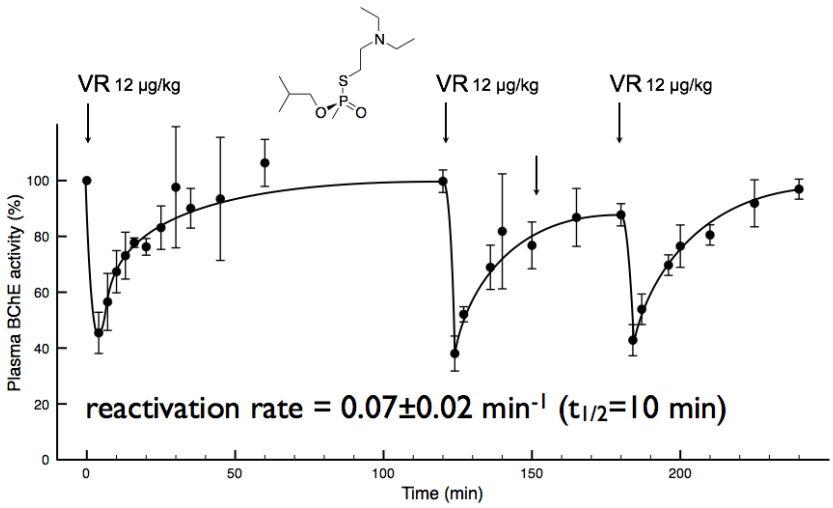


**Figure 47**. Suivi de l'activité butyrylcholinesterasique du plasma chez le porc après de multiples injections iv de VR (12 µg/kg).

L'ensemble de ces données confirme que c'est bien la pBChE plasmatique qui est à l'origine du rebond et que cette enzyme a la capacité de se réactiver rapidement après inhibition par les agents V. Le projet actuel consiste à identifier l'origine moléculaire de la réactivation spontanée rapide de la pBChE pour transposer cette activité à la hBChE et obtenir un bioépurateur des agents V capable de s'autorégénérer.

Une comparaison des séquences de la pBChE et hBChE indique des différences importantes au niveau de quelques régions du site actif, en particulier de la boucle "acyle" et de résidus proches de celle-ci. Cette piste est actuellement explorée dans le cadre d'un programme de recherche qui consiste à :

- Exprimer la pBChE recombinante à partir d'un gène synthétique

- Vérifier les propriétés catalytiques de l'enzyme recombinante avec les substrats et les agents V (mélange racémique et énantiomères pures)

- Résoudre la structure cristallographique de la pBChE recombinante sous forme apo et phosphylée pour tenter de déterminer le mécanisme de réactivation et les résidus impliqués

- Muter les résidus homologues chez la hBChE pour lui transposer l'activité de réactivation spontanée

- Tester les propriétés catalytiques des mutants de hBChE vis à vis des agents V

- Tester la pBChE et les mutants les plus actifs de hBChE pour leur capacité à protéger d'une intoxication par des agents V sur un modèle murin.

Nous avons déjà obtenu quelques succès importants dans ce programme, notamment résolu la structure cristallographique de la pBChE et obtenu un mutant de hBChE dont le $t_{1/2}$

de réactivation avec le VX est de quelques minutes. Ce projet est financé dans le cadre du protocole DGA/SSA BioMeDef PDH-2-NRBC-3-C-301.

### *IV.6 - Projet de production de cholinestérases humaines dans le lait de lapin*

La dose de cholinestérase nécessaire pour le prétraitement et/ou traitement de l'intoxication sera de l'ordre de la dizaine de mg, même pour des variants aux propriétés catalytiques améliorés. Il convient donc d'identifier un moyen de production adapté à la production de milliers de doses. Le projet consiste à produire des cholinestérases humaines recombinantes à moindre coût dans le lait d'animaux transgéniques optimisés pour leur capacités- de glycosylation. Une grande attention sera portée sur la qualité de la glycosylation car les études pharmacocinétiques de la hBChE naturelle ou recombinante injectée montre que la demi-vie biologique est inversement proportionnelle au nombre de sites d'attachement d'acide sialique (acide N-acétylneuraminique) vacants *(Kronman 1995)*. On sait que l'élimination rapide des asialoglycoprotéines de la circulation résulte de leur capture par des récepteurs situés en surface des hépatocytes. Une solution alternative consiste à modifier l'enzyme après purification soit par PEGylation chimique soit par sialylation enzymatique. L'efficacité *in vivo* des enzymes sera ensuite testée sur des modèles rongeurs. *In fine,* le projet permettra d'évaluer la faisabilité de production de cholinestérases recombinantes, dans la perspective de développer ultérieurement un biomédicament pour le prétraitement et/ou le traitement d'intoxications par des OP.

Le projet vise plus précisément à produire la hBChE et hAChE dans le lait de lapines transgéniques. La société française Trans Rabbit Models (TRM), porteur de ce projet, est un spécialiste de la transgénèse chez le lapin et a développé une expertise en matière de production de protéines recombinantes dans le lait de lapines transgéniques. Le lapin présente l'énorme avantage de pouvoir faire l'objet de modifications génétiques dans des délais et dans des coûts raisonnables en comparaison aux autres espèces laitières grâce à des cycles de reproduction notablement plus courts (seulement 6 mois) et une grande souplesse d'élevage (animal de laboratoire). Il est donc possible d'envisager dans cette espèce d'optimiser génétiquement des lignées de lapines transgéniques pour leurs capacités de glycosylation. La lapine offre par ailleurs des rendements laitiers intéressants (10 à 15 litres de lait par lapine et par an), compatibles avec la production industrielle de biomédicaments destinés à des patients humains. Ce système de production transgénique a récemment été approuvé par les autorités

réglementaires, avec la délivrance d'une autorisation de mise sur le marché pour une première protéine recombinante humaine produite dans du lait de lapines transgéniques.

La préparation des lignées transgéniques est effectuée à partir de l'ADNc optimisé codant la hBChE et hAChE. Les transgènes sont synthétisés et micro-injectés dans des embryons transférés par chirurgie. Après la mise-bas, les animaux transgéniques sont identifiés par criblage (PCR, PCRq) puis élevés jusqu'à maturation sexuelle. Les femelles fondatrices F0 sont mises en reproduction pour la production de lait. L'activité cholinestérasique des laits transgéniques est analysée dans notre laboratoire et l'enzyme est purifiée après clarification du lait par chromatographie d'affinité sur une nouvelle résine performante à base d'huprine que nous avons mis au point en collaboration avec Pierre-Yves Renard *(Brazzolotto 2012)*.

Nous avons d'ores et déjà identifié une femelle produisant de la hBChE à un taux d'environ 1 g/L de lait. Nous allons poursuivre par la caractérisation de la glycosylation de l'enzyme, puis procéder à des mesures pharmacocinétiques chez la souris et enfin effectuer des tests de protection contre l'intoxication par le VX.

Pour parer à un défaut de glycosylation, nos collaborateurs de TRM élaborent une lignée de lapins optimisée. Le profil d'expression des gènes dans la glande mammaire de lapines au cours de la lactation est déterminé par RT-PCRq et séquençage. L'analyse du transcriptome de la glande mammaire permet plus particulièrement d'identifier chez la lapine, les gènes impliqués dans les phénomènes de glycosylation des protéines du lait, de connaitre leur niveau d'expression pour déterminer lesquels devront être « dopés » (par surexpression) et en quelle proportion, ou lesquels devront faire l'objet d'une extinction (knock-out fonctionnel). Par la suite, la lignée optimisée pourra être croisée avec la/les lignées produisant la hBChE et hAChE. Les enzymes seront purifiées à partir du lait des nouvelles femelles productrices, leur profil de glycosylation sera analysé et leur propriétés pharmacocinétiques étudiées. Ce projet est financé dans le cadre du projet DGA RAPID EpuraToxNeuro.

### *IV.7 - Projet d'ingénierie d'une lipase pancréatique humaine*

Les cholinestérases humaines ne sont exprimées sous forme active que dans des systèmes eucaryotiques, ce qui alourdit l'optimisation par mutagénèse, voire rend pratiquement impossible ou trop coûteuse les stratégies d'évolution dirigée. Une hydrolase à sérine humaine structuralement proche des cholinestérases, potentiellement capable de piéger les OP, dont l'expression bactérienne et plus aisée et la structure tridimensionnelle est résolue, constituerait une alternative intéressante pour développer un bioépurateur stœchiométrique ou catalytique. L'identification de candidats répondant à ces critères a été réalisée en collaboration avec

Raphaël Terreux de l'IBCP à Lyon grâce à au logiciel "Surfing the Molecules" SuMo développé dans son institut. La structure de la hBChE a été prise comme modèle pour définir un site actif de référence à partir d'éléments clés, et ce site fut comparé à toutes les protéines de la PDB. La fonction d'évaluation fit rapidement ressortir une lipase pancréatique humaine (pdb 1f6w). Cette protéine possède 27 des 36 éléments définissant le site actif de la hBChE est importants pour la liaison aux OP. Sa séquence est identique à 31% à celle de la hBChE et sa structure est globalement très proche, à part que son site actif est beaucoup plus ouvert en raison de la différence de longueur des deux boucles le flanquant : La boucle-Cys Ω est plus longue chez la hBChE et inversement la boucle "acyle" est plus courte (**Figure 48**).

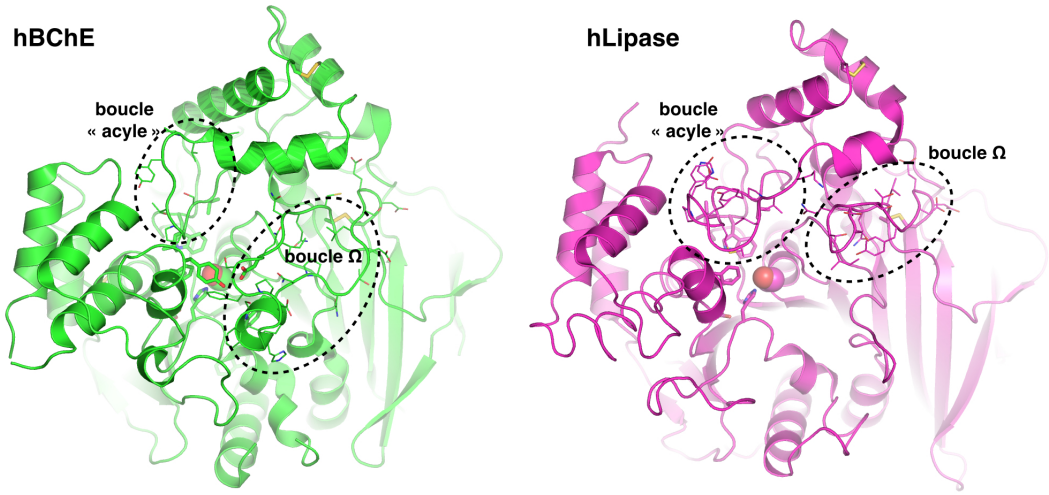


**Figure 48**. Comparaison des structures de hBChE (pdb 1p0i) et de la lipase pancréatique humaine (pdb 1fw6). Les boucles acyle et Ω de la hBChE sont entourée d'une ellipse pointillée, de même que les boucles homologues de la lipase. La chaîne latérale de la sérine catalytique est représentée par des sphères.

Des simulations de docking ont été conduites sur la hBChE et la lipase afin de réaliser une première estimation du potentiel de cette enzyme à piéger les OP. Les dockings ont été réalisés à l'aide du logiciel Surfex-Dock et la fonction d'évaluation consensuelle Cscore (**Tableau 4**).

| OP | Score sur la Lipase | Score sur la hBChE |
|---|---|---|
| VX | 6,64 | 6,68 |
| Paraoxon | 6,23 | 6,65 |
| Echothiophate | 6,18 | 5,24 |
| DFP = Diisopropylfluorophosphate | 5,26 | 4,61 |
| Sarin | 3,88 | 3,97 |
| Soman | 3,72 | 3,61 |
| Tabun | 1,85 | 2,22 |

**Tableau 4**. Résultat de docking moléculaire de Surfex-Dock (Cscore) pour différents OP sur la lipase pancréatique et la hBChE

Les résultats de docking sont globalement comparables ce qui prédit que cette lipase est un bioépurateur potentiel des OP. Sur cette base nous avons décidé d'utiliser cette enzyme comme point de départ une nouvelle famille de bioépurateur dont l'ingénierie est plus aisée, et le coût de revient plus faible que pour la hBChE.

Le projet se décompose en tâches partagées entre mon équipe (Biologie moléculaire, Biochimie, Enzymologie, Cristallographie) et celle de Raphaël Terreux (modélisation) :

- La mise au point de l'expression de la lipase dans *E. coli* à partir d'un ADNc synthétique optimisé (expression sous forme corps d'inclusion suivi d'étapes de dénaturation/renaturation décrit dans la littérature).

- La mesure des constantes d'inhibition de cette lipase par les OP (paraoxon, VX, tabun, sarin...) et éventuellement des constantes de réactivation spontanée.

- La résolution des structures cristallographiques des conjugués formés avec les OP.

- La modélisation des conjugués en dynamique moléculaire afin de proposer des mutations susceptibles d'améliorer l'affinité la réactivité avec les OP.

- La modélisation des conjugués en système hybride mécanique quantique/mécanique moléculaire pour tester des mutations susceptible d'augmenter la vitesse de réactivation spontanée de l'enzyme.

Ce projet est financé dans le cadre du projet ANR ASTRID CatScav et du protocole DGA/SSA BioMedDef PDH-2-NRBC-3-C-301.

### *IV.8 Nouvelle génération de réactivateurs des cholinestérases*

Les conjugués phosphyl-ChE ne peuvent être déphosphylés que par des nucléophiles forts capables d'approcher l'adduit enfoui au fond de la gorge et de déplacer la sérine catalytique par attaque nucléophile du phosphore. La plupart sont des α-nucleophiles (hydroxylamines et oximes)*(Saint-André 2011)*. Si les pyridines aldoximes se sont montrées relativement efficaces pour réactiver l'hAChE avant vieillissement, leur efficacité doit être améliorée. A ce jour et malgré plus de 60 ans de recherches, il n'existe pas de réactivateur universel. Aucun des réactivateurs actuels n'est adapté à la variété des adduits formé par les OP *(Jokanovic 2009; Worek 2004b)*. Certains conjugués sont particulièrement difficiles à réactiver, comme celui formé par le cyclosarin en raison de son substituant cyclique encombrant *(Kuca 2004)* ou celui formé par le tabun en raison de son encombrement stérique et sa faible électrophilie *(Carletti 2010)*. De plus, aucune pyridine aldoxime ne peut déplacer l'acide phosphonique formé par vieillissement. Les réactivateurs actuellement utilisés ont été conçus bien avant que

la structure tridimensionnelle de l'hAChE soit déterminée et n'ont pas bénéficié des avancées récentes dans ce domaine. Il est remarquable que les réactivateurs actuellement les plus efficaces portent un noyau 2- ou 4-pyridinium aldoxime exerçant la fonction réactivatrice, ponté généralement par une chaîne aliphatique à un autre noyau pyridinium capable de se lier au site périphérique de l'hAChE *(Calic 2006)*. Les composés bis pyridinium aldoximes reliés par une chaine carbonée via leur azote quaternaire sont les plus efficaces *(Kassa 2002)*. Comme l'un des pyridiniums aldoximes se lie au niveau du site périphérique de l'AChE, la position de l'autre pyridinium aldoxime par rapport à l'adduit NOP-sérine, et donc sa réactivité, dépend du nombre de groupe méthylène formant la chaîne carbonnée *(Kuca 2004; Wille 2010)*. Ce mode de liaison des bispyridiniums est illustré par la structure de complexes ternaires AChE/NOP/HI-6 ou HLö-7*(Ekstrom 2009; Ekstrom 2006b; Hornberg 2010)* (**Figure 49**). L'un des pyridiniums est pris en sandwich entre les résidus aromatiques Trp286 et Tyr72 du site périphérique, alors que l'autre pyridinium descend dans la gorge pour se rapprocher de la sérine phosphoramidylée.

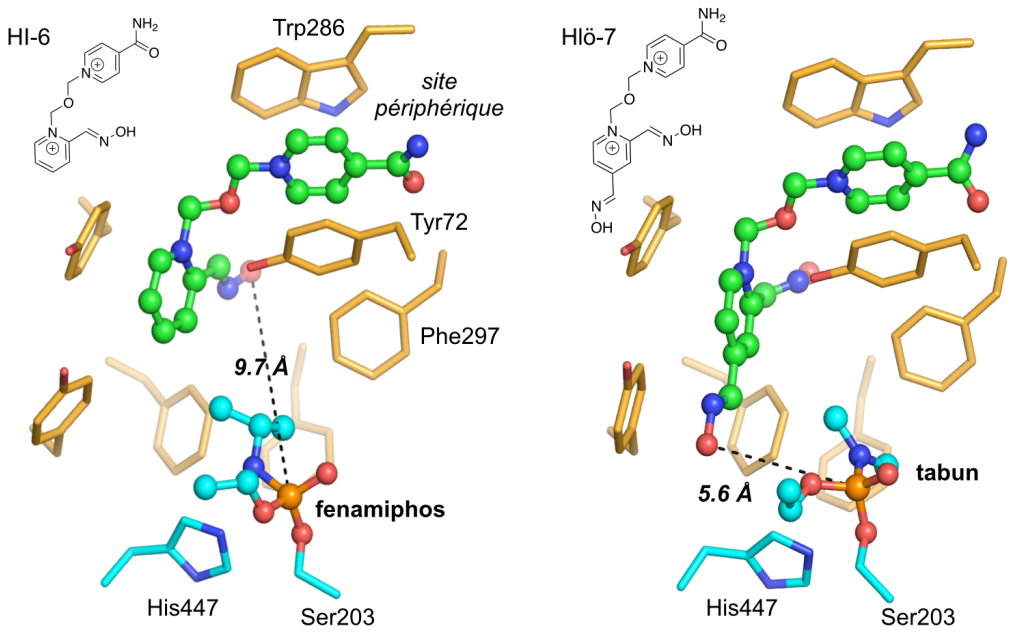


**Figure 49**. Mode de liaison du HI-6 et HLö-7 à l'AChE de souris inhibée par le fenamiphos ou le tabun (pdb 2wu3 et 2jez ; 2.7 Å et 2.6 Å). La distance entre le phosphore de l'adduit et l'oxime la plus proche est indiquée.

Il apparaît clairement sur ces structures ternaires AChE/OP/bispyridinium que la fonction oxime n'est pas située au contact du phosphore et que son orientation est loin d'être optimale pour la réactivation. D'ailleurs il a été montré que des mutations de résidus de la gorge dégageant l'accès à l'adduit accélèrent les vitesses de réactivation *(Kovarik 2007)*. Le point clé pour la conception de réactivateurs plus efficaces apparaît comme étant l'utilisation d'un

ligand du site périphérique permettant de donner une bonne affinité à la molécule pour l'enzyme phosphylée, couplé à une fonction nucléophile capable de s'approcher suffisamment près de la sérine phosphylée et dans la bonne orientation par rapport à la liaison P-O qui doit être clivée. Accessoirement, une fonction nucléophile moins encombrante, comme une alpha-oxo-oxime aliphatique, pourrait plus facilement se faufiler entre les résidus et les substituants jusqu'au phosphore.

Comme la majorité des réactivateurs sont des bispyridiniums, ils ont deux charges positives permanentes. Ils passent donc mal les membranes cellulaires et en particulier la barrière hémato-encéphalique (BHE) assez imperméable aux ions. De fait, le HI-6 pénètre lentement le système nerveux central *(Melchers 1994)* et le rapport moyen de pénétration du 2-PAM est approximativement de 10% *(Sakurada 2003)*. Les bispyridiniums aldoximes n'ont donc pas d'activité réelle dans le système nerveux central, activité qui serait pourtant bénéfique pour le traitement comme démontré pour la MINA, une oxime simple et neutre capable de passer la BHE. La conception de réactivateurs possédant cette activité centrale doit donc être basée sur des fragments ne possédant pas de charge permanente.

Concernant la partie nucléophile, nous avons développé dans le cadre du contrat ANR DetoxNeuro dont j'étais coordinateur, en collaboration avec Pierre-Yves Renard et Rachid Baati (Universités de Rouen et Strasbourg), une nouvelle fonction nucléophile de type oxime, sans charge permanente, et capable de réagir sur les phosphothioesters : la 3-hydroxy-2-pyridinealdoxime *(Saint-André 2011)*. Nous avons montré que cette fonction est au moins aussi réactive que les aldoximes de pyridinium pour la réactivation de l'hAChE inhibée par le VX. De plus cette oxime forme rapidement un isoxasole et un acide phosphonique non toxique par réaction intramoléculaire après déphosphylation de la sérine *(Saint-André 2011)*. Ceci élimine le problème de recapture observé pour les phosphoryloximes générés à partir des 2-pyridiniums aldoximes. Comme attendu en raison de son pKa suffisamment bas (8.2 ± 0.1), cette oxime non quaternaire a montré de bonnes qualités de réactivation de l'hAChE inhibée par le VX ($k_r$ = 0.5 ± 0.1 $min^{-1}$, pH 7.0, 25 °C) avec cependant une faible affinité pour l'enzyme inhibée ($K_D$ = 32 ± 11 mM). Ce dernier point est facilement corrigé par couplage à un ligand du site périphérique de l'hAChE. Cette stratégie de couplage d'une fonction nucléophile à un ligand du site périphérique a été initialement suggérée par Taylor *et al (Taylor 2007)*. Une autre particularité de la fonction 3-hydroxy-2-pyridinealdoxime est que le pKa de la fonction oxime est indépendant de la position du bras de couplage (ortho, méta ou para). En comparaison, l'azote des pyridiniums aldoximes, sur lequel est généralement accroché le bras de couplage, doit former un système conjugué avec la fonction oxime (donc

située en ortho ou para, voir HLö-7 **figure 49**) pour que la forme oximate soit stabilisée à pH physiologique. Cette particularité de la 3-hydroxy-2-pyridinealdoxime permet d'obtenir des orientations plus diverses et éventuellement une orientation optimale de la fonction oxime dans le site actif par rapport à la phosphylsérine.

La fonction 3-hydroxy-2-pyridinealdoxime présente donc toutes les propriétés requises pour être à la base d'une nouvelle famille de réactivateurs plus performants. Nous mettons à profit notre expérience accumulée dans l'étude structurale des cholinestérases inhibées par les neurotoxiques pour concevoir de manière rationnelle une nouvelle génération de réactivateurs, basée sur la nouvelle fonction oxime identifiée. L'orientation de la fonction oxime couplée via différents bras espaceurs à des ligands du site périphérique est systématiquement analysée par docking combiné à la dynamique moléculaire. Ces dernières années, les molécules obtenues par couplage de la 3-hydroxy-2-pyridinealdoxime en position méta avec des phényltetrahydroisoquinoline, tacrine et tryptoline ont démontré l'efficacité de notre stratégie *(Kliachyna 2014; Mercey 2012; Mercey 2011; Renou 2014; Renou 2013)*(**Figure 50**).

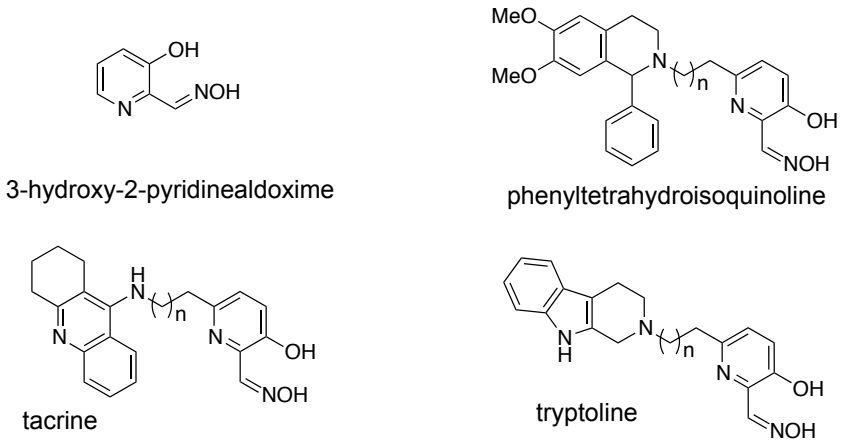


**Figure 50**. Structure de la 3-hydroxy-2-pyridinealdoxime et de ses dérivés phényltétrahydroisoquinoline, tacrine et tryptoline.

Certains réactivateurs sans charge permanente appartenant à ces trois familles sont plus efficaces ou au moins aussi efficaces que les meilleurs réactivateurs connus pris individuellement pour la réactivation de l'hAChE inhibée par le VX, le tabun et le paraoxon. Suite aux résultats très prometteurs obtenus sur ces molécules *in vitro*, nous avons réalisé des expériences *in vivo* pour étudier la pharmacocinétique des dérivés de phényltétrahydroisoquinoline et tacrine sur un modèle de souris, et ainsi déterminer une fenêtre d'action pour le traitement de l'intoxication par le VX par injection *ip*. Bien que les données pharmacocinétiques soient semblables à celles du HI-6, elles ont mis en évidence un problème de biodisponibilité plasmatique liés à la solubilité limitée en solution aqueuse de ces

composés non quaternaires (de l'ordre de 0.2 à 0.5 mM). Notre projet actuel est de contourner cette difficulté en suivant plusieurs approches:

- Modifier la partie ligand périphérique des molécules pour la rendre plus soluble ou pour la coupler à une molécule transportée activement à travers la BHE (ex ascorbate, glucides)
- Travailler sur la formulation galénique des composés sans les modifier (émulsion, sels de chlorhydrates ou mésylate)
- Quaternariser une amine des composés en supposant que des composés monochargés seront plus solubles tout en passant mieux la BHE que les bispyridinium bi-chargé n'en sont capable.
- Remplacer les ligands du site périphérique aromatiques par des ligands à base d'amines tertiaires plus simples (ex, pyrolidine), éventuellement quaternarisées, à l'exemple des travaux récents de Radic *et al (Radic 2012)*.

Parallèlement à ces approches d'ordre stratégique, je cherche à améliorer toute la chaîne de développement des réactivateurs, de la conception des molécules jusqu'à leur évaluation *in vivo* par de multiples actions indépendantes mais cohérentes. Les principales sont: (1) l'amélioration des méthodes de docking moléculaire pour tenir compte de la flexibilité importante de résidus de la gorge du site actif de l'hAChE, en réalisant avec Gianluca Santoni (étudiant en thèse à l'IBS que je co-encadre) une banque de conformations préexistantes des résidus mobiles, basée sur des simulation de dynamique moléculaire. (2) Le passage à l'hAChE pour remplacer la *Tc*AChE et mAChE pour tous les travaux de cristallographie sur la base des avancées récentes de Cheung *et al (Cheung 2012)*. (3) La mise au point d'un modèle transgénique murin à hAChE humaine en collaboration avec Eric Krejci de l'Université Paris Descartes pour évacuer les problèmes potentiels liés au fait que la réactivation *in vivo* est effectuée *in fine* sur l'AChE de souris et non pas sur l'hAChE. En effet, bien que les sites actifs de mAChE et hAChE soient tapissés de résidus identiques, nous avons montré, en collaboration avec Judith Peters de l'IBS/ILL et par des expériences de diffusion de neutrons, que la dynamique globale des deux enzymes est sensiblement différente *(Peters 2012; Trovaslet 2013)*. Des différences de comportement vis-à-vis des réactivateurs sont donc possibles.

L'ensemble de ce projet est financé dans le cadre du projet ANR BLANC ReAChE, de l'ANR ASTRID ReCNS-AChE, du protocole DGA/SSA BioMeDef PDH-2-NRBC-4-C-403 et du programme HDTRA1-11-C-0047 (US Department of Defense).

### *IV.9 Concept de bioépurateur pseudo-catalytique et réactivateurs de hBChE*

Le développement de nouveaux réactivateurs permet d'explorer le concept de bioépurateur pseudocatalytique qui consiste à associer une cholinestérase et un réactivateur, que ce soit l'hAChE *(Kovarik 2007)*, un de ses mutants optimisé pour la réactivation *(Cochran 2011; Kronman 2010)*, ou la hBChE *(Aurbek 2009)*. En cas d'intoxication, la cholinestérase plasmatique exogène va piéger l'OP pour former un conjugué. Ce conjugué pourra être déphosphylé par le réactivateur présent dans la circulation d'où la régénération d'une cholinestérase libre capable de piéger une nouvelle molécule d'OP et ainsi de suite. Ce concept peut être particulièrement attractif pour les agents V qui diffusent lentement dans la circulation sanguine à partir de sites de stockage cutanés, ce qui conduit à une inhibition lente et continue des cholinestérases.

Comme la hBChE est le candidat bioépurateur stœchiométrique le plus avancé, elle a été au cœur de la plupart des tests du concept de bioépurateur pseudocatalytique. Cependant, les premières études ont montré que la hBChE inhibée par le VX, le VR, le sarin, le cyclosarin, le tabun, le méthylparaoxon ou l'éthylparaoxon était réactivée beaucoup trop lentement par les oximes classiques tel que l'obidoxime, la pralidoxime, le HI-6 ou le MMB4 *(Aurbek 2009)*. En 2010, l'équipe de Kovarik testa *in vitro* sur la butyrylcholinestérase phosphylée par le tabun et le paraoxon de nouvelles bispyridinium oximes synthétisées par le groupe de Kuca *(Kovarik 2010)*. Les réactivateurs les plus efficaces vis-à-vis de la hBChE inhibée par le tabun atteignent des taux de réactivation de 70% en moins d'une heure. En revanche, la réactivation de la hBChE inhibée par le paraoxon reste trop lente. Plus récemment, Radic *et al* ont identifiés de nouveaux réactivateurs de hBChE non pyridinium *(Radic 2013)*. Leur molécule la plus efficace, la 2-triméthylammonio-6-hydroxybenzaldoxime, est capable de réactiver la hBChE inhibée par le VX, le cyclosarin, le sarin, le tabun et le paraoxon. Son association avec une quantité sub-stœchiométrique de hBChE améliore la protection de souris exposées au sarin et au paraoxon de l'ordre de 30 à 60% validant son efficacité dans le cadre du concept de pseudocatalyse. Enfin, nous avons montré que les conjugués tryptoline-3-hydroxy-2-pyridinealdoxime sont d'excellents réactivateurs de VX-hBChE, surpassant en efficacité toutes les autres molécules connues *(Renou 2014)*.

Il est remarquable qu'aucun de ces réactivateurs n'ait été spécifiquement conçu pour la hBChE. Ce sont toutes des molécules d'abord conçues pour réactiver l'hAChE qui ont été ensuite testées sur la hBChE. Il est clair qu'il est désormais nécessaire de faire un effort de conception de réactivateurs adaptés aux spécificités de la hBChE, en particulier sa gorge plus

vaste dépourvue d'un important cluster de résidus aromatiques à son entrée. De ce fait, la stratégie de couplage entre ligand de site périphérique et fonction nucléophile n'est pas adaptée *a priori*. *La conception de réactivateurs de hBChE doit être basée sur des squelettes chimiques de ligands spécifiques*. Cependant nous ne disposons actuellement que de très peu de données structurales sur le mode de liaison de ligands spécifiques de la hBChE, l'essentiel de mes travaux de cristallographie ayant été dédiés à l'étude des inhibiteurs irréversibles. J'ai toutefois récemment commencé à étudier la particularité des interactions des ligands réversibles avec la hBChE pour la famille de la tacrine et de l'huprine *(Nachon 2013)*. J'ai également été amené à étudier la liaison non covalente de ligands de type pyridinium à la hBChE vieillie dans le cadre d'un projet d'étude de faisabilité de réalkylation des cholinestérases vieillies, projet en collaboration avec Daan Noort et Martijn de Koning du TNO et financé par l'US Department of Defense (projet HDTRA CBDIF07-THER01-2-0038) *(Wandhammer 2013)*. Ces premières données pointent déjà vers un rôle potentiellement clé de la Tyr332, ce résidu à l'entrée de la gorge que j'avais identifiée par marquage de photoaffinité lors de ma thèse. En parallèle, Macdonald *et al* ont également entrepris d'étudier la topologie du site périphérique de la hBChE mais via une approche assez classique de compétition entre inhibiteurs sur différents mutants de l'enzyme *(Macdonald 2012)*. Je me suis rapproché de cette équipe pour leur proposer une collaboration afin de compléter leur étude par l'obtention des structures cristallographiques des complexes entre les inhibiteurs employés (propidium, phenothiazine, edrophonium...) et la hBChE. A ce jour, nous avons déjà résolu les structures de quelques-uns de ces complexes. Ces données constitueront une bibliothèque complète de modes de liaison de ligands à la hBChE, qui pourront être utilisés pour concevoir des réactivateurs spécifiques.

## V Conclusion et perspectives à plus long terme

Mon travail de ces 15 dernières années a d'abord été basé sur l'amélioration des connaissances de la structure des cholinestérases. La résolution de la structure cristallographique de la butyrylcholinestérase a été une étape clé qui m'a ouvert tout un champ d'investigation tournant autour du mécanisme d'hydrolyse des cholinestérases et du mécanisme d'inhibition par les OP. Combiner la cristallographie aux analyses par spectrométrie de masse m'a permis d'étudier les mécanismes de manière détaillée, et en particulier de caractériser la stéréochimie des réactions, un aspect très important pour les neurotoxiques de guerre, des composés chiraux dont la toxicité est associée généralement à un seul des isomères. Les études comparatives entre AChE et hBChE ont aussi prouvé être très riches en enseignement quant aux mécanismes moléculaires mis en jeu. Ce travail a débouché sur des avancées en matière de conception de nouvelles contremesures médicales pour le prétraitement et le traitement de l'intoxication par les OP: bioépurateurs enzymatiques et réactivateurs.

Côté bioépurateurs, des pistes prometteuses sont identifiées pour augmenter la vitesse de réactivation spontanée des cholinestérases et ainsi pallier à la principale limite de ces enzymes, soit la stœchiométrie 1:1 de la réaction avec les OP. Cependant, il est clair que ceci n'est qu'une étape et qu'à plus long terme, le prétraitement sera à base de bioépurateurs capables d'hydrolyser les OP à grande vitesse, telles que les phosphotriestérases bactériennes et la paraoxonase humaine. Bien que n'ayant pas été personnellement très impliqué, je suis très attentif et soutiens activement la recherche dans ce domaine, en particulier les travaux du Prof. Eric Chabrière de l'Université de Méditerranée. Je garde également comme objectif de résoudre la structure de la paraoxonase humaine, car la liaison des OP à cette enzyme et le mécanisme d'hydrolyse sont encore largement incompris.

La conception rationnelle d'enzymes capables d'hydrolyser les OP fait appel à la dynamique moléculaire pour prédire la formation du complexe Michaëlien. La simulation de la réaction doit quant à elle être modélisée en mécanique quantique. L'hybridation des deux techniques permet de prendre en compte, dans une certaine mesure, la contribution de la dynamique de l'enzyme à la catalyse chimique, contribution dont on commence seulement à percevoir l'importance. Mais je pense que les simulations ne gagneront suffisamment en fiabilité qu'avec les systèmes où toute l'enzyme et son environnement proche sont traités au niveau quantique. Les ressources de calcul nécessaires commencent à être disponible grâce au

développement des processeurs graphiques spécialisés dans le calcul hautement parallélisé. Je suis attentivement les développements techniques dans ce domaine pour pouvoir les intégrés au plus tôt dans mes travaux futurs en ingénierie des enzymes.

Côté réactivateurs, le partenariat fort établi avec des équipes de chimistes organiciens a conduit au développement de nouvelles familles de réactivateurs très prometteurs. Ces études ont montré tout l'intérêt du docking combiné à la dynamique moléculaire pour la conception des molécules qui doivent se fixer dans un site actif aux résidus très mobiles. La validation des motifs proposés par résolution des structures cristallographiques des complexes avec les enzymes inhibées est également d'une aide précieuse pour affiner la structure des molécules les plus actives. Il reste cependant encore beaucoup à faire car de nombreuses questions restent ouvertes sur le mécanisme de réactivation par les oximes: régio- et stéréochimie de la réaction, implications de résidus dans la catalyse... La réponse à ces questions permettra sans aucun doute de concevoir des molécules plus actives. Elle nécessite la mise en œuvre de techniques de modélisations à base de mécanique quantique. Je me rapproche actuellement d'Etienne Derat de l'Université Pierre et Marie Curie pour lancer des travaux dans cette direction.

Enfin, mon but est bien de pousser un candidat réactivateur et un candidat bioépurateur jusqu'à la porte des essais cliniques de phase I. Rappelons que les phases II et III n'étant pas applicables pour les intoxications aux neurotoxiques de guerre, la phase est I est généralement suffisante pour obtenir une autorisation de mise sur le marché. Une fois les molécules candidates identifiées, de nombreuses étapes de validation de l'activité *in vivo* seront nécessaires avant d'y arriver, mais je peux m'appuyer sur l'activité d'expérimentation animale en place dans l'unité de recherche que je dirige au sein de l'Institut de Recherche Biomédicale des Armées. Même si cet objectif à long terme est assez ambitieux et nécessitera sans doute des circonstances favorables pour être atteint, comme le rappelle Louis Pasteur: "La chance ne sourit qu'aux esprits bien préparés".

# Références


Aldridge, W. N. (1954). "Tricresyl phosphates and cholinesterase." *Biochem. J.* **56**(2), 185-9

Aldridge, W. N., and Reiner, E. (1969). "Acetylcholinesterase. Two types of inhibition by an organophosphorus compound: one the formation of phosphorylated enzyme and the other analogous to inhibition by substrate." *Biochem. J.* **115**(2), 147-62

Aldridge, W. N., and Reiner, E. (1972). Enzyme inhibitors as substrates - Interactions of esterases with esters of organophosphorus and carbamic acids. In (Vol. 16 Frontiers of biology ed., pp. 328. North-Holland Pub. Co. - Amsterdam.

Amitay, M., and Shurki, A. (2009). "The structure of G117H mutant of butyrylcholinesterase: nerve agents scavenger." *Proteins* **77**(2), 370-7

Amitay, M., and Shurki, A. (2011). "Hydrolysis of organophosphate compounds by mutant butyrylcholinesterase: a story of two histidines." *Proteins* **79**(2), 352-64

Aracava, Y., Pereira, E. F., Akkerman, M., Adler, M., and Albuquerque, E. X. (2009). "Effectiveness of donepezil, rivastigmine, and (+/-)huperzine A in counteracting the acute toxicity of organophosphorus nerve agents: comparison with galantamine." *J. Pharmacol. Exp. Ther.* **331**(3), 1014-24

Arpagaus, M., Kott, M., Vatsis, K. P., Bartels, C. F., La Du, B. N., and Lockridge, O. (1990). "Structure of the gene for human butyrylcholinesterase. Evidence for a single copy." *Biochemistry* **29**(1), 124-31

Ashani, Y., Grauer, D., Grunwald, J., Allon, N., and Raveh, L. (1998). Current capabilities in extrapolating from animal to human the capacity of human BChE yo detoxify organophosphates. In *Structure and Function of Cholinesterase an related proteins* (B. P. Doctor, P. Taylor, D. M. Quinn, R. L. Rotundo, and M. K. Gentry, Eds.), pp. 255-260. Plenum Press, NY.

Ashani, Y., and Pistinner, S. (2004). "Estimation of the upper limit of human butyrylcholinesterase dose required for protection against organophosphates toxicity: a mathematically based toxicokinetic model." *Toxicol. Sci.* **77**(2), 358-67

Aurbek, N., Thiermann, H., Eyer, F., Eyer, P., and Worek, F. (2009). "Suitability of human butyrylcholinesterase as therapeutic marker and pseudo catalytic scavenger in organophosphate poisoning: a kinetic analysis." *Toxicology* **259**(3), 133-9

Aurbek, N., Thiermann, H., Szinicz, L., Eyer, P., and Worek, F. (2006). "Analysis of inhibition, reactivation and aging kinetics of highly toxic organophosphorus compounds with human and pig acetylcholinesterase." *Toxicology* **224**(1-2), 91-9

Barak, D., Kronman, C., Ordentlich, A., Ariel, N., Bromberg, A., Marcus, D., Lazar, A., Velan, B., and Shafferman, A. (1994). "Acetylcholinesterase peripheral anionic site degeneracy conferred by amino acid arrays sharing a common core." *J. Biol. Chem.* **269**(9), 6296-305

Barak, D., Ordentlich, A., Bromberg, A., Kronman, C., Marcus, D., Lazar, A., Ariel, N., Velan, B., and Shafferman, A. (1995). "Allosteric modulation of acetylcholinesterase activity by peripheral ligands involves a conformational transition of the anionic subsite." *Biochemistry* **34**(47), 15444-52

Barak, D., Ordentlich, A., Kaplan, D., Barak, R., Mizrahi, D., Kronman, C., Segall, Y., Velan, B., and Shafferman, A. (2000). "Evidence for P-N bond scission in phosphoroamidate nerve agent adducts of human acetylcholinesterase." *Biochemistry* **39**(5), 1156-61

Bird, S. B., Dawson, A., and Ollis, D. (2010). "Enzymes and bioscavengers for prophylaxis and treatment of organophosphate poisoning." *Front Biosci (Schol Ed)* **2**, 209-20

Bismuth, C. (1993). "Armes chimiques, description et risques toxiques." *Réanim. Urgence* **2**, 625-633

Bon, S. (1982). "Molecular forms of acetylcholinesterase in developing Torpedo embryos." *Neurochem. Int.* **4**(6), 577-85

Bourne, Y., Radic, Z., Sulzenbacher, G., Kim, E., Taylor, P., and Marchot, P. (2006). "Substrate and product trafficking through the active center gorge of acetylcholinesterase analyzed by crystallography and equilibrium binding." *J. Biol. Chem.* **281**(39), 29256-67

Bourne, Y., Taylor, P., Radic, Z., and Marchot, P. (2003). "Structural insights into ligand interactions at the acetylcholinesterase peripheral anionic site." *EMBO J.* **22**(1), 1-12

Brazzolotto, X., Wandhammer, M., Ronco, C., Trovaslet, M., Jean, L., Lockridge, O., Renard, P. Y., and Nachon, F. (2012). "Human butyrylcholinesterase produced in insect cells: huprine-based affinity purification and crystal structure." *FEBS J.* **279**(16), 2905-16

Bui, J. M., Tai, K., and McCammon, J. A. (2004). "Acetylcholinesterase: enhanced fluctuations and alternative routes to the active site in the complex with fasciculin-2." *J. Am. Chem. Soc.* **126**(23), 7198-205

Calic, M., Vrdoljak, A. L., Radic, B., Jelic, D., Jun, D., Kuca, K., and Kovarik, Z. (2006). "In vitro and in vivo evaluation of pyridinium oximes: mode of interaction with acetylcholinesterase, effect on tabun- and soman-poisoned mice and their cytotoxicity." *Toxicology* **219**(1-3), 85-96

Carletti, E., Colletier, J. P., Dupeux, F., Trovaslet, M., Masson, P., and Nachon, F. (2010). "Structural evidence that human acetylcholinesterase inhibited by tabun ages through O-dealkylation." *J. Med. Chem.* **53**(10), 4002-8

Carr, P. D., and Ollis, D. L. (2009). "Alpha/beta hydrolase fold: an update." *Protein Pept. Lett.* **16**(10), 1137-48

Cheng, Y., Suen, J. K., Radic, Z., Bond, S. D., Holst, M. J., and McCammon, J. A. (2007). "Continuum simulations of acetylcholine diffusion with reaction-determined boundaries in neuromuscular junction models." *Biophys. Chem.* **127**(3), 129-39

Cheung, J., Rudolph, M. J., Burshteyn, F., Cassidy, M. S., Gary, E. N., Love, J., Franklin, M. C., and Height, J. J. (2012). "Structures of human acetylcholinesterase in complex with pharmacologically important ligands." *J. Med. Chem.* **55**(22), 10282-6

Cochran, R., Kalisiak, J., Kucukkilinc, T., Radic, Z., Garcia, E., Zhang, L., Ho, K. Y., Amitai, G., Kovarik, Z., Fokin, V. V., Sharpless, K. B., and Taylor, P. (2011). "Oxime-assisted acetylcholinesterase catalytic scavengers of organophosphates that resist aging." *J. Biol. Chem.*

Colletier, J. P., Fournier, D., Greenblatt, H. M., Stojan, J., Sussman, J. L., Zaccai, G., Silman, I., and Weik, M. (2006). "Structural insights into substrate traffic and inhibition in acetylcholinesterase." *EMBO J.* **25**(12), 2746-56

Cousin, X., Creminon, C., Grassi, J., Meflah, K., Cornu, G., Saliou, B., Bon, S., Massoulie, J., and Bon, C. (1996). "Acetylcholinesterase from Bungarus venom: a monomeric species." *FEBS Lett.* **387**(2-3), 196-200

Coussen, F., Ayon, A., Le Goff, A., Leroy, J., Massoulie, J., and Bon, S. (2001). "Addition of a glycophosphatidylinositol to acetylcholinesterase. Processing, degradation, and secretion." *J. Biol. Chem.* **276**(30), 27881-92

Cowper, M., and Davidson, L. H. (1943). "Phenacyl Bromide." *Organic Syntheses* **2**, 480-481

Dirnhuber, P., French, M. C., Green, D. M., Leadbeater, L., and Stratton, J. A. (1979). "The protection of primates against soman poisoning by pretreatment with pyridostigmine." *J. Pharm. Pharmacol.* **31**(5), 295-9

Dorandeu, F., Foquin, A., Briot, R., Delacour, C., Denis, J., Alonso, A., Froment, M. T., Renault, F., Lallement, G., and Masson, P. (2008). "An unexpected plasma cholinesterase activity rebound after challenge with a high dose of the nerve agent VX." *Toxicology* **248**(2-3), 151-7

Dorandeu, F., Lallement, G., Carpentier, P., Filliat, P., Collombet, J. M., and Ruttimann, M. (2003). Neuroprotection et neurotoxiques organophosphorés : quelle place pour la kétamine ? . In *Arnette* (F. Rueil-Malmaison, Ed.) Eds.), pp. 77-96.

Dougherty, D. A., and Stauffer, D. A. (1990). "Acetylcholine binding by a synthetic receptor: implications for biological recognition." *Science* **250**(4987), 1558-60

Eddleston, M., Buckley, N. A., Eyer, P., and Dawson, A. H. (2008). "Management of acute organophosphorus pesticide poisoning." *Lancet* **371**(9612), 597-607

Ekstrom, F., Akfur, C., Tunemalm, A. K., and Lundberg, S. (2006a). "Structural changes of phenylalanine 338 and histidine 447 revealed by the crystal structures of tabun-inhibited murine acetylcholinesterase." *Biochemistry* **45**(1), 74-81

Ekstrom, F., Hornberg, A., Artursson, E., Hammarstrom, L. G., Schneider, G., and Pang, Y. P. (2009). "Structure of HI-6*sarin-acetylcholinesterase determined by X-ray crystallography and molecular dynamics simulation: reactivator mechanism and design." *PLoS ONE* **4**(6), e5957

Ekstrom, F., Pang, Y. P., Boman, M., Artursson, E., Akfur, C., and Borjegren, S. (2006b). "Crystal structures of acetylcholinesterase in complex with HI-6, Ortho-7 and obidoxime: structural basis for differences in the ability to reactivate tabun conjugates." *Biochem. Pharmacol.* **72**(5), 597-607

Elhanany, E., Ordentlich, A., Dgany, O., Kaplan, D., Segall, Y., Barak, R., Velan, B., and Shafferman, A. (2001). "Resolving pathways of interaction of covalent inhibitors with the active site of acetylcholinesterases: MALDI-TOF/MS analysis of various nerve agent phosphyl adducts." *Chem. Res. Toxicol.* **14**(7), 912-8

Fleisher, J. H., and Harris, L. W. (1965). "Dealkylation as a mechanism for aging of cholinesterase after poisoning with pinacolyl methylphosphonofluoridate." *Biochem. Pharmacol.* **14**(5), 641-50

Fosbraey, P., Wetherell, J. R., and French, M. C. (1990). "Neurotransmitter changes in guinea-pig brain regions following soman intoxication." *J. Neurochem.* **54**(1), 72-9

Fujikawa, Y., Satoh, T., Suganuma, A., Suzuki, S., Niikura, Y., Yui, S., and Yamaura, Y. (2005). "Extremely sensitive biomarker of acute organophosphorus insecticide exposure." *Hum. Exp. Toxicol.* **24**(6), 333-6

Fukuto, T. R. (1990). "Mechanism of action of organophosphorus and carbamate insecticides." *Environ. Health Perspect.* **87**, 245-54

Genovese, R. F., Sun, W., Johnson, C. C., Ditargiani, R. C., Doctor, B. P., and Saxena, A. (2010). "Safety of administration of human butyrylcholinesterase and its conjugates with soman or VX in rats." *Basic Clin. Pharmacol. Toxicol.* **106**(5), 428-34

Getman, D. K., Eubanks, J. H., Camp, S., Evans, G. A., and Taylor, P. (1992). "The human gene encoding acetylcholinesterase is located on the long arm of chromosome 7." *Am. J. Hum. Genet.* **51**(1), 170-7

Geyer, B. C., Kannan, L., Garnaud, P. E., Broomfield, C. A., Cadieux, C. L., Cherni, I., Hodgins, S. M., Kasten, S. A., Kelley, K., Kilbourne, J., Oliver, Z. P., Otto, T. C., Puffenberger, I., Reeves, T. E., Robbins, N., 2nd, Woods, R. R., Soreq, H., Lenz, D. E., Cerasoli, D. M., and Mor, T. S. (2010). "Plant-derived human butyrylcholinesterase, but not an organophosphorous-compound hydrolyzing variant thereof, protects rodents against nerve agents." *Proc. Natl. Acad. Sci. U. S. A.* **107**(47), 20251-6

Gilson, M. K., Straatsma, T. P., McCammon, J. A., Ripoll, D. R., Faerman, C. H., Axelsen, P. H., Silman, I., and Sussman, J. L. (1994). "Open "back door" in a molecular dynamics simulation of acetylcholinesterase." *Science* **263**(5151), 1276-8

Glynn, P. (1999). "Neuropathy target esterase." *Biochem. J.* **344**, 625-31

Gnatt, A., Ginzberg, D., Lieman-Hurwitz, J., Zamir, R., Zakut, H., and Soreq, H. (1991). "Human acetylcholinesterase and butyrylcholinesterase are encoded by two distinct genes." *Cell. Mol. Neurobiol.* **11**(1), 91-104

Goeldner, M. P., and Hirth, C. G. (1980). "Specific photoaffinity labeling induced by energy transfer: application to irreversible inhibition of acetylcholinesterase." *Proc. Natl. Acad. Sci. U. S. A.* **77**(11), 6439-42

Gordon, J. J., Leadbeater, L., and Maidment, M. P. (1978). "The protection of animals against organophosphate poisoning by pretreatment with a carbamate." *Toxicol. Appl. Pharmacol.* **43**(1), 207-16

Grunwald, J., Raveh, L., Doctor, B. P., and Ashani, Y. (1994). "Huperzine A as a pretreatment candidate drug against nerve agent toxicity." *Life Sci.* **54**(14), 991-7

Gunosewoyo, H., Tipparaju, S. K., Pieroni, M., Wang, Y., Doctor, B. P., Nambiar, M. P., and Kozikowski, A. P. (2013). "Structural analogs of huperzine A improve survival in guinea pigs exposed to soman." *Bioorg. Med. Chem. Lett.* **23**(5), 1544-7

Haas, R., Brandt, P. T., Knight, J., and Rosenberry, T. L. (1986). "Identification of amine components in a glycolipid membrane-binding domain at the C-terminus of human erythrocyte acetylcholinesterase." *Biochemistry* **25**(11), 3098-105

Harel, M., Kryger, G., Rosenberry, T. L., Mallender, W. D., Lewis, T., Fletcher, R. J., Guss, J. M., Silman, I., and Sussman, J. L. (2000). "Three-dimensional structures of Drosophila melanogaster acetylcholinesterase and of its complexes with two potent inhibitors." *Protein Sci.* **9**(6), 1063-72

Harel, M., Quinn, D. M., Nair, H. K., Silman, I., and Sussman, J. (1996). "The X-ray Structure of a Transition State Analog Complex Reveals the Molecular Origins of the Catalytic Power and Substrate Specificity of Acetylcholinesterase." *J. Am. Chem. Soc.* **118**, 2340-2346

Harel, M., Schalk, I., Ehret-Sabatier, L., Bouet, F., Goeldner, M., Hirth, C., Axelsen, P. H., Silman, I., and Sussman, J. L. (1993). "Quaternary ligand binding to aromatic residues in the active-site gorge of acetylcholinesterase." *Proc. Natl. Acad. Sci. U. S. A.* **90**(19), 9031-5

Harel, M., Su, C. T., Frolow, F., Ashani, Y., Silman, I., and Sussman, J. L. (1991). "Refined crystal structures of "aged" and "non-aged" organophosphoryl conjugates of gamma-chymotrypsin." *J. Mol. Biol.* **221**(3), 909-18

Harel, M., Sussman, J. L., Krejci, E., Bon, S., Chanal, P., Massoulie, J., and Silman, I. (1992). "Conversion of acetylcholinesterase to butyrylcholinesterase: modeling and mutagenesis." *Proc. Natl. Acad. Sci. U. S. A.* **89**(22), 10827-31

Harris, L. W., Fleisher, J. H., Clark, J., and Cliff, W. J. (1966). "Dealkylation and loss of capacity for reactivation of cholinesterase inhibited by sarin." *Science* **154**(747), 404-7

Hornberg, A., Artursson, E., Warme, R., Pang, Y. P., and Ekstrom, F. (2010). "Crystal structures of oxime-bound fenamiphos-acetylcholinesterases: reactivation involving flipping of the His447 ring to form a reactive Glu334-His447-oxime triad." *Biochem. Pharmacol.* **79**(3), 507-15

Huang, Y. J., Huang, Y., Baldassarre, H., Wang, B., Lazaris, A., Leduc, M., Bilodeau, A. S., Bellemare, A., Cote, M., Herskovits, P., Touati, M., Turcotte, C., Valeanu, L., Lemee, N., Wilgus, H., Begin, I., Bhatia, B., Rao, K., Neveu, N., Brochu, E., Pierson, J., Hockley, D. K., Cerasoli, D. M., Lenz, D. E., Karatzas, C. N., and Langermann, S. (2007). "Recombinant human butyrylcholinesterase from milk of transgenic animals to protect against organophosphate poisoning." *Proc. Natl. Acad. Sci. U. S. A.* **104**(34), 13603-8

Hvistendahl, M. (2013). "In Rural Asia, Locking Up Poisons to Prevent Suicides." *Science* **341**(6147), 738-739

Järv, J. (1984). "Stereochemical aspects of cholinesterase catalysis." *Bioorganic Chemistry* **12**(4), 259-278

Johnson, J. L., Cusack, B., Davies, M. P., Fauq, A., and Rosenberry, T. L. (2003). "Unmasking tandem site interaction in human acetylcholinesterase. Substrate activation with a cationic acetanilide substrate." *Biochemistry* **42**(18), 5438-52

Jokanovic, M. (2009). "Medical treatment of acute poisoning with organophosphorus and carbamate pesticides." *Toxicol. Lett.* **190**(2), 107-15

Kaplan, D., Barak, D., Ordentlich, A., Kronman, C., Velan, B., and Shafferman, A. (2004). "Is aromaticity essential for trapping the catalytic histidine 447 in human acetylcholinesterase?" *Biochemistry* **43**(11), 3129-36

Kassa, J. (2002). "Review of oximes in the antidotal treatment of poisoning by organophosphorus nerve agents." *J. Toxicol. Clin. Toxicol.* **40**(6), 803-16

Kasten, S. A., Kajih, T., Smith, J. R., Oliver, Z., Otto, T. C., Reeves, T. E., Lenz, D. E., and Cerasoli, D. M. The importance of Nerve Agent Stereoselectivity in Stoichiometric and catalytic bioscavengers2010, Hunt Valley, MD, p. 46.

Kersharwani, M. K., Bandyopadhyay, T., and Ganguly, B. (2012). "Probing O-dealkylation and deamination aging processes in tabun-conjugated AChE: a computational study." *Theor. Chem. Acc.* **131**(1175)

Kliachyna, M., Santoni, G., Nussbaum, V., Renou, J., Sanson, B., Colletier, J. P., Arboleas, M., Loiodice, M., Weik, M., Jean, L., Renard, P. Y., Nachon, F., and Baati, R. (2014). "Design, synthesis and biological evaluation of novel tetrahydroacridine pyridine- aldoxime and -amidoxime hybrids as efficient uncharged reactivators of nerve agent-inhibited human acetylcholinesterase." *European journal of medicinal chemistry* **sous presse**

Koellner, G., Kryger, G., Millard, C. B., Silman, I., Sussman, J. L., and Steiner, T. (2000). "Active-site gorge and buried water molecules in crystal structures of acetylcholinesterase from Torpedo californica." *J. Mol. Biol.* **296**(2), 713-35

Kovarik, Z., Katalinic, M., Sinko, G., Binder, J., Holas, O., Jung, Y. S., Musilova, L., Jun, D., and Kuca, K. (2010). "Pseudo-catalytic scavenging: searching for a suitable reactivator of phosphorylated butyrylcholinesterase." *Chem. Biol. Interact.* **187**(1-3), 167-71

Kovarik, Z., Radic, Z., Berman, H. A., and Taylor, P. (2007). "Mutation of acetylcholinesterase to enhance oxime-assisted catalytic turnover of methylphosphonates." *Toxicology* **233**(1-3), 79-84

Kronman, C., Cohen, O., Mazor, O., Ordentlich, A., Raveh, L., Velan, B., and Shafferman, A. (2010). "Next generation OP-bioscavengers: a circulatory long-lived 4-PEG hypolysine mutant of F338A-HuAChE with optimal pharmacokinetics and pseudo-catalytic characteristics." *Chem. Biol. Interact.* **187**(1-3), 253-8

Kronman, C., Ordentlich, A., Barak, D., Velan, B., and Shafferman, A. (1994). "The "back door" hypothesis for product clearance in acetylcholinesterase challenged by site-directed mutagenesis." *J. Biol. Chem.* **269**(45), 27819-22

Kronman, C., Velan, B., Marcus, D., Ordentlich, A., Reuveny, S., and Shafferman, A. (1995). "Involvement of oligomerization, N-glycosylation and sialylation in the clearance of cholinesterases from the circulation." *Biochem. J.* **311 ( Pt 3)**, 959-67

Kryger, G., Harel, M., Giles, K., Toker, L., Velan, B., Lazar, A., Kronman, C., Barak, D., Ariel, N., Shafferman, A., Silman, I., and Sussman, J. L. (2000). "Structures of recombinant native and E202Q mutant human acetylcholinesterase complexed with the snake-venom toxin fasciculin-II." *Acta Crystallogr. D Biol. Crystallogr.* **56**(Pt 11), 1385-94

Kuca, K., and Cabal, J. (2004). "In vitro reactivation of tabun-inhibited acetylcholinesterase using new oximes--K027, K005, K033 and K048." *Cent. Eur. J. Public Health* **12 Suppl**, S59-61

Kwasnieski, O., Verdier, L., Malacria, M., and Derat, E. (2009). "Fixation of the two Tabun isomers in acetylcholinesterase: a QM/MM study." *J. Phys. Chem. B* **113**(29), 10001-7

Lallement, G., Carpentier, P., Pernot-Marino, I., Baubichon, D., Collet, A., and Blanchet, G. (1993). "Transient impairment of the gabaergic function during initiation of soman-induced seizures." *Brain Res.* **629**(2), 239-44

Lallement, G., Veyret, J., Masqueliez, C., Aubriot, S., Burckhart, M. F., and Baubichon, D. (1997). "Efficacy of huperzine in preventing soman-induced seizures, neuropathological changes and lethality." *Fundam. Clin. Pharmacol.* **11**(5), 387-94

Li, H., Schopfer, L. M., Masson, P., and Lockridge, O. (2008). "Lamellipodin proline rich peptides associated with native plasma butyrylcholinesterase tetramers." *Biochem. J.* **411**(2), 425-32

Li, Y., Camp, S., and Taylor, P. (1993). "Tissue-specific expression and alternative mRNA processing of the mammalian acetylcholinesterase gene." *J. Biol. Chem.* **268**(8), 5790-7

Lockridge, O., Bartels, C. F., Vaughan, T. A., Wong, C. K., Norton, S. E., and Johnson, L. L. (1987). "Complete amino acid sequence of human serum cholinesterase." *J. Biol. Chem.* **262**(2), 549-57

Lockridge, O., Blong, R. M., Masson, P., Froment, M. T., Millard, C. B., and Broomfield, C. A. (1997). "A single amino acid substitution, Gly117His, confers phosphotriesterase (organophosphorus acid anhydride hydrolase) activity on human butyrylcholinesterase." *Biochemistry* **36**(4), 786-95

Macdonald, I. R., Martin, E., Rosenberry, T. L., and Darvesh, S. (2012). "Probing the peripheral site of human butyrylcholinesterase." *Biochemistry* **51**(36), 7046-53

Macilwain, C. (1993). "Study proves Iraq used nerve gas." *Nature* **363**(6424), 3

Mallender, W. D., Szegletes, T., and Rosenberry, T. L. (2000). "Acetylthiocholine binds to asp74 at the peripheral site of human acetylcholinesterase as the first step in the catalytic pathway." *Biochemistry* **39**(26), 7753-63

Masson, P., Adkins, S., Gouet, P., and Lockridge, O. (1993). "Recombinant human butyrylcholinesterase G390V, the fluoride-2 variant, expressed in Chinese hamster ovary cells, is a low affinity variant." *J. Biol. Chem.* **268**(19), 14329-41

Masson, P., Fortier, P. L., Albaret, C., Froment, M. T., Bartels, C. F., and Lockridge, O. (1997a). "Aging of di-isopropyl-phosphorylated human butyrylcholinesterase." *Biochem. J.* **327 ( Pt 2)**, 601-7

Masson, P., Froment, M. T., Bartels, C. F., and Lockridge, O. (1996). "Asp7O in the peripheral anionic site of human butyrylcholinesterase." *Eur. J. Biochem.* **235**(1-2), 36-48

Masson, P., Froment, M. T., Gillon, E., Nachon, F., Lockridge, O., and Schopfer, L. M. (2007). "Hydrolysis of oxo- and thio-esters by human butyrylcholinesterase." *Biochim. Biophys. Acta* **1774**(1), 16-34

Masson, P., Legrand, P., Bartels, C. F., Froment, M. T., Schopfer, L. M., and Lockridge, O. (1997b). "Role of aspartate 70 and tryptophan 82 in binding of succinyldithiocholine to human butyrylcholinesterase." *Biochemistry* **36**(8), 2266-77

Masson, P., Nachon, F., Broomfield, C. A., Lenz, D. E., Verdier, L., Schopfer, L. M., and Lockridge, O. (2008). "A collaborative endeavor to design cholinesterase-based catalytic scavengers against toxic organophosphorus esters." *Chem. Biol. Interact.* **175**(1-3), 273-80

Masson, P., Nachon, F., and Lockridge, O. (2010). "Structural approach to the aging of phosphylated cholinesterases." *Chem. Biol. Interact.* **187**(1-3), 157-62

Masson, P., Xie, W., Froment, M. T., Levitsky, V., Fortier, P. L., Albaret, C., and Lockridge, O. (1999). "Interaction between the peripheral site residues of human butyrylcholinesterase, D70 and Y332, in binding and hydrolysis of substrates." *Biochim. Biophys. Acta* **1433**(1-2), 281-93

Massoulie, J. (2002). "The origin of the molecular diversity and functional anchoring of cholinesterases." *Neurosignals* **11**(3), 130-43

Massoulie, J., Sussman, J., Bon, S., and Silman, I. (1993). "Structure and functions of acetylcholinesterase and butyrylcholinesterase." *Prog. Brain Res.* **98**, 139-46

Melchers, B. P., Philippens, I. H., and Wolthuis, O. L. (1994). "Efficacy of HI-6 and HLo-7 in preventing incapacitation following nerve agent poisoning." *Pharmacol. Biochem. Behav.* **49**(4), 781-8

Mercey, G., Renou, J., Verdelet, T., Kliachyna, M., Baati, R., Gillon, E., Arboleas, M., Loiodice, M., Nachon, F., Jean, L., and Renard, P. Y. (2012). "Phenyltetrahydroisoquinoline-pyridinaldoxime conjugates as efficient uncharged reactivators for the dephosphylation of inhibited human acetylcholinesterase." *J. Med. Chem.* **55**(23), 10791-5

Mercey, G., Verdelet, T., Saint-Andre, G., Gillon, E., Wagner, A., Baati, R., Jean, L., Nachon, F., and Renard, P. Y. (2011). "First efficient uncharged reactivators for the dephosphylation of poisoned human acetylcholinesterase." *Chem. Commun. (Camb.)* **47**(18), 5295-7

Michel, H. O., Hackley, B. E., Jr., Berkowitz, L., List, G., Hackley, E. B., Gillilan, W., and Pankau, M. (1967). "Ageing and dealkylation of Soman (pinacolylmethylphosphonofluoridate)-inactivated eel cholinesterase." *Arch. Biochem. Biophys.* **121**(1), 29-34

Millard, C. B., Koellner, G., Ordentlich, A., Shafferman, A., Silman, I., and Sussman, J. L. (1999a). "Reaction Products of Acetylcholinesterase and VX Reveal a Mobile Histidine in the Catalytic Triad." *J. Am. Chem. Soc.* **121**(42), 9883- 9884

Millard, C. B., Kryger, G., Ordentlich, A., Greenblatt, H. M., Harel, M., Raves, M. L., Segall, Y., Barak, D., Shafferman, A., Silman, I., and Sussman, J. L. (1999b). "Crystal structures of aged phosphonylated acetylcholinesterase: nerve agent reaction products at the atomic level." *Biochemistry* **38**(22), 7032-9

Millard, C. B., Lockridge, O., and Broomfield, C. A. (1995). "Design and expression of organophosphorus acid anhydride hydrolase activity in human butyrylcholinesterase." *Biochemistry* **34**(49), 15925-33

Millard, C. B., Lockridge, O., and Broomfield, C. A. (1998). "Organophosphorus acid anhydride hydrolase activity in human butyrylcholinesterase: synergy results in a somanase." *Biochemistry* **37**(1), 237-47

Mollerup, H. M., and Gatke, M. R. (2011). "Butyrylcholinesterase gene mutations in patients with prolonged apnea after succinylcholine for electroconvulsive therapy." *Acta Anaesthesiol. Scand.* **55**(1), 82-6

Myers, T. M., Sun, W., Naik, R. S., Clark, M. G., Doctor, B. P., and Saxena, A. (2012). "Characterization of human serum butyrylcholinesterase in rhesus monkeys: behavioral and physiological effects." *Neurotoxicol. Teratol.* **34**(3), 323-30

Nachon, F., Asojo, O. A., Borgstahl, G. E., Masson, P., and Lockridge, O. (2005). "Role of water in aging of human butyrylcholinesterase inhibited by echothiophate: the crystal structure suggests two alternative mechanisms of aging." *Biochemistry* **44**(4), 1154-62

Nachon, F., Carletti, E., Ronco, C., Trovaslet, M., Nicolet, Y., Jean, L., and Renard, P. Y. (2013). "Crystal structures of human cholinesterases in complex with huprine W and tacrine: elements of specificity for anti-Alzheimer's drugs targeting acetyl- and butyryl-cholinesterase." *Biochem. J.* **453**(3), 393-9

Nachon, F., Stojan, J., and Fournier, D. (2008). "Insights into substrate and product traffic in the Drosophila melanogaster acetylcholinesterase active site gorge by enlarging a back channel." *FEBS J.* **275**(10), 2659-64

Neville, L. F., Gnatt, A., Padan, R., Seidman, S., and Soreq, H. (1990). "Anionic site interactions in human butyrylcholinesterase disrupted by two single point mutations." *J. Biol. Chem.* **265**(34), 20735-8

Ordentlich, A., Barak, D., Kronman, C., Ariel, N., Segall, Y., Velan, B., and Shafferman, A. (1995). "Contribution of aromatic moieties of tyrosine 133 and of the anionic subsite tryptophan 86 to catalytic efficiency and allosteric modulation of acetylcholinesterase." *J. Biol. Chem.* **270**(5), 2082-91

Ordentlich, A., Barak, D., Kronman, C., Ariel, N., Segall, Y., Velan, B., and Shafferman, A. (1996). "The architecture of human acetylcholinesterase active center probed by interactions with selected organophosphate inhibitors." *J. Biol. Chem.* **271**(20), 11953-62

Ordentlich, A., Barak, D., Kronman, C., Flashner, Y., Leitner, M., Segall, Y., Ariel, N., Cohen, S., Velan, B., and Shafferman, A. (1993a). "Dissection of the human acetylcholinesterase active center determinants of substrate specificity. Identification of residues constituting the anionic site, the hydrophobic site, and the acyl pocket." *J. Biol. Chem.* **268**(23), 17083-95

Ordentlich, A., Kronman, C., Barak, D., Stein, D., Ariel, N., Marcus, D., Velan, B., and Shafferman, A. (1993b). "Engineering resistance to 'aging' of phosphylated human acetylcholinesterase. Role of hydrogen bond network in the active center." *FEBS Lett.* **334**(2), 215-20

Perrier, A. L., Massoulie, J., and Krejci, E. (2002). "PRiMA: the membrane anchor of acetylcholinesterase in the brain." *Neuron* **33**(2), 275-85

Peters, J., Trovaslet, M., Trapp, M., Nachon, F., Hill, F., Royer, E., Gabel, F., van Eijck, L., Masson, P., and Tehei, M. (2012). "Activity and molecular dynamics relationship within the family of human cholinesterases." *Phys. Chem. Chem. Phys.*

Poulton, T. J., James, F. M., 3rd, and Lockridge, O. (1979). "Prolonged apnea following trimethaphan and succinylcholine." *Anesthesiology* **50**(1), 54-6

Puu, G. (1988). "Ketamine protects acetylcholinesterase against in vitro inhibition by sarin." *Biochem. Pharmacol.* **37**, 969-970

Qian, N., and Kovach, I. M. (1993). "Key active site residues in the inhibition of acetylcholinesterases by soman." *FEBS Lett.* **336**(2), 263-6

Radic, Z., Dale, T., Kovarik, Z., Berend, S., Garcia, E., Zhang, L., Amitai, G., Green, C., Radic, B., Duggan, B. M., Ajami, D., Rebek, J., and Taylor, P. (2013). "Catalytic detoxification of nerve agent and pesticide organophosphates by butyrylcholinesterase assisted with non-pyridinium oximes." *Biochem. J.* **450**(1), 231-42

Radic, Z., Reiner, E., and Taylor, P. (1991). "Role of the peripheral anionic site on acetylcholinesterase: inhibition by substrates and coumarin derivatives." *Mol. Pharmacol.* **39**(1), 98-104

Radic, Z., Sit, R. K., Kovarik, Z., Berend, S., Garcia, E., Zhang, L., Amitai, G., Green, C., Radic, B., Fokin, V. V., Sharpless, K. B., and Taylor, P. (2012). "Refinement of structural leads for centrally acting oxime reactivators of phosphylated cholinesterases." *J. Biol. Chem.* **287**(15), 11798-809

Radic, Z., and Taylor, P. (2001). "Interaction kinetics of reversible inhibitors and substrates with acetylcholinesterase and its fasciculin 2 complex." *J. Biol. Chem.* **276**(7), 4622-33

Raveh, L., Grunwald, J., Marcus, D., Papier, Y., Cohen, E., and Ashani, Y. (1993). "Human butyrylcholinesterase as a general prophylactic antidote for nerve agent toxicity. In vitro and in vivo quantitative characterization." *Biochem. Pharmacol.* **45**(12), 2465-74

Renou, J., Loiodice, M., Arboleas, M., Baati, R., Jean, L., Nachon, F., and Renard, P. Y. (2014). "Tryptoline-3-hydroxypyridinaldoxime conjugates as efficient reactivators of phosphylated human acetyl and butyrylcholinesterases." *Chem. Commun. (Camb.)*

Renou, J., Mercey, G., Verdelet, T., Paunescu, E., Gillon, E., Arboleas, M., Loiodice, M., Kliachyna, M., Baati, R., Nachon, F., Jean, L., and Renard, P. Y. (2013). "Syntheses and in vitro evaluations of uncharged reactivators for human acetylcholinesterase inhibited by organophosphorus nerve agents." *Chem. Biol. Interact.* **203**(1), 81-4

Riotte, M., Vacquier, M., and Van de valle, M. T. (1988). Un anticonvulsivant efficace en urgence contre l'intoxication par les organophosphorés. *SSA Trav. Sci.* **9**, 115-116.

Rosenberry, T. L., Mallender, W. D., Thomas, P. J., and Szegletes, T. (1999). "A steric blockade model for inhibition of acetylcholinesterase by peripheral site ligands and substrate." *Chem. Biol. Interact.* **119-120**, 85-97

Rousseau, J. M., Besse Bardot, I., Franck, L., Libert, N., Lallement, G., and Clair, P. (2009). "[Interest of Ineurope syringe for nerve agent intoxication]." *Ann. Fr. Anesth. Reanim.* **28**(5), 482-8

Saint-André, G., Kliachyna, M., Sanjeevarao, K., Louise-Leriche, L., Gillon, E., Renard, P. Y., Nachon, F., Baati, R., and Wagner, A. (2011). "Design, synthesis and evaluation of new α-nucleophiles for the hydrolysis of organophosphorus nerve agents: application to the reactivation of phosphorylated acetylcholinesterase." *Tetrahedron* **67**, 6352-61

Sakurada, K., Matsubara, K., Shimizu, K., Shiono, H., Seto, Y., Tsuge, K., Yoshino, M., Sakai, I., Mukoyama, H., and Takatori, T. (2003). "Pralidoxime iodide (2-pAM) penetrates across the blood-brain barrier." *Neurochem. Res.* **28**(9), 1401-7

Sanson, B., Colletier, J. P., Xu, Y., Lang, P. T., Jiang, H., Silman, I., Sussman, J. L., and Weik, M. (2011). "Backdoor opening mechanism in acetylcholinesterase based on X-ray crystallography and molecular dynamics simulations." *Protein Sci.* **20**(7), 1114-8

Sanson, B., Nachon, F., Colletier, J. P., Froment, M. T., Toker, L., Greenblatt, H. M., Sussman, J. L., Ashani, Y., Masson, P., Silman, I., and Weik, M. (2009). "Crystallographic snapshots of nonaged and aged conjugates of soman with acetylcholinesterase, and of a ternary complex of the aged conjugate with pralidoxime." *J. Med. Chem.* **52**(23), 7593-603

Saxena, A., Luo, C., and Doctor, B. P. (2008). "Developing procedures for the large-scale purification of human serum butyrylcholinesterase." *Protein Expr. Purif.* **61**(2), 191-6

Saxena, A., Sun, W., Dabisch, P. A., Hulet, S. W., Hastings, N. B., Jakubowski, E. M., Mioduszewski, R. J., and Doctor, B. P. (2011). "Pretreatment with human serum butyrylcholinesterase alone prevents cardiac abnormalities, seizures, and death in Gottingen minipigs exposed to sarin vapor." *Biochem. Pharmacol.* **82**(12), 1984-93

Schalk, I., Ehret-Sabatier, L., Bouet, F., Goeldner, M., and Hirth, C. (1994). "Trp279 is involved in the binding of quaternary ammonium at the peripheral site of Torpedo marmorata acetylcholinesterase." *Eur. J. Biochem.* **219**(1-2), 155-9

Schopfer, L. M., Ticu-Boeck, A., Broomfield, C. A., and Lockridge, O. (2004). "Mutants of human butyrylcholinesterase with organophosphate hydrolase activity; evidence that His117 serves as a general base catalyst." *J Med Chem Def* **2**, 1-21

Segall, Y., Waysbort, D., Barak, D., Ariel, N., Doctor, B. P., Grunwald, J., and Ashani, Y. (1993). "Direct observation and elucidation of the structures of aged and nonaged phosphorylated cholinesterases by 31P NMR spectroscopy." *Biochemistry* **32**(49), 13441-50

Shafferman, A., Ordentlich, A., Barak, D., Stein, D., Ariel, N., and Velan, B. (1996). "Aging of phosphylated human acetylcholinesterase: catalytic processes mediated by aromatic and polar residues of the active centre." *Biochem. J.* **318 ( Pt 3)**, 833-40

Shafferman, A., Velan, B., Ordentlich, A., Kronman, C., Grosfeld, H., Leitner, M., Flashner, Y., Cohen, S., Barak, D., and Ariel, N. (1992). "Substrate inhibition of acetylcholinesterase: residues affecting signal transduction from the surface to the catalytic center." *EMBO J.* **11**(10), 3561-8

Shih, T. M., and McDonough, J. H., Jr. (1997). "Neurochemical mechanisms in soman-induced seizures." *J. Appl. Toxicol.* **17**(4), 255-64

Soreq, H., Ben-Aziz, R., Prody, C. A., Seidman, S., Gnatt, A., Neville, L., Lieman-Hurwitz, J., Lev-Lehman, E., Ginzberg, D., Lipidot-Lifson, Y., and et al. (1990). "Molecular cloning and construction of the coding region for human acetylcholinesterase reveals a G + C-rich attenuating structure." *Proc. Natl. Acad. Sci. U. S. A.* **87**(24), 9688-92

Suarez, D., Diaz, N., Fontecilla-Camps, J., and Field, M. J. (2006). "A computational study of the deacylation mechanism of human butyrylcholinesterase." *Biochemistry* **45**(24), 7529-43

Sussman, J. L., Harel, M., Frolow, F., Oefner, C., Goldman, A., Toker, L., and Silman, I. (1991). "Atomic structure of acetylcholinesterase from Torpedo californica: a prototypic acetylcholine-binding protein." *Science* **253**(5022), 872-9

Szegletes, T., Mallender, W. D., Thomas, P. J., and Rosenberry, T. L. (1999). "Substrate binding to the peripheral site of acetylcholinesterase initiates enzymatic catalysis. Substrate inhibition arises as a secondary effect." *Biochemistry* **38**(1), 122-33

Taylor, P., Kovarik, Z., Reiner, E., and Radic, Z. (2007). "Acetylcholinesterase: converting a vulnerable target to a template for antidotes and detection of inhibitor exposure." *Toxicology* **233**(1-3), 70-8

Tormos, J. R., Wiley, K. L., Wang, Y., Fournier, D., Masson, P., Nachon, F., and Quinn, D. M. (2010). "Accumulation of tetrahedral intermediates in cholinesterase catalysis: a secondary isotope effect study." *J. Am. Chem. Soc.* **132**(50), 17751-9

Trovaslet, M., Trapp, M., Weik, M., Nachon, F., Masson, P., Tehei, M., and Peters, J. (2013). "Relation between dynamics, activity and thermal stability within the cholinesterase family." *Chem. Biol. Interact.* **203**(1), 14-8

Vale, J. A. (1998). "Toxicokinetic and toxicodynamic aspects of organophosphorus (OP) insecticide poisoning." *Toxicol. Lett.* **102-103**, 649-52

Velan, B., Kronman, C., Ordentlich, A., Flashner, Y., Leitner, M., Cohen, S., and Shafferman, A. (1993). "N-glycosylation of human acetylcholinesterase: effects on activity, stability and biosynthesis." *Biochem. J.* **296 ( Pt 3)**, 649-56

Vellom, D. C., Radic, Z., Li, Y., Pickering, N. A., Camp, S., and Taylor, P. (1993). "Amino acid residues controlling acetylcholinesterase and butyrylcholinesterase specificity." *Biochemistry* **32**(1), 12-7

Viragh, C., Akhmetshin, R., Kovach, I. M., and Broomfield, C. (1997). "Unique push-pull mechanism of dealkylation in soman-inhibited cholinesterases." *Biochemistry* **36**(27), 8243-52

Vyas, S., Beck, J. M., Xia, S., Zhang, J., and Hadad, C. M. (2010). "Butyrylcholinesterase and G116H, G116S, G117H, G117N, E197Q and G117H/E197Q mutants: a molecular dynamics study." *Chem. Biol. Interact.* **187**(1-3), 241-5

Wandhammer, M., de Koning, M., van Grol, M., Loiodice, M., Saurel, L., Noort, D., Goeldner, M., and Nachon, F. (2013). "A step toward the reactivation of aged cholinesterases--crystal structure of ligands binding to aged human butyrylcholinesterase." *Chem. Biol. Interact.* **203**(1), 19-23

Wang, Y., Boeck, A. T., Duysen, E. G., Van Keuren, M., Saunders, T. L., and Lockridge, O. (2004). "Resistance to organophosphorus agent toxicity in transgenic mice expressing the G117H mutant of human butyrylcholinesterase." *Toxicol. Appl. Pharmacol.* **196**(3), 356-66

Wang, Y., Wei, Y., Oguntayo, S., Doctor, B. P., and Nambiar, M. P. (2013). "A combination of [+] and [-]-Huperzine A improves protection against soman toxicity compared to [+]-Huperzine A in guinea pigs." *Chem. Biol. Interact.* **203**(1), 120-4

Wille, T., Ekstrom, F., Lee, J. C., Pang, Y. P., Thiermann, H., and Worek, F. (2010). "Kinetic analysis of interactions between alkylene-linked bis-pyridiniumaldoximes and human acetylcholinesterases inhibited by various organophosphorus compounds." *Biochem. Pharmacol.* **80**(6), 941-6

Wilson, I. B., and Ginsburg, B. (1955). "A powerful reactivator of alkylphosphate-inhibited acetylcholinesterase." *Biochim. Biophys. Acta* **18**(1), 168-70

Winder, C., and Balouet, J. C. (2002). "The toxicity of commercial jet oils." *Environ. Res.* **89**(2), 146-64

Worek, F., Eyer, P., and Szinicz, L. (1998). "Inhibition, reactivation and aging kinetics of cyclohexylmethylphosphonofluoridate-inhibited human cholinesterases." *Arch. Toxicol.* **72**(9), 580-7

Worek, F., Reiter, G., Eyer, P., and Szinicz, L. (2002). "Reactivation kinetics of acetylcholinesterase from different species inhibited by highly toxic organophosphates." *Arch. Toxicol.* **76**(9), 523-9

Worek, F., Szinicz, L., and Thiermann, H. (2005). "Estimation of oxime efficacy in nerve agent poisoning: a kinetic approach." *Chem. Biol. Interact.* **157-158**, 349-52

Worek, F., Thiermann, H., and Szinicz, L. (2004a). "Reactivation and aging kinetics of human acetylcholinesterase inhibited by organophosphonylcholines." *Arch. Toxicol.* **78**(4), 212-7

Worek, F., Thiermann, H., Szinicz, L., and Eyer, P. (2004b). "Kinetic analysis of interactions between human acetylcholinesterase, structurally different organophosphorus compounds and oximes." *Biochem. Pharmacol.* **68**(11), 2237-48

Worek, F., Wille, T., Aurbek, N., Eyer, P., and Thiermann, H. (2010). "Reactivation of organophosphate-inhibited human, Cynomolgus monkey, swine and guinea pig acetylcholinesterase by MMB-4: a modified kinetic approach." *Toxicol. Appl. Pharmacol.* **249**(3), 231-7

Xu, Y., Colletier, J. P., Weik, M., Qin, G., Jiang, H., Silman, I., and Sussman, J. L. (2010). "Long route or shortcut? A molecular dynamics study of traffic of thiocholine within the active-site gorge of acetylcholinesterase." *Biophys. J.* **99**(12), 4003-11

# ANNEXE A

## Curriculum vitae

**Florian NACHON** — **Directeur de Recherche**

**Ingénieur Divisionnaire d'Étude et de Fabrication des Armées**

Né le 29 Décembre 1971 à Besançon (25)
Nationalité Française
Marié, 2 enfants

Département de Toxicologie et Risque C
Institut de Recherche Biomédicale des Armées - BP 73
F-91223 Brétigny-s-Orge

Secrétaire: (33) 178 651 371
Mobile: (33) 645 685 115
Courriel: florian@nachon.net

## 1. Formation

Sep95-Mar99 **Doctorat de Pharmacologie moléculaire et Pharmacochimie** de l'Université Louis Pasteur, Strasbourg, sous la direction du Pr. M. Goeldner: Etudes structurales de la butyrylcholinesterase par marquage irréversible. Financement MRT.

Sep93-Juin94 **DEA de Pharmacologie moléculaire et Pharmacochimie** obtenu avec le grade de Major et la *mention Bien* (ULP - Strasbourg).

Sep92-Juin93 **Licence-Maîtrise de Biochimie**. Options de chimie organique et biologie moléculaire. *Mention Bien* (ULP - Strasbourg)

Sep89-Juin91 **D.E.U.G.) en Biologie** (Option sciences chimiques) obtenu avec le grade de Major et la *mention Très Bien* (Université de Franche Comté)

Juin89 **Baccalauréat Sciences (série C)**, *mention assez bien* (Besançon).

## 2. Expérience Professionnelle

Sep13-Présent **Scientifique visiteur** Institut de Biologie Structurale, Groupe Dynamop de Martin Weik, Grenoble.

Oct10-Présent **Chef de l'unité de Physiopathologie et Traitement de l'Atteinte par les Neurotoxiques**, Département de Toxicologie et Risque Chimique, Institut de Recherche Biomédicale des Armées, Grenoble/Brétigny-s-Orge.

Jan08-Sep10 **Chef de l'unité d'enzymologie**, Département de Toxicologie, Centre de Recherche du Service de Santé des Armées, Grenoble.

Mar02-Fev04 **Scientifique visiteur** dans le laboratoire du Pr. O. Lockridge. Eppley Cancer Research Institute - University of Nebraska Medical Center. Mise en disponibilité pour deux années.

Oct00-Dec08 **Ingénieur d'Etude et de Fabrication** au Centre de Recherche du Service de Santé des Armées, Département de toxicologie, Unité d'enzymologie dirigée par le Pr. P. Masson.

Avr99-Sep99 **Stage Postdoctoral** dans le laboratoire du Pr. O. Lockridge. Eppley Cancer Research Institute - University of Nebraska Medical Center.

## 3. Spécialités

Biologie Moléculaire - Expression hétérologue de protéines (procaryote/eucaryotes) - Purification de protéines - Ingénierie des protéines - Enzymologie - Catalyse enzymatique - Cristallographie des protéines (45 entrées dans la pdb) - Dynamique Moléculaire - Docking Moléculaire - Conception de molécules actives - Chimie computationnelle - Chimie organique.

## 4. Évaluations

Evaluateur pour *JAmChemSoc, Biochemical pharmacology, Biochemistry, PLoS ONE, Chemistry & Biology, Chemical Research in Toxicology, Chemico-Biological Interactions, Bioorganic & Medicinal chemistry Letters, Journal of Molecular Graphics and Modelling, Pharmacogenetics and Genomics, Molecules, Protein Engineering Design and Selection, Biochimie, Molecules.*

Evaluateur de projets pour l'ANR, le Nebraska Research Initiative et la Direction Générale de l'Armement (DGA).

Membre de la commission de recrutement des agents sur contrat de l'IRBA.

## 6. Direction de thèses

**Gianluca Santoni** - Université Joseph Fourier - co-directeur M. Weik – "Dynamique de l'acétylcholinestérase humaine" - Avril 2011-présent. Financement sur contrat ANR.

**Marielle Wandhammer** – Université de Strasbourg – co-directeur Pr. M. Goeldner – "Nouveaux réactivateurs des cholinestérases inhibées par des agents neurotoxiques" - Sept 2008-Fev2012. Financement sur contrat DTRA.

**Eugénie Carletti** – Université Joseph Fourier – Grenoble I – co-directeur Pr. P. Masson – "Études biochimiques et structurales d'enzymes interagissant avec les toxiques organophosphorés" – Sept06-Mars09 – Financement sur contrat de volontaire du SSA.

## 5. Projets financés

**Coordinateur** de deux actions du contrat DGA/SSA BioMedef ; Etude mécanistique et conception de réactivateurs et bioépurateurs catalytiques des neurotoxiques organophosphorés ; **2012-15** ; 5 partenaires.

**Partenaire** du projet ANR ASTRID ReCNS-AChE ; Réactivateurs de l'acétylcholinestérase centrale ; **2014-2017**. 4 partenaires. (coord. R. Baati, Université de Strasbourg)

**Partenaire** du projet ANR ASTRID CatScav ; Conception d'une enzyme catalytique pour les composés de type organophosphorés.; **2013-2015**. (coord. R. Terreux, IBPC Lyon)

**Partenaire** du projet DGA/RAPID Epuratox ; Production d'acétylcholinestérase et butyrylcholinesterase humaine dans le lait de lapines transgéniques ; **2012-2015**. (coord. A. Fouassier, Trans Rabbit Model)

**Partenaire** du contrat Defense Threat Reduction Agency (CB11-MEDCHEM1-1-0008) ; The dynamic personalities of cholinesterases and phosphotriesterases : importance for improving medical countermeasures against poisoning by chemical warfare agents ; **2012-2015**. 4 partenaires. (coord. M. Weik, IBS).

**Partenaire** du contrat Defense Threat Reduction Agency (CB11-MEDCHEM1-2-0013) ; BChE tethered with a reactivating ligand: a pseudo-catalytic nerve agent bioscavenger ; **2011-2014**. 2 partenaires internationaux. (coord. M. de Koning, TNO).

**Partenaire** du projet ANR Blanc ReAChE (ANR09BLAN192) ; Nouveaux réactivateurs de l'AChE empoisonnée ; **2009-12** ; 4 partenaires.

**Coordinateur** du contrat d'objectif DGA 08co501 ; Bioépurateurs catalytiques des neurotoxiques organophosphorés: optimisation et fonctionnalisation ; **2008-11** ; 6 partenaires dont 2 internationaux.

**Partenaire** du contrat Defense Threat Reduction Agency (CBDIF07-THER01-2-0038) ; Novel bi-functional reactivators for aged acetylcholinesterase ; **2009-11** ; 3 partenaires dont 1 international.

**Titulaire** du contrat German-French Military Cooperation (M/SABX/8A001) ; Expression of human paraoxonase based catalytic bioscavengers for prophylaxis and treatment of exposure to nerve agents ; **2008-10**.

**Coordinateur** du projet ANR Blanc DetoxNeuro (ANR06BLAN0163) ; Evaluation d'épurateurs biocompatibles pour la détoxification des neurotoxiques organophosphorés ; **2007-10** ; 4 partenaires.

## 7. Publications

Plus de 90 publications dans des journaux à comité de lecture (h-index = 22).

Sélection de 20 publications sur les 10 dernières années:


1. Renou, J., M. Loiodice, M. Arboleas, R. Baati, L. Jean, F. Nachon, and P.Y. Renard **(2014)**. *Tryptoline-3-hydroxypyridinaldoxime conjugates as efficient reactivators of phosphylated human acetyl and butyrylcholinesterases*. **Chem. Commun. (Camb.)** 50(30): p. 3947-50.
2. Wandhammer, M., M. de Koning, M. van Grol, M. Loiodice, L. Saurel, D. Noort, M. Goeldner, and F. Nachon **(2013)**. *A step toward the reactivation of aged cholinesterases--crystal structure of ligands binding to aged human butyrylcholinesterase*. **Chem. Biol. Interact.** 203(1): p. 19-23.
3. Trovaslet, M., M. Trapp, M. Weik, F. Nachon, P. Masson, M. Tehei, and J. Peters **(2013)**. *Relation between dynamics, activity and thermal stability within the cholinesterase family*. **Chem. Biol. Interact.** 203(1): p. 14-8.
4. Nachon, F., E. Carletti, C. Ronco, M. Trovaslet, Y. Nicolet, L. Jean, and P.Y. Renard **(2013)**. *Crystal structures of human cholinesterases in complex with huprine W and tacrine: elements of specificity for anti-Alzheimer's drugs targeting acetyl- and butyryl-cholinesterase*. **Biochem. J.** 453(3): p. 393-9.
5. Nachon, F., X. Brazzolotto, M. Trovaslet, and P. Masson **(2013)**. *Progress in the development of enzyme-based nerve agent bioscavengers*. **Chem. Biol. Interact.** 206(3): p. 536-44.
6. Carletti, E., J.P. Colletier, L.M. Schopfer, G. Santoni, P. Masson, O. Lockridge, F. Nachon, and M. Weik **(2013)**. *Inhibition pathways of the potent organophosphate CBDP with cholinesterases revealed by X-ray crystallographic snapshots and mass spectrometry*. **Chem. Res. Toxicol.** 26(2): p. 280-9.

7. Trapp, M., M. Trovaslet, F. Nachon, M.M. Koza, L. van Eijck, F. Hill, M. Weik, P. Masson, M. Tehei, and J. Peters **(2012)**. *Energy landscapes of human acetylcholinesterase and its Huperzine A-inhibited counterpart*. **J. Phys. Chem. B** 116(51): p. 14744-53.

8. Mercey, G., T. Verdelet, J. Renou, M. Kliachyna, R. Baati, F. Nachon, L. Jean, and P.Y. Renard **(2012)**. *Reactivators of acetylcholinesterase inhibited by organophosphorus nerve agents*. **Acc Chem Res** 45(5): p. 756-66.

9. Mercey, G., J. Renou, T. Verdelet, M. Kliachyna, R. Baati, E. Gillon, M. Arboleas, M. Loiodice, F. Nachon, L. Jean, and P.Y. Renard **(2012)**. *Phenyltetrahydroisoquinoline-pyridinaldoxime conjugates as efficient uncharged reactivators for the dephosphylation of inhibited human acetylcholinesterase*. **J. Med. Chem.** 55(23): p. 10791-5.

10. Brazzolotto, X., M. Wandhammer, C. Ronco, M. Trovaslet, L. Jean, O. Lockridge, P.Y. Renard, and F. Nachon **(2012)**. *Human butyrylcholinesterase produced in insect cells: huprine-based affinity purification and crystal structure*. **FEBS J.** 279(16): p. 2905-16.

11. Wandhammer, M., E. Carletti, M. Van der Schans, E. Gillon, Y. Nicolet, P. Masson, M. Goeldner, D. Noort, and F. Nachon **(2011)**. *Structural study of the complex stereoselectivity of human butyrylcholinesterase for the neurotoxic V-agents*. **J. Biol. Chem.** 286(19): p. 16783-9.

12. Smirnov, I., E. Carletti, I. Kurkova, F. Nachon, Y. Nicolet, V.A. Mitkevich, H. Debat, B. Avalle, A.A. Belogurov, Jr., N. Kuznetsov, A. Reshetnyak, P. Masson, A.G. Tonevitsky, N. Ponomarenko, A.A. Makarov, A. Friboulet, A. Tramontano, and A. Gabibov **(2011)**. *Reactibodies generated by kinetic selection couple chemical reactivity with favorable protein dynamics*. **Proc. Natl. Acad. Sci. U. S. A.** 108(38): p. 15954-9.

13. Nachon, F., E. Carletti, M. Wandhammer, Y. Nicolet, L.M. Schopfer, P. Masson, and O. Lockridge **(2011)**. *X-ray crystallographic snapshots of reaction intermediates in the G117H mutant of human butyrylcholinesterase, a nerve agent target engineered into a catalytic bioscavenger*. **Biochem. J.** 434(1): p. 73-82.

14. Nachon, F., E. Carletti, F. Worek, and P. Masson **(2010)**. *Aging mechanism of butyrylcholinesterase inhibited by an N-methyl analogue of tabun: implications of the trigonal-bipyramidal transition state rearrangement for the phosphylation or reactivation of cholinesterases*. **Chem. Biol. Interact.** 187(1-3): p. 44-8.

15. Carletti, E., J.P. Colletier, F. Dupeux, M. Trovaslet, P. Masson, and F. Nachon **(2010)**. *Structural evidence that human acetylcholinesterase inhibited by tabun ages through O-dealkylation*. **J. Med. Chem.** 53(10): p. 4002-8.

16. Nachon, F., J. Stojan, and D. Fournier **(2008)**. *Insights into substrate and product traffic in the Drosophila melanogaster acetylcholinesterase active site gorge by enlarging a back channel*. **FEBS J.** 275(10): p. 2659-64.

17. Carletti, E., H. Li, B. Li, F. Ekstrom, Y. Nicolet, M. Loiodice, E. Gillon, M.T. Froment, O. Lockridge, L.M. Schopfer, P. Masson, and F. Nachon **(2008)**. *Aging of cholinesterases phosphylated by tabun proceeds through O-dealkylation*. **J. Am. Chem. Soc.** 130(47): p. 16011-20.

18. Nachon, F., O.A. Asojo, G.E. Borgstahl, P. Masson, and O. Lockridge **(2005)**. *Role of water in aging of human butyrylcholinesterase inhibited by echothiophate: the crystal structure suggests two alternative mechanisms of aging*. **Biochemistry** 44(4): p. 1154-62.

19. Nicolet, Y., O. Lockridge, P. Masson, J.C. Fontecilla-Camps, and F. Nachon **(2003)**. *Crystal structure of human butyrylcholinesterase and of its complexes with substrate and products*. **J. Biol. Chem.** 278(42): p. 41141-7.

20. Nachon, F., Y. Nicolet, N. Viguie, P. Masson, J.C. Fontecilla-Camps, and O. Lockridge **(2002)**. *Engineering of a monomeric and low-glycosylated form of human butyrylcholinesterase: expression, purification, characterization and crystallization*. **Eur. J. Biochem.** 269(2): p. 630-7.

# ANNEXE B

## Articles Choisis

# Progress in the development of enzyme-based nerve agent bioscavengers

**F. Nachon***, X. Brazzolotto, M. Trovaslet, P. Masson

Chemico-Biological Interactions 206 (2013) 536–544

Chemico-Biological Interactions 206 (2013) 536–544

Contents lists available at SciVerse ScienceDirect

Chemico-Biological Interactions

journal homepage: www.elsevier.com/locate/chembioint

# Progress in the development of enzyme-based nerve agent bioscavengers ☆

Florian Nachon [a,*], Xavier Brazzolotto [a], Marie Trovaslet [a], Patrick Masson [a,b,c]

[a] Institut de Recherche Biomédicale des Armées, BP87, 38702 La Tronche Cédex, France
[b] Eppley Institute, University of Nebraska Medical Center, Omaha, NE 68198-5950, United States
[c] Institut de Biologie Structurale J.-P. Ebel, UMR 5075, CNRS-CEA-UJF, F-38042 Grenoble Cédex 9, France

ARTICLE INFO

*Article history:*
Available online 26 June 2013

*Keywords:*
Organophosphate poisoning
Nerve agent
Medical countermeasures
Pretreatment
Treatment
Bioscavenger

ABSTRACT

Acetylcholinesterase is the physiological target for acute toxicity of nerve agents. Attempts to protect acetylcholinesterase from phosphylation by nerve agents, is currently achieved by reversible inhibitors that transiently mask the enzyme active site. This approach either protects only peripheral acetylcholinesterase or may cause side effects. Thus, an alternative strategy consists in scavenging nerve agents in the bloodstream before they can reach acetylcholinesterase. Pre- or post-exposure administration of bioscavengers, enzymes that neutralize and detoxify organophosphorus molecules, is one of the major developments of new medical counter-measures. These enzymes act either as stoichiometric or catalytic bioscavengers.

Human butyrylcholinesterase is the leading stoichiometric bioscavenger. Current efforts are devoted to its mass production with care to pharmacokinetic properties of the final product for extended lifetime. Development of specific reactivators of phosphylated butyrylcholinesterase, or variants with spontaneous reactivation activity is also envisioned for rapid *in situ* regeneration of the scavenger.

Human paraoxonase 1 is the leading catalytic bioscavenger under development. Research efforts focus on improving its catalytic efficiency toward the most toxic isomers of nerve agents, by means of directed evolution-based strategies. Human prolidase appears to be another promising human enzyme. Other non-human efficient enzymes like bacterial phosphotriesterases or squid diisopropylfluorophosphatase are also considered though their intrinsic immunogenic properties remain challenging for use in humans. Encapsulation, PEGylation and other modifications are possible solutions to address this problem as well as that of their limited lifetime.

Finally, gene therapy for *in situ* generation and delivery of bioscavengers is for the far future, but its proof of concept has been established.



## 1. Introduction

The acute toxicity of organophosphorus compounds is due to the rapid phosphylation of acetylcholinesterase (AChE). Irreversible inhibition of AChE leads to an increase in acetylcholine concentration in the synaptic clefts and at neuromuscular junctions, disrupting the cholinergic neurotransmission. These organophosphorus inhibitors are phosphoryl/phosphonyl esters (Fig. 1). Thiono esters, e.g. parathion, need *in vivo* conversion into oxo forms to become cholinesterase inhibitors. While traditional organophosphorus nerve agents (OPNAs) pose the major threat, non-traditional nerve agents such as pesticides (malathion, paraoxon) or drugs (echothiophate) are potential terrorist threats. In addition, other organophosphorus compounds not specifically acting as inhibitors of AChE are potential threats too. For instance, TOCP (tri-o-cresyl phosphate), an anti-wear and flame retardant used in jet engine oils [1] is converted in the body to CBDP (Fig. 1), a potent inhibitor of carboxylesterases (CaEs), neuropathy target esterase and cholinesterases (ChEs) [2]. Also, the bicyclic phosphorus ester TMPP, formed during pyrolysis of synthetic engine oils, is

*Abbreviations:* AChE, acetylcholinesterase; BChE, butyrylcholinesterase; CaE, carboxylesterase; CBDP, 2-(o-cresyl)-4H-1,3,2-benzodioxaphosphoran-2-one or cresyl saligenin phosphate; ChE, cholinesterase; CHO, Chinese hamster ovary; HDL, high density lipoprotein; OPNA, organophosphorus nerve agent; PEG, polyethyleneglycol; hPON-1, human paraoxonase; PRAD, proline rich attachment domain; PTE, phosphotriesterase; TMPP, trimethylolpropane phosphate or ethyl bicylclophosphate; TOCP, triorthocresylphosphate.

☆ The opinions expressed herein are private views of the authors and do not reflect the views of the French Ministry of Defense.

* Corresponding author. Address: Département de Toxicologie, Institut de Recherche Biomédicale des Armées – CRSSA, 24 av. des Maquis du Grésivaudan, 38700 La Tronche, France. Tel.: +33 35205 3703; fax: +33 205 934 7437.
*E-mail address:* florian@nachon.net (F. Nachon).

0009-2797/$ - see front matter © 2013 Elsevier Ireland Ltd. All rights reserved.
http://dx.doi.org/10.1016/j.cbi.2013.06.012

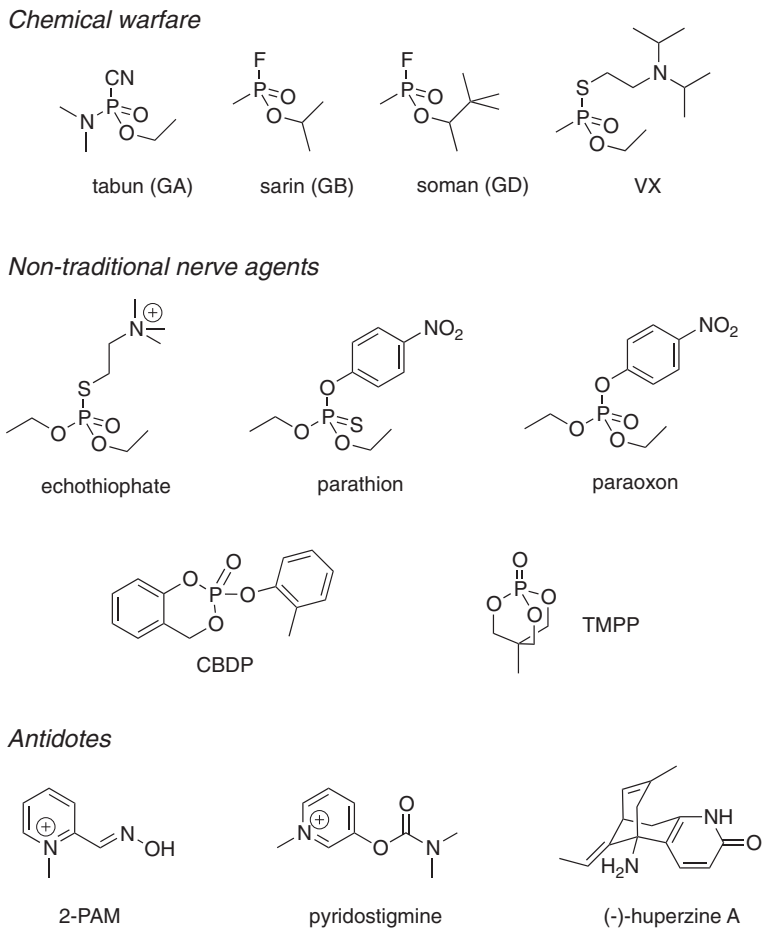


**Fig. 1.** Chemical structures of selected chemical warfare, non-traditional nerve agents, and antidotes.

a potent GABA antagonist. This compound, with a toxicity similar to that of sarin, has been called "the poor man's nerve agent" [3].

Medical treatments against OPNA poisoning aim at counter-acting the inhibition of AChE by the use of oxime reactivators, and prevent the primary and secondary effects of acetylcholine excess by the use of antinicotinic, antimuscarinic and anticonvulsant drugs. These approaches are more or less effective for mitigating the acute, sub-lethal and long-term effects of all agents. In the best case, they improve survival, but do not reduce incapacitation due to irreversible brain damage.

### 1.1. Current pre-treatment of OPNA poisoning

In situations where a risk of exposure to OPNAs is established, pre-treatments have to be implemented systematically for protection of personnel. Current prophylactic treatments consist in masking the active site of AChE from OPNA using specific ligands, which bind transiently to the enzyme (Fig. 2B). For example, this is achieved by the use of the carbamate pyridostigmine, a pseudo-irreversible inhibitor making a labile bond with the catalytic serine of AChE [4]. This strategy is effective only if a sufficient percentage of AChE is transiently inhibited by pyridostigmine, and remain hidden from the OPNA during the exposure time. Yet, pyridostigmine inhibition must remain moderate to keep a sufficient amount of active AChE to preserve cholinergic transmission before intoxication. It results that the balance between active/inhibited AChE can be challenging in terms of dosage. In addition, pyridostigmine does not readily cross the blood brain barrier [5], and leaves central AChE unprotected. In the search of a central AChE reversible inhibitor, (−)-huperzine A (Fig. 1), a natural alkaloid, appears to have the highest potential [6,7]. Nevertheless, it is toxic at those doses required for protection. Yet, a combination of (+)/(−) isomers of lower toxicity improves survival and reduces behavioral abnormalities against 1.2 × $LD_{50}$ of soman [8]. Also, recent huperzine A analogs were demonstrated to improve survival against 2 × $LD_{50}$ of soman in guinea pigs [9]. Other pharmacological pretreatments have been implemented in Western and other armies with known limitations and/or potent adverse effects (for review see Masson, 2011 and van Helden, 2011) [10,11].

### 1.2. Bioscavenger concept

The alternative approach to AChE inhibitors is based on molecules that inactivate OPNA in the bloodstream before they can reach AChE at the physiological sites. Bioscavengers being developed for some 25 years are stoichiometric, pseudo-catalytic, or catalytic. Stoichiometric bioscavengers are specific molecules that irreversibly bind to OPNAs in a mole-to-mole ratio (Fig. 2C). Pseudo-catalytic bioscavengers are stoichiometric bioscavengers in combination with a reactivator (Fig. 2D). Catalytic bioscavengers are OPNA-degrading enzymes with a turnover (Fig. 2E), so that administration of a small dose of a catalytic bioscavenger is thought to provide better protection than large doses of costly stoichiometric bioscavengers [12].

Numerous enzymes and proteins participate in natural defenses against OPNAs [13]. Natural skin, tissues and blood bioscavengers detoxify OPNAs or react with them. In some cases, these natural defenses are sufficient to protect against exposure to low doses

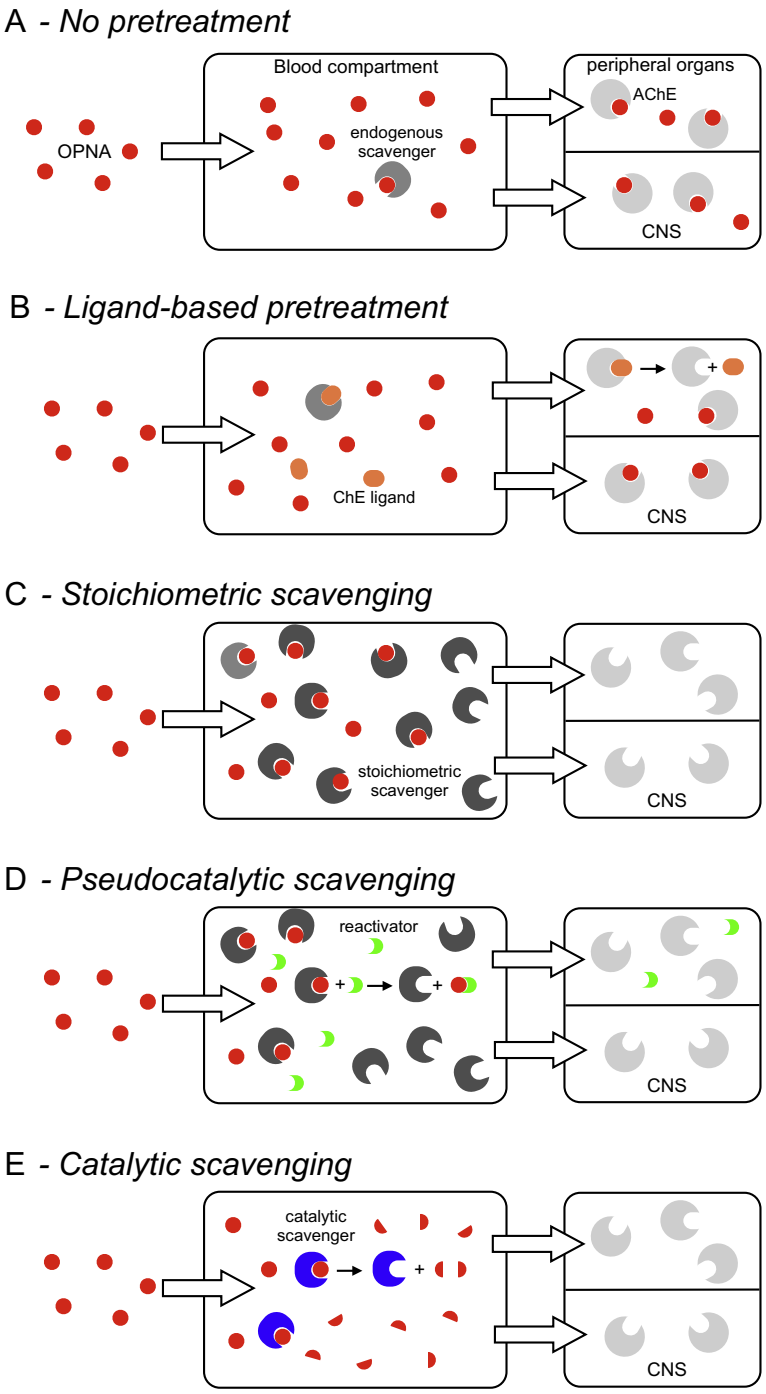


**Fig. 2.** Pretreatment strategies of OPNA poisoning. (A) OPNAs enter the blood compartment and pass to peripheral organs and the central nervous system to inhibit AChE. Endogenous scavengers like plasma BChE trap a small amount of OPNA. (B) The current pretreatment is based on a transient carbamate inhibitor, pyridostigmine, that masks the active site of a percentage of AChE from OPNAs. Active AChE is slowly released by spontaneous decarbamylation of the inhibited enzyme. Central nervous system AChE is not masked because pyridostigmine does not cross the blood–brain barrier. (C) Large amount of exogenous stoichiometric scavenger trap OPNAs in the blood preventing peripheral and central hAChE inhibition. (D) Co-administration of reactivators allows rapid regeneration of inhibited stoichiometric scavengers, thus potentially increasing the protection efficacy. (E) A limited amount of catalytic scavenger can hydrolyze every OPNA molecules in the blood compartment before they pass to peripheral organs and the central nervous system.

of OPNAs. For example, BChE (≈50 nM in human plasma) reacts rapidly with CBDP, the toxic metabolite of TOCP, and likely plays a role in protection against the development of the aerotoxic syndrome that may occur for low dose exposure to TOCP-containing fumes in aircrafts [14]. However, either they are abundant like albumin (≈0.6 mM in plasma and lymph) but react too slowly with toxicants, [15,16], or they are present in too low amount to confer protection against high doses of poisons. For example, CaEs present in plasma of model animals are effective endogenous bioscavengers [12], but human plasma is CaEs-free [17]. Protection in humans can be enhanced by administration of exogenous bioscavengers. Ideally, bioscavengers would protect against exposure to $5 \times LD_{50}$ of a large spectrum of OPNAs. Unlike pharmacological pretreatments, iatrogenic toxicity of bioscavengers should be negligible.

However, administration of large amounts of enzymes displaying promiscuous activities might perturb certain metabolic processes. An important issue is to administer bioscavengers devoid of protein contaminants that may cause side effects, e.g. endotoxins, coagulation factors. Thus, the medical use of bioscavengers imposes re-enforced GMP conditions for their preparation. Finally, we should point out that immunologic adverse effects are expected following repeated administration of non-human enzymes. PEGylation or inclusion of recombinant human and non-human enzymes and bacterial enzymes in nanocontainers should prevent immune responses. Recent reviews on the use of bioscavengers against OPNAs are in Romano et al., 2008 [18] and Gupta, 2009 [19]; see also, [20–22].

## 2. Stoichiometric scavengers

### 2.1. Prophylaxis

Human BChE (hBChE) is the most advanced bioscavenger. A dose of 200 mg of hBChE is predicted to protect a human against $2 \times LD_{50}$ of soman [23]. Animal studies showed that administration of large doses of hBChE confer protection against up to $5.5 \times LD_{50}$ of soman or $8 \times LD_{50}$ of VX [24]. Pre-treatment with 7.5 mg/kg completely prevent toxic signs and physiological abnormalities in minipig exposed for 1 h to sarin vapor (4.1 mg/m$^3$) [25]. The required doses to be injected in humans for such protection appear to be economically prohibitive, so that the current focus is on large-scale production. hBChE can be produced from different sources under GMP conditions. The most accessible natural source is Cohn fraction IV-4 paste, from which hBChE is purified with yields ranging around 7–9 g/100 kg [26]. Plasma-derived hBChE displays days of long-lasting stability in the bloodstream, and does not induce any side effect in rats [27]. Noteworthy, attempts to further extend the long half-life of plasma hBChE by PEGylation were not successful [28]. Behavioral and physiological safety of plasma hBChE was established at 30 mg/kg in rhesus monkeys [29] and 21 mg/kg in mice [30].

Albeit its great effectiveness, plasma hBChE presents the drawback that its source is limited, so that a maximum of 5000 individual doses could be theoretically produced yearly at the scale of a large country like the USA [31]. Therefore, production of recombinant hBChE (rhBChE) has been sought for the last decade. rhBChE has been produced in different expression systems including CHO cells [32], drosophila cells [33], silkworm larvae [34], but economically viable large-scale production are currently limited to transgenic goats [35] and tobacco plants [31,36]. Transgenic goat milk rhBChE used to be considered as the most promising production system, but a compromised lactation performance due to endoplasmic reticulum stress put a halt to development [37,38]. Purification of high-quality rhBChE can be costly due to limited performance of the key procainamide-based affinity chromatography step, but huprine-based resins improve yields and quality and should help to reduce global production costs [33].

Independent of the expression system, rhBChE has a dramatically shorter plasma half-life than the plasma enzyme (hours-long vs days-long) due to lower oligomerization and altered glycosylation pattern, especially incomplete sialylation [35,39,40]. Still, an extended biological life is achievable by simple addition [41] or coexpression [30,42] of a proline-rich peptide enhancing tetramerization such as PRAD, by fusion to albumin [43], chemical polysialylation [30] or PEGylation [35]. PEG-conjugated CHO-derived rhBChE has proved to be safe and not immunogenic [40]. To circumvent plasma half-life problems, aerosolized rhBChE can be delivered unmodified directly into the lung to form a shield against inhaled OPNAs. Such a non-invasive pretreatment 1–40 h prior intoxication by $>1 \times LD_{50}$ of aerosolized paraoxon can prevent inhibition of circulating cholinesterase in a dose-dependent manner [44].

An alternative to hBChE is the physiological target of OPNAs, i.e. human AChE (hAChE). hAChE is more stereoselective than hBChE, which is important in regard to the amount of enzyme required to scavenge one equivalent of racemic nerve agent. Indeed, half an equivalent of hBChE is sufficient if the enzyme binds preferably the same enantiomer as hAChE. At least one equivalent is necessary if hBChE binds equally both enantiomers or preferably the less toxic enantiomer. This last case is met for example with soman: the stereoselectivity ratio of hAChE for the P(S)-C(R)/P(R)-C(R) isomers of soman is $4 \times 10^4$-fold while hBChE has no selectivity [45]. Similar lack of strong selectivity of hBChE is observed for tabun [46] and V-agents [47], and indeed, at equivalent dose, hAChE provides a better protection of mouse exposed to VX compared to hBChE [48]. Yet, hAChE is not in advanced development as a stoichiometric bioscavenger, but mutants of the enzyme are being designed for pseudocatalytic scavenging (see Section 3).

### 2.2. Post-exposure treatment

Blood purification by hemodiafiltration was successfully implemented for a patient severely poisoned by sarin in the Tokyo subway [49]. However, the effectiveness of this approach is questionable, in particular in the case of percutaneous exposure (e.g. VX poisoning) and for OPNAs that store in lipophilic depot sites from which they are slowly released into the bloodstream.

By contrast a bioscavenger with a half-life matching or exceeding that of a nerve agent slowly absorbed via the percutaneous route, can effectively neutralize the agent as it continuously enters the blood compartment. In the case of VX, percutaneous absorption is sufficiently slow that i.m. injection of goat-milk rhBChE (220 mg/kg) 1 h after exposure to 2 and $5 \times LD_{50}$ improve survival rates of guinea pigs from 20% to 90% and 0% to 33%, respectively [50]. PEGylated goat-milk rhBChE (72 mg/kg) with improved residence time allows 100% survival of guinea pigs exposed to $2.5 \times LD_{50}$, with minimal signs of poisoning, despite a late i.m. administration 2 h after exposure [51]. Plasma-derived hBChE also provides 100% protection from lethality by identical conditions, but efficacy was shown to drop when administration was delayed at the onset of signs of poisoning (about 4–5 h) [52]. However, when classical therapy (oxime + anti-muscarinic + anticonvulsant) was concomitantly administered, a synergistic effect was observed as 100% survival was achieved, even for administration after the on-set of symptoms [53]. Synergy results from rapid alleviation of the cholinergic crisis by conventional treatment, while hBChE neutralizes further VX entering the bloodstream, thus preventing it from reaching the target organs.

## 3. Pseudocatalytic scavenging

The limit of a stoichiometric bioscavenger like hBChE is that once it is phosphylated by one molecule of OPNA, it becomes waste. An attractive approach is to recycle phosphylated hBChE by the mean of oxime reactivators. If the reactivation rates were in the same order as the inhibition rates, then a mixture of hBChE and reactivator would act as an effective pseudo-catalytic bioscavenger (Fig. 2D). Unfortunately, reactivation of hBChE by available oximes is too slow for pseudocatalytic scavenging of OPNA [54]. This led to seek better reactivators of hBChE [55]. Combinations of sub-stoichiometric amount of hBChE with last generations of specific hBChE reactivators show improved protective indices in therapy of sarin- and paraoxon-exposed mice [56].

Available oxime reactivators, having been primarily developed to reactivate hAChE, have shown to be more suitable for pseudoscavenging with hAChE than with hBChE. Actually, hAChE based pseudoscavenging has been early explored through one issue hampering the concept: phosphylated cholinesterases age, in a few minutes in the case of soman, and become refractory to oxime reaction [57]. F338A mutant of hAChE with slow aging rate, remaining reactivatable by oximes for extended periods, has enhanced pseudocatalytic properties [58,59]. This slow-aging mutation is effectively combined to the Y337A mutation aimed at enlarging the active site gorge for an easier access to reactivators [60].

## 4. Catalytic bioscavengers

Human enzymes capable of degrading OPNAs at high rate would be the most suitable biocatalytic scavengers. The idea of converting human ChEs into OPNA hydrolases was developed about 20 years ago. Several other human enzymes have been considered, including plasma paraoxonase-1 (PON-1), erythrocyte and liver prolidases, and human liver senescence marker (SMP-30) [61]. For a review on catalytic bioscavengers, see Wales et al. (2012) [62].

### 4.1. Cholinesterase-based catalytic scavengers

Mutagenesis of human cholinesterases into OPNA-degrading enzymes has been attempted. More than 60 mutants of hBChE and hAChE were created by inserting a second nucleophile in the active center (for reviews see: [63,64]). The Y124H/Y72D mutant of hAChE displays up to 110-fold improved spontaneous reactivation rate after inhibition by V-agents (half-life from 25 to 170 min), a performance not so far from the action of oxime reactivators [65]. Yet, this enzyme must be considered as a fast regenerating scavenger rather than a true catalytic scavenger. The G117H mutant of hBChE, that was the first designed ChE mutant capable of hydrolyzing OPNAs, remains the most active of all, but still far too low for practical interest as a catalytic scavenger. Interestingly, transgenic mice expressing G117H hBChE are protected against $1 \times LD_{50}$ echothiophate toxicity not because of echothiophate neutralization, but most likely because G117H hBChE is more slowly inhibited, readily regenerates and finally acts as a surrogate of wild-type mouse AChE and BChE [66]. Besides, G117H/E197Q hBChE, a slow aging/fast regenerating variant expressed in transgenic plants, failed to protect guinea pigs from $2 \times LD_{50}$ challenges of GB/GD/VX, due to 1000-fold decreased phosphylation rates for this particular mutant [31]. Since the X-ray structure has recently been solved [67], there is renewal of effort to improve the dephosphylation rates of the G117H mutant without altering phosphylation rates, its mechanism being now investigated by QM/MM modeling [68,69]. It is believed that these works will lay foundations for future computational re-design of a new generation of hBChE mutants aimed at hydrolyzing OPNAs (Lushchekina et al., unpublished work).

### 4.2. Human paraoxonase 1

A considerable body of data is available on human paraoxonase 1 (hPON-1) as a potential catalytic bioscavenger (for a review see: [70]). hPON-1 is a calcium dependent promiscuous enzyme (lactonase, arylesterase, phosphotriesterase). Promiscuous activities are controlled by position of the catalytic $Ca^{2+}$ in the catalytic center [71]. hPON-1 is produced in the liver, and circulating in the blood bound to HDLs. Expression and plasma concentration can be positively modulated by hypolipemic drugs and polyphenols [72]. hPON-1 hydrolyzes numerous OPNAs at quite a high rate [21]. hPON-1 level is inversely correlated with susceptibility to OPNAs intoxication. For example, *Trichoplusia ni* larvae expressing hPON-1 are protected from exposure to $>100 \times LD_{50}$ of chlorpyrifos [73]. Conversely, KO-mice for hPON-1 are far more sensitive to OPNAs than wild-type mice [74]. Though hPON-1 hydrolyzes preferentially the less toxic soman enantiomers [75], a recent *in vitro* study using hAChE back-titration showed that tabun is efficiently hydrolyzed [76]. In addition, intravenous administration of purified hPON-1 was found to protect guinea pigs against sarin and soman [77,78]. However, exogenous injection of hPON-1 produced in *Trichoplusia ni* larvae or adenovirus-induced expression of hPON-1 do not sufficiently increase the systemic activity in mice to provide *in vivo* protection against nerve agents [79].

A 10- to 100-fold increase in hPON-1's catalytic efficiency ($k_{cat}/K_m$) would be enough to afford protection against nerve agents. Modeling OPNA interactions in a hPON-1's 3D structure model [80] helps to design new mutants of the enzyme by the site-directed mutagenesis approach [81,82]. H115W/Y71A double mutant improve paraoxon hydrolysis rate 8-fold over wild-type, but gains for VX, GA, GB and GD remain below 2-fold [83]. Computer-assisted redesign of hPON-1 mutants with enhanced hydrolase activity and better enantioselectivity would need exact knowledge of the 3D structure and molecular dynamics of the human enzyme, which are still lacking. Alternatively, directed evolution of a chimeric PON-1 (chimPON-1) made via mammalian gene shuffling, combined with high-throughput screening, successfully led in 5 generations to an evolved variant of chimPON-1 that hydrolyzes the most toxic enantiomer of a coumarin analog of cyclosarin with a catalytic enhancement ($k_{cat}/K_m$) of 100,000 [84,85]. This variant protects mice challenged with $1 \times LD_{100}$ cyclosarin analog [84]. Unfortunately, chimPON-1 is expected to be immunogenic, and the catalytic properties of variants are not easily transposable to hPON-1 [81].

Plasma-derived hPON-1 is difficult to purify and its stability depends on the presence of partners and a hydrophobic environment [65,86]. Therefore, its mass production from outdated plasma would present numerous biotechnological problems. Recombinant hPON-1 and mutants are functionally expressed with difficulties in mammalian cells, *Escherichia coli* [87], and insect (*Trichoplusia ni*) larvae [73]. To overcome biotechnology difficulties with production, stabilization and pharmacokinetics of a functional biopharmaceutical, gene delivery of hPON-1 has been attempted. A recent study using an adenoviral vector demonstrates that endogenous production of high levels of hPON-1 is capable of protecting mice against cumulative doses ($4 \times LD_{50}$) of diazoxon [88]. It is therefore quite conceivable that a safe gene-delivered evolved hPON-1 variant would be able to provide excellent protection against OPNAs. Thus, hPON-1 remains the most promising catalytic bioscavenger.

### 4.3. Other phosphotriesterases

Other phosphotriesterases (PTEs) have been considered as potential catalytic bioscavengers. The squid (*Loligo vulgaris*) diisopropyl fluorophosphatase with a β-propeller structure similar to hPON-1, hydrolyzes OPNAs [89]. Rational design allowed to reverse the stereochemical preference of this enzyme for the most toxic OPNA isomers [90]. A PEGylated form of the mutant with improved stereoselectivity prevents death of rats exposed to a subcutaneous $3 \times LD_{50}$ dose of soman [91].

Several bacterial PTEs, mesophilic and extremophilic, have been extensively investigated for some 20 years (for reviews see [92,93]), but screening of new bacterial strains for measurable level of OPNA hydrolase activity is still ongoing [94]. Strategies combining rational design and directed evolution have been extremely

successful at improving native phosphotriesterase activity. Such strategies led to the discovery of the H257Y/L303T mutant of *Pseudomonas diminuta* PTE, with up to 15000-fold improvements in catalytic activity against the most toxic enantiomers of GB, GD and GF, thus reaching $1.2 \times 10^8$, $3 \times 10^7$ and $5 \times 10^7$ $M^{-1}$ $min^{-1}$, respectively [95]. The catalytic activity of a phosphotriesterase from *Deinicoccus radiodurans* toward ethyl and methyl paraoxon was improved respectively 560 fold and 180-fold to reach $k_{cat}/K_M$ about $4.6 \times 10^5$ $M^{-1}$ $min^{-1}$ and $6.3 \times 10^3$ $M^{-1}$ $min^{-1}$[96].

Despites these successes, important issues remain before PTE can be used *in vivo* for OPNA detoxification, notably issues about expression, pharmacokinetics and humanization. Indeed, despite their bacterial origin, large scale-production of PTEs in *E. coli* is problematic due to limited synthesis of the bimetal center [97,98]. Regarding pharmacokinetics, PTE from *Agrobacterium radiobacter* prevents lethality of rat treated with pesticides [99], but has a relatively short mean residence time in primates (57 min) [100]. PEGylation of PTE improves thermal stability [101] and extends mean residence time from a few minutes to a few days in rats, but the modified enzyme remains immunogenic, thus of limited use in humans [65].

### 4.4. Other human and mammalian enzymes

To avoid immunogenicity issues, research groups were led to look for any human protein that has the potential to form the basis of a pretreatment. The drug-metabolizing human liver enzyme carboxylesterase 1 (hCaE1) was found to be a candidate of interest. Wild-type hCaE1 reacts with G-agents and reactivates spontaneously after inhibition by the P-(S) isomer of sarin at a slow rate (half-time = 46 h) [102]. The rate is enhanced by the addition of an oxime according to the pseudocatalytic bioscavenger concept. Like for cholinesterases, the introduction of nucleophilic residues near the triad can enhance the spontaneous reactivation rate up to a half time of 1 h in the case of cyclosarin [103]. But like cholinesterase, the gain is too modest for catalytic scavenging.

Human prolidases from erythrocyte or liver present structural and catalytic properties similar to *Alteromona's* "organophosphorus acid anhydrolase", aka phosphotriesterase [104,105]. Human prolidases are easily expressed in *E. coli* [106] and were found to hydrolyze the G-agents at a higher rate than hPON-1. Prolidase can hydrolyze tabun but not CBDP nor TMPP [14]. Gene-delivered prolidase persistenly expressed in mice, provides only modest protection *in vivo* delaying death by only 4–8 h [107]. However, engineering of this enzyme is just beginning.

The senescence marker protein 30 is another human enzyme of interest [108]. It is a promiscuous metal-containing enzyme lactonase structurally related to hPON-1 and DFPase [109]. Its phosphotriesterase activity is against G-agents, DFP and paraoxon, albeit at modest rates for the mouse homologous enzyme [61]. As for human prolidase, study of this enzyme is still in infancy.

Another mammalian enzyme, the zinc-containing mouse adenosine deaminase, was redesigned for organophosphate hydrolysis [110]. After directed evolution of the initial redesign, the catalytic efficiency ($k_{cat}/K_M$) raised up to $\sim 10^4$ $M^{-1}$ $s^{-1}$ for the hydrolysis of a model organophosphate, a value just one order shy of the efficiency required for a catalytic bioscavenger ($10^5$ $M^{-1}$ $s^{-1}$) [63].

## 5. Future directions

Human BChE is currently the most advanced bioscavenger, but an affordable source of the enzyme is still lacking. Production in transgenic organisms remains the only viable long-term solution, in spite of the complications encountered with transgenic goats. Other animals, like transgenic rabbits are under evaluation, and production in the leaves of tobacco plants gives promising yields [31]. New purification protocols improving yields and quality will also help to reduce production costs [33]. But recombinant hBChE lacks the post-translational modifications necessary to achieve daylong residence time, in particular glycosylation and tetramerization. Solutions for tetramerization already exist, so that the most serious issues revolve around the glycosylation pattern of recombinant hBChE. Chemical modifications like PEGylation or polysialylation [30] extend residence time to a sufficient level, but their cost for hundred grams of enzyme is probably prohibitive. Enzymatic polysialylation by the mean of bacterial sialyltransferases is potentially more affordable [111]. Modification of transgenic hosts to optimize *in vivo* human-like glycosylation with polysialylation during biosynthesis could solve the issue. Though, in the case of the humanization of plants, the endogenous glycosylation pathway must eventually be partially or completely shut down to avoid mixed plant/human patterns. Consequences of such extreme modifications on the plant viability are unclear yet.

Alternatively to glycosylation, encapsulation in nanocarriers lengthens residence time to multiple days: hBChE encapsulated in polylysine/polyethylene oxide copolymers, injected i.m. or i.v. in mice, is capable of crossing the blood brain barrier and remains active for 3 days in the brain [112]. Encapsulation of recombinant and/or non-human enzymes may also offer the advantage of cheating the immune system.

Delivery of protein scavenger in human is also challenging given the mg-dose required for effective protection. In addition to i.v. injection (not compatible with field use) the privileged delivery route is i.m. injection. Yet, very few is known about diffusion of protein bioscavengers following i.m. injection in humans. Related pharmacodynamic/pharmacokinetic models are still lacking. Alternative delivery means must be evaluated in addition to aerosols [44], e.g. intranasal delivery [113] or transdermal means like microneedle patches.

The use of safe and short-induction gene vectors capable of delivering hBChE in the bloodstream would solve both the delivery and cost issues. The excellent protection afforded by gene-delivered hBChE, using an adenoviral system in mice challenged with OPNAs ($5 \times LD_{50}$ VX, $30 \times LD_{50}$ echothiophate) proved the feasibility of this approach [114]. Similar success was recorded for hPON-1 [88] and prolidase [107]. However, before gene delivery becomes operational, further work is needed to engineer safe vectors that do not produce toxic viral proteins and/or induce deleterious immune responses. Also, the use of a gene for pretreatment of healthy human beings poses a delicate ethical issue, regardless of the transient nature of the expression.

With regard to catalytic bioscavengers, human prolidase is a recent candidate that will be further studied. Mutants of rPON-1, bacterial phosphotriesterase with good catalytic efficiencies against the toxic isomers of OPNAs are now identified. But these enzymes are not human enzymes and must be humanized. The directed-evolution work performed on rPON-1 is not transposable to hPON-1 [81]. In that context, the determination of the 3D structure of hPON-1 remains a priority to improve its catalytic efficiency towards nerve agents.

In addition, pharmaceutical biotechnology of hPON-1 is complex. The enzyme is unstable without a proper hydrophobic environment. Binding of engineered hPON-1 to artificial HDL (Tawfik et al., personal communication) appears to be a solution for the future.

Research of novel OPNA-degrading enzymes is actively pursued [94], in particular in extremophile microorganisms [115]. Evolved mutants of *Sulfolobus solfataricus* PTE have been found to degrade nerve agent analogues and CBDP at very fast rate ($k_{cat}/K_m \approx 10^7$–$10^8$ $M^{-1}$ $min^{-1}$) [14,116]. In addition, mass production in *E. coli*, and easy purification of these enzymes seems affordable.

Given the current limited activity spectrum of OPNA-reacting enzymes, operational catalytic bioscavengers should be cocktails of different enzymes.

## Conflict of interest statement

The authors declare that there are no conflicts of interest.

## Acknowledgments

We are thankful to the Direction Générale de l'Armement for sustained funding of research and development of nerve agent bioscavengers, currently under contract DGA/DSP/STTC PDH-2-NRBC-3-C-301.

## References

[1] C. Winder, J.C. Balouet, The toxicity of commercial jet oils, Environ. Res. 89 (2002) 146–164.
[2] E. Carletti, L.M. Schopfer, J.P. Colletier, M.T. Froment, F. Nachon, M. Weik, O. Lockridge, P. Masson, Reaction of cresyl saligenin phosphate, the organophosphorus agent implicated in aerotoxic syndrome, with human cholinesterases: mechanistic studies employing kinetics, mass spectrometry, and X-ray structure analysis, Chem. Res. Toxicol. 24 (2011) 797–808.
[3] N. Antonov, Khimicheskoe oruzhie na rubezhe dvikh stoletii (Chemical Weapon at the Turn of the Century), Progress, Moscow, 1994.
[4] D.M. Maxwell, K.M. Brecht, B.P. Doctor, A.D. Wolfe, Comparison of antidote protection against soman by pyridostigmine, HI-6 and acetylcholinesterase, J. Pharmacol. Exp. Ther. 264 (1993) 1085–1089.
[5] C. Amourette, I. Lamproglou, L. Barbier, W. Fauquette, A. Zoppe, R. Viret, M. Diserbo, Gulf war illness: effects of repeated stress and pyridostigmine treatment on blood-brain barrier permeability and cholinesterase activity in rat brain, Behav. Brain Res. 203 (2009) 207–214.
[6] G. Lallement, V. Baille, D. Baubichon, P. Carpentier, J.M. Collombet, P. Filliat, A. Foquin, E. Four, C. Masqueliez, G. Testylier, L. Tonduli, F. Dorandeu, Review of the value of huperzine as pretreatment of organophosphate poisoning, Neurotoxicology 23 (2002) 1–5.
[7] J. Kassa, J. Bajgar, K. Kuca, K. Musilek, J. Karasova, The present approaches to the development of prophylactic and therapeutic antidotes against nerve agents, Interdiscip. Toxicol. 1 (2008) 18–21.
[8] Y. Wang, Y. Wei, S. Oguntayo, B.P. Doctor, M.P. Nambiar, A combination of [+] and [−]-huperzine A improves protection against soman toxicity compared to [+]-huperzine A in guinea pigs, Chem. Biol. Interact. 203 (2013) 120–124.
[9] H. Gunosewoyo, S.K. Tipparaju, M. Pieroni, Y. Wang, B.P. Doctor, M.P. Nambiar, A.P. Kozikowski, Structural analogs of huperzine A improve survival in guinea pigs exposed to soman, Bioorg. Med. Chem. Lett. 23 (2013) 1544–1547.
[10] P. Masson, Evolution of and perspectives on therapeutic approaches to nerve agent poisoning, Toxicol. Lett. 206 (2011) 5–13.
[11] H.P. van Helden, M.J. Joosen, I.H. Philippens, Non-enzymatic pretreatment of nerve agent (soman) poisoning: a brief state-of-the-art review, Toxicol. Lett. 206 (2011) 35–40.
[12] D.M. Maxwell, K.M. Brecht, Carboxylesterase: specificity and spontaneous reactivation of an endogenous scavenger for organophosphorus compounds, J. Appl. Toxicol. 21 (Suppl. 1) (2001) S103–S107.
[13] M. Jokanovic, Current understanding of the mechanisms involved in metabolic detoxification of warfare nerve agents, Toxicol. Lett. 188 (2009) 1–10.
[14] P. Masson, L.M. Schopfer, A. Saxena, J. Mikler, O. Lockridge, Endogenous human plasma catalytic bioscavengers for organophosphorus compounds do not protect against the toxicity of chemicals implicated in aerotoxic syndrome: an *in vitro* study, J. Biol. Phys. Chem. 12 (2012) 89–97.
[15] B. Li, F. Nachon, M.T. Froment, L. Verdier, J.C. Debouzy, B. Brasme, E. Gillon, L.M. Schopfer, O. Lockridge, P. Masson, Binding and hydrolysis of soman by human serum albumin, Chem. Res. Toxicol. 21 (2008) 421–431.
[16] M.A. Sogorb, E. Vilanova, Serum albumins and detoxication of anticholinesterase agents, Chem. Biol. Interact. 187 (2010) 325–329.
[17] B. Li, M. Sedlacek, I. Manoharan, R. Boopathy, E.G. Duysen, P. Masson, O. Lockridge, Butyrylcholinesterase, paraoxonase, and albumin esterase, but not carboxylesterase, are present in human plasma, Biochem. Pharmacol. 70 (2005) 1673–1684.
[18] J.A. Romano, B.J. Lukey, H. Salem, Chemical Warfare Agents: Chemistry, Pharmacology, Toxicology, and Therapeutics, CRC Press, Boca Raton, 2008.
[19] R.C. Gupta, Handbook of Toxicology of Chemical Warfare Agents, Academic Press, 2009.
[20] D.E. Lenz, D. Yeung, J.R. Smith, R.E. Sweeney, L.A. Lumley, D.M. Cerasoli, Stoichiometric and catalytic scavengers as protection against nerve agent toxicity: a mini review, Toxicology 233 (2007) 31–39.
[21] P. Masson, D. Rochu, Catalytic bioscavengers against toxic esters, an alternative approach for prophylaxis and treatments of poisonings, Acta Naturae 1 (2009) 68–79.
[22] S.B. Bird, A. Dawson, D. Ollis, Enzymes and bioscavengers for prophylaxis and treatment of organophosphate poisoning, Front. Biosci. (Schol Ed) 2 (2010) 209–220.
[23] Y. Ashani, S. Pistinner, Estimation of the upper limit of human butyrylcholinesterase dose required for protection against organophosphates toxicity: a mathematically based toxicokinetic model, Toxicol. Sci. 77 (2004) 358–367.
[24] A. Saxena, W. Sun, J.M. Fedorko, I. Koplovitz, B.P. Doctor, Prophylaxis with human serum butyrylcholinesterase protects guinea pigs exposed to multiple lethal doses of soman or VX, Biochem. Pharmacol. 81 (2011) 164–169.
[25] A. Saxena, W. Sun, P.A. Dabisch, S.W. Hulet, N.B. Hastings, E.M. Jakubowski, R.J. Mioduszewski, B.P. Doctor, Pretreatment with human serum butyrylcholinesterase alone prevents cardiac abnormalities, seizures, and death in gottingen minipigs exposed to sarin vapor, Biochem. Pharmacol. 82 (2011) 1984–1993.
[26] A. Saxena, P. Tipparaju, C. Luo, B.P. Doctor, Pilot-scale production of human serum butyrylcholinesterase suitable for use as a bioscavenger against nerve agent toxicity, Process Biochem. 45 (2010) 1313–1318.
[27] R.F. Genovese, W. Sun, C.C. Johnson, R.C. Ditargiani, B.P. Doctor, A. Saxena, Safety of administration of human butyrylcholinesterase and its conjugates with soman or VX in rats, Basic Clin. Pharmacol. Toxicol. 106 (2010) 428–434.
[28] W. Sun, C. Luo, P. Tipparaju, B.P. Doctor, A. Saxena, Effect of polyethylene glycol conjugation on the circulatory stability of plasma-derived human butyrylcholinesterase in mice, Chem. Biol. Interact. 203 (2013) 172–176.
[29] T.M. Myers, W. Sun, R.S. Naik, M.G. Clark, B.P. Doctor, A. Saxena, Characterization of human serum butyrylcholinesterase in rhesus monkeys: behavioral and physiological effects, Neurotoxicol. Teratol. 34 (2012) 323–330.
[30] D.G. Ilyushin, I.V. Smirnov, A.A. Belogurov Jr., I.A. Dyachenko, T. Zharmukhamedova, T.I. Novozhilova, E.A. Bychikhin, M.V. Serebryakova, O.N. Kharybin, A.N. Murashev, K.A. Anikienko, E.N. Nikolaev, N.A. Ponomarenko, D.D. Genkin, G.M. Blackburn, P. Masson, A.G. Gabibov, Chemical polysialylation of human recombinant butyrylcholinesterase delivers a long-acting bioscavenger for nerve agents *in vivo*, Proc. Natl. Acad. Sci. U.S.A. 110 (2013) 1243–1248.
[31] B.C. Geyer, L. Kannan, P.E. Garnaud, C.A. Broomfield, C.L. Cadieux, I. Cherni, S.M. Hodgins, S.A. Kasten, K. Kelley, J. Kilbourne, Z.P. Oliver, T.C. Otto, I. Puffenberger, T.E. Reeves, N. Robbins 2nd, R.R. Woods, H. Soreq, D.E. Lenz, D.M. Cerasoli, T.S. Mor, Plant-derived human butyrylcholinesterase, but not an organophosphorous-compound hydrolyzing variant thereof, protects rodents against nerve agents, Proc. Natl. Acad. Sci. U.S.A. 107 (2010) 20251–20256.
[32] F. Nachon, Y. Nicolet, N. Viguie, P. Masson, J.C. Fontecilla-Camps, O. Lockridge, Engineering of a monomeric and low-glycosylated form of human butyrylcholinesterase: expression, purification, characterization and crystallization, Eur. J. Biochem. 269 (2002) 630–637.
[33] X. Brazzolotto, M. Wandhammer, C. Ronco, M. Trovaslet, L. Jean, O. Lockridge, P.Y. Renard, F. Nachon, Human butyrylcholinesterase produced in insect cells: huprine-based affinity purification and crystal structure, FEBS J. 279 (2012) 2905–2916.
[34] S. Li, D.T. Ip, H.Q. Lin, J.M. Liu, Y.G. Miao, L.J. Ke, D.C. Wan, High-level expression of functional recombinant human butyrylcholinesterase in silkworm larvae by Bac-to-Bac system, Chem. Biol. Interact. 187 (2010) 101–105.
[35] Y.J. Huang, Y. Huang, H. Baldassarre, B. Wang, A. Lazaris, M. Leduc, A.S. Bilodeau, A. Bellemare, M. Cote, P. Herskovits, M. Touati, C. Turcotte, L. Valeanu, N. Lemee, H. Wilgus, I. Begin, B. Bhatia, K. Rao, N. Neveu, E. Brochu, J. Pierson, D.K. Hockley, D.M. Cerasoli, D.E. Lenz, C.N. Karatzas, S. Langermann, Recombinant human butyrylcholinesterase from milk of transgenic animals to protect against organophosphate poisoning, Proc. Natl. Acad. Sci. U.S.A. 104 (2007) 13603–13608.
[36] B.C. Geyer, L. Kannan, I. Cherni, R.R. Woods, H. Soreq, T.S. Mor, Transgenic plants as a source for the bioscavenging enzyme, human butyrylcholinesterase, Plant Biotechnol. J. 8 (2010) 873–886.
[37] H. Baldassarre, M. Schirm, J. Deslauriers, C. Turcotte, V. Bordignon, Protein profile and alpha-lactalbumin concentration in the milk of standard and transgenic goats expressing recombinant human butyrylcholinesterase, Transgenic Res. 18 (2009) 621–632.
[38] H. Baldassarre, J. Deslauriers, N. Neveu, V. Bordignon, Detection of endoplasmic reticulum stress markers and production enhancement treatments in transgenic goats expressing recombinant human butyrylcholinesterase, Transgenic Res. 20 (2011) 1265–1272.
[39] A. Saxena, Y. Ashani, L. Raveh, D. Stevenson, T. Patel, B.P. Doctor, Role of oligosaccharides in the pharmacokinetics of tissue-derived and genetically engineered cholinesterases, Mol. Pharmacol. 53 (1998) 112–122.
[40] Y.J. Rosenberg, A. Saxena, W. Sun, X. Jiang, N. Chilukuri, C. Luo, B.P. Doctor, K.D. Lee, Demonstration of *in vivo* stability and lack of immunogenicity of a polyethyleneglycol-conjugated recombinant CHO-derived butyrylcholinesterase bioscavenger using a homologous macaque model, Chem. Biol. Interact. 187 (2010) 279–286.
[41] H. Li, L.M. Schopfer, P. Masson, O. Lockridge, Lamellipodin proline rich peptides associated with native plasma butyrylcholinesterase tetramers, Biochem. J. 411 (2008) 425–432.
[42] E.G. Duysen, C.F. Bartels, O. Lockridge, Wild-type and A328W mutant human butyrylcholinesterase tetramers expressed in Chinese hamster ovary cells

have a 16-hour half-life in the circulation and protect mice from cocaine toxicity, J. Pharmacol. Exp. Ther. 302 (2002) 751–758.
[43] Y.J. Huang, P.M. Lundy, A. Lazaris, Y. Huang, H. Baldassarre, B. Wang, C. Turcotte, M. Cote, A. Bellemare, A.S. Bilodeau, S. Brouillard, M. Touati, P. Herskovits, I. Begin, N. Neveu, E. Brochu, J. Pierson, D.K. Hockley, D.M. Cerasoli, D.E. Lenz, H. Wilgus, C.N. Karatzas, S. Langermann, Substantially improved pharmacokinetics of recombinant human butyrylcholinesterase by fusion to human serum albumin, BMC Biotechnol. 8 (2008) 50.
[44] Y.J. Rosenberg, B. Laube, L. Mao, X. Jiang, S. Hernandez-Abanto, K.D. Lee, R. Adams, Pulmonary delivery of an aerosolized recombinant human butyrylcholinesterase pretreatment protects against aerosolized paraoxon in macaques, Chem. Biol. Interact. 203 (2013) 167–171.
[45] A. Ordentlich, D. Barak, C. Kronman, H.P. Benschop, L.P. De Jong, N. Ariel, R. Barak, Y. Segall, B. Velan, A. Shafferman, Exploring the active center of human acetylcholinesterase with stereomers of an organophosphorus inhibitor with two chiral centers, Biochemistry 38 (1999) 3055–3066.
[46] W. Jiang, J.R. Cashman, F. Nachon, P. Masson, L.M. Schopfer, O. Lockridge, Mass spectrometry method to identify aging pathways of SP- and RP-tabun adducts on human butyrylcholinesterase based on the Acid labile P–N bond, Toxicol. Sci. 132 (2013) 390–398.
[47] M. Wandhammer, E. Carletti, M. Van der Schans, E. Gillon, Y. Nicolet, P. Masson, M. Goeldner, D. Noort, F. Nachon, Structural study of the complex stereoselectivity of human butyrylcholinesterase for the neurotoxic V-agents, J. Biol. Chem. 286 (2011) 16783–16789.
[48] O. Cohen, C. Kronman, L. Raveh, O. Mazor, A. Ordentlich, A. Shafferman, Comparison of polyethylene glycol-conjugated recombinant human acetylcholinesterase and serum human butyrylcholinesterase as bioscavengers of organophosphate compounds, Mol. Pharmacol. 70 (2006) 1121–1131.
[49] K. Yokoyama, Y. Ogura, M. Kishimoto, F. Hinoshita, S. Hara, A. Yamada, N. Mimura, A. Seki, O. Sakai, Blood purification for severe sarin poisoning after the Tokyo subway attack, JAMA 274 (1995) 379.
[50] D.E. Lenz, E.D. Clarkson, S.M. Schulz, D.M. Cerasoli, Butyrylcholinesterase as a therapeutic drug for protection against percutaneous VX, Chem. Biol. Interact. 187 (2010) 249–252.
[51] H. Mumford, J.K. Troyer, Post-exposure therapy with recombinant human BuChE following percutaneous VX challenge in guinea-pigs, Toxicol. Lett. 206 (2011) 29–34.
[52] H. Mumford, M.E. Price, D.M. Cerasoli, W. Teschner, H. Ehrlich, H.P. Schwarz, D.E. Lenz, Efficacy and physiological effects of human butyrylcholinesterase as a post-exposure therapy against percutaneous poisoning by VX in the guinea-pig, Chem. Biol. Interact. 187 (2010) 304–308.
[53] H. Mumford, C.J. Docx, M.E. Price, A.C. Green, J.E. Tattersall, S.J. Armstrong, Human plasma-derived BuChE as a stoichiometric bioscavenger for treatment of nerve agent poisoning, Chem. Biol. Interact. 203 (2013) 160–166.
[54] N. Aurbek, H. Thiermann, F. Eyer, P. Eyer, F. Worek, Suitability of human butyrylcholinesterase as therapeutic marker and pseudo catalytic scavenger in organophosphate poisoning: a kinetic analysis, Toxicology 259 (2009) 133–139.
[55] Z. Kovarik, M. Katalinic, G. Sinko, J. Binder, O. Holas, Y.S. Jung, L. Musilova, D. Jun, K. Kuca, Pseudo-catalytic scavenging: searching for a suitable reactivator of phosphorylated butyrylcholinesterase, Chem. Biol. Interact. 187 (2010) 167–171.
[56] Z. Radic, T. Dale, Z. Kovarik, S. Berend, E. Garcia, L. Zhang, G. Amitai, C. Green, B. Radic, B.M. Duggan, D. Ajami, J. Rebek, P. Taylor, Catalytic detoxification of nerve agent and pesticide organophosphates by butyrylcholinesterase assisted with non-pyridinium oximes, Biochem. J. 450 (2013) 231–242.
[57] P. Masson, F. Nachon, O. Lockridge, Structural approach to the aging of phosphylated cholinesterases, Chem. Biol. Interact. 187 (2010) 157–162.
[58] Z. Kovarik, Z. Radic, H.A. Berman, P. Taylor, Mutation of acetylcholinesterase to enhance oxime-assisted catalytic turnover of methylphosphonates, Toxicology 233 (2007) 79–84.
[59] C. Kronman, O. Cohen, O. Mazor, A. Ordentlich, L. Raveh, B. Velan, A. Shafferman, Next generation OP-bioscavengers: a circulatory long-lived 4-PEG hypolysine mutant of F338A-HuAChE with optimal pharmacokinetics and pseudo-catalytic characteristics, Chem. Biol. Interact. 187 (2010) 253–258.
[60] R. Cochran, J. Kalisiak, T. Kucukkilinc, Z. Radic, E. Garcia, L. Zhang, K.Y. Ho, G. Amitai, Z. Kovarik, V.V. Fokin, K.B. Sharpless, P. Taylor, Oxime-assisted acetylcholinesterase catalytic scavengers of organophosphates that resist aging, J. Biol. Chem. 286 (2011) 29718–29724.
[61] T. Belinskaya, N. Pattabiraman, R. diTargiani, M. Choi, A. Saxena, Differences in amino acid residues in the binding pockets dictate substrate specificities of mouse senescence marker protein-30, human paraoxonase 1, and squid diisopropylfluorophosphatase, Biochim. Biophys. Acta 2012 (1824) 701–710.
[62] M.E. Wales, T.E. Reeves, Organophosphorus hydrolase as an *in vivo* catalytic nerve agent bioscavenger, Drug Test. Anal. 4 (2012) 271–281.
[63] P. Masson, F. Nachon, C.A. Broomfield, D.E. Lenz, L. Verdier, L.M. Schopfer, O. Lockridge, A collaborative endeavor to design cholinesterase-based catalytic scavengers against toxic organophosphorus esters, Chem. Biol. Interact. 175 (2008) 273–280.
[64] P. Masson, O. Lockridge, Butyrylcholinesterase for protection from organophosphorus poisons: catalytic complexities and hysteretic behavior, Arch. Biochem. Biophys. 494 (2010) 107–120.
[65] M. Trovaslet-Leroy, L. Musilova, F. Renault, X. Brazzolotto, J. Misik, L. Novotny, M.T. Froment, E. Gillon, M. Loiodice, L. Verdier, P. Masson, D. Rochu, D. Jun, F. Nachon, Organophosphate hydrolases as catalytic bioscavengers of organophosphorus nerve agents, Toxicol. Lett. 206 (2011) 14–23.
[66] Y. Wang, A.T. Boeck, E.G. Duysen, M. Van Keuren, T.L. Saunders, O. Lockridge, Resistance to organophosphorus agent toxicity in transgenic mice expressing the G117H mutant of human butyrylcholinesterase, Toxicol. Appl. Pharmacol. 196 (2004) 356–366.
[67] F. Nachon, E. Carletti, M. Wandhammer, Y. Nicolet, L.M. Schopfer, P. Masson, O. Lockridge, X-ray crystallographic snapshots of reaction intermediates in the G117H mutant of human butyrylcholinesterase, a nerve agent target engineered into a catalytic bioscavenger, Biochem. J. 434 (2011) 73–82.
[68] M. Amitay, A. Shurki, Hydrolysis of organophosphate compounds by mutant butyrylcholinesterase: a story of two histidines, Proteins 79 (2011) 352–364.
[69] S. Lushchekina, P. Masson, F. Nachon, A.V. Nemukhin, S.D. Varfolomeev, QM/MM modeling of the G117H butyrylcholinesterase catalyzed echothiophate hydrolysis reaction mechanism, in: Proceedings Kazan, 2012.
[70] D. Rochu, E. Chabriere, P. Masson, Human paraoxonase: a promising approach for pre-treatment and therapy of organophosphorus poisoning, Toxicology 233 (2007) 47–59.
[71] M. Ben-David, G. Wieczorek, M. Elias, I. Silman, J.L. Sussman, D.S. Tawfik, Catalytic metal ion rearrangements underline promiscuity and evolvability of a metalloenzyme, J. Mol. Biol. 425 (2013) 1028–1038.
[72] L.G. Costa, G. Giordano, C.E. Furlong, Pharmacological and dietary modulators of paraoxonase 1 (PON1) activity and expression: the hunt goes on, Biochem. Pharmacol. 81 (2011) 337–344.
[73] T.C. Otto, S.A. Kasten, E. Kovaleva, Z. Liu, G. Buchman, M. Tolosa, D. Davis, J.R. Smith, R. Balcerzak, D.E. Lenz, D.M. Cerasoli, Purification and characterization of functional human paraoxonase-1 expressed in Trichoplusia ni larvae, Chem. Biol. Interact. 187 (2010) 388–392.
[74] D.M. Shih, L. Gu, Y.R. Xia, M. Navab, W.F. Li, S. Hama, L.W. Castellani, C.E. Furlong, L.G. Costa, A.M. Fogelman, A.J. Lusis, Mice lacking serum paraoxonase are susceptible to organophosphate toxicity and atherosclerosis, Nature 394 (1998) 284–287.
[75] D.T. Yeung, J.R. Smith, R.E. Sweeney, D.E. Lenz, D.M. Cerasoli, A gas chromatographic-mass spectrometric approach to examining stereoselective interaction of human plasma proteins with soman, J. Anal. Toxicol. 32 (2008) 86–91.
[76] M. Valiyaveettil, Y. Alamneh, L. Biggemann, I. Soojhawon, B.P. Doctor, M.P. Nambiar, Efficient hydrolysis of the chemical warfare nerve agent tabun by recombinant and purified human and rabbit serum paraoxonase 1, Biochem. Biophys. Res. Commun. 403 (2010) 97–102.
[77] M. Valiyaveettil, Y. Alamneh, P. Rezk, L. Biggemann, M.W. Perkins, A.M. Sciuto, B.P. Doctor, M.P. Nambiar, Protective efficacy of catalytic bioscavenger, paraoxonase 1 against sarin and soman exposure in guinea pigs, Biochem. Pharmacol. 81 (2011) 800–809.
[78] M. Valiyaveettil, Y.A. Alamneh, B.P. Doctor, M.P. Nambiar, Crossroads in the evaluation of paraoxonase 1 for protection against nerve agent and organophosphate toxicity, Toxicol. Lett. 210 (2012) 87–94.
[79] S.M. Hodgins, S.A. Kasten, J. Harrison, T.C. Otto, Z.P. Oliver, P. Rezk, T.E. Reeves, N. Chilukuri, D.M. Cerasoli, Assessing protection against OP pesticides and nerve agents provided by wild-type HuPON1 purified from Trichoplusia ni larvae or induced via adenoviral infection, Chem. Biol. Interact. 203 (2013) 177–180.
[80] M. Harel, A. Aharoni, L. Gaidukov, B. Brumshtein, O. Khersonsky, R. Meged, H. Dvir, R.B. Ravelli, A. McCarthy, L. Toker, I. Silman, J.L. Sussman, D.S. Tawfik, Structure and evolution of the serum paraoxonase family of detoxifying and anti-atherosclerotic enzymes, Nat. Struct. Mol. Biol. 11 (2004) 412–419.
[81] T.C. Otto, C.K. Harsch, D.T. Yeung, T.J. Magliery, D.M. Cerasoli, D.E. Lenz, Dramatic differences in organophosphorus hydrolase activity between human and chimeric recombinant mammalian paraoxonase-1 enzymes, Biochemistry 48 (2009) 10416–10422.
[82] S.Z. Fairchild, M.W. Peterson, A. Hamza, C.G. Zhan, D.M. Cerasoli, W.E. Chang, Computational characterization of how the VX nerve agent binds human serum paraoxonase 1, J. Mol. Model. 17 (2011) 97–109.
[83] S.D. Kirby, J.R. Norris, J. Richard Smith, B.J. Bahnson, D.M. Cerasoli, Human paraoxonase double mutants hydrolyze V and G class organophosphorus nerve agents, Chem. Biol. Interact. 203 (2013) 181–185.
[84] R.D. Gupta, M. Goldsmith, Y. Ashani, Y. Simo, G. Mullokandov, H. Bar, M. Ben-David, H. Leader, R. Margalit, I. Silman, J.L. Sussman, D.S. Tawfik, Directed evolution of hydrolases for prevention of G-type nerve agent intoxication, Nat. Chem. Biol. 7 (2011) 120–125.
[85] M. Goldsmith, Y. Ashani, Y. Simo, M. Ben-David, H. Leader, I. Silman, J.L. Sussman, D.S. Tawfik, Evolved stereoselective hydrolases for broad-spectrum G-type nerve agent detoxification, Chem. Biol. 19 (2012) 456–466.
[86] F. Renault, T. Carus, C. Clery-Barraud, M. Elias, E. Chabriere, P. Masson, D. Rochu, Integrative analytical approach by capillary electrophoresis and kinetics under high pressure optimized for deciphering intrinsic and extrinsic cofactors that modulate activity and stability of human paraoxonase (PON1), J. Chromatogr. B Anal. Technol. Biomed. Life Sci. 878 (2010) 1346–1355.
[87] R.C. Stevens, S.M. Suzuki, T.B. Cole, S.S. Park, R.J. Richter, C.E. Furlong, Engineered recombinant human paraoxonase 1 (rHuPON1) purified from *Escherichia coli* protects against organophosphate poisoning, Proc. Natl. Acad. Sci. U.S.A. 105 (2008) 12780–12784.

[88] E.G. Duysen, K. Parikh, V. Aleti, V. Manne, O. Lockridge, N. Chilukuri, Adenovirus-mediated human paraoxonase1 gene transfer to provide protection against the toxicity of the organophosphorus pesticide toxicant diazoxon, Gene Ther. 18 (2011) 250–257.
[89] M.M. Blum, C.M. Timperley, G.R. Williams, H. Thiermann, F. Worek, Inhibitory potency against human acetylcholinesterase and enzymatic hydrolysis of fluorogenic nerve agent mimics by human paraoxonase 1 and squid diisopropyl fluorophosphatase, Biochemistry 47 (2008) 5216–5224.
[90] M. Melzer, J.C. Chen, A. Heidenreich, J. Gab, M. Koller, K. Kehe, M.M. Blum, Reversed enantioselectivity of diisopropyl fluorophosphatase against organophosphorus nerve agents by rational design, J. Am. Chem. Soc. 131 (2009) 17226–17232.
[91] M. Melzer, A. Heidenreich, F. Dorandeu, J. Gab, K. Kehe, H. Thiermann, T. Letzel, M.M. Blum, *In vitro* and *in vivo* efficacy of PEGylated diisopropyl fluorophosphatase (DFPase), Drug Test. Anal. 4 (2012) 262–270.
[92] M.A. Sogorb, E. Vilanova, V. Carrera, Future applications of phosphotriesterases in the prophylaxis and treatment of organophosporus insecticide and nerve agent poisonings, Toxicol. Lett. 151 (2004) 219–233.
[93] E. Ghanem, F.M. Raushel, Detoxification of organophosphate nerve agents by bacterial phosphotriesterase, Toxicol. Appl. Pharmacol. 207 (2005) 459–470.
[94] T.C. Otto, J.R. Scott, M.A. Kauffman, S.M. Hodgins, R.C. Ditargiani, J.H. Hughes, E.P. Sarricks, G.A. Saturday, T.A. Hamilton, D.M. Cerasoli, Identification and characterization of novel catalytic bioscavengers of organophosphorus nerve agents, Chem. Biol. Interact. 203 (2013) 186–190.
[95] P.C. Tsai, N. Fox, A.N. Bigley, S.P. Harvey, D.P. Barondeau, F.M. Raushel, Enzymes for the homeland defense: optimizing phosphotriesterase for the hydrolysis of organophosphate nerve agents, Biochemistry 51 (2012) 6463–6475.
[96] R. Hawwa, S.D. Larsen, K. Ratia, A.D. Mesecar, Structure-based and random mutagenesis approaches increase the organophosphate-degrading activity of a phosphotriesterase homologue from *Deinococcus radiodurans*, J. Mol. Biol. 393 (2009) 36–57.
[97] C. Roodveldt, D.S. Tawfik, Directed evolution of phosphotriesterase from *Pseudomonas diminuta* for heterologous expression in *Escherichia coli* results in stabilization of the metal-free state, Protein Eng. Des. Sel. 18 (2005) 51–58.
[98] E. Carletti, L. Jacquamet, M. Loiodice, D. Rochu, P. Masson, F. Nachon, Update on biochemical properties of recombinant *Pseudomonas diminuta* phosphotriesterase, J. Enzyme Inhib. Med. Chem. 24 (2009) 1045–1055.
[99] S.B. Bird, T.D. Sutherland, C. Gresham, J. Oakeshott, C. Scott, M. Eddleston, OpdA, a bacterial organophosphorus hydrolase, prevents lethality in rats after poisoning with highly toxic organophosphorus pesticides, Toxicology 247 (2008) 88–92.
[100] C.J. Jackson, C. Scott, A. Carville, K. Mansfield, D.L. Ollis, S.B. Bird, Pharmacokinetics of OpdA, an organophosphorus hydrolase, in the African green monkey, Biochem. Pharmacol. 80 (2010) 1075–1079.
[101] D. Jun, L. Musilova, M. Link, M. Loiodice, F. Nachon, D. Rochu, F. Renault, P. Masson, Preparation and characterization of methoxy polyethylene glycol-conjugated phosphotriesterase as a potential catalytic bioscavenger against organophosphate poisoning, Chem. Biol. Interact. 187 (2010) 380–383.
[102] A.C. Hemmert, T.C. Otto, M. Wierdl, C.C. Edwards, C.D. Fleming, M. MacDonald, J.R. Cashman, P.M. Potter, D.M. Cerasoli, M.R. Redinbo, Human carboxylesterase 1 stereoselectively binds the nerve agent cyclosarin and spontaneously hydrolyzes the nerve agent sarin, Mol. Pharmacol. 77 (2010) 508–516.
[103] A.C. Hemmert, T.C. Otto, R.A. Chica, M. Wierdl, J.S. Edwards, S.M. Lewis, C.C. Edwards, L. Tsurkan, C.L. Cadieux, S.A. Kasten, J.R. Cashman, S.L. Mayo, P.M. Potter, D.M. Cerasoli, M.R. Redinbo, Nerve agent hydrolysis activity designed into a human drug metabolism enzyme, PLoS One 6 (2011) e17441.
[104] N.K. Vyas, A. Nickitenko, V.K. Rastogi, S.S. Shah, F.A. Quiocho, Structural insights into the dual activities of the nerve agent degrading organophosphate anhydrolase/prolidase, Biochemistry 49 (2010) 547–559.
[105] M. Costante, L. Biggemann, Y. Alamneh, I. Soojhawon, R. Short, S. Nigam, G. Garcia, B.P. Doctor, M. Valiyaveettil, M.P. Nambiar, Hydrolysis potential of recombinant human skin and kidney prolidase against diisopropylfluorophosphate and sarin by *in vitro* analysis, Toxicol. in Vitro 26 (2012) 182–188.
[106] L. Chandrasekaran, T. Belinskaya, A. Saxena, *In vitro* characterization of organophosphorus compound hydrolysis by native and recombinant human prolidase, Toxicol. in Vitro 27 (2013) 499–506.
[107] V. Aleti, G.B. Reddy, K. Parikh, P. Arun, N. Chilukuri, Persistent and high-level expression of human liver prolidase *in vivo* in mice using adenovirus, Chem. Biol. Interact. 203 (2013) 191–195.
[108] R.C. diTargiani, L. Chandrasekaran, T. Belinskaya, A. Saxena, In search of a catalytic bioscavenger for the prophylaxis of nerve agent toxicity, Chem. Biol. Interact. 187 (2010) 349–354.
[109] S. Chakraborti, B.J. Bahnson, Crystal structure of human senescence marker protein 30: insights linking structural, enzymatic, and physiological functions, Biochemistry 49 (2010) 3436–3444.
[110] S.D. Khare, Y. Kipnis, P. Greisen Jr., R. Takeuchi, Y. Ashani, M. Goldsmith, Y. Song, J.L. Gallaher, I. Silman, H. Leader, J.L. Sussman, B.L. Stoddard, D.S. Tawfik, D. Baker, Computational redesign of a mononuclear zinc metalloenzyme for organophosphate hydrolysis, Nat. Chem. Biol. 8 (2012) 294–300.
[111] T. Lindhout, U. Iqbal, L.M. Willis, A.N. Reid, J. Li, X. Liu, M. Moreno, W.W. Wakarchuk, Site-specific enzymatic polysialylation of therapeutic proteins using bacterial enzymes, Proc. Natl. Acad. Sci. U.S.A. 108 (2011) 7397–7402.
[112] A. Gaydess, E. Duysen, Y. Li, V. Gilman, A. Kabanov, O. Lockridge, T. Bronich, Visualization of exogenous delivery of nanoformulated butyrylcholinesterase to the central nervous system, Chem. Biol. Interact. 187 (2010) 295–298.
[113] E.T. Maggio, Intravail: highly effective intranasal delivery of peptide and protein drugs, Expert Opin. Drug Delivery 3 (2006) 529–539.
[114] K. Parikh, E.G. Duysen, B. Snow, N.S. Jensen, V. Manne, O. Lockridge, N. Chilukuri, Gene-delivered butyrylcholinesterase is prophylactic against the toxicity of chemical warfare nerve agents and organophosphorus compounds, J. Pharmacol. Exp. Ther. 337 (2011) 92–101.
[115] G. Gotthard, J. Hiblot, M. Elias, E. Chabriere, Crystallization and preliminary X-ray diffraction analysis of the hyperthermophilic Sulfolobus islandicus lactonase, Acta Crystallogr. Sect. F Struct. Biol. Cryst. Commun. 67 (2011) 354–357.
[116] J. Hiblot, G. Gotthard, E. Chabriere, M. Elias, Characterisation of the organophosphate hydrolase catalytic activity of SsoPox, Sci. Rep. 2 (2012) 779.

# Actions et efficacités des différentes oximes dans le traitement de l'intoxication par les neurotoxiques organophosphorés

M-A. Vonesch, **F. Nachon**, P. Burnat*

Médecine et Armées 39 (2011) 445-452

# Actions et efficacités des différentes oximes dans le traitement de l'intoxication par les neurotoxiques organophosphorés.

M.-A. Vonesch[a], F. Nachon[b], P. Burnat[c].

a Service de pharmacie hospitalière, HIA Sainte-Anne, BP 20545 – 83041 Toulon Cedex 9.
b Département de toxicologie de l'Institut de recherche biomédicale des armées, antenne de la Tronche, 24 avenue des Maquis Grésivaudan – 38702 La Tronche.
c Service de biochimie toxicologie clinique, HIA Bégin, 69 avenue de Paris – 94163 Saint-Mandé Cedex.

Article reçu le 11 mai 2011, accepté le 1er juin 2011.

**Résumé**

Le panel des neurotoxiques organophosphorés disponibles et susceptibles d'être utilisés dans un contexte terroriste, nécessite une actualisation constante des thérapeutiques mises en place dans le cadre d'une intoxication par ces agents chimiques de guerre. Les oximes, dont la pralidoxime présente dans l'auto-injecteur bicompartimenté du Service de santé des armées en France, font partie des antidotes majeurs indiqués dans un tel contexte. La pralidoxime possède une efficacité certaine et potentialisée par l'association d'atropine et d'avizafone mais limitée à certains agents neurotoxiques organophosphorés. D'autres oximes commercialisées ou en développement pourraient présenter un plus grand intérêt permettant d'élargir le spectre d'action de la pralidoxime. La comparaison de ces oximes, d'une part vis-à-vis de leur capacité à réactiver les acétylcholinestérases *in vitro* reflétant leur efficacité *in vivo* et d'autre part, de leur toxicité semble indiquer que l'HI-6 représente le meilleur compromis concernant ces deux paramètres. La stabilité des oximes en vue du développement d'une formulation galénique adaptée et l'amélioration de leur passage au niveau du système nerveux central, constituent des pistes de recherche d'actualité.

Mots-clés : Acétylcholinestérases. Inhibition. Neurotoxiques organophosphorés. Oximes. Pharmacocinétique. Pharmacodynamique. Réactivation.

**Abstract**

**ACTIONS AND EFFICACIES OF DIFFERENT OXIMES IN TREATING INTOXICATION WITH ORGANOPHOSPHORUS NERVE AGENTS.**

The panel of organophosphorus nerve agents available which could be used by terrorists requires a constant update of therapeutics employed in the frame of intoxication by chemical warfare agents. Oximes as pralidoxime, which is an essential component of the French Armed Forces Health Service two compartments auto-injector are part of major drugs used in this context. Pralidoxime has a sure efficiency also potentiated by combining atropine and avizafone yet is limited to certain neurotoxic agents. Other oximes commercialized or in development could be interesting to broaden the action spectrum of pralidoxime. Comparing the oximes through their ability to reactivate *in vitro* acetylcholinesterases reflecting their *in vivo* efficacy and through their toxicity suggests that HI-6 is the best compromise for these two parameters. The research of stable oximes for developing an adapted pharmaceutical formulation and improving their penetration through the blood brain barrier are burning current issues.

Keywords: Acetylcholinesterases. Inhibition. Organophosphorus nerve agents. Oximes. Pharmacodynamic. Pharmacokinetics. Re-activation.

## Introduction.

Dans le cadre de la prise en charge d'une intoxication par les neurotoxiques organophosphorés (NOP), trois médicaments sont classiquement employés aussi bien en auto-traitement sur un théâtre d'opérations qu'en traitement hospitalier. Ainsi, l'auto-injecteur bicompartimenté (AIBC) du Service de santé des armées (SSA) fabriqué par la Pharmacie centrale des armées (PCA) contient, sous forme lyophilisée, du sulfate d'atropine antagonisant les effets de l'acétylcholine au niveau des récepteurs muscariniques, du chlorhydrate d'avizafone qui est un précurseur du diazepam agissant comme un anticonvulsivant et du méthylsulfate de pralidoxime.

M.-A. VONESCH, pharmacien. F. NACHON, IDEF. P. BURNAT, pharmacien chef des services, professeur agrégé du Val-de-Grâce.
**Correspondance** : M.-A. VONESCH. Service de pharmacie hospitalière, HIA Sainte-Anne, BP 20545 – 83041 Toulon Cedex 9.
E-mail : ma.vonesch@gmail.com

La pralidoxime est une oxime permettant la réactivation des acétylcholinestérases inhibées par les NOP. Si la pralidoxime est actuellement la seule oxime commercialisée en France, il en existe cependant de nombreuses autres capables de réactiver les cholinestérases inhibées par les neurotoxiques organophosphorés. La problématique liée à l'emploi de ces oximes est basée sur leurs propriétés très différentes sur le plan galénique, principalement influencée par leur solubilité et leur stabilité, comme d'un point de vue pharmacologique, du fait de leur efficacité variable selon le NOP considéré, sans oublier leur différence de toxicité.

Dans cet article, nous nous attacherons à dégager les avantages et les inconvénients des trois oximes commercialisées au niveau international : la pralidoxime (2-PAM), l'obidoxime (LüH-6) et l'asoxime (HI-6) ; ainsi que de trois autres oximes : la trimédoxime (TMB-4), la méthoxime (MMB-4) et l'HLö-7 vis-à-vis des intoxications par les différents neurotoxiques de guerre. Nous nous intéresserons également à leurs propriétés physico-chimiques, qui conditionnent leur formulation galénique et leur application thérapeutique sur le plan pratique, qu'elle soit effective ou potentielle.

## Le mode d'action des neurotoxiques organophosphorés et le phénomène de vieillissement des acétylcholinestérases.

Les NOP sont des composés chimiques liposolubles, particulièrement toxiques, développés pour les premiers d'entre eux en Allemagne durant l'entre-deux-guerres. Ils se divisent en deux groupes : les agents G qui sont des esters dérivés des acides fluorophosphonique ou phosphoramidique tels que le tabun (GA), le sarin (GB), le soman (GD) ou encore le sarin cyclohexylique (GF) et les agents V qui sont des esters de l'acide thiophosphonique tels que le VX et ses analogues russe (VR) et chinois (VXC). Leurs propriétés physico-chimiques sont variables mais ils possèdent tous une affinité élevée pour les cholinestérases : acétylcholinestérases tissulaires, érythrocytaires et centrales ainsi que les butyrylcholinestérases plasmatiques qu'ils inhibent par phosphylation de la fonction hydroxyl de la sérine située dans leur site catalytique. Cette action inhibitrice sur l'acétylcholinestérase est responsable de son inaptitude à hydrolyser son substrat physiologique, l'acétylcholine, conduisant alors à une accumulation de ce neurotransmetteur. Ce phénomène conduit à une hyperstimulation des récepteurs cholinergiques post-synaptiques, muscariniques et nicotiniques, à la fois au niveau central et périphérique, pouvant être fatale. Lors de cette étape, les oximes peuvent jouer un rôle bénéfique, puisqu'elles vont permettre la déphosphylation des acétylcholinestérases favorisant ainsi la récupération d'une enzyme active. La réactivation spontanée des enzymes n'est pas systématique comme en témoigne l'absence de ce phénomène avec le sarin, le sarin cyclohexylique et le tabun (1).

Cependant, cette réactivation qu'elle soit spontanée pour certains NOP ou induite par les oximes n'est plus possible après la désalkylation du conjugué formé entre le NOP et l'acétylcholinestérase (fig. 1). Ce phénomène correspond au « vieillissement » de l'enzyme également dénommé « aging » (2). Le vieillissement par désalkylation du conjugué enzyme-NOP conduit à la formation d'un adduit acide méthylphosphonique anionique qui forme une liaison ionique forte additionnelle avec l'acétylcholinestérase. De plus, la charge négative de l'acide méthylphosphonique repousse la fonction oximate négative du réactivateur en approche. Le vieillissement entraîne donc à la fois une augmentation de la stabilité et une baisse de réactivité du conjugué

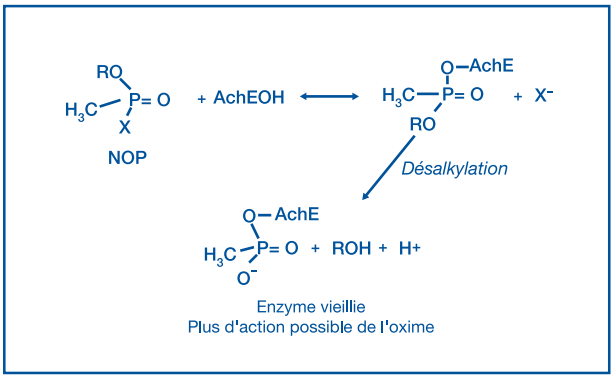


**Figure 1 : Schéma descriptif du phénomène de vieillissement des acétylcholinestérases. R est le groupement alkyl du NOP. $X^-$ est un groupement partant ou un anion.**

formé par l'acétylcholinestérase et le NOP, interdisant toute réactivation ultérieure. La vitesse de vieillissement dépend essentiellement de la nature de l'agent NOP mais aucune corrélation n'a été mise en évidence entre la structure des NOP et leur interaction avec les acétylcholinestérases humaines (1). *In vitro*, le vieillissement des enzymes survient après quelques minutes avec le soman, en cinq à six heures avec le sarin, après 46 heures avec le tabun et au bout de 48 heures avec le VX (tab. I). Le conjugué enzyme-VR possède une demi-vie plus élevée, de plus d'une semaine (12 jours), que celui du conjugué enzyme-VX alors que pour son homologue chinois, le VXC, le vieillissement est plus rapide. La rapidité de l'altération des enzymes inhibées par le soman permet de comprendre la résistance à la réactivation des acétylcholinestérases inhibées par ce NOP. En plus de la nature de l'organophosphoré, la vitesse de vieillissement de l'enzyme varie selon l'espèce animale considérée (3).

**Tableau I. Délai avant l'apparition du phénomène « d'aging » pour différents NOP.**

| NOP | Soman | Sarin | Tabun | VX |
|---|---|---|---|---|
| Délai avant apparition du phénomène « d'aging » (*in vitro*) | Quelques minutes | 5-6 heures | > 46 heures | > 48 heures |

Le vieillissement rapide des acétylcholinestérases conduisant à une inefficacité du traitement à base d'oxime est à l'origine de l'utilisation d'un traitement prophylactique consistant en la prise de bromure de pyridostigmine avant une potentielle intoxication aux NOP et en particulier avec le soman et le tabun. Ce médicament masque une partie des sites catalytiques d'acétylcholinestérase en s'y fixant de façon réversible. Cependant, la pyridostigmine ne franchissant pas la barrière hémato-encéphalique (BHE), la protection octroyée par cette prémédication ne concerne donc pas les cholinestérases centrales et seulement environ 30 % des cholinestérases situées en périphérie. Cette mesure prophylactique est insuffisante, elle est limitée à un usage militaire, et même si de nouveau traitement prophylactique à base d'enzymes bioépuratrices sont en cours de développement (4), il est encore nécessaire de disposer de thérapeutiques à visée curative comme les oximes.

## Le mécanisme d'action général des oximes.

Le mécanisme d'action principal des oximes consiste à hydrolyser la liaison établie entre les enzymes et leur inhibiteur, afin de régénérer les acétylcholinestérases inhibées par les NOP. De façon plus approfondie, les oximes, dont les structures les plus courantes sont représentées sur la figure 2, sont de puissants agents nucléophiles possédant une affinité élevée pour les sites actifs des acétylcholinestérases. L'acétylcholinestérase possède deux sites de liaison pour son substrat et ses inhibiteurs, le site catalytique à proprement parler enfoui au fond d'une gorge ainsi que le site périphérique situé à l'entrée de cette gorge et en contrôlant l'accès. Lorsque l'enzyme est inhibée par un NOP, le fond de la gorge est complètement occupé.

La réactivation de l'enzyme se déroule de la manière suivante. Dans un premier temps, le réactivateur en approche de l'enzyme inhibée va interagir avec le site périphérique à l'entrée de la gorge. Puis, la fonction oximate du réactivateur va descendre dans la gorge pour approcher la phosphylsérine. Quand il est suffisamment proche, l'oximate réagit sur l'atome de phosphore de la phosphylsérine pour former une nouvelle liaison covalente. La formation de cette nouvelle liaison fragilise la liaison entre l'atome de phosphore et la sérine, qui finit par se rompre. L'oxime fraîchement phosphylée sort du site actif. La sérine libérée peut à nouveau jouer son rôle catalytique dans l'hydrolyse de l'acétylcholine. Néanmoins, après avoir réactivé l'acétylcholinestérase, l'oxime phosphylée ou phosphyloxime peut retourner dans le site actif et retransférer le groupement phosphyle à la sérine catalytique. Les phosphyloximes sont elles-mêmes de bons inhibiteurs des cholinestérases.

**Figure 2 : Formule générale d'une oxime, un puissant agent nucléophile.**

L'action régénératrice de l'oxime et la vitesse à laquelle elle réactive les cholinestérases sont dépendantes de nombreux facteurs tels que la nature et la concentration du NOP inhibiteur ; la vitesse de vieillissement, la structure et la localisation de l'enzyme (cérébrale, tissulaire ou érythrocytaire) ; la concentration et la structure chimique de l'oxime et enfin l'espèce animale considérée. En particulier, la structure de l'oxime modifie son affinité pour les acétylcholinestérases et leur réactivité vis-à-vis de celles-ci (1). Le mécanisme d'action principal des oximes correspondant à la réactivation des acétylcholinestérases ne permet pas d'expliquer l'efficacité de certaines d'entre elles comme l'HI-6 vis-à-vis des NOP entraînant un vieillissement extrêmement rapide des enzymes tel que le soman. C'est pourquoi, d'autres propositions de mécanismes d'action des oximes ont été envisagées ; parmi celles-ci nous pouvons évoquer différentes hypothèses :

– une interaction de l'oxime au niveau central, au sein de la voie de transmission GABAergique ;

– une interaction au niveau de la voie de transmission cholinergique des muscles squelettiques ;

– une inhibition du relargage de l'acétylcholine ;

– une altération des neurotransmetteurs ;

– une interaction avec les terminaisons nerveuses pré-synaptiques ou les récepteurs post-synaptiques à l'acétylcholine ;

– un effet anticonvulsivant intrinsèque de l'oxime.

Par ailleurs, certaines hypothèses de mécanismes d'action secondaires ont été confirmées. En effet, d'après Øydvin et al., la pralidoxime et l'HI-6 interagiraient avec les récepteurs nicotiniques, de plus, l'HI-6 et l'HLö-7 inhiberaient partiellement le relargage de l'acétylcholine *in vitro* chez le rat après inactivation des acétylcholinestérases par le soman. Ce mécanisme d'action commun à l'HI-6 et l'HLö-7 pourrait être en partie dû à la fonction aldoxime qu'elles partagent et qui se situe en quatrième position au niveau d'un de leurs deux cycles pyridiniques (5). Les oximes peuvent également avoir un rôle de protection sur les cholinestérases du fait de leur fixation sur leur site actif, empêchant alors le NOP de se fixer.

Cependant, ces mécanismes d'action sont annexes et l'efficacité des oximes dépend essentiellement de leur aptitude à réactiver les acétylcholinestérases.

## La réactivation des différentes cholinestérases.

Les acétylcholinestérases sont localisées au niveau tissulaire (poumon, cœur, muscles squelettiques), érythrocytaire et cérébral. Les butyrylcholinestérases

sont des enzymes sans activité physiologique connue, présentes au niveau plasmatique et cérébral. Mais elles servent de leurre en cas d'intoxication aux NOP, car en réagissant avec eux, elles diminuent leur concentration inhibitrice efficace. Cependant, les butyrylcholinestérases diffèrent des acétylcholinestérases au niveau de la structure de leur site catalytique, ce qui rend les oximes bispyridiniques inadaptées à la réactivation des butyrylcholinestérases. C'est pourquoi, d'autres oximes permettant une réactivation spécifique des butyrylcholinestérases sont actuellement en cours de recherche.

Les répartitions périphérique et centrale des cholinestérases, sont responsables d'une variabilité de l'action des oximes en fonction de leur accessibilité à ces différents compartiments. De la même façon, la perméabilité du passage de la BHE par les NOP, définit le type de cholinestérases qu'ils vont pouvoir inhiber et la prédominance des symptômes observés. Par exemple, le VR et le VX franchissent difficilement la BHE, en revanche ils présentent une forte affinité pour les cholinestérases périphériques (6).

Shih et al. ont étudié la capacité de différentes oximes, dont l'HI-6 (sous forme de dichlorure et de diméthylsulfonate plus hydrosoluble), l'HLö-7, la méthoxime (MMB-4), la trimédoxime (TMB-4) et la pralidoxime (2-PAM), à réactiver les cholinestérases tissulaires, sanguines et cérébrales *in vivo* chez le cochon d'Inde, à la suite d'une administration sous-cutanée de sarin, de sarin cyclohexylique, de VR ou de VX. Les résultats obtenus sont exposés et discutés ci-dessous.

## Les cholinestérases cérébrales.

Globalement, les oximes testées n'ont que peu d'effet sur la réactivation des cholinestérases cérébrales. La plupart des oximes dérivant de pyridiniums éprouvent des difficultés à franchir la BHE du fait de la présence de leur charge positive permanente. Ainsi, au maximum 10 % de la concentration périphérique en oximes sont retrouvés au niveau central (7).

En considérant une concentration périphérique en oximes compatible avec une utilisation thérapeutique, la concentration théorique au niveau central est alors insuffisante pour réactiver efficacement les acétylcholinestérases à ce niveau. Ceci justifie pleinement la co-administration d'atropine et d'avizafone, qui eux franchissent la BHE, afin de contrer les effets cholinergiques centraux induits par les NOP.

La réactivation des acétylcholinestérases humaines du système nerveux central pourrait être considérablement améliorée par les amidine-oximes, récemment synthétisées et testées chez l'animal afin de présenter une alternative à la pralidoxime et plus largement aux oximes dont le passage de la BHE se trouve limité. En effet, ces nouvelles oximes présentent une structure s'affranchissant des charges positives permanentes des oximes bispyridiniques ce qui augmente leur lipophilie et donc leur passage et leur action au niveau cérébral. Mais l'efficacité des amidine-oximes est encore inférieure à celle de la pralidoxime (8). D'autres pistes sont actuellement explorées et un effort conjoint de l'Institut de recherche biomédicale des armées (IRBA) (Département de toxicologie) et de laboratoires mixtes CNRS universitaires de Strasbourg (Faculté de pharmacie) et de Rouen (IRCOF) a récemment permis de mettre au point une nouvelle génération d'oximes non chargées, aussi efficace *in vitro*, voire plus efficace, que toutes les oximes connues sur l'acétylcholinestérase humaine inhibée par le VX et le tabun (9). Toutefois, leur efficacité *in vivo* reste à établir.

## Les cholinestérases tissulaires.

La réactivation des acétylcholinestérases tissulaires varie selon l'oxime employée.

Au niveau pulmonaire, la méthoxime s'est avérée être la plus efficace vis-à-vis du sarin, du cyclosarin et du VX suivi de près par l'HLö-7 (10). L'HI-6, sous forme de dichlorure, s'est montrée supérieure aux autres oximes contre le VR et à la pralidoxime contre le VX.

Au niveau cardiaque, la méthoxime est la plus efficace contre le cyclosarin et le VR. La première position de la méthoxime est supplantée par la pralidoxime pour le cyclosarin et par l'HLö-7 pour le VX.

Au niveau musculaire, l'HLö-7 s'est avérée être la plus efficace contre le sarin, le cyclosarin et le VX alors que l'HI-6 s'est trouvée être la meilleure oxime contre le VR.

## Les cholinestérases sanguines.

Du fait de leur localisation, les cholinestérases sanguines, érythrocytaires et plasmatiques, sont les premières à être inhibées par les NOP et à être réactivées par les oximes. L'effet réactivateur des oximes est majoritairement plus intense du fait de leur concentration plus élevée au niveau sanguin qu'au niveau tissulaire.

Les cholinestérases érythrocytaires sont réactivées plus efficacement par l'HI-6 sous forme de diméthylsulfonate, lorsqu'elles ont été inhibées par le sarin ou le cyclosarin. En revanche, la méthoxime s'avère plus efficace en cas d'intoxication par le VX et le VR.

L'HI-6 et l'HLö-7 seraient dix à dix mille fois plus efficace que la pralidoxime et la méthoxime, dans la réactivation *in vitro* des acétylcholinestérases érythrocytaires inhibées par le sarin, le cyclosarin et le VR chez l'homme (3). Les résultats d'une étude de mesure de l'activité des différentes oximes pour réactiver les acétylcholinestérases érythrocytaires humaines inhibées par le VX, le VR et le VXC, mettent en évidence l'ordre d'efficacité suivant : HLö-7 > HI-6 > MMB-4 ≥ obidoxime > 2-PAM (11).

En résumé, dans l'étude de Shih et al., réalisée chez le cochon d'Inde, la méthoxime est la seule oxime significativement efficace pour réactiver les cholinestérases inhibées par l'un ou l'autre des quatre NOP suivants : sarin, cyclosarin, VX et VR, dans les trois compartiments tissulaires et au niveau sanguin (10).

L'action de l'HLö-7 est plus faible que celle de la méthoxime vis-à-vis des cholinestérases tissulaires inhibées par le VR ou le cyclosarin alors que les autres oximes manquent d'efficacité vis-à-vis de la réactivation des cholinestérases tissulaires inhibées par le cyclosarin.

De manière générale, la pralidoxime s'avère moins efficace sur les cholinestérases périphériques que les autres oximes étudiées.

En outre, les données concernant la réactivation des cholinestérases au niveau sanguin ne peuvent pas être extrapolées au niveau tissulaire, car aucune corrélation n'existe entre l'activité des oximes dans ces deux compartiments.

Par ailleurs, ces résultats peuvent difficilement être extrapolés à l'homme, car d'après Luo et al., la réactivation des cholinestérases inhibées par le VR, le sarin ou le cyclosarin, *in vitro* chez le cochon d'Inde, en utilisant les oximes dont l'HI-6 et l'HLö-7, s'effectue plus lentement que chez l'homme ou le singe (3).

## La comparaison des differentes oximes.

D'un point de vue structurel, les oximes actuellement commercialisées sont divisées en deux groupes : la pralidoxime possédant une structure à un seul cycle pyridinique et les autres constituant le deuxième groupe disposant d'un noyau structural composé de deux cycles pyridiniques.

Sous forme de sels d'ammoniums quaternaires, les oximes passent difficilement la BHE. Ce passage varie selon la posologie de l'oxime considérée, la nature de ses groupements caractéristiques, la co-administration d'un traitement comme l'atropine, voire même selon le type de NOP employé qui pourrait alors faciliter le passage de la BHE (12).

Les oximes substituées en deuxième position de leur cycle pyridinique, comme la pralidoxime et l'HI-6, seraient moins stables que celles substituées en quatrième position comme l'obidoxime (13).

Plusieurs explications concernant la différence d'efficacité des oximes dans la réactivation des acétylcholinestérases ont été proposées. Outre l'affinité même de l'oxime pour l'enzyme, plus l'acidité du groupement oxime mais aussi du proton méthine est forte, plus l'oxime sera un bon réactivateur (1).

La position du groupement oxime au niveau du cycle pyridinique a également son importance. Placé en deuxième position, l'oxime présenterait un intérêt dans l'intoxication par le soman et situé en quatrième position, l'oxime est active lors de l'intoxication par le tabun (14).

En outre, l'efficacité d'une même oxime pourrait varier en fonction de l'effet stérique engendré par le groupement alkyl du NOP considéré (15).

La comparaison de l'activité des différentes oximes est fortement dépendante du choix du modèle animal utilisé (fig. 3). Pour des raisons éthiques évidentes, peu d'études présentent des résultats de l'action des oximes chez l'homme ou chez le singe alors que le modèle primate non humain, même s'il est imparfait, représente le modèle le plus pertinent pour l'étude *in vivo* de la pharmacocinétique et de la pharmacodynamique des oximes afin de permettre une extrapolation des résultats à l'homme. Les résultats obtenus *in vivo* chez le rat et le cochon d'Inde, ce dernier étant majoritairement considéré comme le meilleur modèle non primate, sont à extrapoler à l'homme avec prudence.

En effet, la réactivation des acétylcholinestérases par les oximes de la série H (HI-6, HLö-7, LüH-6) peut être

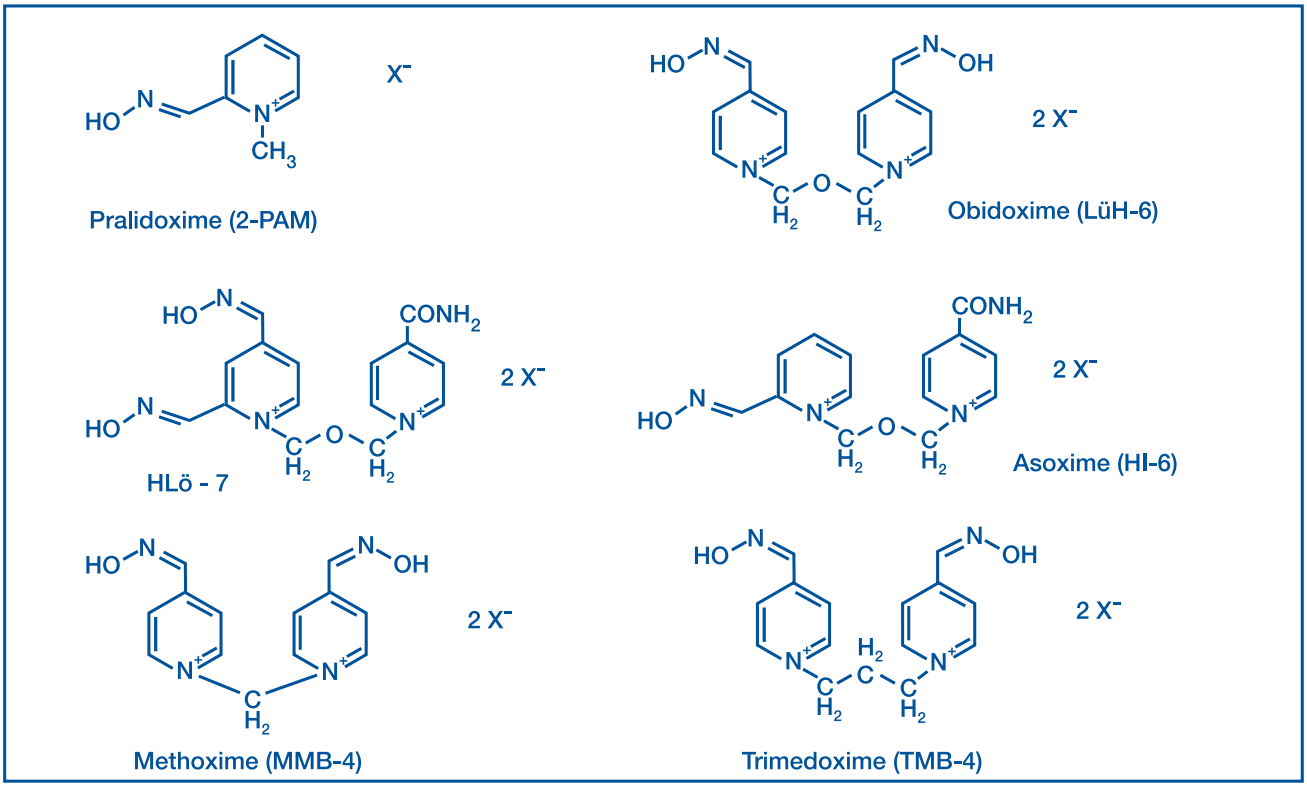


**Figure 3 : Structure chimique des principales oximes. $X^-$ étant le contre-ion.**

quelques centaines de fois plus rapide chez l'homme que chez le cochon d'Inde. En revanche, le modèle d'étude *in vitro* de l'activité réactivatrice des oximes vis-à-vis des acétylcholinestérases érythrocytaires est validé et semble bien corrélé à leur efficacité *in vivo* (3). Il est également nécessaire d'interpréter les résultats des études en fonction de la concentration en oxime employée qui doit être compatible avec une utilisation thérapeutique chez l'homme. En effet, une dose élevée *in vitro* pourra générer de très bons résultats mais reproduire les effets d'un NOP *in vivo* (16).

La formulation des oximes utilise des sels différents : chlorure, iodure, bromure, lactate, méthylsulfate, méthanesulfonate, faisant ainsi varier les propriétés de ces oximes, notamment leur stabilité et leur solubilité. Généralement, la pralidoxime, la trimédoxime et l'obidoxime sont stables et peuvent se conserver en ampoules sous forme liquide tandis que l'HI-6 et l'HLö-7 sont instables en solution aqueuse et ne peuvent être conservées que sous forme sèche, solubilisées juste avant leur administration notamment dans les auto-injecteurs (17).

## La pralidoxime (2-PAM).

La première réactivation des acétylcholinestérases a été effectuée en 1951 par l'hydroxylamine, un réactif fréquemment utilisé dans la synthèse des oximes. Quatre ans plus tard, la synthèse puis l'utilisation de la pralidoxime, ont permis la réactivation de ces enzymes à une vitesse un million de fois supérieure à celle constatée en utilisant l'hydroxylamine (18). La pralidoxime est couramment utilisée aux États-Unis et en France.

Lors de l'attentat au sarin dans le métro de Tokyo en 1995, 700 ampoules de 500 mg de pralidoxime ont été utilisées. Cependant, l'atropine fut beaucoup plus largement employée (19). Si l'efficacité de la pralidoxime est démontrée dans les intoxications par le sarin ou le VX, en revanche, elle est très limitée lorsque d'autres NOP tels que le tabun, le soman, le sarin cyclohexylique ou encore le VR sont utilisés (20).

C'est une des raisons pour laquelle la pralidoxime apparaît aujourd'hui dépassée par des oximes de conception plus récente et est en passe d'être remplacée par l'HI-6 dans l'AIBC du SSA (Ineurope®) ainsi que dans les protocoles de traitement des intoxications par les NOP élaborés par les armées étrangères. Par ailleurs, la pralidoxime pénètre difficilement la BHE et par conséquent, son activité sur les acétylcholinestérases centrales est très limitée.

L'hypothèse selon laquelle l'administration conjointe d'atropine, améliorerait le passage de la pralidoxime au niveau central, est controversée (21).

L'administration d'une dose de 10 mg/kg de pralidoxime en intramusculaire, conduit à une concentration sanguine supérieure à 4 mg/L en cinq à dix minutes et qui se maintient environ une heure. Les effets secondaires notables observés de cette oxime sont : des étourdissements, une vision brouillée, une diplopie, une difficulté d'accommodation, des nausées et des céphalées (22).

## La trimédoxime (TMB-4).

La trimédoxime synthétisée en 1957 est également active dans le traitement de l'intoxication par le tabun, en plus du sarin et du VX. Cependant, il s'agit de l'oxime la plus toxique, car sa dose létale 50 ($DL_{50}$) chez la souris, est trois fois plus faible que celle de l'obidoxime, quatre fois plus faible que celle de la pralidoxime et huit fois plus faible que celle de l'HI-6 (23). Elle présente toutefois une forte efficacité, en lien étroit avec sa toxicité, contre les pesticides organophosphorés. Son efficacité contre le tabun est supérieure à celles des trois oximes actuellement commercialisées.

## L'obidoxime (LüH-6).

L'obidoxime a été synthétisée en 1964 par l'équipe d'Hagedorn à Freiburg (Allemagne). Par rapport à la pralidoxime, elle présente un intérêt certain vis-à-vis de la réactivation des acétylcholinestérases inhibées par les pesticides organophosphorés. En dehors de cette particularité d'action, elle possède le même spectre d'activité que la trimédoxime concernant les cholinestérases inhibées par les NOP, si ce n'est qu'elle semblerait active lorsqu'elle est co-administrée avec de l'atropine, chez des cochons d'Inde prétraités par de la pyridostigmine et intoxiqué par du soman.

En revanche, son action est limitée lors des intoxications par le cyclosarin, mais son efficacité vis-à-vis du tabun est supérieure à celle de la trimédoxime et de l'HI-6. Une posologie de 5 mg/kg administrée en intramusculaire conduit en cinq minutes à des concentrations sanguines supérieures à 4 mg/L, se maintenant environ trois heures (22).

Des effets secondaires sont cependant notés comme : une pâleur, des nausées, une sensation de brûlure, des céphalées et des paresthésies faciales. La toxicité hépatique de l'obidoxime est néanmoins plus faible que celle de la trimédoxime, même si elle représente tout de même 10 % des effets secondaires observés chez les patients traités par cette oxime (24).

L'obidoxime, employée en Allemagne, en Norvège, en Finlande et aux Pays-Bas est une oxime largement utilisée dans le cadre du traitement des intoxications aux pesticides organophosphorés (25). L'oxime K-27 appartenant à la série des K-oximes est actuellement à l'étude ; elle pourrait également être une bonne candidate dans cette indication thérapeutique (26).

## La méthoxime (MMB-4).

La méthoxime est en cours de développement aux États-Unis pour remplacer la pralidoxime. Elle est efficace dans les intoxications par le soman, le sarin, le cyclosarin et le VX mais pas lorsque le tabun est utilisé (20). Son efficacité demeure dix à mille fois plus faible que celle de l'HI-6 et de l'HLö-7 lorsque le toxique en cause est le cyclosarin ou le VR (3). En revanche, sa toxicité est supérieure à celle de l'HI-6.

## L'HI-6.

L'HI-6 ou asoxime, synthétisée en 1966, appartient à la série des oximes d'Hagedorn. Elle a démontré une

efficacité, c'est-à-dire une réactivation supérieure à 10 % de l'activité des acétylcholinestérases (27), dans la réactivation des enzymes inhibées par le sarin, le cyclosarin, le soman, le VX ou le VR chez la souris (28).

Bien que son spectre d'action soit large, son efficacité est faible lors des intoxications par le tabun ainsi que par la majorité des pesticides organophosphorés. D'après Hamilton et al., l'HI-6 en association avec l'atropine et le diazépam, aurait cependant permis à des singes intoxiqués par le tabun de survivre (29). Les enzymes inhibées par le tabun sont particulièrement difficiles à réactiver du fait de la fonction amide de ce NOP qui diminue l'électrophilie de l'atome de phosphore, empêchant ainsi l'attaque nucléophile de l'enzyme par l'oxime. Comme les autres oximes, elle serait peu efficace lors d'intoxications par le soman.

Une injection intramusculaire de 250 mg ou de 500 mg, conduit à une concentration sanguine supérieure à 4 mg/L en quatre à six minutes. Cette concentration sanguine se maintient environ deux heures pour la plus faible posologie et plus de trois heures pour la plus élevée (22).

L'HI-6 est la moins toxique des oximes présentées. Elle existe sous forme de dichlorure et de méthylsulfonate dont les pharmacocinétiques sont similaires, ce dernier sel étant plus soluble. Le méthylsulfonate d'HI-6 semble, à ce jour, représenter le meilleur compromis entre efficacité et toxicité d'une oxime dans le cadre du traitement d'une intoxication par les NOP exceptés, le tabun et le soman.

Son instabilité en solution aqueuse, nécessite de la conserver sous forme lyophilisée jusqu'à sa reconstitution extemporanée avant injection. Le groupement isonicotinamide, présent dans la structure de l'HI-6 et initialement introduit pour en diminuer sa toxicité, aurait une importance dans sa supériorité d'efficacité par rapport à la pralidoxime et à l'obidoxime dans le traitement de l'intoxication par le VX, le VR, le sarin ou le cyclosarin (15). La différence d'efficacité entre l'HI-6 et la pralidoxime serait également due à l'interaction du second cycle pyridinique de l'HI-6, avec le site périphérique allostérique de l'acétylcholinestérase, permettant ainsi une meilleure orientation de l'oxime (30).

Les oximes de la série H auraient un effet réactivateur sur les cholinestérases centrales puisqu'elles antagonisent l'hypothermie centrale induite par le sarin (18).

En France, le *Common Technical Document* (CTD) concernant le dépôt d'AMM visant à remplacer la pralidoxime, dont l'action reste modérée, par l'HI-6 dans l'AIBC du SSA est en cours de constitution. L'emploi de cette oxime dans le cadre de la lutte contre l'intoxication aux NOP est déjà autorisé aux États-Unis, au Canada et en Suède.

### *L'HLö-7.*

L'HLö-7, dont le nom lui fut donné en l'honneur d'Ilse Hagedorn et Marianne Löffler, qui l'ont synthétisée en Allemagne en 1986, possède une efficacité supérieure à l'HI-6 dans les intoxications par le tabun et le VX (18).

En revanche, son activité *in vivo*, co-administrée à de l'atropine est plus faible que celle de l'HI-6 lorsque le sarin, le sarin cyclohexylique ou le soman sont utilisés.

La toxicité de l'HLö-7 est environ trois fois plus élevée que celle de l'HI-6. Tout comme l'HI-6, l'HLö-7 présente une instabilité en milieu aqueux nécessitant un conditionnement du médicament sous forme lyophilisée.

Globalement, sans évoquer leur toxicité et leur disponibilité en France et tout en sachant que les études sont le plus souvent réalisées chez l'animal ou *in vitro*, l'efficacité des oximes en fonction des différents NOP utilisés, pouvant être proposée est représenté dans le tableau II.

**Tableau II. Efficacité des oximes en fonction du NOP.**

| NOP | Soman |
|---|---|
| Tabun | LüH-6, TMB-4 et HLö-7 mais pas HI-6, MMB-4 et 2-PAM. |
| Soman | MMB-4 mais efficacité limitée. |
| Sarin | HI-6, TMB-4, MMB-4 et 2-PAM. |
| Cyclosarin | MMB-4 et HI-6 essentiellement. Très peu d'efficacité pour les autres. |
| VX | TMB-4, LüH-6, MMB-4, HI-6, HLö-7et 2-PAM. |
| VR | HI-6, MMB-4 et LüH-6. |

## Conclusion.

Aucune oxime n'est efficace contre tous les NOP et encore moins contre tous les composés organophosphorés comprenant la majorité des pesticides. Le choix d'une oxime à visée thérapeutique, résulte d'un compromis entre son efficacité et sa toxicité, selon la probabilité du risque encouru, lequel dépend du contexte d'emploi. Le spectre d'action des oximes varie selon de nombreux paramètres, tels que la concentration, étroitement liée à la toxicité de la molécule. La nature de l'oxime influence d'une part, le phénomène de vieillissement des enzymes et d'autre part, son pouvoir de réactivation des cholinestérases.

Actuellement, l'HI-6 semble la meilleure candidate dans le cadre du traitement d'une intoxication aux NOP et elle devrait remplacer à terme la pralidoxime dans l'AIBC fabriqué par la PCA. En effet, bien que présentant une faiblesse d'action vis-à-vis du tabun, elle est efficace contre de nombreux agents notamment le VX et le VR qui sont des toxiques de guerre présentant une place importante dans la menace chimique, du fait de leur haute toxicité et de leur caractère persistant. Cependant, la menace terroriste peut aussi faire appel à des toxiques plus volatils comme ce fut le cas à Tokyo.

L'utilisation thérapeutique d'une oxime requiert une certaine stabilité, en vue de trouver une formulation galénique adaptée. Ce point constitue la limite dans le choix des oximes bispyridiniques comme l'HI-6, puisque leur faible stabilité en solution aqueuse nécessite une conservation du médicament sous forme sèche.

## RÉFÉRENCES BIBLIOGRAPHIQUES


1. Worek F, Thiermann H, Szinicz L, Eyer P. Kinetic analysis of interactions between human acetylcholinesterase, structurally different organophosphorus compounds and oximes. Biochem Pharmacol. 2004;6 (11):2237-48.
2. Masson P, Nachon F, Lockridge O. Structural approach to the aging of phosphylated cholinesterases. Chem Biol Interact. 2010: 187(1-3):157-62.
3. Luo C, Tong M, Maxwell DM, Saxena A. Comparison of oxime reactivation and aging of nerve agent-inhibited monkey and human acetylcholinesterases. Chem Biol Interact. 2008;175(1-3):261-6.
4. Trovaslet-Leroy M, Musilova L, Renault F, Brazzolotto X, Misik J, Novotny L, et al. Organophosphate hydrolases as catalytic bioscavengers of organophosphorus nerve agents. Toxicol Lett. 2011;206(1):14-23.
5. Øydvin OK, Tansø R, Aas P. Pre-junctional effects of oximes on [3H]-acetylcholine release in rat hippocampal slices during soman intoxication. Eur J Pharmacol. 2005;516(3):227-34.
6. Karasova JZ, Bajgar J, Jun D, Pavlikova R, Kuca K. Time-course changes of acetylcholinesterase activity in blood and some tissues in rats after intoxication by Russian VX. Neurotox Res. 2009;16(4):356-60.
7. Sakurada K, Matsubara K, Shimizu K, Shiono H, Seto Y, Tsuge K, et al. Pralidoxime iodide (2-PAM) penetrates across the blood-brain barrier. Neurochem Res. 2003;28(9):1401-7.
8. Kalisiak J, Ralph EC, Zhang J, Cashman JR. Amidine-oximes: reactivators for organophosphate exposure. J Med Chem. 2011.
9. Mercey G, Verdelet T, Saint-André G, Gillon E, Wagner A, Baati R, et al. First efficient uncharged reactivators for the dephosphylation of poisoned human acetylcholinesterase. Chem Commun (Camb). 2011;47(18):5295-7.
10. Shih TM, Skovira JW, O'Donnell JC, McDonough JH. *In vivo* reactivation by oximes of inhibited blood, brain and peripheral tissue cholinesterase activity following exposure to nerve agents in guinea pigs. Chem Biol Interact. 2010;187(1-3):207-14.
11. Aurbek N, Thiermann H, Szinicz L, Eyer P, Worek F. Analysis of inhibition, reactivation and aging kinetics of highly toxic organophosphorus compounds with human and pig acetylcholinesterase. Toxicology. 2006;224(1-2):9.
12. Carpentier P, Delamanche IS, Le Bert M, Blanchet G, Bouchaud C. Seizure-related opening of the blood-brain barrier induced by soman: Possible correlation with the acute neuropathology observed in poisoned rats. NeuroToxicology. 1990;11:493-508.
13. Ashani Y, Bhattacharjee AK, Leader H, Saxena A, Doctor BP. Inhibition of cholinesterases with cationic phosphonyl oximes highlights distinctive properties of the charged pyridine groups of quaternary oxime reactivators. Biochem Pharmacol. 200366(2):191-202.
14. De Jong LP, Verhagen MA, Langenberg JP, Hagedorn I, Löffler M. The bispyridinium-dioxime HLö-7. A potent reactivator for acetylcholinesterase inhibited by the stereoisomers of tabun and soman. Biochem Pharmacol. 1989;38(4):633-40.
15. Maxwell DM, Koplovitz I, Worek F, Sweeney RE. A structure activity analysis of the variation in oxime efficacy against nerve agents. Toxicol Appl Pharmacol. 2008,231:157-64.
16. Pohanka M, Jun D, Kuca K. Amperometric Biosensor for Evaluation of Competitive Cholinesterase Inhibition by the Reactivator HI-6. Anal Lett. 2007;40(12):2351-9.
17. Antonijevic B, Stojiljkovic MP. Unequal efficacy of pyridinium oximes in acute organophosphate poisoning. Clin Med Res. 2007;5(1):71-82.
18. Stojiljkovic MP, Jokanovic M. Pyridinium oximes: rationale for their selection as causal antidotes against organophosphate poisonings and current solutions for auto-injectors. Arh Hig Rada Toksikol. 2006;57(4):435-43.
19. Burnat P, Renaudeau C, Ceppa F, Gidenne S, Vaillant C, Almeras D et al. Attentat au sarin dans le métro de Tokyo. Medecine et Armées. 2001;29:(1):33-4.
20. Kuca K, Jun D, Bajgar J. Currently used cholinesterase reactivators against nerve agent intoxication: comparison of their effectivity *in vitro*. Drug Chem Toxicol. 2007;30(1):31-40.
21. Hasan MY, Petroianu GA, Sheen R, Nurulain SM, Lorke D, Kalasz H. "Paraoxon and atropine do not increase pralidoxime (PXX) passage through the blood brain barrier (BBB)." J. Clin. Pharmacol. 2007;47:1206.
22. Jokanovic M. Medical treatment of acute poisoning with organophosphorus and carbamate pesticides. Toxicol Letters. 2009;190(2):107-15.
23. Clement JG. Toxicology and pharmacology of bispyridinium oximes. Insight into the mechanism of action vs soman poisoning *in vivo*. Fundam. appl. Toxic. 1981;1:193-202.
24. Eyer, P. The role of oximes in the management of organophosphorus pesticide poisoning. Toxicol Rev. 2003;22:165-90.
25. Thiermann H, Szinicz L, Eyer F, Worek F, Eyer P, Felgenhauer N et al. Modern strategies in therapy of organophosphate poisoning. Toxicol Lett. 1999;107:233-9.
26. Nurulain SM, Lorke DE, Hasan MY, Shafiullah M, Kuca K, Musilek K et al. Efficacy of eight experimental bispyridinium oximes against paraoxon-induced mortality: comparison with the conventional oximes pralidoxime and obidoxime. Neurotox Res. 2009;16:60-7.
27. Bajgar J, Fusek J, Kuca K, Bartosova L, Jun D. Treatment of organophosphate intoxication using cholinesterase reactivators: facts and fiction. Mini Rev Med Chem. 2007;7:461-6.
28. Kuca K, Musilek K, Jun D, Pohanka M, Zdarova Karasova J, Novotny L et al. Could oxime HI-6 really be considered as "broad-spectrum" antidote ? J. Appl. Biomed. 2009;7:143-9.
29. Hamilton MG, Lundy PM. HI-6 therapy of soman and tabun poisoning in primates and rodents. Arch Toxicol. 1989;63:144-9.
30. Ashani Y, Radic Z, Tsigelny I, Vellom DC, Pickering NA, Quinn DM, et al. Amino acid residues controlling reactivation of organophosphonyl conjugates of acetylcholinesterase by mono- and bisquaternary oximes. J Biol Chem. 1995;270(11):6370-80.

# Reactivators of Acetylcholinesterase Inhibited by Organophosphorus Nerve Agents

G. Mercey, T. Verdelet, J. Renou, M. Kliachyna, R. Baati, **F. Nachon**, L. Jean, P-Y. Renard

Accounts of Chemical Research 45 (2012) 756-766

ACCOUNTS
of chemical research

# Reactivators of Acetylcholinesterase Inhibited by Organophosphorus Nerve Agents

GUILLAUME MERCEY,[§,†] TRISTAN VERDELET,[§,†] JULIEN RENOU,[§,†] MARIA KLIACHYNA,[∥] RACHID BAATI,[∥] FLORIAN NACHON,[⊥] LUDOVIC JEAN,[§,†] AND PIERRE-YVES RENARD*[,§,†,‡]

[§]*Equipe de Chimie Bio-Organique, COBRA - CNRS UMR 6014 & FR 3038, Rue Lucien Tesnière, 76131 Mont-Saint-Aignan, France,* [†]*Université de Rouen, Place Emile Blondel, 76821, Mont-Saint-Aignan, France,* [∥]*Faculté de Pharmacie, Université de Strasbourg, CNRS UMR 7199, Laboratoire des Systèmes Chimiques Fonctionnels, 74 route du Rhin, BP 60024, 67401 Illkirch, France,* [⊥]*Département de Toxicologie, Institut de Recherche Biomédicale des Armées, 24 Avenue des Maquis du Grésivaudan, BP87, 38702 La Tronche, France, and* [‡]*Institut Universitaire de France, 103 Boulevard Saint Michel, 75005 Paris, France*

RECEIVED ON NOVEMBER 9, 2011

## CONSPECTUS

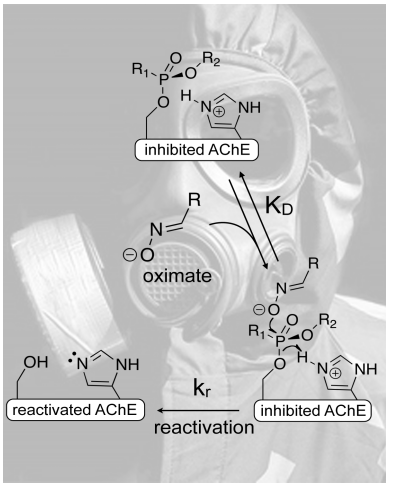


Since the September 11, 2001, terrorist attacks in the United States, the specter of a chemical threat against civilian populations has renewed research interest in chemical warfare agents, their mechanisms of action, and treatments that reverse their effects. In this Account, we focus specifically on organophosphorus nerve agents (OPNAs). Although some OPNAs are used as pest control, the most toxic chemicals in this class are used as chemical warfare agents in armed conflicts. The acute toxicity of OPNAs results from the irreversible inhibition of acetylcholinesterase (AChE, EC 3.1.1.7) via the formation of a covalent P−O bond at the serine hydroxyl group in the enzyme active site. AChE breaks down the neurotransmitter acetylcholine at neuronal synapses and neuromuscular junctions. The irreversible inhibition of AChE causes the neurotransmitter to accumulate in the synaptic cleft, leading to overstimulation of cholinergic receptors, seizures, respiratory arrest, and death.

The current treatment for OPNA poisoning combines an antimuscarinic drug (e.g., atropine), an anticonvulsant drug (e.g., diazepam), and an AChE reactivator of the pyridinium aldoxime family (pralidoxime, trimedoxime, obidoxime, HI-6, HLö-7). Because of their high nucleophilicity, oximes can displace the phosphyl group from the catalytic serine, thus restoring the enzyme's catalytic activity. During 50 years of research in the reactivator field, researchers have synthesized and tested numerous structural modifications of monopyridinium oximes and bispyridinium oximes. In the past decade, medicinal chemists have focused their research on the more efficient bispyridinium reactivators, but all known reactivators have several drawbacks. First, due to their permanent positive charge, they do not cross the blood−brain barrier (BBB) efficiently and do not readily reactivate AChE in the central nervous system. Second, no single oxime is efficient against a wide variety of OPNAs. Third, oximes cannot reactivate "aged" AChE.

This Account summarizes recent strategies for the development of AChE reactivators capable of crossing the BBB. The use of nanoparticulate transport and inhibition of P-glycoprotein efflux pumps improves BBB transport of these AChE reactivators. Chemical modifications that increased the lipophilicity of the pyridinium aldoximes, the addition of a fluorine atom and the replacement of a pyridyl ring with a dihydropyridyl moiety, enhances BBB permeability. The glycosylation of pyridine aldoximes facilitates increased BBB penetration via the GLUT-1 transport system. The development of novel uncharged reactivators that can move efficiently across the BBB represents one of the most promising of these new strategies.



Published on the Web 02/23/2012 www.pubs.acs.org/accounts
10.1021/ar2002864 

## Introduction

Poisoning by organophosphorus-based pesticides is a serious public health issue with over 200 000 fatalities annually worldwide.[1] Organophosphorus warfare agents present a persistent threat to the general population as a consequence of armed conflicts (e.g., Gulf War) and terrorist attacks (e.g., subway attacks in Japan in 1995). These compounds irreversibly inhibit acetylcholinesterase (AChE, EC 3.1.1.7), which plays an essential role in neurotransmission. Over the last 60 years, pyridinium oxime compounds have been widely used as antidotes to treat these intoxications.[2,3] Despite decades of research in this field, there is no efficient and general reactivator for organophosphorus-inhibited AChE. Interest in this field has increased since the September 2001 terrorist attacks in the U.S.A. The purpose of this Account is to highlight the important and recent advances in research on organophosphorus-inhibited AChE.

We will focus most of the discussion on the reactivation of human AChE (hAChE) inhibited by the highly toxic organophosphorus chemical warfare agents. Details on the reactivation of AChE after organophosphorus pesticide poisoning have been recently reviewed extensively.[4] In the first section, the organophosphorus nerve agents will be discussed, as well as the mechanism responsible for AChE irreversible inhibition and the effects caused by this inhibition. In the next section, the main pyridinium oxime reactivators and their mechanism of reactivation will be discussed. Then, the structural modifications of pyridinium and bis-pyridinium oximes, developed in the past decade, will be summarized. Finally, new concepts focused on AChE reactivation in the brain will be discussed.

## Inhibition of AChE by Organophosphorus Nerve Agents

The first generation of organophosphorus (OP) nerve agents, called G-agents (German agents), share a common $O{=}P^{V}(O{-}R)$ moiety. They include the cyanophosphoramidate, tabun (GA), and the methylfluorophosphonates, sarin (GB), soman (GD), and cyclosarin (GF) (Figure 1). After WWII, methylphosphothioates called V-agents (venomous agents) were invented: VX (Great Britain), RVX (Russian isomer), and CVX (Chinese isomer) (Figure 1). V-agents differ from G-agents by their lower volatility, their higher persistency in the environment, and their higher toxicity.[5]

The acute toxicity of OPs is due to their rapid inhibition of AChE. This enzyme is a serine hydrolase and is responsible for the breakdown of the neurotransmitter acetylcholine at

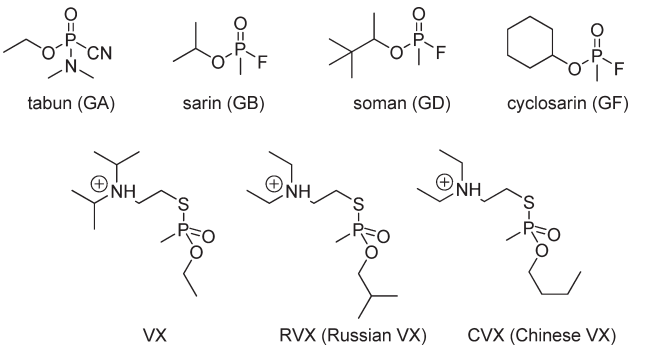


**FIGURE 1.** Chemical structures of the main organophosphorus nerve agents.

neuronal synapses and neuromuscular junctions.[6] The inhibition of AChE leads to an accumulation of acetylcholine, resulting in permanent saturation of muscarinic and nicotinic receptors and ultimately a system-wide cholinergic crisis. Among the many symptoms that appear upon hyperstimulation of the cholinergic system are paralysis, seizures, and respiratory failure causing death.

During normal function of AChE, a serine–histidine–glutamate triad, located in the active site of the enzyme, catalyzes the hydrolysis of acetylcholine (Figure 2A). The catalytic mechanism consists of two steps: (1) the nucleophilic serine attacks acetylcholine to form a tetrahedral transition state that collapses to the acetyl-enzyme with release of choline; (2) a water molecule, activated by the nearby histidine, attacks the acetylserine leading to the formation of a second tetrahedral transition state that collapses to the free enzyme and acetic acid. This mechanism is extremely efficient; AChE hydrolyzes more than $10^4$ molecules of acetylcholine per second.[7]

The mechanism of AChE inhibition by OPs is similar to the initial step of hydrolysis. Once the OP has reached the bottom of the active site gorge, the nucleophilic serine attacks the phosphorus atom, forming a bipyramidal transition state, which is followed by the departure of the leaving group and the formation of the phosphylserine (Figure 2B). The phosphyl adduct is a remarkable mimic of the transition state of the initial step of hydrolysis. However, in the second step, the catalytic histidine cannot fulfill the role of water activation because it is either forced into a nonproductive conformation (e.g., VX[8] and tabun conjugates[9]) or shielded from water (e.g., soman conjugate[10]). Therefore the spontaneous hydrolysis of the phosphylenzyme is extremely slow, varying from hours for dimethylphosphoryl conjugates[11] to days for V-agent AChE conjugates.[12]

Spontaneous hydrolysis of the conjugate is in competition with a time-dependent intramolecular reaction yielding

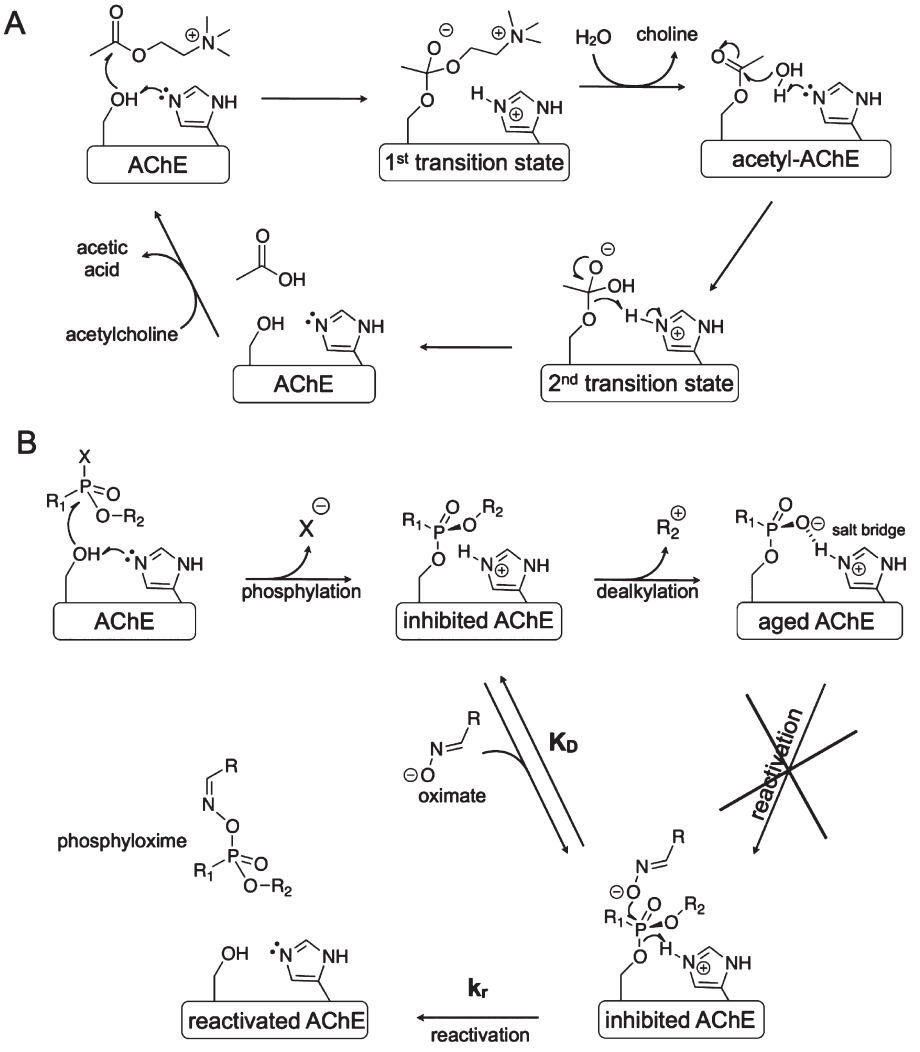


**FIGURE 2.** (A) Mechanism of acetylcholine hydrolysis by AChE. (B) Mechanism of AChE inhibition by organophosphorus nerve agents, aging, and reactivation by oximes.

an "aged" form of the conjugate.[13] The aging reaction of AChE conjugates is generally a dealkylation of the alkoxy substituent present on the phosphorus atom, and it yields a phosphonate adduct (Figure 2B). The aging half-time are 2−4 min for soman, 5 h for sarin, 46 h for tabun, and 48 h for VX.[14] The resulting phosphonic oxyanion forms a salt bridge with the protonated triad histidine[15] that strongly stabilizes the conjugate.[9] Moreover, the phosphonic oxyanion prevents any negatively charged nucleophile from approaching the phosphorus atom. Consequently, aged phosphyl-AChE conjugates do not get hydrolyzed.

## Known Antidotes against OP Poisoning

In the 1950s, Wilson showed that hydroxylamine[16] and nicotinhydroxamic acid[17] were able to reactivate diethylphosphoryl AChE. These initial findings quickly led to the discovery that oximes,[18] 2-oxoaldoximes,[19] and especially 2-pyridinium aldoxime (2-PAM; Figure 3)[20] were powerful reactivators.

The efficiency of reactivators can be estimated by the second-order rate constant for reactivation, $k_{r2}$, which is the ratio of the reactivation rate constant ($k_r$) and the approximate dissociation constant of the reactivator/phosphyl-AChE complex ($K_D$) (Figure 2B).[15] The good activity of 2-PAM was attributed to strong binding of the positively charged pyridinium to the enzyme active site and proper orientation of the oxime group for displacement of the phosphyl moiety. The corresponding oxime, 4-PAM, was less efficient than 2-PAM because its orientation was improper. It was hypothesized that combining 4-PAM with a ligand that is able to strongly bind to the enzyme could yield a compound with both better affinity and proper orientation

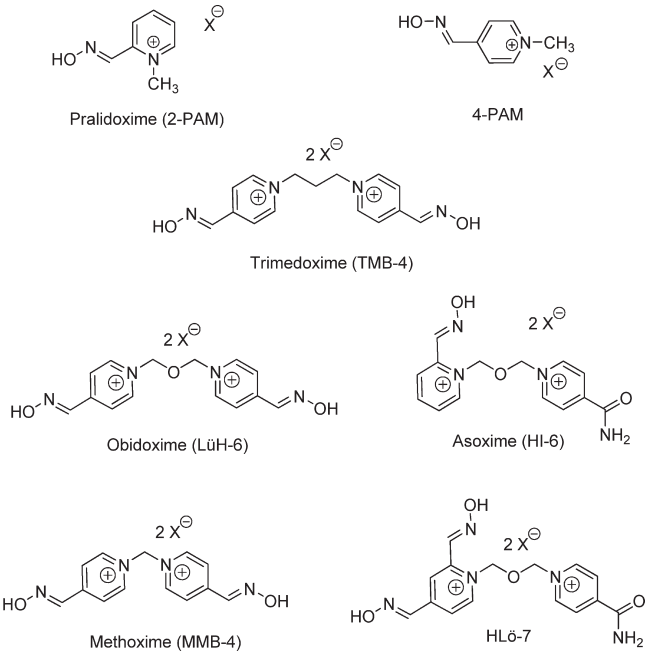


**FIGURE 3.** Chemical structures of the main pyridinium aldoxime reactivators.

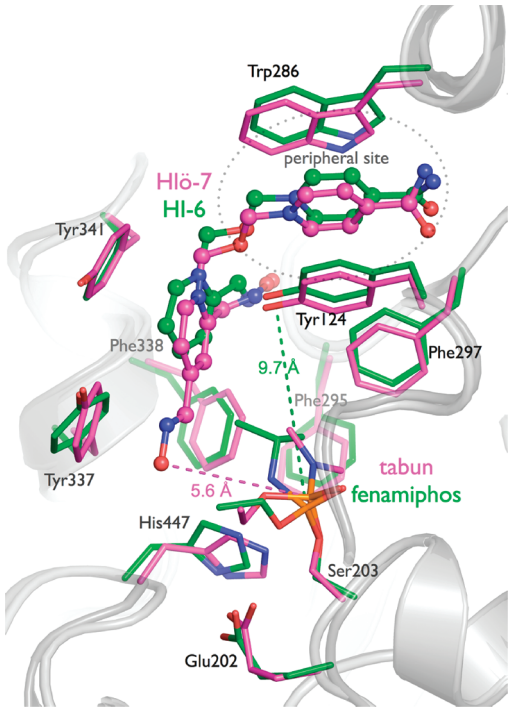


**FIGURE 4.** Active site view of HLö-7–tabun–mouse AChE (carbon atoms in magenta) and HI-6–fenamiphos–mouse AChE (carbon atoms in green). Ser203 and His447 are components of the catalytic triad. Tyr124 and Trp286 are components of the peripheral site at the entrance of the active site gorge.

of the oxime group in the AChE catalytic site. Following this reasoning, the first bispyridium aldoxime, TMB-4 (Figure 3), was prepared. TMB-4 proved to be superior to both 2-PAM and 4-PAM due to an improved affinity.[21] Subsequently, other aldoximes were synthesized based on the TMB-4 structure: LüH-6,[22] HI-6,[23] and HLö-7[24] (Figure 3). Though the bispyridinium aldoximes are effective reactivators, none is a universal reactivator. Their efficiency of reactivation varies greatly with the nature of the phosphyl group on the inhibited AChE.[15] LüH-6 is generally considered as the best reactivator for pesticides (dialkylphosphoryl-AChE).[25] HI-6 is active against soman and VX[15] but is inefficient against tabun.[26] 4-Substituted oximes like TMB-4, HLö-7, and LüH-6 are efficient against tabun inhibition,[27] but their reactivation rates are very slow compared with those obtained for VX-inhibited AChE.[15] This poor reactivity is related to the weak electrophilicity and steric hindrance of the phosphoramidyl-AChE adduct created by tabun.[27]

What is worse, all aged conjugates are completely refractory toward oxime reactivation. The only viable strategy for reactivation of aged adducts seems to be modification of the phosphonic moiety by realkylation *in situ*, using powerful and specific alkylating agents.[13]

The p$K_a$ of oximes is also of pivotal importance since the reactive species is the oximate. To be effective, the oxime must remain partially deprotonated in the range of physiological pH; full deprotonation is unwanted because the reactivity is compromised by the cost in the desolvation energy for formation of the oximate anion.[28] The conjugated ring systems of 2- and 4-alkylpyridinium aldoximes (e.g., 2-PAM, HI-6, and obidoxime) increase the acidity of these oximes yielding p$K_a$ values ranging between 7.3 and 8.0.[28]

The recent X-ray structures of HLö-7 and HI-6 complexed with phosphoramidyl-AChE illustrate the prototypic binding of a bisquaternary oxime to tabun-inhibited enzyme. Association is predominantly via $\pi-\pi$ and cation$-\pi$ interactions.[29,30] One pyridinium moiety is stacked between the aromatic residues of the peripheral site at the entrance of the active site gorge, and the second pyridinium interacts with tyrosines in the middle of the active site gorge (Figure 4). The phosphorus–oximate distance is 5.6 Å for HLö-7 and 9.7 Å for HI-6. The oxime functions are neither in a proper orientation nor at a proper distance to attack the phosphorus atom. These observations suggest that the structure of oxime reactivators could be substantially improved. One such improvement might involve coupling a peripheral site ligand to a nucleophilic function.[31] A major difficulty in designing new reactivators is that the details of the reactivation mechanism are not yet well understood. Some structural work suggests that deprotonation of the oxime is assisted by the catalytic histidine[32] or by a

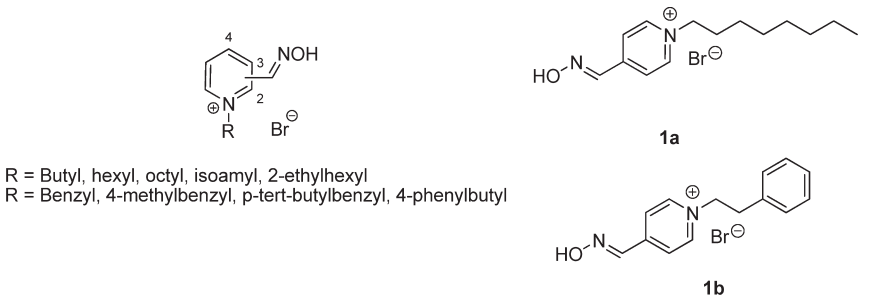


**FIGURE 5.** PAM analogues.

bridging water molecule.[33] It has also been suggested that the nucleophile does not have to attack the face of the phosphyl group opposite to the serine (apical position), but it could also attack the vicinal face if it is open.[34] The wealth of new structural information on complexes of inhibited-AChE and oximes must be considered when designing new generations of reactivators.

## Structural Modifications of Monoquaternary and Bisquaternary Pyridinium AChE Reactivators

Monoquaternary pyridinium reactivators are known to be weak AChE reactivators compared with the bisquaternary reactivators. Still, analogues of monoquaternary pralidoxime (PAM) have been synthesized in an effort to improve their reactivity. Their reactivation abilities were evaluated *in vitro* on organophosphorus inactivated human AChE (hAChE) (Figure 5).[35] These studies have shown that elongation of the side chain (to improve lipophilicity) or the presence of an aromatic group in the side chain (to increase interactions with AChE residues via $\pi-\pi$ interactions) did not improve their reactivation ability compared with 2-PAM (the relative reactivation activity to 2-PAM is 46% and 44% for **1a** and **1b**, respectively). These lipophilic derivates **1a** and **1b** were shown to penetrate the blood−brain barrier (BBB) with a penetration ratio of 30% and 3%, respectively.[36] However, the usefulness of these compounds is limited due to their significant toxicity. Monopyridinium oximes were studied less frequently following the realization that bispyridinium oximes were better reactivators.

To date, the principal modifications carried out on bispyridinium structures have included modifying the position of the oxime on the pyridinium ring, the introduction of various substituents, and especially alterations to the nature and the length of the linker between the pyridinium rings.

To test the effect of the linker chain length on the reactivation of tabun-inhibited AChE, analogues of trimedoxime

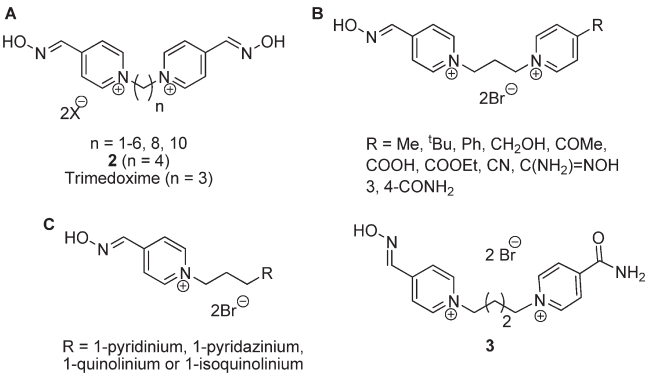


**FIGURE 6.** Analogues of trimedoxime (TMB-4) evaluated in the reactivation of tabun-inhibited hAChE.

(TMB-4) were synthesized. It was determined that the optimal distance between two 4-pyridinium aldoximes was three or four carbons (Figure 6A).[37] Mono-oxime bispyridinium analogues of TMB-4 were also evaluated as potential hAChE reactivators. The nonoxime pyridinium ring was substituted in position 4 with various groups (Figure 6B) or was replaced with a heteroaromatic ring (Figure 6C). Some of these analogues (R = COMe, Ph, or C(NH$_2$)=NOH, refer to Figure 6B) had a slightly lower reactivation potency for tabun-inhibited hAChE than trimedoxime.[38] Of all the synthesized and evaluated analogues, only compound **3** (Figure 6)[39] was more efficient than trimedoxime at reactivating tabun-inhibited hAChE *in vitro* (5-fold more efficient).[40] Interestingly, the presence of a carbamoyl group influences the reactivation ability of the analogue by increasing its affinity for the organophosphorus-inhibited enzyme. Affinity is improved via hydrogen bond interactions with residues at the peripheral site of the enzyme. For example, compound **3** is 6-fold more efficient than compound **2** (Figure 6A) due to its increased affinity.

Modifications to the HI-6 and obidoxime structures have also been evaluated. The research teams of K. Kuča and J. Acharya have independently studied the effects on reactivation of introducing additional heteroatoms into the linker. It was hypothesized that a pair of oxygen atoms in the linker

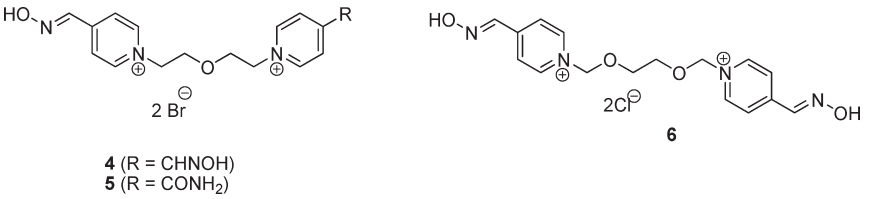


**FIGURE 7.** Structures of reactivators bearing one or two oxygen atoms in the linker between the two pyridinium rings.

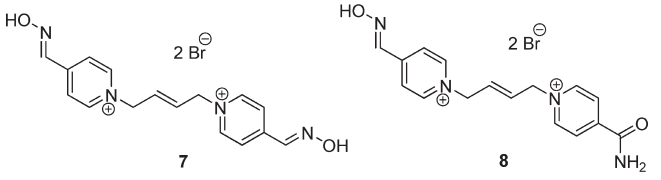


**FIGURE 8.** Reactivators bearing (*E*)- or (*Z*)-but-2-ene linkers between the two pyridinium rings.

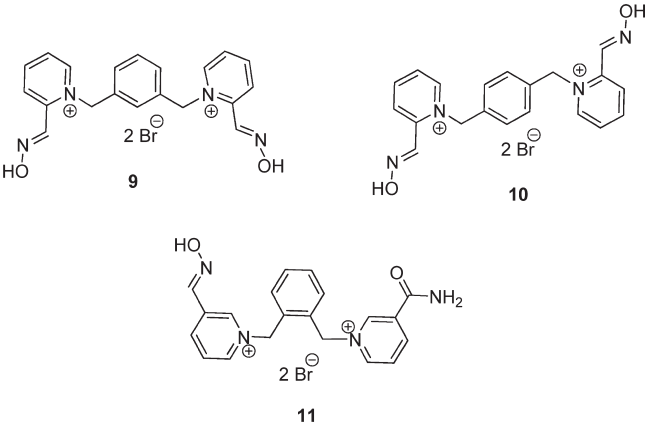


**FIGURE 9.** Reactivators bearing xylene-connecting linkers between the two pyridinium rings.

could interact better with residues in the AChE catalytic site through hydrogen bonds and thus increase reactivator's affinity toward the phosphylated enzyme.[41,42] Biological evaluation of **4** and **5** (Figure 7)[43] showed that the latter is 2-fold more efficient than trimedoxime for the reactivation of tabun-inhibited hAChE. On the other hand, Acharya et al. have prepared and evaluated symmetrical bispyridinium aldoximes with longer linkers bearing two oxygen atoms.[44] Among these compounds, **6** (Figure 7) showed a slightly better ability to reactivate sarin-inhibited hAChE than 2-PAM.

The inclusion of an unsaturated chain to connect the two pyridinium rings has also been evaluated. In comparison with its saturated analogue, **7** (Figure 8) is 2.5-fold more efficient at reactivating tabun-inhibited AChE due to a better affinity and reactivity, and it is 2-fold more efficient than trimedoxime.[40] Interestingly, the substitution of one of the oxime functions by a carbamoyl group dramatically increased the reactivation potency of **8** (5-fold more efficient than **7**).[45] Molecular docking studies have shown that the improved reactivity of **8** (compared with **3**) could be due to supplementary interactions of **8** with AChE, specifically edge-to-face interactions between the double bond and AChE aromatic residues.[46]

With the intention of increasing the reactivator's affinity toward the inhibited enzyme through cation$-\pi$ or $\pi-\pi$ interactions, bispyridinium compounds with xylene connecting linkers were synthesized and evaluated. Compounds **9** and **10** (Figure 9) were 6-fold less efficient than trimedoxime at reactivating tabun-inhibited AChE.[46] However, **10** reactivated 45% of sarin-inhibited hAChE in comparison to, respectively, 34% and 24% reactivation by 2-PAM and obidoxime at the concentration $10^{-3}$ M.[47] A total of 26 xylene-modified, monooxime-monocarbamoyl bispyridinium compounds were tested, and only structure **11** (Figure 9) displayed substantial reactivation potency, but it was 1.6-fold less efficient than trimedoxime at reactivating tabun-inhibited AChE. Moreover, it was 1.5-fold more toxic than trimedoxime.[46]

## Strategies for Blood–Brain Barrier Penetration

The blood–brain barrier (BBB) is composed of an endothelial cell layer, which separates the circulating blood and the brain's extracellular fluid. Tight junctions (TJ) between endothelial cells and limited pinocytic activity[48] make the BBB nearly impenetrable to viruses, bacteria, proteins, and polar molecules.[49] OP nerve agents, being small lipophilic molecules, can easily penetrate the BBB by free diffusion and thereby inhibit AChE in the central nervous system (CNS). However, commonly used reactivators are permanently charged cationic compounds that have difficulty in crossing the BBB.[50] For instance, the BBB penetration of 2-PAM (striatal extracellular/blood concentration ratio) has been estimated to be only approximately 10% by *in vivo* rat brain microdialysis technique with HPLC/UV.[51] Therefore, oximes reactivate AChE in peripheral sites, but they are not effective in the CNS. Consequently they provide little to no protection against the neurological effects of OP exposure, which

includes seizures, convulsions, and behavioral and psychological changes. This dilemma prompted the development of oxime-based agents that can cross the BBB and reverse the effects of OP on AChE in the CNS.

A number of strategies have been developed to circumvent or disrupt the BBB. Direct injections into the brain,[52] local exposure to high-intensity focused ultrasound (HIFU),[53] and osmotic TJ opening (by hypertonic mannitol)[54] represent the most painful and invasive BBB disruption methods. Significant progress in BBB penetration has been achieved by using targeted nanoparticulate drug delivery. Obidoxime dichloride and both HI-6 dichloride monohydrate and HI-6 dimethanesulfonate bound to biodegradable human serum albumin (HSA) nanoparticles were able cross an in vitro BBB model.[55] In general, the oximes transported in nanoparticles exhibited a better reactivation of paraoxon-ethyl and sarin-inhibited AChE than free oximes, resulting from higher BBB crossing. For example, the concentration of HI-6 dimethanesulfonate loaded on NP-ApoE nanoparticles, measured across the BBB, was 44.6 $\mu$M compared with 15.2 $\mu$M for the free oxime (transport difference +193.16%).

Safe and effective modulation of transport across the BBB also represents an attractive approach for targeting drugs into the brain. Inhibition of the active efflux transporter P-glycoprotein (Pgp) located in the endothelial cell membranes was shown to improve the BBB permeability of HI-6.[56] Administration of tariquidar, a specific noncompetitive Pgp pump inhibitor, resulted in a 2-fold increase in HI-6 levels in the brain and, subsequently, twice as much AChE activity after 1 h of treatment, while HI-6 concentration in the blood was not affected. More recently, adenosine receptor (AR) signaling was shown to modulate BBB permeability *in vivo*, facilitating the entry of dextrans and antibodies to $\beta$-amyloid into the brain.[57] AR signaling may be a promising strategy for improvement in the BBB permeability of therapeutically important oximes.

Introduction of a fluorine atom into the heterocyclic ring of pyridinium oximes should enhance their lipophilicity. Increased lipophilicity would enable the oxime to more readily diffuse across the BBB increasing its AChE reactivation potency. According to computer-aided calculations, fluorinated 4-PAM analogues **12** and **13** (Figure 10) are more lipophilic than nonfluorinated 4-PAM. These predictions were confirmed by AChE reactivation experiments[58] and by assessment of BBB permeability using the parallel artificial membrane permeation assays (PAMPA) method.[59] In the PAMPA experiment, the fluorinated *N*-methyl-4-pyridinium oxime **12** exhibited higher permeability than

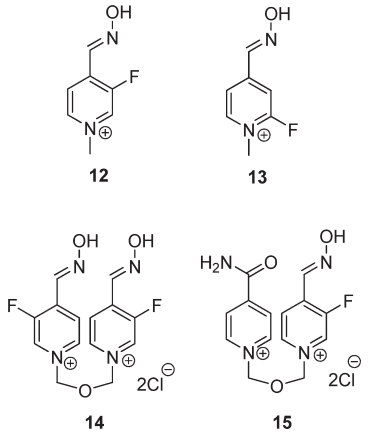


**12** **13** **14** **15**

**FIGURE 10.** Fluorinated mono- and bisquaternary pyridinium aldoximes.

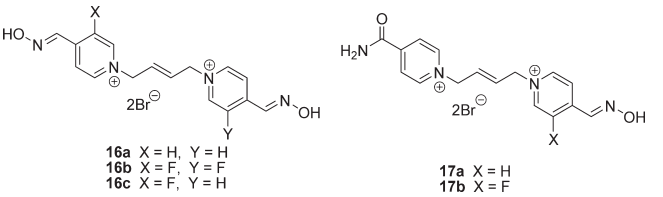


**16a** X = H, Y = H
**16b** X = F, Y = F
**16c** X = F, Y = H

**17a** X = H
**17b** X = F

**FIGURE 11.** Fluorinated analogues of **7** and **8**.

4-PAM (log $P_e = -7.2$ and $-6.4$ for 4-PAM and **12,** respectively, where $P_e$ is effective permeability). In the AChE reactivation experiments, compound **12** showed a reactivation potency toward the paraoxon-inhibited housefly AChE and bovine RBC (red blood cell) AChE that was 2.5-fold and 2.2-fold higher than 4-PAM, respectively.

Fluorinated oximes **14** and **15** both exhibited higher reactivation potencies toward paraoxon-inhibited housefly AChE than obidoxime and HI-6. However, toward paraoxon-inhibited bovine RBC AChE, obidoxime and HI-6 were more active than their fluorinated analogs **14** and **15**.[58] Membrane permeability measurements showed that the BBB permeability increased in proportion to the number of fluorine atoms. However, for the bis-pyridinealdoximes **16a**–**c** and **17a**,**b** (Figure 11) the permeability data did not correlate with the *in vitro* reactivation results.[59]

The modification of pyridine aldoxime with a glucose moiety was proposed to facilitate its BBB penetration. This was confirmed by Heldman et al. These sugar–oxime conjugates are thought to penetrate the BBB due to recognition of the glucose moiety by the facilitative glucose transporters.[60] The most active sugar–oxime, compound **18** (Figure 12), had a reactivation potency toward diisopropyl phosphorofluoridate (DFP)- and paraoxon-inhibited hAChE that was similar to that of 2-PAM.[61] Moreover, the sugar-derivative **19** showed lower toxicity than 4-PAM.

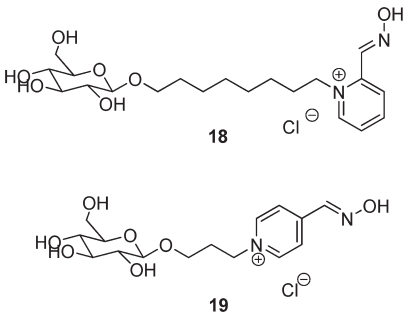


**FIGURE 12.** Sugar–Oximes.

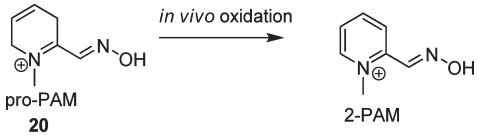


**FIGURE 13.** *In vivo* oxidation of pro-PAM.

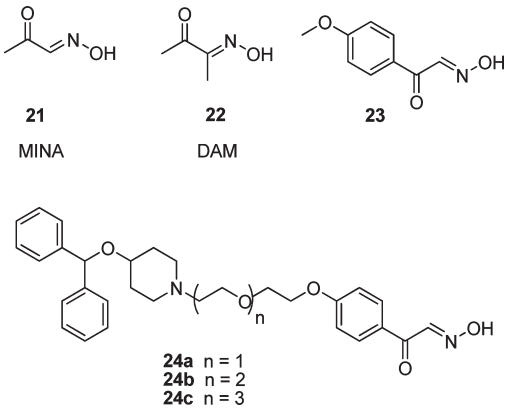


**FIGURE 14.** Neutral reactivators: α-ketoaldoximes and ketoxime.

Yet another approach is based on the use of a prodrug of 2-PAM, in which the highly charged pyridine ring is replaced with a significantly less charged dihydropyridyl moiety.[62,63] Once it has penetrated the BBB, pro-PAM **20** (Figure 13) rapidly undergoes oxidation in the brain to produce a functionally active quaternary oxime 2-PAM, which can then reactivate OP-inhibited AChE in the CNS. Disadvantages of this approach include the difficult synthesis of pro-PAM and its rather low stability due to autoxidation.

A novel strategy used to improve the BBB permeability is the synthesis of uncharged reactivators, which are capable of diffusing across the BBB and reactivating AChEs within the CNS. The neutral oximes monoisonitrosoacetone **21** (MINA) and diacetylmonooxime **22** (DAM) bearing the ketoaldoxime or ketoxime moiety as a reactivator function (Figure 14) are reported to cross the BBB, but their *in vitro* reactivation potency toward OP-inhibited AChE is much lower than that of 2-PAM and other quaternary oximes.[64,65]

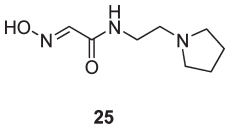


**FIGURE 15.** Uncharged hydroxyiminoacetamide **25**.

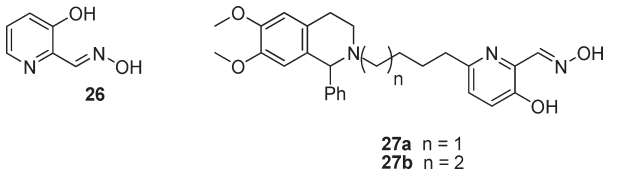


**FIGURE 16.** Phenyl-tetrahydroisoquinoline–pyridinaldoxime conjugates.

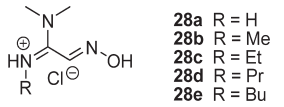


**FIGURE 17.** Amidine-oxime reactivators.

M. de Koning et al. proposed linking the reactivating α-ketoaldoxime moiety to a piperidine-derived peripheral site ligand (PSL) in order to increase the affinity for AChE (Figure 14).[66] The hybrids **24a–c** displayed a remarkable increase in reactivation potency (about 25–36% reactivation of sarin-inhibited hAChE) compared with the reference compound **23** (5% reactivation of sarin-inhibited hAChE), but they still remained inefficient reactivators compared with the commonly used pyridinium oximes. Replacing the ketone moiety with an amide one resulted in compound **25** (Figure 15), which showed reactivation kinetics superior to the reference uncharged compounds **21** and **22**, but in comparison with 2-PAM, this analogue still requires the further refinement.[67]

Nonquaternary pyridinealdoxime, compound **26** (Figure 16), exhibited a high potency for reactivation of VX-inhibited hAChE, but a low affinity toward inhibited enzyme.[68] Linking this oxime to phenyl-tetrahydroisoquinoline (a peripheral site ligand) to create compounds **27a**,**b** enhanced the affinity toward the enzyme, and increased reactivation of VX and tabun-inhibited hAChE. Rates of reactivation equaled and even exceeded those of HI-6, obidoxime, and HLö-7.[69] For example, **27b** is as efficient at reactivating VX–hAChE as HLö-7, which is currently the best bispyridinium oxime reactivator for VX–hAChE. Compound **27b** is also 5-fold more efficient at reactivating tabun-inhibited AChE than trimedoxime, which is currently the best bispyridinium oxime reactivator for tabun–hAChE.

Reactivation of inhibited AChE with pyridinium aldoximes (especially 4-pyridinium aldoximes) results inevitably in the formation of highly reactive phosphyloximes, which

in turn may inhibit AChE (recapture phenomenon).[70] This complication could be limited with oximes **27** due to the presence of the phenol moiety, which takes part in the formation of an isoxazole by a subsequent intramolecular and irreversible reaction.[71]

Amidine−oxime reactivators **28a**−**e** (Figure 17) are expected to possess increased lipophilicity.[72] Although these compounds were found to be less potent than 2-PAM in reactivation of AChE *in vitro*, they have the advantage of being more lipophilic than 2-PAM and were expected to be found at much higher concentrations in the brain. Two amidine-oximes, **28c** and **28d**, were efficacious *in vivo* and protected animals from CNS toxicity of nerve agent model compounds.

## Conclusion and Outlook

During the three decades since the discovery of monopyridinium and bispyridinium oximes as reactivators for OP-inhibited AChE, hundreds of variations have been synthesized and evaluated. All of those reactivators have three major drawbacks: (1) Their permanent positive charge prevents them from crossing the BBB to reactivate brain AChE. (2) They exhibit unequal reactivation abilities against AChE inhibited with different types of OP. (3) they are inefficient at reactivating "aged" AChE. Recent research has developed new and efficient uncharged reactivators that are able to cross the BBB. However, further research is necessary to discover a broad-spectrum reactivator suitable for the whole range of OPs. None of existing pyridinium oximes is a true broad-spectrum reactivator.[73] In the short term, a solution to the broad-spectrum reactivator issue would be to combine two or more oximes that have complementary activities. In this regard, combining obidoxime with HI-6 is a promising approach.[74] Regarding "aged" AChE, further research is necessary, since no existing reactivator is able to reactivate it. Further developments in this field will lead to better protection for the public from OPs used in both pest control and warfare.

*The authors gratefully acknowledge Lawrence M. Schopfer for the critical reading of the manuscript.*

BIOGRAPHICAL INFORMATION

**Guillaume Mercey** received his Ph.D. from the University of Caen (France) in 2009 with Dr. Mihaela Gulea. He is a postdoctoral fellow at the University of Rouen (France) with Professor Pierre-Yves Renard studying syntheses of uncharged AChE reactivators.

**Tristan Verdelet** and **Julien Renou** are completing their Ph.D. programs in bioorganic chemistry at the University of Rouen with Professor Pierre-Yves Renard. They are studying syntheses of uncharged AChE reactivators.

**Maria Kliachyna** received her Ph.D. in 2010 from the Institute of Organic Chemistry, NASU (Ukraine). She is a postdoctoral fellow with Dr. Rachid Baati and Dr. Alain Wagner at the University of Strasbourg (France) working on the syntheses of AChE reactivators.

**Rachid Baati** is a CNRS Researcher at the University of Strasbourg. His research is dedicated to the study of organic chemistry, bio-orthogonal and bio-organic chemistry (AChE reactivation) through methodology development and catalysis.

**Florian Nachon** is the leader of the structural enzymology team at the Department of Toxicology in the Army Institute of Biomedical Research in Grenoble (IRBA, France). His present research interests are focused on the development of nerve agent bioscavengers and the design of new generations of reactivators for inhibited cholinesterases.

**Ludovic Jean** is an assistant professor at the University of Rouen since 2008 in the research team of professor Pierre-Yves Renard. His research topics are focused on organophosphorus nerve agent and reversible AChE inhibitors.

**Pierre-Yves Renard** is a professor in bioorganic chemistry at the University of Rouen and has been the head of the bioorganic chemistry team at the Institut de Recherche en Chimie Organique Fine (IRCOF) since 2003. His research topics are focused on (1) organophosphorus nerve agent and reversible AChE inhibitors and (2) chemical tools for the understanding of biological mechanisms (bioconjugate chemistry, fluorescence, chemiluminescence, self-immolative linkers, probes for *in vivo* imaging).

FOOTNOTES

*To whom correspondence should be addressed. Fax: (+)33 2 35 52 29 59. E-mail: pierre-yves.renard@univ-rouen.fr.
The authors declare no competing financial interest.

REFERENCES

1 Eddleston, M.; Buckley, N. A.; Eyer, P.; Dawson, A.-H. Management of acute organophosphorus pesticide poisoning. *Lancet* **2008**, *371*, 597–607.
2 Jokanović, M.; Prostran, M. Pyridinium oximes as cholinesterase reactivators. Structure−activity relationship and efficacy in the treatment of poisoning with organophosphorus compounds. *Curr. Med. Chem.* **2009**, *16*, 2177–2188.
3 Jung, Y.-S.; Kuča, K. Current study on the development of bis-pyridinium oxime reactivators for the antidotal treatment of poisoning by toxic organophosphorus agents. *Curr. Org. Chem.* **2011**, *15*, 433–444.
4 Musilek, K.; Dolezal, M.; Gunn-Moore, F.; Kuča, K. Design, evaluation and structure−activity relationship studies of the AChE reactivators against organophosphorus pesticides. *Med. Res. Rev.* **2009**, *31*, 548–575.
5 Watson, A.; Opresko, D.; Young, R.; Hauschild, V.; King, J.; Bakshi, K. Organophosphate Nerve Agents. In *Handbook of Toxicology of Chemical Warfare Agents*; Gupta, R. C., Ed.; Academic Press Inc: London, 2009; Chapter 6.
6 Maxwell, D. M.; Brecht, K. M.; Koplovitz, I.; Sweeney, R. E. Acetylcholinesterase inhibition: Does it explain the toxicity of organophosphorus compounds? *Arch. Toxicol.* **2006**, *80*, 756–760.
7 Quinn, D. M. Acetylcholinesterase: Enzyme structure, reaction dynamics, and virtual transition states. *Chem. Rev.* **1987**, *87*, 955–979.
8 Millard, C. B.; Koellner, G.; Ordentlich, A.; Shafferman, A.; Silman, I.; Sussman, J. L. Reaction products of acetylcholinesterase and VX reveal a mobile histidine in the catalytic triad. *J. Am. Chem. Soc.* **1999**, *121*, 9883–9884.
9 Carletti, E.; Colletier, J.-P.; Dupeux, F.; Trovaslet, M.; Masson, P.; Nachon, F. Structural evidence that human acetylcholinesterase inhibited by tabun ages through O-dealkylation. *J. Med. Chem.* **2010**, *53*, 4002–4008.

10 Sanson, B.; Nachon, F.; Colletier, J.-P.; Froment, M.-T.; Toker, L.; Greenblatt, H. M.; Sussman, J. L.; Ashani, Y.; Masson, P.; Silman, I.; Weik, M. Crystallographic snapshots of nonaged and aged conjugates of soman with acetylcholinesterase, and of a ternary complex of the aged conjugate with pralidoxime. *J. Med. Chem.* **2009**, *52*, 7593–7603.

11 Worek, F.; Diepold, C.; Eyer, P. Dimethylphosphoryl-inhibited human cholinesterases: inhibition, reactivation, and aging kinetics. *Arch. Toxicol.* **1999**, *73*, 7–14.

12 Trovaslet-Leroy, M.; Musilova, L.; Renault, F.; Brazzolotto, X.; Misik, J.; Novotny, L.; Froment, M.-T.; Gillon, E.; Loiodice, M.; Verdier, L.; Masson, P.; Rochu, D.; Jun, D.; Nachon, F. Organophosphate hydrolases as catalytic bioscavengers of organophosphorus nerve agents. *Toxicol. Lett.* **2011**, *206*, 14–23.

13 Masson, P.; Nachon, F.; Lockridge, O. Structural approach to the aging of phosphylated cholinesterases. *Chem. Biol. Interact.* **2010**, *187*, 157–162.

14 Worek, F.; Thiermann, H.; Szinicz, L.; Eyer, P. Kinetic analysis of interactions between human acetylcholinesterase, structurally different organophosphorus compounds and oximes. *Biochem. Pharmacol.* **2004**, *68*, 2237–2248.

15 Segall, Y.; Waysbort, D.; Barak, D.; Ariel, N.; Doctor, B. P.; Grunwald, J.; Ashani, Y. Direct observation and elucidation of the structures of aged and nonaged phosphorylated cholinesterases by $^{31}$P NMR spectroscopy. *Biochemistry* **1993**, *32*, 13441–13450.

16 Wilson, I. B. Acetylcholinesterase. XI. Reversibility of tetraethyl pyrophosphate. *J. Biol. Chem.* **1951**, *190*, 111–117.

17 Wilson, I. B.; Meislich, E. K. Reactivation of acetylcholinesterase inhibted by alkylphosphates. *J. Am. Chem. Soc.* **1953**, *75*, 4628–4629.

18 Childs, A. F.; Davies, D. R.; Green, A. L.; Rutland, J. P. The reactivation by oximes and hydroxamic acids of cholinesterase inhibited by organo-phosphorus compounds. *Br. J. Pharmacol.* **1955**, *10*, 462–465.

19 Green, A. L.; Smith, H. J. The reactivation of cholinesterase inhibited with organophosphorus compounds. I. Reactivation by 2-oxoaldoximes. *Biochem. J.* **1958**, *68*, 28–31.

20 Wilson, I. B.; Ginsburg, B. A powerful reactivator of alkylphosphate-inhibited acetylcholinesterase. *Biochim. Biophys. Acta* **1955**, *18*, 168–170.

21 Wilson, I. B.; Ginsburg, S. Reactivation of alkylphosphate inhibited acetylcholinesterase by bis quaternary derivatives of 2-PAM and 4-PAM. *Biochem. Pharmacol.* **1959**, *1*, 200–206.

22 Luettringhaus, A.; Hagedorn, I. Quaternary hydroxyiminomethylpyridinium salts. The dischloride of bis-(4-hydroxyiminomethyl-1-pyridinium-methyl)-ether (lueh6), a new reactivator of acetylcholinesterase inhibited by organic phosphoric acid esters. *Arzneimittelforschung* **1964**, *14*, 1–5.

23 Hagedorn, I.; Gundel, W. H.; Schoene, K. Reactivation of phosphorylated acetylcholine esterase with oximes: contribution to the study of the reaction course. *Arzneimittelforschung* **1969**, *19*, 603–606.

24 Eyer, P.; Hagedorn, I.; Klimmek, R.; Lippstreu, P.; Löffler, M.; Oldiges, H.; Spöhrer, U.; Steidl, I.; Szinicz, L.; Worek, F. HLö-7 dimethanesulfonate, a potent bispyridinium-dioxime against anticholinesterases. *Arch. Toxicol.* **1992**, *66*, 603–621.

25 Worek, F.; Eyer, P.; Aurbek, N.; Szinicz, L.; Thiermann, H. Recent advances in evaluation of oxime efficacy in nerve agent poisoning by in vitro analysis. *Toxicol. Appl. Pharmacol.* **2007**, *219*, 226–234.

26 Worek, F.; Aurbek, N.; Koller, M.; Becker, C.; Eyer., P.; Thiermann, H. Kinetic analysis of reactivation and aging of human acetylcholinesterase inhibited by different phosphoramidates. *Biochem. Pharmacol.* **2007**, *73*, 1807–1817.

27 Carletti, E.; Aurbek, N.; Gillon, E.; Loiodice, M.; Nicolet, Y.; Fontecilla-Camps, J. C.; Masson, P.; Thiermann, H.; Nachon, F.; Worek, F. Structure-activity analysis of aging and reactivation of human butyrylcholinesterase inhibited by analogues of tabun. *Biochem. J.* **2009**, *421*, 97–106.

28 Terrier, F.; Rodriguez-Dafonte, P.; Le Guével, E.; Moutiers, G. Revisiting the reactivity of oximate $\alpha$-nucleophiles with electrophilic phosphorus centers. Relevance to detoxification of sarin, soman and DFP under mild conditions. *Org. Biomol. Chem.* **2006**, *4*, 4352–4363.

29 Ekström, F.; Astot, J. C.; Pang, Y. P. Novel nerve-agent antidote design based on crystallographic and mass spectrometric analyses of tabun-conjugated acetylcholinesterase in complex with antidotes. *Clin. Pharmacol. Ther.* **2007**, *82*, 282–293.

30 Hörnberg, A.; Artursson, E.; Wärme, R.; Pang, Y. P.; Ekström, F. Crystal structures of oxime-bound fenamiphos-acetylcholinesterases: reactivation involving flipping of the His447 ring to form a reactive Glu334-His447-oxime triad. *Biochem. Pharmacol.* **2010**, *79*, 507–515.

31 Taylor, P.; Kovarik, Z.; Reiner, E.; Radić, Z. Acetylcholinesterase: Converting a vulnerable target to a template for antidotes and detection of inhibitor exposure. *Toxicology* **2007**, *233*, 70–78.

32 Hörnberg, A.; Artursson, E.; Wärme, R.; Pang, Y. P.; Ekström, F. Crystal structures of oxime-bound fenamiphos-acetylcholinesterases: reactivation involving flipping of the His447 ring to form a reactive Glu334-His447-oxime triad. *Biochem. Pharmacol.* **2010**, *79*, 507–515.

33 Ekström, F.; Hörnberg, A.; Artursson, E.; Hammarström, L. G.; Schneider, G.; Pang, Y. P. Structure of HI-6/sarin-acetylcholinesterase determined by X-ray crystallography and molecular dynamics simulation: Reactivator mechanism and design. *PLoS One* **2009**, *4*, e5957.

34 Nachon, F.; Carletti, E.; Worek, F.; Masson, P. Aging mechanism of butyrylcholinesterase inhibited by an N-methyl analogue of tabun: Implications of the trigonal-bipyramidal transition state rearrangement for the phosphylation or reactivation of cholinesterases. *Chem. Biol. Interact.* **2010**, *187*, 44–48.

35 Ohta, H.; Ohmori, T.; Suzuki, S.; Ikegaya, H.; Sakurada, K.; Takatori, T. New Safe method for preparation of sarin-exposed human erythrocytes acetylcholinesterase using non-toxic and stable sarin analogue isopropyl p-nitrophenyl methylphosphonate and its application to evaluation of nerve agent antidotes. *Pharm. Res.* **2006**, *23*, 2827–2833.

36 Okuno, S.; Sakurada, K.; Ohta, H.; Ikegaya, H.; Kazui, Y.; Akutsu, T.; Takatori, T.; Iwadate, K. Blood-brain barrier penetration of novel pyridinealdoxime methiodide (PAM)-type oximes examined by brain microdialysis with LC-MS/MS. *Toxicol. Appl. Pharmacol.* **2008**, *227*, 8–15.

37 Cabal, J.; Kuča, K.; Kassa, J. Specification of the structure of oximes able to reactivate tabun-inhibited acetylcholinesterase. *Basic Clin. Pharmacol. Toxicol.* **2004**, *95*, 81–86.

38 Musilek, K.; Komloova, M.; Holas, O.; Horova, A.; Pohanka, M.; Gunn-Moore, F.; Dohnal, V.; Dolezal, M.; Kuča, K. Mono-oxime bisquaternary acetylcholinesterase reactivators with prop-1,3-diyl linkage—Preparation, in vitro screening and molecular docking. *Bioorg. Med. Chem.* **2011**, *19*, 754–762.

39 Kuča, K.; Bielavský, J.; Cabal, J.; Kassa, J. Synthesis of a new reactivator of tabun-inhibited acetylcholinesterase. *Bioorg. Med. Chem. Lett.* **2003**, *13*, 3545–3547.

40 Kassa, J.; Kuča, K.; Karasová, J.; Musilek, K. The development of new oximes and the evaluation of their reactivating, therapeutic and neuroprotective efficacy against tabun. *Mini Rev. Med. Chem.* **2008**, *8*, 1134–1143.

41 Artursson, E.; Akfur, C.; Hornberg, A.; Worek, F.; Ekström, F. Reactivation of tabun-hAChE investigated by structurally analogous oximes and mutagenesis. *Toxicology* **2009**, *265*, 108–114.

42 Ekström, F.; Pang, Y.-P.; Boman, M.; Artusson, E.; Akfur, C.; Börjegren, S. Crystal structures of acetylcholinesterase in complex with HI-6, Ortho-7 and obidoxime: Structural basis for differences in the ability to reactivate tabun conjugates. *Biochem. Pharmacol.* **2006**, *72*, 597–607.

43 Kuča, K.; Cabal, J.; Jung, Y. S.; Musilek, K.; Soukup, O.; Jun, D.; Pohanka, M.; Musilova, L.; Karasová, J.; Novotný, L.; Hrabinova, M. Reactivation of human brain homogenate cholinesterases inhibited by tabun using newly developed oximes K117 and K127. *Basic Clin. Pharmacol. Toxicol.* **2009**, *105*, 207–210.

44 Acharya, J.; Dubey, D. K.; Srivastava, A. K.; Raza, S. K. In vitro evaluation of bis-pyridinium oximes bearing methoxy alkane linker as reactivators of sarin inhibited human acetylcholinesterase. *Toxicol. in Vitro* **2010**, *24*, 1797–1802.

45 Musilek, K.; Jun, D.; Cabal, J.; Kassa, J.; Gunn-Moore, F.; Kuča, K. Design of a potent reactivator of tabun-inhibited acetylcholinesterase synthesis and evaluation of (E)-1-(4-Carbamoylpyridinium)-4-(4-hydroxyiminomethylpyridinium)-but-2-ene Dibromide (K203). *J. Med. Chem.* **2007**, *50*, 5514–5518.

46 Musilek, K.; Holas, O.; Misik, J.; Pohanka, M.; Novotny, L.; Dohnal, V.; Opletalova, V.; Kuča, K. Monooxime-monocarbamoyl bispyridinium xylene-linked reactivators of acetylcholinesterase—Synthesis, in vitro and toxicity evaluation, and docking studies. *ChemMedChem* **2010**, *5*, 247–254.

47 Acharya, J.; Dubey, D. K.; Srivastava, A. K.; Raza, S. K. In vitro reactivation of sarin-inhibited human acetylcholinesterase (AChE) by bis-pyridinium oximes connected by xylene linkers. *Toxicol. in Vitro* **2011**, *25*, 251–256.

48 Ballabh, P.; Bruan, A.; Nedergaard, M. The blood-brain barrier: An overview structure, regulation, and clinical implications. *Neurobiol. Dis.* **2004**, *16*, 1–13.

49 Abbott, N. J.; Ronnback, L.; Hansson, E. Astrocyte-endothelial interactions at the blood-brain barrier. *Nat. Rev. Neurosci.* **2006**, *7*, 41–53.

50 Lorke, D. E.; Kalasz, H.; Petroianu, G. A.; Tekes, K. Entry of oximes into the brain: A review. *Curr. Med. Chem.* **2008**, *15*, 743–753.

51 Sakurada, K.; Matsubara, K.; Shimizu, K.; Shiono, H.; Seto, Y.; Tsuge, K.; Yoshino, M.; Sakai, I.; Mukoyama, H.; Takatori, T. Pralidoxime iodide (2-PAM) penetrates across the blood-brain barrier. *Neurochem. Res.* **2003**, *28*, 1401–1407.

52 Cook, A. M.; Mieure, K. D.; Owen, R. D.; Pesaturo, A. B.; Hatton, J. Intracerebroventricular administration of drugs. *Pharmacotherapy* **2009**, *29*, 832–845.

53 Bradley, W. G., Jr. MR-guided focused ultrasound: A potentially disruptive technology. *J. Am. Coll. Radiol.* **2009**, *6*, 510–513.

54 Neuwelt, E. A.; Frenkel, E. P.; Diehl, J. T.; Maravilla, K. R.; Vu, L. H.; Clark, W. K.; Rapoport, S. I.; Barnett, P. A.; Hill, S. A.; Lewis, S. E.; Ehle, A. L.; Beyer, C. W., Jr.; Moore, R. J. Osmotic blood-brain barrier disruption: A New means of increasing chemotherapeutic agent delivery. *Trans. Am. Neurol. Assoc.* **1979**, *104*, 256–260.

55 Wagner, S.; Kufleitner, J.; Zensi, A.; Dadparvar, M.; Wien, S.; Bungert, J.; Vogel, T.; Worek, F.; Kreuter, J.; von Briesen, A. Nanoparticulate transport of oximes over an in vitro blood-brain barrier model. *PLoS One* **2010**, *5*, No. e14213.

56 Joosen, M. J. A.; van der Schans, M. J.; van Dijk, C. G. M.; Kuijpers, W. C.; Wortelboer, H. M.; van Helden, H. P. M Increasing oxime efficacy by blood-brain barrier modulation. *Toxicol. Lett.* **2011**, *206*, 67–71.

57 Carman, A. J.; Mills, J. H.; Krenz, A.; Kim, D. G.; Bynoe, M. S. Adenosine receptor signaling modulates permeability of the blood-brain barrier. *J. Neurosci.* **2011**, *31*, 13272–13280.

58 Jeong, H. C.; Kang, N. S.; Park, N. J.; Yum, E. K.; Jung, Y. S. Reactivation potency of fluorinated pyridinium oximes for acetylcholinesterases inhibited by paraoxon organophosphorus agent. *Bioorg. Med. Chem. Lett.* **2009**, *19*, 1214–1217.

59 Jeong, H. C.; Park, N. J.; Chae, C. H.; Musilek, K.; Kassa, J.; Kuca, K.; Jung, Y. S. Fluorinated pyridinium oximes as potential reactivators for acetylcholinesterases inhibited by paraoxon organophosphorus agent. *Bioorg. Med. Chem.* **2009**, *17*, 6213–6217.

60 Heldman, E.; Ashani, Y.; Raveh, L.; Rachaman, E. S. Sugar conjugates of pyridinium aldoximes as antidotes against organophosphonate poisoning. *Carbohydr. Res.* **1986**, *151*, 337–347.

61 Garcia, G. E.; Campbell, A. J.; Olson, J.; Moorad-Doctor, D.; Morthole, V. I. Novel oximes as blood-brain barrier penetrating cholinesterase reactivators. *Chem. Biol. Interact.* **2010**, *187*, 199–206.

62 Shek, E.; Higuchi, T.; Bodor, N. Improved delivery through biological membranes. 2. Distribution, excretion, and metabolism of N-methyl-1,6-dihydropyridine-2-carbaldoxime hydrochloride, a pro-drug of N-methylpyridinium-2-carbaldoxime chloride. *J. Med. Chem.* **1976**, *19*, 108–112.

63 Demar, J. C.; Clarkson, E. D.; Ratcliffe, R. H.; Campbell, A. J.; Thangavelu, S. G.; Herdman, C. A.; Leader, H.; Schulz, S. M.; Marek, E.; Medynets, M. A.; Ku, T. C.; Evans, S. A.; Khan, F. A.; Owens, R. R.; Nambiar, M. P.; Gordon, R. K. Pro-2-PAM therapy for central and peripheral cholinesterases. *Chem. Biol. Interact.* **2010**, *187*, 191–198.

64 Shih, T. M.; Skovira, J. W.; O'Donnell, J. C.; McDonough, J. H. Central acetylcholinesterase reactivation by oximes improves survival and terminates seizures following nerve agent intoxication. *Adv. Stud. Biol.* **2009**, *1*, 155–196.

65 Skovira, J. W.; O'Donnell, J. C.; Koplovitz, I.; Kan, R. K.; McDonough, J. H.; Shih, T. M. Reactivation of brain acetylcholinesterase by monoisonitrosoacetone increases the therapeutic efficacy against nerve agents in guinea pigs. *Chem. Biol. Interact.* **2010**, *187*, 318–324.

66 de Koning, M. C.; van Grol, M.; Noort, D. Peripheral site ligand conjugation to a non-quaternary oxime enhances reactivation of nerve agent-inhibited human acetylcholinesterase. *Toxicol. Lett.* **2011**, *206*, 54–59.

67 Sit, R. K.; Radić, Z.; Gerardi, V.; Zhang, L.; Garcia, E.; Katalinić, M.; Amitai, G.; Kovarik, Z.; Fokin, V. V.; Sharpless, K. B.; Taylor, P. New structural scaffolds for centrally acting oxime reactivators of phosphylated cholinesterases. *J. Biol. Chem.* **2011**, *286*, 19422–19430.

68 Saint-André, G.; Kliachyna, M.; Kodepelly, S.; Louise-Leriche, L.; Gillon, E.; Renard, P.-Y.; Nachon, F.; Baati, R.; Wagner, A. Design, synthesis and evaluation of new $\alpha$-nucleophiles for the hydrolysis of organophosphorus nerve agents: application to the reactivation of phosphorylated acetylcholinesterase. *Tetrahedron* **2011**, *67*, 6352–6361.

69 Mercey, G.; Verdelet, T.; Saint-André, G.; Gillon, E.; Wagner, A.; Baati, R.; Jean, L.; Nachon, F.; Renard, P.-Y. First efficient uncharged reactivators for the dephosphorylation of poisoned human acetylcholinesterase. *Chem. Commun.* **2011**, *47*, 5295–5297.

70 Ashani, Y.; Bhattacharjee, A. K.; Leader, H.; Saxena, A.; Doctor, B. P. Inhibition of cholinesterases with cationic phosphonyl oximes highlights distinctive properties of the charged pyridine groups of quaternary oxime reactivators. *Biochem. Pharmacol.* **2003**, *66*, 191–202.

71 Louise-Leriche, L.; Păunescu, E.; Saint-André, G.; Baati, R.; Romieu, A.; Wagner, A.; Renard, P.-Y. A HTS assay for the detection of organophosphorus nerve agents scavengers. *Chem.—Eur. J.* **2010**, *16*, 3510–3523.

72 Kalisiak, J.; Ralph, E. C.; Zhang, J.; Cashman, J. R. Amidine-oximes: Reactivators for organophosphate exposure. *J. Med. Chem.* **2011**, *54*, 3319–3330.

73 Antonijevic, B.; Stojiljkovic, M. P. Unequal efficacy of pyridinium oximes in acute organophosphate poisoning. *Clin. Med. Res.* **2007**, *5*, 71–82.

74 Worek, F.; Aurbek, N.; Thiermann, H. Reactivation of organophosphate-inhibited human AChE by combinaisons of obidoxime and Hl 6 in vitro. *J. Appl. Toxicol.* **2007**, *27*, 582–588.

# Trp82 and Tyr332 Are Involved in Two Quaternary Ammonium Binding Domains of Human Butyrylcholinesterase as Revealed by Photoaffinity Labeling with [$^3$H]DDF

**F. Nachon**, L. Ehret-Sabatier, D. Loew, C. Colas, A. van Dorsselaer, M. Goeldner*

Biochemistry 37 (1998) 10507-10513

# Trp82 and Tyr332 Are Involved in Two Quaternary Ammonium Binding Domains of Human Butyrylcholinesterase as Revealed by Photoaffinity Labeling with [$^3$H]DDF†

Florian Nachon,‡ Laurence Ehret-Sabatier,‡ Damarys Loew,§ Christophe Colas,‡ Alain van Dorsselaer,§ and Maurice Goeldner*,‡

*Laboratoire de Chimie Bio-organique, UMR 7514 CNRS, Faculté de Pharmacie, Université Louis Pasteur Strasbourg, 74 route du Rhin, BP 24, 67401 Illkirch Cedex, France, and Laboratoire de Spectrométrie de Masse Bio-organique, UMR 7509 CNRS, Faculté de Chimie, Université Louis Pasteur Strasbourg, 1 rue Blaise Pascal, 67096 Strasbourg Cedex, France*

*Received March 9, 1998; Revised Manuscript Received May 4, 1998*

ABSTRACT: Purified butyrylcholinesterase (BuChE) was photolabeled by [$^3$H]-*p*-*N*,*N*-dimethylamino benzene diazonium ([$^3$H]DDF) to identify the quaternary ammonium binding sites on this protein [Ehret-Sabatier, L., Schalk, I., Goeldner, M., and Hirth, C. (1992) *Eur. J. Biochem. 203*, 475−481]. The covalent photoincorporation occurs with a stoichiometry of one mole of probe per mole of inactivated site and could be fully prevented by several cholinergic inhibitors such as tacrine or tetramethylammonium. After complete deglycosylation of the enzyme using *N*-glycosidase F, the alkylated protein was trypsinolyzed and the digests were analyzed by HPLC coupled to ES-MS. A direct comparison of tryptic fragments from labeled and unlabeled BuChE allowed us to identify the tryptic peptide Tyr61-Lys103 as carrying the probe. Purification of the labeled peptides by anion-exchange chromatography gave a major radioactive peak which was further fractionated by reversed-phase HPLC leading to three, well-resolved, radioactive peaks. Microsequencing revealed that two of these peaks contained an overlapping sequence starting at Tyr61, while the third peak contained a sequence extending from Thr315. Radioactive signals could be unambiguously attributed to positions corresponding to residues Trp82 and Tyr332. This labeling study establishes the existence of two different binding domains for quaternary ammonium in BuChE and exemplifies additional cation/$\pi$ interactions in cholinergic proteins. This work strongly supports the existence of a peripheral anionic site in BuChE, implying residue Tyr332 as a key element.

Two types of cholinesterases can be distinguished in vertebrates; acetylcholinesterase (AChE,[1] EC 3.1.1.7) and butyrylcholinesterase (BuChE, EC 3.1.1.8). These very homologous enzymes both rapidly hydrolyze the neurotransmitter acetylcholine but show distinct substrate and inhibitor selectivity (*1*). The elucidation of the 3D structure of *Torpedo* AChE (*2*) followed by the description of a series of 3D structures of enzyme−inhibitor complexes (*3*−*6*) have revealed remarkable structural features for this protein. Extensive site-directed mutagenesis and molecular dynamics experiments have tried to assess the different functional characteristics of this enzyme, including the unusual location of the catalytic triad at the bottom of a 20 Å depth (*7*, *8*). Another noteworthy feature of this protein was an allosteric regulation of its activity by molecules binding at the peripheral site located at the entrance of this cavity. The different X-ray structures also allowed us to exemplify very accurately, in a biological model, cation/$\pi$ interactions (*9*, *10*) between quaternary ammonium salts and aromatic residues. The 3D structure of BuChE has not been solved yet, and most of the structure−function investigations rely on a 3D model of this protein (*11*), which is based on the 3D structure of *Torpedo* AChE. Most of these investigations are focused on the functional specificities between aligned amino acids from different ChE species.

Contrary to site-directed mutagenesis analyses, site-directed labeling experiments do not require the existence of a 3D structure or a model of a protein. They lead to structural characterizations of ligand receptor interactions in solution (*12*), and after the publication of the amino acid sequence of AchE (*13*), early structural information resulted from photoaffinity or affinity labeling experiments. These site-directed labeling experiments allowed the identification of residues from the active site, such as Phe330 (14) and Trp84 (*15*), or from the peripheral site, such as Trp279 (*16*, *17*), His280 (*18*), Tyr70, and Tyr121 (*19*), of *Torpedo* AChE. Aromatic diazonium salts proved to be particularly attractive

† This work was supported by the Centre National de la Recherche Scientifique, the Ministère de la Recherche et de la Technologie, and the European Community Biotechnology Program under Grant No. 960081.

* To whom correspondence should be adressed. E-mail: goeldner@bioorga.u-strasbg.fr.

‡ Laboratoire de Chimie Bio-organique.

§ Laboratoire de Spectrométrie de Masse Bio-organique.

[1] Abbreviations: BuChE, butyrylcholinesterase; AChE, acetylcholinesterase; PAS, peripheral anionic site; DDF, *p*-(*N*,*N*-dimethylamino)-benzenediazonium fluoroborate; THA, tacrine; DTT, dithiothreitol; NM7C, *N*-methyl-(7-dimethylcarbamoxy)quinolinium iodide; SDS, sodium dodecyl sulfate; TFA, trifluoroacetic acid; HPLC, high-performance liquid chromatography; MS, mass spectrometry; ES, electrospray; MALDI, matrix-assisted laser-desorption−ionization; PAGE, polyacrylamide gel electrophoresis.

S0006-2960(98)00536-4 CCC: $15.00 
Published on Web 06/26/1998

photoaffinity probes for the structural investigations of the acetylcholine binding site on cholinergic proteins. As a remarkable example, the [$^3$H]-*p*-*N*,*N*-dimethylamino benzene diazonium salt ([$^3$H]DDF) allowed the identification of no less than eight different amino acid residues from the acetylcholine binding site on the nicotinic receptor (*12*).

In this paper, we analyzed, at the molecular level, photoaffinity labeling experiments on BuChE using [$^3$H]DDF (*20*). The specific photoincorporation of the probe allowed, after the deglycosylation of the protein, using MS methods applied on the crude tryptic digest, the identification of the tryptic fragment Tyr61-Lys103 as being alkylated by the photoprobe. In parallel, standard purification and sequencing methods lead to the unambiguous identification of the labeled amino acids Trp82 and Tyr332. These photoaffinity labeling results strongly support the existence of two distinct ammonium binding sites in BuChE, involving cation/$\pi$ interactions.

## MATERIALS AND METHODS

### *Chemicals*

Dithiothreitol, tacrine, 4-vinylpyridine, and *n*-octyl-$\beta$-D-glucopyranoside were purchased from Sigma, and butyrylthiocholine iodide and 5,5′-dithiobis(2-nitrobenzoic acid) were from Aldrich. Porcine pancreatic trypsin (sequencing grade modified) was from Promega and recombinant *N*-glycosidase F from Boehringer Mannheim. *N*-Methyl-7-hydroxyquinolinium iodide and the derived dimethylcarbamic acid ester NM7C were prepared as described (*21*). Tritiated *p*-(*N*,*N*-dimethylamino) benzenediazonium ([$^3$H]DDF; 1−6.25 Ci/mmol) was prepared as previously described (*22*).

### *Butyrylcholinesterase Preparation*

Human butyrylcholinesterase (BuChE) was purified from frozen outdated plasma (gift from the Centre de Transfusion Sanguine, Strasbourg). We used the classical two-step procedure described by Lockridge (*23*) consisting of DEAE ion-exchange chromatography followed by procainamide affinity chromatography. Protein concentration was estimated from absorbance at 280 nm ($e$ = 1.8 mL mg$^{-1}$ cm$^{-1}$) (*23*) using the Bradford assay (Biorad). Activity was assayed spectrophotometrically using butyrylthiocholine as the substrate (*24*). BuChE active serines were titrated using the NM7C method (*21*). The purified enzyme (400 ± 50 units/mg) can be stored at least one year at 4 °C in 50 mM phosphate buffer, pH 7.0, without loss of activity.

### *Photolabeling Experiments*

Photolabeling of BuChE was performed as described (*20*) in 50 mM phosphate buffer, pH 7.2, by irradiation at 295 nm under energy transfer (*25*), 75 $\mu$V for 45 min at 10 °C. The total volume for each irradiation was 1.5 mL. Final concentrations were 300 $\mu$g/mL BuChE, 100 $\mu$M [$^3$H]DDF, and, in the protection experiment, 2 $\mu$M THA. After irradiation, 2 mM DTT was added to destroy unreacted [$^3$H]-DDF. An aqueous dilution−concentration procedure on CM30 filter units (Amicon) was repeated twice and removed up to 90% of the free radioactive ligand before a final lyophilization.

### *[$^3$H]DDF Incorporation Measurement*

Aliquots of alkylated BuChE were analyzed on a 10% SDS−PAGE (*26*). The radioactivity incorporated was quantified after gel slicing, digestion, and counting (*20*).

### *Reduction−Alkylation*

Lyophilized−alkylated BuChE (450 $\mu$g) was redissolved in 0.5 M Tris-HCl buffer, pH 8.5, containing 5 M urea and 40 mM DTT (final volume 100 $\mu$L). The sample was incubated for 1 h in the dark at 50 °C under a stream of argon. 4-Vinylpyridine was added to a final concentration of 450 mM, and incubation was prolonged for 15 min. The protein was then extensively dialyzed against 50 mM $NH_4HCO_3$ buffer, pH 8.

### *Enzymatic Deglycosylation and Proteolytic Cleavage*

Reduced−alkylated BuChE was incubated at 37 °C for 16 h in 50 mM $NH_4HCO_3$ buffer, pH 8, containing 0.01% SDS and *N*-glycosidase F (22 units/mg BuChE). The reaction was either stopped by denaturation and analysis on an 8% SDS−PAGE to ascertain the loss of glycosylation weight or followed by addition of trypsin (w/w; 1/45) and subsequent incubation for 6 h at 37 °C. The trypsinolysis was stopped by the addition of one volume of acetonitrile and/or by acidification.

### *Peptide Purification*

*First Step*. Tryptic digests were loaded onto a cation-exchange HPLC column (Waters S5SCX, 4.6 × 250 mm) equilibrated with 25 mM $AcONH_4$ buffer, pH 4.5, containing 50% acetonitrile. Peptides were eluted with a linear gradient from 0% to 40% of the equilibrating solution containing 1 M NaCl, over 40 min at a flow rate of 1 mL/min. Absorbance was monitored at 214 nm. Fractions (0.5 mL) were collected, and aliquots were assayed for radioactivity. Fractions of interest were concentrated under vacuum (Speedvac) in order to remove acetonitrile before proceeding to the next step.

*Second Step*. Samples were loaded onto a reversed-phase HPLC column (Vydac 218TP52, 2.1 × 250 mm) equilibrated with 95% A/5% B (solvent A, 0.1% TFA in water; solvent B, 0.085% TFA in acetonitrile). Elution was performed at a flow rate of 0.25 mL/min with a linear biphasic gradient of 5−15% B over 5 min then 15−40% B over 100 min. Absorbance was monitored at 214 nm. Fractions (0.25 mL) were collected, and those containing radioactivity were lyophilized.

### *Peptide Sequencing*

Peptides were redissolved in 50% formic acid. Automated Edman degradation was performed on a pulse liquid automatic sequenator (Applied Biosystems Model 473A). The remaining HPLC output from each cycle was collected and counted for radioactivity quantification.

### *Mass Spectrometry Analyses*

For mass spectrometry analysis, BuChE was photolabeled with nonradioactive DDF as described before. After reduction−alkylation steps, the samples, unlabeled (control) and labeled, were deglycosylated and trypsinolyzed replacing

0.01% SDS by 0.4% *n*-octyl-$\beta$-D-glucopyranoside during the deglycosylation procedure. Reaction was stopped by acidification (0.1% TFA) before LC/MS analysis.

*Liquid Chromatography/Mass Spectrometry (LC/MS).* The chromatography was carried out on an Alliance HPLC system (Waters 2690) equipped with a diode array detector (Waters 996). Absorbances were monitored with a chromatography manager Millennium (version 2.15.01). The column was a Nucleosil 300-5C18 (Macherey Nagel, 2.1 mm $\times$ 125 mm) maintained at 35 °C. The solvent system consisted of 0.1% TFA in water (solvent A) and 0.08% TFA in acetonitrile (solvent B). The elution was performed at a flow rate of 0.25 mL/min, using a multiphasic gradient of 0% B (5 min), 0−20% B (15 min), 20−50% B (70 min), and 50−80% B (5 min) successively. The column efluent was flow-splitted via a stainless steel Valco tee (Supelco) with $^1/_{15}$ directed toward the electrospray mass spectrometer by means of fused silica capillary. Fractions of residual effluent were hand-collected. Therefore, for all analyses, both UV and mass measurement detections were obtained.

*Electrospray Mass Spectrometry (ESMS).* The positive ES mass spectra were obtained on a VG BioQ triple quadrupole mass spectrometer (mass to charge (*m*/*z*) range 4000) upgraded by the manufacturer to a Quattro II performance (Micromass Ltd UK, Altrincham). Scanning was performed in the range 500−2000 in 6 s at an extracting cone voltage of 40 V. The mass spectrometer was externally calibrated by using horse heart myoglobin multiply charged ions and the resolution adjusted so that the peak at *m*/*z* 998 was 1.25 wide at 50% on the base.

*Matrix-Assisted Laser-Desorption−Ionization Mass Spectrometry (MALDI-MS).* The collected fractions were concentrated under vacuum and redissolved in 15 $\mu$L of 50% acetonitrile, 1% formic acid. Aliquots of 0.5 $\mu$L were analyzed by MALDI-MS.

The mass spectrometry experiments were performed on a Bruker (Bremen, Germany) Biflex matrix-assisted laser-desorption−ionization time-of-flight mass spectrometer with improved resolution by means of delayed-ion extraction (DE). The samples were prepared by a two-layer method described elsewhere (*27*) and desorbed/ionized using a pulsed nitrogen laser beam ($\lambda$ = 337 nm) at a repetition rate of 3 Hz. All studies were performed in the linear and reflector positive mode at an acceleration potential of 20 and 19 kV, respectively. The spectra were externally calibrated using the $[M + H]^+$ ions of angiotensin II (1046.19) and ACTH 18-39 (2465.69) in the reflector mode and ubiquitin (8564.87) and cytochrome C (12361.09) in the linear mode.

## RESULTS

### *Photolabeling of BuChE Using [$^3$H]DDF*

Purified human BuChE was photolabeled by [$^3$H]DDF (100 $\mu$M) leading to a 50% inactivation after 45 min of irradiation. In the presence of 2 $\mu$M tacrine (Figure 1), BuChE was efficiently protected against this inactivation. Figure 2 shows the incorporation of [$^3$H]DDF on both monomer (85 kDa) and dimer (170 kDa) of BuChE after denaturating electrophoresis. The quantification of incorporated radioactivity allowed us to calculate a stoichiometry close to one mole of [$^3$H]DDF incorporated per inactivated site. The specificity of the labeling was demonstrated by

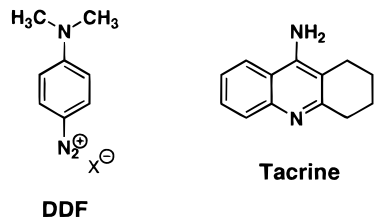


FIGURE 1: Structures of *p*-(*N*,*N*-dimethylamino)benzenediazonium and tacrine.

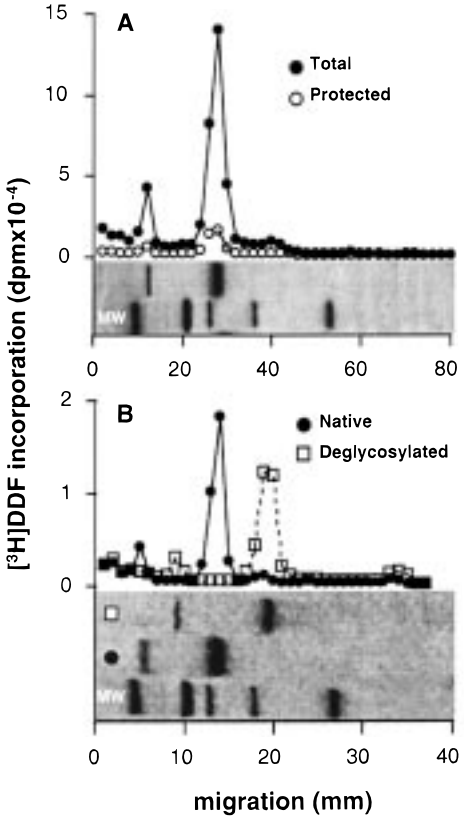


FIGURE 2: SDS−PAGE analysis of [$^3$H]DDF incorporation into BuChE upon iradiation. (A) BuChE was irradiated with [$^3$H]DDF (100 $\mu$M, 6.25 Ci/mmol) in the presence (○, protected) or absence (●, total) of tacrine (2 $\mu$M). Samples were denatured and subjected to a 10% SDS−PAGE (amount BuChE loaded, 10 $\mu$g). Molecular mass protein markers were 200, 116, 97.4, 66, and 45 kDa. The gel lanes were cut into slices which were digested and counted. (B) BuChE was irradiated with [$^3$H]DDF (100 $\mu$M, 1 Ci/mmol). After reduction−alkylation, lyophilized alkylated BuChE was (●) (or not (□)) deglycosylated. Samples were denatured and subjected to electrophoresis on a 8% SDS−acrylamide gel (amount BuChE loaded, 5 $\mu$g). The gel lanes were cut into slices which were digested and counted.

preventing the incorporation of radioactivity with tacrine (Figure 2A). When the labeled BuChE was treated with *N*-glycosidase F, the electrophoresis gel profile (Figure 2B) exhibited a shift of the protein bands concomitant with the radioactivity signals. The observed shift of 25 kDa is in agreement with a complete deglycosylation (*28*).

### *Mass Spectrometric Analysis of Labeled BuChE*

After deglycosylation and trypsinolysis the digests were analyzed by HPLC with multiwavelength detection and coupled to ES-MS. Figure 3 shows the UV profiles of unlabeled (as control) and DDF-labeled digests. The profiles are identical along the entire chromatograms except at

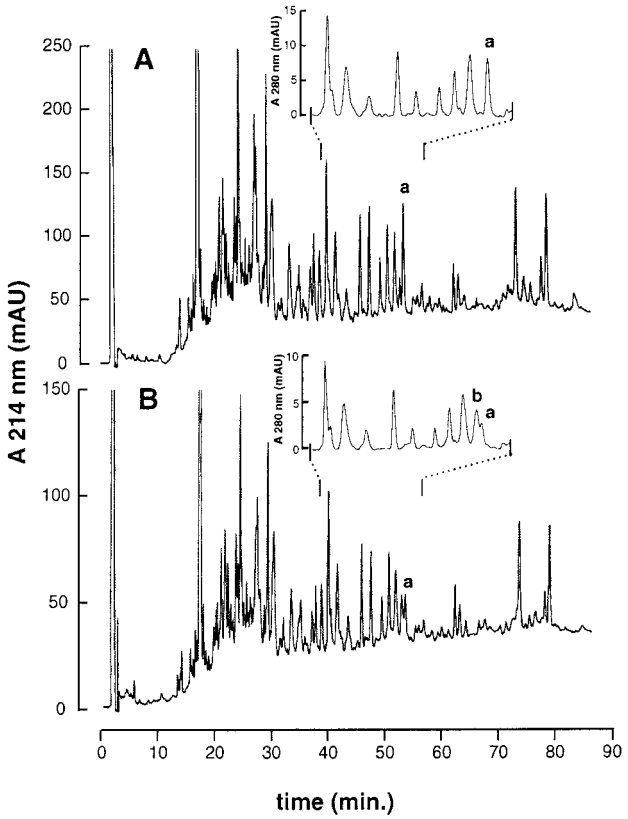


FIGURE 3: Comparison of LC/MS chromatograms from unlabeled (A) and labeled (B) trypsinolyzed BuChE. Samples of DDF-labeled and unlabeled BuChE (75 $\mu$g protein) were deglycosylated, digested, and submitted to LC/MS analysis as described in Materials and Methods. UV absorbance was monitored at 214 and 280 nm. The profiles are given at 214 nm while interesting regions are expanded and shown at 280 nm.

retention times 51−52 min. In this area, the absorbance at 214 nm of one peak (peak a) clearly decreases in the DDF-labeled digest while monitoring the absorbance at 280 nm shows a concomitant appearance of a new peak b. Figure 4 shows the mass spectra sum of peptides eluted in the ion source in this time range. Three ions ($m/z$ = 1069.1, 1336.2, 1780.8) are present only in the labeled digest and correspond to different protonated states (respectively 5, 4, 3) of an average molecular mass of 5340.3 ± 0.6 Da. This measured molecular mass did not fit with any native tryptic peptide and was attributed to a DDF-labeled peptide. As previously indicated, with one mole of probe being incorporated per inactivated site, the difference of mass between native and labeled peptide should correspond to the mass of the incorporated label, that is, 119 Da, after substitution of a hydrogen atom by the photogenerated dimethylaminophenyl cation. Consequently, the measured mass for the labeled peptide (5340.3 ± 0.6 Da) agrees with the labeling of the parent peptide of measured average molecular mass 5221.7 ± 1.8 Da ($m/z$ = 1045.6, 1305.9, 1741.7, Figure 4) and corresponds to the peptide Tyr61-Lys103 (calculated average mass: 5222.9 Da).

The identification of the labeled peptide was confirmed by MALDI-MS analysis of the collected HPLC fractions. The mass of the native peptide Tyr61-Lys103 could be identified in peak a, both in labeled and unlabeled digests, while the mass of the labeled peptide could be detected only in peak b of labeled digest (spectra not shown).

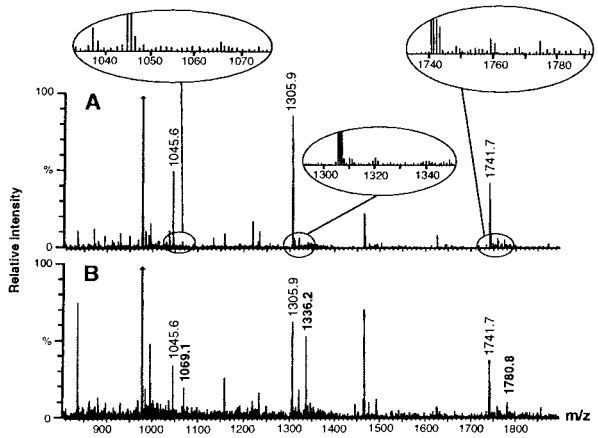


FIGURE 4: Comparison of ES/MS spectra from unlabeled (A) and labeled (B) trypsinolyzed BuChE. Spectra are shown for peptides eluting at retention time 51−52 min (Figure 3). The quoted peaks (1045.6, 1305.9, 1741.7 Da) correspond to three different charge states of a peptide which has a mass of 5221.7 ± 1.8 Da and was identified as Tyr61-Lys103. The three additional bold typed quotations in Figure 4B (1069.1, 1336.2, 1780.8 Da) show the ions corresponding to the labeled peptide (5340.3 ± 0.6 Da). Expanded spectra in Figure 4A show the absence of this peptide in the unlabeled experiment.

In conclusion the results obtained by mass spectrometry, without resorting to extensive purification of labeled peptides, indicate that the peptide Tyr61-Lys103 was specifically labeled by DDF.

### *Identification of [$^3$H]DDF-Labeled BuChE Residues*

First attempts to purify labeled peptides were carried out without deglycosylation of the protein. After photolabeling, BuChE was trypsinolyzed and the peptides fractionated by anion-exchange chromatography (MonoQ) followed by reversed-phase HPLC. However this procedure did not lead to satisfactory results due to glycosylation heterogeneity affording complicated peptide mixtures from which we were unable to unambiguously identify the labeled residues.

Thus, BuChE was deglycosylated before trypsinolysis, and [$^3$H]DDF-labeled peptides could then be purified by a two-step procedure. The first step was cation-exchange chromatography which had the advantage, when compared to the previously used anion exchange, to be compatible with the presence of the anionic detergent SDS used for deglycosylation. Moreover, a concentration of 50% acetonitrile was added to the elution buffer in order to obtain satisfactory yield of radioactivity elution (75%). Figure 5A shows the UV and radioactivity profiles of this chromatography. The fractions containing the major radioactive peak were further treated by simultaneous desalting and purification by reversed-phase HPLC, affording three resolved radioactive peaks 1, 2, and 3 (Figure 5B). The other minor radioactive fractions (Figure 5A) were also analyzed by reversed-phase HPLC and exhibited the same radioactive peaks 1, 2, and 3 but in different relative proportions.

The three peaks 1, 2, and 3 were sequenced (Table 1). Peak 1 contained the sequence extending from Thr315, and the radioactivity was associated with Tyr332. Peaks 2 and 3 both contained sequences beginning at Tyr61 with the radioactivity associated with Trp82. These sequences were thought to be of different length due to incomplete proteolysis.

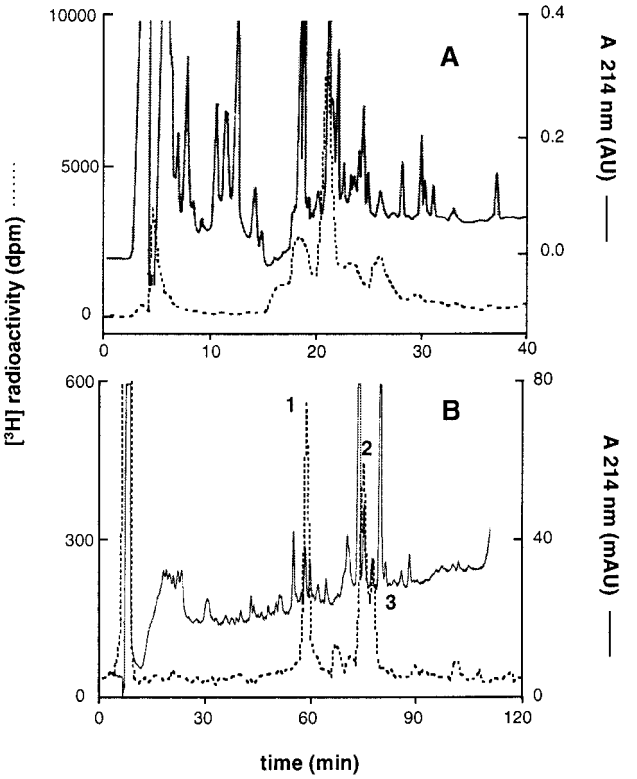


FIGURE 5: HPLC purification steps of [$^3$H]DDF-photolabeled peptides. After irradiation of BuChE in the presence of [$^3$H]DDF (100 $\mu$M, 1 Ci/mmol), samples were deglycosylated and digested by trypsin. (A) Digests were applied onto a cation-exchange column and eluted with a NaCl gradient as described in Materials and Methods. (B) Major radioactive peak from cation-exchange chromatography was further loaded onto a C18 reversed-phase column and purified with an acetonitrile gradient.

Table 1: Amino Acid Sequences from the Purified Peptides

| peak | sequence |
|---|---|
| 1 | $T_{315}$QILVGVNKDEGTAFLV**Y**G... |
| 2 | $Y_{61}$ANSCCQNIDQSFPGFHG**S**EM**W**NP... |
| 3 | $Y_{61}$ANSCCQNIDQSFPGFHGSEM**W**NP... |

## DISCUSSION

Photoaffinity labeling experiments are used to bring structural information on ligand binding sites of biological receptors in solution. DDF (*25*), a small aromatic diazonium salt, has been intensively used to map the acetylcholine binding site on different cholinergic proteins (*12*). This probe combined remarkable photochemical properties to a striking mimic of quaternary ammonium salts for cation/$\pi$ interactions with aromatic amino acid residues. As a new example, the photolabeling of BuChE using the probe [$^3$H]-DDF allowed us to identify two aromatic amino acid residues, Trp82 and Tyr332. This labeling reaction is protectable by tacrine (Figure 2) as well as by tetramethylammonium (*20*). The identification of the labeled amino acids could be assessed by microsequencing of the major labeled peptides (Table 1) which were initially purified to homogeneity by means of HPLC (Figure 5). Importantly, a complete deglycosylation of the labeled protein (Figure 2B) was very helpful in reducing substantially the complexity of the peptide mixture allowing the purification first to proceed successfully and second to identify by MS, directly on the crude tryptic fragments, the peptide Tyr61-Lys103 as being labeled by the probe (Figures 3 and 4).

BuChE, despite its strong sequence homology with AChE, differs markedly from it, in substrate specificity and sensivity (*1*). Considering the different aromatic amino acid residues involved in the binding of quaternary ammonium in the AChE active site (Trp84 and Phe330) and peripheral site (Trp279, Tyr70, and Tyr121), only Trp82(84)[2] is conserved in BuChE, leading to the disruption of the peripheral site of BuChE (*11*). This outcome was confirmed by a series of site-directed mutagenesis experiments, performed on either AChE or BuChE, and consisting mainly of the interchange of the aligned corresponding amino acids (*8*, *11*, *29*−*31*). Interestingly, a mouse AChE peripheral site triple mutant, Y72(70)N, Y124(121)Q, W286(279)A, produced a protein which affected the binding of AChE peripheral site ligands much more strongly when compared to the difference between AChE and BuChE (*30*). The possibility that binding of the peripheral probes at a different locus in AChE and BuChE has been evoked to explain this difference.

The structure−function relationship of BuChE has been studied mainly through site-directed mutagenesis, molecular modeling, and molecular dynamics experiments (*32*−*35*) based on the 3D model of BuChE (*11*). The studies, which were directly oriented to the structural characterization of the ammonium binding sites, determined the contribution of residues Trp82(84) and Asp70(72) to be the predominant residues for the active and peripheral sites, respectively. While the Trp82(84) was easily identified as the key residue for the ammonium binding at the active site, correlating the situation in AChE, the characterization of the peripheral site, was more problematic due notably to the absence of the representative aromatic residues from the AChE PAS (*11*). A series of publications referred to Asp70(72) as the key amino acid residue for the PAS on BuChE (*33*, *34*). The negative charge of the aspartic residue at the rim of the gorge was described as being primarily responsible for the binding of positively charged ligands through ion pair interaction. A three-step binding process successively implying Asp70 and Trp82, and eventually both residues for bis-quaternary ammonium, has been proposed to rationalize the functioning of this enzyme (*34*).

The photogeneration, in our labeling experiment, of a hyper-reactive aryl cation (*36*) allows the exclusion of the fact that such a cationic species diffuses out from a target binding site. According to the measured distance between the two residues Trp82 and Typ332, about 10 Å referring to the BuChE model (*11*), their labeling must result from the occupancy of the DDF probe at two different binding sites. The protection of the labeling reaction by positively charged cholinergic molecules indicates that DDF targeted the quaternary ammonium binding areas of BuChE. Importantly, the observed stoichiometry of labeling of one molecule of probe per active site of BuChE indicates that the labeling at the two ammonium binding sites is mutually exclusive as was the case for the labeling of AChE with DDF (*3*).

Our labeling results first confirm the contribution of Trp82 for the binding of quaternary ammonium at the active site

[2] By convention, the number in parentheses immediately following an amino acid residue refers to the corresponding amino acid residue number in *Torpedo californica* acetylcholinesterase.

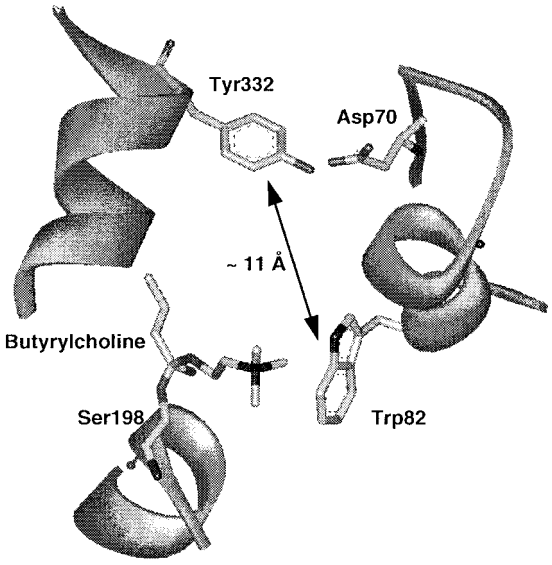


FIGURE 6: Representation of DDF-labeled residues on human BuChE. Trp82 and Tyr332 are shown on a model with docked butyrylcholine (*11*).

and, second, allow us to propose Tyr332 as a predominant residue from the PAS of BuChE to bind quaternary ammonium salts (Figure 6). Interestingly, this residue Tyr332-(334) has been shown to interact directly through a hydrogen bond with Asp70(72) both in the 3D X-ray structure of AChE (*2*) and in the 3D model of BuChE (*11*). This hydrogen bond allows this residue to be indirectly connected to the flexible omega-loop Cys65(67)-Cys92(94) which has been proposed to regulate the functioning of this protein (*34*). Noteworthy, the cation/$\pi$ interactions involving tyrosine residues have been shown to be dependent on the existence of hydrogen bonds, implying that the tyrosyl hydroxyl group (*37*) leads to a strongly increased cation/$\pi$ interaction when existing.

In human AChE, Tyr341(334) residue has been shown to be part of a signal relay from the gorge surface to the catalytic center (*38*) while it has been demonstrated, by site-directed mutagenesis, to affect the binding of bis-quaternary ligands such as BW284C51 and decamethonium (*31*, *39*). Interestingly, the 3D X-ray structure of the mouse AChE complexed with fasciculin revealed, by comparison with the 3D *Torpedo* AChE structure, that after fasciculin binding, the largest conformational motion was observed for residue Tyr341(334) (*6*). However, one should keep in mind that AChE and BuChE are different proteins and the results obtained for the binding of fasciculin on AChE might not be relevant for BuChE. The only study which has been achieved on BuChE Tyr332 residue used the Y332F mutant to evaluate the importance of the hydrogen bond between Tyr332 and Asp70 for the binding of quaternary ammonium ligands (*34*). A moderate decrease in binding affinities of mono- and bis-quaternary ammonium derivatives was observed; however, the Y332F mutant did not abolish the cation/$\pi$ interaction of this residue and additional mutagenesis experiments are required to delineate accurately the importance of Tyr332 in the binding of quaternary ammonium ligands. Although the residue Asp70 was not part of the major labeled peptides by [$^3$H]DDF, we cannot rule out its labeling completely; either it could have been present in minor radiolabeled peptide fragments or the labeling might have been partially lost during the used experimental procedures (i.e., aqueous formic acid treatment during microsequencing). Therefore, the involvement of both residue Asp70 and residue Tyr332 for the binding of quaternary ammonium at the PAS of BuChE is conceivable (Masson, personal communication).

The existence of a PAS at BuChE has been questioned (*11*), due notably to the absence of specific ligands for this site. Evidently, if the BuChE PAS exists, it is structurally very different from the AChE PAS (see above), and this is best illustrated by the striking difference in binding affinities of fasciculin, an AChE peripheral site ligand, for these two proteins (*40*). Our labeling results, besides identifying the well-characterized Trp82 at the active site of BuChE, strongly reinforce the existence of a peripheral site on this protein by identifying Tyr332 as a major participant. This result confirms a complete different location in the 3D structures of the peripheral sites of AChE and BuChE. Work is currently in progress to determine precisely the structural determinants and functional implications of the BuChE peripheral site.

## ACKNOWLEDGMENT

We are grateful to Dr P. Bulet (UPR CNRS 9022, Strasbourg) for sequence analysis as well fruitful discussions.

## REFERENCES

1. Massoulie, J., Pezzementi, L., Bon, S., Krejci, E., and Vallette, F. M. (1993) *Prog. Neurobiol. 41*, 31−91.
2. Sussman, J. L., Harel, M., Frolow, F., Oefner, C., Goldman, A., Toker, L., and Silman, I. (1991) *Science 253*, 872−879.
3. Harel, M., Schalk, I., Ehret-Sabatier, L., Bouet, F., Goeldner, M., Hirth, C., Axelsen, P. H., Silman, I., and Sussman, J. L. (1993) *Proc. Natl. Acad. Sci. U.S.A. 90*, 9031−9035.
4. Harel, M., Kleywegt, G. J., Ravelli, R. B., Silman, I., and Sussman, J. L. (1995) *Structure 3*, 1355−1366.
5. Harel, M., Quinn, D. M., Nair, H. K., Silman, I., and Sussman, J. L. (1996) *J. Am. Chem. Soc. 118*, 2340−2346.
6. Bourne, Y., Taylor, P., and Marchot, P. (1995) *Cell 83*, 503−512.
7. Sussman, J. L., and Silman, I. (1992) *Curr. Opin. Struct. Biol. 2*, 721−729.
8. Taylor, P., and Radic, Z. (1994) *Annu. Rev. Pharmacol. Toxicol. 34*, 281−320.
9. Dougherty, D. A., and Stauffer, D. A. (1990) *Science 250*, 1558−1560.
10. Dougherty, D. A. (1996) *Science 271*, 163−168.
11. Harel, M., Sussman, J. L., Krejci, E., Bon, S., Chanal, P., Massoulie, J., and Silman, I. (1992) *Proc. Natl. Acad. Sci. U.S.A. 89*, 10827−10831.
12. Kotzyba-Hibert, F., Kapfer, I., and Goeldner, M. (1995) *Angew. Chem., Int. Ed. Engl. 34*, 1296−1312.
13. Schumacher, M., Camp, S., Maulet, Y., Newton, M., MacPhee-Quigley, K., Taylor, S. S., Friedmann, T., and Taylor, P. (1986) *Nature 319*, 407−409.
14. Kieffer, B., Goeldner, M., Hirth, C., Aebersold, R., and Chang, J. Y. (1986) *FEBS Lett. 202*, 91−96.
15. Kreienkamp, H. J., Weise, C., Raba, R., Aaviksaar, A., and Hucho, F. (1991) *Proc. Natl. Acad. Sci. U.S.A. 88*, 6117−6121.
16. Schalk, I., Ehret-Sabatier, L., Bouet, F., Goeldner, M., and Hirth, C. (1992) in *Multidisciplinary Approaches to Cholinesterase Functions* (Shafferman, A., and Velan, B., Eds.) pp 117−120, Plenum Press, New York.
17. Schalk, I., Ehret-Sabatier, L., Bouet, F., Goeldner, M., and Hirth, C. (1994) *Eur. J. Biochem. 219*, 155−159.
18. Haas, R., Adams, E. W., Rosenberry, T. L., and Rosenberry, T. L. (1992) in *Multidisciplinary Approaches to Cholinesterase*

*Functions* (Shafferman, A., and Velan, B., Eds.) pp 131−139, Plenum Press, New York.
19. Schalk, I., Ehret-Sabatier, L., Le Feuvre, Y., Bon, S., Massoulie, J., and Goeldner, M. (1995) *Mol. Pharmacol. 48*, 1063−1067.
20. Ehret-Sabatier, L., Schalk, I., Goeldner, M., and Hirth, C. (1992) *Eur. J. Biochem. 203*, 475−481.
21. Rosenberry, T. L., and Bernhard, S. A. (1971) *Biochemistry 10*, 4114−4120.
22. Autelitano, F., Weill, C., Goeldner, M., and Ilien, B. (1997) *Biochem. Pharmacol. 53,* 501−510.
23. Lockridge, O., and LaDu, B. N. (1978) *J. Biol. Chem. 253*, 361−366.
24. Ellman, G. L., Courtney, K. D., Andres, J. V., and Featherstone, R. M. (1961) *Biochem. Pharmacol. 7*, 88−95.
25. Goeldner, M. P., and Hirth, C. G. (1980) *Proc. Natl. Acad. Sci. U.S.A. 77*, 6439−6442.
26. Laemmli, U. K. (1970) *Nature 227*, 680−685.
27. Ravanat, C., Morales, M., Azorsa, D. O., Moog, S., Schuler, S., Grunert, P., Loew, D., van Dorsselaer, A., Cazenave, J. P., and Lanza, F. (1997) *Blood 89*, 3253−3262.
28. Lockridge, O., Bartels, C. F., Vaughan, T. A., Wong, C. K., Norton, S. E., and Johnson, L. L. (1987) *J. Biol. Chem. 262*, 549−557.
29. Vellom, D. C., Radic, Z., Li, Y., Pickering, N. A., Camp, S., and Taylor, P. (1993) *Biochemistry 32*, 12−17.
30. Radic, Z., Pickering, N. A., Vellom, D. C., Camp, S., and Taylor, P. (1993) *Biochemistry 32*, 12074−12084.
31. Barak, D., Kronman, C., Ordentlich, A., Ariel, N., Bromberg, A., Marcus, D., Lazar, A., Velan, B., and Shafferman, A. (1994) *J. Biol. Chem. 269*, 6296−6305.
32. Loewenstein-Lichtenstein, Y., Glick, D., Gluzman, N., Sternfeld, M., Zakut, H., and Soreq, H. (1996) *Mol. Pharmacol. 50*, 1423−1431.
33. Masson, P., Froment, M. T., Bartels, C. F., and Lockridge, O. (1996) *Eur. J. Biochem. 235*, 36−48.
34. Masson, P., Legrand, P., Bartels, C. F., Froment, M. T., Schopfer, L. M., and Lockridge, O. (1997) *Biochemistry 36*, 2266−2277.
35. Saxena, A., Redman, A. M., Jiang, X., Lockridge, O., and Doctor, B. P. (1997) *Biochemistry 36*, 14642−14651.
36. Gasper, S. M., Devadoss, C., and Schuster, G. B. (1995) *J. Am. Chem. Soc. 117*, 5206−5211.
37. Mecozzi, S., West, A. P., Jr., and Dougherty, D. A. (1996) *Proc. Natl. Acad. Sci. U.S.A. 93*, 10566−10571.
38. Shafferman, A., Velan, B., Ordentlich, A., Kronman, C., Grosfeld, H., Leitner, M., Flashner, Y., Cohen, S., Barak, D., and Ariel, N. (1992) *EMBO J. 11*, 3561−3568.
39. Velan, B., Barak, D., Ariel, N., Leitner, M., Bino, T., Ordentlich, A., and Shafferman, A. (1996) *FEBS Lett. 395*, 22−28.
40. Radic, Z., Duran, R., Vellom, D. C., Li, Y., Cervenansky, C., and Taylor, P. (1994) *J. Biol. Chem. 269*, 11233−11239.

BI980536L

# Engineering of a monomeric and low-glycosylated form of human butyrylcholinesterase: Expression, purification, characterization and crystallization

**F. Nachon***, Y. Nicolet, N. Viguié, P. Masson, J-C. Fontecilla-Camps, O. Lockridge

European Journal Biochemistry 269 (2002) 630-637

*Eur. J. Biochem.* **269**, 630–637 (2002) © FEBS 2002

# Engineering of a monomeric and low-glycosylated form of human butyrylcholinesterase

## Expression, purification, characterization and crystallization

**Florian Nachon[1], Yvain Nicolet[2], Nathalie Viguié[1], Patrick Masson[1], Juan C. Fontecilla-Camps[2] and Oksana Lockridge[3]**

[1]*Centre de Recherches du Service de Santé des Armées, Unité d'Enzymologie, La Tronche, France;* [2]*Laboratoire de Cristallographie et Cristallogénèse des Protéines, Institut de biologie structurale 'J.P. Ebel', Grenoble, France;* [3]*University of Nebraska Medical Center, Eppley Research Institute, Omaha, NE, USA*

Human butyrylcholinesterase (BChE; EC 3.1.1.8) is of particular interest because it hydrolyzes or scavenges a wide range of toxic compounds including cocaine, organophosphorus pesticides and nerve agents. The relative contribution of each N-linked glycan for the solubility, the stability and the secretion of the enzyme was investigated. A recombinant monomeric BChE lacking four out of nine N-glycosylation sites and the C-terminal oligomerization domain was stably expressed as a monomer in CHO cells. The purified recombinant BChE showed catalytic properties similar to those of the native enzyme. Tetragonal crystals suitable for X-ray crystallography studies were obtained; they were improved by recrystallization and found to diffract to 2.0 Å resolution using synchrotron radiation. The crystals belong to the tetragonal space group I422 with unit cell dimensions a = b = 154.7 Å, c = 124.9 Å, giving a $V_m$ of 2.73 Å$^3$ per Da (estimated 60% solvent) for a single molecule of recombinant BChE in the asymmetric unit. The crystal structure of butyrylcholinesterase will help elucidate unsolved issues concerning cholinesterase mechanisms in general.

*Keywords*: butyrylcholinesterase; crystallization; N-glycosylation; site-directed mutagenesis; X-ray diffraction.

Acetylcholinesterase (AChE; EC 3.1.1.7) and butyrylcholinesterase (BChE; EC 3.1.1.8) are closely related serine hydrolases with different substrate specificity and inhibitor sensitivity. AChE terminates the action of the neurotransmitter acetylcholine at postsynaptic membranes and neuromuscular junctions. Although BChE is found in various vertebrate tissues (liver, intestine, lung, heart, muscle, brain, serum), its physiological role remains undetermined. However, plasma BChE is of pharmacological and toxicological importance because it hydrolyzes ester-containing drugs such as succinylcholine and cocaine. Consequently, purified BChE has been used for treatment of succinylcholine-induced apnea in humans [1] and it is known to protect rodents from the toxic effects of cocaine [2,3]. To improve the rate of hydrolysis of cocaine, a mutated enzyme has been designed [4]. However, a higher catalytic rate may be necessary if BChE is to be used therapeutically in severe cocaine overdoses.

Human BChE is also known to be a good scavenger of organophosphorus (OP) pesticides and chemical warfare nerve agents [5]. For example, injections of purified BChE as pretreatment against nerve agent poisoning in mice, rats and guinea pigs increased their survival with a higher efficiency than the classical pretreatment with pyridostigmine [6–8]. Similar observations have been reported for monkeys [9,10]. Mutants of human BChE (G117H) capable of hydrolyzing OP have also been designed [11]; however, their catalytic mechanism is unclear [12]. It is noteworthy that the equivalent human AChE mutant (G122H) did not acquire OP hydrolase activity (Lockridge, O. & Bartels, C.F. unpublished results). Thus, BChE could be used in the near future for OP decontamination, pretreatment and treatment of OP poisoning.

Progress in engineering of BChE is currently limited by the lack of a three-dimensional structure. three-dimensional models of human BChE have been built by homology to the *Torpedo californica* acetylcholinesterase X-ray structure [13,14]. Although these models contributed to the understanding of some aspects of the difference in specificity between AChE and BChE, they are not satisfactory for enzyme engineering. The crystal structure of human BChE is expected to provide new insights into unsolved issues such as allosteric modulation of cholinesterase activity (BChE presents substrate activation, whereas AChE has substrate inhibition) or the traffic of substrate, products, and water molecules in and out of the active site gorge [15,16].

*Correspondence to* F. Nachon, Centre de Recherches du Service de Santé des Armées, Unité d'enzymologie, 24 Avenue des Maquis du Grésivaudan, BP 87–38702 La Tronche Cédex, France.
Fax: + 33 4 76 63 69 61, Tel.: + 33 4 76 63 69 88,
E-mail: florian@nachon.net

*Abbreviations*: AChE, acetylcholinesterase; BChE, butyrylcholinesterase, CCD, charge coupled device; ChE, cholinesterase; CHO, Chinese hamster ovary; DMEM, Dulbecco's modified Eagle's medium; $Nbs_2$, 5,5′-dithiobis-2-nitrobenzoic acid; HEK, human embryonic kidney cells; OP, organophosphorus ester.

(Received 6 August 2001, revised 19 November 2001, accepted 20 November 2001)

During the past decade, the crystallization of purified plasma BChE has not been successful, despite an exhaustive screening program in one of our laboratories. Human BChE is a heavily glycosylated homotetramer of 340 kDa with nine N-glycosylation sites per catalytic subunit representing almost 25% of its mass [17,18]. It is known that the glycan moieties often perturb crystallization [19,20]. Human BChE oligosaccharides, which are of the complex biantennary type [21,22], could shield the protein surface and prevent or reduce favorable crystal contacts. Therefore, several attempts to deglycosylate the native enzyme were made. Chemical deglycosylation with trifluoroacetic acid, which was successfully used on horseradish peroxidase [23], as well as enzymatic partial deglycosylation using neuraminidase and galactosidase (Masson, P. unpublished results) led to aggregation. Due to the presence of fucose residues, enzymatic deglycosylation using large amounts of recombinant GST–N-glycosidase F fusion protein [24] was not efficient except under mild denaturing conditions. Thus, we decided to investigate the effects of the suppression of N-glycosylation sites to produce a low-glycosylated recombinant BChE suitable for crystallization.

## MATERIALS AND METHODS

### Mutagenesis

4sugOff$_{17/455/481/486}$ BChE$_{\Delta}$ was obtained by PCR using *Pfu* polymerase. Carbohydrate attachment sites at N17, N455, N481, and N486 were deleted by mutating Asn residues to Gln residues. The tetramerization domain at the C-terminus of BChE was deleted by placing a stop codon at position 530 [25,26]. The stop codon deleted 45 amino acids from the C-terminus to yield a protein containing 529 amino acids and six carbohydrate chains. PCR fragments were cloned into the expression plasmid pGS and resequenced to confirm that only the desired mutations were present. Plasmid pGS has the CMV promoter and rat glutamine synthetase for selection.

Other mutants from which carbohydrate attachment sites were deleted were also constucted by PCR. In each case, a codon for Asn was replaced by a codon for Gln. The expression plasmid pGS was suitable for both transient and stable expression.

### Transient expression

BChE mutants were transiently expressed in human embryonic kidney cell line 293T/17, used with permission from D. Baltimore (Rockefeller University of New York; ATCC No CRL 11268). Cells were grown to 80–90% confluence in 100 mm dishes and then transfected by calcium phosphate co-precipitation of 20 μg plasmid DNA per dish. Four days after transfection, the culture medium [5% fetal bovine serum in Dulbecco's modified Eagle's medium (DMEM)] was harvested for a BChE activity assay. Each mutant BChE was transfected into five dishes.

### Large scale production of recombinant human BChE

4sugOff$_{17/455/481/486}$ BChE$_{\Delta}$ in pGS was expressed in CHO cells and stably transfected as previously described [11]. Selective pressure to retain the plasmid was provided by 25 μM methionine sulfoximine. Secreted BChE was collected into serum-free and glutamine-free culture medium, Ultraculture (BioWhittaker, Walkersville, MD, USA; catalogue no. 12–725B), thus avoiding contamination by AChE present in fetal bovine serum. No antibiotics were added to the culture medium. The cells were grown in 1-L roller bottles. The culture medium (150 mL per bottle) in the roller bottles was changed every 2–4 days. A roller bottle yielded enzyme continuously for as long as 6 months. Each L of culture medium contained 3–5 mg of 4sugOff$_{17/455/481/486}$ BChE$_{\Delta}$.

### Purification of 4sugOff$_{17/455/481/486}$ BChE$_{\Delta}$

Units of activity are expressed as μmoles of substrate hydrolyzed per minute. Protein concentration was estimated from absorbance at 280 nm ($E_{1\%} = 18$). A specific activity of 720 U·mg$^{-1}$, measured at 25 °C with 1 mM butyrylthiocholine in 0.1 M potassium phosphate pH 7.0, was the standard for 100% pure native BChE. All purification steps were conducted at 4 °C.

Serum-free culture medium was collected from roller bottles over a period of 6 months. Twenty-six liters of culture medium containing 100 mg of 4sugOff$_{17/455/481/486}$ BChE$_{\Delta}$ were loaded onto 400 mL of procainamide–Sepharose packed in a XK50/30 Pharmacia column (diameter, 5 cm; flow rate of 1 L·h$^{-1}$). The column was washed with 20 mM potassium phosphate, pH 7.0, 1 mM EDTA (until $D_{280} \approx 0$) and then with 0.1, 0.2 and 0.3 M NaCl in buffer. The BChE activity was eluted with buffer containing 0.3 M NaCl and 0.1 M N(Me)$_4$Br. The eluted enzyme was 21% pure as judged from specific activity. Then, the 4sugOff$_{17/455/481/486}$ BChE$_{\Delta}$ was dialyzed against 20 mM Tris/HCl pH 7.4, and loaded onto 400 mL of DE52 anion exchanger (Whatman; catalog no. 4057200, purchased from Fisher Scientific) packed in Pharmacia C26/100 column. The column was washed with 20 mM Tris/HCl pH 7.4 until $D_{280} \approx 0$. BChE was eluted with a NaCl gradient (0–0.5 M NaCl in 1 L buffer); 80% of the BChE activity was recovered. The cleanest fractions (≈ 80% pure) were loaded directly onto a 10-mL procainamide–Sepharose column packed in Pharmacia C10/20 (0.9 cm diameter × 16 cm). The column was washed with 2 L of 20 mM Tris/HCl pH 7.4. 4sugOff$_{17/455/481/486}$ BChE$_{\Delta}$ (9.3 mg, 6740 U; 98% pure) was eluted with 400 mL of 0.6 M NaCl in 20 mM Tris/HCl pH 7.4, then dialyzed against 5 mM Mes pH 6.5 and concentrated to 10 mg·mL$^{-1}$ (7200 U·mL$^{-1}$) in an Amicon Diaflo apparatus with a PM10 membrane. The dialyzed, concentrated sample was filtered through a 0.2-μm filter and stored at 4 °C.

### Determination of kinetic parameters

Hydrolysis of butyrylthiocholine iodide at 25 °C was measured at concentrations ranging from 0.010 to 50 mM according to the method of Ellman [27]. The buffer was 0.1 M sodium phosphate at pH 7.0 and contained 0.1 mg·mL$^{-1}$ $Nbs_2$ and 0.1% BSA. The active sites were titrated by the method of residual activity using diisopropyl phosphoro fluoridate (DFP) as titrant [28]. Kinetic parameters ($k_{cat}$, $K_m$, $K_{ss}$, $b$ factor) were determined by nonlinear fitting of the apparent rate vs. [S] using the equation described by Radic *et al.* [29].

### Crystallization

A home-made sparse matrix kit similar to the one described by Jancarik & Kim [30] was used to screen for initial crystallization conditions in a hanging drop system [20]. BChE crystallized at a concentration of 6.6 mg·mL$^{-1}$ from a 0.1-M Mes buffer solution, pH 6.5 at 20 °C, containing 2.05–2.15 M $(NH_4)_2SO_4$ (Fluka) and using drops of 3 μL and a protein to reservoir ratio of 1 : 2 (v/v). Crystals grew in about 1 week. Their quality was improved using the recrystallization procedure described by Kryger [31].

### Catalytic activity in the crystals

A recombinant BChE crystal grown at pH 6.5 was washed twice for 5 min in a 100 μL drop of 0.1 M Mes pH 6.5 buffer containing 2.4 M $(NH_4)_2SO_4$. Then the crystal was soaked in a 20-μL drop of the same buffer containing 0.1 mg·mL$^{-1}$ $Nbs_2$ and 5 mM butyrylthiocholine iodide (Sigma). The change in crystal coloration (turning yellow) was followed under a binocular magnifying glass. No spontaneous hydrolysis of the substrate in the soaking liquor was observed when monitored by spectrophotometry at 412 nm.

### Data collection

Diffraction data were collected at $\lambda = 0.932$ Å wavelength to 2.0 Å resolution at the ID14-eh2 beamline of the European Synchrotron Radiation Facility with a MAR-Research CCD detector. To prevent ice formation, crystals were soaked for a few minutes in a 2.4-M $(NH_4)_2SO_4$, 15% glycerol, 0.1 M Mes pH 6.5 buffer just before flash-cooling at 100 K in a nitrogen stream. Collected data were indexed, integrated and reduced using MOSFLM and SCALA from the CCP4 suite [32].

## RESULTS AND DISCUSSION

### Engineering of a low-glycosylated truncated BChE

Glycosylation influences the folding, secretion, stability, and solubility of ChE as well as the clearance of their plasmatic forms [22,33–35]. Heavy glycosylation of BChE contributes to its long residence time in blood circulation and protects it against proteolysis. For example, the glycosylation patterns may change with the tissue localization, but do not seem to play a critical role in the catalytic properties of the enzyme [36]. Our goal was to favor the crystallization of BChE by designing an enzyme with the fewest possible glycosylation sites, while preserving its solubility, stability and functional properties. Amino-acid sequences of AChE and BChE from different species were aligned to pinpoint the conserved N-glycosylation sites (Table 1). BChEs are generally more glycosylated than AChEs. AChEs from different species contain three to six N-glycosylation sites, three of which are conserved in BChE. Therefore, our first attempt was to construct a recombinant BChE containing only these three glycosylation sites (positions 256, 341 and 455). This was achieved by mutating six Asn residues in Asn-X-Ser/Thr recognition sites into Gln residues.

These studies overlooked the possibility that a mutation of Asn486 might unmask a glycosylation site at Asn485. Three glycosylation recognition sites are present in the sequence $N_{481}$ETQNNSTS$_{489}$, but the peptide sequencing of human BChE showed that positions 481 and 486 were glycosylated, and position 485 was not [18]. Because Asn485 and Asn486 are adjacent, the nonglycosylation of Asn485 may be due to steric hindrance. Therefore, we assume that all of the constructs with the double mutation N481Q/N486Q should be glycosylated at position 485.

**Table 1. Comparison of the N-glycosylation positions for various cholinesterases.**

| | Potential N-glycosylation sites (human BChE numbering) | | | | | | | | | |
|---|---|---|---|---|---|---|---|---|---|---|
| Enzyme | 17 | 57 | 106 | 241 | 256 | 341 | 455 | 481 | 486 | Others |
| BChE | | | | | | | | | | |
| human | X | X | X | X | X | X | X | X | X | |
| monkey | X | X | X | X | X | X | X | X | X | |
| cat | | X | X | X | X | X | X | X | X | |
| tiger | | X | X | X | X | X | X | X | X | |
| rabbit | | X | X | X | X | X | X | X | X | |
| mouse | | X | X | X | | X | X | X | X | |
| horse | | X | X | X | X | X | X | X | X | |
| rat | | X | X | X | | X | X | X | X | 1 |
| AChE | | | | | | | | | | |
| human | | | | | X | X | X | | | |
| cat | | | | | X | X | X | | | |
| rabbit | | | | | X | X | X | | | |
| mouse | | | | | X | X | X | | | |
| cow | | X | | | X | X | X | | | |
| Torpedo fish | | X | | | | | X | | | 2 |
| rat | | | | | X | X | X | | | |
| Bungarus | | | | | X | X | X | | | 2 |
| eel | | | X | | X | X | X | | | 2 |
| zebrafish | | | X | | X | X | X | | | 2 |

**Table 2. Influence of the number and position of N-glycosylation sites on the expression level of secreted human BChE.** The presence or absence of the oligomerization domain at the C-terminus is indicated by yes or no. Transient transfection in 293T cells was repeated in five dishes. The relative expression unit corresponds to 0.2 μmol butyrylthiocholine hydrolyzed per minute.

| | | Potential N-glycosylation sites | | | | | | | | | | |
|---|---|---|---|---|---|---|---|---|---|---|---|---|
| Number sites off | Oligomeric domain | 17 | 57 | 106 | 241 | 256 | 341 | 455 | 481 | 485 | 486 | Relative expression level |
| 0[a] | Yes | | X | X | X | X | X | X | | X | 1[a] | |
| 2 | Yes | X | X | X | X | X | X | X | | X | | 1.45 |
| 3 | Yes | X | X | X | X | X | X | | | X | | 1.15 |
| 4 | Yes | X | X | X | X | | X | | | X | | 1 |
| 4 | No | X | X | X | X | | X | | | X | | 7.2 |
| 4[b] | No | X | X | X | X | X | X | | | X | | 6[b] |
| 5 | Yes | | X | X | X | | | | | X | | 0.2 |
| 6 | Yes | X | X | | | X | X | X | | X | | 0.1 |
| 7 | Yes | | | | | X | X | | | X | | 0.1 |
| 9 | Yes | | | | | | | | | X | | 0.025 |

[a] Wild-type human BchE. [b] Clone chosen for crystallization trials.

A recombinant BChE containing the three conserved glycosylation sites, N256, N341 and N455 plus the one unmasked at position 485, was transiently expressed in 293T cells. Unfortunately, the expression level in the culture medium was ≈ 10-fold lower than for the native enzyme (Table 2, six sites off). The suppression of seven or nine sites yielded poor expression levels as well (Table 2, seven and nine sites off) due to retention of the protein inside the cell, as shown by Western blotting. As the expression level of these clones was not high enough to produce large amounts of BChE, new constructs were tested in which the N-glycosylation sites were suppressed empirically.

Suppression of sites N481 and N486 (Table 2, two sites off) led to 45% higher expression levels than native BChE. Suppression of sites N455, N481 and 486 led to a 15% greater expression level than the native enzyme (Table 2, three sites off). When an additional site was suppressed at position N256, the expression level was similar to that of the native enzyme (Table 2, four sites off; oligomeric domain: 'yes'). The additional N341Q mutation resulted in a fivefold lower active enzyme (Tables 2, five sites off). Consequently, the five glycosylation sites mutant was not used any further. Interestingly, the N341 site is also conserved in *Candida rugosa* lipase, where it plays an important role in the stabilization of the open conformation of the enzyme [37]. Such a role has not yet been observed in cholinesterases.

The tetramerization domain is located at the C-termini of AChE and BChE. In human BChE, this domain comprises 40 amino acids, encoded by exon 4. Its deletion leads to higher levels of secretion into the culture medium and expression of monomers [25]. Crystallization of monomeric cholinesterases is more favorable than for oligomeric forms, even if they form a noncovalent dimer by association of a four-helix bundle (helices 383–372 and 526–543; human

```
Rec.  BChE   ----EDDIIIATKNGKVRGMQLTVFGGTVTAFLGIPYAQPPLGRLRFKKPQSLTKWSDIWNATKYANSCCQNIDQSFPGFHGSEMWNPNTDLSEDCLYLNVWIPAPKPKN-ATVLIWIYG 115
Human BChE   ----EDDIIIATKNGKVRGMNLTVFGGTVTAFLGIPYAQPPLGRLRFKKPQSLTKWSDIWNATKYANSCCQNIDQSFPGFHGSEMWNPNTDLSEDCLYLNVWIPAPKPKN-ATVLIWIYG 115
Torca AChE    --DDHSELLVNTKSGKVMGTRVPVLSSHISAFLGIPFAEPPVGNMRFRRPEPKKPWSGVWNASTYPNNCQQYVDEQFPGFSGSEMWNPNREMSEDCLYLNIWVPSPRPKS-TTVMVWIYG 117
Human AChE   EGREDAELLVTVRGGRLRGIRLKTPGGPVSAFLGIPFAEPPMGPRRFLPPEPKQPWSGVVDATTFQSVCYQYVDTLYPGFEGTEMWNPNRELSEDCLYLNVWTPYPRPTSPTPVLVWIYG 120
Mouse AChE   EGREDPQLLVRVRGGQLRGIRLKAPGGPVSAFLGIPFAEPPVGSRRFMPPEPKRPWSGVLDATTFQNVCYQYVDTLYPGFEGTEMWNPNRELSEDCLYLNVWTPYPRPASPTPVLIWIYG 120
                    ...  . *.. *  .      ..******.*.**.*  **  *.    ** .  *. .   * * .*  .*** *.****** ..********.* * *.*   . *..****

Rec.  BChE   GGFQTGTSSLHVYDGKFLARVERVIVVSMNYRVGALGFLALPGNPEAPGNMGLFDQQLALQWVQKNIAAFGGNPKSVTLFGESAGAASVSLHLLSPGSHSLFTRAILQSGSFNAPWAVTS 235
Human BChE   GGFQTGTSSLHVYDGKFLARVERVIVVSMNYRVGALGFLALPGNPEAPGNMGLFDQQLALQWVQKNIAAFGGNPKSVTLFGESAGAASVSLHLLSPGSHSLFTRAILQSGSFNAPWAVTS 235
Torca AChE    GGFYSGSSTLDVYNGKYLAYTEEVVLVSLSYRVGAFGFLALHGSQEAPGNVGLLDQRMALQWVHDNIQFFGGDPKTVTIFGESAGGASVGMHILSPGSRDLFRRAILQSGSPNCPWASVS 237
Human AChE   GGFYSGASSLDVYDGRFLVQAERTVLVSMNYRVGAFGFLALPGSREAPGNVGLLDQRLALQWVQENVAAFGGDPTSVTLFGESAGAASVGMHLLSPPSRGLFHRAVLQSGAPNGPWATVG 240
Mouse AChE   GGFYSGAASLDVYDGRFLAQVEGAVLVSMNYRVGTFGFLALPGSREAPGNVGLLDQRLALQWVQENIAAFGGDPMSVTLFGESAGAASVGMHILSLPSRSLFHRAVLQSGTPNGPWATVS 240
            *** .*...* ** *..*   *  ..**. ****. ***** *  *****.** **..*****. *.  *** * .**.****** *** .*.**  *. ** **.****. * ***

Rec.  BChE   LYEARNRTLNLAKLTGCSRE----NETEIIKCLRNKDPQEILLNEAFVVPYGTPLSVNFGPTVDGDFLTDMPDILLELGQFKKTQILVGVNKDEGTAFLVYGAPGFSKDNNSIITRKEFQ 351
Human BChE   LYEARNRTLNLAKLTGCSRE----NETEIIKCLRNKDPQEILLNEAFVVPYGTPLSVNFGPTVDGDFLTDMPDILLELGQFKKTQILVGVNKDEGTAFLVYGAPGFSKDNNSIITRKEFQ 351
Torca AChE    VAEGRRRAVELGRNLNCNLN----SDEELIHCLREKKPQELIDVEWNVLPFDSIFRFSFVPVIDGEFFPTSLESMLNSGNFKKTQILLGVNKDEGSFFLLYGAPGFSKDSESKISREDFM 353
Human AChE   MGEARRRATQLAHLVGCPPGGTGGNDTELVACLRTRPAQVLVNHEWHVLPQESVFRFSFVPVVDGDFLSDTPEALINAGDFHGLQVLVGVVKDEGSYFLVYGAPGFSKDNESLISRAEFL 360
Mouse AChE   AGEARRRATLLARLVGCPPGGAGGNDTELIACLRTRPAQDLVDHEWHVLPQESIFRFSFVPVVDGDFLSDTPEALINTGDFQDLQVLVGVVKDEGSYFLVYGVPGFSKDNESLISRAQFL 360
              * * *.  * .  .*        . *.. *** .  * ..  *  *.*  .     * * .**.*     . ..  * *.  *.*.** ****. **.** ******  * *.*  *

Rec.  BChE   EGLKIFFPGVSEFGKESILFHYTDWVDDQRPENYREALGDVVGDYNFICPALEFTKKFSEWGNNAFFYYFEHRSSKLPWPEWMGVMHGYEIEFVFGLPLERRDQYTKAEEILSRSIVKRW 471
Human BChE   EGLKIFFPGVSEFGKESILFHYTDWVDDQRPENYREALGDVVGDYNFICPALEFTKKFSEWGNNAFFYYFEHRSSKLPWPEWMGVMHGYEIEFVFGLPLERRDNYTKAEEILSRSIVKRW 471
Torca AChE    SGVKLSVPHANDLGLDAVTLQYTDWMDDNNGIKNRDGLDDIVGDHNVICPLMHFVNKYTKFGNGTYLYFFNHRASNLVWPEWMGVIHGYEIEFVFGLPLVKELNYTAEEEALSRRIMHYW 473
Human AChE   AGVRVGVPQVSDLAAEAVVLHYTDWLHPEDPARLREALSDVVGDHNVVCPVAQLAGRLAAQGARVYAYVFEHRASTLSWPLWMGVPHGYEIEFIFGIPLDPSRNYTAEEKIFAQRLMRYW 480
Mouse AChE   AGVRIGVPQASDLAAEAVVLHYTDWLHPEDPTHLRDAMSAVVGDHNVVCPVAQLAGRLAAQGARVYAYIFEHRASTLTWPLWMGVPHGYEIEFIFGLPLDPSLNYTTEERIFAQRLMKYW 480
              *...  *   .   ...  .****.       *. .  .*** * .**      . .  *   . * * **.* * ** **** *******.**.**    .**  *   .. ... *

Rec.  BChE   ANFAKYGNPQETQNQST-SWPVFKSTEQKYLTLNTESTRIMTKLRAQQCRFWTSFFPKV---------------------------------------------- 529
Human BChE   ANFAKYGNPNETQNNST-SWPVFKSTEQKYLTLNTESTRIMTKLRAQQCRFWTSFFPKVLEMTGNIDEAEWEWKAGFHRWNNYMMDWKNQFNDYTSKKESCVGL 574
Torca AChE    ATFAKTGNPNEPHSQES-KWPLFTTKEQKFIDLNTEPMKVHQRLRVQMCVFWNQFLPKLLNATAC---------------------------------------- 537
Human AChE   ANFARTGDPNEPRDPKAPQWPPYTAGAQQYVSLDLRPLEVRRGLRAQACAFWNRFLPKLLSAT---------------------------------------- 543
Mouse AChE   TNFARTGDPNDPRDSKSPQWPPYTTAAQQYVSLNLKPLEVRRGLRAQTCAFWNRFLPKLLSATATEAP---------------------------------- 548
             ..**. * *.. .   .  ** . .  *... *      .   ** * * **. * **.
```

**Fig. 1. Alignment of the amino-acid sequences of 4sugOff$_{17/455/481/486}$ BChE$_{\Delta}$, human BChE, and crystallized forms of human AChE, mouse AChE and *Torpedo californica* AChE.** 4sugOff$_{17/455/481/486}$ BChE$_{\Delta}$ (Rec. BChE), human BChE [18], human AChE [44], mouse AChE [38] and *T. californica* AChE (Torca AChE) [45] were aligned using CLUSTALW. Asterisks denote identity, and full stops show high similarity.

AChE numbering) under the protein concentrations used for crystallization [31,38]. Therefore, a truncated BChE lacking both the tetramerization domain and the N256, N455, N481 and N486 N-glycosylation sites was constructed. Deletion of the tetramerization domain was achieved by introducing a stop codon at position 530 according to Blong *et al.* [25]. As expected, activity measured in culture media was about sevenfold higher for the monomeric form ($BChE_{\Delta}$) than for the oligomeric form (Tables 2, four sites off; oligomeric domain: 'no'). In another effort, a second truncated clone also lacking four N-glycosylation sites (N17, N455, N481 and N486) was constructed. The activity level of this enzyme was slightly lower than that of the previous clone but sufficiently high to produce significant amounts of enzyme. Consequently, this clone ($4sugOff_{17/455/481/486}$ $BChE_{\Delta}$) was chosen for large scale expression. Figure 1 shows how the amino-acid sequence of $4sugOff_{17/455/481/486}$ $BChE_{\Delta}$ compares to the native human BChE enzyme and to the crystallized forms of *Torpedo californica*, human and mouse AChEs. According to this alignment, the X-ray structure of *Torpedo californica* AChE should provide a good probe model to solve the structure of $4sugOff_{17/455/481/486}$ $BChE_{\Delta}$ by a molecular-replacement procedure.

### Preparation of $4sugOff_{17/455/481/486}$ $BChE_{\Delta}$

The mutated $BChE_{\Delta}$ cloned into the pGS expression vector, that expresses Gln-synthethase for selection purposes, was transfected into CHO cells. Stable clones secreting high levels of recombinant $BChE_{\Delta}$ were selected for large-scale production. Purification was carried out by anion-exchange and affinity chromatography. Axelsen *et al.* reported that decamethonium, used during the last affinity chromatography step of *T. californica* AChE, was present in the crystals despite extensive dialysis of the purified enzyme [39]. Thus, to avoid contamination by a ligand, NaCl was used for elution of BChE from affinity chromatography gels. The purity of the final enzyme preparation was estimated to be greater than 98% based on its specific activity and the presence of a single band on SDS/PAGE.

### Characterization of $4sugOff_{17/455/481/486}$ $BChE_{\Delta}$

The kinetics of butyrylthiocholine hydrolysis by recombinant BChE under standard conditions (0.1 M phosphate buffer, pH 7.0) can be described by the model of Radic [29]. The kinetic parameters are very close to the values reported previously for the native BChE [40], with $k_{cat} = 28\,000\ min^{-1}$ and $K_m = 25.6 \pm 0.4\ \mu M$ ($n = 3$). The native enzyme and recombinant BChE display similar substrate activation with $K_{ss} = 510 \pm 35\ \mu M$ ($n = 3$) and $b$ factor $= 2.85 \pm 0.15$ ($n = 3$). Thus, the catalytic properties of the recombinant enzyme can be considered to be the same as the plasma enzyme.

SDS/PAGE analysis of the purified recombinant BChE monomer displayed a single broad band in the 70–75 kDa molecular mass range. In contrast, the purified plasma BChE showed a faint band at 170 kDa (nonreducible dimer) and a major broad band at 85 kDa (monomer) under reducing conditions (Fig. 2A). The apparent molecular mass of the recombinant monomer is consistent with the expected molecular mass for the truncated BChE after the deletion of 45 residues at the C-terminal sequence and

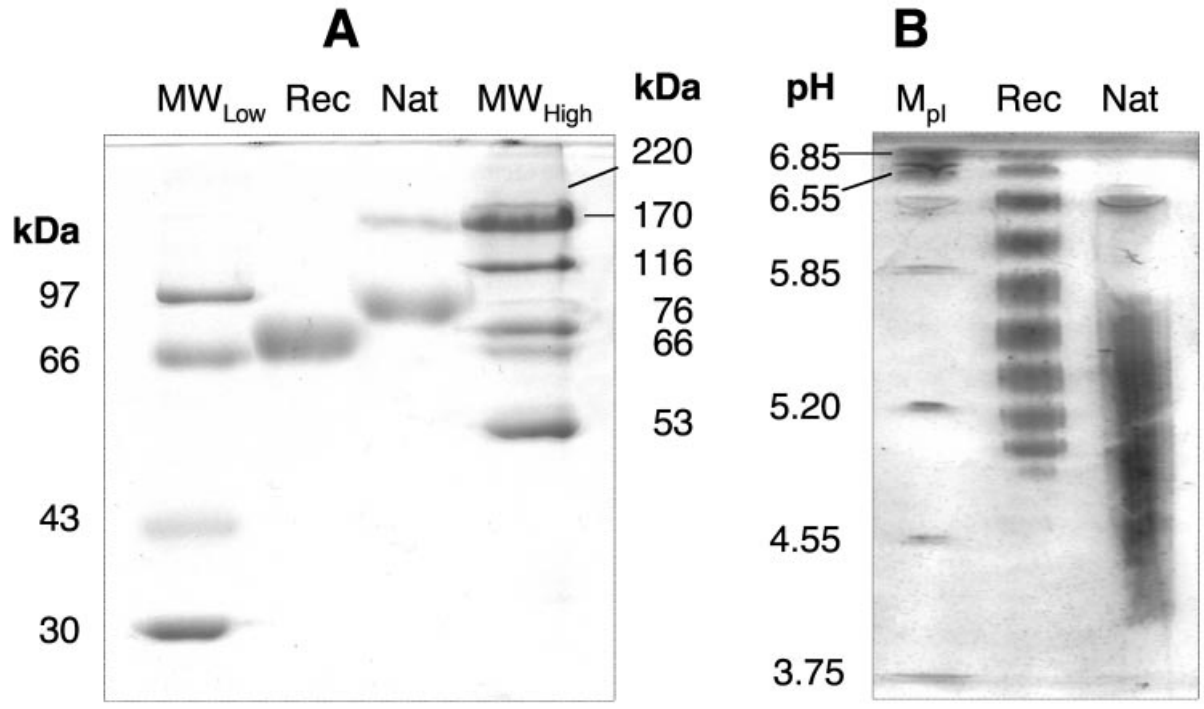


**Fig. 2. Gel electrophoresis analysis of $4sugOff_{17/455/481/486}$ $BChE_{\Delta}$ (Rec) and human native BChE (Nat).** (A) SDS/PAGE (4.5% stacking/10% separating) was carried out under reducing conditions according to Laemmli [46] using the Biorad MiniProtean II gel system and Coomassie blue staining. (B) Isoelectrofocusing gel was carried out on a Pharmacia Phast System using Phast gel (4–6.5; pH range) and silver staining [47].

four N-glycosylation sites. The broadness of the band suggests that the purified 4sugOff$_{17/455/481/486}$ BChE$_{\Delta}$ still displays a significant glycosylation-related heterogeneity. This issue was addressed using IEF analysis. The carbohydrate chains of BChE are partly capped by sialic acids [22], which directly influence the pI of the enzyme. Whereas plasma BChE displayed a continuous smear extending from pH 4.0 to 5.7, thus reflecting high sialylation heterogeneity, 4sugOff$_{17/455/481/486}$ BChE$_{\Delta}$ displayed 10 well-resolved bands between pH 5.0 and 6.5 (Fig. 2B). This was a definite improvement of the enzyme homogeneity, and encouraged us to start BChE crystallization trials.

### Crystallization of 4sugOff$_{17/455/481/486}$ BChE$_{\Delta}$ and data collection

Initial crystallization conditions were screened according to Jancarick & Kim [30] using the hanging drop method. Tetragonal crystals appeared within 1 week in a pH 6.5 0.1 M Mes buffer solution containing 2.1 M $(NH_4)_2SO_4$ (Fig. 3A). Interestingly, these crystals appear morphologically similar to the crystals of fully glycosylated equine serum BChE obtained in 1944 [41]. However these BChE crystals were not further characterized due to technical limitations at that time.

To check whether the crystallized recombinant BChE was still active, one crystal was soaked in Ellman's buffer containing 5 mM butyrylthiocholine and 2.4 M $(NH_4)_2SO_4$. This higher concentration of precipitant was necessary to avoid the dissolution of the crystal. After a few minutes, the colorless crystal turned yellow, the color of the product of the Ellman's reaction (Fig. 3B). The crystalline enzyme seems to be sufficiently flexible to display an observable catalytic activity, and small molecules such as butyrylthiocholine, $Nbs_2$ and the product of the Ellman's reaction may easily diffuse in a short period of time inside and outside the crystals. However we cannot rule out the possibility that the substrate might have been hydrolyzed by the protein located in the crystal surface, which is likely to solubilize during the soaking experiment.

The crystals that measured up to 0.3 mm in their longest dimension diffracted to 2.2–2.3 Å resolution at 100 K, using 15% glycerol (v/v) as a cryoprotectant, and synchrotron radiation at the ESRF ID14-eh1 beamline. As recrystallization improved the quality of human AChE crystals [31], we reproduced the procedure by transferring crystal-containing drops over reservoirs of water until the crystals dissolved. The drops were then placed over the original reservoir solution, or a solution with slightly lower precipitant concentration, for recrystallization. As reported for human AChE, these new crystals were fewer but larger with longest dimensions of up to 0.6 mm. They diffracted to 2.0 Å at 100 K, using 15% glycerol (v/v) as a cryoprotectant, and synchrotron radiation at the ESRF ID14-eh2 beamline. Analysis of the collected data (Table 3) indicated that BChE crystals belong to the tetragonal space group I422 with unit cell dimensions a = b = 154.7 Å, c = 127.9 Å, giving a $V_m$ of 2.73 Å$^3$ per Da (estimated 60% solvent) for a crystal containing a single molecule of recombinant BChE (≈ 70 kDa) per asymmetric unit [42]. A total of 371 832 observations were obtained at 2.0 Å resolution giving ≈ 49 298 unique reflections (98.6% complete, $R_{sym}$ = 0.073). The structure has been successfully solved by molecular replacement starting from the model of native *T. californica* AChE, PDB code 2ace [43]. The refinement of the model is underway.

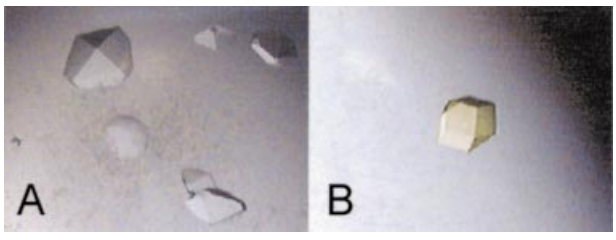


**Fig. 3. Tetragonal crystals of 4sugOff$_{17/455/481/486}$ BChE$_{\Delta}$.** (A) The larger crystal has dimension of 0.5 × 0.5 × 0.3 mm$^3$. (B) Crystal after a 10-min soaking in Ellman's buffer with precipitant and 5 mM butyrylthiocholine.

**Table 3. Data collection and processing.** Values for the highest resolution shell are given in parentheses.

| | |
|---|---|
| Space group | I422 |
| Unit-cell parameters | a = b = 154.66 Å, c = 127.89 Å, α = β = γ = 90° |
| X-ray source | ESRF |
| Beamline | ID14-eh2 |
| Wavelength | 0.933 Å |
| Diffraction limit | 2.0 Å |
| No. of measured reflections | 371 832 |
| No. of unique reflections | 49 298 |
| Highest resolution shell | 2.1 → 2.0 Å |
| Completeness | 98.6% (99.1%) |
| Multiplicity | 7.1 (6.4) |
| $R_{sym}$ (on I) | 0.073% (0.431%) |
| I/σ | 6.5 (1.7) |
| *b* Factor average | 30.65 Å$^2$ |

In summary, a recombinant human butyrylcholinesterase suitable for crystallization has been constructed by suppressing four out of nine N-glycosylation sites and deleting its oligomerization domain. Large amounts of pure recombinant enzyme were obtained by expression in CHO cells and purification by anion-exchange and affinity chromatographies. The recombinant enzyme showed less heterogeneity than the natural form while conserving identical catalytical properties. Crystals were grown at pH 6.5 using $(NH_4)_2SO_4$ as the precipitant. After their quality was improved by recrystallization, they diffracted to 2.0 Å resolution. The first three-dimensional structure of a butyrylcholinesterase is expected to improve our knowledge regarding ChE mechanism, such as allosteric modulation, product clearance outside the active site gorge and motion of water molecules. Moreover, the three-dimensional structure of human BChE should provide a template for the design of new mutants capable of hydrolyzing nerve agents and drugs such as cocaine with increased efficiency.

## ACKNOWLEDGEMENTS

This work was supported by the US Army Medical Research and Materiel Command under contract DAMD 17-97-1-7349 to O. L. and

the Délégation Générale de l'Armement under contract DGA/DSP/STTC-PEA 990802/99 CO 029 (ODCA, Washington, DC, 00-2-032-0-00) to P. M. We thank, respectively, Hassan Belrhali and Joanne McCarthy for the opportunity to collect data at the ID14-eh1 and ID14-eh2 beamline at the ESRF in Grenoble.

## REFERENCES

1. Viby-Mogensen, J. (1981) Succinylcholine neuromuscular blockade in subjects heterozygous for abnormal plasma cholinesterase. *Anesthesiology* **55**, 231–235.
2. Hoffman, R.S., Morasco, R. & Goldfrank, L.R. (1996) Administration of purified human plasma cholinesterase protects against cocaine toxicity in mice. *J. Toxicol. Clin. Toxicol.* **34**, 259–266.
3. Lynch, T.J., Mattes, C.E., Singh, A., Bradley, R.M., Brady, R.O. & Dretchen, K.L. (1997) Cocaine detoxification by human plasma butyrylcholinesterase. *Toxicol. Appl. Pharmacol.* **145**, 363–371.
4. Xie, W., Altamirano, C.V., Bartels, C.F., Speirs, R.J., Cashman, J.R. & Lockridge, O. (1999) An improved cocaine hydrolase: the A328Y mutant of human butyrylcholinesterase is 4-fold more efficient. *Mol. Pharmacol.* **55**, 83–91.
5. Lockridge, O. & Masson, P. (2000) Pesticides and susceptible populations: people with butyrylcholinesterase genetic variants may be at risk. *Neurotoxicology*. **21**, 113–126.
6. Raveh, L., Grunwald, J., Marcus, D., Papier, Y., Cohen, E. & Ashani, Y. (1993) Human butyrylcholinesterase as a general prophylactic antidote for nerve agent toxicity. *In vitro* and *in vivo* quantitative characterization. *Biochem. Pharmacol.* **45**, 2465–2474.
7. Ashani, Y., Shapira, S., Levy, D., Wolfe, A.D., Doctor, B.P. & Raveh, L. (1991) Butyrylcholinesterase and acetylcholinesterase prophylaxis against soman poisoning in mice. *Biochem. Pharmacol.* **41**, 37–41.
8. Allon, N., Raveh, L., Gilat, E., Cohen, E., Grunwald, J. & Ashani, Y. (1998) Prophylaxis against soman inhalation toxicity in guinea pigs by pretreatment alone with human serum butyrylcholinesterase. *Toxicol. Sci.* **43**, 121–128.
9. Broomfield, C.A., Maxwell, D.M., Solana, R.P., Castro, C.A., Finger, A.V. & Lenz, D.E. (1991) Protection by butyrylcholinesterase against organophosphorus poisoning in nonhuman primates. *J. Pharmacol. Exp. Ther.* **259**, 633–638.
10. Wolfe, A.D., Blick, D.W., Murphy, M.R., Miller, S.A., Gentry, M.K., Hartgraves, S.L. & Doctor, B.P. (1992) Use of cholinesterases as pretreatment drugs for the protection of rhesus monkeys against soman toxicity. *Toxicol. Appl. Pharmacol.* **117**, 189–193.
11. Lockridge, O., Blong, R.M., Masson, P., Froment, M.T., Millard, C.B. & Broomfield, C.A. (1997) A single amino acid substitution, Gly117His, confers phosphotriesterase (organophosphorus acid anhydride hydrolase) activity on human butyrylcholinesterase. *Biochemistry*. **36**, 786–795.
12. Albaret, C., Masson, P., Broomfield, C.A., El Kaim, L. & Fortier, P.L. (1998) Mechanical aspects of the phosphotriesterase activity of human butyrylcholinesterase G117H mutant. In *Structure and Function of Cholinesterases and Related Proteins* (Doctor, B.P., ed.), pp. 339–405. Plenum Press, New York, NY.
13. Millard, C.B. & Broomfield, C.A. (1992) A computer model of glycosylated human butyrylcholinesterase. *Biochem. Biophys. Res. Commun.* **189**, 1280–1286.
14. Harel, M., Sussman, J.L., Krejci, E., Bon, S., Chanal, P., Massoulie, J. & Silman, I. (1992) Conversion of acetylcholinesterase to butyrylcholinesterase: modeling and mutagenesis. *Proc. Natl Acad. Sci. USA* **89**, 10827–10831.
15. Gilson, M.K., Straatsma, T.P., Mccammon, J.A., Ripoll, D.R., Faerman, C.H., Axelsen, P.H., Silman, I. & Sussman, J.L. (1994) Open back door in a molecular dynamics simulation of acetylcholinesterase. *Science* **263**, 1276–1278.
16. Henchman, R., Tai, K., Shen, T.B., Börjesson, U., Philippopoulos, M. & Mccammon, J.A. (2001) *A Structural and Dynamical Analysis of Water in Acetylcholinesterase* (Paper presented at the American Chemical Society National Meeting 2001). The American Chemical Society, San Diego, CA, USA.
17. Lockridge, O., Eckerson, H.W. & Du La, B.N. (1979) Interchain disulfide bonds and subunit organization in human serum cholinesterase. *J. Biol. Chem.* **254**, 8324–8330.
18. Lockridge, O., Bartels, C.F., Vaughan, T.A., Wong, C.K., Norton, S.E. & Johnson, L.L. (1987) Complete amino acid sequence of human serum cholinesterase. *J. Biol. Chem.* **262**, 549–557.
19. Davis, S.J., Puklavec, M.J., Ashford, D.A., Harlos, K., Jones, E.Y., Stuart, D.I. & Williams, A.F. (1993) Expression of soluble recombinant glycoproteins with predefined glycosylation: application to the crystallization of the T-cell glycoprotein CD2. *Protein Eng.* **6**, 229–232.
20. Mcpherson, A. (1982) *Preparation and Analysis of Protein Crystals*. John Wiley & Sons, New York, NY.
21. Ohkura, T., Hada, T., Higashino, K., Ohue, T., Kochibe, N., Koide, N. & Yamashita, K. (1994) Increase of fucosylated serum cholinesterase in relation to high risk groups for hepatocellular carcinomas. *Cancer Res.* **54**, 55–61.
22. Saxena, A., Raveh, L., Ashani, Y. & Doctor, B.P. (1997) Structure of glycan moieties responsible for the extended circulatory life time of fetal bovine serum acetylcholinesterase and equine serum butyrylcholinesterase. *Biochemistry* **36**, 7481–7489.
23. Tams, J.W. & Welinder, K.G. (1995) Mild chemical deglycosylation of horseradish peroxidase yields a fully active, homogeneous enzyme. *Anal. Biochem.* **228**, 48–55.
24. Grueninger-Leitch, F., D'Arcy, A., D'Arcy, B. & Chene, C. (1996) Deglycosylation of proteins for crystallization using recombinant fusion protein glycosidases. *Protein Sci.* **5**, 2617–2622.
25. Blong, R.M., Bedows, E. & Lockridge, O. (1997) Tetramerization domain of human butyrylcholinesterase is at the C-terminus. *Biochem. J.* **327**, 747–757.
26. Altamirano, C.V. & Lockridge, O. (1999) Conserved aromatic residues of the C-terminus of human butyrylcholinesterase mediate the association of tetramers. *Biochemistry* **38**, 13414–13422.
27. Ellman, G.L., Courtney, K.D., Andres, J.V. & Featherstone, R.M. (1961) A new and rapid colorimetric determination of acetylcholinesterase activity. *Biochem. Pharmacol.* **7**, 88–95.
28. Leuzinger, W. (1971) The number of catalytic sites in acetylcholinesterase. *Biochem. J.* **236**, 139–141.
29. Radic, Z., Pickering, N.A., Vellom, D.C., Camp, S. & Taylor, P. (1993) Three distinct domains in the cholinesterase molecule confer selectivity for acetyl- and butyrylcholinesterase inhibitors. *Biochemistry* **32**, 12074–12084.
30. Jancarik, J. & Kim, S.H. (1991) Sparse matrix sampling: a screening method for crystallization of proteins. *J. Appl. Crystallogr.* **24**, 409–411.
31. Kryger, G., Harel, M., Giles, K., Toker, L., Velan, B., Lazar, A., Kronman, C., Barak, D., Ariel, N., Shafferman, A., Silman, I. & Sussman, J.L. (2000) Structures of recombinant native and E202Q mutant human acetylcholinesterase complexed with the snake-venom toxin fasciculin-II. *Acta Crystallogr.* **D56**, 1385–1394.
32. Collaborative Computational Computer Project 4. . (1994) The CCP4 suite: programs for protein crystallography. *Acta Crystallogr.* **D50**, 760–763.
33. Kronman, C., Chitlaru, T., Elhanany, E., Velan, B. & Shafferman, A. (2000) Hierarchy of post-translational modifications involved in the circulatory longevity of glycoproteins. Demonstration of concerted contributions of glycan sialylation and subunit assembly to the pharmacokinetic behavior of bovine acetylcholinesterase. *J. Biol. Chem.* **275**, 29488–29502.
34. Wang, C., Eufemi, M., Turano, C. & Giartosio, A. (1996) Influence of the carbohydrate moiety on the stability of glycoproteins. *Biochemistry* **35**, 7299–7307.

35. Kronman, C., Velan, B., Marcus, D., Ordentlich, A., Reuveny, S. & Shafferman, A. (1995) Involvement of oligomerization, N-glycosylation and sialylation in the clearance of cholinesterases from the circulation. *Biochem. J.* **311**, 959–967.
36. Liao, J., Heider, H., Sun, M.C. & Brodbeck, U. (1992) Different glycosylation in acetylcholinesterases from mammalian brain and erythrocytes. *J. Neurochem.* **58**, 1230–1238.
37. Brocca, S., Persson, M., Wehtje, E., Adlercreutz, P., Alberghina, L. & Lotti, M. (2000) Mutants provide evidence of the importance of glycosydic chains in the activation of lipase 1 from *Candida rugosa*. *Protein Sci.* **9**, 985–990.
38. Marchot, P., Ravelli, R.B., Raves, M.L., Bourne, Y., Vellom, D.C., Kanter, J., Camp, S., Sussman, J.L. & Taylor, P. (1996) Soluble monomeric acetylcholinesterase from mouse: expression, purification, and crystallization in complex with fasciculin. *Protein Sci.* **5**, 672–679.
39. Axelsen, P.H., Harel, M., Silman, I. & Sussman, J.L. (1994) Structure and dynamics of the active site gorge of acetylcholinesterase: synergistic use of molecular dynamics simulation and X-ray crystallography. *Protein Sci.* **3**, 188–197.
40. Masson, P., Froment, M.T., Bartels, C.F. & Lockridge, O. (1996) Asp70 in the peripheral anionic site of human butyrylcholinesterase. *Eur. J. Biochem.* **235**, 36–48.
41. Baden, R., Schutz, F. & Stacey, M. (1944) A crystalline serum mucoprotein with high cholinesterase activity. *Nature* **154**, 183–184.
42. Matthews, B.W. (1968) Solvent content of protein crystals. *J. Mol. Biol.* **33**, 491–497.
43. Raves, M.L., Harel, M., Pang, Y.P., Silman, I., Kozikowski, A.P. & Sussman, J.L. (1997) Structure of acetylcholinesterase complexed with the nootropic alkaloid, (–)-huperzine A. *Nat. Struct. Biol.* **4**, 57–63.
44. Soreq, H., Ben-Aziz, R., Prody, C.A., Seidman, S., Gnatt, A., Neville, L., Lieman-Hurwitz, J., Lev-Lehman, E., Ginzberg, D. & Lipidot-Lifson, Y. (1990) Molecular cloning and construction of the coding region for human acetylcholinesterase reveals a G + C-rich attenuating structure. *Proc. Natl Acad. Sci. USA* **87**, 9688–9692.
45. Schumacher, M., Camp, S., Maulet, Y., Newton, M., Macphee-Quigley, K., Taylor, S.S., Friedmann, T. & Taylor, P. (1986) Primary structure of *Torpedo californica* acetylcholinesterase deduced from its cDNA sequence. *Nature* **319**, 407–409.
46. Laemmli, U.K. (1970) Cleavage of structural proteins during the assembly of the head of bacteriophage T4. *Nature* **227**, 680–685.
47. Morrissey, J.H. (1981) Silver stain for proteins in polyacrylamide gels: a modified procedure with enhanced uniform sensitivity. *Anal. Biochem.* **117**, 307–310.

# Crystal Structure of Human Butyrylcholinesterase and of Its Complexes with Substrate and Products

Y. Nicolet, O. Lockridge, P. Masson, J-C. Fontecilla-Camps*,

**F. Nachon**,

The Journal of Biological Chemistry 278 (2003) 41141-41147

THE JOURNAL OF BIOLOGICAL CHEMISTRY
Vol. 278, No. 42, Issue of October 17, pp. 41141–41147, 2003

*Printed in U.S.A.*

# Crystal Structure of Human Butyrylcholinesterase and of Its Complexes with Substrate and Products*

Received for publication, October 7, 2002, and in revised form, July 2, 2003
Published, JBC Papers in Press, July 17, 2003, DOI 10.1074/jbc.M210241200

**Yvain Nicolet‡§, Oksana Lockridge¶, Patrick Masson‖, Juan C. Fontecilla-Camps‡**, and Florian Nachon¶‖**

*From the ‡Laboratoire de Cristallographie et Cristallogénèse des Protéines, Institut de Biologie Structurale "Jean-Pierre Ebel," CEA, UJF, CNRS, 41 rue Jules Horowitz, 38027 Grenoble Cedex 1, France, the ¶University of Nebraska Medical Center, Eppley Research Institute, Omaha, NE 68198-6805, and the ‖Centre de Recherches du Service de Santé des Armées, Unité d'Enzymologie, 24 Avenue des Maquis du Grésivaudan, BP 87-38702 La Tronche CEDEX, France*

**Cholinesterases are among the most efficient enzymes known. They are divided into two groups: acetylcholinesterase, involved in the hydrolysis of the neurotransmitter acetylcholine, and butyrylcholinesterase of unknown function. Several crystal structures of the former have shown that the active site is located at the bottom of a deep and narrow gorge, raising the question of how substrate and products enter and leave. Human butyrylcholinesterase (BChE) has attracted attention because it can hydrolyze toxic esters such as cocaine or scavenge organophosphorus pesticides and nerve agents. Here we report the crystal structures of several recombinant truncated human BChE complexes and conjugates and provide a description for mechanistically relevant non-productive substrate and product binding. As expected, the structure of BChE is similar to a previously published theoretical model of this enzyme and to the structure of *Torpedo* acetylcholinesterase. The main difference between the experimentally determined BChE structure and its model is found at the acyl binding pocket that is significantly bigger than expected. An electron density peak close to the catalytic Ser$^{198}$ has been modeled as bound butyrate.**

Cholinesterases are divided into two subfamilies according to their substrate and inhibitor specificities: acetylcholinesterase (AChE[1]; EC 3.1.1.7) and butyrylcholinesterase (BChE; EC 3.1.1.8). Acetylcholinesterase is responsible for the hydrolysis of acetylcholine released at the synaptic cleft and the neuromuscular junction in response to nerve action potential (1). In addition, both AChE and BChE seem to be involved in roles that are independent of their catalytic activities, such as cell differentiation and development (2, 3). The catalytic mechanism of AChE is extremely efficient approaching diffusion-controlled rates (4). Unexpectedly, the crystal structure of the *Torpedo californica* enzyme (*Tc*AChE) showed that the active site catalytic Ser-His-Glu triad is found at the bottom of a 20-Å deep gorge lined mostly with aromatic residues (5). The structure also revealed the nature and the location of the previously described peripheral and "anionic" sites; the former, located at the outer rim of the gorge, has been postulated to be the initial substrate binding site (6). The binding of ligand to this site has been proposed to slow down the traffic of substrate and product at the acylation site (6, 7). Although a similar peripheral site has been described for human BChE, site-directed mutagenesis and photo-affinity labeling studies showed that its location and the response upon ligand binding differ significantly from those of AChE (8, 9).

The site to which the positively charged quaternary ammonium of choline moiety productively binds is found half-way down the gorge, in between the peripheral and acylation sites. Originally, there was a great deal of controversy concerning the nature of the residues involved in this site. Both the crystal structure and labeling experiments showed that positively charged ligands form $\pi$-cation interactions with Phe$^{330}$ and Trp$^{84}$ (numbering in italics corresponds to that of torpedo AChE) (10).

The physiological role of BChE remains unclair (11, 12). Although it is capable of hydrolyzing ACh and other acylcholines, so far no endogenous natural substrate has been described for this enzyme. Because BChE is relatively abundant in plasma (about 3 mg/liter), and can degrade a large number of ester-containing compounds, it plays important pharmacological and toxicological roles (13). For instance, BChE is a potential detoxifying enzyme to be used as a prophylactic scavenger against neurotoxic organophosphates such as the nerve gas soman (14–16).

We have recently published the engineering and crystallization of a monomeric and partially glycosylated recombinant human BchE (17). Here we report several crystal structures of BChE complexed with a substrate, products, and conjugated to soman after aging. From these structures we propose alternative substrate and product binding that may be related to the high catalytic efficiency of the choline esterases.

## EXPERIMENTAL PROCEDURES

*Crystallization of Recombinant BChE and Its Complexes*—Recombinant human BChE suitable for crystallization was obtained, purified, and crystallized as described previously (17). No butyrate was present in the culture medium and none was added during any step of the purification procedure. The 3-bromopropionate-BChE complex was obtained by soaking crystals for a few minutes in the mother liquor containing 100 mM bromopropionate (Sigma). The BChE-choline complex was obtained by soaking BChE crystals grown from a 2.1 M

* The costs of publication of this article were defrayed in part by the payment of page charges. This article must therefore be hereby marked "*advertisement*" in accordance with 18 U.S.C. Section 1734 solely to indicate this fact.

*The atomic coordinates and structure factors (code P0I, 1P0Q, 1P0M, and 1P0P) have been deposited in the Protein Data Bank, Research Collaboratory for Structural Bioinformatics, Rutgers University, New Brunswick, NJ (http://www.rcsb.org/).*

§ Present address: Dept. of Chemistry, Massachusetts Inst. of Technology, Cambridge, MA 02139.

** To whom correspondence should be addressed. Tel.: 33-438785920; Fax: 33-438785122; E-mail: juan@lccp.ibs.fr.

[1] The abbreviations used are: AchE, acetylcholinesterase; BchE, butyrylcholinesterase; *Tc*AChE, *Torpedo californica* acetylcholinesterase; *Dm*AChE, *Drosophila melanogaster* acetylcholinesterase; BTC, butyrylthiocholine; Bicine, *N*,*N*-bis(2-hydroxyethyl)glycine; MES, 4-morpholineethanesulfonic acid.

TABLE I
*Data and refinement statistics*

| Data set | Native BChE | 3-Bromopropionate | Choline[a] | Soman-aged | Soman-aged/BSCh |
|---|---|---|---|---|---|
| Space group | I422 | I422 | I422 | I422 | I422 |
| Unit cell axes, $a = b$, $c$ (Å) | 154.659 127.890 | 154.920 126.939 | 154.657 128.570 | 154.616 127.307 | 154.924 127.909 |
| X-ray source | ID14-eh2 | ID14-eh4 ($\lambda$ = 0.915Å) | BM30 | ID14-eh1 | ID14-eh2 |
| Resolution range (Å) | 55.0–2.0 | 2.7 | 2.32 | 40.6–2.43 | 54.7–2.3 |
| No. of unique reflections | 51,326 | 37,108[b] | 29,378 | 25,868 | 28,730 |
| Completeness (%) | 98.6 (99.6) | 94.1 (69.9) | 87.4 (77.7) | 90.8 (88.6) | 86.5 (49.6) |
| $R_{sym}$ | 0.074 (0.448) | 0.103 (0.506) | 0.061 (0.398) | 0.071 (0.217) | 0.081 (0.264) |
| $I\sigma(I)$ | 6.8 (1.7) | 11.75 (2.72) | 23.7 (4.3) | 7.6 (3.3) | 8.1 (2.8) |
| Multiplicity | 7.3 (6.4) | 4.97 (4.08) | 9.9 (6.7) | 10.2 (6.2) | 6.4 (5.5) |
| $R$-factor (free $R$-factor) | 0.195 (0.225) | 0.227 (0.229) | 0.215 (0.244) | 0.199 (0.235) | 0.199 (0.242) |
| No. atoms | | | | | |
| Protein | 4,199 | | 4,207 | 4,157 | 4,175 |
| Others | 155 | | 154 | 126 | 147 |
| Solvent | 496 | | 264 | 286 | 337 |
| $B$ (Å$^2$) | 36.5 | | 49.2 | 38.3 | 35.1 |
| Root mean square from ideality | | | | | |
| Bond length (Å) | 0.014 | | 0.008 | 0.006 | 0.006 |
| Angles (°) | 1.6 | | 1.4 | 1.3 | 1.4 |
| Dihedrals (°) | 23.7 | | 23.4 | 23.4 | 23.6 |
| Impropers (°) | 1.08 | | 0.88 | 0.83 | 0.81 |

[a] The choline-BChE complex was refined to 2.38-Å resolution.
[b] 3-Bromopropionate-BChE data processing was carried out without merging the Friedel mates to evaluate the anomalous signal from the bromine atom.

$(NH_4)_2SO_4$ 100 mM Bicine (Fluka), pH 9.0, crystallization solution, in the mother liquor containing 100 mM choline chloride. Crystallization of soman-aged BChE: racemic soman (pinacolyl methylphosphonofluoridate) was obtained from CEB Le Bouchet (Vert-le-Petit, France). The purified enzyme (6.6 mg/ml) was inhibited in the presence of 0.5 mM soman (~5.5-fold molar excess) in 10 mM MES buffer, pH 6.5. The reaction mixture was further incubated for 3 days at 4 °C, allowing enough time for completion of the aging reaction and the disappearance of the remaining unreacted soman. The inhibited enzyme was crystallized under the same conditions as the uninhibited BChE except that the mother liquor was buffered at pH 8.0 using a 0.1 M Tris/HCl buffer solution. Soman-aged BChE and butyrylthiocholine (BTC) were cocrystallized at pH 6.5 (0.1 M MES buffer, 2.1 M $(NH_4)_2SO_4$) with 10 mM BTC (Sigma). X-ray data were collected from a 4-day-old crystal to limit the loss of substrate by spontaneous hydrolysis.

*X-ray Data Collection and Structure Solution*—All crystals were flash-cooled at 100 K in a nitrogen stream using 15–20% glycerol in the mother liquor as cryoprotectant. Data sets were collected at the following beamlines of the European Synchrotron Radiation Facility (Grenoble, France): ID14-eh1 for the soman-aged BChE, ID14-eh2 for the native BChE, BM30 for the choline-BChE complex and the soman-aged BTC complex, and ID14-eh4 for the 3-bromopropionate-BChE complex (see Table I). Data sets for the native, the soman-aged BchE, and soman-aged BChE-BTC complex crystals were integrated, scaled, and reduced using MOSFLM, SCALA, and TRUNCATE from the CCP4 suite (18). Data sets from the choline-BChE complex and the 3-bromopropionate-BChE species were processed using the program XDS (19). Data collection from the 3-bromopropionate-BChE crystal was performed at a wavelength of 0.915 Å to measure the Br anomalous scattering signal. Subsequent data processing was performed without merging the Friedel mates to better evaluate the anomalous signal of the bromine atom. Molecular replacement was carried out with the native data set between 15- and 3.5-Å resolution using the program AMoRe (20) and the *Tc*AChE structure (Protein Data Bank ID code: 2ACE) as a search model. A well constrasted solution with $R$-factor = 42.4% and correlation coefficient = 46.7% was obtained for one monomer per asymmetric unit. This solution was used as a starting model for manual rebuilding and refinement of BChE against all data to 2.0-Å resolution with the programs TURBO (21) and CNS (22), respectively. Observed structure factors were scaled anisotropically and a bulk solvent correction was applied. Several cycles of refinement, manual rebuilding, and solvent addition led to a model with good statistics (Table I). Residues 1–3, 378–379, and 455 did not have matching electron density and, consequently, were not included in the model. Carbohydrate chains corresponding to five of the six expected glycosylation sites (17) have been included in the crystallographic model. They correspond to those connected to $Asn^{57}$, $Asn^{106}$, $Asn^{241}$, $Asn^{341}$, and $Asn^{485}$. Although $Asn^{256}$ was expected to be glycosylated, no electron density was observed for carbohydrate. Further examination of the electron density maps led to the inclusion of three molecules of glycerol, used as cryoprotectant, two sulfate ions, the precipitanting agent, one molecule of MES buffer, and two chloride ions. During refinement, an unexpected residual positive electron density was observed around the O$\gamma$ atom of the catalytic serine. At the final stages of refinement and after several attempts at modeling this density as corresponding to chemicals added either during purification or crystallization, a very good fit was only obtained when butyrate was used as a model (see Fig. 2).

The soman-aged BChE structure was solved using the rigid body refinement from the program CNS. The refined model statistics are shown in Table I. Residues 1–3, 378–379, and 455 and carbohydrates bonded to $Asn^{256}$ and $Asn^{485}$ had no significant matching electron density and consequently were not included in the final model. The soman-aged BChE structure also contains the three glycerol molecules, the two chloride ions, and one of the two sulfate ions previously observed in the native structure. The same refinement scheme was applied to this and the choline-BChE structure (Table I). The structure of the 3-bromopropionate-BChE complex was solved using the native BChE structure as a starting coordinate set in which the modeled butyrate had been removed. Anomalous difference and $F_{obs} - F_{calc}$ difference Fourier maps were calculated with the program CNS. The starting Protein Data Bank coordinates, parameters, and topology files for 3-bromopropionate were obtained using PRODRG (23). Subsequently, it was manually positioned to fit the electron density maps. Comparable $B$-factors for bromine and the other 3-bromopropionate atoms were obtained when fixing the occupancy to 0.5, suggesting that the putative butyryl moiety was only partially substituted during the soaking process.

## RESULTS

*Crystallographic Analysis of Uninhibited Butyrylcholinesterase*—The BChE crystal structure was originally solved by the molecular replacement method and subsequently refined to 2.0-Å resolution using CNS (see "Experimental Procedures" and Table I). As expected (24–28), the overall structure of BChE is very similar to that of *Tc*AChE. However, BChE does not form the dimer observed in previous structures of *Tc*AChE (5, 29), mouse AChE (30, 31), and human AChE (32). In AChEs, the four helices involved in the subunit-subunit interaction are antiparallel and the active site openings are located on opposite sides of the dimer. Although homologous helices are found at the BChE dimer interface (residues 362–375 and 514–529), they are not antiparallel but form a ≈45° angle, and the active site openings are located on the same side of the dimer (not shown). Constraints resulting from the crystal packing could be responsible for these differences.

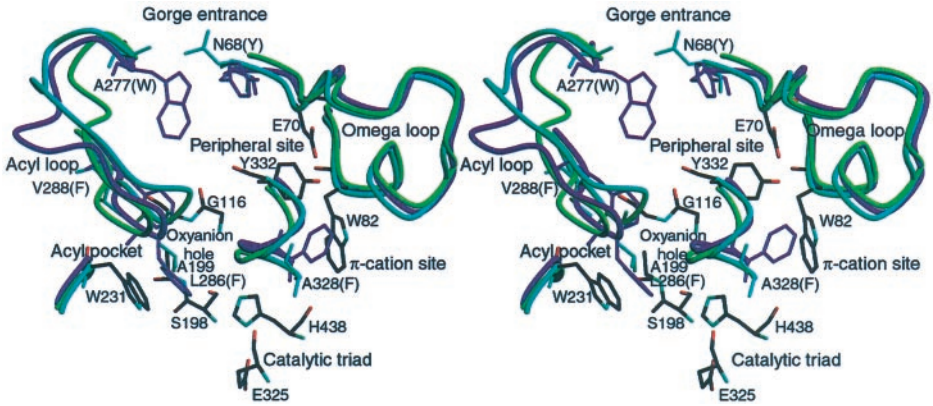


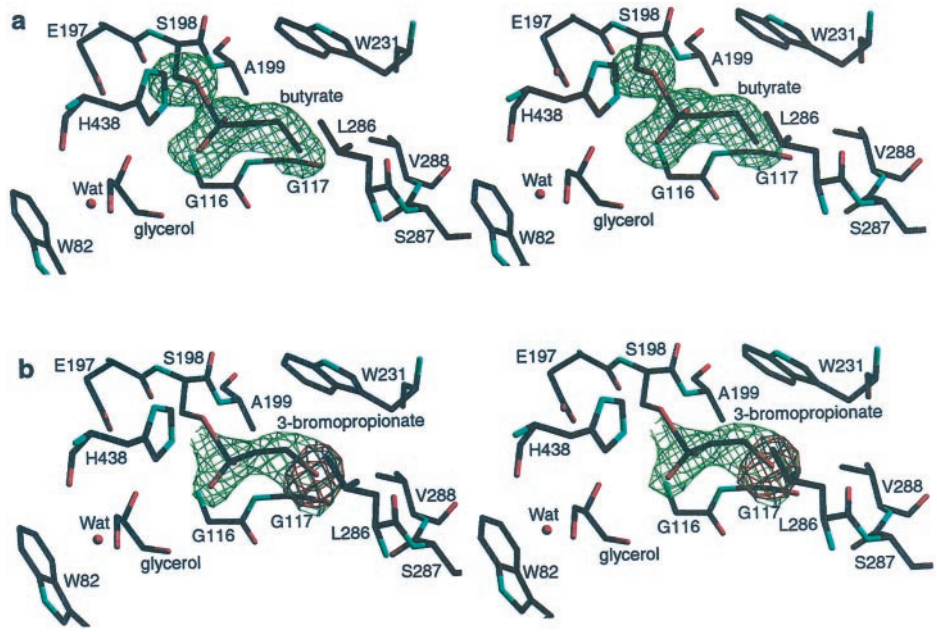


FIG. 1. **Stereo view of the superposition of native BChE (*cyan*), *Tc*AChE (*pink*), and *Dm*AChE (*green*) around the active site gorge.** Only the acyl loop exhibits significantly different conformations in all three enzymes. Amino acids that differ in BChE and *Tc*AChE are depicted in *cyan* and *pink*, respectively. This figure and Figs. 2–4 were generated with MOLSCRIPT (44), BOBSCRIPT (45), and RASTER3D (46).

FIG. 2. *a*, stereo pair of the active site viewed from the gorge entrance. The depicted electron density was calculated at 2.0-Å resolution with the putative butyryl moiety and the side chain of the catalytic $Ser^{198}$ absent from both phase and structure factor calculations (omit map) and is contoured at the 3 $\sigma$ level. There are no residual negative electron density peaks for this model. *b*, stereo view of the active site of a crystal that was soaked in a 100 mM 3-bromopropionate solution. The anomalous and difference Fourier maps are depicted in *red* and *green*, respectively. Both omit maps were calculated at 2.7-Å resolution. The shape of the electron density is basically the same in *a* and *b*, and the anomalous peak at 6 $\sigma$ corresponds to the expected position for the bromine atom. This figure is in the same orientation as *a*.

Most differences between BChE and *Tc*AChE are confined to 1) the residues lining the gorge, where the former enzyme has replaced several of the aromatic groups of the latter by hydrophobic ones; 2) the acyl-binding pocket, with the replacements of $Phe^{288}$ and $Phe^{290}$ of *Tc*AChE by $Leu^{286}$ and $Val^{288}$, respectively; these changes make it possible for the binding of the bulkier butyrate substrate moiety in BChE (as discussed below); and 3) the conformation of the acyl loop (Fig. 1). In addition, the catalytic serine is connected to a large electron density peak whose identity is discussed in the next section. We note, in passing, that a previously modeled structure of BChE (24) differs from the actual structure precisely at these regions, indicating a strong bias toward the AChE starting atomic coordinate set. As an example, the acyl pocket of the model is significantly smaller than the one observed in the crystal structure.

*A Putative Butyryl Moiety Bound to the Catalytic Serine*—During the crystallographic refinement procedure, it became evident that the catalytic serine 198 was bound to an unidentified moiety that was eventually modeled as butyrate with well matching electron density (Fig. 2*a* and "Experimental Procedures"). To confirm this result, we soaked native crystals with the butyrate isosteric analog 3-bromopropionate in which the $\gamma$ carbon is replaced by a bromine atom. Subsequently, we collected x-ray data at 0.915-Å wavelength where bromine gives rise to a strong anomalous signal. Fig. 2*b* clearly indicates extensive substitution of the putative butyryl moiety by its brominated analog with essentially no changes in the shape of the corresponding electron density. In the case of the butyrated enzyme the length of the bond connecting the acyl group to the catalytic serine refined to values >2.0 Å, with no residual peaks in the Fourier difference electron density maps. On the other hand, maps calculated after crystallographic refinement of either restrained non-bonded butyrate or the tetrahedral intermediate display significant negative peaks, suggesting that neither one is a good model for the $Ser^{198}$-butyrate interaction (Fig. 3). We are currently investigating the plausibility of the long bond using density function theory calculations. Although the source of the butyryl moiety is unknown, it seems to be essential for crystallization because "butyrate-depleted" samples were extremely difficult to crystallize. In fact, the few crystals grown from these samples had the putative butyrate still bound to $Ser^{198}$. Furthermore, crystals were readily obtained when butyrate, or BTC, was added to the crystallization

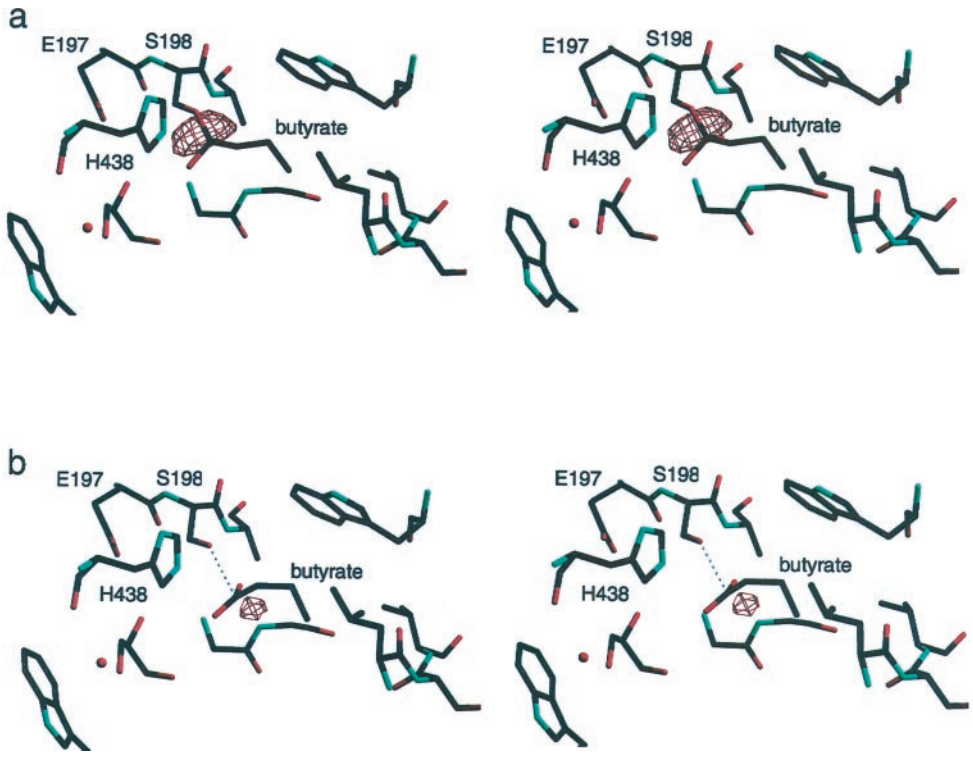


FIG. 3. **Difference Fourier electron density maps for bonded and non-bonded butyrate.** *a*, tetrahedral model. Despite the restrains applied the C–O$\gamma$ distance is 1.47 Å, and there is a residual negative electron density peak at $-5.7$ $\sigma$ between these two atoms. The average *B*-factor for the buryrate moiety is 44 Å$^2$ and that of the tetrahedral C atom is 51.1 Å$^2$ (comparable values for the model with a 2.16-Å-long C–O$\gamma$ bond depicted in Fig. 2 are 41.7 and 41.4 Å, respectively). *b*, non-bonded butyrate model. The C–O$\gamma$ distance refines to 2.6 Å, and there is a negative peak at $-3.7$ $\sigma$ below the carboxylate carbon atom. The average *B*-factor for the buryrate moiety is 41.7 Å$^2$ and that of the carboxylate carbon atom is 45.8 Å$^2$.

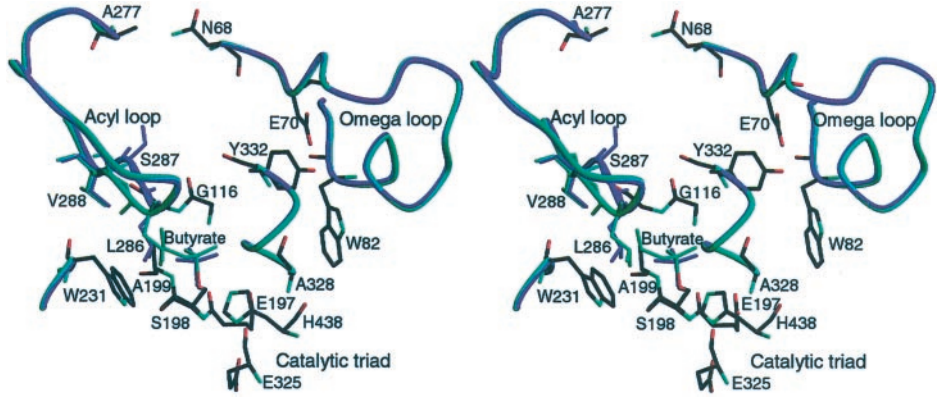


FIG. 4. **Stereo view of the superposition of native (*cyan*) and soman-aged (*pink*) BChE in the same orientation as Fig. 1.** The two structures have an overall root mean square deviation of 0.12 Å for 511 C$\alpha$s. However, there are shifts of 1.63 and 1.53 Å for the C$\alpha$s of Ser$^{287}$ and Leu$^{286}$, respectively, and the peptide plane between Leu$^{286}$ and Ser$^{287}$ is rotated by about 60°. This movement is the only structural difference detected when the putative butyrate is substituted by methylphosphonate and results in a reduction of the size of the acyl pocket. Acyl loop conformational changes have also been reported for phosphonylfluoridate-aged *Tc*AChE (35). The fact that this loop is more flexible than other parts of the protein suggests that it may be involved in product release.

solutions.[2] This phenomenon may be related to the stabilization of the extensive acyl pocket in BChE by butyrate.

*A Mobile Acyl Loop*—As we already noticed when comparing the native hBChE, *Tc*AChE, and *Dm*AChE structures, although the omega loop has the same conformation (see Fig. 1), residues belonging to the acyl loop have appreciably different orientations in the three cholinesterases. Furthermore, in BChE the acyl loop changes conformation depending on the substitution at the catalytic serine by butyrate or soman (Fig. 4). The reaction of soman and other related organophosphate esters with the catalytic serine of cholinesterases can be reversed initially by nucleophilic agents such as oximes (reviewed in (33)). However, with time, serine phosphonylation becomes irreversible through dealkylation of an alkoxy chain on the phosphorus atom, a process called "aging" (34). Except for its size, the resulting "aged" phosphonyl adduct is a structural analog of both the butyryl-serine association we have detected in the original BChE crystals and of the postulated deacylation tetrahedral intermediate. The protonated His$^{438}$ forms a salt bridge with one oxygen atom of the methylphosphonyl moiety. Such a bridge was also observed in the crystal structures of soman-, sarin-, and phosphonylfluoridate-aged *Tc*AChE (35). A conformational change of the acyl loop has also been reported for the crystal structure of phosphonylfluoridate-

[2] J. Colletíer, personal communication.

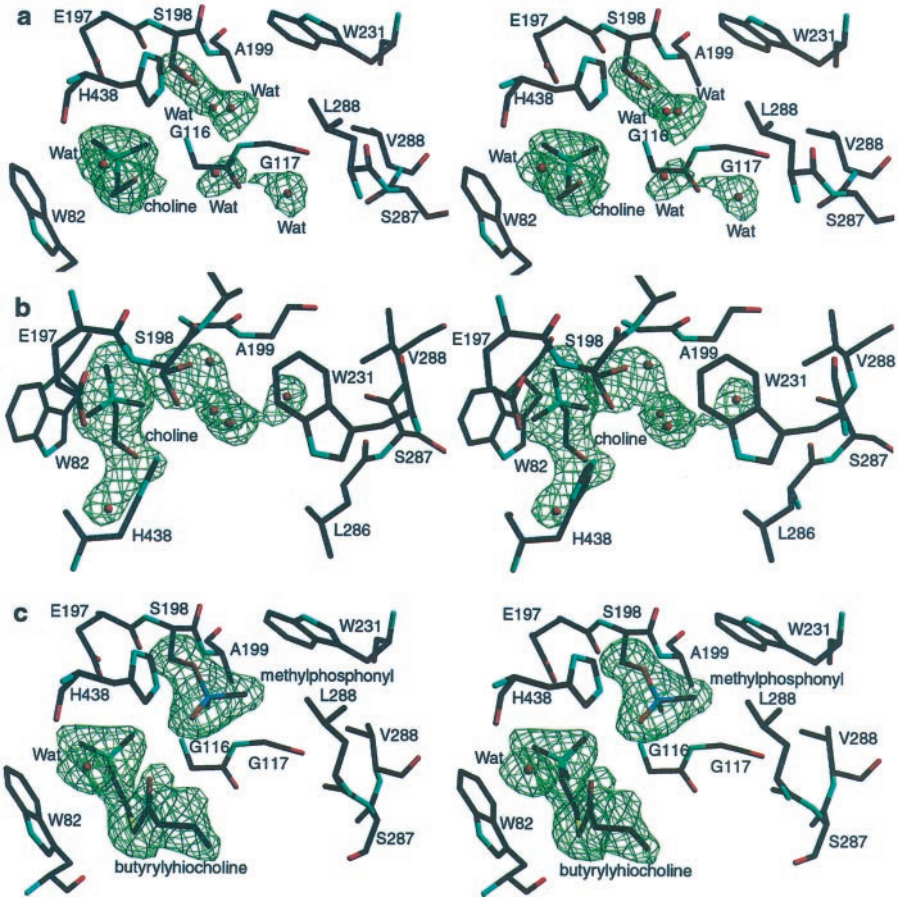


FIG. 5. *a*, stereo view of the active site after soaking one of the original crystals in a 100 mM choline solution. The orientation is the same as in Fig. 2. *b*, stereo view of the same structure rotated by 90° around an *horizontal axis* relative to *a*. The catalytic serine side chain adopts two different conformations: one where the O$\gamma$ interacts with His$^{438}$ and the other where it replaces a water molecule that interacted with the main chain nitrogen of Ala$^{199}$, in the oxyanion hole. *c*, stereo view of the active site of the soman-aged butyrylthiocholine-BChE complex oriented as in Fig. 1. The 2.3-Å resolution difference Fourier omit map is depicted in *green*. The covalently bound methylphosphonyl moiety occupies the same position as in soman-aged *Tc*AChE (35). As expected, the quaternary ammonium group of butyrylthiocholine is located in the $\pi$-cation site, but the substrate adopts a non-productive orientation (see "Results"). The omit Fourier electron density maps show that choline and butyrylthiocholine occupy very similar positions and that the alcohol function of the former and the carbonyl oxygen of the latter establish hydrogen bonds with equivalent water molecules. In all three panels the omit maps are depicted in *green* and are contoured at a 3$\sigma$ level.

aged *Tc*AChE. Taken together, these changes in cholinesterases show that the acyl loop is flexible and are consistent with molecular dynamic studies, indicating that acetate could leave the AChE active site either directly through the gorge, "above" this loop or through an alternative exit located "below" it (36). As mentioned above, stabilization of the acyl loop by butyrate seems to be required for crystallization.

*Alternative Choline Binding Site at the Active Site*—To obtain an image of the unsubstituted Ser$^{198}$ in BChE, we soaked our crystals in a 100 mM choline chloride solution, pH 9.0. Indeed, maps calculated with x-ray data collected from a choline-soaked crystal displayed no electron density corresponding to the putative butyryl moiety. In this structure the O$\gamma$ from Ser$^{198}$ displays two approximately equally occupied conformations: a classical one where it forms a hydrogen bond with the catalytic His$^{438}$, and a much less expected one, where it has turned away from the histidine and establishes a hydrogen bond with the main chain N-H from Ala$^{199}$ at the oxyanion hole (Fig. 5, *a* and *b*). It is unlikely that this is solely due to the deprotonation of His$^{438}$ at pH 9.0, because identical crystals grown at pH 6.5 display similar Ser$^{198}$ conformations when soaked with cocaine, tacrine, or decamethonium, and a native structure solved at pH 9.0 still has the putative butyrate bound to the active site (not shown). Another surprising feature in this structure is the orientation of the bound choline. Although, as expected, its quaternary ammonium group binds close to Trp$^{82}$ through a $\pi$-cation interaction, the alcohol group points roughly toward the gorge entrance and forms a hydrogen bond with a water molecule that, in turn, interacts with the main chain carbonyl O from His$^{438}$. Although choline binding may not be physiologically relevant (given the high choline concentration in the soaking solution and the basic pH), it shows that this reaction product may adopt at least two conformations at the active site: the productive one, as part of butyrylcholine bound to the active site region, and an alternative one, as observed here (Fig. 5, *a* and *b*).

The existence of an alternative choline binding mode prompted us to perform an additional experiment where crystals obtained from protein previously inhibited with soman were soaked in a solution containing the substrate BTC. In the complex between soman-aged BChE and BTC (pH 6.5) (Fig. 5*c*), the latter binds very much like choline, with its ammonium group close to Trp$^{82}$ and its carbonyl group hydrogen-bonded to a water molecule topologically equivalent to the one described above for the BChE-choline complex (Fig. 5). This confirms the above-stated notion that substrate binding through $\pi$-cation interactions is bimodal and that a tetrahedral adduct bound to the catalytic serine is sterically compatible with intermediate site substrate binding as defined here by the soman-aged BChE-BTC complex. Crystallographic data for all the structures are presented in Table I.

## DISCUSSION

Taken together, the results presented here, in conjuction with data from the literature, shed new light concerning the catalytic mechanism of cholinesterases. These enzymes appear to function through an assembly line approach where every step in the reaction is tightly controlled by the protein environment and extremely efficient use is made of the available substrate binding sites. Peripheral sites serve as attraction centers for substrate at the outer rim of the gorge (an observation confirmed by a BChE-decamethonium complex; not shown). From one or several of these positions, substrate can move into an intermediate site, equivalent to the one observed in the soman-aged BChE-BTC complex. Computer graphics simulations show that, as predicted by Masson *et al.* (9), a simple rotation of the molecule around its quaternary ammonium group, bound at the $\pi$-cation site, can bring the substrate to productive binding. Hydrogen bonding of the carbonyl group of BTC to a water molecule, rather than to protein, may facilitate this transition. It has been proposed that the position of the catalytic triad in cholinesterases, at the bottom of a 20-Å-deep gorge allows the exothermic formation of the transition state in a "dry" environment (37). The results presented here provide an additional explanation for the location of the buried catalytic triad as the presence of peripheral and intermediate sites at the gorge allow for a drastic reduction of substrate mobility, leading it to the active site in a most efficient way.

The presence of a putative butyrate bound to $Ser^{198}$ could be related to the reactivity and/or stability of the catalytic serine. This is supported by the recent observation by Bourne *et al.* (38) who described a carbonate or acetate molecule found close to the catalytic serine of mouse AChE in complex with a peripheral site inhibitor. Interestingly, other structures of AChE also display electron densitiy peaks very close to the catalytic serine (39, 40).

Although the distance between O$\gamma$ of $Ser^{198}$ and N$\epsilon$2 of $His^{438}$ of 2.8 Å is compatible with hydrogen bonding, the angle between C$\delta$2, N$\epsilon$2, and O$\gamma$ is about 170°, a value that is unfavorable for that type of interaction. In fact, if this hydrogen bond geometry were better, proton transfer to the alcoholate of the choline moiety would be less favorable (similar observations have been made on serine proteases. For example, the *Streptomyces griseus* protease A structure refined at 1.8-Å resolution (41, 42) shows a Ser-His hydrogen bond distance of 3.1 Å and the orientation is far from optimal, suggesting that the bond is very weak or even absent). One way to overcome the problem of poor geometry of the His-Ser hydrogen bond is to propose that the side chain of $His^{438}$ rotates to optimize hydrogen bonding to $Ser^{198}$ when this residue is free. However, our observations do not support this hypothesis: $His^{438}$ seems to be well ordered and be similarly oriented in all the structures discussed here. On the other hand, we have observed that in several butyrate-free BChE complexes the O$\gamma$ atom of $Ser^{198}$ is highly disordered and shows no tendency to bind to $His^{438}$ (see, for example, Fig. 5). Furthermore, a very recent report by Masson *et al.* (43) indicates that in the presence of excess substrate and low pH, BChE is still active, although $His^{438}$ should remain protonated under these conditions. Consequently, neither our results, nor previously reported data (41–43), favor the deprotonation of the catalytic serine by $His^{438}$ during turnover. One alternative to deprotonation of the catalytic serine by $His^{438}$ during turnover would be a concerted product release/substrate binding at $Ser^{198}$, whose O$\gamma$ would remain deprotonated throughout the catalytic cycle. The presence of a putative serine-bound butyrate moiety in the purified BChE hints at this possibility.

As discussed above, upon productive substrate binding at the active site the C=O bond becomes polarized through its interaction with the oxyanion hole: a lone pair orbital develops on the oxygen atom, and an empty orbital forms on the carbon atom, facilitating the nucleophilic attack of the O$\gamma$ atom of $Ser^{198}$ on the partially positive carbon atom. This makes the first step of the reaction easier by lowering the energy barrier toward the formation of the first tetrahedral intermediate. A similar mechanism would operate when a water molecule hydrolyzes the acyl-enzyme intermediate.

X-ray structures of both "native" and soman-aged BChE have a glycerol molecule bound to the $\pi$-cation site. As glycerol was used only as cryoprotectant (see the "Experimental Procedures"), its presence in the active site gorge confirms the broad specificity of the $\pi$-cation site and that the substrate specificity is mainly due to residues $Val^{288}$ and $Leu^{286}$ lining the acyl pocket.

The presence of a moiety next to the catalytic serine is intriguing. Several lines of evidence indicate that in our case it is most likely butyrate as it can be replaced by 3-bromopropionate, it is displaced by choline, and the presence of butyrate is essential for crystrallization. However, additional experiments will be required to definetively establish its identity.

Atomic coordinates and structure factors have been deposited with the Protein Data Bank codes 1P0I (BChE with butyrate), 1P0Q (BChE with aged soman), 1P0M (BChE plus choline), and 1P0P (BChE with aged soman and BTC) and will be released upon publication.

*Acknowledgments*—We are grateful to the staffs of ID14 and FIP beamlines from the European Synchrotron Radiation facility. Julien Lescar is especially thanked for his help with data collection from the 3-bromopropionate-BChE crystal.

## REFERENCES

1. Massoulie, J., Sussman, J., Bon, S., and Silman, I. (1993) *Prog. Brain Res.* **98,** 139–146
2. Meshorer, E., Erb, C., Gazit, R., Pavlovsky, L., Kaufer, D., Friedman, A., Glick, D., Ben-Arie, N., and Soreq, H. (2002) *Science* **295,** 508–512
3. Behra, M., Cousin, X., Bertrand, C., Vonesch, J. L., Biellmann, D., Chatonnet, A., and Strahle, U. (2002) *Nat. Neurosci.* **5,** 111–118
4. Quinn, D. (1987) *Chem. Rev.* **87,** 955–979
5. Sussman, J. L., Harel, M., Frolow, F., Oefner, C., Goldman, A., Toker, L., and Silman, I. (1991) *Science* **253,** 872–879
6. Szegletes, T., Mallender, W. D., Thomas, P. J., and Rosenberry, T. L. (1999) *Biochemistry* **38,** 122–133
7. De Ferrari, G. V., Mallender, W. D., Inestrosa, N. C., and Rosenberry, T. L. (2001) *J. Biol. Chem.* **276,** 23282–23287
8. Nachon, F., Ehret-Sabatier, L., Loew, D., Colas, C., van Dorsselaer, A., and Goeldner, M. (1998) *Biochemistry* **37,** 10507–10513
9. Masson, P., Legrand, P., Bartels, C. F., Froment, M. T., Schopfer, L. M., and Lockridge, O. (1997) *Biochemistry* **36,** 2266–2277
10. Harel, M., Schalk, I., Ehret-Sabatier, L., Bouet, F., Goeldner, M., Hirth, C., Axelsen, P. H., Silman, I., and Sussman, J. L. (1993) *Proc. Natl. Acad. Sci. U. S. A.* **90,** 9031–9035
11. Chatonnet, A., and Lockridge, O. (1989) *Biochem. J.* **260,** 625–634
12. Mack, A., and Robitzki, A. (2000) *Prog. Neurobiol.* **60,** 607–628
13. Lockridge, O., and Masson, P. (2000) *Neurotoxicology* **21,** 113–126
14. Allon, N., Raveh, L., Gilat, E., Cohen, E., Grunwald, J., and Ashani, Y. (1998) *Toxicol. Sci.* **43,** 121–128
15. Broomfield, C. A., Maxwell, D. M., Solana, R. P., Castro, C. A., Finger, A. V., and Lenz, D. E. (1991) *J. Pharmacol. Exp. Ther.* **259,** 633–638
16. Raveh, L., Grunwald, J., Marcus, D., Papier, Y., Cohen, E., and Ashani, Y. (1993) *Biochem. Pharmacol.* **45,** 2465–2474
17. Nachon, F., Nicolet, Y., Viguie, N., Masson, P., Fontecilla-Camps, J. C., and Lockridge, O. (2002) *Eur. J. Biochem.* **269,** 630–637
18. Collaborative Computational Project No. 4 (1994) *Acta Crystallogr. Sect. D Biol. Crystallogr.* **50,** 760–763
19. Kabsch, W. (1993) *J. Appl. Crystallogr.* **26,** 795–800
20. Navaza, J. (1994) *Acta Crystallogr. Sect. A* **50,** 157–163
21. Roussel, A., and Cambillaud, C. (1989) *TURBO computer program*, Silicon Graphics, Mountain View, CA
22. Brünger, A. T., Adams, P. D., Clore, G. M., DeLano, W. L., Gross, P., Grosse-Kunstleve, R. W., Jiang, J. S., Kuszewski, J., Nilges, M., Pannu, N. S., Read, R. J., Rice, L. M., Simonson, T., and Warren, G. L. (1998) *Acta Crystallogr.* **D54,** 905–921
23. van Aalten, D. M. F., Bywater, R., Findlay, J. B. C., Hendlich, M., Hooft, R. W., and Vriend, G. W. (1996) *J. Comput. Aided Mol. Des.* **10,** 255–262
24. Harel, M., Sussman, J. L., Krejci, E., Bon, S., Chanal, P., Massoulie, J., and Silman, I. (1992) *Proc. Natl. Acad. Sci. U. S. A.* **89,** 10827–10831
25. Kaplan, D., Ordentlich, A., Barak, D., Ariel, N., Kronman, C., Velan, B., and Shafferman, A. (2001) *Biochemistry* **40,** 7433–7445
26. Radic, Z., Pickering, N. A., Vellom, D. C., Camp, S., and Taylor, P. (1993) *Biochemistry* **32,** 12074–12084

27. Saxena, A., Redman, A. M. G., Jiang, X. L., Lockridge, O., and Doctor, B. P. (1997) *Biochemistry* **36,** 14642–14651
28. Vellom, D. C., Radic, Z., Li, Y., Pickering, N. A., Camp, S., and Taylor, P. (1993) *Biochemistry* **32,** 12–17
29. Harel, M., Kleywegt, G. J., Ravelli, R. B., Silman, I., and Sussman, J. L. (1995) *Structure* (*Lond.*) **3,** 1355–1366
30. Bourne, Y., Taylor, P., and Marchot, P. (1995) *Cell* **83,** 503–512
31. Bourne, Y., Taylor, P., Bougis, P. E., and Marchot, P. (1999) *J. Biol. Chem.* **274,** 2963–2970
32. Kryger, G., Harel, M., Giles, K., Toker, L., Velan, B., Lazar, A., Kronman, C., Barak, D., Ariel, N., Shafferman, A., Silman, I., and Sussman, J. L. (2000) *Acta Crystallogr. Sect. D Biol. Crystallogr.* **56,** 1385–1394
33. Dawson, R. M. (1994) *J. Appl. Toxicol.* **14,** 317–331
34. Harris, L. W., Fleisher, J. H., Clark, J., and Cliff, W. J. (1966) *Science* **154,** 404–407
35. Millard, C. B., Kryger, G., Ordentlich, A., Greenblatt, H. M., Harel, M., Raves, M. L., Segall, Y., Barak, D., Shafferman, A., Silman, I., and Sussman, J. L. (1999) *Biochemistry* **38,** 7032–7039
36. Enyedy, I., J., Kovach, I. M., and Brooks, B. R. (1998) *J. Am. Chem. Soc.* **120,** 8043–8050
37. Harel, M., Quinn, D. M., Haridasan, K. N., Silman, I., and Sussman, J. L. (1996) *J. Am. Chem. Soc.* **118,** 2340–2346
38. Bourne, Y., Taylor, P., Radic, Z., and Marchot, P. (2003) *EMBO J.* **22,** 1–12
39. Harel, M., Kryger, G., Rosenberry, T. L., Mallender, W. D., Lewis, T., Fletcher, R. J., Guss, J. M., Silman, I., and Sussman, J. L. (2000) *Protein Sci.* **9,** 1063–1072
40. Weik, M., Ravelli, R. B., Kryger, G., McSweeney, S., Raves, M. L., Harel, M., Gros, P., Silman, I., Kroon, J., and Sussman, J. L. (2000) *Proc. Natl. Acad. Sci. U. S. A.* **97,** 623–628
41. Matthews, D. A., Alden, R. A., Birktoft, J. J., Freer, T., and Kraut, J. (1977) *J. Biol. Chem.* **252,** 8875–8883
42. Sielecki, A. R., Hendrickson, W. A., Broughton, C. G., Delbaere, L. T., Brayer, G. D., and James, M. N. (1979) *J. Mol. Biol.* **134,** 781–804
43. Masson, P., Nachon, F., Bartels, C. F., Froment, M. T., Ribes, F., Matthews, C., and Lockridge, O. (2003) *Eur. J. Biochem.* **270,** 315–324
44. Kraulis, P. J. (1991) *J. Appl. Crystallogr.* **24,** 946–950
45. Esnouf, R. M. (1997) *J. Mol. Graph.* **15,** 132–134
46. Merrit, E. A., and Bacon, D. J. (1997) *Methods Enzymol.* **277,** 505–524

# The Reactant State for Substrate-Activated Turnover of Acetylthiocholine by Butyrylcholinesterase is a Tetrahedral Intermediate

J.R. Tormos, K.L. Wiley, J. Seravalli, **F. Nachon**, P. Masson, Y. Nicolet, D.M. Quinn*

Journal of the American Chemical Society 127 (2005) 14538-14539

J|A|C|S
COMMUNICATIONS

Published on Web 09/30/2005

# The Reactant State for Substrate-Activated Turnover of Acetylthiocholine by Butyrylcholinesterase is a Tetrahedral Intermediate

Jose R. Tormos,[†] Kenneth L. Wiley,[†,¶] Javier Seravalli,[†,#] Florian Nachon,[‡] Patrick Masson,[‡] Yvain Nicolet,[§] and Daniel M. Quinn*[,†]

*Department of Chemistry, The University of Iowa, Iowa City, Iowa 52242, Centre de Recherches du Service de Santé Armées, Unité d'Enzymologie, BP 87-38702 La Tronche CEDEX, France, and Institut de Biologie Structurale, Laboratoire de Cristallographie et Cristallogénèse des Protéines, 38027 Grenoble, France*

Received April 13, 2005; E-mail: daniel-quinn@uiowa.edu

Acetylcholinesterase (AChE[1]) and butyrylcholinesterase (BuChE[1]) catalyze the hydrolysis of choline esters with very high catalytic efficiency. At neutral pH, cholinesterase reactions are $\sim 10^{13}$-fold faster than spontaneous substrate hydrolysis, a factor that corresponds to 74 kJ mol$^{-1}$ of transition state stabilization.[2] Though many structural features that contribute to the catalytic mechanism have been illuminated[3,4]—the Ser-His-Glu catalytic triad, the oxyanion hole, the acyl binding site, the quaternary ammonium binding site—a decisive understanding of cholinesterase catalytic power is yet to be had.

Recently, Nicolet et al.[5] reported crystal structures of human BuChE and complexes of the enzyme. Surprisingly, in the supposed unliganded enzyme structure, determined at a resolution of 2.0 Å, electron density that was proximal to the nucleophilic oxygen of the active site Ser198 was interpreted as a bound butyrate. This ligand could be displaced with 3-bromopropionate, which placed the structural assignment on a firm footing. However, it was not possible to differentiate cleanly between a complex in which the ligand is bound as a tetrahedral intermediate and one which is a BuChE−carboxylate complex. Though angular distortions toward tetrahedrality were noted about the carbonyl carbon of the bound butyrate, the resolution of the structure and the rather long Ser198 $\gamma$O to butyrate carbonyl carbon distance (2.16 Å) suggest that the complex may be a mixture of tetrahedral intermediate and EP complexes, and perhaps also a covalent acylenzyme.

These unusual observations beg for an experimental probe of the catalytic behavior of BuChE that can address the nature of substrate hybridization changes that accompany catalytic turnover in the steady state. Herein we report on the measurements of secondary $\beta$-deuterium kinetic isotope effects with isotopomers of acetylthiocholine (i.e., acetyl-L$_3$-thiocholine, L = $^1$H or $^2$H) that provide such a probe.[6] Secondary deuterium isotope effects are inverse (<1.00) when a sp$^2$ hybridized reactant is converted to a quasi-tetrahedral transition state and normal (>1.00) when an sp$^3$ reactant state is converted to a transition state that has greater trigonal planar character.[7]

BuChE-catalyzed reactions often show substrate activation at high substrate concentrations.[3] An interaction mechanism that accords with substrate activation is outlined in Scheme 1. E and A are the enzyme and substrate, respectively, EA is the Michaelis complex, F is the acylenzyme intermediate, and EAA is the ternary complex of enzyme with substrate monomers bound at both the active and substrate activation sites. The active site of BuChE is at the bottom of a 20 Å deep gorge,[5] and the substrate activation site is thought to coincide with the peripheral site at the mouth of the gorge.[9] Substrate activation is observed because turnover of EAA via $\beta k_{cat}$ ($= \beta V_{max}/[E]_T$) is faster than turnover of EA by a factor $\beta$. As Figure 1 shows, the dependence of human BuChE-catalyzed hydrolysis of acetyl-$^1$H$_3$-thiocholine on substrate concentration shows deviations from Michaelis−Menten kinetics that are consistent with substrate activation. The data in Figure 1 were fit to eq 1, derived for the kinetic mechanism of Scheme 1 (see Supporting Information for derivation of eq 1). The fit yielded the following parameters: $V_{max} = 20 \pm 2$ m*A* min$^{-1}$, $K_m = 80 \pm 20$ $\mu$M, $K_a = 3.5 \pm 0.5$ mM, and $\beta = 2.6 \pm 0.2$. Hence, the ternary EAA complex of Scheme 1 turns over to product 2.6 times faster than does the EA complex. Though substrate activation has long been observed for BuChE-catalyzed reactions, an understanding of its functional origins remains elusive. Fortunately, the $\beta$-secondary deuterium kinetic isotope effects detailed below shed important new light on this phenomenon.

***Scheme 1.*** Kinetic Mechanism for Substrate Activation of BuChE-Catalyzed Reactions

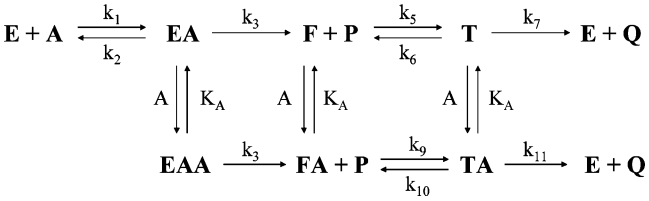


$$v_i = \frac{V_{max}[A](1 + \beta[A]/K_A)}{K_m(1 + \beta[A]/K_A) + [A](1 + [A]/K_A)} \qquad (1)$$

The least-squares uncertainties that result from the fit in Figure 1 preclude determination of secondary isotope effects on the kinetic parameters from such experiments. An alternate approach is to determine the secondary isotope effect on the initial rate (i.e., $^{D3}v_i = v_i^{H3}/v_i^{D3}$) as a function of substrate concentration. As Figure 2 shows, the isotope effect on the initial rate increases hyperbolically as the substrate concentration increases. These data were fit to eq 2, which provides a quantitative analysis and extrapolation of the isotope effects:

$$^{D3}v_i = {}^{D3}V_{max}\frac{1 + \frac{\beta[A]}{K_A}}{1 + \frac{\beta[A]}{K_A{}^{D3}\beta}} \times \frac{[A]\left(1 + \frac{[A]}{K_A}\right) + K_m\left(1 + \frac{\beta[A]}{K_A{}^{D3}\beta}\right)}{[A]\left(1 + \frac{[A]}{K_A}\right) + K_m\left(1 + \frac{\beta[A]}{K_A}\right)} \qquad (2)$$

[†] The University of Iowa.
[‡] Centre de Recherches du Service de Santé des Armées.
[§] Institut de Biologie Structurale.
[¶] Current address: Department of Molecular and Cellular Biology, Harvard University, Cambridge, MA 02138.
[#] Current address: Department of Biochemistry, University of Nebraska, Lincoln, NE 68588-0664.


10.1021/ja052401q CCC: $30.25 

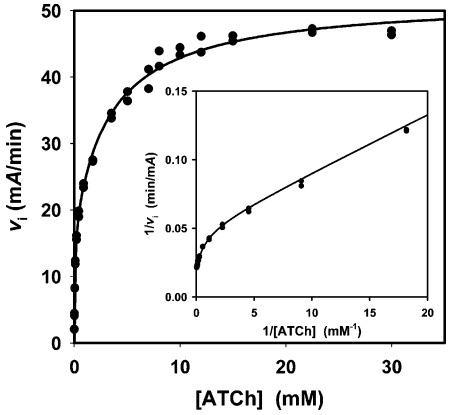


***Figure 1.*** Dependence of initial rate on concentration of acetyl-$^1H_3$-thiocholine. Reactions were monitored by the coupled assay of Ellman et al.[8] at 27.0 ± 0.1 °C and pH = 7.24 in 0.1 M sodium phosphate buffer that contained 0.5 mM DTNB, 0.03 mg/mL of BSA, and 93 pM recombinant human BuChE. Reactions were followed at $\lambda$ = 412 nm on a Molecular Devices SPECTRA$_{MAX}$ PLUS$^{384}$ UV−visible microplate spectrophotometer. The solid line is least-squares fit to eq 1 of the text. The double-reciprocal plot in the inset clearly shows substrate activation.

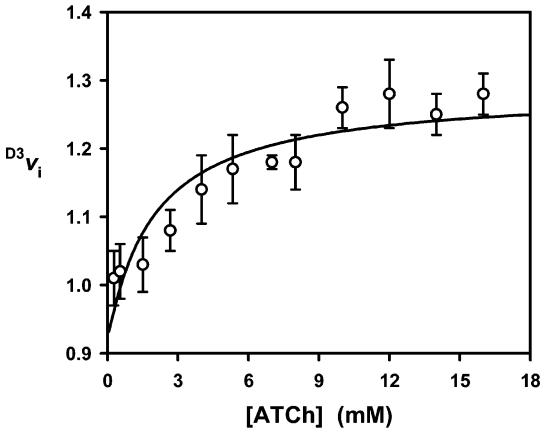


***Figure 2.*** $\beta$-Secondary deuterium kinetic isotope effects versus substrate concentration for the recombinant human BuChE-catalyzed hydrolysis of acetyl-$L_3$-thiocholine (L = H or D). The solid line is a least-squares fit to eq 2 of the text.

The isotope effect extrapolated to zero concentration is $^{D3}V/K$ (the isotope effect on $V_{max}/K_m$), and $^{D3}\beta$ is the asymptotic value of the isotope effect on substrate activation of $V_{max}$ at infinite concentration. Figure 2 shows a least-squares fit of the isotope effects to eq 2. In determining this fit, the parameters $\beta$, $K_A$, and $K_m$ were constrained to the values determined in the substrate activation plot in Figure 1. The isotope effects that result from the fit in Figure 2 are $^{D3}V/K = 0.93 \pm 0.03$ and $^{D3}\beta = 1.38 \pm 0.06$. Hence, the isotope effect on $\beta V_{max}$ is 1.29 ± 0.06.

The experiment in Figure 2 does not provide the value of the isotope effect on $V_{max}$, the parameter that monitors nonsubstrate-activated turnover via the EA complex of Scheme 1. To determine $^{D3}V_{max}$ and to provide a check on the value of $^{D3}V/K$ determined in Figure 2, time course data for the isotopic acetyl-$L_3$-thiocholines were fit to the integrated form of the Michaelis−Menten equation.[10] The experiments utilized an initial substrate concentration $[A]_0$ = 0.2 mM that was well below $K_A$, and therefore, the kinetics were not complicated by substrate activation. These experiments gave the following values for the isotope effects on the Michaelis−Menten parameters: $^{D3}V_{max} = 1.02 \pm 0.05$ and $^{D3}V/K = 0.97 \pm 0.06$. Both values are within experimental error of an isotope effect of 1.00, and the value for $^{D3}V/K$ indeed agrees with that determined in Figure 2. Importantly, neither isotope effect approaches the normal isotope effect on substrate-activated $V_{max}$. Only upon substrate activation is the marked normal isotope effect expressed.

The observation of a covalent tetrahedral adduct in the crystal structure of human BuChE[5] suggests that turnover of the acylenzyme intermediate is rate limiting for $V_{max}$. Therefore, the sizable normal isotope effect on substrate-activated $V_{max}$ suggests that in the FA complex allosteric modulation of the active site is accompanied by stabilization of the tetrahedral adduct, which then becomes the predominant accumulating species in the steady state. The turnover of the tetrahedral adduct would be marked by rehybridization from $sp^3$ toward $sp^2$ in the developing acetate product, consistent with the observed normal isotope effect. Hence, observations from X-ray crystallography and from isotope effects conspire to suggest that an important element in the catalytic power of cholinesterases is their ability to stabilize tetrahedral intermediates that are, in corresponding nonenzymatic reactions, high-energy and metastable species.

**Acknowledgment.** K.L.W. was supported by the Predoctoral Training Program in Biotechnology, NIH Grant T32 GM008365.

**Supporting Information Available:** Kinetic parameters ($V_{max}$, $V/K$) from fits of time courses to the integrated Michaelis−Menten equation for BuChE-catalyzed hydrolyses of acetyl-$L_3$-thiocholines. Derivations of eqs 1 and 2. This material is available free of charge via the Internet at http://pubs.acs.org.

## References

(1) Abbreviations: AChE, acetylcholinesterase; ATCh, acetylthiocholine; BuChE, butyrylcholinesterase; BSA, bovine serum albumin; DTNB, 5,5′-dithiobis(2-nitrobenzoic acid); mA, milli-absorbance unit.
(2) Quinn, D. M. *Chem. Rev.* **1987**, *87*, 955−979.
(3) Taylor, P.; Radić, Z. *Annu. Rev. Pharmacol. Toxicol.* **1994**, *34*, 281−320.
(4) Harel, M.; Quinn, D. M.; Nair, H. K.; Silman, I.; Sussman, J. L. *J. Am. Chem. Soc.* **1996**, *118*, 2340−2346.
(5) Nicolet, Y.; Lockridge, O.; Masson, P.; Fontecilla-Camps, J. C.; Nachon, F. *J. Biol. Chem.* **2003**, *278*, 41141−41147.
(6) Malany, S.; Sawai, M.; Sikorski, R. S.; Seravalli, J.; Quinn, D. M.; Radić, Z.; Taylor, P.; Kronman, C.; Velan, B.; Shafferman, A. *J. Am. Chem. Soc.* **2000**, *122*, 2981−2987.
(7) (a) Hogg, J. L. In *Transition States of Biochemical Processes*; Gandour, R. D., Schowen, R. L., Eds.; Plenum Press: New York and London, 1978; pp 201−224. (b) Kirsch, J. F. In *Isotope Effects on Enzyme-Catalyzed Reactions*; Cleland, W. W., O'Leary, M. H., Northrop, D. B., Eds.; University Park Press: Baltimore, MD, 1977; pp 100−122.
(8) Ellman, G. L.; Courtney, K. D.; Andreas, V., Jr.; Featherstone, R. M. *Biochem. Pharmacol.* **1961**, *7*, 88−95.
(9) Masson, P.; Legrand, P.; Bartels, C. F.; Froment, M.-T.; Schopfer, L. M.; Lockridge, O. *Biochemistry* **1997**, *36*, 2266−2277.
(10) Acheson, S. A.; Barlow, P. N.; Lee, G. C.; Swanson, M. L.; Quinn, D. M. *J. Am. Chem.* Soc. **1987**, *109*, 246−252.

JA052401Q

# Role of Water in Aging of Human Butyrylcholinesterase Inhibited by Echothiophate: The Crystal Structure Suggests Two Alternative Mechanisms of Aging

**F. Nachon***, O.A. Asojo, G.E.O. Borgstahl, P. Masson, O. Lockridge

Biochemistry 44 (2005) 1154-1162

# Role of Water in Aging of Human Butyrylcholinesterase Inhibited by Echothiophate: The Crystal Structure Suggests Two Alternative Mechanisms of Aging[†,‡]

Florian Nachon,[*,§,||] Oluwatoyin A. Asojo,[§] Gloria E. O. Borgstahl,[§] Patrick Masson,[||] and Oksana Lockridge[§]

*The Eppley Institute for Research in Cancer and Allied Diseases, University of Nebraska Medical Center, Omaha, Nebraska 68198-6805, and Unité d'enzymologie, Département de Toxicologie, Centre de Recherches du Service de Santé des Armées, 24 avenue des Maquis du Grésivaudan BP87, 38702 La Tronche Cedex, France*

*Received August 14, 2004; Revised Manuscript Received November 12, 2004*

ABSTRACT: Organophosphorus poisons (OP) bind covalently to the active-site serine of cholinesterases. The inhibited enzyme can usually be reactivated with powerful nucleophiles such as oximes. However, the covalently bound OP can undergo a suicide reaction (termed aging) yielding nonreactivatable enzyme. In human butyrylcholinesterase (hBChE), aging involves the residues His438 and Glu197 that are proximal to the active-site serine (Ser198). The mechanism of aging is known in detail for the nerve gases soman, sarin, and tabun as well as the pesticide metabolite isomalathion. Aging of soman- and sarin-inhibited acetylcholinesterase occurs by C−O bond cleavage, whereas that of tabun- and isomalathion-inhibited acetylcholinesterase occurs by P−N and P−S bond cleavage, respectively. In this work, the crystal structures of hBChE inhibited by the ophthalmic reagents echothiophate (nonaged and aged) and diisopropylfluorophosphate (aged) were solved and refined to 2.1, 2.25, and 2.2 Å resolution, respectively. No appreciable shift in the position of the catalytic triad histidine was observed between the aged and nonaged conjugates of hBChE. This absence of shift contrasts with the aged and nonaged crystal structures of *Torpedo californica* acetylcholinesterase inhibited by the nerve agent VX. The nonaged hBChE structure shows one water molecule interacting with Glu197 and the catalytic triad histidine (His438). Interestingly, this water molecule is ideally positioned to promote aging by two mechanisms: breaking either a C−O bond or a P−O bond. Pesticides and certain stereoisomers of nerve agents are expected to undergo aging by breaking the P−O bond.

Organophosphorus compounds (OP)[1] are widely used as pesticides, plasticizers, pharmaceuticals, in hydraulic fluid, and in jet engine fuel. Some are feared chemical warfare agents. Acute toxicity from exposure to organophosphorus agents is due to inhibition of acetylcholinesterase (AChE; EC 3.1.1.7). Butyrylcholinesterase (BChE; EC 3.1.1.8), a closely related serine hydrolase found in vertebrates and sharing about 55% sequence identity with AChE, is also inhibited. But BChE inhibition is thought to serve a protective role, by scavenging OP molecules. Plasma BChE scavenges OPs, thus preventing inhibition of neuromuscular and neuronal AChEs. Monkeys pretreated with human BChE (hBChE) can be fully protected against OP toxicity, for example, up to 5 $LD_{50}$ of soman (*1*−*3*).

Aging is defined as a time-dependent process leading to nonreactivatable enzyme. For example, soman-inhibited acetylcholinesterase ages by dealkylation (departure of the pinacolyl side chain) of the OP moiety (*4*). Many OP react faster with BChEs than with AChEs (*5*−*7*), and many OP−BChE conjugates age faster than OP−AChE conjugates (Table 1). The goal of this study was to understand the particularities of the BChE aging mechanism. For this purpose we solved the crystal structures of OP-inhibited human BChE before and after aging.

We focused on hBChE inhibited by the ophthalmic agents echothiophate iodide and diisopropylfluorophosphate (DFP) (see structures in Figure 1). Echothiophate was used because (a) the diethylphosphoryl conjugate ages slowly, with a half-life of 12 h at pH 7.0 (*8*), allowing isolation of the first nonaged conjugate of hBChE to date, as well as the aged structure; (b) the aged derivative is close in size to butyrate, making the aged structure analogous to the deacylation tetrahedral intermediate during hydrolysis of butyrylcholine; (c) echothiophate iodide is soluble and stable in aqueous solvent and therefore readily soaks into a crystal; (d)

[†] Supported by U.S. Army Medical Research and Materiel Command, Grant DAMD17-01-2-0036 (to O.L.); UNMC Eppley Cancer Center Support, Grant P30CA36727-19; Contract 00-2-032-0-00 from the Office of the Defense Cooperation Attache, République Française, Washington, DC, part of DGA 99CO-029/PEA (to P.M.); DGA/DSP/STTC-PEA 010807 (to P.M. and O.L.); and the Nebraska Tobacco Settlement Biomedical Research Development Fund (to G.B.).

[‡] Protein Data Bank entry codes are 1XLW for nonaged echothiophate-inhibited hBChE, 1XLV for aged echothiophate-inhibited hBChE, and 1XLU for aged DFP-inhibited hBChE.

* To whom correspondence should be addressed: Telephone (+33) 476 63 9765; fax (+33) 476 63 6962; e-mail florian@nachon.net.

[§] University of Nebraska Medical Center.

[||] Centre de Recherches du Service de Santé des Armées.

[1] Abbreviations: OP, organophosphate; AChE, acetylcholinesterase; BChE, butyrylcholinesterase; DFP, diisopropyl fluorophosphate; DP, diethylphosphoryl; VX, *O*-ethyl-*S*-[2-[bis(1-methylethyl)amino]ethyl]-methylphosphonothioate; PDB, Protein Data Bank.

10.1021/bi048238d CCC: $30.25 
Published on Web 01/06/2005

Table 1: Rates of Aging of OP-Inhibited Human BChE and Human AChE

| Enzyme | OP | Substituent $R_1$,$R_2$ | Aging half-life | pH | T in°C | Reference |
|---|---|---|---|---|---|---|
| hBChE | | | | | | |
| | Paraoxon | EtO, EtO | 11.6 h | 8 | 20 | (*8*) |
| | Triazophos | EtO, EtO | 12.6 h | 7.4 | 37 | (*31*) |
| | DFP | iPrO, iPrO | 1 h | 8 | 25 | (*32*) |
| | Cyclosarin |  , Me | 2.2 h | 7.4 | 37 | (*33*) |
| | Soman (racemic) |  , Me | 9 min | 8 | 25 | (*32*) |
| | Soman PsCs |  , Me | 3.9 min | 8 | 25 | (*27*) |
| hAChE | | | | | | |
| | Paraoxon | EtO, EtO | 41 h | | 37 | (*34*) |
| | Ethyldichlorvos | EtO, EtO | 58 h | 7.4 | 37 | (*35*) |
| | DFP | iPrO, iPrO | 4.6 h | | 37 | (*34*) |
| | Cyclosarin |  , Me | 8.7 h | 7.4 | 37 | (*33*) |
| | Cyclosarin |  , Me | 4.6 h | 7.1-7.3 | 25 | (*36*) |
| | Soman |  , Me | 6.3 min | 8 | 27 | (*37*) |

echothiophate is not volatile, making it relatively safe in a laboratory setting; (e) echothiophate is of clinical interest because it has been used as an anti-glaucoma drug; (f) echothiophate is positively charged and does not cross the blood−brain barrier; and last, (g) echothiophate is a prototype of the VX nerve agent family. DFP was used to allow comparison of DFP-phosphorylated hBChE with the DFP-inhibited *Torpedo californica* AChE (*Tc*AChE) structure (*9*).

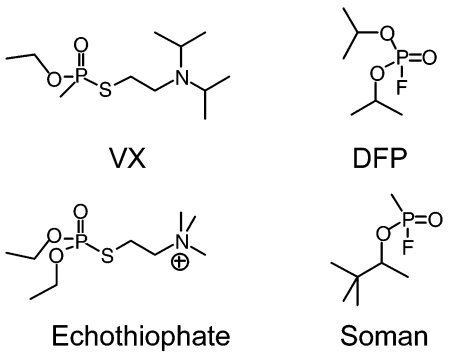


FIGURE 1: Chemical structures of VX, DFP, echothiophate, and soman.

Of particular interest was to compare the OP-hBChE and OP-*Tc*AChE structures in order to understand why they age at different rates. Millard et al. (*10*) reported the crystal structure of nonaged VX-inhibited *Tc*AChE (PDB entry 1VXO). They found that the catalytic His440[2] shifted 4.5 Å away from its triad partner Glu327 to interact with Glu199. They suggested disruption of the catalytic triad could explain the slow spontaneous reactivation of the VX−*Tc*AChE conjugate. In the aged structure, the imidazole ring of His440 had returned to its idle position. It was of interest to determine whether the catalytic His of hBChE displayed a similar mobility during aging. Aged *Tc*AChE structures, resulting from reaction with soman, sarin, DFP, or VX, are essentially identical and provide an explanation for the resistance to reactivation of the aged OP conjugates (*9*, *10*). The present work asked whether the mechanism of aging was equivalent in phosphylated AChE and BChE.

## MATERIALS AND METHODS

*Crystals of Nonaged Echothiophate-Inhibited hBChE*. The recombinant hBChE was a truncated monomer containing residues 1−529 (*11*). The tetramerization domain at the carboxy terminus was deleted. The carbohydrate content was reduced by site-directed mutagenesis from 9 to 6 glycans (*11*). The recombinant hBChE gene was expressed in Chinese hamster ovary (CHO) cells. The enzyme secreted into serum-free culture medium was purified by affinity and ion-exchange chromatography and crystallized as described (*11*). The mother liquor was 0.1 M MES buffer, pH 6.5, with 2.1

[2] *Tc*AChE's amino acid numbering corresponds to hBChE's amino acid numbering + 2.

Table 2: Data Collection and Refinement Statistics

| | MIP-BChE (DFP aged) | DEP-BChE (echothiophate) | EFS-BChE (echothiophate aged) |
|---|---|---|---|
| | | Data | |
| space group | *I*422 | *I*422 | *I*422 |
| unit cell axes, $a = b, c$ (Å) | 154.49, 127.29 | 154.46, 127.01 | 154.59, 126.70 |
| no. of reflections | 294 819 | 402 015 | 247 056 |
| unique reflections | 37 851 | 43 695 | 31,580 |
| resolution (Å) | 50−2.20 (2.20−2.28) | 50-2.10 (2.18−2.10) | 50-2.25 (2.33−2.25) |
| completeness (%) | 96.3 (100.0) | 97.3 (98.2) | 86.1 (91.1) |
| $R_{merge}$[a] (%) | 6.3 (40.1) | 5.8 (46.2) | 5.1 (43.9) |
| $I/\sigma(I)$ | 27.9 (4.6) | 29.0 (5.5) | 32.2 (3.3) |
| redundancy | 7.8 (7.7) | 9.2 (9.0) | 7.8 (6.3) |
| | | Refinement Statistics | |
| *R*-factor[b](*R*-free[c]) | 19.3 (24.2) | 18.4 (22.3) | 18.3 (24.6) |
| no. of atoms | | | |
| protein | 4273 | 4225 | 4285 |
| solvent | 255 | 290 | 220 |
| others | 158 | 192 | 172 |
| mean *B*-factor (Å$^2$) | 45.8 | 42.3 | 48.3 |
| RMS from ideality | | | |
| bond length (Å) | 0.017 | 0.018 | 0.018 |
| angles (deg) | 1.600 | 1.714 | 1.744 |
| chiral (Å$^3$) | 0.109 | 0.127 | 0.115 |

[a] $R_{merge} = (\Sigma|I - \langle I\rangle|)/\Sigma I$, where $I$ is the observed intensity and $\langle I\rangle$ is the average intensity obtained from multiple observations of symmetry-related reflections after rejections. [b] *R*-factor $= \Sigma|F_o - |F_c||/\Sigma|F_o|$, where $F_o$ are observed and $F_c$ are calculated structure factors. [c] *R*-free set uses 5% of randomly chosen reflections defined in Brunger et al. (*38*).

M $(NH_4)_2SO_4$. The echothiophate iodide (Wyeth-Ayerst, Rouses Point, NY) stock solution was 50 mM in water. The echothiophate−hBChE conjugate was obtained by soaking crystals for 1 h in 0.1 M MES buffer, pH 6.5, with 2.4 M $(NH_4)_2SO_4$ containing 1 mM echothiophate iodide. Data were collected right after the incubation to avoid aging ($t_{1/2}$ aging ≈ 12 h at pH 7.0, 25 °C).

*Crystallization of DFP and Echothiophate-Aged hBChE*. The purified enzyme (6.6 mg/mL) was inhibited in the presence of 0.5 mM DFP (Sigma) in 10 mM MES buffer, pH 6.5. The reaction mixture was incubated for 1 day at 4 °C, allowing enough time for completion of the aging reaction ($t_{1/2}$ aging ≈ 1 h at pH 7.0, 25 °C). The inhibited enzyme was crystallized by the hanging drop method as described (*12*). Crystals grew to 0.5 × 0.5 × 0.3 mm in one week at 20 °C. The echothiophate-aged hBChE crystals were produced following a similar process after the enzyme was inhibited in the presence of 1 mM echothiophate iodide in 10 mM MES buffer, pH 6.5. The length of time between the phosphorylation step and the data collection was sufficiently long (>1 week) to achieve completion of the aging reaction.

*X-ray Data Collection and Structure Solution*. Data were collected at the University of Nebraska Medical Center Structural Biology Laboratory. The crystals were washed with a cryoprotectant solution [0.1 M MES buffer with 2.4 M $(NH_4)_2SO_4$ containing 18% glycerol] and then flash-cooled at −160 °C in a nitrogen stream provided by an X-Stream 2000 system (Rigaku MSC). The X-ray diffraction equipment consisted of a Rigaku rotating anode FR-E SuperBright X-ray generator, Osmic mirrors for focusing, and a RAXIS-IV ++detector.

All data sets were processed with HKL2000 (*13*). The structures were solved by use of the CCP4 suite (*14*). An initial solution model was determined by molecular replacement with MolRep (*15*) starting from the recombinant BChE structure (PDB entry 1P0I) from which all ligands (butyrate, glycerol, ions) and glycan chains had been removed. For all diffraction data sets, the model was refined by the following strategy: an initial rigid-body refinement with REFMAC5 (*16*), followed by iterative cycles of model building, with PyMol (*17*) and O (*18*), and restrained refinement with REFMAC5.

## RESULTS

*X-ray Crystallography*. Data were collected from tetragonal crystals of space group *I*422 and refined to 2.20 Å (DFP-phosphorylated enzyme), 2.10 Å (nonaged echothiophate−BChE conjugate), and 2.25 Å (aged echothiophate−BChE conjugate). Data and refinement statistics are shown in Table 2. In the original structure (PDB entry 1P0I) the catalytic serine was within 2.16 Å of a butyrate molecule. The butyrate was removed in the starting model used for the molecular replacement. Therefore the peak of positive density within covalent bond distance of the O$\gamma$ of the catalytic serine, observed in the omit electron density maps of the three OP structures, confirms the presence of the covalently bound inhibitor.

A peak of positive density was found close to Cys66 in the three structures. This density was refined as a sulfur atom covalently bound to Cys66 (*S*-mercaptocysteine). While this particular modification of residue 66 is present in the enzyme preparation we used in this work, it was clearly absent in the previously solved structures of hBChE (*12*).

*Induced Fit of the Acyl Loop*. One side of the active-site gorge is delimited by a loop, called the acyl-loop, because it extends from residue 276 at the gorge entrance to residue 289 in the acyl-binding pocket. The acyl-binding pocket of hBChE is defined by side chains of residues Leu286, Val288, and Trp231. The function of this pocket is to bind the acyl moiety of carboxyl ester substrates. This pocket also binds one isopropoxy group of DFP in the DP conjugate and the methyl group of soman-phosphonylated BChE (Figure 2A). The conformation of the acyl-loop in the DFP-phosphorylated

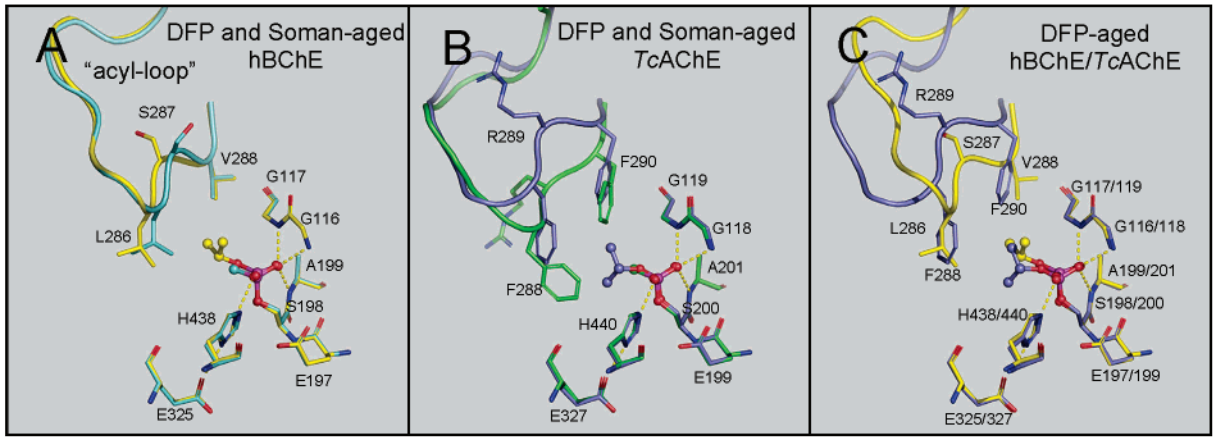


FIGURE 2: Superposition of the active-site structures of aged hBChE and aged *Tc*AChE emphasizing the differences in the "acyl-loop" conformations. (A) Superposition of aged DFP-inhibited hBChE, carbon atoms in yellow, and aged soman-inhibited hBChE (PDB entry 1P0Q) (*12*), carbon atoms in light blue. (B) Aged DFP-inhibited *Tc*AChE (PDB entry 2DFP) (*9*), carbon atoms in slate, and aged Soman-inhibited *Tc*AChE (PDB entry 1SOM) (*9*), carbon atoms in green. (C) Aged DFP-inhibited hBChE, carbon atoms in yellow, and aged DFP-inhibited *Tc*AChE, carbon atoms in slate. The backbone of the acyl-loops is represented as a thick wire. Key residues are represented as sticks with nitrogen atoms in blue and oxygen atoms in red. The phosphoryl- (DFP) and phosphonyl- (soman) heads are represented as ball-and-sticks with the phosphorus atoms in magenta. Hydrogen bonds are represented by yellow dashes.

enzyme structure is the same as in the butyrate−hBChE structure (PDB entry 1P0I). However, its conformation is different from the soman-aged hBChE structure. The van der Waals volume of the methylphosphonyl moiety derived from soman inhibition is smaller than the one occupied by the monoisopropylphosphoryl aged moiety resulting from DFP inhibition. The size difference results from moiety-induced fit of the acyl-loop. In the soman-aged structure, Leu286 is shifted inward by 2.0 Å, clasping the acyl-binding pocket around the methyl group. The Leu286 shift is accompanied by a flip of the adjacent residue, Ser287.

The acyl-binding pocket of *Tc*AChE is shaped by Trp233 and two additional bulky aromatic residues, Phe288 and Phe290, both much bulkier than their aliphatic counterparts in hBChE, Leu286 and Val288. The acyl-binding pocket of *Tc*AChE is therefore more restrictive than that of hBChE. The restrictive acyl pocket of AChE provides a good fit for the small methyl group of the soman-aged *Tc*AChE structure. However, the pocket is too small to accommodate larger groups, such as the isopropoxy group of the DP moiety, without adjustment. Figure 2B shows the shift in the acyl-loop backbone reported by Millard et al. (*9*). The conformational change is accompanied by a flip of Arg289, the residue between Phe288 and Phe290. This is similar to the flip of Ser287, the equivalent residue in hBChE.

As a consequence of the conformational change following inhibition by DFP, the size of the acyl-binding pocket in *Tc*AChE has expanded to become similar in size to the acyl-binding pocket in hBChE, even though the conformations of the acyl-loop backbones are very different (2.74 Å rms deviation). This is shown in Figure 2C. With the exception of the acyl-loop, the active-site residues have the same positions in DFP-aged hBChE and AChE. The isopropyl groups do not superimpose in *Tc*AChE and hBChE, reflecting the specificity of the interactions with the different side chains of the two pockets.

*No Change in the Position of His438 in Echothiophate-Inhibited, Nonaged hBChE*. The crystal structure of the nonaged, echothiophate-inhibited hBChE shows the phosphorus atom covalently bound to the O$\gamma$ of the catalytic Ser198. One oxygen of the phosphate fits in the oxyanion hole, strongly hydrogen-bonded to the backbone NH of Gly116, Gly117, and Ala199 (Figure 3A). The distances are 2.81 Å to Gly116, 2.75 Å to Gly117, and 2.94 Å to Ala199. One ethoxy group fills the acyl-binding pocket. The second ethoxy group points toward the mouth of the gorge. The oxygen atom of the second ethoxy group is at hydrogen-bonding distance to N$\epsilon$2 of His438 (3.32 Å).

The catalytic triad of hBChE consists of Ser198, His438, and Glu325. These residues are interconnected by hydrogen bonds in hBChE when Ser198is not interacting with a ligand. This situation is observed for one of the alternate conformations of the catalytic serine in the choline−hBChE complex (PDB entry 1P0M). However, the Ser198−His438 connection is disrupted in the diethylphosphoryl conjugate of hBChE (Figure 3A). Though the N$\epsilon$2 of His438 is at hydrogen-bonding distance to O$\gamma$ of Ser198 (3.22 Å), the angle is about 80°, a value unfavorable for making a H-bond. This was also observed in the butyrate−hBChE complex (PDB entry 1P0I). By contrast, His438 retains its connection to Glu325 in the diethylphosphoryl conjugate. The interaction with Glu325 maintains the histidine in the same position in all hBChE crystal structures observed to date. The disruption of the H-bond between O$\gamma$ of the serine and N$\epsilon$2 of His438 when a ligand is bound to the serine does not mean that the catalytic residues adopt an improper position for catalytic function. Actually, it is necessary that the relative positions of the serine and histidine side chains adjust during the catalytic cycle. This allows efficient proton transfer between the serine, the leaving alcohol product, and the water molecule that hydrolyzes the acyl-enzyme.

*A Possible Second Mechanism of Aging*. Another important feature of the diethylphosphoryl−hBChE conjugate (Figure 3A) is the location of water molecule 101. Water 101 is within interaction distance to N$\epsilon$2 of His438 (2.90 Å) and the carboxyl group of Glu197 (2.82 Å). Therefore, water 101 serves as a relay for Glu197 to stabilize the positive charge on protonated His438. Because of its interaction with Glu197, Water 101 is activated. This water molecule is ideally positioned to catalyze two mechanisms of aging.

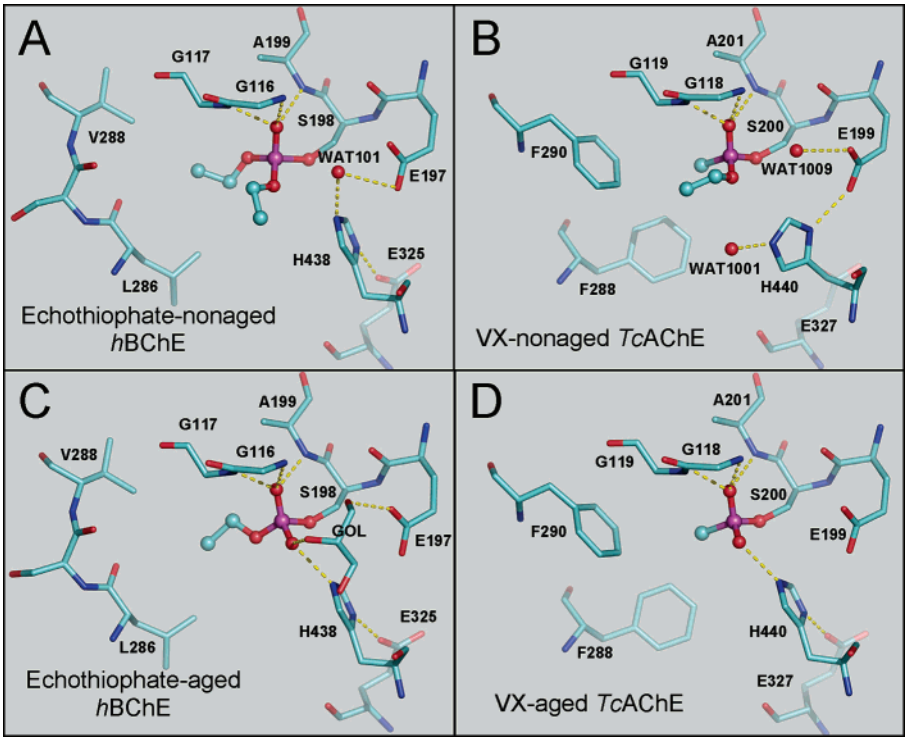


FIGURE 3: Active-site structures of hBChE and *Tc*AChE before and after aging. (A) hBChE inhibited by echothiophate yields a diethylphosphoryl conjugate (nonaged). (B) Diethylphosphoryl-hBChE aged to a monoethylphosphoryl conjugate. (C) *Tc*AChE inhibited by VX yields the *O*-ethylmethylphosphonyl conjugate (nonaged; PDB entry 1VXR) (*10*). (D) TcAChE-conjugate aged into a methylphosphonyl conjugate (PDB entry 1VXO) (*9*). Key active-site residues and glycerol (GOL) are represented as sticks, the OP as ball-and-sticks, and water molecules as red spheres. Water 101 in BChE is positioned to carry out aging by either C−O or P−O bond breakage.

In the first aging mechanism the C−O bond of the ethoxy group is broken. This is the accepted mechanism of aging of acetylcholinesterase for soman (*4*, *19*) and sarin (*20*). The positively charged imidazolium ion stabilizes the developing negative charge on the $C-O^{\delta-}$ oxygen. Water 101 is at a good distance to attack the carbocationic center that appears on the $C^{\delta+}-O$ carbon.

In the second aging mechanism the P−O bond is broken. Water 101 is ideally positioned to attack the electrophilic phosphorus atom to form a bipyramidal intermediate. The leaving group has to be on the opposite side of the attacking water molecule (in-line inversion). Therefore, the leaving group is the ethoxy group that fills the acyl-binding pocket. This second mechanism is a novel result from this work.

The diethylphosphoryl−hBChE conjugate has the ability to age by both mechanisms. Though the energy needed to break C−O and P−O bonds is of the same order, that is, about 360 kJ·mol$^{-1}$, local geometry, polarity, and dielectric constraints may dramatically alter the activation energy needed for covalent bond breakage. Therefore, it is risky to predict which mechanism predominates.

*Comparison of Echothiophate-Inhibited Nonaged hBChE to VX-Inhibited Nonaged TcAChE*. The structure of VX-inhibited *Tc*AChE before aging is shown in Figure 3B (PDB entry 1VXR) (*10*). The similarities with the hBChE structure in Figure 3A are the following. The oxygen of the phosphonate is locked in the oxyanion hole, the methyl group is in the acyl pocket, and the ethoxy group points toward the mouth of the gorge. Water 1009 in *Tc*AChE is in a position equivalent to that of water 101 in hBChE. However, water 1009 is not within hydrogen-bond distance of His440 because His440 has shifted its position. This contrasts with hBChE, whose catalytic histidine does not shift position after inhibition by OP. Although the position of Water 1009 is compatible with an attack on the phosphorus atom, the reaction cannot take place. The reason is that in the VX-inhibited *Tc*AChE, the group on the opposite side of the bipyramidal intermediate is a methyl group directly bound to the phosphorus atom, that is, not a leaving group. Thus, the second aging mechanism involving breaking of a P−O bond is not possible for VX-inhibited *Tc*AChE. The same is probably true for dealkylation of sarin- and soman-inhibited *Tc*AChE.

The connection between glutamate Glu327 of the catalytic triad and His440 is disrupted in *Tc*AChE but not in hBChE (compare Figure 3 panels A and B). The consequence is that the imidazolium ion does not directly stabilize the negative charge on the oxygen of the C−O bond. Millard et al. (*10*) concluded this explains the slow aging of VX-inhibited *Tc*AChE.

However, Water 1001 in Figure 3B is part of a hydrogen-bonded network, including Glu199 and His440. Water 1001 is 3.58 Å away from the primary carbon of the ethoxy group. This water molecule is activated and may stabilize the formation of the developing carbocation. An equivalent water molecule is not present in echothiophate-phosphorylated hBChE (Figure 3A).

*Aged hBChE and TcAChE*. The dealkylation leads to a new negative charge on one of the oxygens of the phosphyl group. This has major consequences. The presence of this negative charge decreases the electrophilicity of the phosphorus atom so that nucleophiles, like oximes, are unable to displace the phosphyl group. As a result, aged forms of *Tc*AChE and hBChE cannot be reactivated.

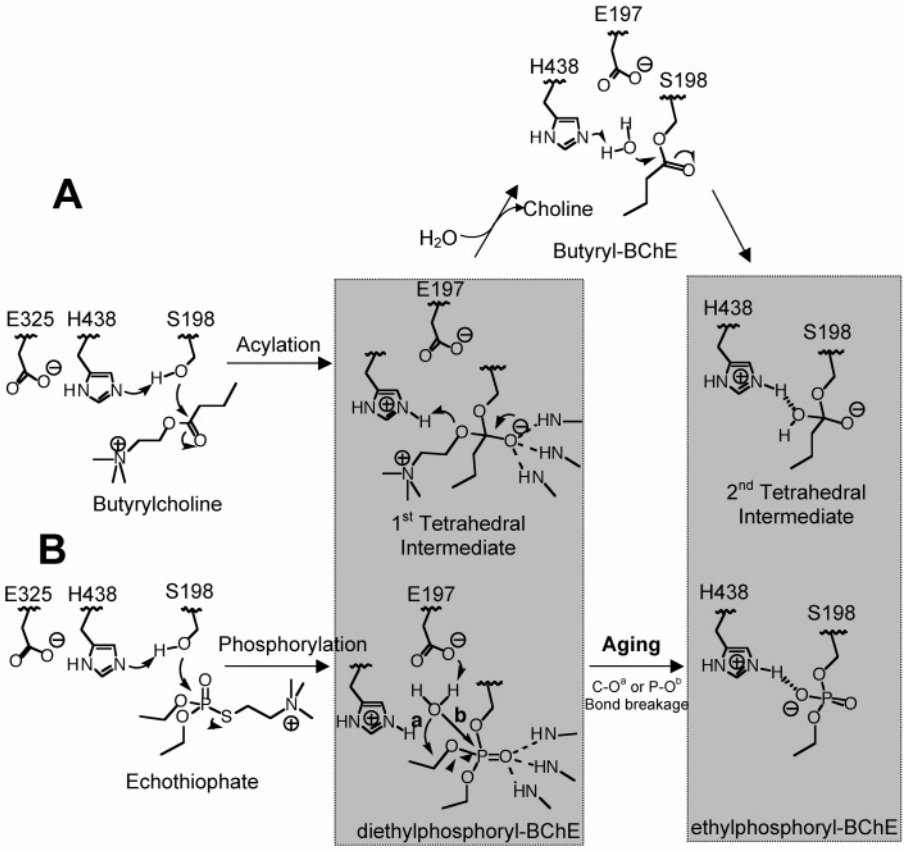


FIGURE 4: Catalytic hydrolysis mechanism of butyrylcholine by hBChE (A) and phosphorylation mechanism with the inhibitor echothiophate (B). The gray boxes indicate the similarities between the intermediates for the two mechanisms.

A second consequence is that a salt bridge forms between His438/440 and the oxyanion of the dealkylated OP, stabilizing the negative charge. Figure 3 panels C and D show that the salt bridge imposes identical orientations on His438/440 and on the dealkylated phosphyl group in echothiophate-inhibited hBChE and in VX-inhibited *Tc*AChE. This salt bridge raises the energy of activation necessary for the oxime-mediated enzyme reactivation. Moreover, the proton of the catalytic His, captured in the salt bridge, cannot be easily transferred to the serine as is required in the reactivation mechanism. In hBChE, formation of the salt bridge induces a slight rotation/shift of the phosphoryl moiety, aligning the negatively charged oxygen with His438 (Figure 3A,C). In *Tc*AChE, formation of the salt bridge forces the catalytic His440 to return to its classical position where it is hydrogen-bonded to Glu327 (Figure 3B,D).

*Glycerol in the Aged Structure Displaces Water Molecules Present in Nonaged hBChE*. There is a molecule of glycerol in the active site of the aged monoethylphosphoryl−hBChE (Figure 3C). The presence of glycerol is an artifact related to its use as a cryoprotectant during X-ray diffraction experiments. Two hydroxyls of glycerol roughly superimpose with the location of water molecules 207 and 72 present before aging in the diethylphosphoryl−hBChE (not shown). These two hydroxyls are at hydrogen-bond distance with the negatively charged oxygen of the dealkylated phosphoryl. The third hydroxyl is within hydrogen-bond distance of Glu197. The glycerol binds to the aged active site because the negatively charged oxygen resulting from the dealkylation is a better hydrogen-bond acceptor than the equivalent phosphoester oxygen in the nonaged hBChE. The butyrate−hBChE complex also has an equivalent glycerol in the active site.

*OP Conjugates as Analogues of Catalytic Intermediates*. The mechanism of hydrolysis of butyrylcholine is illustrated in Figure 4A. The carboxylic ester undergoes a nucleophilic attack by the catalytic serine to form the first tetrahedral intermediate. This intermediate collapses to the butyryl-enzyme intermediate with release of choline. Then a water molecule makes a nucleophilic attack on the butyryl−enzyme to form the second tetrahedral intermediate that collapses into the butyrate−enzyme complex. This butyrate−enzyme complex was seen in the crystal structure of native hBChE (PDB entry 1P0I).

The mechanism of inhibition and aging by echothiophate is illustrated in Figure 4B. The phosphoric acid thioester undergoes a nucleophilic attack by the catalytic serine to form a bipyramidal intermediate (not shown). This intermediate collapses to diethylphosphoryl−hBChE with release of the thiocholine. The diethylphosphoryl−hBChE intermediate (Figure 4B) is analogous to the first tetrahedral intermediate (Figure 4A) because both have the same tetrahedral geometry and the choline carboxyl ester function is analogous to one of the ethyl phosphoryl ester functions. One of the ethoxy groups points to the mouth of the gorge (Figure 4A). Similarly, in the nonaged VX−*Tc*AChE structure, the ethoxy group points toward the mouth of the gorge (Figure 4B). It was previously suggested that the orientation of the charged leaving group of cationic OPs is directed toward the mouth of the gorge (*21*). In the first tetrahedral intermediate, the choline head may similarly point toward Tyr332 of the peripheral anionic site.

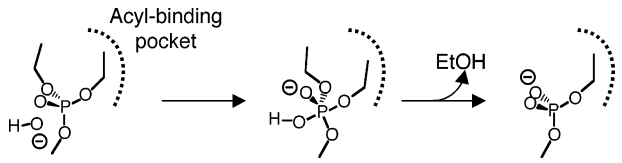


FIGURE 5: Aging mechanism by P−O bond breaking.

A water molecule hydrogen-bonded to Glu197 was observed in the crystal structure of the diethylphosphoryl−hBChE. Although the first tetrahedral intermediate structure has never been directly observed, an equivalent water molecule is likely to be present in the same location. This water molecule is in the right position to attack the butyryl−hBChE complex to form the second tetrahedral intermediate (*22*).

Both the second tetrahedral intermediate, that is, butyrate−hBChE, and the ethylphosphoryl hBChE were directly observed in crystal structures. These structures are analogous in the following ways. The isosteric butyryl and ethoxy chains interact with the acyl-binding pocket. The butyrate and ethoxy atoms superimpose. Both the carbonyl oxygen of the butyrate and the (oxy)phosphoryl oxygen are locked into the oxyanion hole. The anionic phosphoryl oxygen in the ethylphosphoryl−hBChE forms a salt bridge with the imidazolium, similar to the electrostatic interaction between the natural substrate and His438 in the second tetrahedral intermediate. In the ethylphosphoryl−hBChE the formal negative charge is distributed on the oxygen in the oxyanion hole and the oxygen in the salt bridge with His438. Both the oxyanion hole and the charged histidine stabilize the negative charge. In the second tetrahedral intermediate the negative charge is similarly stabilized by the oxyanion hole and the imidazolium. This dual stabilization may explain why butyrate−hBChE was found as a stable complex in the crystal.

## DISCUSSION

*Mechanism of Aging by Breaking P−O Bond*. The crystal structure of nonaged, echothiophate-inhibited hBChE shows one water molecule ideally positioned to catalyze aging by two mechanisms: by breaking the C−O bond and/or by breaking the P−O bond. An aging mechanism that involves breaking of the P−O bond has never been reported. Breaking of a P−O bond is chemically feasible as demonstrated by the fact that a P−O bond between the OP and serine is broken during reactivation of OP-inhibited BChE.

Our hypothesis requires a specific OP stereochemistry for aging by P−O bond breaking. Common pesticides have no chiral phosphorus atom. Their active forms are usually dimethyl or diethyl phosphate. Therefore, pesticides always place an alkoxy group in the acyl-binding pocket, which is a requirement for P−O bond breaking (nucleophilic substitution by in-line inversion). A bipyramidal intermediate is formed when the water molecule close to Glu197 attacks the phosphorus atom (Figure 5). The stereochemistry of the phosphorus atom imposes that the leaving group be on the opposite side of the attacking molecule of water, that is, in the acyl-binding pocket. As a consequence, OP pesticides are expected to age through P−O bond breaking, in addition to aging through C−O bond breaking.

By contrast, nerve agents have a chiral phosphorus atom. Their stereoisomers do not systematically fulfill the requirement for P−O bond breaking. A stereoisomer that places an alkyl group in the acyl-binding pocket cannot undergo P−O bond breaking. For example, VX is a mixture of P(*S*) and P(*R*) stereoisomers. The P(*S*) stereoisomer reacts stereospecifically with *Tc*AChE, so that the methyl group of the moiety lies in the acyl-binding pocket, whereas the P(*R*) stereoisomer yields the ethoxy group in the acyl-binding pocket. The P(*S*) stereoisomer can age only by C−O bond cleavage, whereas the P(*R*) stereoisomer can age only by breaking of the P−O bond.

The acyl-binding pocket of hBChE can accommodate bigger substituents than *Tc*AChE. Consequently, unlike *Tc*AChE, hBChE does not exert stereoselectivity for OP bearing small substituents. This is the case for sarin (methyl and isopropyloxy groups) and VX (methyl and ethoxy groups) (*23*). hBChE can react with both stereoisomers of sarin or VX, while *Tc*AChE reacts preferentially with the stereoisomer that yields the smallest substituent in the acyl-binding pocket. *Tc*AChE does not present a potential leaving group in the acyl-binding pocket when it is inhibited by sarin or VX; therefore aging occurs exclusively by C−O bond breaking. The C−O bond breaking is always the favored aging mechanism for compounds with branched alkoxy groups, like soman, sarin, and DFP. The intermediate carbocation is not stabilized by neighboring carbons for nonbranched alkoxy groups such as ethoxy and methoxy. As a result the C−O bond breaking is slower. We expect both *Tc*AChE and hBChE to age by P−O bond breaking as well as by C−O bond breaking when the conjugate is a dimethoxy or diethoxy phosphate.

The P−O bond breaking mechanism of aging is similar to the aging mechanism described for *Tc*AChE and hBChE inhibited by (1*S*,3*S*)-isomalathion (*24*, *25*). (1*S*,3*S*)-Isomalathion conjugates of AChE and BChE aged via an $S_N2$ mechanism with loss of diethyl thiosuccinate, that is, by breaking of P−S bond. The P−S bond breakage is so favorable that the fast rate of aging was impossible to measure by conventional methods. It is expected that the rate of P−O bond breaking is much slower because of the nature of the leaving group, thiols being better leaving groups than alcohols.

Regarding phosphoramidyl conjugates, NMR studies showed that tabun ages slowly through a mechanism involving the P−N bond scission (*26*). It is possible that the P−N bond scission occurs via an $S_N2$ mechanism similar to the P−O bond mechanism of aging we propose.

*Role of Protonated Histidine in Aging by P−O Bond Breaking*. Because His438 is positively charged, it reinforces the electrophilicity of the phosphorus atom by withdrawing the electrons on the neighboring alkoxy oxygen. A second role of His438 is to hold water molecule 101 by H-bonding, at the optimum location for the nucleophilic attack of the phosphorus atom. It is noteworthy that His438 cannot participate in the activation of the water molecule because it cannot accept a second proton. The activation of water relies on Glu197.

The catalytic histidine cannot play these two roles when it is shifted like in the nonaged VX-inhibited *Tc*AChE structure. In this case, His440 is away from the alkoxy oxygen so that it does not provide an electrostatic environment favorable to the $S_N2$ mechanism. Since His440 is unavailable, water molecule 1009 interacts only with Glu199.

Unlike the position of His438, the position of His440 is unfavorable for P−O bond breaking.

*Evidence for Aging by $S_N2$ Reaction?* pH dependence studies were helpful to understand the mechanism of aging of soman-inhibited cholinesterase (*27*). The dealkylation rate of soman-inhibited huBChE is faster when both His438 and Glu197 are ionized because the imidazolium ion stabilizes a negative charge on the ethoxy oxygen while the negatively charged glutamate stabilizes the carbocation intermediate. Hobbiger (*28*) showed earlier that the aging of diethylphosphoryl- bovine AChE is faster at pH 6.0 than 8.0 and dependent on the protonation of a residue of p$K_a$ about 7.3, that is, the catalytic histidine. This pH dependence study supports that aging of diethylphosphoryl AChE occurs principally by dealkylation. However, it is not clear that the pH dependence of the $S_N2$ reaction would be much different from that of the dealkylation, even in this pH range, because as described above, a protonated catalytic histidine also constitutes a driving force for the $S_N2$ reaction. Besides, the $S_N2$ rate may not be significantly enhanced by the higher concentration of hydroxyl ions at high pH because Glu197 repulses approaching anions. The rate of the $S_N2$ reaction should be enhanced at low pH close to the p$K_a$ of Glu197, where Glu197 can act as a general base catalyst to activate water. Therefore a pH-dependence study is not appropriate to discriminate between the two mechanisms.

A better method to provide evidence of the $S_N2$ mechanism is to age in the presence of $H_2{}^{18}O$ and then analyze the aged products by mass spectrometry. $^{18}O$ will be incorporated on the monoethylphosphoryl group only if aging results from the nucleophilic attack of $H_2{}^{18}O$. Thus, there will be a mass difference of +2 Da between the $S_N2$ product and the dealkylation product, that can be detected by mass spectrometry analysis of tryptic peptides. This experiment is underway.

*Why BChE Ages Faster than AChE*. Comparison of the rates of aging of hBChE and *Tc*AChE in Table 1 shows that diethoxy and diisopropoxy conjugates of hBChE age about 4-fold faster than the conjugates with *Tc*AChE. A possible explanation for this difference is that His438 in hBChE is always well positioned to carry out the dealkylation reaction, whereas His440 in *Tc*AChE shifts to a position unfavorable for aging (*10*). The absence of a histidine shift in hBChE is supported by NMR studies. Viragh et al. (*29*) observed only one short strong hydrogen bond in aged hBChE, between His438 and Glu325. In contrast, Massiah et al. (*30*) observed two short strong hydrogen bonds in aged-hAChE, one between His440 and Glu327 and one between His440 and Glu199. This suggests a conformational heterogeneity of the catalytic histidine in hAChE that does not exist in hBChE.

In summary, the crystal structures of DFP-, soman-inhibited hBChE, and *Tc*AChE show that the acyl-loop adapts its conformation to fit moderate-size substituents in the acyl-binding pocket. The crystal structures of aged and nonaged echothiophate-inhibited hBChE show the conformational stability of the catalytic histidine and the presence of a molecule of water able to promote aging by an $S_N2$ mechanism involving P−O bond cleavage.

## ACKNOWLEDGMENT

We thank Larry M. Schopfer for helpful scientific discussions.

## REFERENCES

1. Broomfield, C. A., Maxwell, D. M., Solana, R. P., Castro, C. A., Finger, A. V., and Lenz, D. E. (1991) Protection by butyrylcholinesterase against organophosphorus poisoning in nonhuman primates, *J. Pharmacol. Exp. Ther. 259*, 633−638.
2. Wolfe, A. D., Blick, D. W., Murphy, M. R., Miller, S. A., Gentry, M. K., Hartgraves, S. L., and Doctor, B. P. (1992) Use of cholinesterases as pretreatment drugs for the protection of rhesus monkeys against soman toxicity, *Toxicol. Appl. Pharmacol. 117*, 189−193.
3. Ashani, Y., and Pistinner, S. (2004) Estimation of the upper limit of human butyrylcholinesterase dose required for protection against organophosphates toxicity: a mathematically based toxicokinetic model, *Toxicol. Sci. 77*, 358−67.
4. Michel, H. O., Hackley, B. E., Jr., Berkowitz, L., List, G., Hackley, E. B., Gillilan, W., and Pankau, M. (1967) Aging and dealkylation of Soman (pinacolylmethylphosphonofluoridate)-inactivated eel cholinesterase, *Arch. Biochem. Biophys. 121*, 29−34.
5. Amitai, G., Moorad, D., Adani, R., and Doctor, B. P. (1998) Inhibition of acetylcholinesterase and butyrylcholinesterase by chlorpyrifos-oxon, *Biochem. Pharmacol. 56*, 293−299.
6. Skrinjaric-Spoljar, M., Simeon, V., and Reiner, E. (1973) Spontaneous Reactivation and Aging of dimethylphosphorylated Acetylcholinesterase and Cholinesterase, *Biochim. Biophys. Acta 315*, 363−369.
7. Kovarik, Z., Radic, Z., Berman, H. A., Simeon-Rudolf, V., Reiner, E., and Taylor, P. (2003) Acetylcholinesterase active centre and gorge conformations analysed by combinatorial mutations and enantiomeric phosphonates, *Biochem. J. 373*, 33−40.
8. Masson, P., Froment, M. T., Bartels, C. F., and Lockridge, O. (1997) Importance of aspartate-70 in organophosphate inhibition, oxime re- activation and aging of human butyrylcholinesterase, *Biochem. J. 325*, 53−61.
9. Millard, C. B., Kryger, G., Ordentlich, A., Greenblatt, H. M., Harel, M., Raves, M. L., Segall, Y., Barak, D., Shafferman, A., Silman, I., and Sussman, J. L. (1999) Crystal structures of aged phosphonylated acetylcholinesterase: nerve agent reaction products at the atomic level, *Biochemistry 38*, 7032−7039.
10. Millard, C. B., Koellner, G., Ordentlich, A., Shafferman, A., Silman, I., and Sussman, J. (1999) Reaction products of acetylcholinesterase and VX reveal a mobile histidine in the catalytic triad, *J. Am. Chem. Soc. 121*, 9883−9884.
11. Nachon, F., Nicolet, Y., Viguie, N., Masson, P., Fontecilla-Camps, J. C., and Lockridge, O. (2002) Engineering of a monomeric and low-glycosylated form of human butyrylcholinesterase: expression, purification, characterization and crystallization, *Eur. J. Biochem. 269*, 630−637.
12. Nicolet, Y., Lockridge, O., Masson, P., Fontecilla-Camps, J. C., and Nachon, F. (2003) Crystal structure of human butyrylcholinesterase and of its complexes with substrate and products, *J. Biol. Chem. 278*, 41141−7.
13. Otwinowski, Z. (1997) Processing of X-ray diffraction data collected in oscillation mode, *Methods Enzymol. 276*, 307−326.
14. Collaborative Computational Project Number 4. (1994) The CCP4 suite: Programs for Protein Crystallography, *Acta Crystallogr. D 50*, 760−763.
15. Vagin, A., and Teplyakov, A. (1997) MOLREP: an automated program for molecular replacement, *J. Appl. Crystallogr. 30*, 1022−1025.
16. Murshudov, G. N. (1997) Refinement of macromolecular structures by the maximum-likelihood method, *Acta Crystallogr. D 53*, 240−55.
17. Delano, W. L. (2002) The PyMOL Molecular Graphics System, DeLano Scientific, San Carlos, CA.
18. Jones, T. A., Zou, J. Y., Cowan, S. W., and Kjeldgaard. (1991) Improved methods for building protein models in electron density maps and the location of errors in these models, *Acta Crystallogr. A 47*, 110−9.
19. Viragh, C., Kovach, I. M., and Pannell, L. (1999) Small molecular products of dealkylation in soman-inhibited electric eel acetylcholinesterase, *Biochemistry 38*, 9557−9561.
20. Harris, L. W., Fleisher, J. H., Clark, J., and Cliff, W. J. (1966) Dealkylation and loss of capacity for reactivation of cholinesterase inhibited by sarin, *Science 154*, 404−7.
21. Hosea, N. A., Radic, Z., Tsigelny, I., Berman, H. A., Quinn, D. M., and Taylor, P. (1996) Aspartate 74 as a primary determinant in acetylcholinesterase governing specificity to cationic organophosphonates, *Biochemistry 35*, 10995−11004.

22. Nair, H. K., Seravalli, J., Arbuckle, T., and Quinn, D. M. (1994) Molecular recognition in acetylcholinesterase catalysis: free-energy correlations for substrate turnover and inhibition by trifluoro ketone transition-state analogues, *Biochemistry 33*, 8566−8576.
23. Hosea, N. A., Berman, H. A., and Taylor, P. (1995) Specificity and orientation of trigonal carboxyl esters and tetrahedral alkylphosphonyl esters in cholinesterases, *Biochemistry 34*, 11528−11536.
24. Doorn, J. A., Talley, T. T., Thompson, C. M., and Richardson, R. J. (2001) Probing the active sites of butyrylcholinesterase and cholesterol esterase with isomalathion: conserved stereoselective inactivation of serine hydrolases structurally related to acetylcholinesterase, *Chem. Res. Toxicol. 14*, 807−813.
25. Doorn, J. A., Thompson, C. M., Christner, R. B., and Richardson, R. J. (2003) Stereoselective inactivation of *Torpedo californica* acetylcholinesterase by isomalathion: inhibitory reactions with (1*R*)- and (1*S*)-isomers proceed by different mechanisms, *Chem. Res. Toxicol. 16*, 958−65.
26. Barak, D., Ordentlich, A., Kaplan, D., Barak, R., Mizrahi, D., Kronman, C., Segall, Y., Velan, B., and Shafferman, A. (2000) Evidence for P−N bond scission in phosphoroamidate nerve agent adducts of human acetylcholinesterase, *Biochemistry 39*, 1156−1161.
27. Saxena, A., Viragh, C., Frazier, D. S., Kovach, I. M., Maxwell, D. M., Lockridge, O., and Doctor, B. P. (1998) The pH dependence of dealkylation in soman-inhibited cholinesterases and their mutants: further evidence for a push−pull mechanism, *Biochemistry 37*, 15086−15096.
28. Hobbiger, F. (1956) Chemical reactivation of phosphorylated human and bovine true cholinesterases, *Br. J. Pharmacol. 11*, 295−303.
29. Viragh, C., Harris, T. K., Reddy, P. M., Massiah, M. A., Mildvan, A. S., and Kovach, I. M. (2000) NMR evidence for a short, strong hydrogen bond at the active site of a cholinesterase, *Biochemistry 39*, 16200−16205.
30. Massiah, M. A., Viragh, C., Reddy, P. M., Kovach, I. M., Johnson, J., Rosenberry, T. L., and Mildvan, A. S. (2001) Short, strong hydrogen bonds at the active site of human acetylcholinesterase: proton NMR studies, *Biochemistry 40*, 5682−5690.
31. Mason, H. J., Waine, E., Stevenson, A., and Wilson, H. K. (1993) Aging and spontaneous reactivation of human plasma cholinesterase activity after inhibition by organophosphorus pesticides, *Hum. Exp. Toxicol. 12*, 497−503.
32. Masson, P., Fortier, P. L., Albaret, C., Froment, M. T., Bartels, C. F., and Lockridge, O. (1997) Aging of di-isopropyl-phosphorylated human butyrylcholinesterase, *Biochem. J. 327*, 601−607.
33. Worek, F., Eyer, P., and Szinicz, L. (1998) Inhibition, reactivation and aging kinetics of cyclohexylmethylphosphonofluoridate-inhibited human cholinesterases, *Arch. Toxicol. 72*, 580−587.
34. Main, A. R. (1979) Mode of action of anticholinesterases, *Pharmacol. Ther. 6*, 579−628.
35. Clothier, B., Johnson, M. K., and Reiner, E. (1981) Interaction of some trialkyl phosphorothiolates with acetylcholinesterase. Characterization of inhibition, aging and reactivation, *Biochim. Biophys. Acta 660*, 306−316.
36. Berry, W. K., and Davies, D. R. (1966) Factors influencing the rate of "aging" of a series of alkyl methylphosphonyl-acetylcholinesterases, *Biochem. J. 100*, 572−576.
37. Shafferman, A., Ordentlich, A., Barak, D., Stein, D., Ariel, N., and Velan, B. (1996) Aging of phosphylated human acetylcholinesterase: Catalytic processes mediated by aromatic and polar residues of the active centre, *Biochem. J. 318*, 833−840.
38. Brunger, A. T. (1992) Free *R* value: a novel statistical quantity for assessing the accuracy of crystal structures, *Nature 355*, 472−475.

BI048238D

# Aging Pathways for Organophosphate-Inhibited Human Butyrylcholinesterase, Including Novel Pathways for Isomalathion, Resolved by Mass Spectrometry

H. Li, L.M. Schopfer, **F. Nachon**, M-T. Froment, P. Masson,
O. Lockridge*

Toxicological Sciences 100 (2007) 136-145

TOXICOLOGICAL SCIENCES **100(1)**, 136–145 (2007)
doi:10.1093/toxsci/kfm215
Advance Access publication August 13, 2007

# Aging Pathways for Organophosphate-Inhibited Human Butyrylcholinesterase, Including Novel Pathways for Isomalathion, Resolved by Mass Spectrometry

He Li,* Lawrence M. Schopfer,* Florian Nachon,† Marie-Thérèse Froment,† Patrick Masson,† and Oksana Lockridge*,[1]

*Eppley Institute and Department of Biochemistry and Molecular Biology, University of Nebraska Medical Center, Omaha, Nebraska 68198-6805; and †Centre de Recherches du Service de Santé des Armées, Département de Toxicologie-Unité d'Enzymologie, 24 avenue des Maquis du Grésivaudan-BP87, 38702 La Tronche cedex, France

Received June 27, 2007; accepted July 24, 2007

**Some organophosphorus compounds are toxic because they inhibit acetylcholinesterase (AChE) by phosphylation of the active site serine, forming a stable conjugate: Ser–O–P(O)–(Y)–(XR) (where X can be O, N, or S and Y can be methyl, OR, or SR). The inhibited enzyme can undergo an aging process, during which the X–R moiety is dealkylated by breaking either the P–X or the X–R bond depending on the specific compound, leading to a non-reactivatable enzyme. Aging mechanisms have been studied primarily using AChE. However, some recent studies have indicated that organophosphate-inhibited butyrylcholinesterase (BChE) may age through an alternative pathway. Our work utilized matrix-assisted laser desorption/ionization-time-of-flight mass spectrometry to study the aging mechanism of human BChE inhibited by dichlorvos, echothiophate, diisopropylfluorophosphate (DFP), isomalathion, soman, sarin, cyclohexyl sarin, VX, and VR. Inhibited BChE was aged in the presence of $H_2O^{18}$ to allow incorporation of $^{18}O$, if cleavage was at the P–X bond. Tryptic-peptide organophosphate conjugates were identified through peptide mass mapping. Our results showed no aging of VX- and VR-treated BChE at 25°C, pH 7.0. However, BChE inhibited by dichlorvos, echothiophate, DFP, soman, sarin, and cyclohexyl sarin aged exclusively through O–C bond cleavage, i.e., the classical X–R scission pathway. In contrast, isomalathion aged through both X–R and P–X pathways; the main aged product resulted from P–S bond cleavage and a minor product resulted from O–C and/or S–C bond cleavage.**

*Key Words:* **butyrylcholinesterase; organophosphate; aging; mass spectrometry.**

## INTRODUCTION

Butyrylcholinesterase (BChE) is a serine hydrolase that catalyzes the hydrolysis of a variety of choline and noncholine esters (Lockridge and Masson, 2000). BChE is more abundant than acetylcholinesterase (AChE) in mouse and human (Li *et al.*, 2000). BChE reacts with a broad range of toxicants more effectively than AChE. BChE has been suggested to function as a scavenger protein that protects the cholinergic system against anticholinesterase poisons (Lockridge and Masson, 2000).

Organophosphorus (OP) compounds account for a large portion of pesticides and chemical warfare agents. These compounds exert their acute toxicity mainly through inhibition of AChE. OP inhibition of AChE and BChE proceeds in a progressive manner by phosphorylation of the active site Ser, to form a Ser–O–P(O)–(Y)–(XR) adduct (where X can be O, N, or S and Y can be methyl, OR, or SR). The phosphorylated enzyme can be reactivated by treating with strong nucleophilic agents such as oximes. The phosphorylated enzyme can also undergo a spontaneous time-dependent process called "aging" during which the P–X–R component of the OP-serine conjugate is dealkylated, leaving the enzyme irreversibly inhibited (Casida and Quistad, 2004).

Aging has been studied in detail using AChE as the model enzyme. The generally accepted aging mechanism for alkoxy-OP adducts invokes the catalytic participation of residues from the enzyme. Dealkylation of the OP adduct is facilitated primarily by the protonated histidine of the catalytic triad, a glutamic acid residue adjacent to the catalytic serine, and a nearby tryptophan residue (Shafferman *et al.*, 1996; Viragh *et al.*, 1997). It is agreed that these residues combine to promote the cleavage of the O–C bond with formation of a carbocation on the leaving alkyl group and a negatively charged phospho-oxygen (Shafferman *et al.*, 1996; Viragh *et al.*, 1997). The resultant carbocation is then vulnerable to nucleophilic attack by water. A variety of pH, mutational, crystallographic, and kinetic studies support the catalytic involvement of the amino acid residues (Barak *et al.*, 1997; Harris *et al.*, 1966; Jennings *et al.*, 2003; Michel *et al.*, 1967; Millard *et al.*, 1999; Saxena *et al.*, 1993; Shafferman *et al.*, 1996). Studies on BChE inhibited with diisopropylfluorophosphate (DFP) are also consistent with this mechanism (Masson *et al.*, 1997a).

[1] To whom correspondence should be addressed at Eppley Institute, University of Nebraska Medical Center, Box 986805, 600 South 42nd Street, Omaha, NE 68198. Fax: (402) 559-4651. E-mail: olockrid@unmc.edu.

On the other hand, recent studies have provided evidence for alternative aging pathways. First, studies on aging of tabun-inhibited human AChE suggested a P–N bond cleavage and elimination of the dimethylamine moiety from the tabun-enzyme conjugate (Barak *et al*., 2000). This result is also corroborated by the x-ray structure of tabun-aged murine AChE (Ekstrom *et al*., 2006). Second, isomalathion-inhibited equine BChE was shown to age through breaking the P–S bond and releasing either a thiomethyl or a diethylthiosuccinate moiety (Doorn *et al*., 2001a). Third, a crystal structure study on echothiophate-inhibited human BChE presented the possibility of aging through both P–O scission and O–C scission (Nachon *et al*., 2005). Given the diversity of aging pathways invoked for various OP compounds and the indication that different aging pathways may be used by BChE and AChE when inhibited by the same OP, systematic investigation of the BChE aging pathway was needed. The use of BChE as an antidote against OP toxicity also calls for a better understanding of its aging mechanism.

In the current study, we investigated the possibility that OP-inhibited human BChE ages through breakage of the P–X bond (where X may be O or S), as opposed to the classical pathway, i.e., breaking the X–C bond. We evaluated the aging pathway by using matrix-assisted laser desorption/ionization-time-of-flight (MALDI-TOF) mass spectrometry to determine the mass of the aged product. Including $H_2O^{18}$ in the aging medium enabled us to distinguish between the two pathways. Discrimination was possible because the inhibition step employed OP made with common $^{16}O$. If aging occurred via cleavage at P–$^{16}O$, then the phosphorus would pick up an $^{18}OH$ from the medium to form P–$^{18}O$–H. If the cleavage occurred at O–C, then the carbon would pick up the $^{18}OH$ and the phosphorus would retain the $^{16}O$ as P–$^{16}OH$. The net effect would be a 2-Da increase in the mass of the aged adduct if cleavage of the P–O bond occurred. Consequently, the mass of the aged OP-enzyme conjugate revealed which aging pathway had been taken (Fig. 1). The aged enzyme was digested with trypsin, and the resulting tryptic peptides were analyzed by MALDI-TOF mass spectrometry to determine the mass of the OP-labeled, active-site peptide conjugate. Nine OP compounds were tested, including dichlorvos, echothiophate, DFP, soman, sarin, cyclohexyl sarin (GF), VX, VR (Russian VX), and isomalathion (Fig. 2).

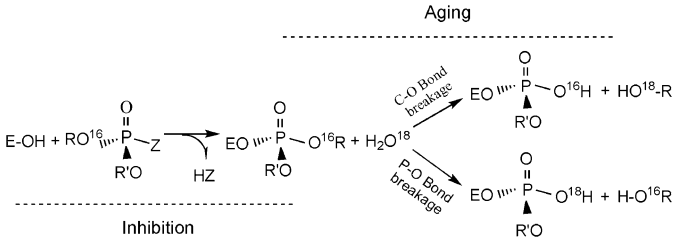


**FIG. 1.** Inhibition and aging of BChE with organophosphate in a $H_2O^{18}$ environment. Two aging pathways give two OP-BChE conjugates with the same chemical structure, but a mass difference of 2 Da, which can be detected by MALDI-TOF mass spectrometry. The generalized OP structure in the scheme represents dichlorvos, echothiophate, and DFP. Aging of isomalathion-, soman-, sarin-, cyclohexyl sarin–, VX-, and VR-inhibited BChE can be studied in the same fashion. E–OH: catalytic serine; R, R′: alkyl groups; Z: OP leaving group.

Aging of all the alkoxy adducts followed the classical pathway, with cleavage of the O–C bond. Isomalathion-inhibited BChE, however, gave two aged products. Besides the main aged product resulting from breaking the P–S bond, a minor product resulted from breaking the O–C and/or S–C bond, which had not been reported before.

## MATERIALS AND METHODS

***Chemicals and reagents.*** Dichlorvos and isomalathion were from CIL Cluzeau Info Labo (Sainte-Foy-La-Grande, France). Echothiophate iodide was from Wyeth-Ayerst (Rouses Point, NY). DFP was from Acros (Belgium). Soman, sarin, cyclohexyl sarin, VX, and VR were from Centre d'Etudes du Bouchet (Vert-le-Petit, France). $H_2O^{18}$ (95% pure) was from Aldrich (Milwaukee, WI). Sequence-grade modified trypsin was from Promega (Madison, WI). α-Cyano-4-hydroxycinnamic acid (CHCA) matrix-assisted laser desorption/ionization (MALDI) matrix and external MALDI mass calibration standard mix were purchased from Applied Biosystems (Framingham, MA).

***Purification and deglycosylation of human BChE.*** Human BChE (gi:116353; Swiss protein P06276) was purified from plasma as previously described (Lockridge *et al*., 2005). Recombinant GST-PNGaseF was expressed and purified as previously described (Grueninger-Leitch *et al*., 1996). Two milligrams of purified human BChE was deglycosylated by treating with 3.2 mg of GST-PNGaseF for 5 min at 37°C in 6.66 ml of 100mM Tris-HCl, pH 7.5. GST-PNGaseF was removed by loading the sample onto GSH-agarose (Sigma, St Louis, MO) packed in a 5-ml column, equilibrated with 100mM Tris-HCl, pH 8.0. The flow through containing human BChE was concentrated to 4.5 mg/ml in a Centricon PM 10 microconcentrator (Millipore, Bedford, MA). BChE was deglycosylated because the deglycosylated protein released the active-site tryptic peptide upon digestion with trypsin. By contrast, when the BChE was not deglycoslyated, the active-site peptide was not available to trypsin unless the protein was first denatured and its disulfide bonds reduced and alkylated.

***Organophosphate treatment of BChE.*** A 10-μl aliquot of deglycosylated human BChE stock at a concentration of 53μM enzyme (4.5 mg/ml) was diluted with 90 μl of $H_2O^{16}$ or $H_2O^{18}$ and 1 μl of 1M sodium phosphate pH 7.0. Each 100-μl diluted BChE sample received 1 μl of dichlorvos (6.5M stock), echothiophate (10mM stock), DFP (50mM stock), soman (27.4mM stock), sarin (35.6mM stock), cyclohexyl sarin (27.7mM stock), VX (18.6mM stock), VR (18.6mM stock), or isomalathion (32mM stock). The final concentration of OP is at least 20 times higher than the BChE concentration in the reaction system, ensuring that the inhibition and aging reaction can reach completion under the experimental conditions. The excess OP should not affect the aging reaction pathways. The $H_2O^{18}$ level in the final reaction mixture was at least 85%. Enzyme inhibition and aging proceeded at room temperature for 4 days or more. The BChE used in this study was purified from sterilized human plasma, and we kept the sterilization condition throughout the OP treatment to prevent the microbial contamination. Samples were stored at − 80°C.

***Tryptic digestion of BChE.*** To remove excess OP, $H_2O^{18}$, and salts, 50 μl of OP-treated BChE was subjected to buffer exchange using Millipore Microcon YM-3 centrifuge filters with 3000 MW cutoff. The protein was diluted with 25mM ammonium bicarbonate pH 8.3, concentrated to 50 μl,

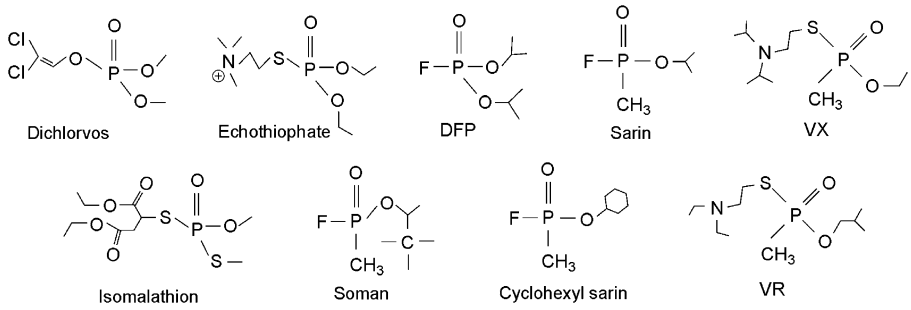


**FIG. 2.** Chemical structures of dichlorvos, echothiophate, DFP, soman, sarin, cyclohexyl sarin, VX, VR, and isomalathion.

rediluted, and reconcentrated 5 times before digestion. The final $H_2O^{18}$ level was no more than 0.5% of the total volume. The BChE was incubated with modified porcine trypsin at a trypsin:BChE ratio of 1:30, at room temperature, overnight. To wash off salts from the digestion that may interfere with mass spectrometric analysis, trypsinized BChE was adsorbed onto a C18 ZipTip (Millipore) and washed with 0.1% trifluoroacetic acid (TFA). Peptides were eluted from the ZipTip with 15 µl of 30% acetonitrile, 0.1% TFA, followed by 15 µl of 60% acetonitrile, 0.1% TFA. The active-site peptide was eluted with 60% acetonitrile, 0.1% TFA.

***MALDI-TOF mass spectrometry.*** All MALDI-TOF mass spectrometry experiments were performed on an Applied Biosystems Voyager DE-PRO workstation equipped with a 337-nm pulsed nitrogen laser. The OP-labeled, trypsinized, BChE active-site peptide that had been adsorbed to a reverse phase C18 ZipTip was eluted into a microcentrifuge tube with 15 µl of 60% acetonitrile, 0.1% TFA. One microliter of eluant was mixed 1:1 (vol/vol) with the matrix solution CHCA (10 mg/ml in 50% acetonitrile, 0.3% TFA) on the MALDI target plate and allowed to dry at room temperature.

Mass spectra were acquired in positive ion, linear, or reflector mode under delayed extraction conditions, using an acceleration voltage of 20 kV. Laser intensity was adjusted so that the strongest ion intensity in a spectrum did not exceed 80% of the maximum, saturated intensity value. Laser positioning on the sample spot was monitored with a video camera. Spectra shown are the average of 500 laser shots collected from multiple locations on the target spot. Calibration for the mass spectra was performed both externally using adrenocorticotropic hormone peptides (amino acid residues 1–17, 18–39, and 7–38) and internally by reference to BChE tryptic fragments other than the labeled, active-site peptide. The sequence of human BChE (accession number: P06276) was obtained from the SwissProt database (http://ca.expasy.org/cgi-bin/sprot-search-ful). The reference masses of the tryptic BChE peptides were obtained using the MS-Digest feature of ProteinProspector version 4.0.6 (http://prospector.ucsf.edu/), a comprehensive proteomic data analysis software package. The MS-Fit feature of ProteinProspector was used to identify human BChE from MALDI peptide mass data, where the mass tolerance was set at 100 ppm.

***Half-life of aging.*** To determine the aging half-life of echothiophate-inhibited BChE, a time course experiment was conducted. Twenty-five microliters of deglycosylated human BChE (150µM enzyme in 15mM 2-(N-morpholino)ethanesulfonic acid buffer, pH 6.5) was mixed with 25 µl of 100mM Tris-Cl, pH 8.6 to give a final pH of 8.4. Five microliters of enzyme solution were taken immediately after mixing and diluted into 100 µl of 25mM ammonium bicarbonate, pH 8.3. This enzyme fraction served as the 0-min time point and was stored in the − 80°C freezer until trypsin digestion. After the 0-min time point had been taken, a 2.2-fold molar excess of echothiophate (1 µl of 7.5mM echothiophate iodide dissolved in water) was added to the enzyme solution. The OP inhibition and aging process proceeded in a 37°C water bath. A total of nine time points were taken (5 min, 1 h, 2 h, 4 h, 8 h, 12 h, 16 h, 23 h and 28 h). For each time point, a 5-µl aliquot was taken from the reaction solution and diluted to 100 µl with 25mM ammonium bicarbonate. Excess OP was removed from the mixture by gel filtration on a spin column (Performa SR gel filtration cartridge, Edge BioSystems, Gaithersburg, MD). Samples were stored at –80°C until trypsin digestion.

When all times points had been collected, the samples were thawed, subjected to tryptic digestion (as described under Tryptic digestion of BChE), and prepared for MALDI-TOF mass spectrometry (as described under MALDI-TOF mass spectrometry).

The Data Explorer software for the Voyager DE-PRO mass spectrometer provided the area of the peptide peaks for the initial and aged adduct in each spectrum. The aging half-life was calculated from a semilog plot of the normalized peak area for unaged OP peptide against time. The normalized peak area was obtained by taking the ratio of the unaged peak area to the sum of the areas for the aged and unaged peak areas, at each time point. This ratio compensated for the variation in MALDI peak intensities from shot-to-shot and sample-to-sample. It was assumed that the signal response of the aged and unaged peptides would be essentially the same in the same sample (i.e., each individual time point) because there is only a small difference between the structures of the two peptides (i.e., an ethoxy phosphate in the unaged form is converted to a hydroxy in the aged form). SigmaPlot (SigmaPlot for Windows version 10.0, Systat Software, Inc.) was used to generate the equation describing the plot and to run statistic tests on the data. The data set passed the Durbin-Watson test, the normality test, and the constant variance test.

## RESULTS

### *Identification of the BChE Tryptic Peptide Containing the Catalytic Serine*

MALDI mass spectra of trypsinized BChE were obtained in both reflector mode for high peak resolution and in linear mode for maximum signal intensity. In reflector mode, the isotopic envelope of each peptide can be resolved and the observed peak values represent the mass of each isotope of a peptide. Peak values observed in linear mode are the average mass of the isotopic variants of the peptides. For a molecule that has a monoisotopic mass around 3000 Da, as the OP-BChE peptides in this study, the average mass of the molecule will be about 2 Da heavier than the monoisotopic mass.

Amino acid numbers are for the mature secreted protein, which has no signal peptide and is therefore shorter by 28 amino acids than the sequence in accession number P06276. Tryptic digestion of BChE generates a 29 amino acid, active-site peptide extending from Ser 191 to Arg 219, where Ser 198 (in bold) is the catalytic Ser: $^{191}$SVTLFGE**S**AGAASVSLHLLSPGSHSLFTR$^{219}$. In the reflector mode

spectrum, 11 peaks can be assigned to the tryptic peptides of BChE (Fig. 3A). The isotopic peaks for each peptide are well resolved. The theoretical monoisotopic m/z for the singly protonated $[M+H]^+$ active-site peptide is 2928.5, the observed m/z is 2928.4. In the linear mode spectrum (Fig. 3B), 13 peaks can be assigned to tryptic peptides of human BChE, including the active-site peptide. The average mass of the active-site peptide is 2930.3 m/z.

The peptide mass data acquired in both linear and reflector mode were submitted to the protein identification program MS-Fit to validate the peptide assignments. The *Homo sapiens* subset of the SwissProt database (2005.01.06 released version) was selected for the search. Human BChE was successfully identified as the first hit using either monoisotopic or average peptide mass.

### *Aging of Echothiophate-, DFP-, Dichlorvos-, Soman-, Sarin-, and Cyclohexyl Sarin–Inhibited BChE Occurs via O–C Bond Breakage*

Aging of echothiophate-treated BChE was allowed to occur in $^{18}O$ water. The active-site tryptic peptide was analyzed by MALDI-TOF. It was calculated that if aging resulted from P–O bond breakage (predicted monoisotopic mass 3038.5 Da), the active-site peptide would be 2 Da heavier than if aging resulted from O–C bond breakage (predicted monnoisotopic mass 3036.5 Da) (Table 1). As shown in Figure 4, a peak with m/z of 3036.3 can be matched to the theoretical monoisotopic m/z of the echothiophate peptide conjugate, indicating O–C bond scission. Neither peak 2928.5 (monoisotopic m/z of unlabeled BChE) nor peak 3064.5 (for unaged BChE) were detected, indicating that all the BChE had been inhibited and that the aging was complete. The observed isotopic distribution is exactly that expected for the aged, active-site conjugate (data not shown). The absence of any trace of a peak at 3038.5 m/z indicates that for echothiophate-inhibited human BChE, aging follows the O–C bond breaking pathway exclusively, under the applied experimental conditions.

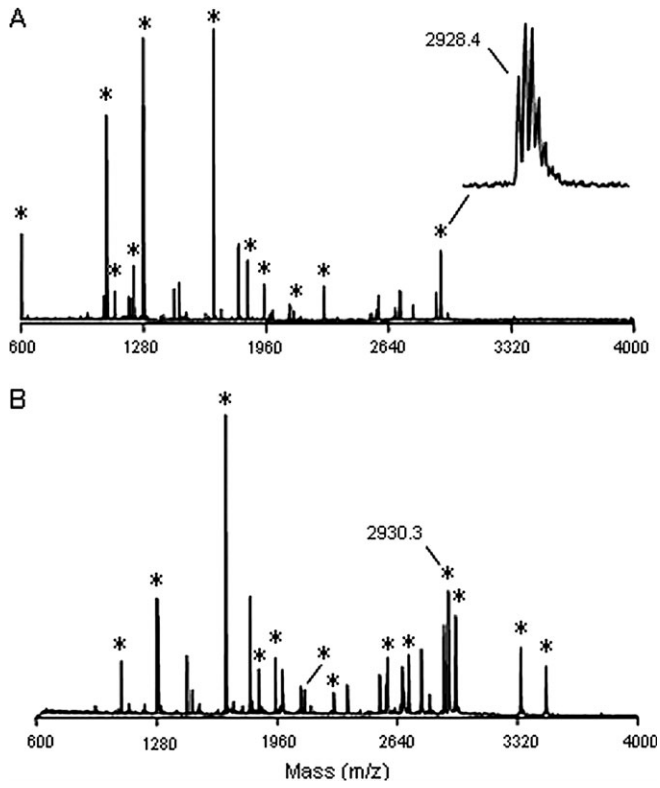


**FIG. 3.** MALDI mass spectrum of BChE tryptic peptides. BChE was subjected to tryptic digestion, and the resulting peptides were analyzed by MALDI-TOF mass spectrometry. Peptide mass spectra were acquired in reflector mode (A) as well as linear mode (B). Peaks labeled with an asterisk match the theoretical masses of BChE tryptic peptides. Peak 2928.4 in A represents the monoisotopic m/z of the active-site peptide. Peak 2930.3 in B represents the average m/z of the active-site peptide.

To rule out the possibility that peak 3036.3 observed in the spectrum from echothiophate-treated BChE (Fig. 4) may be from an unknown peptide which happens to have the same m/z value as the aged echothiophate BChE peptide conjugate, we monitored the disappearance of unaged echothiophate peptide conjugate (average m/z: 3066.4, Table 1) and the appearance of aged echothiophate peptide conjugate (average m/z: 3038.3, Table 1) as a function of time. To avoid confusion, the 3038.3 m/z mass observed in this experiment is the average mass for the aged, active-site peptide; the monoisotopic mass for this peptide is 3036.3 m/z, as described in Figure 3. A total of nine time points were taken after adding echothiophate into the enzyme solution. A MALDI mass spectrum was acquired for each time point, as shown in Figure 5. The predominant peak after 5 min incubation with OP was peak 3066.4, corresponding to the unaged echothiophate BChE peptide conjugate. Peak 3066.4 diminished while peak 3038.3 grew, as the incubation time became longer. After 28 h incubation, peak 3066.4 almost completely disappeared from the spectrum, indicating that aging was essentially complete. This result confirmed that peak 3038.3 was the echothiophate active-site peptide conjugate resulting from O–C bond breakage during aging. The aging half-life of echothiophate-inhibited human BChE was calculated to be 7.2 ± 0.7 h (Fig. 6) under the experimental conditions, which is consistent with previous studies on BChE inhibited by OP with diethoxy moieties on the phosphorus atom (Mason *et al.*, 1993, Masson et al., 1997b).

DFP-treated BChE was analyzed the same way as echothiophate-treated BChE in Figure 4. The peptide mass spectrum of aged, DFP-inhibited BChE revealed a new monoisotopic peak at 3050.4 Da, indicting that aging of this OP-enzyme conjugate is through breaking the O–C bond of one of the isopropoxy groups (Fig. 7, Table 1). The observed isotopic distribution was consistent with that expected for the 3050.4 Da peptide.

Similarly, the O–C bond was cleaved during aging of dichlorvos-inhibited BChE (spectrum not shown).

**TABLE 1**
**Structures and Theoretical Monoisotopic m/z of Organophosphate-Peptide Conjugates**

| | | After aging | |
|---|---|---|---|
| Before aging | | thru O-C bond | thru P-O bond |
| Echothiophate[a] | 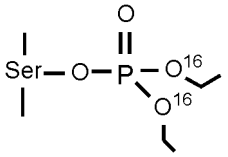 | 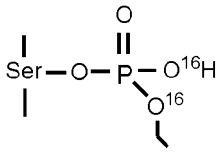 | 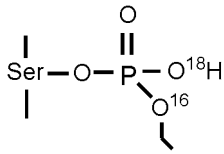 |
| | m/z: 3064.5 | 3036.5 | 3038.5 |
| DFP | 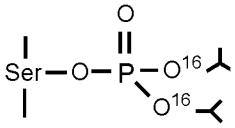 | 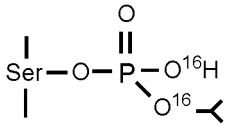 | 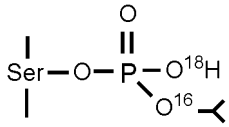 |
| | m/z: 3092.5 | 3050.5 | 3052.5 |
| Soman | 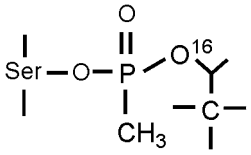 | 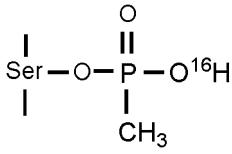 | 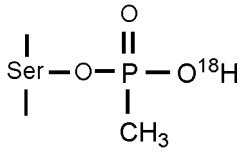 |
| | m/z: 3090.6 | 3006.5 | 3008.5 |
| Sarin | 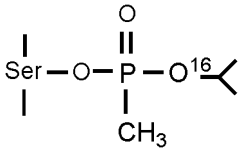 | 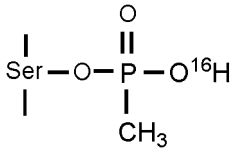 | 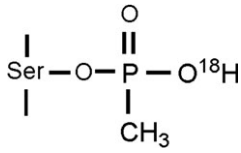 |
| | m/z: 3048.6 | 3006.5 | 3008.5 |
| Cyclohexyl sarin | 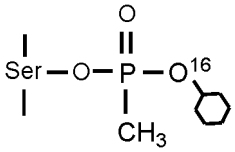 | 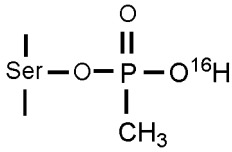 | 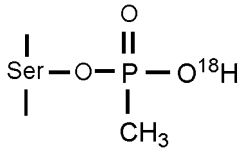 |
| | m/z: 3088.6 | 3006.5 | 3008.5 |
| VX | 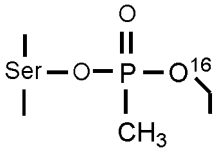 | 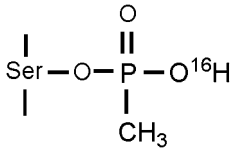 | 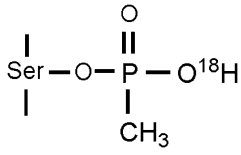 |
| | m/z: 3034.5 | 3006.5 | 3008.5 |
| VR | 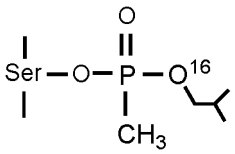 | 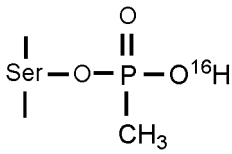 | 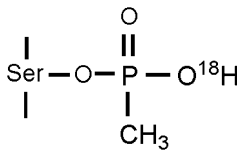 |
| | m/z: 3062.6 | 3006.5 | 3008.5 |

[a]The theoretical average m/z of unaged echothiophate-peptide conjugate, the aged echothiophate-peptide conjugate from the O–C bond bteakage and the P–O bond breakage are 3066.4, 3038.3, and 3040.3, respectively.

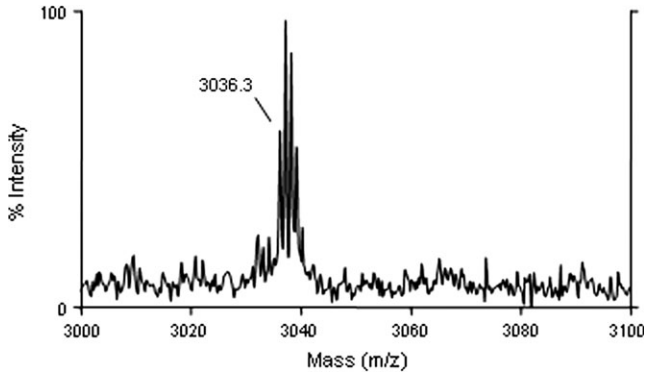


**FIG. 4.** MALDI mass spectrum of tryptic peptides from echothiophate-inhibited BChE. The spectrum was acquired in positive ion reflector mode. Peak 3036.3 represents the monoisotopic mass of the aged, echothiophate-labeled, active-site peptide conjugate resulting from O–C bond breakage.

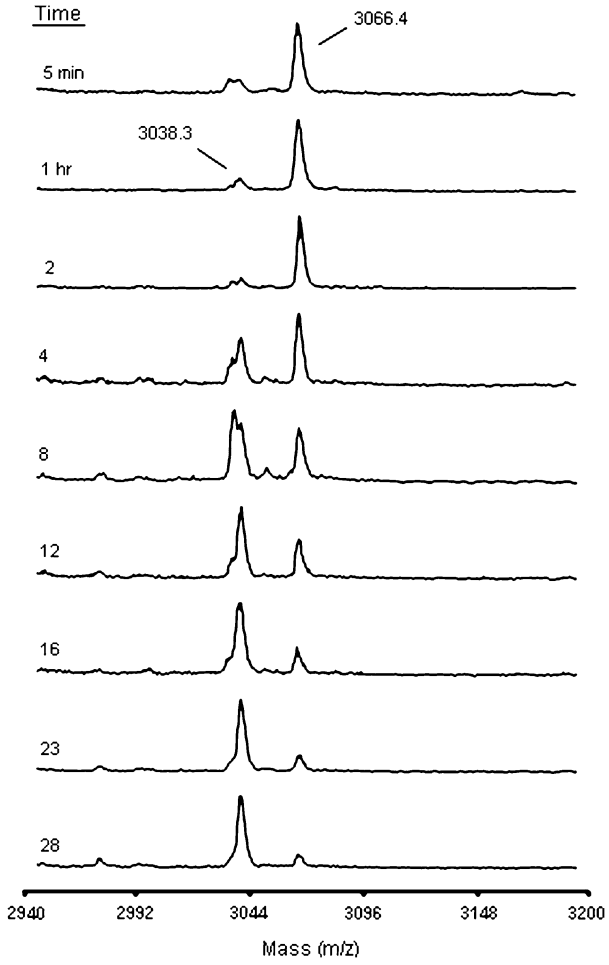


**FIG. 5.** A time course for the aging of echothiophate-inhibited BChE. Mass spectra were acquired in linear mode from samples with various echothiophate incubation times, as indicated. Peaks 3066.4 and 3038.3 represent the average m/z of echothiophate active-site peptide conjugates before and after aging, respectively.

We also investigated the aging pathways for sarin- (Fig. 8, Table 1), cyclohexyl sarin–, and soman- (Table 1, spectra not shown) inhibited BChE. Aging of these three compounds involved only O–C bond cleavage of the alkoxy groups. Peak 3048.4 in Figure 8 and peak 3088.6 (see Table 1, spectrum not shown) represent the monoisotopic m/z of unaged sarin and cyclohexyl sarin BChE conjugate peptides, respectively, indicating that the aging of BChE treated with these two compounds was not complete under the experimental conditions applied in this study.

Aging of VX-inhibited human AChE and human BChE has been previously found to be slow. Seventy percent of the human erythrocyte AChE activity can be restored by incubation with 2-pralidoxime (2-PAM) 48 h after VX inhibition (Sidell and Groff, 1974). Aging half-life of VX- and VR-inhibited human erythrocyte AChE has recently been measured to range between 36 and 138 h, respectively (Aurbek *et al.*, 2006). Aging of VX-inhibited BChE is so slow that BChE spontaneously reactivates to 50% of its original activity, without any need of 2-PAM treatment (van der Schans *et al.*, 2004). In our experiment, the expected peak of the aged VX active-site peptide conjugate with monoisotopic m/z of 3006.5 was absent from the sample spectrum, whereas peak 3034.7 matched the unaged VX active-site peptide conjugate. This result indicated that aging of VX-inhibited BChE did not occur under our experimental conditions (Fig. 9, Table 1). Similarly, the VR-inhibited BChE did not age (spectrum not shown).

### *Trypsin Proteolysis of Echothiophate-Inhibited BChE in $H_2O^{18}$ Medium*

These experiments are controls to prove that a two mass unit shift can be detected in linear mode. The mass spectra in Figures 3A,4, and 7–9 had been acquired in reflector mode. However, signal intensities for isomalathion- and tabun-inhibited BChE were not high enough to support data collection in reflector mode. Mass spectra were therefore acquired using linear mode settings because linear mode data have better signal intensities than those acquired using reflector mode settings. However, the linear mode spectrum is less well resolved than a reflector mode spectrum, and the observed mass represents the average mass of the isotopes of a peptide rather than the monoisotopic mass. For a molecule that has a monoisotopic mass around 3000 Da, as the OP-BChE peptide conjugates in this study, the average mass of the molecule will be 2 Da heavier than the monoisotopic mass (as shown in Figure 3 for BChE active-site peptide and in Table 1 for echothiophate BChE peptide conjugates). To prove that a two mass unit shift, occurring as a consequence of adding the hydroxyl group from $H_2O^{18}$ to a peptide, can be detected from linear mode spectra, we carried out the tryptic digestion of echothiophate-treated BChE without removing the $H_2O^{18}$ from the reaction medium. The hydroxyl group from water is added

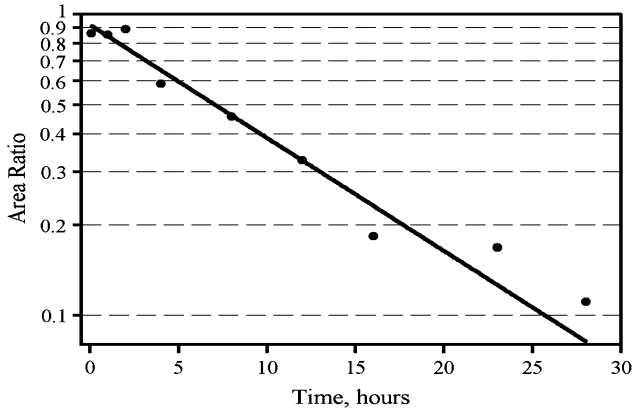


**FIG. 6.** Aging half-life of echothiophate-inhibited BChE. At each time point, the area of peak 3066.4 was divided by the sum of the peak areas of peaks 3066.4 and 3038.3 to generate an area ratio. The area ratio was plotted against its corresponding time point in a semilog fashion using SigmaPlot. The plot can be described by equation: $y = a \times \exp(-bx)$, where ''$a$'' is a proportionality constant = 0.92 ± 0.039 and ''$b$'' is the apparent rate constant = 0.086 ± 0.0090/h. Aging half-life was measured from the plot as 7.2 ± 0.7 h, representing the time when there are equal amounts of aged and unaged OP-peptide conjugates, i.e., the time when the area ratio equals 0.5 on the plot.

to the C-terminus of a tryptic peptide when the amide bond is cleaved. Thus, peptides created in $H_2O^{18}$ will be two mass units heavier than comparable peptides made in $H_2O^{16}$.

The echothiophate-treated BChE was digested with trypsin in 85% $H_2O^{18}$. Thus 85% of each tryptic peptide, including the echothiophate active-site peptide conjugate, will carry an $^{18}O$ hydroxyl group at the C-terminus. The observed mass of a peptide from this $H_2O^{18}$ digestion medium should be 2 Da heavier than the same peptide digested in $H_2O^{16}$ medium. We observed a peak with an m/z of 3040.2 from this sample (spectrum not shown), which is two units heavier than the mass of the aged, echothiophate-labeled, active-site peptide conjugate resulting from tryptic digestion in an $H_2O^{16}$ medium. Seven other peaks in the spectrum from the $H_2O^{18}$ medium were found to be 2 Da heavier than the theoretical masses of the same peptides digested in $H_2O^{16}$ medium. This result demonstrates that MALDI data collected in linear mode are capable of discerning a two mass unit shift resulting from incorporation of an $^{18}O$ hydroxyl group into a peptide.

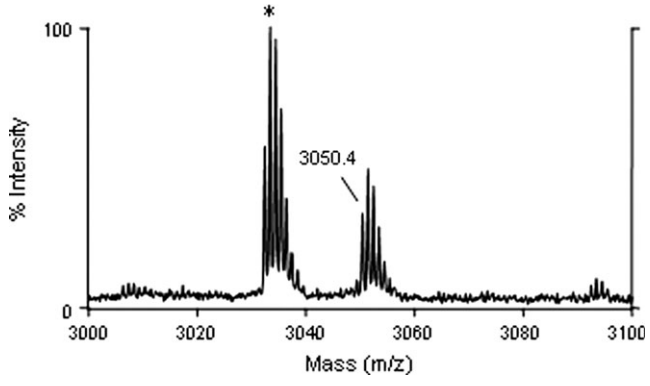


**FIG. 7.** MALDI mass spectrum of tryptic peptides from DFP-inhibited BChE. The spectrum was acquired in positive ion reflector mode. Peak labeled with an asterisk has a monoisotopic m/z of 3032.4, which matches a BChE tryptic peptide. Peak 3050.4 represents the monoisotopic m/z of the aged DFP active-site peptide conjugate resulting from O–C bond breakage. Trace amount of unaged DFP-peptide conjugate can also be seen in the spectrum at m/z of 3092.6.

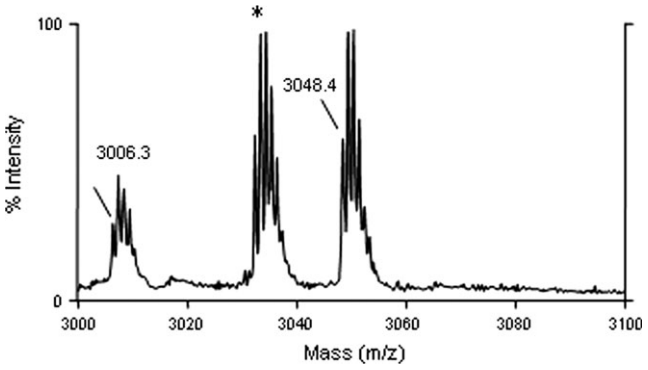


**FIG. 8.** MALDI mass spectrum of tryptic peptides from sarin-inhibited BChE. The spectrum was acquired in positive ion reflector mode. The peak labeled with an asterisk has a monoisotopic m/z of 3032.4, which matches a BChE tryptic peptide. Peak 3006.3 represents the monoisotopic m/z of the aged, sarin-labeled, active-site peptide conjugate resulting from O–C bond breakage. Peak 3048.4 represents the monoisotopic m/z of the unaged, sarin-labeled, active-site peptide conjugate.

### *Aging of Isomalathion-Inhibited BChE Occurs via both P–S and O–C/S–C Bond Breakage*

Previous studies showed that stereoisomers of isomalathion take different inhibitory and aging pathways when reacting with BChE, depending on the stereo configuration of the inhibitor. Inhibition of the enzyme with (1R)-isomalathion proceeds with loss of diethylthiosuccinate as the primary leaving group, resulting in an O,S-dimethyl phosphate adduct;

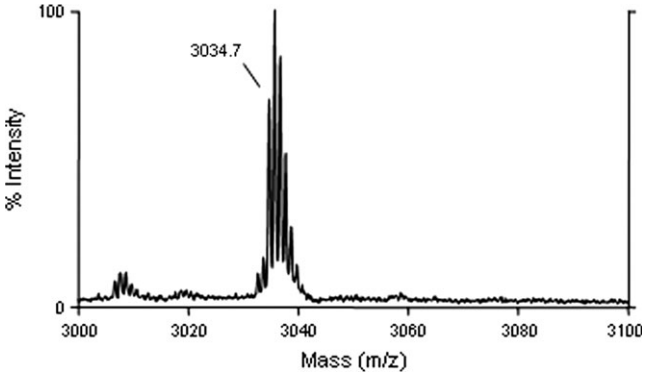


**FIG. 9.** MALDI mass spectrum of tryptic peptides from VX-inhibited BChE. The spectrum was acquired in positive ion reflector mode. Peak 3034.7 represents the monoisotopic m/z of the unaged, VX-labeled, active-site peptide conjugate.

aging of this adduct occurs through breaking the P–S bond and loss of the thiomethyl moiety. On the other hand, the primary leaving group for (1S)-isomalathion inhibition of the enzyme is the thiomethyl group. Inhibition is followed by a quick aging reaction, which also involves breaking a P–S bond. In this case, the diethylthiosuccinate moiety is released (Doorn *et al.*, 2001a,b). In both cases, aging of isomalathion-inhibited BChE occurs via the P–X bond scission pathway.

The isomalathion used in the present study was a mixture of all stereoisomers. The chemical structures and corresponding theoretical masses after inhibition of BChE are summarized in Table 2. The mass spectrum of tryptic peptides of isomalathion-treated BChE (Fig. 10) does not have peaks matching the unaged isomalathion active-site peptide conjugates, regardless of the primary leaving group (theoretical m/z should be 3054.4 when diethylthiosuccinate is the primary leaving group or 3198.5 when thiomethyl is the primary leaving group). This indicates that aging is complete. Peak 3026.6 in the spectrum matches the theoretical m/z of an aged isomalathion peptide conjugate formed as a result of a P–S bond scission. Formation of this fragment can occur from either primary adduct (see Table 2). This result is consistent with the reports in the literature (Doorn *et al.*, 2001a,b).

In addition, a comparatively minor peak with m/z of 3040.6 is present, which matches the theoretical m/z of the aged isomalathion peptide conjugate resulting from O–C or S–C bond scission. An O–C cleavage pathway would generate this mass only from a primary adduct that was formed by elimination of the diethylthiosuccinate moiety, whereas the 3040.6 mass is consistent with an S–C cleavage starting with either primary adduct. This result indicates that isomalathion-inhibited human BChE can age not only via the P–X pathway, as indicated in previous studies, but also via the X–R pathway. The relative intensities of peaks 3026.6 and 3040.6 suggest that the P–X pathway is the predominant aging pathway under the experimental conditions of this study.

## DISCUSSION

### *Direct Evidence Supporting the X–R Scission Pathway for Aging of Human BChE Inhibited by Alkoxy-OP*

Classical aging theory for alkoxy-OP–inhibited cholinesterases states that aging involves activation of the alkoxy oxygen, O–C bond scission, and formation of a carbonium ion (Shafferman *et al.*, 1996; Viragh *et al.*, 1997). Numerous studies involving a wide range of alkoxy-type OP have demonstrated that aging results in the net loss of an alkyl group (Doorn *et al.*, 2001b; Michel *et al.*, 1967; Millard *et al.*, 1999; Nachon *et al.*, 2005; Viragh *et al.*, 1999). However, cleavage at either the P–O or the O–C bond could account for these observations. Only in the case of soman-inhibited AChE has cleavage of the O–C bond been conclusively demonstrated (Michel *et al.*, 1967; Viragh *et al.*, 1999).

To test whether aging of other alkoxy-OP adducts proceeds via an O–C cleavage, we studied the aging of human BChE inhibited by dichlorvos, echothiophate, DFP, soman, sarin, cyclohexyl sarin, VX, and VR. Our results showed that for all of these OP except VX and VR (in which aging did not occur), aging did indeed occur via cleavage of the O–C bond, i.e., they aged through the X–R scission pathway (see Figs. 4,7,8, and related text). Based on these observations, it seems fair to predict that whenever BChE is inhibited by an OP that leaves an alkoxy group in the inhibited adduct, aging will proceed

**TABLE 2**
**Structues and Theoretical Average m/z of Isomalathion-Peptide Conjugates Aged in $^{18}O$ Water**

| | After aging | | | |
|---|---|---|---|---|
| Before aging | thru O-C bond | thru S-C bond | thru P-O bond | thru P-S bond |
| 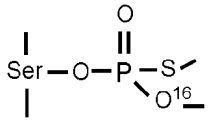 | 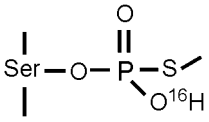 | 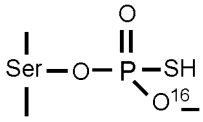 | 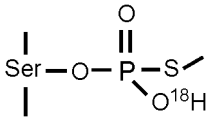 | 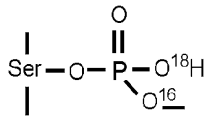 |
| m/z: 3054.4[a] | 3040.4 | 3040.4 | 3042.4 | 3026.5 |
| 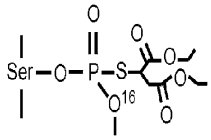 | 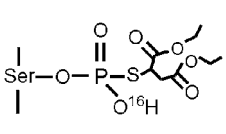 | 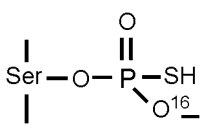 | 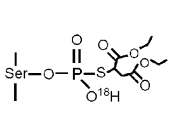 | 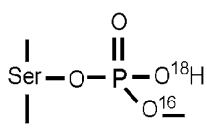 |
| m/z: 3212.5 [b] | 3198.5 | 3040.4 | 3200.5 | 3026.5 |

[a]This OP-peptide conjugate results from the inhibition of BChE by (1R)-isomalathion, where diethylthiosuccinate is the primary leaving group (Droom et al. 2001a).

[b]This OP-peptide conjugate results from the inhibition of BChE by (1S)-isomalathion, where thiomethyl is the primary leaving group (Droom et al. 2001a).

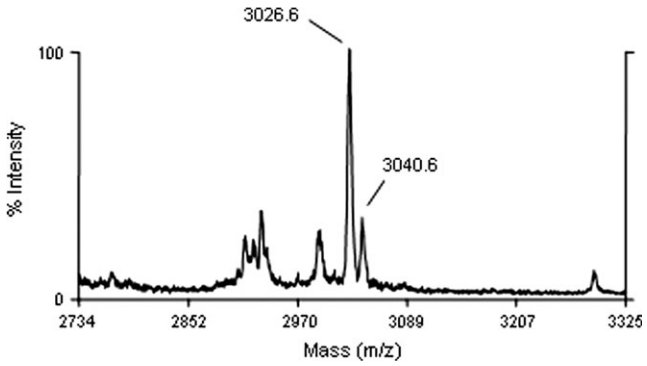


**FIG. 10.** MALDI mass spectrum of tryptic peptides from isomalathion-inhibited BChE. The spectrum was acquired in positive ion linear mode. Peaks 3026.6 and 3040.6 represent the aged isomalathion active-site peptide conjugate resulting from P–S and O–C/S–C bond breakage, respectively.

through the X–R scission pathway. Although AChE demonstrates different kinetic characteristics from BChE upon OP treatment (Giacobini, 2003), it is reasonable to predict that AChE conjugated with an OP retaining an alkoxy group after inhibition will age through the same pathway.

### *Isomalathion-Inhibited Human BChE Ages via both X–R and P–X Scission Pathways*

The two asymmetric centers of isomalathion, one at the phosphorus and the other at the α-carbon of the diethylthiosuccinate group, yield four stereoisomers for this compound. Among the four stereoisomers, two belong to the (1R)-stereoisomer group and the other two belong to the (1S)-stereoisomer group, based on the phosphorus asymmetric center (Berkman *et al*., 1993b). Previous studies have demonstrated that (1R)- and (1S)-isomers have different inhibition and aging mechanisms when reacting with cholinesterases (Berkman *et al*., 1993a; Doorn *et al*., 2001a,b; Jianmongkol *et al*., 1999). For (1R) isomers, the primary leaving group upon conjugation with the catalytic serine is the diethylthiosuccinate, yielding an O,S-dimethyl phosphate adduct; aging of this adduct appears to proceed through a P–X scission reaction where the P–S bond is cleaved and the end product is the *o*-methyl phosphate adduct (refer to Table 2). For (1S)-isomers, the inhibitory reaction is believed to proceed with loss of the thiomethyl. The aging reaction follows quickly with release of the bulky diethylthiosuccinate, through breakage of the P–S bond, another P–X scission reaction. These reaction pathways have been investigated in rat and bovine AChE and horse BChE (Berkman *et al*., 1993a; Doorn *et al*., 2001a,b; Jianmongkol *et al*., 1999).

We have reexamined this reaction with human BChE. The isomalathion used in our study was from a commercial source and was a mixture of stereoisomers. It is thus necessary for us to consider all the possible OP-BChE conjugates that can result from the primary inhibition and aging (see Table 2). The OP was added to human BChE at room temperature, and the reaction proceeded for at least 4 days. Due to this relatively long incubation time, we did not see peaks for the unaged isomalathion conjugates (3054.4 and 3198.5 m/z), and there was no unmodified active-site peptide in the spectrum (2930.3 m/z), indicating that the BChE was completely inhibited and had completely aged (see Fig. 10). A peak with m/z of 3026.5, for the *o*-methyl phosphate adduct containing $O^{18}H$, appeared in the spectrum as expected for a P–X bond scission. This confirmed the results from previous studies.

More interestingly, a minor peak with m/z corresponding to the aged OP adduct resulting from either O–C or S–C bond scission (3040.4 m/z) appeared in the spectrum. This minor peak was not observed in tryptic peptide spectra of isomalathion-treated equine BChE (Doorn *et al*., 2001a). We suggest that this new aged product is due to subtle differences in the geometry of the active-site gorge between human and equine BChE (e.g., Phe398 in human BChE is an Ile in equine BChE at the equivalent position, which may affect the conformation stability of the catalytic histidine) that render either O–C or S–C bond cleavage possible for human BChE but not for equine BChE.

It is noteworthy that a consistent difference was found in the reactivation rates of human BChE inhibited with the (1S, 3R) or the (1S, 3S) isomers of isomalathion (Doorn *et al*., 2001b). The (1S, 3S)-isomer–inhibited enzyme cannot be reactivated at all, whereas a small portion of the (1S, 3R)-isomer–inhibited enzyme was reactivated after adding 2-PAM. This suggests that there is something different about the two 1S adducts. Possibly, one of the (1S)-isomers ages via the P–S bond scission, which proceeds very fast after initial enzyme inhibition, thus leaves no opportunity for reactivation; and the other ages via the relatively slow S–C bond scission, so a partial reactivation was observed.

In conclusion, the aging pathways for BChE inhibited by nine different organophosphates were studied. The organophosphates which were chosen included nerve agents such as soman, sarin, and cyclohexyl sarin. The toxicity of the nerve agents is generally considered to be due to their rapid rate of aging, which results in irreversible inhibition of AChE. BChE is being considered for use as a prophylactic against nerve agent exposure. The nature of the aging pathways for these compounds, as described herein, may help in designing a mutant BChE that has better resistance to aging and thus serves as a more potent anti-organophosphate intoxication drug.

## FUNDING

U.S. Army Medical Research and Materiel Command Contract (W81XWH-06-1-0102); Edgewood Biological Chemical Center Contract (W911SR-04-C-0019); Eppley Cancer Center grant (P30CA36727); National Institute of Health (1 U01 NS058056-01); and grants DGA/DSP/STTC-PEA 010807 and EMA/LR 06 from France.

## ACKNOWLEDGMENTS

Mass spectra were obtained with the support of the Protein Structure Core Facility at the University of Nebraska Medical Center.

## REFERENCES

Aurbek, N., Thiermann, H., Szinicz, L., Eyer, P., and Worek, F. (2006). Analysis of inhibition, reactivation and aging kinetics of highly toxic organophosphorus compounds with human and pig acetylcholinesterase. *Toxicology* **224,** 91–99.

Barak, D., Ordentlich, A., Kaplan, D., Barak, R., Mizrahi, D., Kronman, C., Segall, Y., Velan, B., and Shafferman, A. (2000). Evidence for P-N bond scission in phosphoroamidate nerve agent adducts of human acetylcholinesterase. *Biochemistry* **39,** 1156–1161.

Barak, D., Ordentlich, A., Segall, Y., Velan, B., Benshop, H. P., De Jong, L. P. A., and Shafferman, A. (1997). Carbocation-mediated processes in biocatalysts. Contribution of aromatic moieties. *J. Am. Chem. Soc.* **119,** 3157–3158.

Berkman, C. E., Ryu, S., Quinn, D. A., and Thompson, C. M. (1993a). Kinetics of the postinhibitory reactions of acetylcholinesterase poisoned by chiral isomalathion: A surprising nonreactivation induced by the RP stereoisomers. *Chem. Res. Toxicol.* **6,** 28–32.

Berkman, C. E., Thompson, C. M., and Perrin, S. R. (1993b). Synthesis, absolute configuration, and analysis of malathion, malaoxon, and isomalathion enantiomers. *Chem. Res. Toxicol.* **6,** 718–723.

Casida, J. E., and Quistad, G. B. (2004). Organophosphate toxicology: Safety aspects of nonacetylcholinesterase secondary targets. *Chem. Res. Toxicol.* **17,** 983–998.

Doorn, J. A., Schall, M., Gage, D. A., Talley, T. T., Thompson, C. M., and Richardson, R. J. (2001a). Identification of butyrylcholinesterase adducts after inhibition with isomalathion using mass spectrometry: Difference in mechanism between (1R)- and (1S)-stereoisomers. *Toxicol. Appl. Pharmacol.* **176,** 73–80.

Doorn, J. A., Talley, T. T., Thompson, C. M., and Richardson, R. J. (2001b). Probing the active sites of butyrylcholinesterase and cholesterol esterase with isomalathion: Conserved stereoselective inactivation of serine hydrolases structurally related to acetylcholinesterase. *Chem. Res. Toxicol.* **14,** 807–813.

Ekstrom, F., Akfur, C., Tunemalm, A. K., and Lundberg, S. (2006). Structural changes of phenylalanine 338 and histidine 447 revealed by the crystal structures of tabun-inhibited murine acetylcholinesterase. *Biochemistry* **45,** 74–81.

Giacobini, E. (2003). Cholinesterases and Cholinesterase Inhibitors. pp. 1–19. Informa Healthcare, London.

Grueninger-Leitch, F., D'Arcy, A., D'Arcy, B., and Chene, C. (1996). Deglycosylation of proteins for crystallization using recombinant fusion protein glycosidases. *Protein Sci.* **5,** 2617–2622.

Harris, L. W., Fleisher, J. H., Clark, J., and Cliff, W. J. (1966). Dealkylation and loss of capacity for reactivation of cholinesterase inhibited by sarin. *Science* **154,** 404–407.

Jennings, L. L., Malecki, M., Komives, E. A., and Taylor, P. (2003). Direct analysis of the kinetic profiles of organophosphate-acetylcholinesterase adducts by MALDI-TOF mass spectrometry. *Biochemistry* **42,** 11083–11091.

Jianmongkol, S., Marable, B. R., Berkman, C. E., Talley, T. T., Thompson, C. M., and Richardson, R. J. (1999). Kinetic evidence for different mechanisms of acetylcholinesterase inhibition by (1R)- and (1S)-stereoisomers of isomalathion. *Toxicol. Appl. Pharmacol.* **155,** 43–53.

Li, B., Stribley, J. A., Ticu, A., Xie, W., Schopfer, L. M., Hammond, P., Brimijoin, S., Hinrichs, S. H., and Lockridge, O. (2000). Abundant tissue butyrylcholinesterase and its possible function in the acetylcholinesterase knockout mouse. *J. Neurochem.* **75,** 1320–1331.

Lockridge, O., and Masson, P. (2000). Pesticides and susceptible populations: People with butyrylcholinesterase genetic variants may be at risk. *Neurotoxicology* **21,** 113–126.

Lockridge, O., Schopfer, L. M., Winger, G., and Woods, G. H. (2005). Large scale purification of butyrylcholinesterase from human plasma suitable for injection into monkeys; a potential new therapeutic for protection against cocaine and nerve agent toxicity. *J. Med. CBR. Def.* **3,** online.

Mason, H. J., Waine, E., Stevenson, A., and Wilson, H. K. (1993). Aging and spontaneous reactivation of human plasma cholinesterase activity after inhibition by organophosphorus pesticides. *Hum. Exp. Toxicol.* **12,** 497–503.

Masson, P., Fortier, P. L., Albaret, C., Froment, M. T., Bartels, C. F., and Lockridge, O. (1997a). Aging of di-isopropyl-phosphorylated human butyrylcholinesterase. *Biochem. J.* **327**(Pt. 2), 601–607.

Masson, P., Froment, M. T., Bartels, C. F., and Lockridge, O. (1997b). Importance of aspartate-70 in organophosphate inhibition, oxime re-activation and aging of human butyrylcholinesterase. *Biochem. J.* **325**(Pt. 1), 53–61.

Michel, H. O., Hackley, B. E., Jr, Berkowitz, L., List, G., Hackley, E. B., Gillilan, W., and Pankau, M. (1967). Ageing and dealkylation of Soman (pinacolylmethylphosphonofluoridate)-inactivated eel cholinesterase. *Arch. Biochem. Biophys.* **121,** 29–34.

Millard, C. B., Kryger, G., Ordentlich, A., Greenblatt, H. M., Harel, M., Raves, M. L., Segall, Y., Barak, D., Shafferman, A., Silman, I., *et al.* (1999). Crystal structures of aged phosphonylated acetylcholinesterase: Nerve agent reaction products at the atomic level. *Biochemistry* **38,** 7032–7039.

Nachon, F., Asojo, O. A., Borgstahl, G. E., Masson, P., and Lockridge, O. (2005). Role of water in aging of human butyrylcholinesterase inhibited by echothiophate: The crystal structure suggests two alternative mechanisms of aging. *Biochemistry* **44,** 1154–1162.

Saxena, A., Doctor, B. P., Maxwell, D. M., Lenz, D. E., Radic, Z., and Taylor, P. (1993). The role of glutamate-199 in the aging of cholinesterase. *Biochem. Biophys. Res. Commun.* **197,** 343–349.

Shafferman, A., Ordentlich, A., Barak, D., Stein, D., Ariel, N., and Velan, B. (1996). Aging of phosphylated human acetylcholinesterase: Catalytic processes mediated by aromatic and polar residues of the active centre. *Biochem. J.* **318**(Pt. 3), 833–840.

Sidell, F. R., and Groff, W. A. (1974). The reactivatibility of cholinesterase inhibited by VX and sarin in man. *Toxicol. Appl. Pharmacol* **27,** 241–252.

van der Schans, M. J., Polhuijs, M., van Dijk, C., Degenhardt, C. E., Pleijsier, K., Langenberg, J. P., and Benschop, H. P. (2004). Retrospective detection of exposure to nerve agents: Analysis of phosphofluoridates originating from fluoride-induced reactivation of phosphylated BuChE. *Arch. Toxicol.* **78,** 508–524.

Viragh, C., Akhmetshin, R., Kovach, I. M., and Broomfield, C. (1997). Unique push-pull mechanism of dealkylation in soman-inhibited cholinesterases. *Biochemistry* **36,** 8243–8252.

Viragh, C., Kovach, I. M., and Pannell, L. (1999). Small molecular products of dealkylation in soman-inhibited electric eel acetylcholinesterase. *Biochemistry* **38,** 9557–9561.

# Aging of Cholinesterases Phosphylated by Tabun Proceeds through O-Dealkylation

E. Carletti, H. Li, B. Li, F. Ekström, Y. Nicolet, M. Loiodice, E. Gillon, M-T. Froment, O. Lockridge, L.M. Schopfer, P. Masson, **F. Nachon***

Journal of the American Chemical Society 130 (2008) 16011-16020

J|A|C|S
ARTICLES

Published on Web 11/01/2008

# Aging of Cholinesterases Phosphylated by Tabun Proceeds through O-Dealkylation

Eugénie Carletti,[†] He Li,[‡] Bin Li,[‡] Fredrik Ekström,[§] Yvain Nicolet,[#] Mélanie Loiodice,[†] Emilie Gillon,[†] Marie T. Froment,[†] Oksana Lockridge,[‡] Lawrence M. Schopfer,[‡] Patrick Masson,[†] and Florian Nachon*[,†]

*Département de Toxicologie, Centre de Recherches du Service de Santé des Armées (CRSSA), 24 avenue des Maquis du Grésivaudan, 38700 La Tronche, France, Eppley Institute and Department of Biochemistry and Molecular Biology, University of Nebraska Medical Center, Omaha, Nebraska 68198-6805, FOI CBRN Defence and Security, S-901 82 Umeå, Sweden, and Laboratoire de Cristallogenèse et Cristallographie des Protéines, Institut de Biologie Structurale (CEA-CNRS-UJF), 41 rue Jules Horowitz, 38027 Grenoble, France*

Received June 27, 2008; E-mail: fnachon@crssa.net

***Abstract:*** Human butyrylcholinesterase (hBChE) hydrolyzes or scavenges a wide range of toxic esters, including heroin, cocaine, carbamate pesticides, organophosphorus pesticides, and nerve agents. Organophosphates (OPs) exert their acute toxicity through inhibition of acetylcholinesterase (AChE) by phosphylation of the catalytic serine. Phosphylated cholinesterase (ChE) can undergo a spontaneous, time-dependent process called "aging", during which the OP−ChE conjugate is dealkylated. This leads to irreversible inhibition of the enzyme. The inhibition of ChEs by tabun and the subsequent aging reaction are of particular interest, because tabun−ChE conjugates display an extraordinary resistance toward most current oxime reactivators. We investigated the structural basis of oxime resistance for phosphoramidated ChE conjugates by determining the crystal structures of the non-aged and aged forms of hBChE inhibited by tabun, and by updating the refinement of non-aged and aged tabun-inhibited mouse AChE (mAChE). Structures for non-aged and aged tabun−hBChE were refined to 2.3 and 2.1 Å, respectively. The refined structures of aged ChE conjugates clearly show that the aging reaction proceeds through O-dealkylation of the P(*R*) enantiomer of tabun. After dealkylation, the negatively charged oxygen forms a strong salt bridge with protonated His438N$\epsilon$2 that prevents reactivation. Mass spectrometric analysis of the aged tabun-inhibited hBChE showed that both the dimethylamine and ethoxy side chains were missing from the phosphorus. Loss of the ethoxy is consistent with the crystallography results. Loss of the dimethylamine is consistent with acid-catalyzed deamidation during the preparation of the aged adduct for mass spectrometry. The reported 3D data will help in the design of new oximes capable of reactivating tabun−ChE conjugates.

## Introduction

Acetylcholinesterase (AChE; EC 3.1.1.7) and butyrylcholinesterase (BChE; EC 3.1.1.8) are closely related serine hydrolases with different substrate specificities and inhibitor sensitivities. AChE terminates the action of the neurotransmitter acetylcholine at postsynaptic membranes and neuromuscular junctions. Although BChE is present in numerous vertebrate tissues, its physiological role remains unclear.[1,2]

Human butyrylcholinesterase (hBChE) is toxicologically relevant because it hydrolyzes or scavenges a wide range of toxic esters, including heroin, cocaine, carbamate pesticides, organophosphorus pesticides, and nerve agents.[3] Organophosphates (OPs) exert their acute toxicity through inhibition of AChE by phosphylation of the catalytic serine. Subsequent accumulation of acetylcholine at neuronal synapses and neuromuscular junctions results in paralysis, seizures, and other symptoms of cholinergic syndrome.[4,5]

Phosphylated ChEs can be reactivated by nucleophilic agents such as oximes. The most effective oximes used for emergency treatment of nerve agent poisoning are the monopyridinium oximes (2-PAM and HI-6) and bispyridinium oximes (TMB-4, MMB-4, obidoxime, and HLö-7).[6] Kinetic analysis of the interactions between different AChE-OP conjugates and different oximes shows that the most effective oximes are HLö-7 for phosphonylated AChE and obidoxime for phosphorylated AChE.[6] Unfortunately, a universal antidote, efficient against all known nerve agents and capable of crossing the blood−brain barrier, is not yet available.

Subsequent to formation of the OP−ChE adduct, the phosphylated ChEs can undergo a spontaneous, time-dependent

[†] Département de Toxicologie, CRSSA.
[‡] University of Nebraska Medical Center.
[§] FOI CBRN Defence and Security.
[#] Institut de Biologie Structurale.

(1) Chatonnet, A.; Lockridge, O. *Biochem. J.* **1989**, *260*, 625–634.
(2) Mack, A.; Robitzki, A. *Prog. Neurobiol.* **2000**, *60*, 607–628.
(3) Lockridge, O.; Masson, P. *Neurotoxicology* **2000**, *21*, 113–126.
(4) Eddleston, M.; Mohamed, F.; Davies, J. O.; Eyer, P.; Worek, F.; Sheriff, M. H.; Buckley, N. A. *Qjm* **2006**, *99*, 513–522.
(5) Konradsen, F.; Dawson, A. H.; Eddleston, M.; Gunnell, D. *Lancet* **2007**, *369*, 169–170.
(6) Worek, F.; Thiermann, H.; Szinicz, L.; Eyer, P. *Biochem. Pharmacol.* **2004**, *68*, 2237–2248.

  

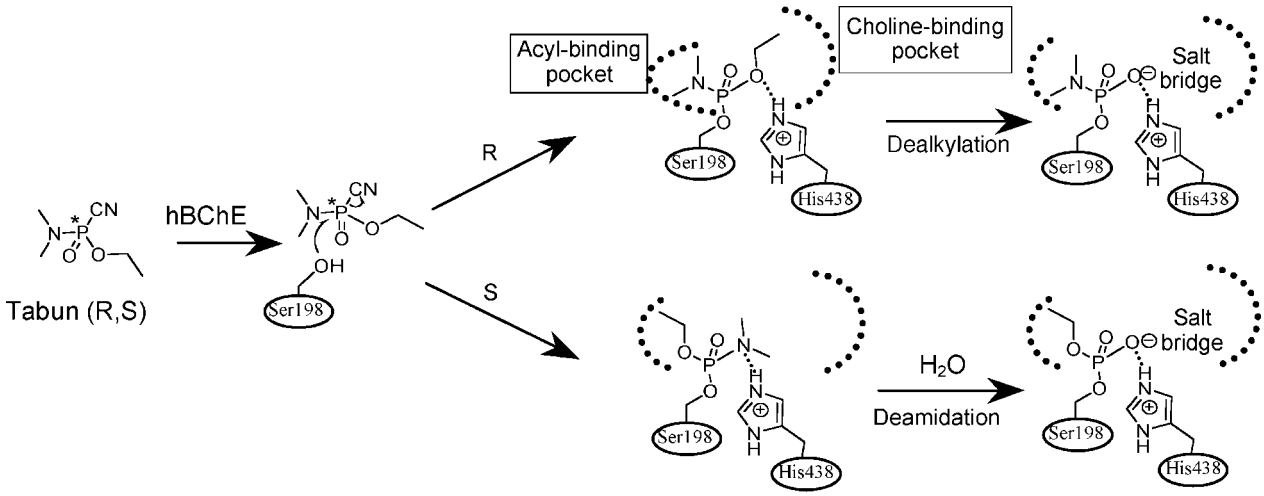


***Figure 1.*** Mechanism proposed for aging of hBChE phosphorylated by tabun.

process called "aging", during which the OP−ChE conjugate is dealkylated. This leads to irreversibly inhibited enzyme.[7−10] The rate of aging depends on the nature of the OP. The $t_{1/2}$ is a few minutes for ChE inhibited by soman[11] and several hours for ChE inhibited by tabun.[12]

Early studies showed that tabun-inhibited ChEs from different animals display different rates of aging.[13] The rate constant for aging of tabun-inhibited human AChE (hAChE) *in vitro* was found to be $8.7 \times 10^{-4}$ $min^{-1}$ (i.e., $t_{1/2}$ =13.3 h) at 37° and pH 7.4.[12]

Inhibition of ChEs by tabun and the subsequent aging reaction are of particular interest, because tabun−ChE conjugates display an extraordinary resistance toward most oxime reactivators. As tabun is racemic, the two enantiomers, P(*R*) and P(*S*), can react with the enzyme and form adducts with different stereochemistry. These adducts could respectively age through "dealkylation" or "deamination" (Figure 1).

Mass spectrometry (MS) studies on the aging of hAChE inhibited by tabun suggested that the mechanism involved a P−N bond cleavage and elimination of the dimethylamine group.[14,15] Intriguingly, the 2.5 Å crystal structure of non-aged *Mus musculus* AChE (mAChE) inhibited by tabun suggested that the ethoxy moiety is placed close to the catalytic His447, with the dimethylamine group distant from catalytic residues able to facilitate the aging reaction.[16] In the structure, the His447 and Phe338 side chains have undergone a structural change relative to the conformation found in the apoenzyme structure. The authors proposed that this displacement might interfere with the accessibility of oximes, thereby contributing to the high resistance of tabun conjugates to reactivators.

Kinetic analysis of the oxime-induced reactivation and aging of hAChE inhibited by various tabun-related *N*-monoalkyl phosphoramidates showed that the rate constants for both were dependent on the length of the *N*-alkyl chain.[17]

In order to better understand the structural basis of both the oxime resistance of the conjugates and the aging mechanism of tabun-inhibited ChEs, we analyzed peptides from tabun−hBChE by MS, determined the crystal structures of non-aged and aged forms of hBChE inhibited by tabun, and updated the previous crystal structure model of tabun−mAChE. The X-ray structures will help in the design of new oximes capable of reactivating tabun−ChEs conjugates.

## Materials and Methods

**Caution:** *As tabun is highly toxic and is classified as a schedule 1 chemical as defined in the Chemical Weapons Convention, all work with tabun is regulated by the convention. The handling of tabun is dangerous and requires suitable personal protection, training, and facilities.*

**Titration of Tabun by Ionometry and NMR.** Racemic tabun in solution in 2-propanol was from CEB (Vert-le-Petit, France). $^{31}P$, $^{1}H$, and $^{13}C$ NMR spectra for tabun in 2-propanol were recorded to determine its purity and integrity. After complete hydrolysis at pH 13.6, tabun was titrated by ionometry using a thermostatted ionometer (Radiometer IONcheck 45) equipped with an ion-selective electrode for cyanide (Radiometer Analytical ISE25CN-9), as described by the electrode provider.

**Production of Recombinant hBChE.** The recombinant hBChE was a truncated monomer containing residues 1−529.[18] The 45-amino acid tetramerization domain at the carboxy terminus was deleted. The carbohydrate content was reduced by site-directed mutagenesis from nine to six glycans.[18] The recombinant hBChE gene was expressed in Chinese hamster ovary (CHO) cells. The enzyme, secreted into serum-free culture medium, was purified by affinity and ion-exchange chromatographies and crystallized as

(7) Benschop, H. P.; Keijer, J. H. *Biochim. Biophys. Acta* **1966**, *128*, 586–588.
(8) Viragh, C.; Kovach, I. M.; Pannell, L. *Biochemistry* **1999**, *38*, 9557–9561.
(9) Millard, C. B.; Kryger, G.; Ordentlich, A.; Greenblatt, H. M.; Harel, M.; Raves, M. L.; Segall, Y.; Barak, D.; Shafferman, A.; Silman, I.; Sussman, J. L. *Biochemistry* **1999**, *38*, 7032–7039.
(10) Nachon, F.; Asojo, O. A.; Borgstahl, G. E.; Masson, P.; Lockridge, O. *Biochemistry* **2005**, *44*, 1154–1162.
(11) Saxena, A.; Viragh, C.; Frazier, D. S.; Kovach, I. M.; Maxwell, D. M.; Lockridge, O.; Doctor, B. P. *Biochemistry* **1998**, *37*, 15086–15096.
(12) Heilbronn, E. *Biochem. Pharmacol.* **1963**, *12*, 25–36.
(13) Heilbronn, E. *Biochim. Biophys. Acta* **1962**, *58*, 222–230.
(14) Barak, D.; Ordentlich, A.; Kaplan, D.; Barak, R.; Mizrahi, D.; Kronman, C.; Segall, Y.; Velan, B.; Shafferman, A. *Biochemistry* **2000**, *39*, 1156–1161.
(15) Elhanany, E.; Ordentlich, A.; Dgany, O.; Kaplan, D.; Segall, Y.; Barak, R.; Velan, B.; Shafferman, A. *Chem. Res. Toxicol.* **2001**, *14*, 912–918.
(16) Ekstrom, F.; Akfur, C.; Tunemalm, A. K.; Lundberg, S. *Biochemistry* **2006**, *45*, 74–81.
(17) Worek, F.; Aurbek, N.; Koller, M.; Becker, C.; Eyer, P.; Thiermann, H. *Biochem. Pharmacol.* **2007**, *73*, 1807–1817.
(18) Nachon, F.; Nicolet, Y.; Viguié, N.; Masson, P.; Fontecilla-Camps, J. C.; Lockridge, O. *Eur. J. Biochem.* **2002**, *269*, 630–637.

described.[18] The active-site concentration of highly purified enzyme was determined using diisopropyl fluorophosphate as the titrant.[19]

**Production of Recombinant hAChE.** The recombinant L544Stop mutant of human AChE (monomeric) was inserted into a pGS vector carrying the glutamine synthetase gene marker. CHO-K1 cells were maintained in serum-free Ultraculture Medium (Bio-Whittaker). Cells were transfected using DNA−calcium phosphate precipitation. Transfected clones were selected by incubation in media containing methionine sulfoximide. When cell death subsided, individual clones were manually transferred to 24 well plates. Clones with high expression of AChE were expanded and transferred to roller bottles for large-scale protein production. The used growth media contained up to 30 mg of hAChE per liter. Protein was precipitated from the media by ammonium sulfate. The pellets were dialyzed against 20 mM Tris-HCl buffer, pH 7.4, and loaded onto an affinity column (Sepharose-4B/procainamide). Human AChE was eluted with 20 mM Tris-HCl buffer, pH 7.4, containing 1 M NaCl, 0.5 M tetramethylammonium iodide, and 1 mM decamethonium chloride. The enzyme was dialyzed against 20 mM Tris-HCl buffer, pH 7.4, and further purified by ion-exchange chromatography (monoQ; Amersham Bioscience) on a fast protein liquid chromatography system (Pharmacia). Fractions containing high hAChE activity were pooled and concentrated using a Centricon-30 ultrafiltration microconcentrator (30 000 MW cutoff, from Amicon). The concentration of the pure, homogeneous hAChE was determined from its absorbance at 280 nm using $\epsilon_{1\ \mathrm{mg/mL}} = 1.7$.[20]

**Inhibition of hChEs by Tabun.** Phosphylation rates were determined by incubating the ChE with different concentrations of tabun in 50 mM sodium phosphate buffer, pH 7.0, containing 5% 2-propanol and 1 mg/mL bovine serum albumin (BSA) and measuring the enzyme residual activity of aliquots at various times after initiation of inhibition at 25 °C. Human ChE activities were assayed according to Ellman[21] with 1 mM butyrylthiocholine for hBChE and 0.75 mM acetylthiocholine (ATC) for hAChE in the presence of 1 mg/mL BSA, 0.5 mM 5,5′-dithiobis(2-nitrobenzoic-acid), and 50 mM sodium phosphate buffer, pH 7.0, at 25 °C using a Uvikon943 spectrophotometer. The stability of tabun under the assay conditions was verified by ionometry (measurement of $CN^-$ release) and by testing the invariant ability of tabun solution to inhibit hBChE as a function of time. No significant spontaneous hydrolysis of tabun was observed after more than 10 h of incubation. Analysis of the kinetic data was performed using GOSA-fit, a fitting software based on a simulated annealing algorithm (BioLog, Toulouse, France; http://www.bio-log.biz).

Cholinesterases are well-known to favor one stereoisomer over another. Therefore, it is prudent to analyze the tabun inhibition kinetics as if the ChE were behaving in a stereoselective manner. The rate of dissociation of the ChE−tabun adduct is slow relative to its rate of formation; therefore, the phosphylation reaction can be treated as an irreversible process for analytical purposes.

Irreversible inhibition by a racemic inhibitor (*R*,*S*) can be described by Scheme 1. The apparent bimolecular phosphylation rate constants ($k_i = k_{iR} + k_{iS}$, see Scheme 1) determined under pseudo-first-order conditions ([tabun] > 20[hChE]) were computed from the slopes of ln *E* vs time plots at different tabun concentrations.

Determination of inhibition enantioselectivity was performed under second-order conditions. The concentration of hBChE was 31.5 nM, while that of tabun ranged between 25 and 200 nM. The concentration of hAChE was 7.4 nM, while that of tabun ranged between 5 and 150 nM. Assuming that the enzymes were enantioselective, with one enantiomer much more efficient than the other (i.e, $k_{iR} \gg k_{iS}$), the fraction of enzyme inhibited by the lowest active

***Scheme 1***[a]

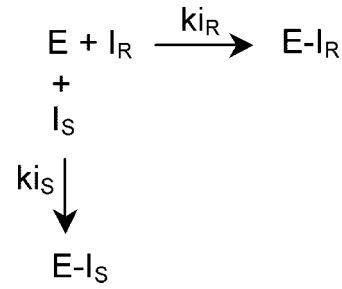


[a] E is the enzyme, $I_R$ is the *R* enantiomer, $I_S$ is the *S* enantiomer, E-$I_R$ and E-$I_S$ are the conjugates, and $k_{iR}$ and $k_{iS}$ are the bimolecular rate constants.

enantiomer is negligible, and the concentration of residual active enzyme follows eq 1 (derived from Scheme 1) as a function of time:

$$E = E_0 \frac{E_0 - I_0/n}{E_0 - (I_0/n)\, e^{(I_0/n - E_0)k_{iR}t}} \quad (1)$$

where *E* is the concentration of residual active enzyme at time *t*, $E_0$ the concentration of enzyme at time $t = 0$, $I_0$ the concentration of racemic inhibitor at $t = 0$, *n* the number of enantiomers, and $k_{iR}$ the bimolecular rate constant of the most active enantiomer (taken to be enantiomer *R* in this case).

**Tabun-Inhibited hBChE Samples for Mass Spectrometry.** Human BChE was reacted with tabun in $H_2{}^{18}O$. Oxygen-18 was used so that the mechanism of dealkylation during aging could be more clearly defined. Evidence from the crystal structure of aged tabun-inhibited hBChE indicates that aging involves dealkylation of the ethoxy moiety. This reaction requires hydrolysis of the P−O−C linkage. In principle, such a hydrolysis could occur by cleavage of the P−O bond or the O−C bond. In the former case, a hydroxyl from water would replace the ethoxy. In the latter case, a hydroxyl from water would add to the ethyl, leaving the original oxygen on the phosphorus. By using $H_2{}^{18}O$, the site of cleavage can be distinguished. If hydrolysis is at the O−C bond, the mass of the phosphorus component will reflect the presence of the original $^{16}O$. If the hydrolysis is at the P−O bond, the phosphorus component will gain an $^{18}O$ from the medium and its mass will increase by 2 amu. This strategy was employed by Li et al. to characterize the aging reactions for a variety of hBChE−OP adducts.[22]

For the inhibition reaction, 10 $\mu$L of recombinant hBChE (13 mg/mL in 15 mM 2-(*N*-morpholino)ethanesulfonic acid (MES) buffer at pH 6.5) was mixed with 90 mL of $H_2{}^{18}O$, 1 mL of 1 M Tris buffer at pH 8.5, and 1 mL of tabun (10 mg/mL in 2-propanol). Samples for analysis of the non-aged adduct were frozen to −80 °C shortly after preparation. Samples for analysis of the aged adduct were incubated at room temperature for 2 days, after which the preparation was stored at −80 °C until use. Final concentrations of hBChE and tabun were 15 and 720 mM, respectively. Unlabeled hBChE was treated in the same manner, except that the tabun was omitted.

To prepare peptides for MS, frozen samples were thawed and 50 mL of sample was mixed with 50 mL of 25 mM ammonium bicarbonate buffer at pH 8.3. The mixture was concentrated to about 20 mL by centrifugation at 6700*g* using a Microcon YM-3 ultrafiltration microconcentrator (3000 MW cutoff, from Millipore). The process was repeated five times to remove the $H_2{}^{18}O$ and excess tabun and to change the buffer. The product was diluted to 50 mL with 25 mM ammonium bicarbonate, mixed with porcine trypsin (0.5 mg/mL from Promega) to a final hBChE/trypsin ratio of 30:1 (w/w), and incubated overnight at room temperature with constant,

(19) Amitai, G.; Moorad, D.; Adani, R.; Doctor, B. P. *Biochem. Pharmacol.* **1998**, *56*, 293–299.
(20) Rosenberry, T. L.; Scoggin, D. M. *J. Biol. Chem.* **1984**, *259*, 5643–5652.
(21) Ellman, G. L.; Courtney, K. D.; Andres, V.; Featherstone, R. M. *Biochem. Pharmacol.* **1961**, *7*, 88–95.
(22) Li, H.; Schopfer, L. M.; Nachon, F.; Froment, M. T.; Masson, P.; Lockridge, O. *Toxicol. Sci.* **2007**, *100*, 136–145.

gentle mixing. Peptides were concentrated and washed using ZipTips (Millipore), as described in the sections on MALDI-TOF mass spectrometry and Q-Trap mass spectrometry.

**MALDI-TOF Mass Spectrometry.** MALDI-TOF MS experiments were performed on an Applied Biosystems Voyager DE-PRO mass spectrometer equipped with a 337 nm pulsed nitrogen laser (Framingham, MA). Peptides that had been adsorbed onto a reverse-phase C-18 ZipTip were eluted into a microcentrifuge tube with 15 $\mu$L of 60% acetonitrile and 0.1% trifluoroacetic acid (TFA). One microliter of eluant was mixed 1:1 (v/v) with α-cyano-4-hydroxycinnamic acid (matrix, 10 mg/mL in 50% acetonitrile and 0.3% TFA) on the MALDI target plate and allowed to dry at room temperature. Mass spectra were acquired in positive-ion, linear mode under delayed extraction conditions, using an acceleration voltage of 20 kV. Laser intensity was adjusted so that the most intense ion in the spectrum did not exceed 80% of the maximum, saturated intensity value. Laser positioning on the sample spot was monitored with a video camera. Spectra shown are the average of 500 laser shots collected from multiple locations on the target spot. Calibration for the mass spectra was performed internally by reference to hBChE tryptic fragments. The sequence of hBChE (accession no. gi:158429457) was obtained from the NCBInr database. The reference masses of the tryptic hBChE peptides were obtained using the MS-Digest feature of ProteinProspector version 4.0.6 (http://prospector.ucsf.edu/).

**Q-Trap Mass Spectrometry.** The amino acid sequence of the aged peptide from tabun-inhibited hBChE was determined by collision-induced dissociation in a QTrap 2000, hybrid, tandem-quadrupole, linear-ion trap mass spectrometer equipped with a nanospray interface (Applied Biosystems). The spectrometer was calibrated daily on selected fragments from the MSMS spectrum of [Glu]fibrinopeptide B. Tryptic peptides from tabun-inhibited hBChE (25 $\mu$L total volume) were subjected to ZipTip cleanup to remove salts before they were delivered into the QTrap. Ten microliters of an 80% acetonitrile and 0.1% formic acid solution was used to elute the peptides from the ZipTip. Two 25-$\mu$L aliquots were cleaned and the eluents combined. Eight microliters of the peptide solution was introduced into the mass spectrometer by static infusion using an Econo12 emitter (New Objective, Woburn, MA). The ion spray voltage was 1300 V (which creates a voltage differential of 1300 V between the emitter and the curtain plate). The emitter position was optimized to obtain maximum signal intensity. All mass spectra were collected in the enhanced mode, i.e., using the ion trap, and by convention are referred to as enhanced spectra. Enhanced product ion (EPI) spectra were obtained using low-energy collision-induced dissociation. The collision cell was pressurized to 40 $\mu$Torr with pure nitrogen. The collision energy was 40 V. The trap fill time for each EPI scan was 20 ms. A total of 200 EPI scans were accumulated to generate the final EPI spectrum. The EPI spectra were manually analyzed to determine the sequence of the peptide.

**Crystals of Non-aged Tabun-Inhibited hBChE Conjugate.** The mother liquor was 0.1 M MES buffer, pH 6.5, with 2.1 M ammonium sulfate. The tabun stock solution was 10 mM in 2-propanol. The tabun−hBChE conjugate was prepared by soaking crystals for 10 min in 0.1 M MES buffer, pH 6.5, with 2.1 M ammonium sulfate containing 1 mM tabun. The crystals were washed with a cryoprotectant solution (0.1 M MES buffer with 2.1 M ammonium sulfate, containing 20% glycerol) and then flash-cooled in liquid nitrogen.

**Crystallization of Aged Tabun−hBChE Conjugate.** The purified enzyme (9 mg/mL) was inhibited in the presence of 1 mM tabun in 10 mM Tris-HCl buffer, pH 7.4. The reaction mixture was incubated for 1 day at 4 °C. The inhibited enzyme was crystallized using the hanging drop method as described.[23] Crystals grew in 1 week at 20 °C. The length of time between phosphylation and data collection was sufficiently long (>1 week) to achieve completion of the aging reaction.

**X-ray Data Collection and Structure Solution of Tabun−hBChE Conjugate.** Diffraction data were collected at the European Synchrotron Radiation Facility (ESRF, Grenoble, France), at the ID14-eh2 beam line using $\lambda = 0.932$ Å wavelength with ADSC Quantum 4 for non-aged conjugate, and at the ID23-2 beam line using $\lambda = 0.873$ Å wavelength with MAR-Research CCD detector for aged conjugate. All data sets were processed with XDS. The structures were solved by use of the CCP4 suite.[24] An initial solution model was determined by molecular replacement with MolRep,[25] starting from the recombinant hBChE structure (PDB entry 1P0I) from which all ligands (butyrate, glycerol, ions) and glycan chains were removed. For all diffraction data sets, the model was refined as follows: an initial rigid-body refinement with REFMAC5[26] was followed by iterative cycles of model building with Coot,[27] and then restrained refinement was carried out with REFMAC5 and Phenix.[28] The bound ligands and their descriptions were built using the Dundee PRODRG2.5 server including energy minimization using GROMOS96.1 force field.

**Updated Refinement of Aged and Non-aged Tabun-Inhibited mAChE.** Coordinates and structure factors of non-aged (PDB entry 2C0Q) and aged (PDB entry 2C0P) tabun-inhibited mouse AChE were retrieved from the Protein Data Bank. The models were refined by iterative cycles of model building with Coot and restrained refinement with REFMAC5 and Phenix.

## Results

**Inhibition of Human Cholinesterases by Tabun.** The bimolecular rate constants, $k_i$, for inhibition of hAChE and hBChE by racemic tabun are respectively $(3.0 \pm 0.4) \times 10^6$ and $(2.0 \pm 0.2) \times 10^6$ $M^{-1}\cdot min^{-1}$ (data not shown). These values are in agreement with reported literature values.[29]

The time dependence of the inhibition of hAChE and hBChE by tabun, under second-order conditions, is shown in Figure 2. Both human ChEs are enantioselective. Fitting the AChE data to eq 1 yields $k_{iR} = (6.9 \pm 0.2) \times 10^6$ $M^{-1}\cdot min^{-1}$ and $n = 2.1 \pm 0.1$. This corresponds to enantioselectivity of hAChE for one enantiomer of tabun. For hBChE, fitting yields $k_{iR} = (6.0 \pm 0.4) \times 10^6$ $M^{-1}\cdot min^{-1}$ and $n = 2.7 \pm 0.1$. The latter $n$ value also suggests an enantioselectivity of hBChE. However, the fact that more than 2 equiv of tabun was required to achieve full enzyme inhibition is puzzling. The value $n = 2.7$ was systematically found for inhibition of both highly purified tetrameric plasma BChE and monomeric recombinant BChE. Because both tabun and BChE preparations were accurately titrated, and because no spontaneous hydrolysis of tabun was observed in buffer, a tentative hypothesis is that hydrolysis of tabun was promoted by a BChE nucleophile group other than Ser198. This requires further investigations.

**Mass Spectrometry Analysis of Tabun−hBChE Adducts.** The initial reaction of hBChE with tabun is expected to result in formation of a covalent adduct with loss of the CN moiety from tabun. This would cause the mass of the singly charged, active-

(23) Nicolet, Y.; Lockridge, O.; Masson, P.; Fontecilla-Camps, J. C.; Nachon, F. *J. Biol. Chem.* **2003**, *278*, 41141–41147.

(24) Collaborative-Computational-Project 4. *Acta Crystallogr. D, Biol. Crystallogr.* **1994**, *50*, 760−763.

(25) Vagin, A.; Teplyakov, A. *J. Appl. Crystallogr.* **1997**, *30*, 1022–1025.

(26) Murshudov, G. N.; Vagin, A. A.; Dodson, E. J. *Acta Crystallogr. D, Biol. Crystallogr.* **1997**, *53*, 240–255.

(27) Emsley, P.; Cowtan, K. *Acta Crystallogr. D, Biol. Crystallogr.* **2004**, *60*, 2126–2132.

(28) Adams, P. D.; Grosse-Kunstleve, R. W.; Hung, L. W.; Ioerger, T. R.; McCoy, A. J.; Moriarty, N. W.; Read, R. J.; Sacchettini, J. C.; Sauter, N. K.; Terwilliger, T. C. *Acta Crystallogr. D, Biol. Crystallogr.* **2002**, *58*, 1948–1954.

(29) Raveh, L.; Grunwald, J.; Marcus, D.; Papier, Y.; Cohen, E.; Ashani, Y. *Biochem. Pharmacol.* **1993**, *45*, 2465–2474.

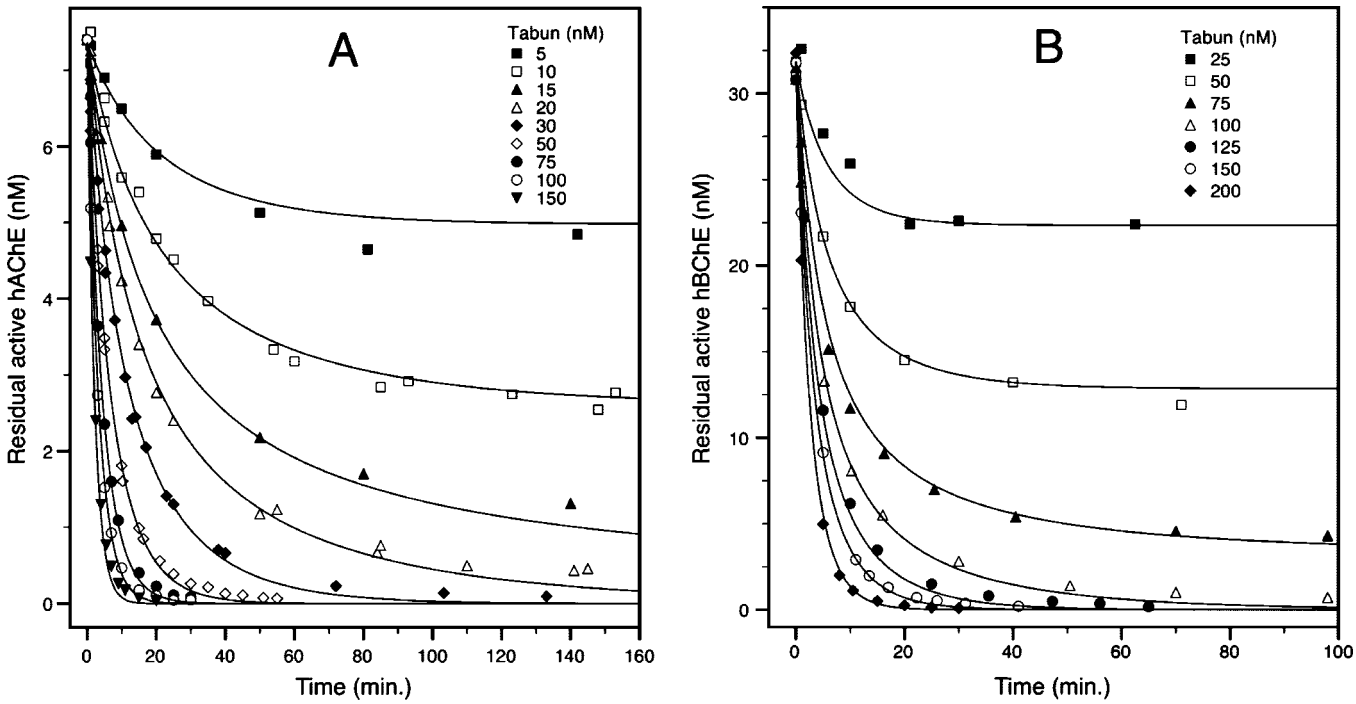


***Figure 2.*** Irreversible inhibition of hAChE (A) and hBChE (B) by racemic tabun under second-order conditions. Human ChEs were inhibited by various concentrations of tabun, and the residual active concentration of enzyme was monitored as a function of time.

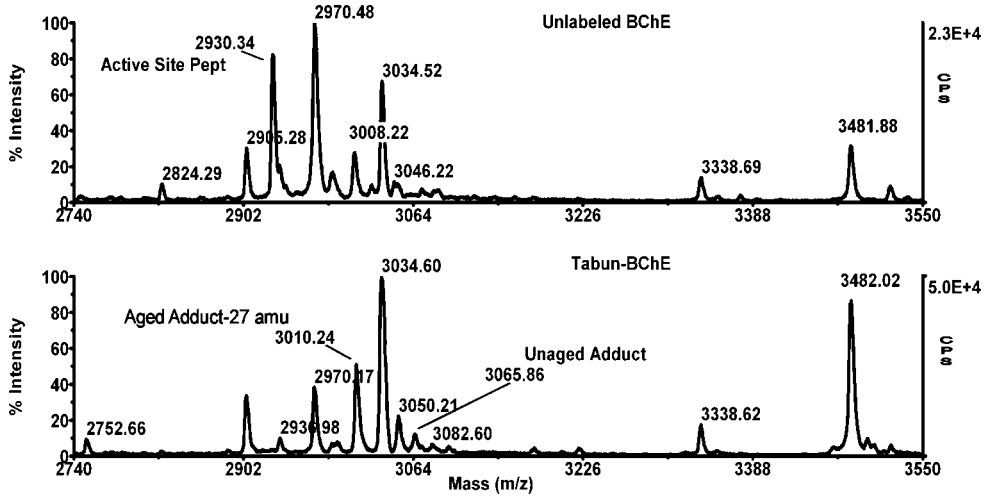


***Figure 3.*** Mass spectra of tryptic digests of hBChE with and without tabun. Spectra were taken in linear mode on a MALDI-TOF mass spectrometer. Peptides were prepared and MALDI-TOF mass spectra were taken as described in the methods section. The upper panel is for unlabeled hBChE. It was internally calibrated using the average masses for hBChE peptides at 3482.07 (residues 148−180) and 3034.59 amu (residues 428−452). The lower panel is for the aged tabun−hBChE adduct. The peak labeled "Aged Adduct-27 amu" is the peak for tabun−hBChE after loss of the dimethylamine and ethoxy groups. It was internally calibrated using the hBChE peptides at 3482.07 (residues 148−180), 3050.59 (residues 428−452 with one oxidized methionine), and 3034.59 amu (residues 428−452). Calibration was performed using peak height as a weighting factor.

site, tryptic peptide to increase by 135 amu, from 2930.3 to 3065.3 amu (average masses). This transformation is evident in the MALDI-TOF mass spectra shown in Figure 3, where the tryptic digest of unlabeled hBChE (upper panel) shows a prominent peak at 2930.34 amu and no mass at 3065 amu, while the tryptic digest of the non-aged tabun−hBChE adduct (lower panel) shows no mass at 2930 amu and a distinct mass at 3065.86 amu.

Following its initial formation, the tabun−hBChE adduct will age. Aging would be expected to result in loss of either a dimethylamine or an ethoxy group. Such losses would lead to reduction in the mass of the active-site peptide adduct to either 3038.3 (for loss of dimethylamine) or 3037.3 amu (for loss of ethoxy). Neither of these masses was detected in the MALDI-TOF mass spectra for the aged tabun−hBChE adduct. The large peak at 3034 amu (from hBChE peptide residues 428−452) could obscure peaks of small intensity at 3037 or 3038 amu. However, high-resolution, reflector-mode MALDI-TOF spectra showed that the peak at 3034 amu (average mass) was composed only of isotopes from a 3032 amu monoisotopic mass. There was no evidence in the isotopic pattern for additional mass at 3037 or 3038 amu. This finding was unexpected since the tabun−hBChE adduct had been allowed to age for several days before digestion and aged product should have been present.

Comparison of the two mass spectra in Figure 3 reveals a shift in the mass of the 3008 amu peak in unlabeled hBChE to

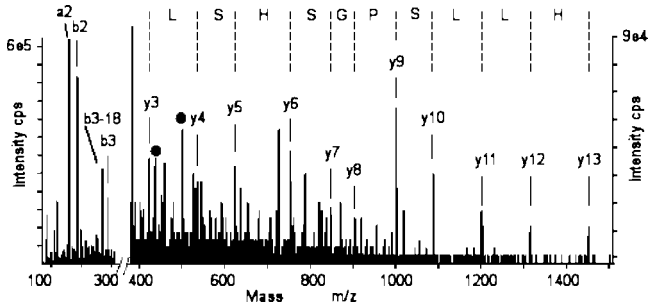


***Figure 4.*** Tandem mass spectrum (MSMS) of the putative aged tabun-labeled active-site peptide from hBChE. An MSMS spectrum was taken of the 753.4 *m/z*, quadruply charged form of the 3010 amu ion using the QTrap 2000 hybrid tandem-quadrupole, linear ion-trap mass spectrometer. The *x*-axis is divided into two intensity ranges. For masses from 400 to 1500 *m/z*, the intensity of the data has been expanded 6.7-fold. The intensities for this region are given in counts per second (cps) on the scale to the right. For masses from 50 to 350 *m/z*, the intensities are given in cps on the scale to the left. Selected y- and b-ions that are characteristic of hBChE active-site peptide are indicated. The amino acid sequence corresponding to the y-ion series is indicated by single-letter abbreviations for the amino acids. The spots indicate the 437.3 and 501.4 amu fragments; see the text for a description of these fragments.

3010 amu in the aged tabun−hBChE sample. The 3008 amu mass is consistent with the mass of a tryptic peptide from hBChE (residues 549−570 having one oxidized methionine). The 3010 amu mass appeared repeatedly in the spectra of aged tabun−hBChE. A mass of 3010 amu would be consistent with loss of both the dimethylamine and the ethoxy groups from the tabun adduct, leaving phosphate (added mass of 80 amu) attached to the active-site peptide.

Justification for the loss of both substituents can be made. The crystallography results indicate that the ethoxy group is lost through the aging process. Hydrolysis of dimethylamine from tabun is known to occur at low pH.[30] During preparation of peptides for positive-mode MALDI-TOF mass spectrometry, samples were routinely exposed to 0.1% TFA. Thus, loss of the dimethylamine could occur. The combination would have resulted in reduction of the tabun adduct to a phosphate adduct.

Confirmation of the identity of the 3010 amu mass was obtained by tandem mass spectrometry. Tryptic peptides from hBChE were infused into a QTrap 2000 tandem-quadrupole mass spectrometer. A mass equal to the quadruply charged form of the 3010 amu ion was observed at 753.4 *m/z*. This mass was subjected to collision-induced dissociation in the mass spectrometer. The resulting MSMS mass spectrum was consistent with that of the active-site peptide from hBChE (Figure 4).

The sequence of the active-site peptide is SVTLFGE**S**AGAASVSLHLLSPGSHSLFTR, where the bold-type S at position 8 is the serine that is expected to be labeled. A singly charged, y-ion series identical to the C-terminal portion of the active-site peptide, HLLSPGSHSL(FTR), was clearly defined in the MSMS spectrum. Singly charged fragments from the N-terminal were also found (a2 at 159.1 amu for SV minus CO, b2 at 187.2 amu for SV, b3 at 288.1 amu for SVT, and b3 minus water at 270.1 amu). Most convincing, however, were two doubly charged masses, at 437.3 and 501.4 *m/z*, which are consistent with phosphoserine fragments $b9^{2+}$ (SVTLFGE**S**A) and $b11^{2+}$ (SVTLFGE**S**AGA) that have lost 98 amu. Both fragments include the labeled serine. Loss of 98 amu from a phosphoserine is a commonly observed consequence of collision-induced dissociation. It represents loss of the phosphate (−80 amu) and transformation of the serine into dehydroalanine (−18 amu).

Thus, both the MALDI-TOF and tandem mass spectrometry results are consistent with the presence of a phosphoserine-containing, active-site peptide in the aged form of tabun-labeled hBChE. The most logical scenario to explain this species is loss of the ethoxy ligand through aging and loss of the dimethylamine ligand through acid-catalyzed hydrolysis during preparation of the sample for mass spectrometry. Only evidence of deamination was found in earlier mass spectrometry studies on human AChE.[14,15] This suggests that only the product of the acid-catalyzed deamination could be observed under those experimental conditions.

This analysis of aged tabun−hBChE utilizes an added mass of 80 amu for phosphate, which is the mass expected if natural abundance oxygen-16 is present for all of the oxygens on the phosphorus. If aging had involved release of the dimethylamine, then one of the phosphorus oxygens should have been derived from the $H_2{}^{18}O$ in the medium, making the added mass of the phosphate 82 amu. Similarly, if aging involved release of the ethoxy moiety via P−O bond cleavage, then the added mass would have been 82 amu. It follows that the added mass is consistent with elimination of the ethoxy moiety during aging via O−C bond cleavage.

**X-ray Structure of Non-aged Tabun-Inhibited hBChE.** Data were collected from tetragonal crystals of space group *I*422 and refined to 2.1 Å. Data and refinement statistics are shown in Table 1. There is no significant displacement of residue side chains compared to the native enzyme (PDB entry 1P0I). A strong peak of positive electronic density (19$\sigma$) within covalent bond distance of the catalytic serine was observed in the initial $|F_o| - |F_c|$ map. This confirms that inhibitor was bound to the active-site serine after 5 min of soaking. The structure was refined as a conjugate of the P(*R*) enantiomer of tabun (Figure 5A). The phosphorus atom is found at covalent bonding distance of 1.65 Å from the Ser198O$\gamma$ atom. O2 of the phosphoramidate moiety is at hydrogen-bonding distance from the main-chain amide nitrogen of residues forming the oxyanion hole, Gly116 (2.9 Å), Gly117 (2.8 Å), and Ala199 (2.9 Å). The ethoxy moiety is pointing toward the top of the active-site gorge, with O3 at hydrogen-bonding distance from His438N$\epsilon$2 (3.2 Å). The dimethylamino moiety is located in the acyl-binding pocket with the two methyl groups pointing toward the top of the gorge. Despite the fact that the P−N distance was refined to 1.8 Å, there is still a residual peak of positive density (4$\sigma$) above the two methyl groups. This density could correspond to low occupancy of the butyrate-like molecule that is always found in the native enzyme structure.[23] The C1 methyl group of the dimethylamine is interacting with Leu286C$\delta$2 and Phe398CZ (both at 3.5 Å) and the C2 methyl group is at 3.2 Å from Gly117C$\alpha$ and 3.8 Å from Trp231C$\epsilon$3. There is a peak of positive density in the initial $|F_o| - |F_c|$ map (5.4$\sigma$) close to Trp82 that could not be reasonably modeled. A similarly shaped density was found in the choline-binding pocket in several structures of native hBChE. In those structures, it was modeled as glycerol (1P0I or 1XLV).[10,23] This unknown ligand appears to be stacked against Trp82 and seems to interact with Glu197O$\epsilon$2, a water molecule from the cluster along Trp430 and Tyr440, and the water molecule H-bonded to Thr120.

**X-ray Structure of Aged Tabun-Inhibited hBChE.** Data were collected from a crystal of aged tabun-inhibited hBChE and were refined to 2.3 Å. A strong peak of positive electronic density

(30) Larsson, L. *Acta Chim Scand* **1958**, *12*, 783–785.

***Table 1.*** Data Collection and Refinement Statistics

| | tabun−hBChE | | tabun−mAChE | |
|---|---|---|---|---|
| | non-aged (3DJY) | aged (3DKK) | non-aged (3DL4) | aged (3DL7) |
| space group | *I*422 | *I*422 | *P*212121 | *P*212121 |
| unit cell axes, *a*, *b*, *c* (Å) | 156.58, 127.74 | 155.24, 127.47 | 79.62, 112.94, 226.16 | 79.02, 110.88, 226.38 |
| no. of measured reflections | 305 954 | 236 247 | n.d.[d] | n.d.[d] |
| unique reflections | 45 888 | 34 165 | 71 021 | 69 074 |
| resolution (Å) | 55.4−2.1 (2.2−2.1) | 28.2−2.3 (2.4−2.3) | 29.2−2.5 (2.6−2.5) | 29.0−2.5 (2.6−2.5) |
| completeness (%) | 99.0 (99.6) | 98.2 (93.0) | 99.6 (100.0) | 99.3 (99.0) |
| $R_{merge}$[a] (%) | 6.3 (50.5) | 6.6 (42.7) | 9.0 (59.0) | 7.0 (51.0) |
| $I/\sigma(I)$ | 22.0 (4.4) | 27.6 (5.1) | 14.4 (3.3) | 17.6 (7.5) |
| redundancy | 6.7 (7.0) | 6.9 (7.3) | 6.2 (6.2) | 7.4 (7.5) |
| Refinement Statistics | | | | |
| *R*-factor[b] (*R*-free[c]) | 21.2 (24.8) | 19.6 (24.6) | 19.6 (24.5) | 18.8 (22.7) |
| no. of atoms | | | | |
| protein | 4213 | 4192 | 8444 | 8403 |
| solvent | 285 | 275 | 133 | 439 |
| others | 154 | 154 | 168 | 72 |
| mean *B*-factor (Å$^2$) | 39.8 | 40.1 | 47.2 | 49.6 |
| rms from ideality | | | | |
| bond length (Å) | 0.017 | 0.022 | 0.014 | 0.013 |
| angles (deg) | 1.764 | 2.068 | 1.501 | 1.461 |
| chiral (Å$^3$) | 0.123 | 0.140 | 0.105 | 0.097 |

[a] $R_{merge} = (\sum|I - \langle I\rangle|)/\sum I$, where $I$ is the observed intensity and $\langle I\rangle$ is the average intensity obtained from multiple observations of symmetry-related reflections after rejections. [b] R-factor $= \sum||F_o| - |F_c||/\sum|F_o|$, where $F_o$ and $F_c$ are observed and calculated structure factors. [c] *R*-free set uses 5% of randomly chosen reflections defined by Brunger et al.[38] [d] Structure factors come from the PDB: 2C0Q (non-aged) and 2C0P (aged).

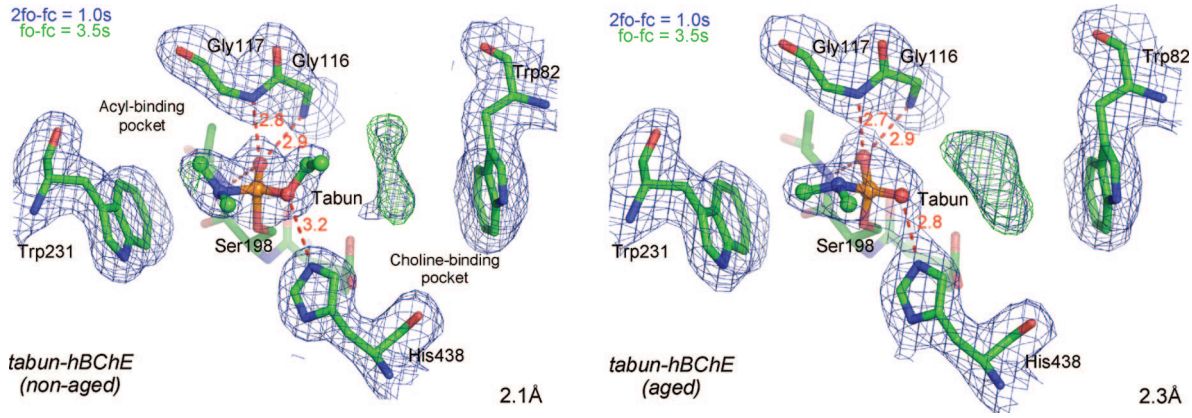


***Figure 5.*** Active site of non-aged and aged tabun−hBChE conjugates. Key residues are represented as sticks with carbon atoms in green, nitrogen atoms in blue, phosphorus in orange, and oxygen atoms in red. Hydrogen bonds are represented by red dashes. Electron density $2|F_o| - |F_c|$ is represented by a blue mesh, contoured at 1.0$\sigma$, and $|F_o| - |F_c|$ is represented by green/red mesh contoured at 3.5$\sigma$.

(13$\sigma$) within covalent bond distance of the catalytic serine in the initial $|F_o| - |F_c|$ map confirms the presence of the bound inhibitor. The refined structure clearly shows that aging proceeds through O-dealkylation of the P(*R*) enantiomer of tabun (Figure 5B). The phosphorus atom is found at a covalent bonding distance of 1.62 Å from the Ser198O$\gamma$ atom. O2 of the phosphoramidate moiety is at hydrogen-bonding distance from the main-chain amide nitrogens of the residues forming the oxyanion hole, Gly116 (2.9 Å), Gly117 (2.7 Å), and Ala199 (2.7 Å). As a result of the loss of the ethoxy substituent, the O3 moiety of the phosphorus is negatively charged and forms a strong salt bridge with His438N$\epsilon$2 (2.8 Å). The dimethylamino moiety is located in the acyl-binding pocket, but in contrast to the non-aged form, the two methyl groups point downward from Phe398. The C2 methyl group interacts with the indole ring of Trp231, about 3.5 Å from each aromatic carbon of the six-atom ring, while C1 is at least 3.7 Å from Phe398, Phe329, and Leu286. The P−N distance was refined to 1.7 Å. The peak of positive density that was close to Trp82 in the non-aged tabun−hBChE $|F_o| - |F_c|$ map is still present but is much stronger (9.1$\sigma$). It is likely that the occupancy of this ligand is higher because there is no steric hindrance from the ethoxy, and there is a possibility for stronger H-bond interactions with the negatively charged O3 of the phosphoramidate.

**Updated Refinement of Non-aged Tabun-Inhibited mAChE.** The original geometry of the aged and non-aged tabun moiety was based on calculations using the monomer library sketcher of the CCP4 program suite.[24] However, a careful examination of the crystal structure of non-aged tabun-inhibited mAChE reveals questionable geometry for the phosphoramidate adduct in both monomers (PDB code 2C0Q). For example, the N−P−Ser203O$\gamma$ angle was refined to 83°, which is at odds with the angle of 103° determined using the GROMOS96.1 force field analysis. The 103° value is in better agreement with the tetrahedral shape of the adduct. In addition, the P and N atoms and the two methyl groups were modeled as strictly coplanar, whereas molecular modeling based on GROMOS96.1 force field indicates an sp$^3$ orbital hybridization of N. However, quantum mechanics computation at the BP86/TZVP level indicates a hybridization of N between sp$^2$ and sp$^3$. This mixed hybridization is supported by two small-molecule structures in

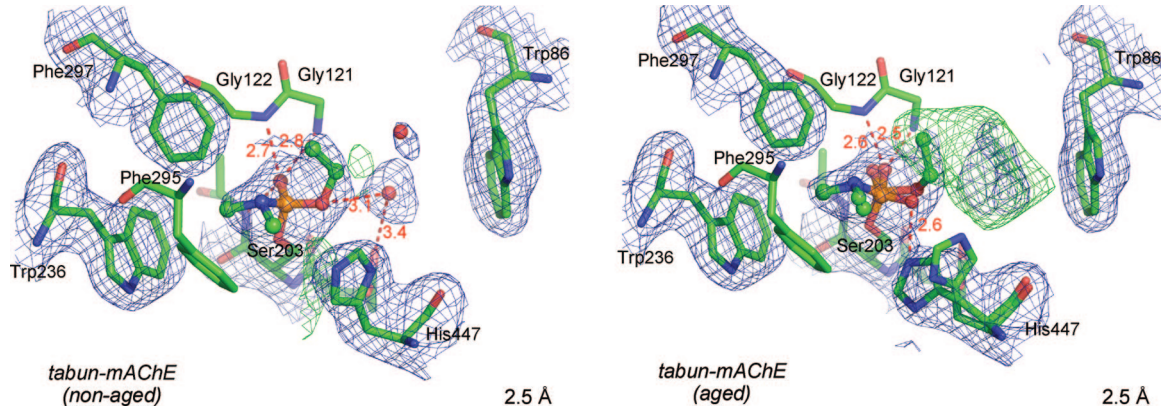


***Figure 6.*** Active site of non-aged and aged tabun−mAChE conjugates. Key residues are represented as sticks, with carbon atoms in green, nitrogen atoms in dark blue, phosphorus in orange, and oxygen atoms in red. Hydrogen bonds are represented by red dashes. Electron density $2|F_o| - |F_c|$ is represented by a blue mesh, contoured at $1.0\sigma$, and $|F_o| - |F|$ is represented by green/red mesh contoured at $3.5\sigma$.

the Cambridge Structural Database (QOQWOI[31] and ZEXBAF[32]) in which dimethylamino groups are attached to phosphorus. Because of these ambiguities, a new refinement was made using better constraints for tabun (Figure 6A).

In the new refinement, the methyl groups of the dimethylamine are pointing downward, in a conformation similar to that found in aged tabun-inhibited hBChE. The C2 methyl group interacts with Trp236C$\zeta$3 (3.5 Å) and Phe295C$\epsilon$1, whereas C1 is 3.4 Å from Phe295C$\zeta$. As previously reported, the imidazolium ring of His447 has shifted toward Phe338. There is a residual peak of density ($4.5\sigma$) in the $|F_o| - |F|$ map between Ser203 and Glu334 of both monomers that suggests some low-occupancy conformations of His447. Two water molecules were added to explain residual density close to Trp86 at the bottom of the gorge. The remainder of the gorge is apparently free of ligands. There is a noteworthy "blob" of density (up to $5.4\sigma$) close to Trp286, which indicates that the peripheral anionic site is occupied by an unknown ligand (data not shown).

**Updated Refinement of Aged Tabun-Inhibited mAChE.** In the original refinement (PDB code 2C0P), the modeled tabun−mAChE adduct underwent aging through displacement of the dimethylamine moiety from the acyl-binding pocket, while the ethoxy substituent was left intact in the choline-binding pocket, pointing toward the top of the gorge. The actual electronic density shows that the dimethylamine group is still attached to the phosphorus atom. While there is clearly some electron density in the $2|F_o| - |F|$ map corresponding to an ethoxy substituent in monomer A, there appears to be none in monomer B. In addition, a peak of positive density next to His447 in both monomers suggests that His447 may adopt an alternate conformation. There were large "blobs" of unexplained density in the $|F_o| - |F|$ map stretching from the peripheral site (Trp286) to the choline-binding site (Trp86), hinting that the whole gorge is occupied by unknown ligands. This material has perturbed the conformation of Tyr337. On the basis of these observations, it was concluded that an improved model should be built.

For monomer A, the presence of electronic density in the choline binding site indicated that the aged conjugate underwent incomplete dealkylation. Accordingly, both aged and non-aged forms of the tabun conjugates were included in the new model. They were assigned an occupancy of 0.5 each, based on *B*-factor values, though a large uncertainty exists on this ratio (Figure 6B). The position and the array of interactions in the non-aged tabun adduct in monomer A are similar to those in the non-aged structure of mAChE. In the aged form, the phosphorus atom is found at a covalent bonding distance of 1.6 Å from the Ser203O$\gamma$ atom. O2 of the phosphoramidate moiety is at hydrogen-bonding distance from the main-chain amide nitrogens of the residues forming the oxyanion hole, Gly121 (2.8 Å), Gly122 (2.6 Å), and Ala204 (2.8 Å). The dimethylamino moiety is still located in the acyl-binding pocket, with the two methyl groups pointing downward. The C2 methyl group is interacting with the indole ring of Trp236, CH2 (3.5 Å), whereas C1 is 3.5 Å from Phe295C$\zeta$ and 3.3 Å from Phe338C$\zeta$. The electron density of His447 is not clearly defined and was modeled as two conformers, despite features indicating that there is more likely a continuum of conformations between the two average positions. In the first conformer, His447N$\epsilon$2 forms a salt bridge with O3 of the phosphorus (2.6 Å), and His447N$\delta$1 is strongly H-bonded to Glu334O$\epsilon$1 (2.5 Å). The second conformer is similar to the conformation of the non-aged conjugate. These two models highlight the fact that dealkylation is accompanied by a shift of the phosphoramidate moiety toward His447N$\epsilon$2 (0.7 Å shift for O3). In addition, nearby residues Tyr337 and Phe338 are extremely perturbed. Their side chains were refined to occupancies of 0.6 and 0.8, respectively. The perturbation of the Tyr337 conformation, in particular, appears to be related to the presence of an unknown ligand close to Trp86. This is indicated by the strong unexplained positive electron density in the $|F_o| - |F|$ map (peak at $8.8\sigma$). We tried to fit this electron density to (1) components of the crystallization buffer, polyethylene glycol monomethyl ether 750, HEPES; and (2) procainamide, the ligand that was used for the last affinity chromatography purification step,[16] without success.

For monomer B, at first sight the weak electron density for the ethyl substituent suggested that complete dealkylation of the conjugate had occurred. However, it became apparent during the refinement process that the weak residual density was better explained by modeling both aged and non-aged forms of the tabun adduct into the structure. For example, when the adduct was modeled solely as the aged form, a peak of positive density in the $|F_o| - |F|$ map developed between His447N$\epsilon$2 and O3. This indicated that the refinement software was placing O3 too far away from the imidazolium. This would arise if the software was trying to fit density corresponding to trace amounts

(31) Gholivand, K.; Tadjarodi, A.; Taeb, A.; Garivani, G.; Ng, S. W. *Acta Crystallogr.* **2001**, *E57*, o472–o473.
(32) Shih, Y.-E.; Wang, F.-C.; Maa, S.-H.; Liu, L.-K. *Bull. Inst. Chem. Acad. Sin.* **1994**, *41*, 9.

of the ethoxy substituent. Accordingly, models for both the aged and non-aged forms of the tabun adduct were refined into the structure with occupancies of 0.6 and 0.4, respectively. This ratio was based on a *B*-factor value of about 41 Å$^2$. The position and the array of interactions in the non-aged and aged tabun adducts are similar to those in monomer A: the two methyl groups point downward and make contacts with Trp236, Phe295, and Phe338, and there is a slight shift of the phosphoramidate toward His447NE2 (0.6 Å for O3). His447 is again perturbed and, consequently, is modeled as two alternate conformations displaying average positions like those in monomer A. Nearby residues, Phe338 and Tyr337, are extremely perturbed and were refined with partial occupancy. This perturbation, at least that of Tyr337, is related to the presence of an unknown ligand in the active site, which is indicated by strong positive peaks in the $|F_o| - |F|$ maps ($7.2\sigma$).

## Discussion

The kinetics for inhibition of hBChE and hAChE by tabun show that both enzymes are enantioselective. This is in agreement with a previous study showing that (−)-tabun reacts about 6.3 times faster than (+)-tabun with electric eel AChE.[33] However, for hBChE and hAChE, the enantioselectivity may be larger than 1 order of magnitude.

Assuming in-line substitution, the X-ray structure of non-aged tabun−hBChE reveals that the enzyme is mainly inhibited by P(*R*)-tabun with the dimethylamine group located in the acyl-binding pocket. Stereoselectivity may result from preferred H-bonding of His438 to the ethoxy substituent and interaction of Trp231 with the dimethylamine moiety. The same considerations apply for the structure of non-aged tabun−mAChE,[16] the refinement of which was improved in the present study. The X-ray structure of aged tabun−hBChE also showed enantioselectivity for P(*R*)-tabun; i.e., the electron density shows that the dimethylamine moiety is located in the acyl-binding pocket. The same enantioselectivity was found in the updated refinements of aged tabun−mAChE and from the structure of aged tabun−TcAChE.[34] These observations provide structural evidence that there is a selectivity of cholinesterases for the P(*R*) enantiomer of tabun. This has important implications for the aging pathway. Combining the enantioselectivity results from the solution kinetics with those from the X-ray crystal structures suggests that (−)-tabun is P(*R*)-tabun.

The first X-ray structure of an aged tabun−cholinesterase was made with mouse AChE (PDB code 2C0P).[16] This structure was determined following 4 weeks of aging, which, with an aging half-time of a few hours, should have been sufficient to complete the reaction. Still, an incomplete dealkylation led to an adduct model with the ethoxy group present in the choline-binding pocket and the *N*-dimethyl group substituted by hydroxyl.

That model implied that aging occurs through nucleophilic attack by water on the P−N bond and subsequent scission of that bond. However, the conformation of the adduct in the active site was peculiar. First, the oxygen arising from loss of the dimethylamine was located in the acyl-binding pocket with no possibility for stabilization through formation of a salt bridge. Previous structural data for aged AChEs indicated that the phosphorus oxygen resulting from aging was stabilized by formation of a salt bridge with His447.[9,10,23,34,35] Second, there were no groups in the acyl pocket that could promote aging. It is generally accepted that the active site of cholinesterase accelerates the aging process. This acceleration is generally thought to involve the histidine from the catalytic triad and the tryptophan from the choline-binding pocket. If the aging process for tabun required similar assistance, the dimethylamine moiety would have been located in the choline-binding pocket. Since the de-dimethylamidated moiety was located in the acyl-binding pocket in the mAChE model, there would have been a rearrangement of the substituents around the phosphorus after aging. Such motions are doubtful in a constrained active-site pocket like that of mAChE. All of these factors suggest that the aged tabun−mAChE model requires refinement.

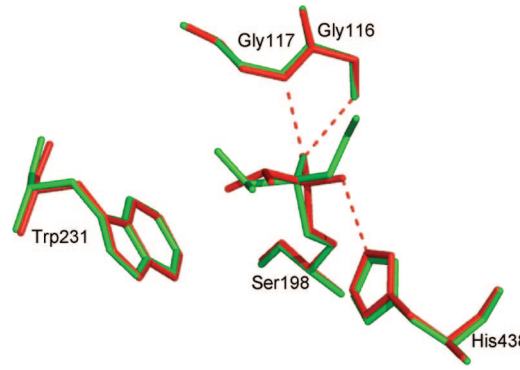


***Figure 7.*** Superimposition of active sites of the non-aged (green) and aged (red) tabun−hBChE conjugates.

The new model for aged tabun−mAChE shows unambiguously that the ethoxy substituent underwent dealkylation. The X-ray structure of aged tabun−hBChE and the structure of aged tabun−TcAChE[34] both support this interpretation. The negatively charged phosphoryl oxygen that results from aging forms a salt bridge with the catalytic imidazolium in each case. There is no doubt that aging of these three phosphoramidated cholinesterases proceeds through the classic aging pathway worked out for phosphonylated human AChE.[10,22,35,36] In that mechanism, the imidazolium stabilizes a developing negative charge on the $C-O^{\delta-}$ oxygen, and a water molecule activated by Glu202 (197 in hBChE) attacks the carbocationic center that appears on the $C^{\delta+}-O$ carbon, thus leading to scission of the C−O bond, release of the alkoxy moiety, and subsequent formation of the salt bridge between the phosphorus O3-oxygen and the imidazolium.

This mechanism can be extended to tabun−hAChE via the following logical argument. Knowing that (1) dealkylation of tabun−ChE conjugates occurs in three different ChEs, (2) residues lining the active-site gorge of mAChE and hAChE are identical, and (3) hAChE is enantioselective for tabun stereoisomers, we can reasonably state that aging of tabun−hAChE proceeds through dealkylation of the ethoxy substituent.

The formation of the salt bridge between the phosphorus O3-oxygen and the imidazolium of His438 in aged tabun−hBChE induces a small rearrangement of the phosphoramidyl-serine, while the active-site residues, notably His438, do not move (Figure 7). His438 is stabilized by a strong hydrogen bond with

(33) Degenhardt, C.; Van Den Berg, G.; De Jong, L.; Benschop, H. *J. Am. Chem. Soc.* **1986**, *108*, 8290–8291.
(34) Millard, C. B.; Olson, M. A.; Carlacci, L.; Ordentlich, A.; Barak, D.; Shafferman, A.; Silman, I.; Sussman, J. L. Presented at the International Meeting on Cholinesterases, Perugia, Italy, Sept 26−30, 2004.
(35) Millard, C.; Koellner, G.; Ordentlich, A.; Shafferman, A.; Silman, I.; Sussman, J. L. *J. Am. Chem. Soc.* **1999**, *121*, 9883–9884.
(36) Shafferman, A.; Ordentlich, A.; Barak, D.; Stein, D.; Ariel, N.; Velan, B. *Biochem. J.* **1997**, *324*, 996–998 (Pt 3)

Glu335 and interactions with Phe398 that restrict its mobility (data not shown). The phosphoramidate moiety has to tilt toward His438N$\epsilon$2 in order to promote formation of the salt bridge. There is also a significant reinforcement of the interactions between the phosphoryl oxygen and the oxyanion hole in the aged form of tabun−hBChE. This is likely related to an increase in electron density in the oxyanion hole oxygen linked to the delocalization of the new negative charge on the phosphorus O2-oxygen. Similar observations were made during the aging of soman−hBChE (Weik, M., personal communication) and echothiophate−hBChE.[10] These features, taken together, are thought to raise the activation energy needed for the dephosphylation reaction, thus rendering oxime-mediated reactivation virtually impossible after aging.

Interestingly, as a result of aging, the phosphoramidate tilts so that the dimethylamine moiety is less constrained and the two methyls point toward Trp231 to better fill in the acyl-binding pocket.

By contrast to hBChE, the catalytic histidine of AChEs (His447 in hAChE) is mobile. This was shown in NMR studies of the short strong hydrogen bond of aged TcAChE[37] and in crystal structure studies on non-aged VX−TcAChE.[35] It was suggested that this mobility was related to the lack of aromatic trapping.[38] Indeed, AChEs lack the aromatic residue equivalent to Phe398 in hBChE that provides stabilization for His438. A valine is found at the equivalent position in mAChE, hAChE, and TcAChE. The mobility of His447 is again illustrated in non-aged tabun−mAChE, as described by Ekstrom et al.[16] and reaffirmed in the present study. His447 and Phe338 shift in concert to avoid unfavorable contacts with the phosphoramidate moiety. Surprisingly, His447 adopts a continuum of conformations in the aged form. This was unexpected because the dealkylation and subsequent formation of a salt bridge normally releases the steric constraints on His447 and stabilizes the imidazolium into a well-defined conformation. The continuum of conformations could be due to the partial dealkylation, and to the coexistence of non-aged and aged conformations (Figure 8). The presence of an unknown ligand interfering with Tyr337 and indirectly with Phe338 might also contribute to the conformation disturbance of His447. Despite the conformational heterogeneity, the phosphoramidate moiety tips slightly toward His437 when the His occupies its usual triad position. This leads to formation of the salt bridge as observed in other aged AChE-OP conjugates.[9,35]

Nonaged cholinesterases inhibited by tabun are known to be resistant to most oxime reactivators.[6] It is acknowledged that oximes based on pyridinium aldoxime like HI-6 are too bulky to achieve a favorable orientation of the reactive group in the narrow active site of hAChE.[39−41] A smaller nucleophile capable of slipping in between the aromatic residues would be highly desirable to improve the efficiency of oxime reactivators. However, limited accessibility of the active site might not be the sole cause for the poor reactivation of tabun−ChE conjugates. The reactivation rate for tabun−hBChE is slow despite the fact that the active site is wide. This suggests that reactivation might be limited by the chemistry of the reaction. Partial delocalization of electron density from the nitrogen lone pair in the P−N bond on the phosphorus atom could reduce its electrophilicity, making it less susceptible to nucleophiles. Quantum mechanics/molecular mechanics (QM/MM) studies of the reactivation reaction based on tabun−mAChE and tabun−hBChE X-ray structures could clarify this point.

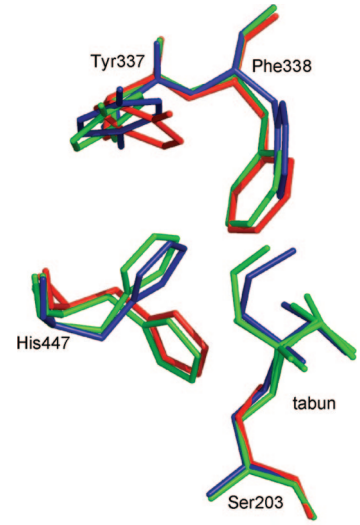


***Figure 8.*** Superimposition of active sites of apo (red), non-aged (blue), and aged (green; two conformations, reflecting partial dealkylation of the tabun, are shown) tabun−mAChE conjugates. This figure highlights the conformational heterogeneity of His447, Tyr337, and Phe338.

Finally, the X-ray structures of tabun−ChEs provide a template on which to design mutants of human cholinesterases that can spontaneously and more efficiently reactivate from OP inhibition. G117H hBChE[42] is a model for such mutations, but more efficient variants are needed. The mutagenesis strategy based on computational design (QM/MM) that was successfully implemented for designing a mutant of hBChE with improved cocaine hydrolase activity[43] could be applied to the design of more active hBChE mutants capable of hydrolyzing OPs.

Efficient BChE-based catalytic bioscavengers would provide a great improvement in prophylaxis, decontamination, and treatment of organophosphate poisoning.

**Acknowledgment.** This work was supported by DGA grant 03co10-05/PEA 01 08 7 to P.M. and by DGA/PEA 08co501 and ANR-06-BLAN-0163 to F.N.

JA804941Z

(37) Massiah, M. A.; Viragh, C.; Reddy, P. M.; Kovach, I. M.; Johnson, J.; Rosenberry, T. L.; Mildvan, A. S. *Biochemistry* **2001**, *40*, 5682–5690.
(38) Kaplan, D.; Barak, D.; Ordentlich, A.; Kronman, C.; Velan, B.; Shafferman, A. *Biochemistry* **2004**, *43*, 3129–3136.
(39) Wong, L.; Radic, Z.; Bruggemann, R. J.; Hosea, N.; Berman, H. A.; Taylor, P. *Biochemistry* **2000**, *39*, 5750–5757.
(40) Kovarik, Z.; Radic, Z.; Berman, H. A.; Simeon-Rudolf, V.; Reiner, E.; Taylor, P. *Biochemistry* **2004**, *43*, 3222–3229.
(41) Luo, C.; Leader, H.; Radic, Z.; Maxwell, D. M.; Taylor, P.; Doctor, B. P.; Saxena, A. *Biochem. Pharmacol.* **2003**, *66*, 387–392.
(42) Millard, C. B.; Lockridge, O.; Broomfield, C. A. *Biochemistry* **1995**, *34*, 15925–15933.
(43) Pan, Y.; Gao, D.; Yang, W.; Cho, H.; Yang, G.; Tai, H. H.; Zhan, C. G. *Proc. Natl. Acad. Sci. U.S.A.* **2005**, *102*, 16656–16661.

# Structural Evidence That Human Acetylcholinesterase Inhibited by Tabun Ages through O-Dealkylation

E. Carletti, J-P Colletier, F. Dupeux, M. Trovaslet, P. Masson,

**F. Nachon***

Journal of Medicinal Chemistry 53 (2010) 4002-4008

4002 J. Med. Chem. 2010, 53, 4002–4008
DOI: 10.1021/jm901853b

Journal of Medicinal Chemistry Article

# Structural Evidence That Human Acetylcholinesterase Inhibited by Tabun Ages through O-Dealkylation†

Eugénie Carletti,‡,§ Jacques-Philippe Colletier,‡ Florine Dupeux,∥ Marie Trovaslet,§ Patrick Masson,‡,§ and Florian Nachon*,§

‡Laboratoire de Biophysique Moléculaire, Institut de Biologie Structurale (CEA-CNRS-UJF), 41 rue Jules Horowitz, 38027 Grenoble, France, §Département de Toxicologie, Centre de Recherches du Service de Santé des Armées (CRSSA), 24 av des Maquis du Grésivaudan, 38700 La Tronche, France, and ∥European Molecular Biology Laboratory, Grenoble Outstation Polygon Scientific, 6 rue Jules Horowitz, 38000 Grenoble, France

Received December 15, 2009

Tabun is a warfare agent that inhibits human acetylcholinesterase (hAChE) by rapid phosphylation of the catalytic serine. A time-dependent reaction occurs on the tabun adduct, leading to an "aged" enzyme, resistant to oxime reactivators. The aging reaction may proceed via either dealkylation or deamidation, depending on the stereochemistry of the phosphoramidyl adduct. We solved the X-ray structure of aged tabun−hAChE complexed with fasciculin II, and we show that aging proceeds through O-dealkylation, in agreement with the aging mechanism that we determined for tabun-inhibited human butyrylcholinesterase and mouse acetylcholinesterase. Noteworthy, aging and binding of fasciculin II lead to an improved thermostability, resulting from additional stabilizing interactions between the two subdomains that face each other across the active site gorge. This first structure of hAChE inhibited by a nerve agent provides structural insight into the inhibition and aging mechanisms and a structural template for the design of molecules capable of reactivating aged hAChE.

## Introduction

Acetylcholinesterase (AChE;[a] EC 3.1.1.7) is the target of numerous natural and synthetic inhibitors, for example, fasciculin, a polypeptide neurotoxin found in mamba snake venom;[1] therapeutic drugs, in particular the first generation of anti-Alzheimer drugs;[2] and a wide range of toxic esters, including organophosphate (OP) pesticides and nerve agents.[3] AChE regulates cholinergic transmission in the peripheral and central nervous systems by hydrolyzing acetylcholine (ACh) with a high catalytic efficiency. Although butyrylcholinesterase (BChE; EC 3.1.1.8), a closely related enzyme, is present in numerous vertebrate tissues, its physiological role remains unclear.[4] While BChE inhibition appears harmless, AChE inhibition results in accumulation of ACh at neuronal synapses and neuromuscular junctions and results in paralysis, seizures, and other symptoms of cholinergic syndrome.[5,6]

The AChE catalytic site, featuring a Ser203−His447−Glu334 triad [residue numbering refers to human AChE (hAChE) throughout the manuscript, unless stated otherwise], is at the bottom of a deep and narrow gorge[7] (Figure 1). AChE inhibition can result from binding either to the gorge entrance, called the "peripheral anionic site" (PAS) (viz. fasciculin), or to the active site (viz. OP). Inhibition of human AChE by OP compounds involves phosphylation of the catalytic serine and leads to the formation of stable inactive phosphyl−AChE adducts. Within the active site, substantial contributions to the stabilization of bound OP within the active site arises from hydrogen bonding of the phosphyl oxygen within the oxyanion hole, viz. Gly121, Gly122, and Ala204, and one of its substituents in the "acyl pocket", viz. Trp236, Phe295, Phe297, and Phe338. Reaction of OP−hAChE conjugates with oxime antidotes can restore the function of the inhibited enzyme. The efficiency of the reactivation reaction depends on several factors, notably the chemical structures of OPs and reactivators and the topography of the AChE active center.[8]

Following phosphylation, a time-dependent elimination reaction occurs on the OP−ChE conjugate that leads to a so-called "aged" enzyme. This reaction can proceed either via dealkylation or deamidation of the phosphorus conjugate, depending on the OP structure.[9−12] The aging reaction results in a very stable anionic conjugate that is resistant to oxime reactivation. Crystal structures of aged phosphyl−AChE conjugates have been produced for *Torpedo califonica* and mouse enzymes inhibited by soman, sarin, tabun, VX, fenamiphos, and diisopropyl fluorophosphate (DFP).[13−19]

Inhibition of hAChE by tabun and the subsequent aging reaction are of particular interest; the conjugate indeed displays an extraordinary resistance toward most oxime reactivators.[20] On the basis of a mass spectrometry (MS) analysis of aged products of tabun-inhibited hAChE, it was suggested that the aging mechanism of tabun−AChE conjugate involved deamination of the phosphoramidate moiety.[4,21] A first crystallographic study on mouse AChE (mAChE) seemed to support a deamination-based aging mechanism,

†The atomic coordinates and structure factors (code 2X8B) have been deposited in the RCSB Protein Data Bank (www.rcsb.org).

*To whom correspondence should be addressed. Tel: +33476639765. Fax: +33476636962. E-mail: florian@nachon.net.

[a]Abbreviations: ACh, acetylcholine; AChE, acetylcholinesterase; BChE, butyrylcholinesterase; ChE, cholinesterase; CHO, Chinese hamster ovary; FAS-II, fasciculin-II; HEPES, *N*-2-hydroxyethylpiperazine-*N*-2-ethanesulfonic acid; hAChE, human AChE; mAChE, mouse AChE; OP, organophosphate; PAS, peripheral anionic site; *Tc*AChE, *Torpedo californica* AChE; $T_m$, melting temperature.

 Published on Web 04/21/2010 

but incomplete aging blurred the interpretation.[22] However, a recent MS study of tabun-inhibited human BChE (hBChE) peptide fragments showed that the loss of the dimethylamine substituent is rather an acid-catalyzed hydrolysis, which occurs during preparation of MS samples,[16] leading to uncertainties on the tabun aging mechanism.

Crystallographic studies on hBChE inhibited by tabun and reinterpretation of mAChE data were at the time undertaken and evidenced that aging of these ChEs proceeds through dealkylation of the ethoxy group.[16] According to the proposed mechanism, the His447 imidazolium stabilizes a developing negative charge on the C−$O^{\delta-}$ oxygen of the ethoxy substituent of the tabun−ChE conjugate, thus polarizing and weakening the C−O bond. Then, a water molecule, stabilized by Glu202, assists the bond breakage by trapping the short-lived developing carbocationic center on the $C^{\delta+}$−O carbon (Scheme 1). This role of water during the dealkylation of an ethoxy substituent was originally suggested by a crystallographic study of hBChE inhibited by echothiophate.[23] However, aging of the tabun−mAChE conjugate was incomplete in the earlier crystallographic studies, complicating the interpretation of the electron density maps. A crystal structure of fully aged tabun-inhibited AChE was needed, especially that of hAChE.

Crystallization of hAChE requires that it is complexed with fasciculin-II (FAS-II), a three-fingered toxin.[24] FAS-II binds tightly to AChE PAS[1] and promotes crystal contacts.[25] The hAChE/FAS complex is reminiscent of the complexes form by FAS with mAChE[26] and *T. californica* AChE (*Tc*AChE).[27] The main feature of the complexes is a sulfur−$\pi$ interaction between Met33 from FAS-II and Trp286 (Trp279 in *Tc*AChE) at the rim of the active site gorge (Figure 1). The toxin completely caps the gorge entrance (interacting surface: 1045 Å$^2$), thereby preventing access to the active site. The interaction surface involves all conserved structural elements that constitute the gorge, viz. the Ω loop (C69−C96), the PAS, the acyl loop (W286−S298), and helix 334−341.

To conclude on the aging pathway of tabun-inhibited hAChE, we undertook its crystal structure determination following formation of the aged conjugate in solution. Effects of FAS-II and tabun aging on hAChE thermal denaturation were also investigated and drew insights into the stabilization mechanism in hAChE; our results indicate that the interaction of the two subdomains that face one another across the active site gorge is the main contributor to AChE resilience.

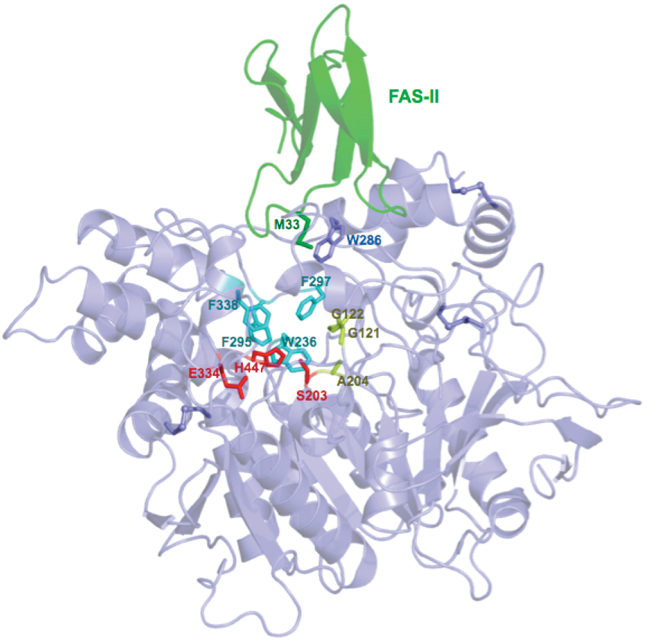


**Figure 1.** Overview of hAChE/FAS-II complex. hAChE (blue) and fasciculin (green) are represented by cartoons. Key residues are represented as sticks with the catalytic triad in red, the acyl-binding pocket in cyan, and the oxyanion hole in yellow.

## Materials and Methods

Racemic tabun solution (2 mg/mL) in isopropanol was from CEB (Vert-le-Petit, France). FAS-II from *Bungarus* venom was purchased from Latoxan (Valence, France). Tabun is a highly toxic chemical warfare agent that belongs to schedule 1 Chemicals (Chemical Weapons Convention). All works with tabun are regulated by the convention. Handling of tabun is dangerous and requires trained personal protection and secured facilities.

**Production of Recombinant hAChE.** The full cDNA of hAChE was inserted into pGS vector carrying the Glutamine Synthetase gene marker and expressed in Chinese hamster ovary (CHO)-K1 cells. The cells were maintained in serum-free Ultraculture Medium (BioWhittaker) and transfected using DNA−calcium phosphate coprecipitation. Transfected clones were selected by incubation in media containing methionine sulfoximide. The enzyme, secreted into the culture medium, was purified by affinity chromatography and ion-exchange chromatography as described previously.[16] The enzyme was concentrated to 15 mg/mL using a Centricon-30 ultrafiltration microconcentrator (30000 MW cutoff, from Amicon). The enzyme concentration was determined from its absorbance at 280 nm using a molar extinction coefficient of 1.7 for 1 mg/mL of protein.[28]

**Melting Temperature ($T_m$) Determination.** The fluorescent dye "Sypro-orange" is sensitive to the polarity of its environment and thus can be used to monitor protein unfolding. Unfolding results in exposure of protein hydrophobic regions, to which the dye binds; this leads to a large increase in fluorescence intensity of dye upon binding.[29] Each hAChE complex (free hAChE, aged tabun−hAChE, hAChE/FAS-II, and aged tabun−hAChE/FAS-II) was diluted to a final concentration of 5 $\mu$M in a solution containing 20 mM *N*-2-hydroxyethylpiperazine-*N*-2-ethanesulfonic acid (HEPES), pH 7.5, 0.15 M NaCl, and 0.15 mM Sypro Orange (Molecular Probes). Samples were brought from 25 to 95 °C at a heating rate of 1 °C/min in a real-time PCR machine (Stratagene Mx3005P; accuracy, ±0.25 °C).

**Scheme 1.** Tabun Inhibition Mechanism on ChEs and Subsequent Aging Mechanism

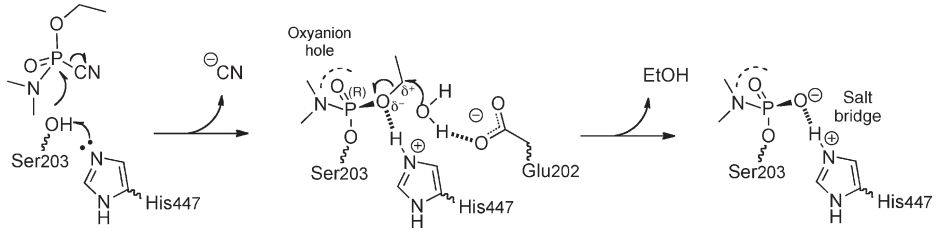

Protein unfolding was monitored through the increase in fluorescence of the Sypro Orange probe and was recorded every minute using the Sybr-Green parameters (wavelength excitation/emission: 492/516 nm). The fluorescence intensity change rate ($dF/dT$) was plotted as a function of temperature and then normalized. The $T_m$, corresponding to the temperature at the inflection point, that is, the midtransition of unfolding, was estimated through a nonlinear fit.

**Crystallization of Aged Tabun−hAChE Conjugate Complexed with FAS-II.** Purified hAChE (0.1 mM) was inhibited in solution, in the presence of 1 mM tabun in 10 mM HEPES buffer, pH 7.4. The reaction mixture was incubated for 1 h at 4 °C. The inhibited enzyme was then combined with FAS-II (0.2 mM) in 10 mM HEPES buffer, pH 7.4, as described.[25] The ternary complex was crystallized at a concentration of 0.1 mM, using the hanging drop method. The mother liquor solution was 0.1 M HEPES buffer, pH 7.4, and 1.3 M ammonium sulfate. An equal amount of the protein and the mother liquor were mixed to yield a 3 $\mu$L drop. Crystals grew within a week at 10 °C. The crystals were transferred to a cryoprotecting solution (0.1 M HEPES buffer, pH 7.4, 1.6 M ammonium sulfate, and 18% glycerol) for few seconds before they were flash cooled in liquid nitrogen. The time span between tabun phosphylation of hAChE and flash cooling was > 2 weeks and thus was sufficient for completion of the aging reaction.

**X-ray Data Collection, Structure Determination, and Refinement of Tabun−hAChE/FAS-II Conjugate.** Diffraction data were collected at the European Synchrotron Radiation Facility (ESRF, Grenoble) on beamline ID14-eh1, at a wavelength of 0.933 Å. Data sets were processed with XDS.[30] The structure was solved by molecular replacement with Phaser,[31] using a starting model of the structure of recombinant hAChE in complex with FAS-II (PDB code: 1B41) without ligands, carbohydrates, and waters. The model was refined using REFMAC5[32] and PHENIX.[33] Iterative cycles of model building were performed with Coot.[34] Ligand descriptions were generated by the PRODRG2.5 server (http://davapc1.bioch.dundee.ac.uk/prodrg/).[35] TLS refinement was performed and yielded significant decreases in $R_{cryst}$ and $R_{free}$ values. TLS groups were defined using the TLSMD server (http://skuld.bmsc.washington.edu/~tlsmd/index.html).[36] A SA composite omit map was calculated, allowing to decrease bias from the model. Protein structures were illustrated using the program PyMOL (http://www.pymol.org).[37]

## Results and Discussion

**Aged Tabun−hAChE Structure and Inferred Aging Mechanisms.** hAChE was inhibited and aged in solution, thus avoiding any possible bias that could arise from inhibition and aging in crystallo. Cocrystals of the aged tabun−hAChE/FAS-II complex diffracted to 2.95 Å. Data and refinement statistics are shown in Table 1. The structure is globally similar to the native hAChE/FAS-II complex (PDB code: 1B41; rmsd = 0.3 Å). Despite expression of the full-length enzyme, residues after 543 are not defined in the electron density maps. Surface loop residues 259−264 are not visible, but external loop residues 493−494, which were not seen in the original structure (PDB code: 1B41), could be modeled.

In the experimental $|F_o| - |F_c|$ map, a strong positive peak is observed (11.7$\sigma$) at covalent bonding distance of the catalytic Ser203 hydroxyl oxygen (distance, 1.6 Å), a signature for the phosphorus atom of the tabun adduct. The structure was unambiguously refined as a *N*,*N*-dimethylphosphoramidyl adduct, indicating that the aged adduct results from the dealkylation of tabun P(R) enantiomer (Figure 2). This is faithfully in agreement with the aging mechanism described for tabun-inhibited hBChE and mAChE.[16] The dimethylamino substituent is located in the acyl-binding pocket, with its methyl groups interacting with Trp236 and Phe338 aromatic rings (closest distance between carbon atoms, 3.5 Å to Trp236CZ and Phe338CZ). The oxygen O2 of the phosphoramidate moiety is H-bonded to the main chain nitrogens of the three constituents of the oxyanion hole, viz. Gly121 (2.5 Å), Gly122 (2.7 Å), and Ala204 (3.0 Å). Another strong positive peak is observed in the initial $|F_o| - |F_c|$ map, in the vicinity of Trp86 (5.4$\sigma$). We were not able to correctly model this density, but the electron-rich microenvironment provided by the phosphoramidate oxyanion O3, Glu202, and the $\pi$-system of Trp86 suggests that it is a positively charged molecule, eventually a weakly coordinated cation. X-ray fluorescence spectra indicate the presence of zinc in the crystals, eventually coming from the plasticware used in the crystallization setup. However, an anomalous map did not confirm the of presence zinc in the active site.

It was already shown that hAChE reacts preferably with one enantiomer of tabun,[16] in accordance with earlier measurements showing that (−)-tabun reacts 6.3 times faster than (+)-tabun with electric eel AChE.[38] However, the absolute configuration of (−)-tabun is unknown. Although the absolute configuration of the nonaged hAChE conjugate can be predicted from the crystal structure, we cannot ascertain which of the two enantiomers is preferred without making assumptions as per the inhibition mechanism. It is

**Table 1.** Data Collection and Refinement Statistics

| data | aged tabun−hAChE/FAS-II PDB code: 2X8B |
|---|---|
| space group | *H*32 |
| unit cell axes, *a*, *b*, *c* (Å) | 151.31, 247.24 |
| no. of measured reflections | 206989 |
| unique reflections | 22948 |
| resolution (Å) | 46.3−2.95 (3.0−2.95) |
| completeness (%) | 98.2 (98.8) |
| *R*sym (%)[a] | 8.2 (66.7) |
| $I/\acute{o}(I)$ | 25.0 (3.5) |
| redundancy | 7.2 (7.0) |
| refinement statistics | |
| *R*-factor[b] (*R*-free[c]) | 18.3 (25.3) |
| no. of atoms | |
| protein | 4 655 |
| water | 235 |
| ligands | 47 |
| Wilson *B*-factor (Å$^2$) | 61.3 |
| average *B*-factor (Å$^2$) | |
| protein | 59.5 |
| water | 105.4 |
| ligands | 72.7 |
| Ramachandran statistics (%) | |
| core | 84.2 |
| allowed regions | 14.1 |
| generously allowed region | 0.8 |
| disallowed regions | 0.8 |
| rms from ideality | |
| bond length (Å) | 0.006 |
| angles (deg) | 0.999 |
| chiral (Å$^3$) | 0.066 |

[a] $R_{sym} = (\Sigma|I - \langle I\rangle|)/\Sigma I$, where $I$ is the observed intensity and $\langle I\rangle$ is the average intensity obtained from multiple observations of symmetry-related reflections after rejections. [b] *R* factor $= \Sigma||F_o| - |F_c||/\Sigma|F_o|$, where $F_o$ and $F_c$ are observed and calculated structure factors. [c] *R*-free set uses 5% of randomly chosen reflections.

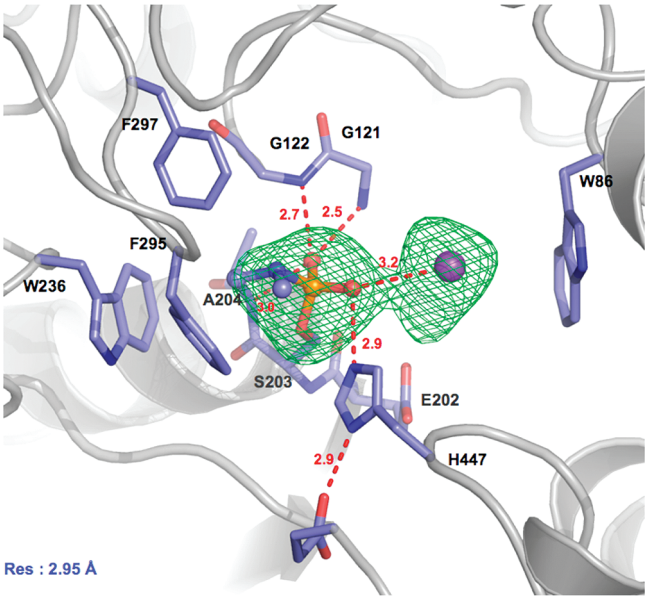


**Figure 2.** Active site of aged tabun−hAChE/FAS-II conjugate. Key residues are represented as sticks with carbon atoms in blue, nitrogen atoms in deep blue, the phosphorus atom in orange, and oxygen atoms in red. Hydrogen bonds are represented by red dashes. The electron density $|F_o| - |F_c|$ omit map is represented by green mesh contoured at $3\sigma$. The blob of electron density between Trp86 and the phosphyl moiety was interpreted as a disordered cation interacting with the $\pi$-system of Trp86, the phosphyl oxyanion, and the negatively charged Glu202 residue.

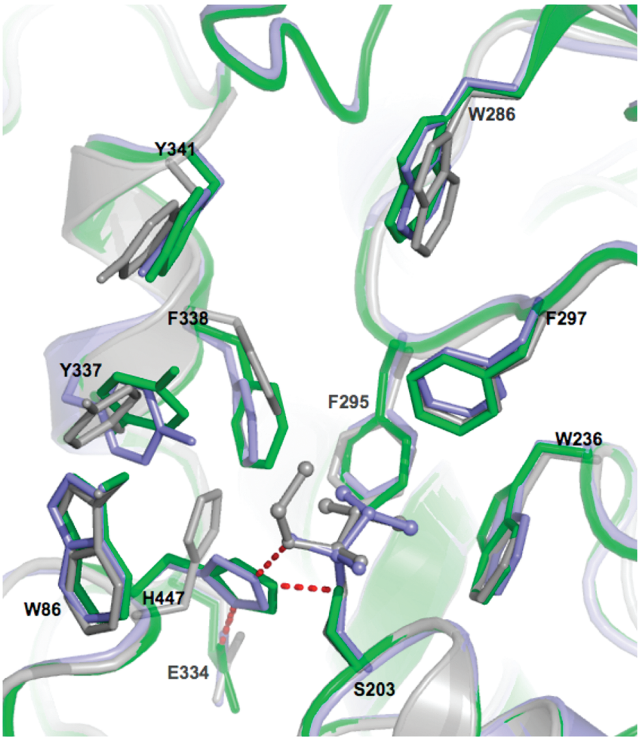


**Figure 3.** Superimposition of X-ray structures of hAChE/FAS-II in green (1B41), nonaged tabun−mAChE in gray (3DL4), and aged tabun−hAChE/FAS-II in blue (2X8B).

usually assumed that phosphylation occurs "in-line", that is, with the leaving group (CN) oriented opposite to the catalytic serine.[39] According to this mechanism, (*R*)-tabun reacts with hAChE to form the observed P(R) ethyl *N*,*N*-dimethylphosphoramidyl adduct. However, a recent QM/MM study reported that the "in-line" reaction is energetically less favorable than that which would occur if the departing group were adjacent to the catalytic serine.[40] In this proposed mechanism, (*S*)-tabun enatiomer should react with hAChE to form the observed P(R) ethyl *N*,*N*-dimethylphosphoramidyl adduct. This hypothesis is supported by the phosphylation mechanism of optically active dioxaphosphadecalins.[41] Its confirmation will require determination of the absolute configuration of (±)-tabun and crystallographic studies of hAChE inhibited by the pure tabun enantiomers.

**Comparison of Free- and Tabun-Inhibited hAChE/FAS-II Complexes.** The structures of hAChE/FAS-II and aged tabun−hAChE/FAS-II are very similar. Only limited conformational changes occurs upon aging of the enzyme (Figure 3). A slight tilt of His447 is observed (changes in $\chi1$ and $\chi2$ are 15° for both), resulting from the formation of a salt bridge between phosphoramidate O3 and His447N$\varepsilon$2. The most important conformational change concerns Tyr337, whose C$\alpha$ shifts by 0.9 Å, while its side chain adopts a new rotamer (changes in $\chi1$ and $\chi2$ are +70 and −27°, respectively). The conformation of Tyr337 in the aged tabun−hAChE/FAS-II structure results in interaction between the Tyr337OH and the cation bound in the choline-binding pocket. This conformer of Tyr337 is further stabilized by a parallel aromatic stacking with Phe338, whose side chain $\chi2$ angle also changes by +40°. This conformation is actually very close to that observed in mAChE−FAS-II complex[42] (PDB code: 1KU6). By contrast, both aromatics are involved in a T-stacking interaction in the hAChE−FAS-II complex. Still, Tyr337 orientation in hAChE−FAS-II is likely influenced by the presence of a ligand visible in the electron density map, modeled as a tight group of three water molecules.[25] We note that Tyr337 in hAChE is equivalent to Phe330 in *Tc*AChE; this residue was also shown to rotate toward the active site upon binding of substrate and substrate reaction product, thereby acting as a bouncer that prevents access to the active site when it is already occupied.[43]

**Conformational Changes upon Aging.** Recently, we reported the structures of nonaged and aged forms of tabun conjugate with mAChE.[16] The fact that aging was incomplete in mAChE made impossible the characterization of conformational changes that occur upon aging. Here, we report the structure of a completely aged conjugate of tabun with hAChE. Because FAS is required for hAChE to crystallize, it was not possible to obtain the nonaged tabun−hAChE structure. Therefore, we are left with no better option than to critically compare the nonaged tabun−mAChE and aged tabun−hAChE structures. This interspecies structural comparison is yet likely of relevance, since all key residues in the active site gorge, apart from Tyr337 (discussed earlier), are identical and adopt the same conformation in mAChE and hAChE (rmsd < 0.5 Å). Thus, it is expected that conformational differences between the nonaged tabun−mAChE and the aged tabun−hAChE structures mostly reflect the rearrangement of residues upon aging.

Changes resulting from aging of tabun−hAChE are not limited to catalytic histidine movement as seen for the aged VX−*Tc*AChE conjugate;[13] rather, they extend to residues in helix 334−341, one constituent of the active site gorge wall. The large concerted movement of helix 334−341 originates from the release of steric strain upon dealkylation of bound tabun. In the nonaged conjugate structure, the side chain of

catalytic His447 is pushed away from its native position ($\chi1 = 178°$, and $\chi2 = 80°$) by the ethoxy substituent of tabun ($\chi1 = 48°$, and $\chi2 = 61°$). Upon aging, it is allowed to switch back to its original conformation and to reform a strong hydrogen bond with its catalytic triad partner, Glu334, on top of the above-mentioned salt bridge with phosphoramidate O3. Noteworthy is the 3 Å shift of the Phe338 aromatic ring that allows it to maintain contact with the side chain of His447, while stacking against that of Phe295. Together with the reorientation of Tyr337, this leads to the formation of an aromatic stacking pile made of Tyr337, Phe338, and Phe295.

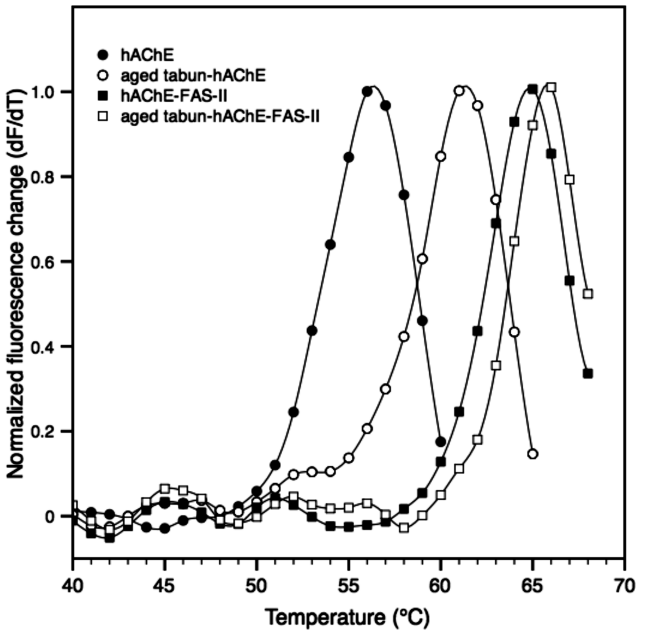


**Figure 4.** Thermostability of hAChE and its complexes with tabun and FAS-II was determined by a fluoresence-based thermal shift assay. Normalized plots of fluorescence change as a function of temperature were represented for hAChE (●), aged tabun−hAChE (○), hAChE/FAS-II (■), and aged tabun−hAChE/FAS-II (□). The $T_m$ determined at the maximum of fluorescence change was about 56.1, 61.1, 64.8, and 65.8 °C, respectively.

An important question is whether dealkylation precedes His447 reorientation or vice versa. Data gathered so far on the role of His447 (or its equivalent) in the aging of ChEs boils down to the following: (i) Catalytic His447 (or its equivalent) is mobile in AChEs[13,44−46] and immobile in hBChE.[16,23] (ii) The absence of mobility of hBChE's catalytic His438 arises from stabilization by adjacent aromatic residue Phe398: Phe398 restricts the conformational freedom of His438 and stabilizes its protonated form by a $\pi$-charge interaction. hAChE lacks this stabilizing effect as Phe398 is replaced by aliphatic residue Val407.[45] (iii) The locked hBChE's histidine is in a conformation always favorable for water-assisted dealkylation of OP ethoxy-substituted adducts by contrast to the mobile histidine of AChEs, which explains why BChEs generally age faster than AChEs.[11,23,47] Altogether, these data suggest that the catalytic His447 should be in its native position to promote tabun dealkylation. It is likely, however, that the steric strain imposed by the presence of the adduct disfavors this conformation in hAChE, thereby delaying aging. Accordingly, any mutation stabilizing the non-native conformation of His447 should slow down the aging process. We believe that this explains the 160-fold decrease in soman−hAChE aging rate for the F338A mutation.[48] Indeed, the mutation leads to the apparition of a void in between Tyr337 and Phe295, where it is possible that the His447 side chain may fit in a conformation unfavorable to aging, similar to that observed in the nonaged tabun−mAChE. Such slow-aging mutants of AChE are of particular interest as pseudo catalytic bioscavengers.[49,50]

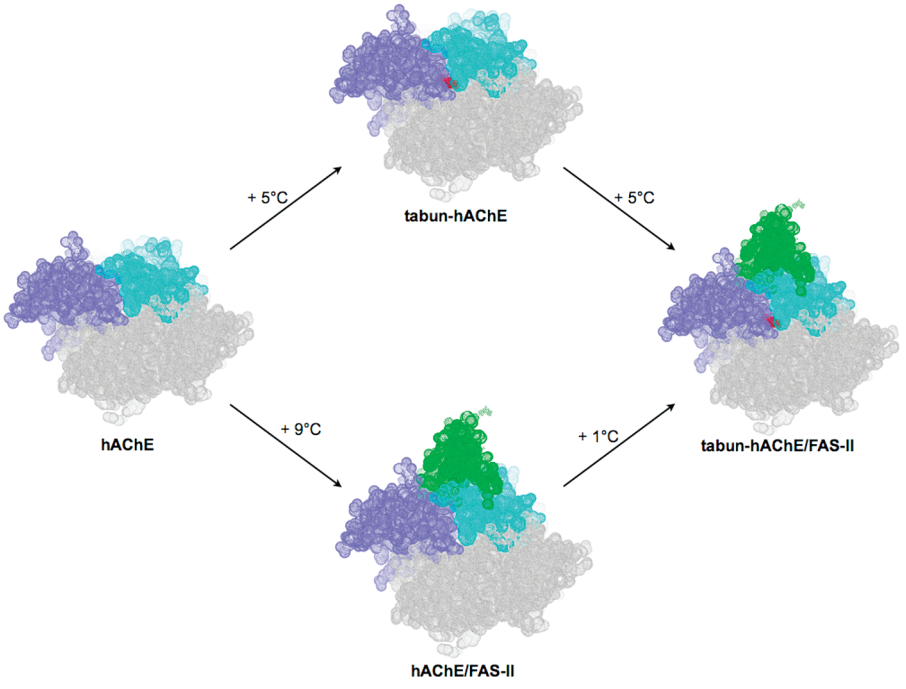


**Figure 5.** Structural representation of the stabilizing effect of tabun (in red) and fasciculin (in green) on both hAChE subdomains that face one another across the active site gorge. Residues of hAChE are represented by dots and colored in cyan for the first helical subdomain containing the acyl loop and three-helix bundle (241−288) and in blue for the helical second subdomain containing the Ω loop and residues (334−409 and 526−544). The rigid core of hAChE is colored in gray.

**Thermostability Screening of hAChE Complexes.** Thermostability of cholinesterases (ChEs) has been shown to increase in the presence of bound ligands or upon aging.[51,52] To estimate the relative contributions of FAS-II and aging on the stability of hAChE, we determined the midpoint denaturation temperature ($T_m$) of native hAChE, aged tabun−hAChE, hAChE/FAS-II, and aged tabun−hAChE/FAS-II. The $T_m$, corresponding to the temperature where $dF/dt = 0$, that is, at mid-denaturation, are 56.1, 61.1, 64.8, and 65.8 °C for native hAChE, aged tabun−hAChE, hAChE/FAS-II, and aged tabun−hAChE/FAS-II, respectively (Figure 4). There is a significant increase in $T_m$ of hAChE inhibited by aged tabun as compared to native hAChE (+5 °C) and a much larger one for hAChE complexed with FAS-II (+9 °C). This indicates that the stabilizing effect arising from the complexation of FAS-II with hAChE is stronger than that coming from the aged adduct. In view of the hAChE/FAS-II structure, this is faithfully understandable; while the aged adduct stabilizes the enzyme by interactions mostly confined in the active site and the bottom part of the acyl loop, interaction with FAS tightly associates the two subdomains that face one another across the active site gorge, the acyl loop, and the Ω loop (Figure 5). There is a marginal increase in the $T_m$ of aged tabun−hAChE/FAS-II ternary complex as compared to that of hAChE/FAS-II (+1 °C), indicating no significant additional contribution of the aged adduct to the stabilization provided by fasciculin (Figure 5).

In summary, we report the first structure of human AChE inhibited by a nerve agent. This structure provides structural insight on the inhibition and aging mechanisms and infers that tabun aging proceeds via dealkylation of the ethoxy substituent. It also provides a structural template to design new molecules for reactivating aged hAChE.

**Acknowledgment.** We gratefully acknowledge the ESRF for beam time under long-term projects MX498 and MX722 (IBS BAG) and the ESRF staff for providing efficient help during data collection. Financial support by the Agence Nationale de la Recherche (ANR) under project ANR-06-BLAN-0163, DTRA under contract CBDIF07-THER01-2-0038, and Direction Générale pour l'Armement (DGA) Grants PEA/08co501 and DGA-REI 2009-34-0023.

**Supporting Information Available:** Morphing movie between nonaged tabun-inhibited mouse AChE and aged tabun-inhibited human AChE structure. This material is available free of charge via the Internet at http://pubs.acs.org.

## References

(1) Karlsson, E.; Mbugua, P. M.; Rodriguez-Ithurralde, D. Fasciculins, anticholinesterase toxins from the venom of the green mamba Dendroaspis angusticeps. *J. Physiol.* (*Paris*) **1984**, *79*, 232–240.
(2) Greenblatt, H. M.; Dvir, H.; Silman, I.; Sussman, J. L. Acetylcholinesterase: A multifaceted target for structure-based drug design of anticholinesterase agents for the treatment of Alzheimer's disease. *J. Mol. Neurosci.* **2003**, *20*, 369–383.
(3) Moretto, A. Experimental and clinical toxicology of anticholinesterase agents. *Toxicol. Lett.* **1998**, *102*−*103*, 509–513.
(4) Barak, D.; Ordentlich, A.; Kaplan, D.; Barak, R.; Mizrahi, D.; Kronman, C.; Segall, Y.; Velan, B.; Shafferman, A. Evidence for P-N bond scission in phosphoroamidate nerve agent adducts of human acetylcholinesterase. *Biochemistry* **2000**, *39*, 1156–1161.
(5) Eddleston, M.; Mohamed, F.; Davies, J. O.; Eyer, P.; Worek, F.; Sheriff, M. H.; Buckley, N. A. Respiratory failure in acute organophosphorus pesticide self-poisoning. *QJM* **2006**, *99*, 513–522.
(6) Konradsen, F. Acute pesticide poisoning—A global public health problem. *Danish Med. Bull.* **2007**, *54*, 58–59.
(7) Sussman, J. L.; Harel, M.; Frolow, F.; Oefner, C.; Goldman, A.; Toker, L.; Silman, I. Atomic structure of acetylcholinesterase from Torpedo californica: a prototypic acetylcholine-binding. *Protein Sci.* **1991**, *253*, 872–879.
(8) Worek, F.; Thiermann, H.; Szinicz, L.; Eyer, P. Kinetic analysis of interactions between human acetylcholinesterase, structurally different organophosphorus compounds and oximes. *Biochem. Pharmacol.* **2004**, *68*, 2237–2248.
(9) Michel, H. O.; Hackley, B. E., Jr.; Berkowitz, L.; List, G.; Hackley, E. B.; Gillilan, W.; Pankau, M. Ageing and dealkylation of Soman (pinacolylmethylphosphonofluoridate)-inactivated eel cholinesterase. *Arch. Biochem. Biophys.* **1967**, *121*, 29–34.
(10) Benschop, H. P.; Keijer, J. H. On the mechanism of ageing of phosphonylated cholinesterases. *Biochim. Biophys. Acta* **1966**, *128*, 586–588.
(11) Li, H.; Schopfer, L. M.; Nachon, F.; Froment, M. T.; Masson, P.; Lockridge, O. Aging pathways for organophosphate-inhibited human butyrylcholinesterase, including novel pathways for isomalathion, resolved by mass spectrometry. *Toxicol. Sci.* **2007**, *100*, 136–145.
(12) Carletti, E.; Aurbek, N.; Gillon, E.; Loiodice, M.; Nicolet, Y.; Fontecilla-Camps, J. C.; Masson, P.; Thiermann, H.; Nachon, F.; Worek, F. Structure-activity analysis of aging and reactivation of human butyrylcholinesterase inhibited by analogues of tabun. *Biochem. J.* **2009**, *421*, 97–106.
(13) Millard, C. B.; Kryger, G.; Ordentlich, A.; Greenblatt, H. M.; Harel, M.; Raves, M. L.; Segall, Y.; Barak, D.; Shafferman, A.; Silman, I.; Sussman, J. L. Crystal structures of aged phosphonylated acetylcholinesterase: Nerve agent reaction products at the atomic level. *Biochemistry* **1999**, *38*, 7032–7039.
(14) Millard, C. B.; Koellner, G.; Ordentlich, A.; Shafferman, A.; Silman, I.; Sussman, J. L. Reaction Products of Acetylcholinesterase and VX Reveal a Mobile Histidine in the Catalytic Triad. *J. Am. Chem. Soc.* **1999**, *121*, 9983–9984.
(15) Hornberg, A.; Tunemalm, A. K.; Ekstrom, F. Crystal structures of acetylcholinesterase in complex with organophosphorus compounds suggest that the acyl pocket modulates the aging reaction by precluding the formation of the trigonal bipyramidal transition state. *Biochemistry* **2007**, *46*, 4815–4825.
(16) Carletti, E.; Li, H.; Li, B.; Ekstrom, F.; Nicolet, Y.; Loiodice, M.; Gillon, E.; Froment, M. T.; Lockridge, O.; Schopfer, L. M.; Masson, P.; Nachon, F. Aging of cholinesterases phosphylated by tabun proceeds through O-dealkylation. *J. Am. Chem. Soc.* **2008**, *130*, 16011–16020.
(17) Sanson, B.; Nachon, F.; Colletier, J. P.; Froment, M. T.; Toker, L.; Greenblatt, H. M.; Sussman, J. L.; Ashani, Y.; Masson, P.; Silman, I.; Weik, M. Crystallographic snapshots of nonaged and aged conjugates of soman with acetylcholinesterase, and of a ternary complex of the aged conjugate with pralidoxime (dagger). *J. Med. Chem.* **2009**, *52*, 7593–7603.
(18) Ekstrom, F.; Hornberg, A.; Artursson, E.; Hammarstrom, L. G.; Schneider, G.; Pang, Y. P. Structure of HI-6*sarin-acetylcholinesterase determined by X-ray crystallography and molecular dynamics simulation: Reactivator mechanism and design. *PLoS One* **2009**, *4*, e5957.
(19) Ekstrom, F. J.; Astot, C.; Pang, Y. P. Novel nerve-agent antidote design based on crystallographic and mass spectrometric analyses of tabun-conjugated acetylcholinesterase in complex with antidotes. *Clin. Pharmacol. Ther.* **2007**, *82*, 282–293.
(20) Worek, F.; Aurbek, N.; Koller, M.; Becker, C.; Eyer, P.; Thiermann, H. Kinetic analysis of reactivation and aging of human acetylcholinesterase inhibited by different phosphoramidates. *Biochem. Pharmacol.* **2007**, *73*, 1807–1817.
(21) Elhanany, E.; Ordentlich, A.; Dgany, O.; Kaplan, D.; Segall, Y.; Barak, R.; Velan, B.; Shafferman, A. Resolving pathways of interaction of covalent inhibitors with the active site of acetylcholinesterases: MALDI-TOF/MS analysis of various nerve agent phosphyl adducts. *Chem. Res. Toxicol.* **2001**, *14*, 912–918.
(22) Ekstrom, F.; Akfur, C.; Tunemalm, A. K.; Lundberg, S. Structural changes of phenylalanine 338 and histidine 447 revealed by the crystal structures of tabun-inhibited murine acetylcholinesterase. *Biochemistry* **2006**, *45*, 74–81.
(23) Nachon, F.; Asojo, O. A.; Borgstahl, G. E.; Masson, P.; Lockridge, O. Role of water in aging of human butyrylcholinesterase inhibited by echothiophate: the crystal structure suggests two alternative mechanisms of aging. *Biochemistry* **2005**, *44*, 1154–1162.
(24) le Du, M. H.; Housset, D.; Marchot, P.; Bougis, P. E.; Navaza, J.; Fontecilla-Camps, J. C. Structure of fasciculin 2 from green mamba snake venom: evidence for unusual loop flexibility. *Acta Crystallogr., Sect. D: Biol. Crystallogr.* **1996**, *52*, 87–92.
(25) Kryger, G.; Harel, M.; Giles, K.; Toker, L.; Velan, B.; Lazar, A.; Kronman, C.; Barak, D.; Ariel, N.; Shafferman, A.; Silman, I.;

Sussman, J. L. Structures of recombinant native and E202Q mutant human acetylcholinesterase complexed with the snake-venom toxin fasciculin-II. *Acta Crystallogr., Sect. D: Biol. Crystallogr.* **2000**, *56*, 1385–1394.
(26) Bourne, Y.; Taylor, P.; Marchot, P. Acetylcholinesterase inhibition by fasciculin: crystal structure of the complex. *Cell* **1995**, *83*, 503–512.
(27) Harel, M.; Kleywegt, G. J.; Ravelli, R. B.; Silman, I.; Sussman, J. L. Crystal structure of an acetylcholinesterase-fasciculin complex: interaction of a three-fingered toxin from snake venom with its target. *Structure* **1995**, *3*, 1355–1366.
(28) Rosenberry, T. L.; Scoggin, D. M. Structure of human erythrocyte acetylcholinesterase. Characterization of intersubunit disulfide bonding and detergent interaction. *J. Biol. Chem.* **1984**, *259*, 5643–5652.
(29) Lo, M. C.; Aulabaugh, A.; Jin, G.; Cowling, R.; Bard, J.; Malamas, M.; Ellestad, G. Evaluation of fluorescence-based thermal shift assays for hit identification in drug discovery. *Anal. Biochem.* **2004**, *332*, 153–159.
(30) Kabsch, W. XDS. *Acta Crystallogr., Sect. D: Biol. Crystallogr.* **2010**, *66*, 125–132.
(31) McCoy, A. J.; Grosse-Kunstleve, R. W.; Adams, P. D.; Winn, M. D.; Storoni, L. C.; Read, R. J. Phaser crystallographic software. *J. Appl. Crystallogr.* **2007**, *40*, 658–674.
(32) Murshudov, G. N.; Vagin, A. A.; Dodson, E. J. Refinement of macromolecular structures by the maximum-likelihood method. *Acta Crystallogr., Sect. D: Biol. Crystallogr.* **1997**, *53*, 240–255.
(33) Adams, P. D.; Afonine, P. V.; Bunkoczi, G.; Chen, V. B.; Davis, I. W.; Echols, N.; Headd, J. J.; Hung, L. W.; Kapral, G. J.; Grosse-Kunstleve, R. W.; McCoy, A. J.; Moriarty, N. W.; Oeffner, R.; Read, R. J.; Richardson, D. C.; Richardson, J. S.; Terwilliger, T. C.; Zwart, P. H. PHENIX: A comprehensive Python-based system for macromolecular structure solution. *Acta Crystallogr., Sect. D: Biol. Crystallogr.* **2010**, *66*, 213–221.
(34) Emsley, P.; Cowtan, K. Coot: Model-building tools for molecular graphics. *Acta Crystallogr., Sect. D: Biol. Crystallogr.* **2004**, *60*, 2126–2132.
(35) Schüttelkopf, A. W.; Van Aalten, D. M. F. PRODRG: A tool for high-throughput crystallography of protein-ligand complexes. *Acta Crystallogr., Sect. D: Biol. Crystallogr.* **2004**, *D60*, 1355–1363.
(36) Painter, J.; Merritt, E. A. Optimal description of a protein structure in terms of multiple groups undergoing TLS motion. *Acta Crystallogr., Sect. D: Biol. Crystallogr.* **2006**, *62*, 439–450.
(37) DeLano, W. L. *The PyMol Molecular Graphics System*; DeLano Scientific LLC: San Carlos, CA, 2002.
(38) Degenhardt, C. E.; Van Den Berg, G. R.; De Jong, L. P. A.; Benschop, H. P.; Van Genderen, J.; Van De Meent, D. Enantiospecific complexation gas chromatography of nerve agents. Isolation and properties of the enantiomers of ethyl N,N-dimethylphosphoramidocyanidate (tabun). *J. Am. Chem. Soc.* **1986**, *108*, 8290–8291.
(39) Järv, J. Stereochemical aspects of cholinesterase catalysis. *Bioorg. Chem.* **1984**, *12*, 259–278.
(40) Kwasnieski, O.; Verdier, L.; Malacria, M.; Derat, E. Fixation of the two tabun isomers in acetylcholinesterase: A QM/MM study. *J. Phys. Chem. B* **2009**, *113*, 10001–10007.
(41) Furegati, S.; Zerbe, O.; Ruedi, P. The stereochemistry of the inhibition of acetylcholinesterase with acetylcholine-mimetic 7-aza-2,4-dioxaphosphadecalins. *Chem.-Biol. Interact.* **2005**, *157−158*, 418–420.
(42) Bourne, Y.; Taylor, P.; Radic, Z.; Marchot, P. Structural insights into ligand interactions at the acetylcholinesterase peripheral anionic site. *EMBO J.* **2003**, *22*, 1–12.
(43) Colletier, J. P.; Fournier, D.; Greenblatt, H. M.; Stojan, J.; Sussman, J. L.; Zaccai, G.; Silman, I.; Weik, M. Structural insights into substrate traffic and inhibition in acetylcholinesterase. *EMBO J.* **2006**, *25*, 2746–2756.
(44) Massiah, M. A.; Viragh, C.; Reddy, P. M.; Kovach, I. M.; Johnson, J.; Rosenberry, T. L.; Mildvan, A. S. Short, strong hydrogen bonds at the active site of human acetylcholinesterase: Proton NMR studies. *Biochemistry* **2001**, *40*, 5682–5690.
(45) Kaplan, D.; Barak, D.; Ordentlich, A.; Kronman, C.; Velan, B.; Shafferman, A. Is aromaticity essential for trapping the catalytic histidine 447 in human acetylcholinesterase? *Biochemistry* **2004**, *43*, 3129–3136.
(46) Hornberg, A.; Artursson, E.; Warme, R.; Pang, Y. P.; Ekstrom, F. Crystal structures of oxime-bound fenamiphos-acetylcholinesterases: reactivation involving flipping of the His447 ring to form a reactive Glu334-His447-oxime triad. *Biochem. Pharmacol.* **2010**, *79*, 507–515.
(47) Aldridge, W. N.; Reiner, E. *Enzyme Inhibitors as Substrates*; North-Holland Publishing Co.: Amsterdam, 1972.
(48) Shafferman, A.; Ordentlich, A.; Barak, D.; Stein, D.; Ariel, N.; Velan, B. Aging of phosphylated human acetylcholinesterase: catalytic processes mediated by aromatic and polar residues of the active centre. *Biochem. J.* **1996**, *318* (Part 3), 833–840.
(49) Shafferman, A.; Barak, D.; Stein, D.; Kronman, C.; Velan, B.; Greig, N. H.; Ordentlich, A. Flexibility versus "rigidity" of the functional architecture of AChE active center. *Chem.-Biol. Interact.* **2008**, *175*, 166–172.
(50) Shafferman, A. Next generation of OP-bioscavengers. International Meeting on Cholinesterases, Sibenik, Croatia **2009**, oral communication.
(51) Masson, P.; Clery, C.; Guerra, P.; Redslob, A.; Albaret, C.; Fortier, P. L. Hydration change during the aging of phosphorylated human butyrylcholinesterase: importance of residues aspartate-70 and glutamate-197 in the water network as probed by hydrostatic and osmotic pressures. *Biochem. J.* **1999**, *343* (Part 2), 361–369.
(52) Rochu, D.; Clery-Barraud, C.; Renault, F.; Chevalier, A.; Bon, C.; Masson, P. Capillary electrophoresis versus differential scanning calorimetry for the analysis of free enzyme versus enzyme-ligand complexes: in the search of the ligand-free status of cholinesterases. *Electrophoresis* **2006**, *27*, 442–451.

# Structure–activity analysis of aging and reactivation of human butyrylcholinesterase inhibited by analogues of tabun

E. Carletti, N. Aurbek, E. Gillon, M. Loiodice, Y. Nicolet, J-C Fontecilla-Camps, P. Masson, H. Thiermann, **F. Nachon***, F. Worek

Biochemical Journal 421 (2009) 97-106

BJ www.biochemj.org

BJ Structure

Biochem. J. (2009) **421**, 97–106 (Printed in Great Britain) doi:10.1042/BJ20090091



# Structure–activity analysis of aging and reactivation of human butyrylcholinesterase inhibited by analogues of tabun

Eugénie CARLETTI*, Nadine AURBEK†, Emilie GILLON*, Mélanie LOIODICE*, Yvain NICOLET‡, Juan-Carlos FONTECILLA-CAMPS‡, Patrick MASSON*, Horst THIERMANN†, Florian NACHON*[1] and Franz WOREK†

*Unité d'Enzymologie, Département de Toxicologie, Centre de Recherches du Service de Santé des Armées (CRSSA), 24 av des Maquis du Grésivaudan, 38700 La Tronche, France, †Bundeswehr Institute of Pharmacology and Toxicology, Neuherbergstrasse 11, 80937 Munich, Germany, and ‡Laboratoire de Cristallogenèse et Cristallographie des Protéines, Institut de Biologie Structurale (CEA-CNRS-UJF), 41 rue Jules Horowitz, 38027 Grenoble, France

hBChE [human BChE (butyrylcholinesterase)] naturally scavenges OPs (organophosphates). This bioscavenger is currently in Clinical Phase I for pretreatment of OP intoxication. Phosphylated ChEs (cholinesterases) can undergo a spontaneous time-dependent process called 'aging' during which the conjugate is dealkylated, leading to creation of an enzyme that cannot be reactivated. hBChE inhibited by phosphoramidates such as tabun displays a peculiar resistance to oxime-mediated reactivation. We investigated the basis of oxime resistance of phosphoramidyl–BChE conjugates by determining the kinetics of inhibition, reactivation (obidoxime {1,1′-(oxybis-methylene) bis[4-(hydroxyimino) methyl] pyridinium dichloride}, TMB-4 [1,3-trimethylene-bis(4-hydroxyiminomethylpyridinium) dibromide], HLö 7 {1-[[[4-(aminocarbonyl) pyridinio]methoxy]methyl]-2,4-bis-[(hydroxyimino)methyl] pyridinium dimethanesulfonate)}, HI-6 {1-[[[4-(aminocarbonyl) pyridinio] methoxy] methyl]-2-[(hydroxyimino)methyl]pyridinium dichloride monohydrate} and aging, and the crystal structures of hBChE inhibited by different N-monoalkyl and *N*,*N*-dialkyl tabun analogues. The refined structures of aged hBChE conjugates show that aging proceeds through O-dealkylation of the P(R) enantiomer of *N*,*N*-diethyl and *N*-propyl analogues, with subsequent formation of a salt bridge preventing reactivation, similarly to a previous observation made on tabun–ChE conjugates. Interestingly, the N-methyl analogue projects its amino group towards the choline-binding pocket, so that aging proceeds through deamination. This orientation results from a preference of hBChE's acyl-binding pocket for larger than 2-atoms linear substituents. The correlation between the inhibitory potency and the N-monoalkyl chain length is related to increasingly optimized interactions with the acyl-binding pocket as shown by the X-ray structures. These kinetics and X-ray data lead to a structure–activity relationship that highlights steric and electronic effects of the amino substituent of phosphoramidate. This study provides the structural basis to design new oximes capable of reactivating phosphoramidyl-hBChE conjugates after intoxication, notably when hBChE is used as pretreatment, or to design BChE-based catalytic bioscavengers.

Key words: aging, butyrylcholinesterase, kinetics, oxime reactivation, tabun analogues, X-ray crystallography.



## INTRODUCTION

Human plasma BChE (butyrylcholinesterase; EC 3.1.1.8) is a toxicologically relevant enzyme because it hydrolyses or scavenges a wide range of toxic esters, including heroin, cocaine, carbamate pesticides, organophosphorus pesticides and nerve agents [1,2]. OPs (organophosphates) exert their acute toxicity through inhibition of AChE (acetylcholinesterase; E.C. 3.1.1.7) by phosphylation of the catalytic serine [2]. Subsequent accumulation of acetylcholine at neuronal synapses and neuromuscular junctions results in paralysis, seizures and other symptoms of cholinergic syndrome [3,4]. hBChE (human BChE) is a potential drug candidate that may be employed in several therapeutic fields. This is due to the unique structure of the enzyme that allows accommodation of a large variety of substrates and inhibitors, some of which are excluded from the catalytic gorge of acetylcholinesterase [5]. BChE-based biopharmaceuticals are under research and development as stoichiometric and catalytic bioscavengers for neutralization or detoxification of poisonous esters. Recombinant and plasma-purified hBChEs are in Clinical Phase I as the first stoichiometric bioscavengers for the pretreatment of OP intoxication. In case of intoxication, reactivation of hBChE used in pretreatment will improve protection against high dose or repetitive OP exposure. For this reason, it is essential to design efficient reactivators for hBChE.

Phosphylated ChEs (cholinesterases) can be reactivated by specific nucleophiles such as oximes [6,7]. The most effective oximes used for emergency treatment of nerve agent poisoning are the monopyridinium oximes (2-PAM) and bispyridinium oximes (TMB-4 [1,3-trimethylene-bis(4-hydroxyiminomethylpyridinium) dibromide], MMB-4 {1,1′-methylene-bis[4-(hydroxyimino)methyl]pyridinium dibromide}, obidoxime {1,1′-(oxybis-methylene) bis[4-(hydroxyimino) methyl] pyridinium dichloride}, HI-6 {1-[[[4-(aminocarbonyl) pyridinio] methoxy] methyl]-2-[(hydroxyimino)methyl]pyridinium dichloride monohydrate} and HLö 7 {1-[[[4-(aminocarbonyl) pyridinio]methoxy]methyl]-2,4-bis-[(hydroxyimino)methyl] pyridinium dimethanesulfonate)}) [6]. Kinetic analysis of the interactions between different AChE–OP conjugates and different oximes shows that the most effective oximes are HLö 7 for phosphonylated AChE and obidoxime for phosphorylated AChE [6]. Unfortunately, a universal antidote, efficient against all nerve

Abbreviations used: AChE, acetylcholinesterase; BChE, butyrylcholinesterase; BTCh, butyrylthiocholine; ChE, cholinesterase; DTNB, 5, 5′-dithiobis-(2-nitrobenzoic-acid); hBChE, human BChE; HI-6, 1-[[[4-(aminocarbonyl) pyridinio] methoxy] methyl]-2-[(hydroxyimino)methyl]pyridinium dichloride monohydrate; HLö 7, 1-[[[4-(aminocarbonyl) pyridinio]methoxy]methyl]-2,4-bis-[(hydroxyimino)methyl] pyridinium dimethanesulfonate); obidoxime, 1,1′-(oxybis-methylene) bis[4-(hydroxyimino) methyl] pyridinium dichloride; OP, organophosphate; TMB-4, 1,3-trimethylene-bis(4-hydroxyiminomethylpyridinium) dibromide.

[1] To whom correspondence should be addressed (email fnachon@crssa.net).

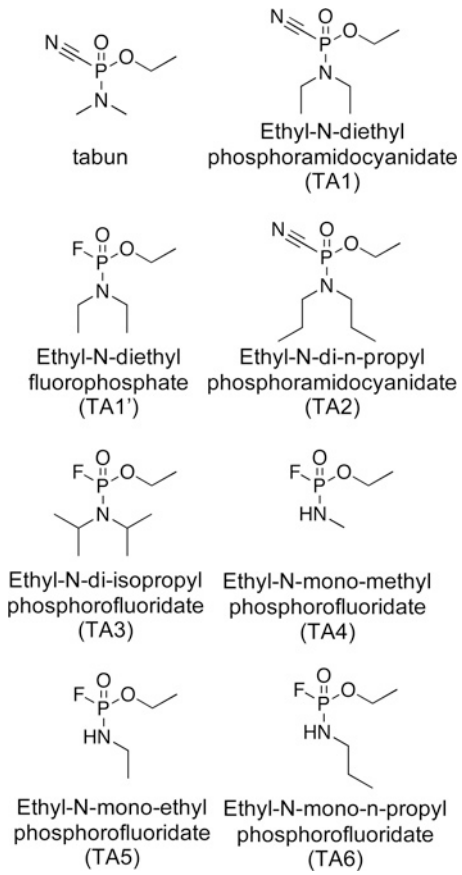


**Figure 1 Chemical structures of tabun analogues (TA)**

agents and capable of crossing the blood brain barrier, is not yet available.

Reactivation of inhibited ChEs is complicated by a side reaction. Indeed, phosphylated ChEs undergo a spontaneous, time-dependent process called 'aging' during which the OP–ChE conjugates are O-dealkylated, leading to non-reactivatable enzyme [8–10].

Inhibition of BChE by tabun and the subsequent aging reaction of adducts are of interest, because tabun–ChE conjugates are particularly resistant to most oxime reactivators. Recent studies detail the mode of interaction of tabun with ChEs and show that tabun–ChE conjugates age through O-dealkylation [11]. An extension of this study to various phosphoramidate anologues of tabun provides the basis of a structure–activity relationship analysis of phosphoramidate adducts. The analogues of tabun differ in their amino substituents (Figure 1). The reactivation of hBChE inhibited by tabun and its analogues was studied with obidoxime, TMB-4, HI-6 and HLö 7 (Figure 2). This study provides a better understanding of the resistance of phosphoramidate-hBChE conjugates to oximes and gives some insights into the design of new oximes capable of reactivating tabun–ChE conjugates, and ChEs inhibited by related agents.

## MATERIAL AND METHODS

### Materials

DTNB (5,5′-dithio-bis-2-nitrobenzoic acid) and TMB-4 dibromide were obtained from Sigma Chemical Co. Obidoxime dichloride was purchased from Duphar. HI-6 dichloride was kindly provided by Dr J. G. Clement (Defence Research and

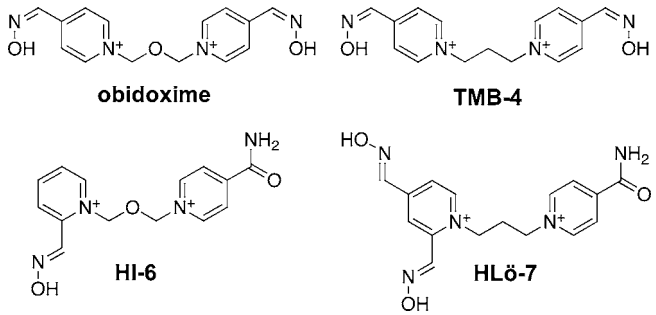


**Figure 2 Chemical structures of oximes used in the present study**

Development Canada, Suffield, Canada) and HLö-7 dimethanesulfonate was a custom synthesis by Dr J. Braxmeier (Chemisches Labor, Döpshofen, Germany). Tabun and its analogues (TA 1–6) (> 98 % by GC-MS, $^{1}$H-NMR and $^{31}$P-NMR) were made available by the German Ministry of Defence, all other chemicals were from Merck Eurolab GmbH. BTCh (butyrylthiocholine, in the form of *S*-butyrylthiocholine iodide) was obtained from Sigma.

Stock solutions of tabun and compounds 1–6 (1 % v/v; Figure 1) were prepared in propan-2-ol, stored at 4 °C and were appropriately diluted in distilled water just before the experiment. Oximes (200 mM) were prepared in distilled water, stored at − 60 °C and diluted as required in distilled water on the day of the experiment. Human plasma was obtained from heparinized whole blood by centrifugation (1000 ***g***, 10 min, 4 °C) and was stored in aliquots at − 60 °C until use. Research was carried out in accordance with the Declaration of Helsinki (2000) of the World Medical Association and with national law. Written informed consent was obtained from all blood donors.

### Isolated plasma hBChE

Isolated hBChE (E.C. 3.1.1.8) was obtained from Sigma. This enzyme was used for kinetic assays.

### Production of recombinant hBChE

Recombinant hBChE was produced in CHO (Chinese hamster ovary) cells and secreted into serum-free culture medium [12]. Briefly, recombinant hBChE was a truncated monomer containing residues 1–529, where the tetramerization domain at the C-terminus was deleted. The glycan chain number was reduced by site-directed mutagenesis from 9 to 6. Enzyme purification was implemented by affinity and ion-exchange chromatography as described in [12]. The active-site concentration of highly purified enzyme was determined using diisopropyl fluorophosphate as the titrant as described [13]. This enzyme was used for crystallographic assays and for testing of enantioselectivity.

### Enzyme assays

hBChE activities were measured spectrophotometrically (Cary 3Bio, Varian, Darmstadt, Germany) at 436 nm with a modified Ellman assay at 37 °C [14,15]. However, the regular Ellman assay at 412 nm works as well. The assay mixture (3.16 ml) contained 1 mM BTCh as substrate and 0.3 mM DTNB as chromogen in 0.1 M phosphate buffer (pH 7.4).

### Determination of inhibition rate constants ($k_i$)

The inhibition rate constants were determined at pseudo-first-order reaction conditions as described previously [6]. In brief,

appropriately diluted OP was added to temperature-equilibrated (37 °C) isolated hBChE at $t = 0$, an aliquot was removed after specified time intervals (1–9 min) and transferred to a cuvette for the determination of residual hBChE activity. $k_i$ was calculated from eqn (1):

$$k_i = \frac{1}{[OP] \times t} \times \ln \frac{v_0}{v_t} \quad (1)$$

where [OP] is the initial concentration of the tested OP, $v_0$ and $v_t$ are the reaction rates at zero time and at time $t$ respectively. The concentration ranges of OP used in the experiment were: tabun, 20–80 nM; TA1, 100–250 nM; TA1′, 1200–1800 nM; TA2, 200–500 nM; TA3, 20–50 $\mu$M; TA4, 50–125 nM; TA5, 70–100 nM; and TA6, 50–90 nM.

### Test of enantioselectivity for TA 4–6

Determination of inhibition enantioselectivity of recombinant hBChE was performed under second-order conditions as described [11]. Briefly, incubation was performed at 25 °C in 50 mM sodium phosphate buffer, pH 7.0, containing 5 % propan-2-ol, 1 mg/ml BSA, a concentration of hBChE of approx. 30 nM, whereas that of tabun analogues ranged between 15 and 200 nM. Residual activity was monitored at 25 °C and pH 7.0, according to Ellman's method using 1 mM BTCh and 0.5 mM DTNB. Under second order conditions, the concentration of residual active enzyme follows eqn 2, as a function of time [11]:

$$E = E_0 \frac{E_0 - \frac{[OP_0]}{n}}{E_0 - \frac{[OP_0]}{n} e^{\left(\frac{[OP_0]}{n} - E_0\right) ki' \cdot t}} \quad (2)$$

where $E$ is the concentration of residual active enzyme at time $t$, $E_0$ the initial concentration of active enzyme, $[OP_0]$ the initial concentration of racemic OP, $n$ the number of enantiomers, and $ki'$ the bimolecular rate constant of the most active enantiomer assuming the inhibition rate of the other enantiomer is negligible. Analysis of the kinetic data was performed using GOSA-fit, a fitting software based on a simulated annealing algorithm (BioLog, Toulouse, France; http://www.bio-log.biz), allowing simultaneous fitting of all the data at once.

### Oxime screening for the reactivation of OP-inhibited hBChE

Human plasma was incubated with a small volume (1 % v/v) of appropriate concentrations of tabun and compounds TA 1–6 for 30 min at 37 °C to achieve an hBChE inhibition of > 90 %. Thereafter, the treated samples were dialysed (phosphate buffer, 0.1 M, pH 7.4) overnight at 4 °C to remove residual inhibitor. The inhibitory activity of the samples was tested by 30 min of incubation at 37 °C of treated plasma and control hBChE in order to verify the absence of residual inhibitor. OP-inhibited hBChE was incubated at 37 °C with 1 mM obidoxime, TMB-4, HI-6 or HLö 7 and the hBChE activity was measured at specified time intervals (1–120 min). Enzyme activities were referred to control activity and the percentage reactivation was calculated according to de Jong and Wolring [16]. Experiments were performed in duplicate.

### Kinetics of obidoxime reactivation

Owing to low reactivating potency, the reactivation kinetics were determined at 37 °C by a discontinuous procedure as described previously [6,17], which allowed the use of high obidoxime concentrations in the incubation mixture (up to 5 mM). OP-inhibited hBChE was incubated with different obidoxime concentrations and 1 mM BTCh. Aliquots were transferred to cuvettes after specified time intervals (2–45 min) for measurement of hBChE activity. The dissociation constant $K_d$ of the enzyme–obidoxime complex, the reactivity rate constant $k_r$ and the second order reactivation rate constant $k_{r2}$ were calculated by a standard procedure [6]. Eight to ten obidoxime concentrations, 100–5000 $\mu$M with tabun- and TA3-inhibited BChE and 50–3000 $\mu$M with TA4–6-inhibited enzyme, were used for the determination of reactivation rate constants.

### Determination of rate constants for aging ($k_a$) and spontaneous reactivation ($k_s$)

OP-inhibited hBChE was brought to 37 °C ($t = 0$). Then, aliquots were taken after various time intervals for determination of BChE activity (spontaneous reactivation) and of the decrease of oxime-induced reactivation (aging). Next, small aliquots were incubated for 1 h with 1 mM obidoxime. Data from duplicate experiments were referred to control activities and the percentage reactivation was calculated. The pseudo-first-order rate constants $k_s$ (spontaneous reactivation) and $k_a$ (aging) were calculated using a non-linear regression model [6].

### Crystallization of non-aged TA1, TA4, TA5 and TA6-inhibited hBChE

The buffer used was 0.1 M Mes, pH 6.5, with 2.1 M ammonium sulfate. Stock solutions of tabun analogues were 10 mM in propan-2-ol. Native enzyme was crystallized using the hanging drop method [12]. Crystals grew in 1 week at 20 °C. Then, the OP-hBChE conjugates were prepared by soaking crystals for 10 min in 0.1 M Mes buffer, pH 6.5, with 2.1 M ammonium sulfate, containing 2 mM tabun analogue. The crystals were washed with a cryoprotectant solution (0.1 M Mes buffer with 2.1 M ammonium sulfate, containing 20 % glycerol), and then flash-cooled in liquid nitrogen.

### Crystallization of aged TA1, TA4 and TA5-hBChE

Purified enzyme (9 mg/ml) was inhibited by 2 mM tabun analogue compounds, in 10 mM Tris/HCl buffer, pH 7.4. The inhibited enzyme was crystallized using the hanging drop method [12]. Crystals grew in 1 week at 20 °C. The time between phosphylation and data collection was sufficiently long (> 2 weeks) to achieve completion of the aging reaction (aging half time < 70 h).

### X-ray data collection and structure solution of hBChE

Diffraction data were collected at $\lambda = 0.932$ Å (1 Å = 0.1 nm) wavelength at the ID14-eh2 beamline of the European Synchrotron Radiation Facility (ESRF, Grenoble, France) with a MAR-Research CCD (charge-coupled-device) detector. All data sets were processed with XDS and the structures were solved by use of the CCP4 suite [18]. An initial solution model was determined by molecular replacement with MolRep [19], starting with the recombinant hBChE structure (PDB entry 1P0I) from which all ligands (butyrate, glycerol, ions) and glycan chains were removed. For all diffraction data sets, the model was refined as follows: an initial rigid-body refinement with REFMAC5 [20] was followed by iterative cycles of model building with Coot [21], and finally restrained refinement was carried out with REFMAC5 and Phenix [22]. The covalently-bound inhibitors and their descriptions were built using the Dundee PRODRG2.5 server including energy minimization using the GROMOS96.1 forcefield.

**Table 1 Rate constants for inhibition ($k_i$), obidoxime-induced reactivation ($K_d$, $k_r$, $k_{r2}$), aging ($k_a$) and spontaneous reactivation ($k_s$) of hBChE phosphorylated with tabun and its analogues**

| | N-group | $k_i$ ($10^6$) ($M^{-1} \cdot min^{-1}$) | $K_d$ ($\mu$M) | $k_r$ ($min^{-1}$) | $k_{r2}$ ($mM^{-1} \cdot min^{-1}$) | $k_a$ ($h^{-1}$) | $k_s$ ($h^{-1}$) |
|---|---|---|---|---|---|---|---|
| tabun |  | 30 ± 8 | 1470 ± 250 | 0.02 ± 0.002 | 0.017 ± 0.006 | 0.1 ± 0.01 | ø[c] |
| TA1 |  | 1 ± 0.0 | ø[a] | ø[a] | ø[a] | ø[b] | ø[c] |
| TA1′ |  | 0.06 ± 0.003 | ø[a] | ø[a] | ø[a] | ø[b] | ø[c] |
| TA2 |  | 0.3 ± 0.03 | ø[a] | ø[a] | ø[a] | ø[b] | ø[c] |
| TA3 |  | 0.012 ± 0.001 | 920[d] | 0.09[d] | 0.098[d] | 0.09 ± 0.0001 | ø[c] |
| TA4 |  | 4 ± 0.5 | 370 ± 40 | 0.042 ± 0.001 | 0.117 ± 0.010 | 0.011 ± 0.0003 | 0.004 ± 0.0001 |
| TA5 |  | 8 ± 0.6 | 630 ± 60 | 0.072 ± 0.003 | 0.114 ± 0.002 | 0.012 ± 0.0002 | 0.008 ± 0.0001 |
| TA6 |  | 17 ± 0.3 | 660 ± 50 | 0.069 ± 0.002 | 0.108 ± 0.002 | 0.015 ± 0.0005 | 0.019 ± 0.0004 |

[a]Failure of oximes to reactivate inhibited hBChE.
[b]Not feasible.
[c]No spontaneous reactivation of inhibited hBChE activity during the observation period.
[d]Single experiment.

## RESULTS

### Inhibition of hBChE by tabun analogues

The bimolecular rate constants, $k_i$, for inhibition of human BChE by tabun and its analogues (TA1–TA6) in the absence of substrate are in Table 1. Phosphoramidocyanidates react faster than homologous phosphoramidofluoridate: TA1 with cyanide as leaving group reacts 17 times faster than TA1′ with fluoride as leaving group. Therefore the inhibitory potency was related to the chain length of the N-alkyl group. With tabun and its closest analogues, TA1 and TA2, bearing a cyanide leaving group and dialkyl chains, $k_i$ values decreased with increasing chain length. In contrast, for TA4, TA5 and TA6, bearing a mono-N-alkyl group, the inhibitory potency increased with chain length, each carbon addition doubling the bimolecular rate constant.

### Determination of enantioselectivity

The time dependence of the inhibition of hBChE by TA4, TA5 and TA6, under second-order conditions, is shown in Figure 3. Fitting the data to equation 2 yields $ki' = 2.4 \pm 0.2 \times 10^6$ $M^{-1} \cdot min^{-1}$ and $n = 1.8 \pm 0.1$ for TA4, $ki' = 8.4 \pm 0.5 \times 10^6$ $M^{-1} \cdot min^{-1}$ and $n = 2.0 \pm 0.1$ for TA5, and $ki' = 24 \pm 2 \times 10^6$ $M^{-1} \cdot min^{-1}$ and $n = 2.0 \pm 0.1$ for TA6. It follows that hBChE reacts preferentially with one enantiomer of tabun analogues. A similar enantiomeric preference was observed for inhibition of hBChE by tabun [11]. In this regard, $ki$ differs from $ki'$ because it is determined under pseudo first-order conditions and describes the reaction of both enantiomers. Moreover, experimental conditions concerning temperature, pH and propan-2-ol-concentration were different.

### Reactivation of phosphoramidate-inhibited hBChE by oximes

The reactivation of OP-inhibited hBChE by oximes was tested with 1 mM obidoxime, TMB-4, HI-6 and HLö 7 (Figure 4). Tabun-inhibited hBChE could be partially reactivated by oximes, and the extent of reactivation decreased in the order obidoxime > TMB-4 > HLö 7 > HI-6. Oxime-induced reactivation was rather ineffective with hBChE inhibited by TA1 and TA2. Interestingly, reactivation of hBChE inhibited by TA3 followed a different pattern. All oximes were capable of reactivating the inhibited enzyme, and after a 120 min incubation the recovery in hBChE activity was in the range of 60–85 %.

In contrast, all oximes reactivated hBChE inhibited by N-monoalkyl tabun analogues, i.e. TA4, TA5 and TA6 completely, although there were some differences between oximes regarding velocity and extent of reactivation (Figure 4).

The reactivation kinetics of hBChE inhibited by tabun and its analogues TA3–TA6 were determined with obidoxime. The reactivation constants are given in Table 1. $K_d$ is the dissociation constant of the oxime–OP–hBChE complex, $k_r$ the reactivation constant and $k_{r2}$ describes the specific reactivity. No rate constants could be determined with hBChE inhibited by TA1 and TA2, due to the low reactivation extent. TA3-inhibited hBChE was, compared with tabun, substantially more susceptible towards reactivation.

The reactivation of hBChE inhibited by N-monoalkyl tabun analogues, TA4, TA5 and TA6, resulted in comparable second-order rate constants $k_{r2}$ (Table 1). There was only a small difference in $K_d$ and $k_r$ between TA5 and TA6, and both values were substantially lower with TA4.

### Aging and spontaneous reactivation of phosphoramidate-inhibited hBChE

Aging and spontaneous reactivation constants are given in Table 1. The kinetics of aging were not determined for TA1 and TA2 due to the insufficient reactivation extent by oximes. Tabun and its *N*,*N*-di-i-propyl analogue (TA3) showed comparable aging kinetics, with $k_a$ values of 0.1 $h^{-1}$ and 0.094 $h^{-1}$ respectively. hBChE inhibited by the *N*-monoalkyl tabun analogues TA4, TA5 and TA6 was susceptible towards aging and spontaneous reactivation. Therefore the velocity of spontaneous reactivation increased with the chain length of the N-alkyl group, whereas the aging rates are comparable and noticeably slower than for tabun-inhibited hBChE (Table 1).

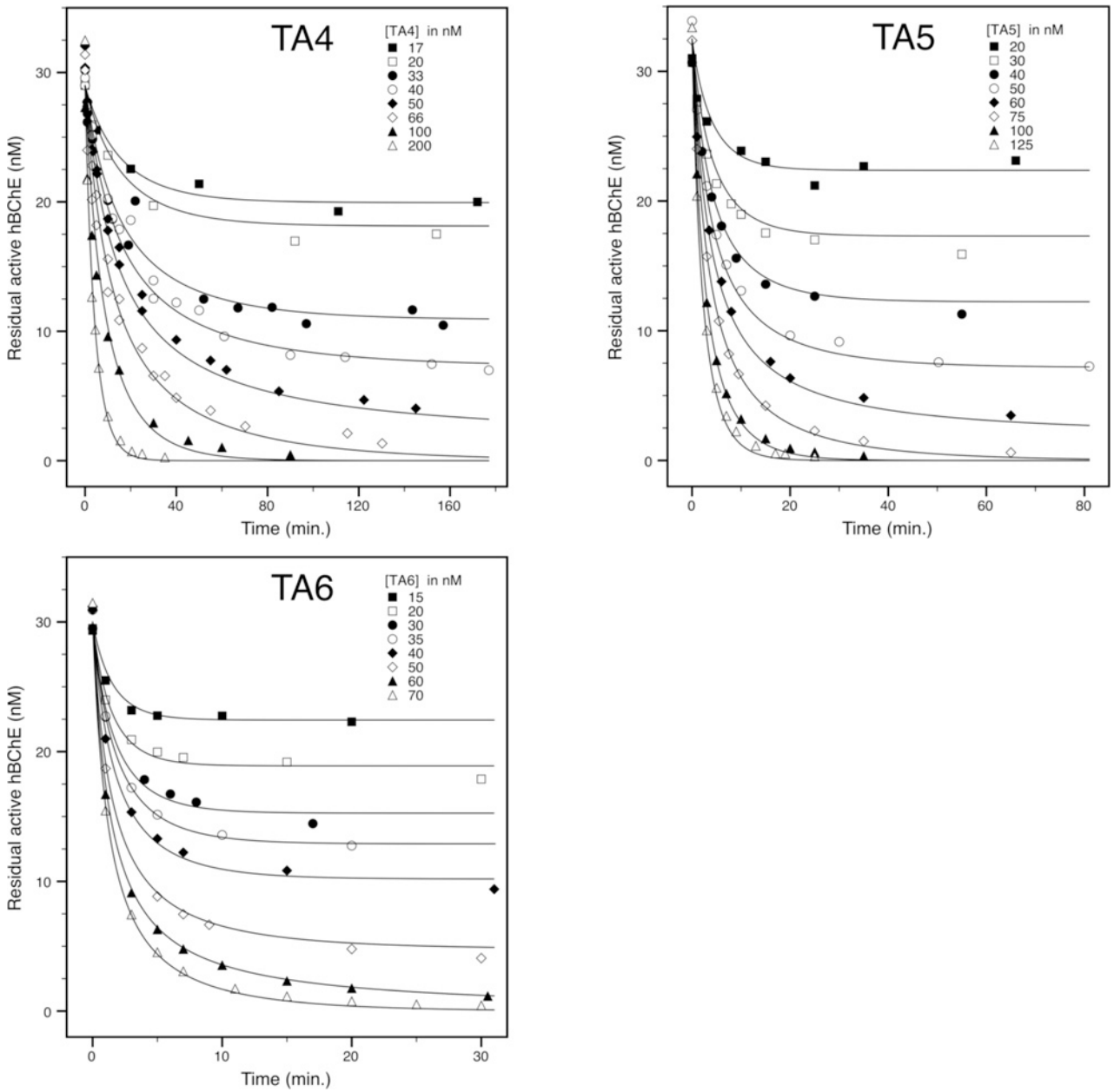


**Figure 3 Irreversible inhibition of hBChE by racemic tabun analogues performed under second-order conditions**

hBChE (29, 32.5 and 30 nM) was inhibited by various concentrations of TA4, TA5 and TA6 respectively, and the residual enzyme activity was monitored as a function of time.

### X-ray structures of non-aged tabun analogue–hBChE conjugates

Data were collected from tetragonal crystals of space group *I*422 and refined to 2.3 Å, 2.15 Å, 2.1 Å and 2.1 Å for TA1, TA4, TA5 and TA6 respectively. Corresponding data and refinement statistics are shown in Table 2. A strong peak of positive electron density (10–15 $\sigma$) within covalent bond distance of the catalytic serine was observed in the initial |Fo|-|Fc| map for each conjugate. This confirms that inhibitors were bound to the active site serine after 5 min of soaking. The refinement yields an adduct that exhibits P(R) stereochemistry for the chiral phosphorus atom, except for TA4 that exhibits P(S) stereochemistry (Figure 5). Given the good resolution (2.15 Å) and the map quality, there is no ambiguity in TA4 stereochemistry assignment. As a control, we also modelled the presumably incorrect stereoisomer of TA4 and performed one round of structural refinement. Distinct positive and negative difference density (|Fo| – |Fc| map) peaks support the conclusion that the adduct intermediate observed in the structures is in the S conformation. There was no significant movement of residue side-chains compared with the native enzyme (PDB code: 1P0I).

There is a strong peak of positive electron density in the initial |Fo| – |Fc| map close to $Trp^{82}$. This density could not be reasonably modelled. It is most likely due to the presence of the small ligand that was previously observed in other structures of hBChE [23,24]. This unknown ligand appears stacked against $Trp^{82}$ and interacts with water molecules. For TA1 there is no large blob of density, but electron density corresponding to two water molecules. The phosphorus atoms were found at covalent bonding distance from the $Ser^{198}O\gamma$ atoms (approx. 1.6 Å) and the P–N distance was refined to values ranging from 1.6 Å to 1.7 Å. $O^2$ of the

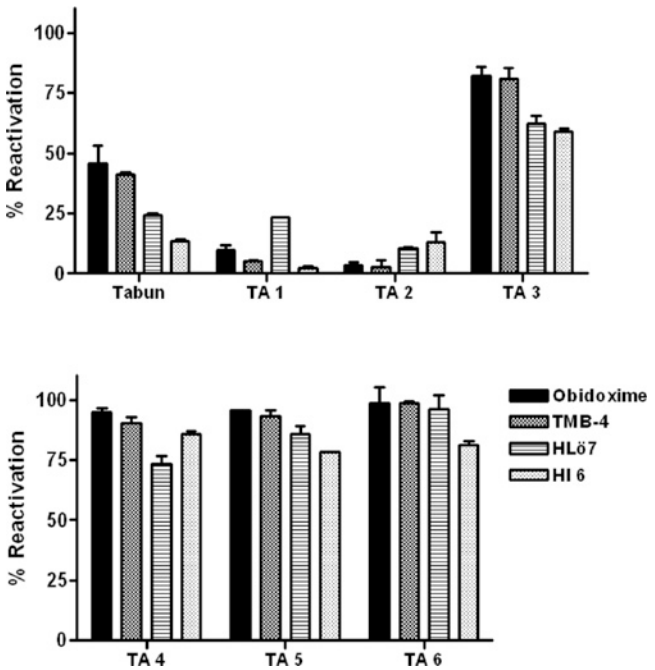


**Figure 4 Reactivation of OP-inhibited hBChE by obidoxime (black column), TMB-4 (dark grey column), HLö 7 (horizontally striped column) or HI-6 (light grey column)**

hBChE inhibited by tabun and its analogues (Figure 1) was incubated with 1 mM oxime and the hBChE activity was determined after 120 min incubation. Data are given as % reactivation (means ± S.D. of two experiments).

phosphoramidate moiety is at hydrogen-bonding distance of the main chain amide nitrogen of residues forming the oxyanion hole (Ala[199]/Gly[116]/Gly[117]). The N-alkyl subsituents were located in the acyl-binding pocket with the alkyl groups pointing towards the top of the gorge, except for TA4. For the latter, the N-alkyl group projects towards the choline-binding pocket, and the ethoxy moiety, located in the acyl-binding pocket, weakly interacts with Leu[286] and Phe[398]. On the choline-binding pocket side, ethoxy oxygen $O^2$ of TA1, TA5, TA6 and N of TA4 are at hydrogen bonding distance of His[438]Nε2.

For TA1, the N-ethyl group makes van der Waals contact with Trp[231] and Phe[329]. The N-diethyl substituent of TA1 imposes much more stress on the residue of the acyl-binding pocket such that we observed a concerted shift of approx. 0.5 Å for Phe[398], Phe[329] and Leu[286].

### X-ray structure of aged tabun analogue–hBChE conjugates

The structures of aged forms were obtained by crystallization of inhibited enzyme in solution. X-ray crystallographic data were collected from tetragonal crystals of space group *I*422, except for TA5 (P4212), and refined to 2.25 Å, 2.0 Å and 3.1 Å for TA1, TA4 and TA5 respectively. Corresponding data and refinement statistics are shown in Table 3. The orientation of aged conjugates is identical to the non-aged conjugates and confirms that the stereoselectivity of the inhibition is identical *in cristallo* and in solution (Figure 5). This also confirms the initial stereochemistry of TA4. As expected in aged forms, the alkyl group projecting towards the choline-binding pocket is missing. This shows that TA1 and TA5 undergo classical O-dealkylation as previously observed for tabun [11], phosphates and phosphonates [8]. On the other hand, TA4 probably undergoes deamination. As a result of aging, $O^3$ forms a salt bridge with protonated His[438]Nε2 (2.7–2.8 Å). For each conjugate, the phosphoramidyl moiety has tilted toward His[438] as a consequence of the salt bridge formation. For TA1, this also translates into a release of stress in the acyl-binding pocket so that only Phe[329] remains shifted. For TA4 and TA5, van der Waals contacts with Trp[231] and Phe[329] are similar as in their non-aged form. The small ligand is still present stacked against Trp[82] and interacts with $O^3$ of the aged adducts of TA1, TA4 and is replaced by two water molecules in the structure of the aged TA5–hBChE conjugate.

**Table 2 Data collection and refinement statistics for non-aged compounds**

RMS, root mean square.

| | TA1–hBChE | TA4–hBChE | TA5–hBChE | TA6–hBChE |
|---|---|---|---|---|
| Data | | | | |
| Space group | *I*422 | *I*422 | *I*422 | *I*422 |
| Unit cell axes, $a = b$, $c$ (Å) | 155.04, 126.21 | 155.01, 126.84 | 155.02, 127.22 | 155.24, 127.25 |
| Number of reflections | 240729 | 302893 | 328846 | 314110 |
| Unique reflections | 34103 | 41918 | 45161 | 45258 |
| Resolution (Å) | 47.8–2.3 (2.4–2.3) | 49.0–2.15 (2.2–2.15) | 55.1–2.1 (2.2–2.1) | 55.1–2.1 (2.2–2.1) |
| Completeness (%) | 99.3 | 99.7 | 99.9 | 99.6 |
| *R*merge* (%) | 8.5 (34.9) | 8.1 (29.6) | 8.6 (28.4) | 9.7 (35.5) |
| $I/\acute{o}(I)$ | 23.1 (5.3) | 25.8 (4.3) | 24.7 (4.4) | 16.6 (3.4) |
| Redundancy | 7.1 (7.2) | 7.2 (7.2) | 7.3 (7.4) | 6.9 (5.9) |
| Refinement statistics | | | | |
| *R*-factor† (*R*-free‡) | 18.9 (25.5) | 18.9 (25.3) | 20.0 (25.3) | 21.3 (27.6) |
| Number of atoms | | | | |
| Protein | 4240 | 4227 | 4213 | 4208 |
| Solvent | 335 | 343 | 342 | 384 |
| Others | 167 | 163 | 162 | 164 |
| Mean *B*-factor (Å$^2$) | 37.6 | 35.3 | 35.9 | 37.4 |
| RMS from ideality | | | | |
| Bond length (Å) | 0.017 | 0.018 | 0.017 | 0.033 |
| Angles (deg) | 1.757 | 1.875 | 1.782 | 2.897 |
| Chiral (Å$^3$) | 0.128 | 0.114 | 0.121 | 0.229 |

*$R\text{merge} = (\Sigma|- < I > |)/\Sigma I$, where $I$ is the observed intensity and $< I >$ is the average intensity obtained from multiple observations of symmetry-related reflections after rejections.
†$R\text{-factor} = \Sigma|\text{Fo-|Fc}||/\Sigma|\text{Fo}|$, Fo and Fc are observed and and calculated structure factors.
‡*R*-free set uses approx. 1000 of randomly chosen reflections.

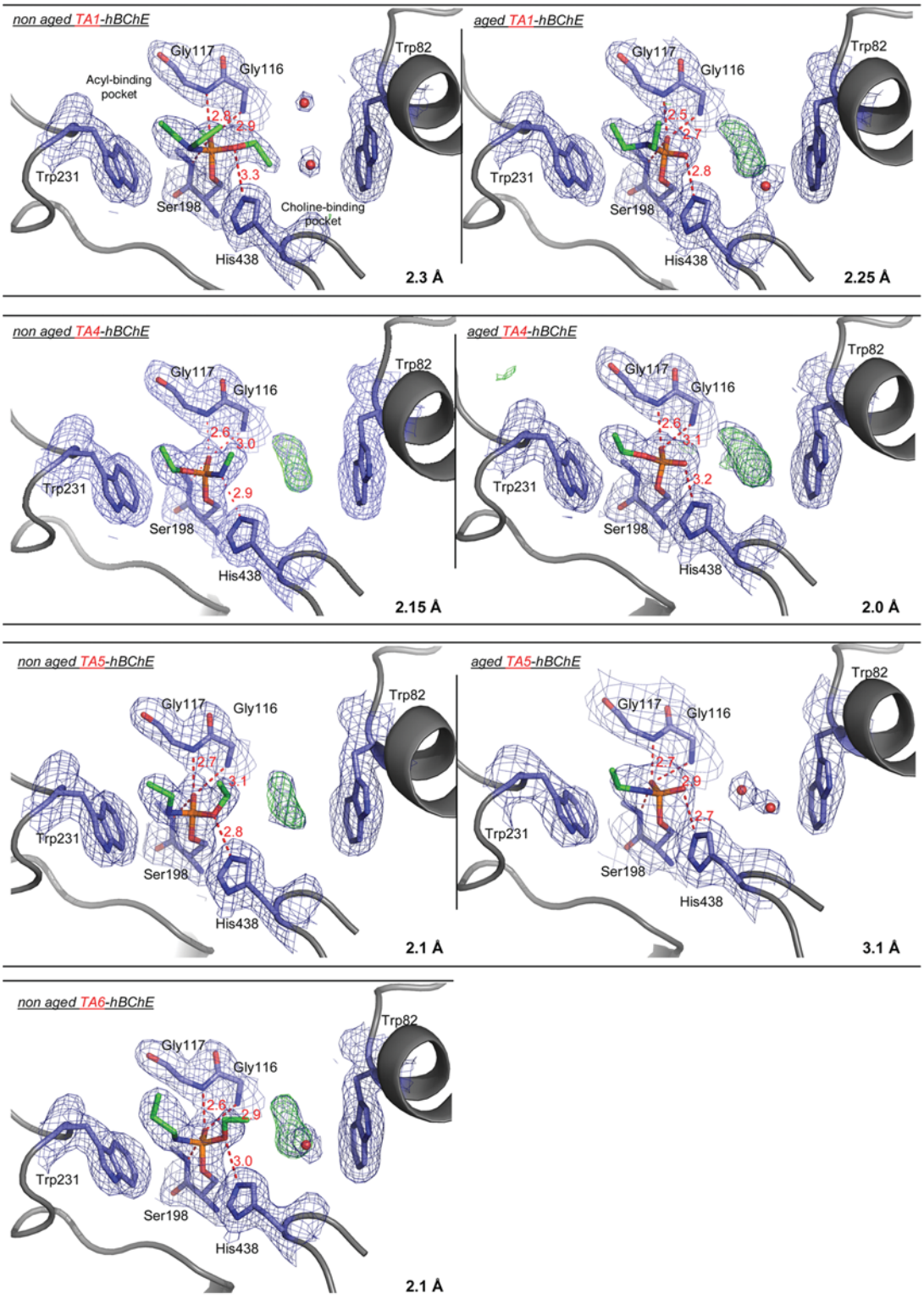


**Figure 5 Active site of non-aged and aged TA–hBChE conjugates**

Key residues are represented as sticks with carbon in green for OP and dark blue for hBChE residues, nitrogen atoms in blue, oxygen atoms in red and phosphorus atom in orange. Water molecules are represented by red spheres and hydrogen bonds by red dashes. Electron density 2|Fo| – |Fc| is represented by a blue mesh, contoured at 1.0 $\sigma$ and |Fo| – |Fc| is represented by green/red mesh contoured at 3.5 $\sigma$.

**Table 3 Data collection and refinement statistics for aged compounds**

RMS, root mean square.

| | TA1-hBChE | TA4-hBChE | TA5-hBChE |
|---|---|---|---|
| Data | | | |
| Space group | *I*422 | *I*422 | *P*4212 |
| Unit cell axes, $a = b$, $c$ (Å) | 155.04, 126.21 | 154.9, 126.01 | 150.35, 139.43 |
| Number of reflections | 248 419 | 391 729 | 167 928 |
| Unique reflections | 35 245 | 51 417 | 28 167 |
| Resolution (Å) | 47.7–2.25 (2.3–2.25) | 48.9–2.0 (2.1–2.0) | 48.4–3.1 (3.2–3.1) |
| Completeness (%) | 96.3 | 98.3 | 98.2 |
| *R*merge* (%) | 10.1 (48.1) | 8.8 (37.5) | 10.1 (30.5) |
| $I/\acute{o}(I)$ | 15.3 (4.0) | 24.8 (5.4) | 29.2 (8.6) |
| Redundancy | 7.1 (7.3) | 7.6 (7.4) | 5.7 (5.9) |
| Refinement statistics | | | |
| *R*-factor† (*R*-free‡) | 20.7 (27.5) | 23.4 (22.0) | 22.0 (25.3) |
| Number of atoms | | | |
| Protein | 4 216 | 4 263 | 8 396 |
| Solvent | 369 | 396 | 136 |
| Others | 163 | 156 | 268 |
| Mean *B*-factor (Å$^2$) | 38.01 | 27.9 | 73.7 |
| RMS from ideality | | | |
| Bond length (Å) | 0.025 | 0.011 | 0.012 |
| Angles (deg) | 2.238 | 1.351 | 1.415 |
| Chiral (Å$^3$) | 0.218 | 0.101 | 0.087 |

*$R\text{merge} = (\Sigma|I - \langle I \rangle|)/\Sigma I$, where $I$ is the observed intensity and $\langle I \rangle$ is the average intensity obtained from multiple observations of symmetry-related reflections after rejections.

†$R\text{-factor} = \Sigma||Fo|-|Fc||/\Sigma|Fo|$, Fo and Fc are observed and calculated structure factors.

‡*R*-free set uses approx. 1000 of randomly chosen reflections.

## DISCUSSION

The higher inhibitory potency of phosphoramidocyanidates compared with homologous phosphoramidofluoridates (Table 1) could be related to the electron-withdrawing effect of cyanide that is stronger than that of fluorine. Cyanide is also a mesomer acceptor in contrast with fluorine. It follows that the phosphorus atom of phosphoramidocyanidates is more electrophilic and more reactive. It is also possible that, during the approach of the inhibitor, the cyanide substituent makes more favourable interactions with the enzyme than does fluorine.

Non-aged and aged structures were obtained for the tabun analogues TA1, TA4, TA5 and non-aged structures for TA6 (Figure 5). We failed to obtain conjugates with TA3 and TA2, most likely because of their poor reactivity with hBChE in relation to their large size. The X-ray structures and second order kinetic data show that there is enantioselectivity for reaction with fluorophosphoramidate analogues (Figures 3 and 5).

We observed that the *N*,*N*-dialkyl substituent of TA1 is located in the acyl-binding pocket, similarly to tabun [11]. The bulky *N*,*N*-diethyl substituent of TA1 fits in the acyl-binding pocket, only inducing slight rotation of Leu$^{286}$, and the phosphoramidate head is pushed toward the choline-binding pocket compared with TA5 and TA6 (Figure 6). The steric hindrance resulting from the *N*,*N*-diethyl group forces the O-ethoxy substituent to orientate towards the bottom of the choline-binding pocket. This notably prevents the binding of the unknown ligand, just leaving enough room for two water molecules (Figures 5 and 6). As for tabun, the orientation of TA1 is explained by delocalization of the N-lone pair and subsequent cation–$\pi$ interactions between the diethylamino and Trp$^{231}$.

For N-monoalkyl analogues (TA4–TA6), the orientation of the OP follows different rules. The larger substituent, whether the ethoxy or amino group, is located in the acyl-binding pocket, forming more van der Waals interactions than the smaller substituent and suggesting that cation–$\pi$ interactions of the N-monoalkyl group and Trp$^{231}$ are secondary in importance. Indeed, we expect weaker cation–$\pi$ interactions because delocalization of the nitrogen lone pair is less stabilized for primary amines compared with secondary amines, thus leading to a lesser positive partial charge on the amino group. For the N-monoalkyl analogues, the optimal length of the alkylamino or ethoxy substituent appears to be of prime importance for preferential interaction with the acyl-binding pocket. Actually, this could result from the preference of hBChE's acyl-binding pocket for larger than 2-atoms linear substituents. Indeed, when the substituent is shorter, for example a single atom, as for soman-aged hBChE conjugate (PDB code: 1p0q), it induces a rearrangement of the acyl-loop (Val$^{279}$–Asn$^{289}$). Thus for TA4, the O-ethyl (3-atom chain) substituent is located in the acyl-binding pocket and the shorter N-methyl (2-atom chain) towards the choline-binding pocket (Figure 5).

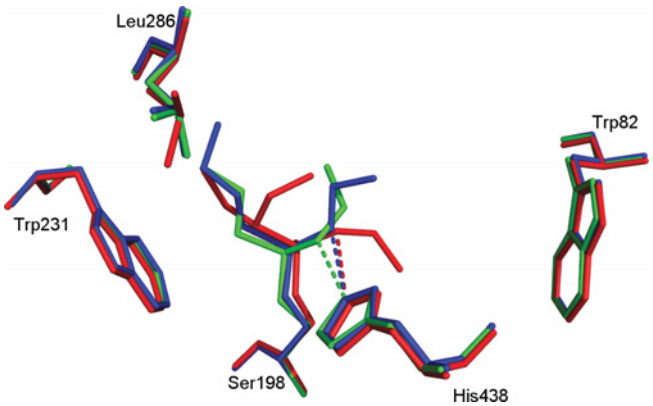


**Figure 6 Superimposition of the active site of the non-aged forms of TA1-hBChE (red), TA5-hBChE (green) and TA6-hBChE (blue) conjugates**

For TA5, we cannot conclude regarding the orientation, as both substituents are indistinguishable by X-ray crystallography. However, second order kinetics shows that hBChE reacts specifically with one enantiomer of TA5. Since van der Waals interactions should be equivalent for both substituents, we suppose that the ethylamino group interacts preferably with Trp$^{231}$ through cation–$\pi$ interactions, whereas the ethoxy oxygen interacts with His$^{438}$N$\varepsilon$2.

Crystallographic data show that aging occurs through classical O-dealkylation for TA1, TA6 (Figure 5), similarly to previous observations made on tabun–ChE conjugates [11]. Unexpectedly, there was also aging for TA4, although the ethoxy group is located in the acyl-binding pocket (Figure 5). These results show that aging of phosphoramidates systematically involves departure of the substituent in the choline-binding pocket. The mechanism differs, depending on the nature of the substituent O-alkyl or N-alkyl group (Figure 7). When this substituent is the ethoxy, aging proceeds through dealkylation: His$^{438}$ imidazolium stabilizes a developing negative charge on the C-O$^{\delta-}$ oxygen, and a water molecule activated by Glu$^{197}$ attacks the carbocationic centre that appears on the C$^{\delta+}$-O carbon. This leads to scission of the C–O bond, release of the ethoxy moiety, and subsequent formation of the salt bridge between the phosphorous O$^3$-oxygen and the imidazolium. This is illustrated with TA1, TA6 and previous solved structures of aged hBChE inhibited by tabun, soman, $iPr_2P$-F (di-isopropyl fluorophosphate) and echothiophate [11,23,24].

For TA4, the N-methyl substituent projects towards the choline-binding site so that aging proceeds through deamination: His$^{438}$ imidazolium protonates the methylamine group. Extremely rapid deamination after nucleophilic attack by water can be assumed

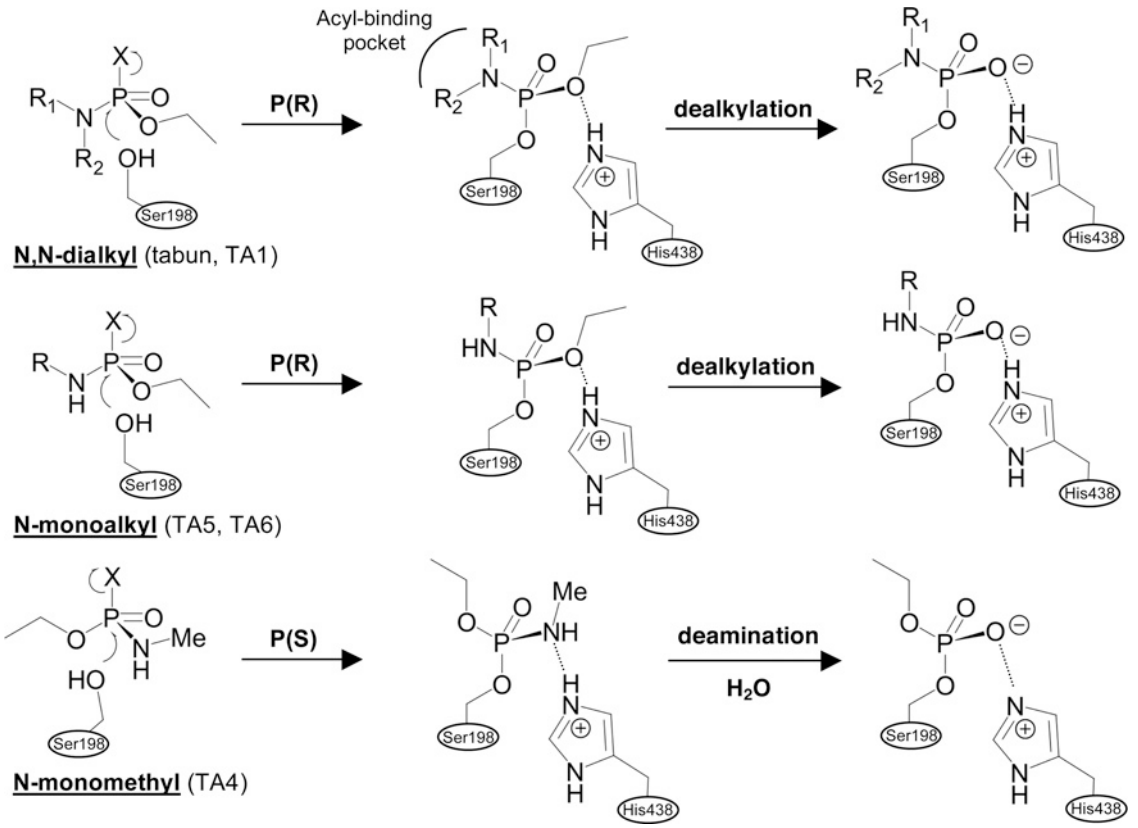


**Figure 7 Aging mechanisms of phosphoramidyl–hBChE conjugates**

since a protonated methylamine is an excellent leaving group. This mechanism, similar to dealkylation, leads to the formation of a salt bridge with a short interatomic distance, as shown by the crystal structure ($His^{438}N\varepsilon2$ and $O^{3} = 2.7$Å). Remarkably, aging rates of all monoalkyl analogues are comparable despite the difference in mechanism.

N,N-dialkyl compounds are generally less potent inhibitors of hBChE than N-monoalkyl analogues (Table 1). N,N-dialkyl compounds are less reactive because steric hindrance from the two alkyl side-chains prevents a correct approach of the OP to the catalytic serine. Moreover, the two alkyl chains have an electron-releasing effect that favours delocalization of the nitrogen lone pair on the phosphorus atom, thus decreasing the electrophilicity of the latter. Additionally, $Trp^{231}$ could stabilize positive partial charges on the amino group when the dialkylamino substituent is in the acyl-binding pocket, thus further favouring delocalization of the N-lone pair.

The remarkable correlation between the inhibitory potency and the N-monoalkyl chain length is most likely related to increasingly optimized interactions with the acyl-binding pocket as shown by the X-ray structures (Figure 5).

The electronic and steric effects have similar influence on the reactivation reaction by oximes of N,N-dialkyl compared with N-monoalkyl compounds (Figure 4). In addition to the poorer reactivity of the phosphorus atom, the two alkyl side-chains prevent a correct approach of the oxime in the apical position, as illustrated in Figure 6.

Obidoxime, TMB-4, HLö 7 and HI-6 have a similar efficiency for reactivating each phosphoramidyl–hBChE conjugate. The increase in chain length of N-monoalkyl compounds does not affect the affinity of oximes for hBChE conjugates in contrast with hAChE [7] because the long chain can easily fit in the acyl-binding pocket.

These bispyridinium oximes are much less efficient than for phosphoramidyl-hAChE [7], despite $Tyr^{124}$, which hinders the phosphorus atom of hAChE conjugates for an optimal apical approach, not being conserved in hBChE ($Gln^{119}$). This is due to a lower affinity of oximes for phosphoramidyl–hBChE conjugates. Indeed, these bispyridinium oximes bind to the peripheral site of hAChE through aromatic stacking and cation–$\pi$ interactions between one pyridinium moiety and peripheral site residues ($Trp^{286}$, $Tyr^{124}$ and $Tyr^{72}$) [25]. In hBChE, these aromatic residues are not conserved and bispyridinium oximes cannot interact in the same fashion. Considering that the OPs occupy the bottom of the active site gorge, and that the nucleophile function must be in the apical position for optimal in-line attack, efficient reactivators must bind to the gorge entrance of hBChE. Efforts should be pursued in designing such reactivators.

In summary, this work provides a better understanding of inhibition of hBChE by phosphoramidates and aging of the conjugates, and provides a structural basis for rational design by molecular modelling of hBChE-based catalytic bioscavengers and oximes able to reactivate phosphoramidyl–hBChE. Great improvement in prophylaxis, decontamination and treatment of organophosphate poisoning are expected in the near future as hBChE is close to FDA (Food and Drug Administration) approval.

## AUTHOR CONTRIBUTION

Eugénie Carletti performed the crystallographic study, including protein purification and crystallogenesis, and wrote the manuscript. Nadine Aurbek and Emilie Gillon did the kinetic studies, Mélanie Loiodice was involved in the production of the enzyme, Yvain Nicolet and

Juan-Carlos Fontecilla-Camps helped in the diffraction data collection. Patrick Masson and Horst Thiermann participated in the editing of the manuscript prior to submission. Florian Nachon and Franz Worek supervised the work and wrote the manuscript.

## ACKNOWLEDGEMENTS

The authors are grateful to T. Hannig and L. Windisch for their skilful and enthusiastic technical assistance.

## FUNDING

This work was supported by DGA (Délègation Générale pour l'Armement) grants [grant numbers 03co10–05/PEA 01 08 7 (to P. M.), and DGA/PEA 08co501 and ANR-06-BLAN-0163 (to F. N.)].

## REFERENCES

1 Lockridge, O. and Masson, P. (2000) Pesticides and susceptible populations: people with butyrylcholinesterase genetic variants may be at risk. Neurotoxicology **21**, 113–126
2 Masson, P., Carletti, E. and Nachon, F. (2009) Structure, activities and biomedical applications of human butyrylcholinesterase, Pep. Prot. Letters., in the press
3 Eddleston, M. (2008) The pathophysiology of organophosphorus pesticide self-poisoning is not so simple. Neth. J. Med. **66**, 146–148
4 Konradsen, F., Dawson, A. H., Eddleston, M. and Gunnell, D. (2007) Pesticide self-poisoning: thinking outside the box. Lancet **369**, 169–170
5 Saxena, A., Redman, A. M., Jiang, X., Lockridge, O. and Doctor, B. P. (1997) Differences in active site gorge dimensions of cholinesterases revealed by binding of inhibitors to human butyrylcholinesterase. Biochemistry **36**, 14642–14651
6 Worek, F., Thiermann, H., Szinicz, L. and Eyer, P. (2004) Kinetic analysis of interactions between human acetylcholinesterase, structurally different organophosphorus compounds and oximes. Biochem. Pharmacol. **68**, 2237–2248
7 Worek, F., Aurbek, N., Koller, M., Becker, C., Eyer, P. and Thiermann, H. (2007) Kinetic analysis of reactivation and aging of human acetylcholinesterase inhibited by different phosphoramidates. Biochem. Pharmacol. **73**, 1807–1817
8 Li, H., Schopfer, L. M., Nachon, F., Froment, M. T., Masson, P. and Lockridge, O. (2007) Aging pathways for organophosphate-inhibited human butyrylcholinesterase, including novel pathways for isomalathion, resolved by mass spectrometry. Toxicol. Sci. **100**, 136–145
9 Shafferman, A., Ordentlich, A., Barak, D., Stein, D., Ariel, N. and Velan, B. (1997) Aging of somanyl-acetylcholinesterase adducts: facts and models. Biochem. J. **324**, 996–998
10 Kovach, I. M., Akhmetshin, R., Enyedy, I. J. and Viragh, C. (1997) A self-consistent mechanism for dealkylation in soman-inhibited acetylcholinesterase. Biochem. J. **324**, 995–996
11 Carletti, E., Li, H., Li, B., Ekström, F., Nicolet, Y., Loiodice, M., Gillon, E., Froment, M. T., Lockridge, O., Schopfer, L. M. et al. (2008) Aging of cholinesterases phosphylated by tabun proceeds through O-dealkylation. J. Am. Chem. Soc. **130**, 16011–16020
12 Nachon, F., Nicolet, Y., Viguie, N., Masson, P., Fontecilla-Camps, J. C. and Lockridge, O. (2002) Engineering of a monomeric and low-glycosylated form of human butyrylcholinesterase: expression, purification, characterization and crystallization. Eur. J. Biochem. **269**, 630–637
13 Amitai, G., Moorad, D., Adani, R. and Doctor, B. P. (1998) Inhibition of acetylcholinesterase and butyrylcholinesterase by chlorpyrifos-oxon. Biochem. Pharmacol. **56**, 293–299
14 Worek, F., Mast, U., Kiderlen, D., Diepold, C. and Eyer, P. (1999) Improved determination of acetylcholinesterase activity in human whole blood. Clin. Chim. Acta **288**, 73–90
15 Eyer, P., Worek, F., Kiderlen, D., Sinko, G., Stuglin, A., Simeon-Rudolf, V. and Reiner, E. (2003) Molar absorption coefficients for the reduced Ellman reagent: reassessment. Anal. Biochem. **312**, 224–227
16 de Jong, L. P. and Wolring, G. Z. (1978) Effect of 1-(AR)alkyl-2-hydroxyiminomethyl-pyridinium salts on reactivation and aging of acetyl-cholinesterase inhibited by ethyl dimethylphosphoramidocyanidate (tabun). Biochem. Pharmacol. **27**, 2229–2235
17 Wang, R. I. and Henschel, E. O. (1967) Semiquantitative determination of cholinesterase activity in human plasma: test-paper method. Anesth. Analg. **46**, 281–285
18 Collaborative Computational Project 4 (1994) The CCP4 suite: programs for protein crystallography. Acta. Crystallogr. D Biol. Crystallogr. **50**, 760–763
19 Vagin, A. and Teplyakov, A. (1997) MOLREP: an automated program for molecular replacement. J. Appl. Crystallogr. **30**, 1022–1025
20 Murshudov, G. N., Vagin, A. A. and Dodson, E. J. (1997) Refinement of macromolecular structures by the maximum-likelihood method. Acta. Crystallogr. D Biol. Crystallogr. **53**, 240–255
21 Emsley, P. and Cowtan, K. (2004) Coot: model-building tools for molecular graphics. Acta. Crystallogr. D Biol. Crystallogr. **60**, 2126–2132
22 Adams, P. D., Grosse-Kunstleve, R. W., Hung, L. W., Ioerger, T. R., McCoy, A. J., Moriarty, N. W., Read, R. J., Sacchettini, J. C., Sauter, N. K. and Terwilliger, T. C. (2002) PHENIX: building new software for automated crystallographic structure determination. Acta. Crystallogr. D Biol. Crystallogr. **58**, 1948–1954
23 Nachon, F., Asojo, O. A., Borgstahl, G. E., Masson, P. and Lockridge, O. (2005) Role of water in aging of human butyrylcholinesterase inhibited by echothiophate: the crystal structure suggests two alternative mechanisms of aging. Biochemistry **44**, 1154–1162
24 Nicolet, Y., Lockridge, O., Masson, P., Fontecilla-Camps, J. C. and Nachon, F. (2003) Crystal structure of human butyrylcholinesterase and of its complexes with substrate and products. J. Biol. Chem. **278**, 41141–41147
25 Ekstrom, F. J., Astot, C. and Pang, Y. P. (2007) Novel nerve-agent antidote design based on crystallographic and mass spectrometric analyses of tabun-conjugated acetylcholinesterase in complex with antidotes. Clin. Pharmacol. Ther. **82**, 282–293

Received 14 January 2009/2 April 2009; accepted 15 April 2009
Published as BJ Immediate Publication 15 April 2009, doi:10.1042/BJ20090091

# Aging mechanism of butyrylcholinesterase inhibited by an N-methyl analogue of tabun: Implications of the trigonal–bipyramidal transition state rearrangement for the phosphylation or reactivation of cholinesterases

**F. Nachon***, E. Carletti, F. Worek, P. Masson

Chemico-Biological Interactions 187 (2010) 44-48

Chemico-Biological Interactions 187 (2010) 44–48

Contents lists available at ScienceDirect

Chemico-Biological Interactions

journal homepage: www.elsevier.com/locate/chembioint

# Aging mechanism of butyrylcholinesterase inhibited by an N-methyl analogue of tabun: Implications of the trigonal–bipyramidal transition state rearrangement for the phosphylation or reactivation of cholinesterases

Florian Nachon[a,*], Eugenie Carletti[a], Franz Worek[b], Patrick Masson[a]

[a] Département de Toxicologie, Centre de Recherches du Service de Santé des Armées (CRSSA), 38702 La Tronche Cedex, France
[b] Bundeswehr Institute of Pharmacology and Toxicology, Neuherbergstrasse 11, 80937 Munich, Germany

ARTICLE INFO

*Article history:*
Available online 8 April 2010

*Keywords:*
Acetylcholinesterase
Butyrylcholinesterase
Transition state
Nerve agents
Aging
Reactivation

ABSTRACT

Cholinesterases are the main target of organophosphorus nerve agents (OPs). Their inhibition results in cholinergic syndrome and death. The enzymes are inhibited by phosphylation of the catalytic serine enzyme, but can be reactivated by oximes to some extent. However, phosphylated cholinesterases undergo a side reaction that progressively prevents their reactivatability. This unimolecular reaction, termed "aging", has been investigated for decades. It was shown that most OP–ChE conjugates aged by O-dealkylation of an alkoxy substituent of the phosphorus atom, a mechanism involving the stabilization of a transient carbocation. In this paper we present structural data supporting a substitution-based mechanism for aging of the huBChE conjugate of an N-mono-methyl analogue of tabun. This mechanism involves an adjacent nucleophilic attack followed by Berry pseudorotation. A similar adjacent attack and subsequent rearrangement of the transition state have been recently proposed for tabun phosphylation of AChE. We suggest that a similar mechanism is also possible for oxime reactivation of phosphylated cholinesterases. This opens new perspectives in terms of reactivator design.



## 1. Introduction

Human acetylcholinesterase (huAChE; EC 3.1.1.7) and butyrylcholinesterase (huBChE; EC 3.1.1.8) are closely related serine hydrolases with different substrate specificity and inhibitor sensitivity. huAChE regulates cholinergic transmission in the peripheral and central nervous systems by hydrolyzing acetylcholine with a high catalytic efficiency, whereas huBChE's role is unclear despite its presence in numerous tissues [1]. huAChE is the main target of organophosphorus nerve agents (OPs) while huBChE is their main natural bioscavenger [2]. Accordingly, considerable works have been performed for some 20 years on the medical interest of huBChE administration for protection against organophosphorus poisoning. Clinical phase I for the use of huBChE as a pretreatment of nerve agent exposure has been completed. In case of OP poisoning, huBChE, susceptible toward reactivation by oximes, administered as pretreatment would greatly increase its potency, by turning it into a "pseudo-catalytic" bioscavenger. But there is a lack of efficient reactivators of phosphylated huBChE [3], and there is now great interest to look for efficient huBChE reactivators. Besides, current huAChE reactivators were empirically designed in the absence of the knowledge of the tridimensional structure of ChEs and their OP-conjugates. It is expected that the information gathered from available X-ray structures can help to design improved huAChE reactivators.

Inhibition of huAChE by OP compounds involves phosphylation of the catalytic serine [4]. The resulting serine adduct is slowly or not hydrolyzed likely because the histidine of the catalytic triad cannot stabilize and activate a water molecule on the proper face of the phosphylserine, i.e., opposite to the serine. However, the conjuguate can be reactivated by more potent nucleophiles like oximes. But the efficiency of oximes varies upon the nature of the OP, and for example, huAChE inhibited by tabun is poorly reactivated [5].

Following phosphylation, a time-dependent intramolecular reaction occurs on the OP–ChE conjugate that leads to a loss of reactivatability by oximes [6]. The resultant enzyme is "aged". The aging reaction of cholinesterase conjugates generally corresponds to the O-dealkylation of one alkoxy substituent of the phosphorus atom [7,8]. O-dealkylation is catalyzed by the protonated triad histidine and the deprotonated glutamate vicinal to the catalytic serine [9,10]. The dealkylation results in an oxyanion that forms a salt bridge with the protonated histidine [8,11]. The salt bridge sta-

*Abbreviations:* huBChE, human butyrylcholinesterase; huAChE, human acetylcholinesterase; ChE, cholinesterase; TA4, N-methyl-ethylphosphoramidofluoridate; OPs, organophosphorous compounds.

* Corresponding author at: Unité d'enzymologie, Département de toxicologie, IRBA–CRSSA, 24 avenue des Maquis du Grésivaudan, 38700 La Tronche, France.
*E-mail address:* florian@nachon.net (F. Nachon).

0009-2797/$ – see front matter © 2010 Elsevier Ireland Ltd. All rights reserved.
doi:10.1016/j.cbi.2010.03.053

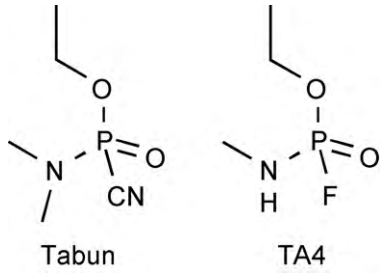


**Fig. 1.** Chemical structure of tabun and N-methyl-ethylphosphoramidofluoridate (TA4).

bilizes the adduct and raises the energy barrier for the reactivation reaction. Besides, the protonated histidine can no more serve as a general base to assist reactivation by nucleophiles. It follows that aged enzymes are not reactivatable by oximes.

The dealkylation mechanism has been confirmed for ChEs conjugated to many different OP, including phosphates (DFP and echothiophate), phosphonates (soman, VX and sarin) and phosphoramidates (fenamiphos and tabun). But it has been shown that aging of phosphorodithioate conjugated to AChE (isomalathion–AChE) likely occurs by attack of a water molecule on the phosphorus atom and release of a thioalkyl substituent [12]. It has also been suggested based on crystallographic data that aging of phosphylated huBChE could involve a nucleophilic substitution by water [13]. To date, this nucleophilic substitution mechanism for huBChE has been confirmed by mass spectrometry for the enzyme inhibited by enantiomers of isomalathion [14] and mipafox, a phosphoramidate [15]. A similar acid-catalyzed hydrolysis has been suggested for aging of mipafox-inhibited huAChE to account for the loss of both isopropylamine groups [16]. Noteworthy, aging of mipafox-inhibited neuropathy target esterase does not involve protonation but abstraction of the amine hydrogen by the catalytic histidine [17]. Though, this form of aging does not lead to substituent loss and is fully reversible.

Here we discuss structural data showing that substitution-based aging also occurs for the huBChE adduct of an N-methyl tabun analogue (TA4, N-methyl-ethylphosphoramidofluoridate; Fig. 1) and involves a rearrangement of the trigonal–bipyramidal transition state. We also discuss general implications of this particular nucleophilic substitution mechanism for the stereochemistry of the phosphylation or the reactivation mechanisms of cholinesterases.

## 2. X-ray structure of non-aged and aged TA4–huBChE conjugates

Crystals of the non-aged TA4 conjugate were obtained by inhibition *in crystallo*, i.e., by a 5-min soaking of native huBChE crystals in a solution containing the OP [18]. Crystals of the aged conjugate were obtained by inhibition and aging in solution then crystallization of the aged enzyme. Noteworthy, long soaking of native huBChE crystals in a solution containing TA4 resulted in the same structure (data not shown). The crystal structures of the non-aged and aged conjugates were subsequently solved to 2.15 Å and 2.0 Å resolution, respectively (pdb code 2wig and 2wsl).

Refinement of non-aged TA4–huBChE yields an adduct that exhibits $P_S$ stereochemistry for the chiral phosphorus (Fig. 2): the phosphorus atom forms a covalent bond with the catalytic serine (1.6 Å); the phosphoramidate oxygen is H bonded with the main chain amide nitrogen of residues forming the oxyanion hole (Ala199/Gly116/Gly117); the ethoxy group is in close contact with residues Phe398/Trp231/Leu286/Val288 of the acyl-pocket; the N-methyl group projects toward the catalytic histidine with the nitrogen at H-bond distance to His438Nε2. Given the good resolution and the electron density map quality there is no ambiguity in the stereochemistry assignment. In this configuration the catalytic histidine is away from the ethoxy group and cannot assist O-dealkylation. Noteworthy, the N-propyl analogue of tabun (TA6) projects its amino group toward the acyl-binding pocket, so that aging proceeds through dealkylation [18]. The situation is not clear for the N-ethyl analogue (TA5) because electron density corresponding to N-ethyl and O-ethyl is undistinguishable, so that the adduct stereochemistry cannot be determined. However, we modeled the N-ethyl substituent in the acyl-pocket, postulating preferred interaction with this pocket (pdb code 2wij). Obviously, this assignment remains largely arbitrary and cannot reasonably be used to conclude on the aging mechanism of the TA5 conjugate.

In the aged TA4 conjugate structure, the ethoxy substituent also fits in the acyl-pocket but the methylamino is lost. The very short distance (2.7 Å) between the atom found at the place of the former methylamino group and His438Nε2 implies a salt bridge involving a negative oxygen atom (Fig. 2). The phosphyl moiety has notably tilted toward His438 as a consequence of the salt bridge formation. This slightly weakens the hydrogen bonds with the oxyanion hole.

These combined structures lead to the following conclusions: (i) huBChE displays stereoselectivity for one enantiomer of TA4 in agreement with kinetic data [18]; (ii) identical position of the ethoxy group in both structures relieves any doubts that huBChE displays the same stereoselectivity in solution and *in crystallo*; (iii) the substitution of the methylamino substituent by oxygen suggests aging by nucleophilic attack of a water molecule and departure of the protonated methylamino substituent. Thus, the aging mechanism is neither a O-dealkylation nor a N-dealkylation but likely a nucleophilic substitution, similar to the acid-catalyzed aging mechanism suggested for mipafox-inhibited huAChE and huBChE [15,16].

## 3. Aging by nucleophilic substitution

Usually, the most favorable substitution corresponds to the nucleophile approaching the phosphorus atom from the opposite face of the leaving group because this leads to the formation of a bipyramidal–trigonal transition state, with the nucleophile and the leaving group, both occupying the apical positions. The bonds between apical atoms and the phosphorus atom are longer, thus weaker, than those with equatorial atoms, so that the scission of the bond with the leaving group is favorable. But here, a nucleophilic water molecule cannot access the crowded face opposite to the methylamino. It means that a water molecule can only attack from one of the open faces, adjacent to the methylamino substituent. This leaves two possibilities: either water approaches the face opposite to the catalytic serine or the face opposite to the ethoxy. Actually, an approach by the face opposite to the ethoxy seems a more favorable situation because the face is wide open, and the water molecule can be stabilized by H-bonding to Glu197 and activated by His438. This attack is expected to lead to the formation of a transition state with the water molecule and the ethoxy in apical position (Fig. 3). The transition state must rearrange to move the methylamino and the oxygen in the oxyanion hole in apical positions favorable for bond cleavage. The energy barrier for such a rearrangement by Berry pseudorotation [19] is not necessarily considerable, because catalytic residues can change their orientation and that of the adduct along the pathway. Especially Ser198, which has a usually high-energy conformation, or His438 that can easily exchange H-bonding partners during the phosphorus moiety displacement accompanying the rearrangement (Ser198-Oγ; hydroxyl, methylamino). Other factors like the electron withdrawing effect of the oxyanion hole or the imidazolium, or stabilization by the acyl-pocket can significantly alter the geometry and length of

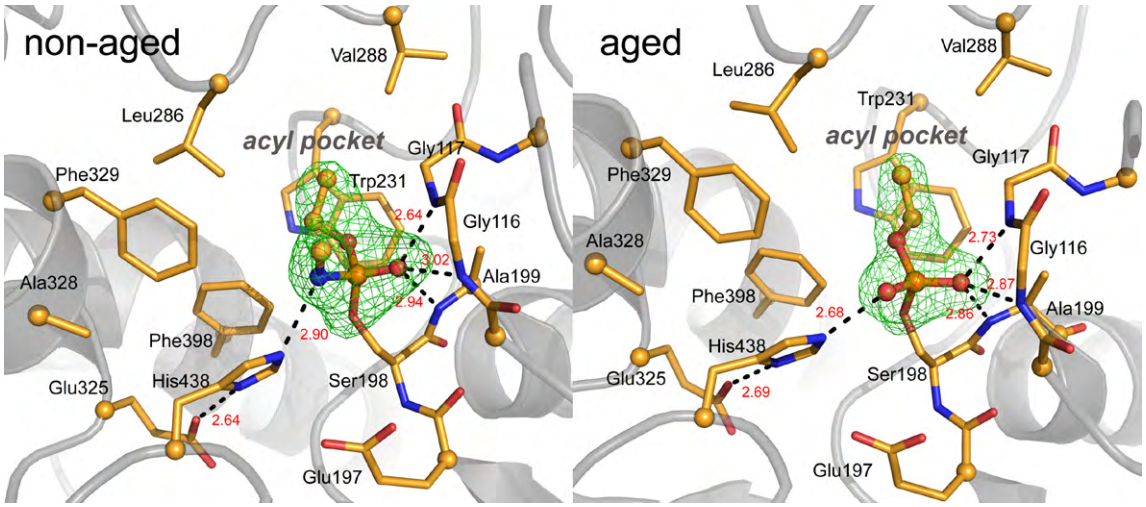


**Fig. 2.** Active site of non-aged (left panel) and aged (right panel) TA4–huBChE conjugates. Key residues are represented as sticks with carbon atoms in bright orange, nitrogen atoms in blue, phosphorus in orange, and oxygen atoms in red. Hydrogen bonds are represented by black dashes with distances in Å. The phosphyl adduct is represented in ball and stick. The green mesh represents a |Fo|−|Fc| omit map contoured at 3.0$\sigma$. The catalytic triad is composed of residues Ser198/His438/Glu325 and residues Leu286/Val288/Trp231/Phe398 delimit the acyl-pocket.

the substituent-phosphorus bond, thus favoring rearrangement of the bipyramidal intermediate. For example, it was recently demonstrated by theoretical calculations that the pathway involving a rearrangement was energetically favored in the case of mouse AChE phosphylation by tabun despite its active site is more buried than that of huBChE [20]. There is sufficient room in both AChE and BChE, to allow a rearrangement of the substituents pointing toward the choline-binding pocket and toward the gorge entrance without steric clash. Then, His438 can trigger the departure of the methylamino by protonation, since a protonated methylamine is an excellent leaving group. We expect that the aging reaction should be optimum when His438 is fully protonated, so that the proposed mechanism could be further confirmed by a pH-dependence study.

The aging rate of TA4–huBChE is noticeably 10-fold slower than that of tabun-inhibited huBChE ($0.011 \pm 0.0003\ h^{-1}$ vs $0.1 \pm 001\ h^{-1}$), but nearly identical to that of N-mono-propyl tabun analogue, TA6, which was shown to dealkylate ($0.015 \pm 0.0005\ h^{-1}$) [18]. The fact that the aging rates of TA4 and TA6 are close despite a different mechanism, and the fact that TA6 ages 6 times slower than tabun despite both do so by dealkylation of their ethoxy group, show that the rates do not provide an argument supporting either identical or different mechanisms. The rates depend apparently upon more factors than the nature of the aging substituent. The close aging rates for TA4 and TA6 also mean that the substitution mechanism is as efficient as dealkylation for these N-mono-alkyl compounds.

Remarkably, the spontaneous reactivation rate of TA4 is only 3-fold slower than the aging rate ($0.004 \pm 0.0001\ h^{-1}$), suggesting competition between both reactions, which share the same initial step: the nucleophilic attack by a water molecule. This suggests that the reaction is at a crossroad at the time of the rearrangement of the transition state because both aging and reactivation pathways remain possible. Indeed, if His438 protonates the serine instead of the methylamino, this leads to the scission of the serine phosphorus bond, i.e., spontaneous reactivation.

## 4. Rearrangement of the transition state during phosphylation and reactivation

Most OPs have a stereogenic phosphorus atom, which leads to the presence of equal amounts of enantiomers in the synthesis product. The two enantiomers have different inhibition potency because the active site of ChEs is asymmetric and thus displays reaction stereoselectivity [4]. It is assumed that the most potent enantiomer is that whose substituents can easily fit the pockets surrounding the catalytic serine and satisfies the requirements for a nucleophilic substitution by in-line displacement: during phosphylation, the leaving group L is in an axial position of the trigonal–bipyramidal transition state, opposite to the axially entering serine hydroxyl group, with the position of phosphoryl oxygen fixed via hydrogen bonding to the oxyanion hole [4] (Fig. 4A). This substitution mechanism by in-line displacement has been confirmed for AChE inhibited by OP which absolute configuration is assumed from stereochemical synthetic pathways [8,21]. This includes soman, sarin and VX: The comparisons of the absolute configuration of the most reactive enantiomer determined by kinetic studies, to the absolute configuration of the serine adduct obtained from X-ray structures of the OP–ChE conjugates, permit the determination of the phosphylation mechanism. However the

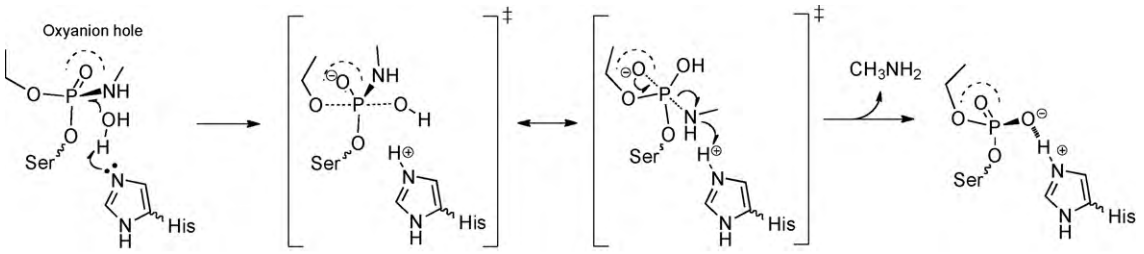


**Fig. 3.** Proposed aging mechanism of the TA4–hBChE conjugates. Pseudorotation leads to reorganization of the methylamino group from equatorial position to apical position in the trigonal–bipyramidal transition state.

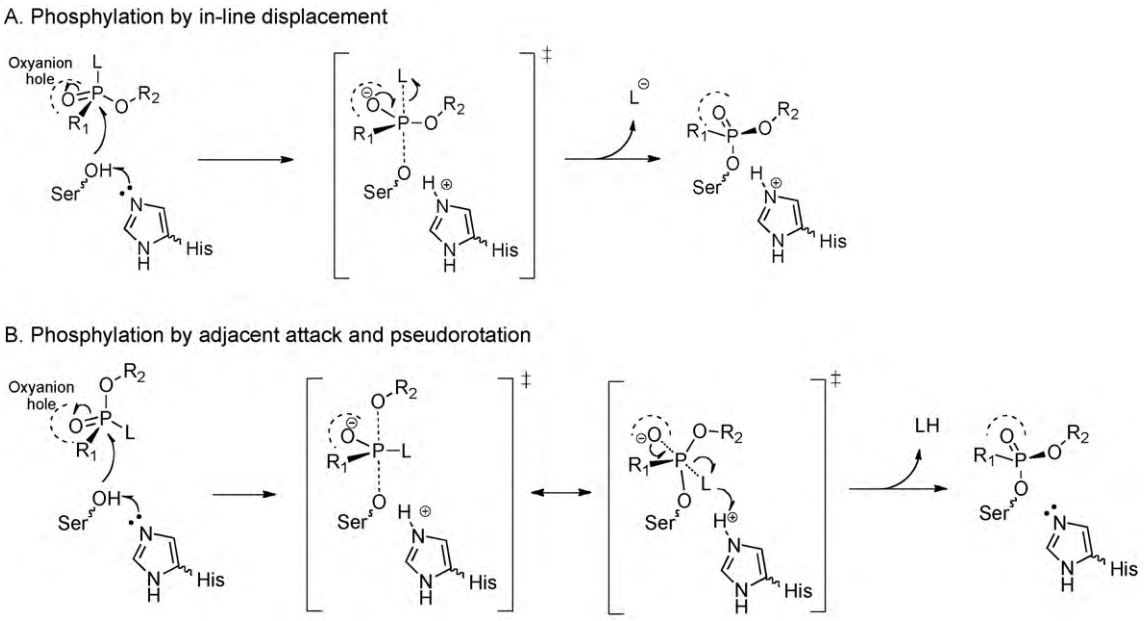


**Fig. 4.** Phosphylation and reactivation mechanism of phosphylated cholinesterases based on assumed in-line displacement.

situation is not so clear for OP like TA4 or tabun, their absolute configurations still being unknown. Despite the crystal structures of tabun–AChE and BChE conjugates have been solved, showing that the serine adduct is of configuration $P_R$, we can only guess the absolute configuration of the most reactive enantiomer by making an assumption on the phosphylation mechanism [22]. For example, assuming in-line displacement, in case of tabun leads to the conclusion that the most reactive enantiomer should be $P_R$. Note that both configurations are R despite the inversion due to a change in the substituent priority. But the Quantum Mechanics/Molecular Mechanics study by Kwasnieski et al. indicates that the most energetically favorable mechanism for tabun inhibition of mouse AChE is that with the leaving group adjacent to the catalytic serine (adjacent attack; Fig. 4B) [20]. This suggests that the most reactive enantiomer of tabun is $P_S$. Much like in the proposed aging mechanism of TA4–huBChE, this attack adjacent to the serine implies a rearrangement of the leaving group position from equatorial to apical by Berry pseudorotation. It suggests that such rearrangement is more common that previously assumed and must be considered as a possible pathway for the reactions involving phosphylated serine hydrolases.

This opens new perspective for the reactivation of phosphylated ChE by oximes. Indeed it is assumed that the oximate must attack from the apical position, opposite to the catalytic serine, because the resulting trigonal–bipyramidal transition state can readily collapse by cleavage of the serine phosphorus bond (Fig. 5A). Actually, the face opposing the catalytic serine is the sole open face for soman due to the bulkiness of the pinacolyl substituent [23], so that the

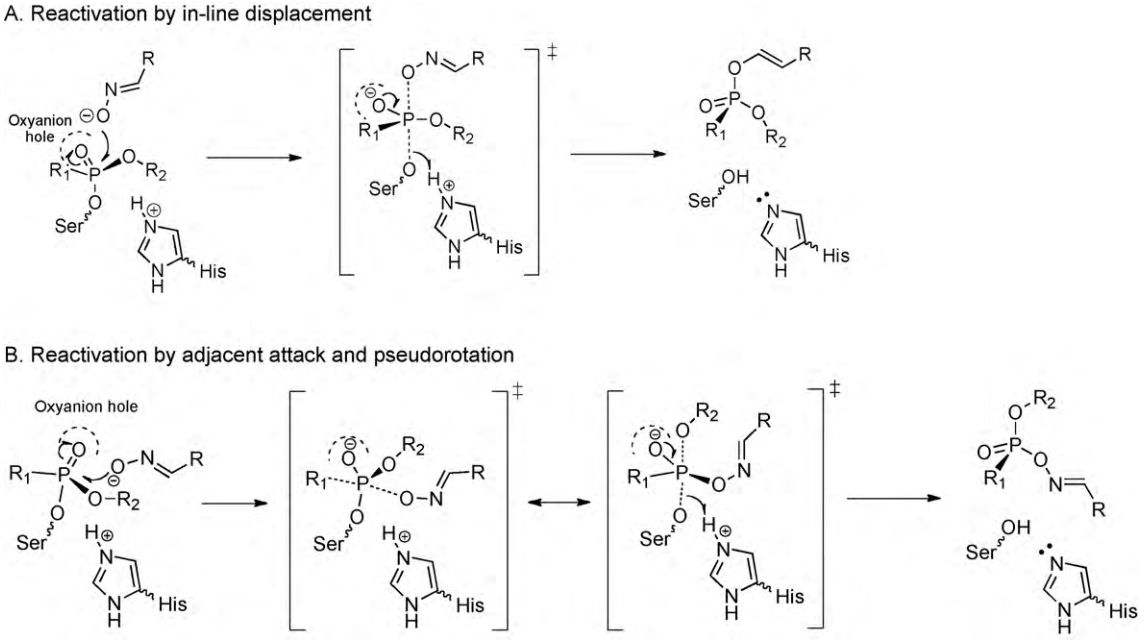


**Fig. 5.** Phosphylation and reactivation mechanism of cholinesterases based on a rearrangement of the trigonal–bipyramidal transition state by Berry pseudorotation following an adjacent attack by the catalytic serine or an oximate.

attack of the oximate from that face remains the only viable solution for soman–AChE conjugates. But the situation is different for other OP like VX, tabun or even sarin which alkoxy substituents are reasonably small (ethoxy, ethoxy and isopropyloxy respectively). The crystal structures of these three OP–AChE conjugates show that their alkoxy group tend to bend back over the phosphorus *à la* "scorpion tail", crowding the face opposite to the serine, and leaving the face adjacent to the serine and vicinal glutamate well open [21,22,24]. This suggests that the oximate could favorably attack from the side according to the rearrangement-based mechanism described in Fig. 5B. None of the current oximes used for reactivating ChEs were designed with that mechanism in mind for the obvious reason that they have been synthesized well before any ChE tridimensionnal structure was known. Anyway, there is a lot of room for improvement, as actually none of the known oximes bind to phosphylated enzyme with their reactive function in a proper orientation for reactivation according to the two possible pathways described above [23–26]. While designing oximes based on in-line nucleophilic substitution is certainly a good option, we suggest that oximes based on adjacent nucleophilic attack and pseudorotation should be investigated.

## Conflict of interest statement

None.

## Acknowledgements

This work was supported by the Direction Générale de l'Armement under contract DGA/PEA 08CO501, and Agence Nationale de la Recherche grant numbers ANR-06-BLAN-0163 and ANR-09-BLAN-0192 to F.N.

## References

[1] B. Li, J.A. Stribley, A. Ticu, W. Xie, L.M. Schopfer, P. Hammond, S. Brimijoin, S.H. Hinrichs, O. Lockridge, Abundant tissue butyrylcholinesterase and its possible function in the acetylcholinesterase knockout mouse, J. Neurochem. 75 (3) (2000) 1320–1331.
[2] O. Lockridge, P. Masson, Pesticides and susceptible populations: people with butyrylcholinesterase genetic variants may be at risk, Neurotoxicology 21 (1–2) (2000) 113–126.
[3] N. Aurbek, H. Thiermann, F. Eyer, P. Eyer, F. Worek, Suitability of human butyrylcholinesterase as therapeutic marker and pseudo catalytic scavenger in organophosphate poisoning: a kinetic analysis, Toxicology 259 (3) (2009) 133–139.
[4] J. Järv, Stereochemical aspects of cholinesterase catalysis, Bioorg. Chem. 12 (4) (1984) 259–278.
[5] F. Worek, H. Thiermann, L. Szinicz, P. Eyer, Kinetic analysis of interactions between human acetylcholinesterase, structurally different organophosphorus compounds and oximes, Biochem. Pharmacol. 68 (11) (2004) 2237–2248.
[6] F Berends, C.H. Posthumus, I.v.d. Sluys, F.A. Deierkauf, The chemical basis of the "ageing process" of DFP-inhibited pseudocholinesterase, Biochim. Biophys. Acta 34 (1959) 567–568.
[7] H.O. Michel, B.E. Hackley Jr., L. Berkowitz, G. List, E.B. Hackley, W. Gillilan, M. Pankau, Ageing and dealkylation of soman (pinacolylmethylphosphonofluoridate)-inactivated eel cholinesterase, Arch. Biochem. Biophys. 121 (1) (1967) 29–34.
[8] C.B. Millard, G. Kryger, A. Ordentlich, H.M. Greenblatt, M. Harel, M.L. Raves, Y. Segall, D. Barak, A. Shafferman, I. Silman, J.L. Sussman, Crystal structures of aged phosphonylated acetylcholinesterase: nerve agent reaction products at the atomic level, Biochemistry 38 (22) (1999) 7032–7039.
[9] A. Bencsura, I. Enyedy, I.M. Kovach, Origins and diversity of the aging reaction in phosphonate adducts of serine hydrolase enzymes: what characteristics of the active site do they probe? Biochemistry 34 (28) (1995) 8989–8999.
[10] A. Shafferman, A. Ordentlich, D. Barak, D. Stein, N. Ariel, B. Velan, Aging of phosphylated human acetylcholinesterase: catalytic processes mediated by aromatic and polar residues of the active centre, Biochem. J. 318 (Pt 3) (1996) 833–840.
[11] Y. Segall, D. Waysbort, D. Barak, N. Ariel, B.P. Doctor, J. Grunwald, Y. Ashani, Direct observation and elucidation of the structures of aged and nonaged phosphorylated cholinesterases by 31P NMR spectroscopy, Biochemistry 32 (49) (1993) 13441–13450.
[12] J.A. Doorn, D.A. Gage, M. Schall, T.T. Talley, C.M. Thompson, R.J. Richardson, Inhibition of acetylcholinesterase by (1S, 3S)-isomalathion proceeds with loss of thiomethyl: kinetic and mass spectral evidence for an unexpected primary leaving group, Chem. Res. Toxicol. 13 (12) (2000) 1313–1320.
[13] F. Nachon, O.A. Asojo, G.E. Borgstahl, P. Masson, O. Lockridge, Role of water in aging of human butyrylcholinesterase inhibited by echothiophate: the crystal structure suggests two alternative mechanisms of aging, Biochemistry 44 (4) (2005) 1154–1162.
[14] H. Li, L.M. Schopfer, F. Nachon, M.T. Froment, P. Masson, O. Lockridge, Aging pathways for organophosphate-inhibited human butyrylcholinesterase, including novel pathways for isomalathion, resolved by mass spectrometry, Toxicol. Sci. 100 (1) (2007) 136–145.
[15] T.J Kropp, R.J. Richardson, Mechanism of aging of mipafox-inhibited butyrylcholinesterase, Chem. Res. Toxicol. 20 (3) (2007) 504–510.
[16] T.J. Kropp, R.J. Richardson, Aging of mipafox-inhibited human acetylcholinesterase proceeds by displacement of both isopropylamine groups to yield a phosphate adduct, Chem. Res. Toxicol. 19 (2) (2006) 334–339.
[17] T.J. Kropp, P. Glynn, R.J. Richardson, The mipafox-inhibited catalytic domain of human neuropathy target esterase ages by reversible proton loss, Biochemistry 43 (12) (2004) 3716–3722.
[18] E. Carletti, N. Aurbek, E. Gillon, M. Loiodice, Y. Nicolet, J.C. Fontecilla-Camps, P. Masson, H. Thiermann, F. Nachon, F. Worek, Structure-activity analysis of aging and reactivation of human butyrylcholinesterase inhibited by analogues of tabun, Biochem. J. 421 (1) (2009) 97–106.
[19] R.S. Berry, Correlation of rates of intramolecular tunneling processes, with application to some group V compounds, J. Chem. Phys. 32 (3) (1960).
[20] O Kwasnieski, L. Verdier, M. Malacria, E. Derat, Fixation of the two Tabun isomers in acetylcholinesterase: a QM/MM study, J. Phys. Chem. B 113 (29) (2009) 10001–10007.
[21] C.B. Millard, G. Koellner, A. Ordentlich, A. Shafferman, I. Silman, J.L. Sussman, Reaction products of acetylcholinesterase and VX reveal a mobile histidine in the catalytic triad, J. Am. Chem. Soc. 121 (42) (1999) 9983–9984.
[22] E. Carletti, H. Li, B. Li, F. Ekstrom, Y. Nicolet, M. Loiodice, E. Gillon, M.T. Froment, O. Lockridge, L.M. Schopfer, P. Masson, F. Nachon, Aging of cholinesterases phosphylated by tabun proceeds through O-dealkylation, J. Am. Chem. Soc. 130 (47) (2008) 16011–16020.
[23] B. Sanson, F. Nachon, J.P. Colletier, M.T. Froment, L. Toker, H.M. Greenblatt, J.L. Sussman, Y. Ashani, P. Masson, I. Silman, M. Weik, Crystallographic snapshots of nonaged and aged conjugates of soman with acetylcholinesterase, and of a ternary complex of the aged conjugate with pralidoxime, J. Med. Chem. 52 (23) (2009) 7593–7603.
[24] F Ekstrom, A. Hornberg, E. Artursson, L.G. Hammarstrom, G. Schneider, Y.P. Pang, Structure of HI-6*sarin-acetylcholinesterase determined by X-ray crystallography and molecular dynamics simulation: reactivator mechanism and design, PLoS One 4 (6) (2009) e5957.
[25] F.J. Ekstrom, C. Astot, Y.P. Pang, Novel nerve-agent antidote design based on crystallographic and mass spectrometric analyses of tabun-conjugated acetylcholinesterase in complex with antidotes, Clin. Pharmacol. Ther. 82 (3) (2007) 282–293.
[26] A. Hornberg, E. Artursson, R. Warme, Y.P. Pang, F. Ekstrom, Crystal structures of oxime-bound fenamiphos-acetylcholinesterases: reactivation involving flipping of the His447 ring to form a reactive Glu334-His447-oxime triad, Biochem. Pharmacol. 79 (3) (2010) 507–515.

# Structural Study of the Complex Stereoselectivity of Human Butyrylcholinesterase for the Neurotoxic V-agents

M. Wandhammer, E. Carletti, M. Van der Schans, E. Gillon, Y. Nicolet, P. Masson, M. Goeldner, D. Noort, **F. Nachon***

The Journal of Biological Chemistry 286 (2011) 16783-16789

THE JOURNAL OF BIOLOGICAL CHEMISTRY VOL. 286, NO. 19, pp. 16783–16789, May 13, 2011


# Structural Study of the Complex Stereoselectivity of Human Butyrylcholinesterase for the Neurotoxic V-agents*

Received for publication, December 6, 2010, and in revised form, February 28, 2011 Published, JBC Papers in Press, March 23, 2011, DOI 10.1074/jbc.M110.209569

**Marielle Wandhammer[‡§], Eugénie Carletti[‡], Marcel Van der Schans[¶], Emilie Gillon[‡], Yvain Nicolet[‖], Patrick Masson[‡], Maurice Goeldner[§], Daan Noort[¶], and Florian Nachon[‡1]**

*From the [‡]Département de Toxicologie, Institut de Recherche Biomédicale des Armées-CRSSA, 38700 La Tronche, France, the [§]Laboratoire de Conception et Application de Molécules Bioactives, UMR 7199, Faculté de Pharmacie, 67400 Illkirch, France, the [¶]Research Group Diagnosis and Therapy, Business Unit Biological and Chemical Protection, TNO Defence, Security and Safety, 2288 GJ Rijswijk, The Netherlands, and the [‖]Laboratoire de Cristallographie et Cristallogenèse des Protéines, Institut de Biologie Structurale, 38027 Grenoble, France*

**Nerve agents are chiral organophosphate compounds (OPs) that exert their acute toxicity by phosphorylating the catalytic serine of acetylcholinesterase (AChE). The inhibited cholinesterases can be reactivated using oximes, but a spontaneous time-dependent process called aging alters the adduct, leading to resistance toward oxime reactivation. Human butyrylcholinesterase (BChE) functions as a bioscavenger, protecting the cholinergic system against OPs. The stereoselectivity of BChE is an important parameter for its efficiency at scavenging the most toxic OPs enantiomer for AChE. Crystals of BChE inhibited in solution or in cristallo with racemic V-agents (VX, Russian VX, and Chinese VX) systematically show the formation of the $P_S$ adduct. In this configuration, no catalysis of aging seems possible as confirmed by the three-dimensional structures of the three conjugates incubated over a period exceeding a week. Crystals of BChE soaked in optically pure $VX_R$-(+) and $VX_S$-(−) solutions lead to the formation of the $P_S$ and $P_R$ adduct, respectively. These structural data support an in-line phosphonylation mechanism. Additionally, they show that BChE reacts with $VX_R$-(+) in the presence of racemic mixture of V-agents, at odds with earlier kinetic results showing a moderate higher inhibition rate for $VX_S$-(−). These combined results suggest that the simultaneous presence of both enantiomers alters the enzyme stereoselectivity. In summary, the three-dimensional data show that BChE reacts preferentially with $P_R$ enantiomer of V-agents and does not age, in complete contrast to AChE, which is selectively inhibited by the $P_S$ enantiomer and ages.**

The acute toxicity of organophosphorus nerve agents (OPs)[2] is due to rapid phosphorylation of acetylcholinesterase (AChE; EC 3.1.1.7) at the neuronal synapses and neuromuscular junctions (1, 2). What follows is an accumulation of acetylcholine that leads, among other cholinergic symptoms, to respiratory failure and even death. One strategy to prevent AChE inhibition is to scavenge the nerve agent before it can reach its synaptic target. Butyrylcholinesterase (BChE; EC 3.1.1.8), abundant in human (3), functions as a natural bioscavenger of nerve agents (4, 5). A large amount of BChE injected intravenously or intramuscularly scavenges the nerve agents and protect animals against 3–5 $LD_{50}$ of soman and VX (6). BChE purified from human plasma (Baxter Healthcare Corporation) is one enzyme source. This product is under consideration for its development as a stoichiometric bioscavenger for pretreatment of OP intoxication.

The catalytic serine of cholinesterases is located at the bottom of a gorge, surrounded by pockets, named from the part of the native substrate they bind. In AChE, the acyl-binding pocket is much smaller than the choline-binding pocket. Therefore, AChE exerts a strong enantioselectivity on chiral OPs, bearing substituents of different sizes. For example, hAChE reacts about $5 \times 10^4$ times more rapidly with $P_S$ diastereoisomers of soman because the large pinacolyl and small methyl substituents fit, respectively, in the choline-binding pocket and acyl-binding pocket (7). The acyl-binding pocket of BChE is much wider than that of AChE and is therefore expected to be less selective for some OPs. This is important in regard to the amount of enzyme required to scavenge one equivalent of racemic nerve agent. Indeed, half an equivalent of BChE is sufficient if the enzyme binds preferably the same enantiomer as AChE. At least one equivalent is necessary if BChE binds equally both enantiomers or preferably the less toxic enantiomer.

Several lines of evidence suggest that BChE and hAChE have a different stereoselectivity for V-agents: VX, Russian VX (VR), and Chinese VX (CVX) (Scheme 1). One piece of evidence comes from a spontaneous time-dependent dealkylation of the V-agent adduct of cholinesterases, called aging, which leads to a resistance toward oxime reactivation (8). The dealkylation mechanism for alkoxy-OP adducts is stereoselective because it involves residues located in the choline-binding pocket of BChE. Accordingly, no aging will occur if the alkoxy substituent of V-agents is not pointing toward this pocket. A marginal aging rate is reported for VX-inhibited BChE ($t_{1/2}$ = 77 h), and

* This work was supported by Direction Générale de l'Armement under Programme d'Etude Amont Grants 08co501, ANR-06-BLAN-0163, and ANR-09-BLAN-0192 (to F. N.) and Defense Threat Reduction Agency Grant CBDIF07-THER01-2-0038 (to D. N., F. N., and M. G.).

*The atomic coordinates and structure factors (codes 2XQF, 2XQG, 2XQI, 2XQJ, and 2XQK) have been deposited in the Protein Data Bank, Research Collaboratory for Structural Bioinformatics, Rutgers University, New Brunswick, NJ (http://www.rcsb.org/).*

[1] To whom correspondence should be addressed: Département de Toxicologie, Institut de Recherche Biomédicale des Armées-CRSSA, 24 av. des Maquis du Grésivaudan, 38700 La Tronche, France. Fax: 205-934-7437; E-mail: florian@nachon.net.

[2] The abbreviations used are: OP, organophosphate; AChE, acetylcholinesterase; BChE, butyrylcholinesterase; CVX, Chinese VX; h, human; PDB, Protein Data Bank; VR, Russian VX; TLS, translation libration screw motion.

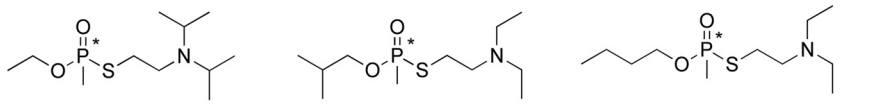

Diisopropylamino-ethyl-O-ethyl methylphosphonothioate (VX)

Diethylamino-ethyl-O-isobutyl methylphosphonothioate (VR)

Diethylamino-ethyl-O-butyl methylphosphonothioate (CVX)

SCHEME 1. **Chemical structures of V-agents, VX, VR, and CVX.**

no aging could be detected for VR-inhibited BChE (9). Furthermore, mass spectrometry analysis shows that no aged adduct was detectable for BChE treated with an excess solution of racemic VX or VR (10). This suggests that for these adducts, the alkoxy substituent is usually not located in the choline-binding pocket. This contrasts with the view offered by the x-ray structure of *Torpedo californica* AChE inhibited by VX with the ethoxy substituent located in the choline-binding pocket and able to age (11). This leads to the conclusion that BChE and AChE have opposite stereoselectivity.

However, measurements of the inhibition rate of separated VX isomers by independent laboratory showed that $VX_S$-(−) inhibits BChE a few-fold faster than $VX_R$-(+), whereas the difference in rate is more than 2 orders of magnitude for hAChE (12, 13). This in turn leads to the conclusion that both cholinesterases share the same stereoselectivity for $VX_S$-(−) but that AChE is much more stereoselective than BChE. This is consistent with recent *in vivo* experiment showing that a molar equivalent of BChE is required to protect against racemic VX (14).

Interestingly, these early results puzzlingly suggest that the stereoselectivity of BChE differs when exposed to racemic or optically pure solutions of VX. In this structural study, we investigate, at the molecular level, which enantiomer of VX, VR, and CVX reacts preferentially with BChE. We determine the inhibition mechanism for both enantiomers of VX and give a rational explanation for the absence of aging in crystallography and mass spectrometry experiments.

## EXPERIMENTAL PROCEDURES

### *Caution*

V-agents (VX, CVX, and VR) are highly toxic and are classified as a schedule 1 chemical as defined in the Chemical Weapons Convention. The handling of V-agents is dangerous and requires suitable personal protection, training, and facilities.

### *Chemicals*

Racemic VX, *O*-ethyl-S-[2[bis(1-methyl-ethyl)amino] ethyl] methylphosphonothioate, VR, and CVX, were obtained from the Centre d'Étude du Bouchet-Maîtrise NRBC (Vert-le-Petit, France). Optically pure enantiomers of $VX_R$-(+) and $VX_S$-(−) were obtained from TNO (Rijswijk, The Netherlands). For the assignment of absolute configuration *R* or *S* of VX-(+/−), see Ref. 15.

### *Recombinant Human Butyrylcholinesterase*

BChE was expressed in Chinese hamster ovary (CHO) cells and secreted into serum-free culture medium, and purified by affinity and ion-exchange chromatography as described earlier (16). The BChE enzyme was a truncated monomer containing residues 1–529 whose tetramerization domain was deleted.

### *Measurement of Inhibition Rate Constants for Pure Enantiomers of VX*

BChE activities were assayed according to Ellman's method (17). BChE solution (17 nM final) was mixed with $VX_S$-(−) or $VX_R$-(+) (respectively, 21 and 88 nM final) in 100 mM phosphate buffer, pH 8.0. Each minute, 5 $\mu$l of the mixture was added to a well (96-well plate) filled with 100 $\mu$l of 0.8 mM 5,5′-dithiobis-(2-nitrobenzoic acid) in 100 mM phosphate buffer, pH 8.0. After the 7th aliquot (7 min), the wells were filled with 100 $\mu$l of 0.8 mM butyrylthiocholine in water. Absorbance was read at 412 nm immediately, then 5 min later. The net raise of absorbance is a direct measure of BChE activity. The initial concentration of $VX_S$-(−) is less than 2-fold the initial concentration of BChE which means that the inhibition follows second-order kinetics. The inhibition rate $ki_S$ of BChE by $VX_S$-(−) was determined with the following equation,

$$\frac{1}{C - Ei} = \frac{1}{C} \cdot ki_S \cdot t \qquad \text{(Eq. 1)}$$

where $C$ is the average concentration of enzyme and inhibitor (enzyme+inhibitor/2), $Ei$ is the concentration of the inhibited enzyme, $ki_S$ is the inhibition rate, and $t$ is time.

The initial concentration of $VX_R$-(+) is more than 5 times the initial concentration of BChE which means that the inhibition follows pseudo-first-order kinetics. The inhibition rate $ki_R$ of BChE by $VX_R$-(+) was determined with the following equation,

$$\log\frac{A_t}{A_0} = -\frac{ki_R \cdot I \cdot t}{2.303} \qquad \text{(Eq. 2)}$$

where $A_t$ is the activity of human BChE at time $t$ and $A_0$ at time 0, $I$ is the initial concentration of $VX_R$-(+), $ki_R$ is the inhibition rate, and $t$ is time.

### *Crystals of V-agent-inhibited BChE Conjugates*

BChE crystallized at a concentration of 8 mg/ml from 0.1 M MES, pH 6.5, supplemented with 2.1 M ammonium sulfate, using the hanging-drop system. The VX, CVX, and VR stock solutions were at 10 mM in 2-propyl alcohol. Crystals of conjugates were obtained using three different procedures.

*Flash Soaking*—Crystals of native BChE were flash-soaked into a solution containing 1 mM racemic V-agents or pure enantiomers VX for 5 min and flash-cooled in liquid nitrogen to prevent postinhibition reactions such as aging and/or spontaneous reactivation. Three soaking solutions were tested for racemic V-agents, from either 0.1 M MES, pH 6.5, or 0.1 M phosphate buffer, pH 7.4 or pH 8.0.

**TABLE 1**
**X-ray data collection and refinement statistics**

| Enzyme | Racemate | | | Pure enantiomer | |
|---|---|---|---|---|---|
| | VX in cristallo | VR in solution | CVX in solution | $VX_S$-(−) | $VX_R$-(+) |
| PDB entry code | 2XQF | 2XQG | 2XQI | 2XQK | 2XQJ |
| **Data collection** | | | | | |
| Space group | *I422* | *I422* | *I422* | *I422* | *I422* |
| Unit cell axes, $a = b$, $c$ (Å) | 155.1 128.1 | 154.6 127.6 | 155.2 127.0 | 154.9 127.4 | 155.8 128.3 |
| X-ray source | ID14-eh4 (λ = 0.981) | ID14-eh1 (λ = 0.933) | ID14-eh2 (λ = 0.933) | ID23-eh1 (λ = 0.954) | |
| No. of reflections | 409,037 | 249,879 | 223,406 | 214,798 | 284,598 |
| Unique reflections | 45,286 | 34,420 | 23,438 | 30,395 | 31,042 |
| Resolution (Å) | 48.0-2.1 (2.5-2.1) | 41.5-2.3 (2.5-2.3) | 49.1-2.6 (2.9-2.6) | 41.5-2.4 (2.5-2.4) | 49.3-2.4 (2.5-2.4) |
| Completeness (%) | 99.2 (98.5) | 99.7 (99.6) | 96.0 (97.7) | 99.5 (99.6) | 99.9 (99.9) |
| $R_{meas}$[a] (%) | 6.8 (30.8) | 7.2 (48.8) | 15.5 (50.4) | 7.9 (48.9) | 8.1 (41.5) |
| $I/\acute{o}$(I) | 22.3 (7.9) | 27.3 (4.8) | 9.9 (4.1) | 20.5 (5.3) | 19.9 (6.2) |
| Redundancy | 9.0 (8.7) | 7.3 (7.4) | 9.5 (9.0) | 7.1 (6.9) | 9.2 (9.7) |
| **Refinement statistics** | | | | | |
| $R$-factor[b] ($R_{free}$)[c] | 15.0 (18.9) | 16.2 (21.4) | 18.4 (24.7) | 15.7 (21.7) | 16.7 (22.3) |
| No. of atoms | | | | | |
| Protein | 4269 | 4258 | 4258 | 4265 | 4246 |
| Solvent | 432 | 419 | 247 | 323 | 346 |
| Others | 193 | 185 | 186 | 183 | 161 |
| Mean $B$-factor (Å$^2$) | 37.1 | 38.1 | 54.0 | 41.2 | 39.7 |
| Root mean square deviation from ideality | | | | | |
| Bond length (Å) | 0.030 | 0.023 | 0.020 | 0.022 | 0.022 |
| Angles (deg) | 2.291 | 2.051 | 1.877 | 1.954 | 1.976 |
| Chiral (Å$^3$) | 0.207 | 0.144 | 0.127 | 0.136 | 0.139 |

[a] $R_{meas}$ as defined in Ref. 31.
[b] $R$-factor = $\Sigma \mid F_o - \mid F_c \mid \mid / \Sigma \mid F_o \mid$, $F_o$, and $F_c$ are observed and calculated structure factors.
[c] $R_{free}$ set uses about 1000 of randomly chosen reflections.

*Long Soaking*—Crystals were long-soaked into a solution containing 1 mM racemic V-agents for 10 days to allow sufficient time for *in cristallo* aging.

*Crystallization after Inhibition*—Crystals were obtained from a solution of BChE first inhibited by 0.4 mM racemic V-agents in 5 mM MES, pH 6.5. In all three cases, the crystals were washed with a cryoprotectant solution (0.1 M MES, pH 6.5, with 2.3 M ammonium sulfate, containing 20% glycerol) and then flash-cooled in liquid nitrogen.

### *X-ray Data Collection and Structure of V-agent-BChE Conjugates*

Diffraction data were collected at the European Synchrotron Radiation Facility (ESRF, Grenoble, France), at the ID29, ID23-1, ID14-1, ID14-2, and ID14-4 beam lines. All datasets were processed with XDS (18). The structures were solved by use of the CCP4 suite (19). An initial solution model was determined by molecular replacement, starting from the recombinant BChE structure (Protein Data Bank (PDB) entry 1P0I) from which all ligands (butyrate, glycerol, ions) and glycan chains were removed. For all diffraction data sets, the model was refined with REFMAC5 (20). An initial rigid body refinement was followed by iterative cycles of model building with Coot (21), and then restrained and TLS refinement was carried out with REFMAC5. The bound ligands and their descriptions were built using the Dundee PRODRG 2.5 server including energy minimization using GROMOS 96.1 force field.

Significant drops in $R$-factor and $R_{free}$ occurred with TLS refinement. TLS groups were defined with the help of the TLS Motion Determination server (22). Refined TLS parameters are included in the deposited PDB file for each entry. Simulated annealing composite omit maps were calculated using Phenix (23) to check any bias in the model. Protein structures were illustrated using the program PyMOL.

## RESULTS

*Inhibition Rate Constants for Optically Pure VX Enantiomers*—The bimolecular rate constant for the inhibition of recombinant BChE is $1.09 \pm 0.07 \times 10^7$ min$^{-1}$ · M$^{-1}$ ($n = 12$) for $VX_S$-(−) and $2.01 \pm 0.10 \times 10^6$ min$^{-1}$ · M$^{-1}$ ($n = 12$) for $VX_R$-(+). Thus, $VX_S$-(−) is only 5.4-fold more potent than $VX_R$-(+), in good agreement with literature data (12, 13).

*X-ray Structure of Racemic V-agent-BChE Conjugates*—We followed three different procedures to obtain the crystal structures of the conjugates. The flash-soaking procedure was aimed at obtaining the conjugate structure before any aging or spontaneous reactivation can take place. The long-soaking procedure intended to obtain the structure of the aged conjugate, and the procedure using inhibition in solution before crystallization was aimed at avoiding a possible enantioselectivity or aging bias introduced by the crystal packing. Still, we cannot exclude that a bias could persist during crystallization, if for example one enantiomeric conjugate crystallizes more favorably.

Whatever the procedure used, we systematically obtained identical conjugate structures with all three racemic V-agents, without any evidence for aging. The crystals belonged to the usual space group *I422*. The structures were refined at resolutions ranging from 2.1 to 2.6 Å. Data and refinement statistics for one dataset per V-agent are presented in Table 1. For each structure, a strong peak of electron density (>11$\sigma$) is observed in the $F_o - F_c$ map at covalent bonding distance of the catalytic serine Oγ, in agreement with the presence of the bound inhibitor. The oxygen of the phosphonate moiety is nested in the oxyanion hole, well stabilized by three hydrogen bonds with the main chain amide nitrogen of Gly-116, Gly-117, and Ala-199 (Fig. 1).

For all conjugates, the methyl group of the phosphonyl adducts points toward the catalytic histidine whereas the

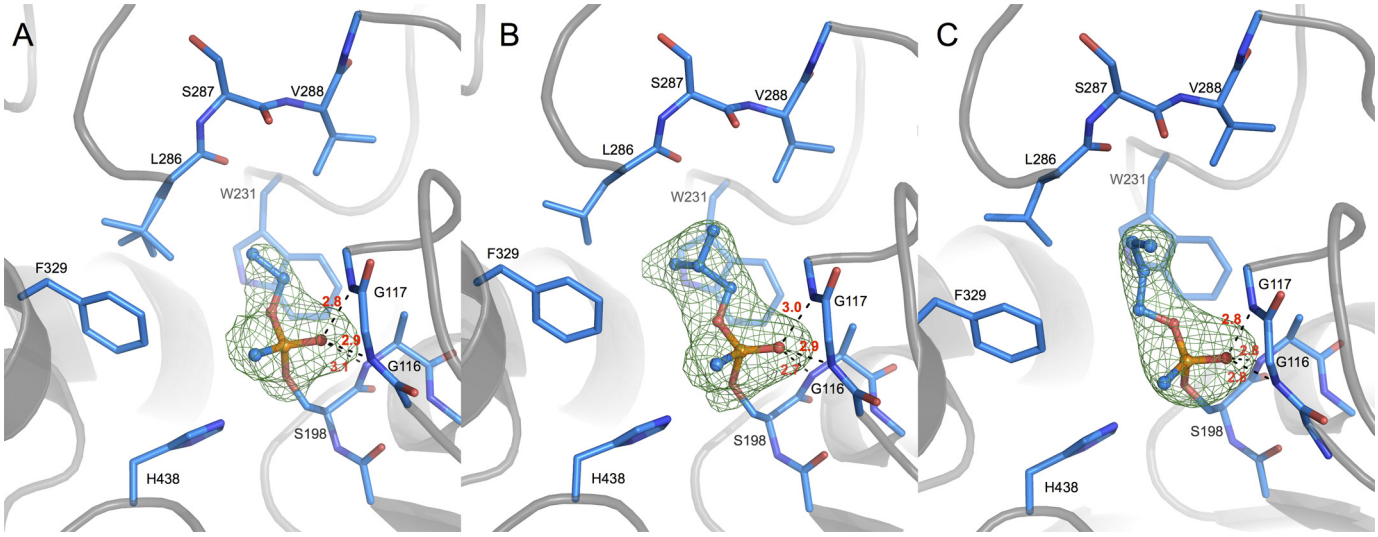


FIGURE 1. **Active site of VX-BChE (*A*), VR-BChE (*B*), and CVX-BChE (*C*) conjugates.** Crystals are obtained either by long soaking of BChE crystal in a 1 mM solution of racemic VX (*A*) or by crystallization of a solution containing 0.1 mM BChE inhibited by 0.4 mM of racemic VR (*B*) or CVX (*C*). Key residues are represented by *sticks* with carbon atoms in *blue*, oxygen atoms in *red*, nitrogen atoms in *dark blue*, and phosphorus atom in *orange*. Hydrogen bonds are represented by *black dashes*, and atomic distances are indicated in *red* (Å). Omit maps are represented in *green mesh*, contoured at 3.0 $\sigma$.

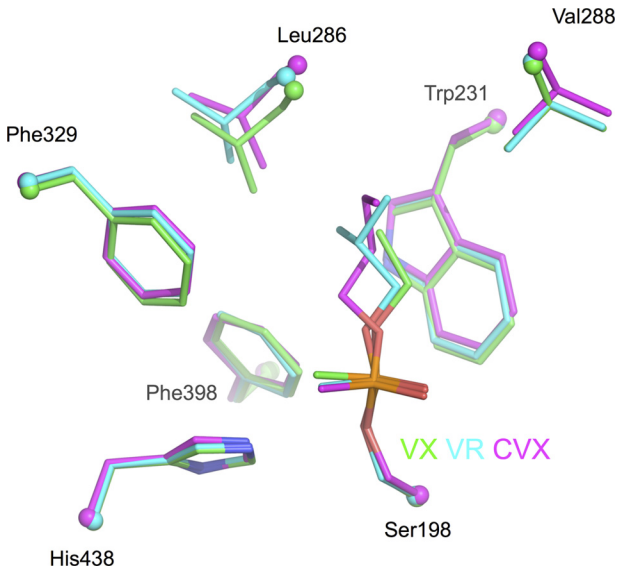


FIGURE 2. **Superimposition of the acyl-binding pocket region of VX-BChE (*cyan*), VR-BChE (*green*), and CVX-BChE (*magenta*) conjugates.** Key residues are represented by *sticks* with oxygen atoms in *red*, nitrogen atoms in *dark blue*, phosphorus atoms in *orange*. C$\alpha$ atoms are represented as *spheres*.

alkoxy substituent is located in the acyl-binding pocket delimited by Trp-231, Leu-286, and Val-288 (Fig. 1). There is no doubt about the configuration assignment. The electron density maps show no evidence for the presence of the alternate configuration, *i.e.* the alkoxy group pointing toward the choline-binding pocket.

Adjustment of the acyl loop residues is observed, depending on the bulkiness of the alkoxy substituent (Fig. 2). Compared with the ethoxy substituent in the VX adduct, the isobutyloxy group of the VR adduct induces a 0.7 Å shift of Leu-286, and the *n*-butyloxy group of CVX adduct induces a 0.4-Å shift of Val-288 and 0.8-Å shift of Leu-286. Rearrangement of the acyl loop conformation was already observed for soman (24) and phosphoramidyl adducts (25). In addition, strain in the acyl-binding pocket translates into a slightly different position of the phosphonyl head for VX and CVX. The phosphorus atom shifts by 0.3 Å away from the pocket, and the phosphonyl moiety rotates about 20° around the SerO$\gamma$-P bond (Fig. 2). No other significant displacement of residues is observed compared with the native enzyme (PDB entry 1P0I).

Thus, the absolute configuration of the phosphorus atom for each adduct is $P_S$. The orientation of VX is identical to that observed in the recently solved structure of the VX-G117H mutant of BChE (PDB entry 2XMG) (26). This is the mirror image of the VX-*Tc*AChE adduct which is of configuration $P_R$: in this latter, the methyl substituent is located in the acyl-binding pocket, and the ethoxy group points toward the catalytic histidine inducing a conformational change (11).

The formation of the $P_S$ adduct could result either from an in-line attack of $VX_R$-(+) with inversion of the phosphorus or an adjacent attack of $VX_S$-(−) and subsequent pseudorotation (27). In an effort to understand which VX enantiomer leads to the formation of the $P_S$ adduct and what is the underlying mechanism, we solved the x-ray structure of BChE crystals flash-soaked in solutions containing pure enantiomers.

*X-ray Structure of BChE Inhibited by Pure VX Enantiomers*—The structures of $VX_R$-(+) and $VX_S$-(−) conjugates were solved to 2.4-Å resolution. Data and refinement statistics for one dataset per isomer are presented in Table 1.

The ethoxy substituent of $VX_R$-(+)-BChE conjugate is located in the acyl-binding pocket whereas the methyl points toward the catalytic histidine (Fig. 3*A*). The phosphorus atom is of absolute configuration $P_S$. This conformation is identical to that obtained by inhibition using a racemic mixture and in agreement with in-line phosphorylation (Scheme 2).

By contrast, the ethoxy substituent of $VX_S$-(−)-BChE points toward the catalytic histidine whereas the methyl group is located in the acyl-binding pocket (Fig. 3*B*). The phosphorus atom is of absolute configuration $P_R$, in agreement with in-line phosphorylation (Scheme 2). The two residues known to promote aging by dealkylation are close to the ethoxy group, His-

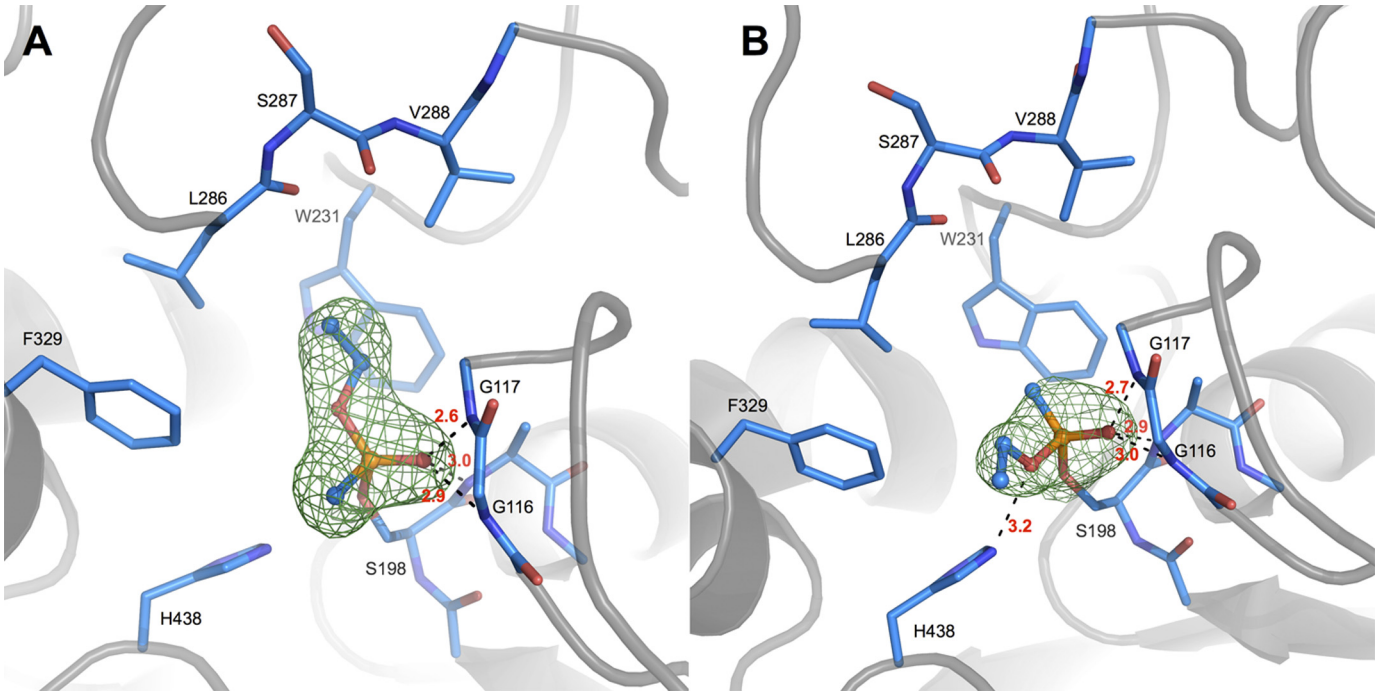


FIGURE 3. **Active site of $VX_R$-(+)-BChE (*A*) and $VX_S$-(−)-BChE (*B*) conjugates.** BChE crystals were flash-soaked in a 1 mM solution of $VX_R$-(+) (*A*) or $VX_S$-(−) (*B*). Key residues are represented by *sticks* with carbon atoms in *blue*, oxygen atoms in *red*, nitrogen atoms in *dark blue*, phosphorus atoms in *orange*. Hydrogen bonds are represented by *black dashes*, and atomic distances are indicated in *red* (Å). Omit maps are represented by a *green mesh*, contoured at 3.0 $\sigma$.

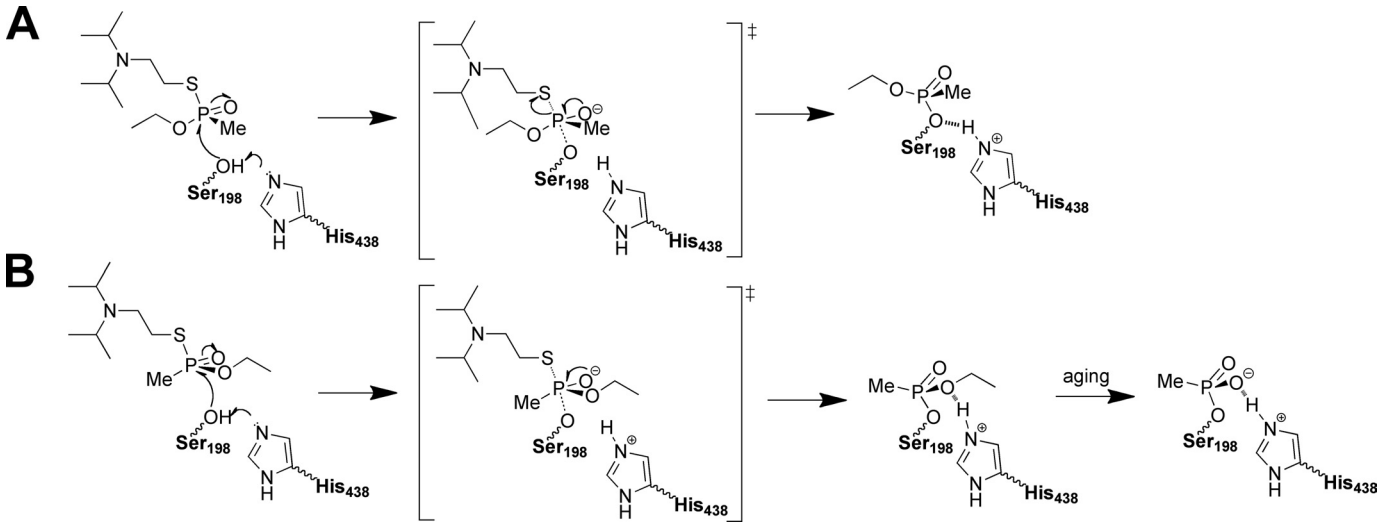


SCHEME 2. **Mechanism of inhibition of BChE by $VX_R$-(+) (*A*) and $VX_S$-(−) (*B*).**

438-Nϵ and the ethoxy oxygen being notably at H-bond distance (3.2 Å). This configuration is identical to that observed when *Tc*AChE was inhibited by racemic VX, except that no conformational change of the catalytic histidine is observed. The absence of conformational change of His-438 shows one more time that this catalytic residue is not mobile in BChE (25). These combined results suggest that in the presence of both enantiomers at submillimolar concentration, BChE will react preferentially with $VX_R$-(+).

## DISCUSSION

We do not observe identical stereoselectivity for experiments performed in the presence of one or both enantiomers of V-agents. On the one hand, three different experiments using racemic VX, *i.e. in vivo* protection (14), mass spectrometry (10), and x-ray crystallography, show that BChE reacts preferentially with $VX_R$-(+) and does not age. On the other hand, kinetic experiments performed with separated $VX_R$-(+) or $VX_S$-(−) show a slight selectivity for $VX_S$-(−). Slow aging has been observed with $VX_S$-(−), $t_{1/2} \approx 50$ h, and no aging could be detected with $VX_R$-(+).[3] The absence of aging with $VX_R$-(+) is in agreement with the structural and mass spectrometry data. Noteworthy, very slow aging has been recently reported for BChE inhibited by racemic VX, $t_{1/2} = 77$ h (9). This half-time value seems to be intermediate between those of the $VX_R$-(+) and the $VX_S$-(−) conjugates.

[3] F. Worek, unpublished data.

There can be many different explanations for this discrepancy. A first hypothesis is that a shift in selectivity originates from the ability to bind multiple molecules at the same time in the active site gorge, especially at high concentrations. This is illustrated in the x-ray structure of aged soman-BChE conjugate in complex with butyrylthiocholine (24). Multiple binding affects the catalytic behavior of the enzyme. For example, at a high substrate concentration, binding of a second molecule of butyrylthiocholine in the active site gorge of BChE accelerates the turnover about three times (28). Thus, it is possible that in the presence of a racemic mixture, both enantiomers bind simultaneously in the active site gorge and interfere so that $VX_R$-(+) is in a position more favorable for the phosphonylation. This may be favored by the high concentrations of VX required for x-ray crystallography and mass spectrometry. Aging kinetic of BChE inhibited by racemic VX could provide some clues regarding this hypothesis, but the exact concentration of inhibitor was not reported (9). Although unexplained electron density is visible in the active site gorge of the conjugate, next to Trp-82, it does not correspond to a second molecule of V-agents in which P and S atoms large electron density is easily recognizable. An alternative hypothesis is that an unknown ligand corresponding to this unexplained electron density, often present in the choline-binding pocket of BChE (24–26), could alter the binding of $VX_S$-(−). Yet another hypothesis could be that even if both conjugates form in solution, the $VX_R$-(+)-BChE conjugate crystallizes more easily. In this case there would be a crystallization artifact for inhibited BChE. But this hypothesis also requires that there should be also a crystal packing artifact, $VX_R$-(+) binding more favorably to crystallized BChE. At this point we have no evidence to favor one of these nonmutually exclusive hypotheses.

Predicting the stereoselectivity of BChE for VR and CVX uniquely from the active site topology is not straightforward. The question is whether the large substituent of VR and CVX can fit in the acyl-binding pocket of BChE. Some clues were provided by structural data showing that a diethylamino group (TA1) or a *N*-propylamino group (TA6) do fit in that pocket (25). Here, the x-ray structures of VR- and CVX-BChE confirm that the long *n*-butyloxy of CVX or the bulky isobutyloxy of VR do fit as well. This explains why no aging was observed during mass spectrometry analysis of the VR-BChE conjugate or kinetics experiments (9). By extrapolation from VX, the $P_S$ adducts results likely from the in-line attack by $VR_R$ and $CVX_R$, whereas we expect a strong selectivity of human AChE for $VR_S$ and $CVX_S$, knowing that $VX_S$-(−) is at least already 100-fold more reactive than $VX_R$-(+) (12, 13).

From a stereoselectivity point of view, hAChE appears as a better V-agents bioscavenger than hBChE. However, titration studies show that one equivalent of hAChE or hBChE is necessary to neutralize one equivalent of racemic VX in conditions simulating the estimated initial concentrations of VX during *in vivo* experiments (13). Actually, the phosphonylation rate of both VX enantiomers is higher than $10^6\ M^{-1} \cdot min^{-1}$ for both enzymes, so that the incubation time over 30 min was too long to discriminate their behavior. However, *in vivo* experiment shows that administration of hAChE gives a better survival rate of VX-exposed mouse (13).

Regarding the stereoselectivity of cholinesterases for G-agents tabun and soman, it has been established that human BChE and human AChE share the same selectivity (24, 29). Regarding sarin, bovine AChE reacts more than $4 \times 10^3$-fold faster with $sarin_S$-(−), the isopropyloxy substituent being too bulky for the AChE acyl-binding pocket, whereas the enantiomers inhibit horse serum BChE with virtually equal rates (30). Indeed, the structural data presented here and elsewhere show that the acyl-binding pocket of BChE can accommodate quite large substituents like isobutyloxy (VR) or diethylamino (TA1) (25). Moreover, mass spectrometry shows that the sarin-BChE conjugate does age by dealkylation, albeit partially (10). Aging by dealkylation suggests that the isopropyloxy substituent points toward His-438, *i.e.* the absolute configuration of the adduct is *R*, which in turn means that the enzyme reacted with $sarin_S$-(−). Incomplete aging could results either from insufficient reaction time or a significant portion of the enzyme inhibited by $sarin_R$-(+). In the latter case, both the kinetic experiment with horse serum BChE and the mass spectrometry analysis with human BChE show that these enzymes are not sufficiently enantioselective for sarin by contrast to AChE. This remains to be eventually supplemented by a structural study.

## REFERENCES


1. Holmstedt, B. (1959) Pharmacol. Rev. **11,** 567–688
2. Silman, I., and Sussman, J. L. (2005) Curr. Opin. Pharmacol. **5,** 293–302
3. Li, B., Stribley, J. A., Ticu, A., Xie, W., Schopfer, L. M., Hammond, P., Brimijoin, S., Hinrichs, S. H., and Lockridge, O. (2000) J. Neurochem. **75,** 1320–1331
4. Saxena, A., Sun, W., Luo, C., Myers, T. M., Koplovitz, I., Lenz, D. E., and Doctor, B. P. (2006) J. Mol. Neurosci. **30,** 145–148
5. Masson, P., and Lockridge, O. (2010) Arch. Biochem. Biophys. **494,** 107–120
6. Lenz, D. E., Maxwell, D. M., Koplovitz, I., Clark, C. R., Capacio, B. R., Cerasoli, D. M., Federko, J. M., Luo, C., Saxena, A., Doctor, B. P., and Olson, C. (2005) Chem. Biol. Interact. **157–158,** 205–210
7. Ordentlich, A., Barak, D., Kronman, C., Benschop, H. P., De Jong, L. P., Ariel, N., Barak, R., Segall, Y., Velan, B., and Shafferman, A. (1999) Biochemistry **38,** 3055–3066
8. Masson, P., Nachon, F., and Lockridge, O. (2010) Chem. Biol. Interact. **187,** 157–162
9. Aurbek, N., Thiermann, H., Eyer, F., Eyer, P., and Worek, F. (2009) Toxicology **259,** 133–139
10. Li, H., Schopfer, L. M., Nachon, F., Froment, M. T., Masson, P., and Lockridge, O. (2007) Toxicol. Sci. **100,** 136–145
11. Millard, C. B., Koellner, G., Ordentlich, A., Shafferman, A., Silman, I., and Sussman, J. L. (1999) J. Am. Chem. Soc. **121,** 9883–9884
12. Reiter, G., Mikler, J., Hill, I., Weatherby, K., Thiermann, H., and Worek, F. (2008) J. Chromatogr. B Analyt. Technol. Biomed. Life Sci. **873,** 86–94
13. Cohen, O., Kronman, C., Raveh, L., Mazor, O., Ordentlich, A., and Shafferman, A. (2006) Mol. Pharmacol. **70,** 1121–1131
14. Kasten, S. A., Kajih, T., Smith, J. R., Oliver, Z., Otto, T. C., Reeves, T. E., Lenz, D. E., and Cerasoli, D. M. (2010) in Proceedings of the 2010 Medical Defense Bioscience Review, Hunt Valley, MD, May 24–27, 2010, p. 46, U.S. Army Medical Research and Development Command, Washington, DC
15. Hall, C. R., Inch, T. D., Inns, R. H., Muir, A. W., Sellers, D. J., and Smith, A. P. (1977) J. Pharm. Pharmacol. **29,** 574–576
16. Nachon, F., Nicolet, Y., Viguié, N., Masson, P., Fontecilla-Camps, J. C., and Lockridge, O. (2002) Eur. J. Biochem. **269,** 630–637
17. Ellman, G. L., Courtney, K. D., Andres, V., Jr., and Feather-Stone, R. M. (1961) Biochem. Pharmacol. **7,** 88–95
18. Kabsch, W. (2010) Acta Crystallogr. D Biol. Crystallogr. **66,** 125–132
19. Collaborative Computational Project 4 (1994) Acta Crystallogr. D Biol.

Crystallogr. **50,** 760–763
20. Murshudov, G. N., Vagin, A. A., and Dodson, E. J. (1997) Acta Crystallogr. D Biol. Crystallogr. **53,** 240–255
21. Emsley, P., and Cowtan, K. (2004) Acta Crystallogr. D Biol. Crystallogr. **60,** 2126–2132
22. Painter, J., and Merritt, E. A. (2006) Acta Crystallogr. D Biol. Crystallogr. **62,** 439–450
23. Adams, P. D., Grosse-Kunstleve, R. W., Hung, L. W., Ioerger, T. R., McCoy, A. J., Moriarty, N. W., Read, R. J., Sacchettini, J. C., Sauter, N. K., and Terwilliger, T. C. (2002) Acta Crystallogr. D Biol. Crystallogr. **58,** 1948–1954
24. Nicolet, Y., Lockridge, O., Masson, P., Fontecilla-Camps, J. C., and Nachon, F. (2003) J. Biol. Chem. **278,** 41141–41147
25. Carletti, E., Aurbek, N., Gillon, E., Loiodice, M., Nicolet, Y., Fontecilla-Camps, J. C., Masson, P., Thiermann, H., Nachon, F., and Worek, F. (2009) Biochem. J. **421,** 97–106
26. Nachon, F., Carletti, E., Wandhammer, M., Nicolet, Y., Schopfer, L. M., Masson, P., and Lockridge, O. (2011) Biochem. J. **434,** 73–82
27. Nachon, F., Carletti, E., Worek, F., and Masson, P. (2010) Chem. Biol. Interact. **187,** 44–48
28. Masson, P., Legrand, P., Bartels, C. F., Froment, M. T., Schopfer, L. M., and Lockridge, O. (1997) Biochemistry **36,** 2266–2277
29. Carletti, E., Colletier, J. P., Dupeux, F., Trovaslet, M., Masson, P., and Nachon, F. (2010) J. Med. Chem. **53,** 4002–4008
30. Boter, H. L., and van Dijk, C. (1969) Biochem. Pharmacol. **18,** 2403–2407
31. Diederichs, K., and Karplus, P. A. (1997) Nat. Struct. Biol. **4,** 269–275

# Crystallographic Snapshots of Nonaged and Aged Conjugates of Soman with Acetylcholinesterase, and of a Ternary Complex of the Aged Conjugate with Pralidoxime

B. Sanson, **F. Nachon**, J-P Colletier, M-T Froment, L. Toker, H.M. Greenblatt, J.L Sussman, Y. Ashani, P. Masson, I. Silman, M. Weik*

Journal of Medicinal Chemistry 52 (2009) 7593-7603

Journal of Medicinal Chemistry Article

*J. Med. Chem.* **2009,** *52,* 7593–7603 **7593**
DOI: 10.1021/jm900433t

# Crystallographic Snapshots of Nonaged and Aged Conjugates of Soman with Acetylcholinesterase, and of a Ternary Complex of the Aged Conjugate with Pralidoxime[†,‡]

Benoît Sanson,[§] Florian Nachon,[∥] Jacques-Philippe Colletier,[§] Marie-Thérèse Froment,[∥] Lilly Toker,[#] Harry M. Greenblatt,[⊥] Joel L. Sussman,[⊥] Yaacov Ashani,[#] Patrick Masson,[∥,§] Israel Silman,[#] and Martin Weik*[,§]

[§]*Laboratoire de Biophysique Moléculaire, Institut de Biologie Structurale Jean-Pierre Ebel, Commissariat à l'Énergie Atomique, Centre National de la Recherche Scientifique, Université Joseph Fourier, 41 Rue Jules Horowitz, 38027 Grenoble, France,* [∥]*Département de Toxicologie, Centre de Recherches du Service de Santé des Armées, 24 Avenue des Maquis du Grésivaudan, 38700 La Tronche, France,* [⊥]*Department of Structural Biology and* [#]*Department of Neurobiology, Weizmann Institute of Science, Rehovot 76100, Israel*

*Received April 3, 2009*

Organophosphate compounds (OP) are potent inhibitors of acetylcholinesterases (AChEs) and can cause lethal poisoning in humans. Inhibition of AChEs by the OP soman involves phosphonylation of the catalytic serine, and subsequent dealkylation produces a form known as the "aged" enzyme. The nonaged form can be reactivated to a certain extent by nucleophiles, such as pralidoxime (2-PAM), whereas aged forms of OP-inhibited AChEs are totally resistant to reactivation. Here, we solved the X-ray crystal structures of AChE from *Torpedo californica* (*Tc*AChE) conjugated with soman before and after aging. The absolute configuration of the soman stereoisomer adduct in the nonaged conjugate is $P_SC_R$. A structural reorientation of the catalytic His440 side chain was observed during the aging process. Furthermore, the crystal structure of the ternary complex of the aged conjugate with 2-PAM revealed that the orientation of the oxime function does not permit nucleophilic attack on the phosphorus atom, thus providing a plausible explanation for its failure to reactivate the aged soman/AChE conjugate. Together, these three crystal structures provide an experimental basis for the design of new reactivators.

## Introduction

The principal role of acetylcholinesterase (AChE,[a] EC 3.1.1.7) is termination of nerve impulse transmission at cholinergic synapses by rapid hydrolysis of the neurotransmitter acetylcholine (ACh).[1] In keeping with its biological role, AChE is a very rapid enzyme, with a turnover number of $10^3-10^4$ $s^{-1}$, depending on the species. The first X-ray structure of an AChE, that from *Torpedo californica* (*Tc*AChE), revealed that its active site is buried at the bottom of a deep and narrow gorge.[2] It features a catalytic triad (Ser200, His440, Glu327), typical of serine hydrolases, and a catalytic anionic subsite (CAS), in which the choline moiety of ACh is stabilized via cation$-\pi$ interactions with Trp84 and Phe330 and by an electrostatic interaction with Glu199.[2,3] Stabilization of ACh in the active site also involves interactions of its carbonyl oxygen within the oxyanion hole (Gly118, Gly119, Ala201) and of the methyl moiety of its acetyl group in the acyl pocket (Trp233, Phe288, Phe290, Phe331).[4] At the rim of the gorge, Trp279 is the main component of a so-called "peripheral" anionic site (PAS) that interacts allosterically with the active site[5] and mediates trapping of the substrate en route to the active site.[3,6]

AChE is the target of numerous inhibitors, both covalent (irreversible) and noncovalent (reversible), including most approved anti-Alzheimer drugs, and neurotoxins such as the fasciculins, carbamates, and organophosphates (OPs).[1] OPs include both insecticides and chemical warfare agents that lead to irreversible inhibition of AChE. Intoxication by OP-based insecticides is a serious public health problem, causing the death of some 200000 people per year throughout the world.[7] The lethality of OP nerve agents was evident both when they were employed by Iraqi troops against Iranian troops and Kurd civilians in 1988[8−11] and in the Tokyo subway terrorist attack in 1995.[12] Detailed understanding of the mechanism of AChE inhibition by OPs is thus of major importance in a toxicological context, inasmuch as it may provide crucial information for the rational design of new antidotes.

Soman, *O*-(1,2,2-trimethylpropyl) methylphosphonofluoridate, is one of the most toxic OPs. Inhibition of AChE by soman involves covalent modification of Ser200 (*Tc*AChE residue numbering throughout the manuscript unless stated otherwise), by a mechanism that implicates nucleophilic attack of the latter on the phosphorus atom of soman, with concomitant departure of its fluoride atom (Scheme 1).

[†] We acknowledge the 100th anniversary of the Division of Medicinal Chemistry of the American Chemical Society.

[‡] The atomic coordinates and structure factors (codes 2wfz, 2wg0, and 2wg1) have been deposited in the RCSB Protein Data Bank, www.rcsb.org.

*To whom correspondence should be addressed. Phone: (33) 4 38 78 95 69. Fax: (33) 4 38 78 54 94. E-mail: weik@ibs.fr.

[a] Abbreviations: AChE, acetylcholinesterase; OP, organophosphate; *Tc*, *Torpedo californica*; 2-PAM, pralidoxime, *N*-methylpyridin-1-ium 2-aldoxime methiodide; ACh, acetylcholine; CAS, catalytic anionic subsite; PAS, peripheral anionic site; BChE, butyrylcholinesterase; TMB-4, trimedoxime bromide; CE1, carboxylesterase 1; PEG, polyethyleneglycol; MES, morpholinoethylsulphonic acid; NAG, *N*-acetylglucosamine; FUC, fucose.



Published on Web 07/30/2009

**Scheme 1.** Irreversible Iinhibition of AChE by Soman (Upper Panel) and Reactivation of the Nonaged Enzyme with 2-PAM (Lower Panel)[a]

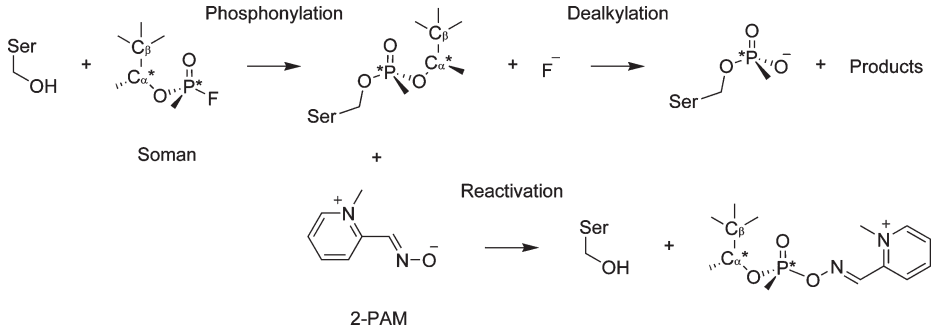


[a] The catalytic Ser200 first performs a nucleophilic attack on the phosphorous atom. Then the enzyme catalyzes departure of the pinacolyl group (dealkylation or "aging"). Prior to "aging", reactivation of AChE can occur via nucleophilic attack of the oxime group of 2-PAM on the phosphorus atom of the phosphonyl adduct, resulting in its cleavage from Ser 200 O$\gamma$. Asterisks denote chiral centers.

Subsequently, AChE catalyzes the dealkylation of the OP adduct at a rate ca. $10^{10}$ higher than that at which non-enzymatic dealkylation would occur.[13] This second step has been termed "aging" and transforms the nonaged soman/AChE conjugate into an aged conjugate that can no longer be rescued by the available reactivators.[14] Among all OPs known to date, with the exception of $CH_3POF_2$ and $CH_3POCl_2$,[15,16] soman is the one that produces an aged enzyme most rapidly. Extrapolated half-lives of aging of soman/AChE conjugates range from seconds to several minutes under near physiological conditions.[13,17−19] For the soman/*Tc*AChE conjugate, half-lives for aging of 1.9 and 3.9 min were reported at pH 6.5 and 7.5, respectively, at room temperature.[17]

The mechanism of enzyme-induced aging is not fully understood, and the chemical basis for the unusually fast rate of dealkylation of soman/AChE conjugates requires further clarification. Two pathways were considered in which either protonation of the pinacolyl oxygen[14,19] or methyl migration from C$\beta$ to C$\alpha$ of the pinacolyl group[13,17,20] were proposed to be rate-determining. Regardless of the mechanistic details, it is agreed that dealkylation is accompanied by O−C scission of the P−O−$CH(CH_3)C(CH_3)_3$ chain (Scheme 1) and that Glu199, Phe331, Glu443, His440, and in particular, Trp84, play important roles in the aging process.[13,17,19,20] It is of interest that the aged soman/AChE conjugate is analogous to the deacylation tetrahedral intermediate of acetylated AChE.[21−23]

Soman contains two chiral centers, the P and C$\alpha$ atoms, and thus occurs as four stereoisomers. AChEs react preferentially with the $P_S$ enantiomers, with phosphylation rates $\sim 5 \times 10^4$ higher for the $P_S$ than for the $P_R$ enantiomers.[24,25] An in-line displacement of fluoride by Ser200 has been proposed,[26] implying that the stereochemistry of the phosphorus atom is reversed following conjugation to the enzyme. The $P_R$ configuration in the crystal structure of the nonaged phosphonylated *Tc*AChE conjugate obtained by use of the *O*-ethyl methylphosphonyl OP, VX, is indeed consistent with inversion at the P atom.[27] As for the preference of AChE for the configuration at the C$\alpha$ atom, the rates of inhibition of human (hu) AChE,[25] bovine AChE,[28] eel AChE,[28] equine butyrylcholinesterase (BChE ; EC 3.1.1.8),[25] and huBChE[18,29] by the $P_SC_S$ stereoisomer are consistently (though only slightly) higher than by the $P_SC_R$ stereoisomer.

Oximes are capable of reactivating nonaged OP/AChE conjugates[30,31] by nucleophilic attack of the oxime group ($R_1R_2C{=}NOH$) on the phosphorus atom.[32,33] So far, only a few oximes have been included in therapeutic regimens for treatment of OP intoxication, viz. *N*-methylpyridin-1-ium 2-aldoxime methiodide (pralidoxime, 2-PAM), trimedoxime bromide (TMB-4), and toxogonin.[34] The bis-quaternary oximes, HI-6 and HLö-7, have, so far, been the most effective in reactivation of most nonaged OP/huAChE conjugates.[35] The nonaged soman/huAChE conjugate obtained by use of the $P_SC_S$ isomer has been reported to be significantly more amenable to reactivation by HI-6 than the $P_SC_R$ adduct.[36] Although great efforts are being made to produce more potent reactivators,[37] no single broad-spectrum reactivator has, so far, been described that is capable of reactivating all nonaged nerve agent/AChE conjugates.[38] Furthermore, it has been observed that phosphonylated oximes, which are formed during reactivation, are capable of reinhibiting AChE.[39,40]

The X-ray structures of several nonaged and aged OP/AChE conjugates have been solved in recent years. Those of the nonaged VX/*Tc*AChE conjugate[27] and of the nonaged tabun conjugate of murine AChE[41] (mAChE) both showed that a reorientation of the side chain of the catalytic histidine is necessary to accommodate the ethoxy group common to the two inhibitors. Upon aging, these structural changes are reversed and the catalytic histidine in the aged OP/AChE conjugate reverts to its native conformation. The structure of the aged soman/*Tc*AChE was determined by crystallizing the inhibited enzyme, and here, too, the side chain of the catalytic His residue was seen to be in its native orientation.[23] However, due to the experimental difficulties imposed by the rapidity of the aging process, the crystal structure of the nonaged soman/AChE conjugate had not been reported.

Here, we present the crystal structures of nonaged and in crystallo aged soman/*Tc*AChE conjugates and of a ternary complex of the aged conjugate with the oxime reactivator, 2-PAM. These structures provide important information that can be utilized in clarifying: (a) the influence of the architecture of the catalytic site and of water molecules within the gorge on the rate and mechanism of the aging reaction and (b) the resistance of aged OP-AChE conjugates to reactivation. Hopefully, such clarifications will facilitate the quest for new reactivators of OP-inhibited AChE.

## Results

**Nonaged Soman/TcAChE Conjugate.** Trapping of the nonaged soman/*Tc*AChE was achieved by reducing the

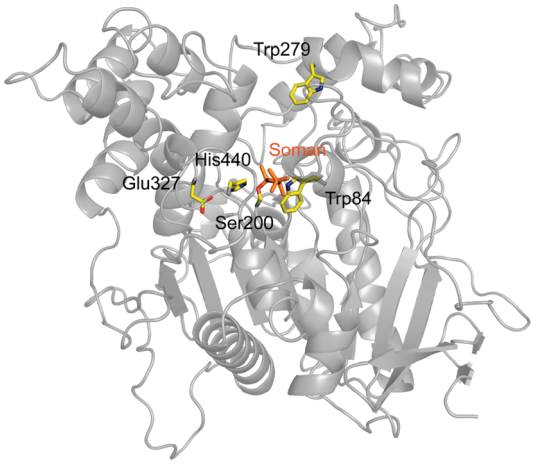


**Figure 1.** Overall view of the nonaged soman/*Tc*AChE conjugate. The backbone of the enzyme is displayed as a gray ribbon, with the entrance to the active-site gorge at the top. The catalytic triad residues (Ser200, His440, and Glu327), as well as the main residues of the CAS and PAS, Trp84, and Trp279, respectively, are represented as yellow sticks and the OP moiety as orange sticks.

soaking time to 6 min and raising the pH to 8.2, a pH value at which aging is significantly retarded.[13,14]

The structure, solved at 1.95 Å resolution, is displayed in Figure 1. The initial $F_o - F_c$ electron density map featured a 12$\sigma$ peak at covalent bonding distance from Ser200 O$\gamma$, clearly revealing the position of the phosphorus atom of the phosphonyl group. At lower $\sigma$ levels, the pinacolyl group is clearly defined (Figure 2A). It is stabilized by hydrophobic interaction with Trp84; thus, one of the methyl groups of the pinacolyl C$\beta$ atom (Scheme 1) is 3.6 Å from the nearest nonhydrogen atom of Trp84.

The catalytic His440 is H-bonded to both Ser200 O$\gamma$ (2.7 Å) and Glu327 O$\varepsilon$1 (2.6 Å) through its N$\varepsilon$2 and N$\delta$1 nitrogens, respectively. The soman O2 atom is within H-bonding distance (3.2 Å) of His440 N$\varepsilon$2, although the bond angle is unfavorable. Thus, the proton on His440 N$\varepsilon$2 is preferentially oriented toward Ser200 O$\gamma$ (N$\varepsilon$2−H−O$\gamma$ angle 142°, H−O$\gamma$ distance 1.8 Å), rather than toward soman O2 (N$\varepsilon$2−H−O2 angle 118°, H−O2 distance 2.6 Å). Mimicking the carbonyl oxygen of the natural substrate, ACh, soman O1 establishes three H-bonds within the oxyanion hole with Gly118 N (2.7 Å), Gly119 N (2.6 Å), and Ala201 N (3.0 Å; not shown in Figure 2A). Noteworthy, also, is a weak H-bond between soman O2 and water 1001, located up the gorge (3.3 Å), which is also within H-bonding distance (3.3 Å) of Tyr121 O$\zeta$. Glu199 O$\varepsilon$1 is 3.1 Å from the methyl group on the C$\alpha$ atom and 4.0 Å from the closest methyl group on the C$\beta$ atom of soman (not shown). Glu199 itself is stabilized by Glu443 through hydrogen bonds with the bridging water 1002, just as was observed for native *Tc*AChE.[2,42]

The pinacolyl moiety in the nonaged conjugate perturbs the position of the imidazole ring of His440; consequently, its N$\varepsilon$2 nitrogen is shifted by 0.5 Å relative to its position in the native structure. This is in contrast to the total disruption of the catalytic triad observed in the nonaged VX/*Tc*AChE conjugate.[27] Several other residues in the vicinity of the active site are slightly affected by phosphonylation of Ser200. These include Trp84, Trp233, Phe330, Tyr334, and Tyr442, all located in the bottom half of the gorge. Their movements result in a small (6%) decrease in the volume of the active-site gorge relative to native *Tc*AChE.

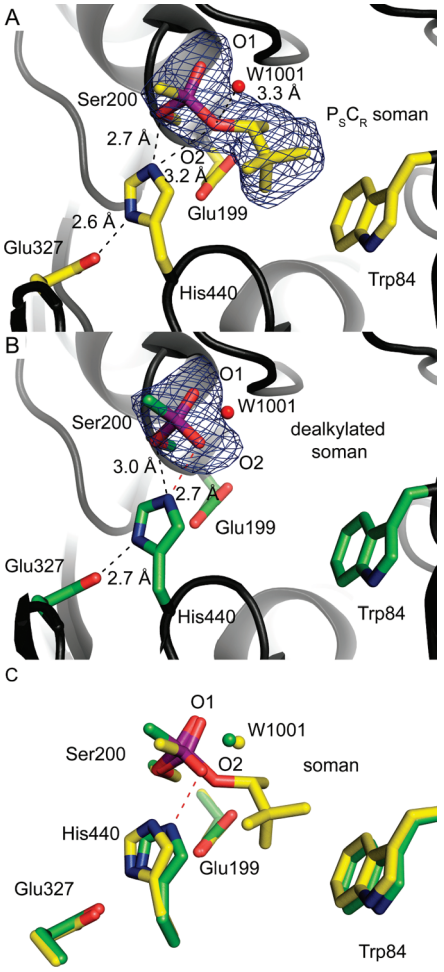


**Figure 2.** Active sites of the nonaged (A) and aged (B) soman/*Tc*AChE conjugates and their superposition (C). The $F_o - F_c$ omit maps are contoured at 3$\sigma$. The catalytic triad residues (Ser200, His440, and Glu327), Trp84, and the OP adducts are displayed as sticks, with oxygen atoms in red, nitrogen atoms in blue, and the phosphorus atom in purple. Carbon atoms of the nonaged conjugate are shown in yellow and those of the aged conjugate in green. A water molecule (1001) interacting with soman O2 is represented as a red ball in (A) and (B), and as yellow and green balls in the nonaged and aged structures, respectively, in (C). Hydrogen bonds and a salt bridge are represented as black and red dashed lines, respectively. The apical nitrogen atom of His440 forms a salt bridge (dashed line) with the negatively charged O2 atom of the soman adduct in the aged conjugate.

The soman soaked into the crystals was a mixture of the four stereoisomers, $P_{R/S}C_{R/S}$. As mentioned above,[23] in aqueous solution, AChE reacts preferentially with the $P_S$ enantiomers of soman (Figure 2A). The crystal structure permits assignment of the absolute configuration of the phosphorus atom as $P_S$ and the fact that the pinacolyl group is retained in the nonaged conjugate permits assignment of the absolute configuration of the C$\alpha$ carbon to be $C_R$. It should be noted that the methyl group on the C$\alpha$ carbon hinders its direct interaction with the carboxyl group of Glu199 (distance C$\alpha$−O$\varepsilon$1 4.2 Å; Figure 2A).

**Aged Soman/TcAChE Conjugate.** To favor the dealkylation reaction,[13,14] the pH of the soaking solution was decreased relative to that used to obtain the nonaged conjugate and the time of soaking was increased. The structure of the aged conjugate was solved at 2.2 Å resolution (Figure 2B). No electron density is observed for the pinacolyl group,

demonstrating that the in crystallo dealkylation of soman, viz., aging of the conjugate, had indeed occurred. The phosphorus atom adopts a tetrahedral conformation, being linked to Ser200 O$\gamma$, to the methyl carbon, and to the two oxygens. As observed in the nonaged conjugate, the O1 atom of the phosphonyl moiety is stabilized by H-bonds with the three components of the oxyanion hole, viz. Gly118 N (2.7 Å), Gly119 N (2.6 Å), and Ala201 N (2.8 Å; not shown in Figure 2B). The negatively charged O2 atom points toward Trp84 and establishes a salt bridge[43,44] with His440 N$\varepsilon$2 (2.7 Å). This interaction distance value is in agreement with that reported by Shafferman et al. (2.8 Å)[19] and with that previously observed in the crystal structure of the aged soman/*Tc*AChE conjugate (2.6 Å).[23] His440 is also hydrogen-bonded to Ser200 O$\gamma$ through its N$\varepsilon$2 nitrogen (3.0 Å) and to Glu327 through its N$\delta$1 nitrogen (2.7 Å). The methyl group of the phosphonyl moiety points toward the acyl pocket (distance of 3.6 Å between closest non-hydrogen atoms). The limited conformational changes reduce the volume of the gorge by 3% compared to the volume of the gorge of the native enzyme.

No significant difference was observed between our crystal structure and that reported earlier after crystallization of the aged conjugate,[23] showing that aging in solution and in crystallo produce the same final state.

Superposition of the structures of the nonaged and aged conjugates reveals a small, yet crucial, movement within the active site (Figure 2C): the imidazole ring of His440 is tilted back (N$\varepsilon$2 shifts by 0.8 Å) to a native-like conformation after aging. The resulting proximity between soman O2, which is negatively charged, and His440 N$\varepsilon$2, results in formation of a salt bridge (2.7 Å) (Figure 2B). It should be noted that water molecule 1001, which interacts with soman O2 in the non-aged crystal structure (Figure 2A), is not within H-bonding distance (3.7 Å) of O2 in the aged crystal structure (Figure 2B).

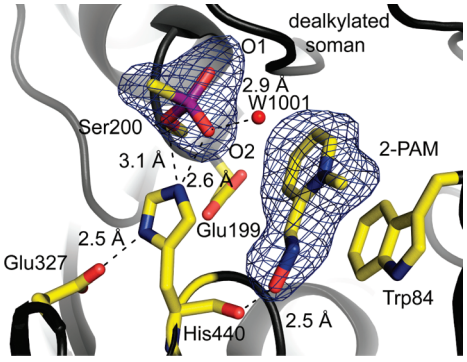


**Figure 3.** Ternary complex of 2-PAM with the aged soman/*Tc*AChE conjugate. The $F_o - F_c$ omit map is contoured at 3$\sigma$. The catalytic triad residues (Ser200, His440, and Glu327) and Trp84 are represented as sticks, and color-coding of these residues, of the OP adduct and of 2-PAM, are as in Figure 2A. A water molecule (1001) interacting with O2 of soman and with the nitrogen atom of 2-PAM is represented as a red ball. Hydrogen bonds are shown as dashed lines.

**Ternary Complex of 2-PAM with the Aged Soman/*Tc*AChE Conjugate.** The structure of the ternary complex of the aged conjugate with the oxime reactivator, 2-PAM, was solved at 2.2 Å resolution. A molecule of 2-PAM is seen at the CAS but not at the PAS. 2-PAM interacts via parallel $\pi$-stacking with the indole moiety of Trp84 (distance of 3.5 Å between closest non-hydrogen atoms) (Figure 3). The oxime oxygen is 2.5 Å from His440 O. The conformation of the phosphonyl adduct on Ser200 is not affected by the presence of 2-PAM, and the oxime oxygen is 6.8 Å from the phosphorus atom. This distance precludes nucleophilic attack at the soman phosphorus atom by the oxime, which would be essential for displacing it from Ser200 O$\gamma$. Water molecule 1001 (Figure 3) bridges 2-PAM and the phosphonyl adduct; it is H-bonded to soman O2 (2.8 Å) and interacts electrostatically with 2-PAM N1 (3.4 Å). Noteworthy is the rotation of Phe330 $\chi$1 and $\chi$2 angles, both by ~50°, which brings the residue across the gorge. It should be noted that a PEG molecule spans the gorge (not shown) from the vicinity of Tyr70/Trp279 down to residues Tyr334/Phe330/Phe331, in the middle of the gorge; yet it does not interact with 2-PAM (distance of 5.9 Å between closest non-hydrogen atoms). The crystal structure presented was solved after soaking crystals of the aged conjugate with 2-PAM at pH 5.6. A structure solved after soaking in 2-PAM at pH 8.2 reproduced all the structural details shown in Figure 3 (data not shown). Thus, the ionization state of the oxime group in solution (p$K_a$ = 7.8)[45] does not appear to influence the mode of 2-PAM binding, which is likely to be governed principally by the hydrophobic interaction with Trp84.

## Discussion

This study presents, for the first time, the crystal structure of a nonaged soman/AChE conjugate that was obtained by rapid flash-cooling of crystals of *Tc*AChE soaked with soman at high pH and low temperature, so as to preclude significant aging. The corresponding aged conjugate was generated in crystallo by a longer incubation of the soman-soaked crystals at a lower pH. The aged conjugate was further used to obtain a tertiary complex with the oxime reactivator, 2-PAM. These structures provide valuable information for understanding: (a) the molecular details of the rapid phosphonylation of AChE by soman and of the aging process and (b) the resistance of the aged enzyme to the theoretically possible

**Scheme 2.** Phosphylation Reaction Scheme of AChE with Either Soman (Upper Panel) or VX (Lower Panel)

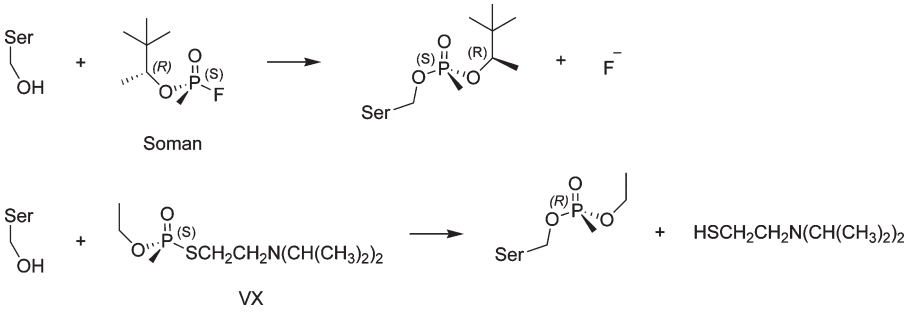

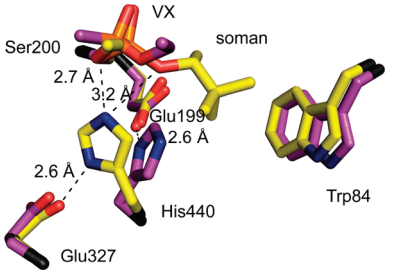


**Figure 4.** Superposition of the active sites of the nonaged soman/*Tc*AChE and nonaged VX/*Tc*AChE conjugates. Carbon atoms of the soman/*Tc*AChE conjugate are shown in yellow, and those of the VX/*Tc*AChE conjugate in purple. Oxygen and nitrogen atoms are in red and blue, respectively, for the two structures, and phosphorus atoms in orange. Hydrogen bonds are represented as dashed lines.

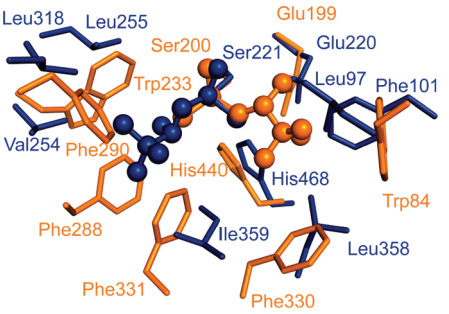


**Figure 5.** Superposition of the active sites of nonaged soman/*Tc*AChE (orange) and soman/huCE1 (blue) conjugates. The residues and the OP moieties are represented as ball-and-stick models. Labels for *Tc*AChE and huCE1 residues are in orange and blue, respectively.

reactivation. These, in turn, may provide a basis for designing more efficient antidotes against nerve agent intoxication.

**Soman Inhibition of *Tc*AChE.** It is well established that the $P_SC_S$ stereoisomer of soman is the one that interacts preferentially with AChE.[25,28] Examination of the 3D structure of the nonaged soman/*Tc*AChE conjugate permits unequivocal assignment of the chirality of the covalently bound OP moiety. This is seen to be $P_SC_R$. The observation that the same absolute configuration (viz., $P_S$) is retained at the P atom in the nonaged adduct is attributed to stereoinversion at the P atom and to replacement of the fluoride leaving group by Ser200 O$\gamma$, which has lower priority order than the fluorine atom in assignment of the absolute configuration (Scheme 2). Similar inversion and retention of the absolute configuration of the P atom was reported by Cygler et al.,[46] who determined the crystal structure of a lipase conjugated to a methyl hexylphosphonate transition state analogue. Stereoinversion at the P atom was also observed for the VX-*Tc*AChE adduct,[27] as well as for the VX/mAChE adduct;[47] however, in these cases, the $P_R$ configuration was assigned because the $O-CH_2CH_3$ moiety has lower priority order than Ser 200 in determining the absolute configuration (Figure 4; Scheme 2). Recently, inversion of the configuration at the P atom was reported for reaction of tabun with mAChE and huBChE.[48] Thus, an in-line displacement is envisaged in all the cases reported for ChEs, regardless of the nature of the leaving group or the size of the O-alkyl substituent on the OP. This mode of nucleophilic attack is due to the steric constraints within the catalytic site that enforce the approach of the catalytic serine from the face opposite to the leaving group (Figure 4).

The $P_S$ configuration of the soman/*Tc*AChE adduct was anticipated on the assumption that phosphonylation proceeds via an in-line displacement mechanism. However, the $C_R$ stereochemistry of the pinacolyl C$\alpha$ atom seen in the crystal structure is at odds with the kinetic measurements performed on various AChEs and BChEs, all of which slightly favor the $P_SC_S$ diastereoisomer.[25,28] Two possible explanations may be provided: (a) Even though the $P_SC_S$ isomer can be docked computationally into the active site without its distortion (not shown), steric constraints produced by crystal packing could change the chiral preference at C$\alpha$. (b) A second possibility is that inhibition of *Tc*AChE by the $P_SC_S$ isomer is followed by a rapid rearrangement at the C$\alpha$ atom, resulting from formation of a planar pinacolyl carbenium ion species that realkylates the oxygen of the OP moiety. This would preferentially generate the more stable $P_SC_R$ adduct under the experimental conditions employed. Furthermore, we cannot rule out the possibility that *Tc*AChE preferentially selects the $P_SC_R$ epimer. It would, therefore, be of interest, not only to compare the 3D crystal structures of soman/*Tc*AChE conjugates obtained from the individual $P_SC_S$ and $P_SC_R$ epimers but also to investigate the kinetics of their reaction with soluble *Tc*AChE. We note that similar rates of aging were observed for various AChEs inhibited with either the $P_SC_R$ or the $P_SC_S$ diastereoisomer.[13,18,25]

**Comparison of the Inhibition of *Tc*AChE and of Human Carboxylesterase by Soman.** It is of interest to compare the nonaged soman/*Tc*AChE crystal structure with that of the corresponding nonaged conjugate of human carboxylesterase 1 (huCE1; EC 3.1.1.1). It should be noted that the soman/huCE1 crystals were obtained by crystallization of the soman/huCE1 conjugate produced with soman (stereoisomeric mixture $P_{R/S}C_{R/S}$), which thus displayed no tendency to age over a period of 1−4 weeks,[49] as already reported for the rat CE1 conjugate.[50] huCE1 is a cholinesterase-like $\alpha/\beta$ hydrolase that contains a catalytic triad, an oxyanion hole, and a glutamate equivalent to Glu199. Figure 5 shows that all these residues can be superposed on the homologous residues in *Tc*AChE. However, the substrate specificity pockets in the two enzymes differ in size. Whereas the acyl-binding pocket in *Tc*AChE is too small to accommodate the bulky pinacolyl goup of soman, the analogous pocket in huCE1 is large enough to do so. In contrast, the pocket in huCE1 that is homologous to the large choline-binding pocket in *Tc*AChE is much smaller. Thus, the two enzymatic active sites bear a "mirror image" relation. This explains the difference in enantioselectivity between *Tc*AChE and huCE1 with respect to their reaction with soman. It was indeed recently shown that huCE1 reacts preferentially with the $P_R$ isomer of soman in aqueous solution (Matthew Redinbo, personal communication), and it is the $P_R$ configuration that is observed in the crystal structure of the soman/huCE1 conjugate.[49] This suggests that phosphonylation of huCE1 proceeds by a mechanism similar to the standard in-line displacement proposed for ChEs and lipases.[46]

**Structural Comparison of the Nonaged Conjugates of AChEs with Soman, VX, and Tabun.** Comparison of the crystal structure of the nonaged soman/*Tc*AChE conjugate with those of the nonaged VX/*Tc*AChE conjugate[27] and of the nonaged tabun/mAChE conjugate[48] reveals an interesting difference. In the VX/*Tc*AChE conjugate, there is a disruption of the catalytic triad, resulting in H440 N$\varepsilon$2

forming an H-bond with Glu199 instead of with Glu327, while in the tabun/mAChE conjugate, catalytic His447 and Phe338 shift in concert to avoid unfavorable contacts with the phosphoramidate group. In contrast, inhibition of *Tc*AChE by soman results in only a slight reorientation of the imidazole ring of His440 without disruption of the catalytic triad. A movement similar to that occurring upon phosphonylation with VX is precluded by the presence of the pinacolyl moiety, which is much more bulky than the ethoxy group of VX (Figure 4). Indeed, His440 N$\varepsilon$2 would be only 2.3 Å from the nearest methyl carbon of the pinacolyl moiety if it adopted the same conformation as in the nonaged VX/*Tc*AChE conjugate. The absence of a major conformational change of the catalytic histidine during aging of the soman/*Tc*AChE conjugate could explain partially its accelerated rate of aging relative to the VX/TcAChE conjugate. By contrast, in the nonaged tabun/huBChE conjugate, catalytic His438 is restrained by Phe398, a residue that is absent in the AChEs.[48]

**Mechanism of Aging of the Soman/TcAChE Conjugate.** The mechanism of aging (viz., dealkylation of the OP moiety) of conjugates of OP nerve agents with ChEs has been the topic of intense investigation and debate over the past 50 years. Aging of the soman/AChE conjugate has been a particular focus because its rapid rate presents a paramount toxicological challenge. The availability of a high-resolution crystal structure of the nonaged soman/*Tc*AChE conjugate, together with that of the homologous aged conjugate, at last permits a critical examination of the proposed mechanisms at the atomic level.

The proposed mechanisms were generated on the basis of kinetic data[51] and product analysis.[14] After the 3D structures of *Tc*AChE,[2] and subsequently of mAChE[52] and huAChE,[53] became available, dynamic modeling was attempted[19] and various mechanistic proposals were tested by site-directed mutagenesis.[19] On the basis of the pH-rate profile of aging[13,18] and the increased resistance of certain mutants to aging,[17,54] the following residues have been implicated in the aging of soman/AChE conjugates (*Tc*AChE numbering, with huAChE numbering in brackets): His440 (447), Trp84 (86), Glu199(202), Glu443(450), Phe331(338).[17,19,54]

Comparison of the crystal structures of the nonaged and aged soman/*Tc*AChE conjugates reveals a small, yet significant, movement of the imidazole ring of His440 (displacement of N$\varepsilon$2 by ~0.8 Å) that results in formation of a salt bridge with soman O2 in the aged conjugate (Figure 2C). In the case of the VX/*Tc*AChE conjugate, there is a much larger movement, which involves reformation of the catalytic triad and concomitant establishment of a salt bridge homologous to that seen in both the aged soman and aged sarin conjugates.[23] In the case of the tabun/mAChE conjugate, inspection of the crystal structure of the aged conjugate revealed a continuum of conformations that was ascribed, at least in part, to incomplete aging.[48]

The pH/rate profile of aging provides evidence that His440 is involved in the process. In the nonaged soman/*Tc*AChE conjugate, N$\varepsilon$2 of its imidazole ring is within H-bonding distance of both Ser 200 O$\gamma$ (2.7 Å) and O2 of the pinacolyl moiety (3.2 Å). The unfavorable bond angle for the H-bond with the pinacolyl O2, taken together with the restricted movement of the imidazole ring imposed by the bulky pinacolyl group, render it unlikely that His440 is directly involved in the aging process by protonation of O2. However, the proximity of the protonated N$\varepsilon$2 may confer a stabilizing electrostatic effect that could contribute to the observed pH-dependence.

Mutation of Glu199 (huAChE 202) to Gln slows the aging of soman-inhibited *Tc*AChE and huAChE to a similar extent.[17,19] In the electrostatic push−pull mechanism for dealkylation proposed by Viragh et al.,[13] Glu199 is proposed to play the "pusher" role, in conjunction with Trp84, triggering methyl migration from C$\beta$ to C$\alpha$, with concomitant transformation of C$\beta$ into a positively charged carbenium atom, resulting in C$\alpha$−O2 bond breakage. Because C$\beta$ is near Trp84 in the crystal structure of nonaged soman/*Tc*AChE (4.6 Å; Figure 2A), the carbenium ion may indeed be stabilized by a cation−$\pi$ interaction as proposed.[13] Once the carbenium ion is formed, it undergoes rapid rearrangement that could explain the composition of the low molecular weight products of "aging" as identified by Michel et al.[14] Because Glu199 is actually closer to C$\alpha$ than to C$\beta$ in the crystal structure, it seems unlikely that it would indeed play a "pushing" role. It may, however, stabilize the developing carbenium ion. Such an electrostatic stabilization is supported by the effect of mutagenesis of Glu199 to Gln (see above) and also by mutation of Glu443 (Glu450 in hAChE) to Ala; this latter residue is linked to Glu199 via a conserved water molecule (numbered 1002) and may thus be expected to stabilize its position.[2,42] Arguing against the push−pull mechanism as proposed by Viragh et al.[13] is the contention that methyl migration prior to carbenium ion formation would be most unfavored in energetic terms. We were unable to find an example in the literature in which methyl migration preceded carbenium ion formation. But methyl migration following carbenium ion formation is an accepted mechanism.[55] Indeed, in studies on the dealkylation of model OP compounds,[56] the composition of the observed olefin products was in line with the initial formation of a pinacolyl ion. The crystal structure of the nonaged conjugate described in the present paper provides a plausible mechanism for enhancement of carbenium ion formation as follows. The conserved water molecule 1001, which is hydrogen-bonded to Tyr121 O$\zeta$, may enhance cleavage of the O2−C$\alpha$ bond by increasing its polarity through hydrogen bonding to O2 (Figure 2A), while His440 would stabilize the partial charge on O2, thus releasing the unstable pinacolyl carbenium ion. This species immediately rearranges by methyl migration from C$\beta$ to C$\alpha$ to form the 2,3-dimethylbutyl carbenium ion that accounts for the principal olefin isolated. Trp84 may contribute to acceleration of dealkylation by stabilizing the developing positive charge on the pinacolyl moiety. In this context, it is interesting to note that the pinacolyl O2−C$\alpha$ bond is elongated by 0.3 Å and thus weakened, if geometric restraints of this bond are down weighted in an alternate refinement of the nonaged soman/*Tc*AChE conjugate (see Supporting Information). The role of water 1001 in dealkylation could be checked experimentally by mutagenesis of Tyr121 (Tyr124 in huAChE). This mutation does not significantly affect the rate of phosphonylation,[57] but the aging rate of an OP conjugate of the mutant enzyme has not been compared to that of the corresponding conjugate of the wild-type enzyme.

In huAChE, mutation to Ala of Phe338 (Phe331 in *Tc*AChE) decreased the rate of aging of the soman conjugate by 160-fold,[19] whereas no effect was observed upon similar mutation of Phe337 (Phe330 in *Tc*AChE). Visual inspection of the 3D structure of the nonaged conjugate suggests that this mutation opens up a cavity into which the imidazole ring

of the catalytic His residue can move. This, in turn, could weaken the electrostatic stabilization of the developing carbocationic charge on the pinacolyl moiety.

Finally, it should be noted that the solvent-accessible volume of the gorge in the nonaged conjugate is decreased (6%) compared to the native structure. This decrease in gorge volume may generate a more suitably tuned vessel for catalyzing the dealkylation reaction by relevant enzyme residues. After dealkylation, a slight volume increase of 3% is observed but the volume of the gorge of the aged enzyme is still 3% less than that of the native form. Osmotic vs hydrostatic pressure, differential scanning calorimetry, and neutron scattering studies indicate that the thermodynamic stability of aged ChEs is strongly increased and that enzyme dynamics is altered compared to native enzymes.[58−60] Increased thermodynamic stability of aged ChEs was explained by dehydration at the bottom of the gorge so that the salt bridge between His440 and the phosphonyl moiety is in a low dielectric environment.

**Nonfunctional Orientation of 2-PAM in the Ternary Complex with the Aged Soman/TcAChE Conjugate.** The crystal structure of the ternary complex of 2-PAM with the aged soman/*Tc*AChE conjugate clearly reveals how 2-PAM binds within the CAS of the aged enzyme. The aromatic ring of 2-PAM stacks against the side chain of Trp84 in such a way that the oxime group points toward His440 O (the main-chain oxygen), at a distance of 2.5 Å; not only does it point away from the soman phosphorus atom, with its oxygen atom at a distance of 6.8 Å, but it is also on the wrong side for direct nucleophilic attack on the P-Ser200 O$\gamma$ bond. The orientation of 2-PAM differs from that seen in the complex of 2-PAM with native *Tc*AChE (Harel, Silman & Sussman, unpublished; PDB code 2VQ6). In this structure, too, the 2-PAM moiety is stacked against Trp84, but in a reversed orientation, so that its oxygen atom is 4.8 Å from Ser200 O$\gamma$ and could be substantially closer to the P atom in a putative OP conjugate.

Attempts were made to trap and solve the 3D structure of the ternary complex of 2-PAM with the nonaged soman/*Tc*AChE conjugate. To this end, crystallographic data were collected on a *Tc*AChE crystal that had been soaked for 5 min in a solution containing soman, at pH 8.2, followed by 5 min soaking in a 10 mM solution of 2-PAM at the same pH. No electron density was found that could account for the presence of 2-PAM, whereas the pinacolyl moiety of non-dealkylated soman was observed at the same position as in the nonaged soman/*Tc*AChE conjugate, viz., in proximity to Trp84, which would preclude binding of 2-PAM at that position as observed for the native enzyme and for the aged soman/*Tc*AChE conjugate (data not shown).

2-PAM thus binds poorly to the nonaged phosphonylated enzyme and binds in an unfavorable conformation after aging. Apart from 2-PAM, the oximes in use or under consideration for treatment of OP intoxication are elongated molecules and it was tacitly assumed that they span the active-site gorge, linking the PAS and the CAS, just like such potent bivalent AChE inhibitors as decamethonium[61,62] and heptylene-linked bistacrine.[63,64] Indeed, such an assumption was made in the design of an effective heptylene-linked bis-pyridinium aldoxime reactivator, Ortho-7.[65] However, the crystal structures of the complexes of three bis-quaternary oximes with mAChE, including Ortho-7,[66] provide strong evidence that their oximate groups attack OP/AChE conjugates from a position up the gorge axis, remote from the Trp residue in the CAS, and it is plausible that 2-PAM also acts on phosphylated conjugates from a similar angle and not as might be inferred from the crystal structures of the 2-PAM/*Tc*AChE complex or of its ternary complex with the aged soman/*Tc*AChE conjugate.

These findings should stimulate new approaches for improvement in the design of reactivators with better affinity for the nonaged conjugate or that could bind in the proper orientation after aging. Furthermore, because a nucleophilic attack is not prevented by the negative charge on the phosphonyl group,[67,68] reactivation of aged enzymes should in principle be made possible.

**Template for Designing Novel Reactivators.** A large number of putative reactivators have already been synthesized, some of which are currently being tested.[66,69] As already mentioned, they are mostly elongated molecules designed to bind simultaneously at the CAS and PAS of AChE. However, no molecule able to reactivate an aged OP/ChE conjugate has yet been found. Furthermore, there is scope for improving the potency of reactivators such as 2-PAM, HI-6, HLö-7, and MMB-4.

2-PAM, and its bisquaternary analogue, HI-6, are both 2-pyridinium monoaldoximes and yet, as mentioned above, display substantially different potencies in the reactivation of soman/AChE adducts.[70] Bimolecular rate constants of the reactivation for soman-inhibited AChEs by various oximes showed that in the case of human AChE HI-6 is $4\times10^5$-fold more potent than its monoquaternary parent analogue, 2-PAM. Furthermore, HI-6 was shown to reactivate the conjugate of mAChE obtained with the $P_SC_S$ isomer significantly faster than that generated with the $P_SC_R$ isomer[36] Similar results were reported for electric eel AChE inhibited with the same two potent soman epimers.[28] In this context, the crystal structure of the nonaged soman/*Tc*AChE conjugate presented here provides a valuable template for designing more potent reactivators. In particular, we propose to conduct molecular dynamics (MD) simulations of the nonaged soman/*Tc*AChE conjugate and take minor conformations accessed during the simulation into account in the design process. Indeed, a recent study showed that side chain conformations of gorge residues in crystallographic AChE−ligand complexes, which differ from those observed in native AChE, are already accessed in a MD simulation of native AChE.[71,72] Conformational changes upon ligand-binding in AChE thus involve pre-existing equilibrium dynamics, rather than an induced fit, and can be predicted to a certain extent. In the light of the considerations referred to above, it should also be of value to conduct docking experiments for 2-PAM and suitable bifunctional reactivators utilizing the crystal structures of native *Torpedo* and mammalian AChEs as well as of the nonaged and aged soman/*Tc*AChE conjugates.

## Experimental Section

**Materials.** Polyethyleneglycol (PEG) 200 and morpholinoethylsulphonic acid (MES) were from Sigma Chemical Co. (St Louis, MO). *O*-(1,2,2-trimethylpropyl) methylphosphonofluoridate (soman) was obtained from the CEB (Centre d'Étude du Bouchet, Vert-le-Petit, France) and pralidoxime (*N*-methylpyridin-1-ium 2-aldoxime methiodide, 2-PAM) from EGA-Chemie (Steinheim, Germany). *Tc*AChE was purified as described previously.[2]

**Crystallization and Soaking Procedures.** Trigonal crystals of *Tc*AChE (space group $P3_121$) were obtained by the vapor diffusion

**Table 1.** Crystallographic and Refinement Statistics

| | nonaged soman/TcAChE | aged soman/TcAChE | ternary 2-PAM/aged soman/TcAChE complex |
|---|---|---|---|
| PDB entry code | 2wfz | 2wg0 | 2wg1 |
| ESRF beamline | ID14−4 | ID14−2 | ID14−2 |
| temperature (K) | 100 | 100 | 100 |
| no. of frames | 120 | 100 | 90 |
| exposure time (s/frame) | 1 (transmission 20%) | 2 | 4 |
| wavelength (Å) | 0.939 | 0.933 | 0.933 |
| space group | $P3_121$ | $P3_121$ | $P3_121$ |
| unit cell parameters (Å) | | | |
| $a = b$ | 111.4 | 111.6 | 111.9 |
| $c$ | 137.4 | 136.8 | 137.2 |
| resolution range (Å)[a] | 20.00−1.95 (2.00−1.95) | 20.00−2.20 (2.30−2.20) | 20.00−2.20 (2.30−2.20) |
| completeness (%)[a] | 99.3 (98.8) | 99.4 (99.9) | 99.5 (99.4) |
| $R_{sym}$ (%)[a,b] | 7.3 (59.8) | 13.7 (48.8) | 8.0 (49.5) |
| $I/\sigma(I)$[a] | 17.64 (3.12) | 10.02 (3.25) | 16.12 (3.30) |
| unique reflections[a] | 71726 (5103) | 50212 (6216) | 50657 (6244) |
| redundancy | 7.1 | 5.6 | 5.5 |
| $R_{cryst}$ (%) | 16.62 | 17.72 | 16.58 |
| $R_{free}$ (%) | 19.56 | 22.89 | 21.18 |
| rmsd bond length (Å) | 0.012 | 0.014 | 0.013 |
| rmsd bond angles (deg) | 1.3 | 1.5 | 1.4 |
| no. of non-hydrogen atoms in ASU | | | |
| total | 5206 | 5113 | 5221 |
| protein | 4395 | 4297 | 4449 |
| water | 660 | 620 | 555 |
| ligands | 151 | 196 | 217 |
| carbohydrates | 52 | 56 | 38 |
| soman | 10 | 4 | 4 |
| 2-PAM | | | 10 |
| $B$ factor (Å$^2$) | | | |
| overall | 31.4 | 25.4 | 31.2 |
| protein | 28.3 | 22.4 | 28.2 |
| water | 45.7 | 37.1 | 42.7 |
| ligands | 57.7 | 54.0 | 64.3 |
| carbohydrates | 61.2 | 56.6 | 64.6 |
| soman | 32.6 | 20.8 | 21.1 |
| 2-PAM | | | 33.3 |

[a] Values in brackets refer to the highest resolution shell. [b] $R_{sym} = \frac{\sum_{hkl}\sum_{i}\left|I_i(hkl) - \overline{I(hkl)}\right|}{\sum_{hkl}\sum_{i} I_i(hkl)}$

method at 4 °C in hanging drops in 32−34% PEG 200 and 150 mM MES, at pH 5.8−6.1. Conjugates and complexes were formed by soaking crystals of the native enzyme at 4 °C into solutions based on either 36% PEG 200/150 mM MES, pH 5.8 (referred to as *soaking solution A*) or 36% PEG 200/150 mM Tris/HCl, pH 8.2 (referred to as *the soaking solution B*). To obtain the nonaged soman/*Tc*AChE conjugate, crystals were soaked for 6 min in *soaking solution B* containing 1.3 mM soman (mixture of the four stereoisomers $P_{R/S}C_{R/S}$). Because of the cryoprotective capacity of PEG 200 itself, no additional cryoprotectant was necessary and the crystal was directly loop-mounted and flash-cooled in liquid nitrogen. The aged soman/*Tc*AChE conjugate was obtained by soaking crystals for 2 h in *soaking solution A* containing 1.3 mM soman. Crystals of the ternary complex of the aged soman/*Tc*AChE conjugate with 2-PAM were obtained in two stages: first, crystals of the aged conjugate were obtained as described above; these crystals were then transferred for 12 h into *soaking solution A* or *B* containing 10 mM 2-PAM (solubilized initially at 100 mM in 150 mM Tris/HCl, pH 8). All soaking and flash-cooling operations were performed at the Centre de Recherches du Service de Santé des Armées (La Tronche).

**Data Collection and Processing.** All data collection was performed at the European Synchrotron Radiation Facility (ESRF, Grenoble) on beamlines ID14−2 and ID14−4. The loops containing flash-cooled crystals were transferred on the goniometer head into the cryostream of a cooling device (700 series, Oxford Cryosystems, Oxford, UK) operating at 100 K. For details concerning data collection, see Table 1. Reflections were indexed and integrated using XDS.[73] The intensities of integrated reflections were scaled using XSCALE, and structure factors were calculated using XDSCONV. Refinement of the models was carried out using Refmac5,[74] with the native structure of *Tc*AChE (PDB entry code 1EA5) as the starting model. For calculation of $R_{free}$, the same structure factors as the ones used for refinement of the starting model (1EA5) were flagged. For all three structures (viz., the nonaged soman/*Tc*AChE conjugate, the aged conjugate, and the ternary complex of the aged conjugate with 2-PAM), a rigid-body refinement was first carried out using reflections in the range of 20−4 Å. All model building and graphic operations were carried out using Coot.[75] In each model, the first set of water molecules was added automatically using the water-picking feature in Coot. Solvent molecules, ligands, and sugar residues of the covalently attached glycan chains, viz., *N*-acetylglucosamine (NAG) and fucose (FUC), were added subsequently. The occupancies of the soman adduct in the nonaged and in the aged conjugates were estimated to be 90% and 100%, respectively. 2-PAM and soman in the ternary complex were estimated to display full occupancy. Successive alternation of refinement cycles and manual model building were performed until $R_{cryst}$ and $R_{free}$ did not decrease any further. Refinement comprised energy minimization and individual isotropic $B$ factor refinement, using the full range of recorded reflections for each data set. The simulated-annealing omit maps shown in Figures 2 and 3 were calculated using CNS

version 1.2[76] after omitting soman adducts and/or 2-PAM. Figures were produced with Pymol.[77] Active-site gorge volumes were calculated using the CASTP server[78] after removal of ligands and water molecules from the models. Alignment of huCE1 and *Tc*AChE structures was achieved with Theseus.[79] Final models were validated using MOLPROBITY[80] and WHATCHECK.[81] Parameters and topologies of PEG, MES, NAG, FUC, 2-PAM, and of nondealkylated and dealkylated soman adducts were generated using the PRODRG server at Dundee University.[82]

**Acknowledgment.** We gratefully acknowledge the ESRF for beam-time under long-term projects MX498, MX609, and MX722 (IBS BAG) and MX551 and MX666 (radiation-damage BAG), and the ESRF staff for providing efficient help during data collection. Financial support by the CEA, the CNRS, and the UJF is acknowledged, as well as a grant to M. W. from the Agence Nationale de la Recherche (ANR) (project no. JC05_45685), grants to F.N. from the ANR (ANR-06-BLAN-0163) and from the DGA (08co501), and a DGA grant (03co10-05/PEA 010807) to P.M. This study was supported by the European Commission Sixth Framework Research and Technological Development Program "SPINE2-COMPLEXES" Project, under contract no. 031220, a research grant from Erwin Pearl, the Benoziyo Center for Neurosciences, the Divadol Foundation, the Nalvyco Foundation, the Bruce Rosen Foundation, and the Neuman Foundation. J.L.S. is the Morton and Gladys Pickman Professor of Structural Biology. We thank Dr. Matthew Redinbo (Department of Chemistry, University of North Carolina at Chapel Hill) for permission to quote his unpublished data and Prof. David Milstein (Department of Organic Chemistry, Weizmann Institute of Science) for valuable discussions.

**Supporting Information Available:** Alternate refinement of the nonaged soman/*Tc*AChE conjugate. This material is available free of charge via the Internet at http://pubs.acs.org.

## References

(1) Silman, I.; Sussman, J. L. Acetylcholinesterase: "Classical" and "Nonclassical" Functions and Pharmacology. *Curr. Opin. Pharmacol.* **2005**, *5*, 293–302.
(2) Sussman, J. L.; Harel, M.; Frolow, F.; Oefner, C.; Goldman, A.; Toker, L.; Silman, I. Atomic Structure of Acetylcholinesterase from *Torpedo californica*: A Prototypic Acetylcholine-Binding Protein. *Science*. **1991**, *253*, 872–879.
(3) Colletier, J. P.; Fournier, D.; Greenblatt, H. M.; Stojan, J.; Sussman, J. L.; Zaccai, G.; Silman, I.; Weik, M. Structural Insights into Substrate Traffic and Inhibition in Acetylcholinesterase. *EMBO J.* **2006**, *25*, 2746–2756.
(4) Harel, M.; Quinn, D. M.; Nair, H. K.; Silman, I.; Sussman, J. L. The X-Ray Structure of a Transition State Analog Complex Reveals the Molecular Origins of the Catalytic Power and Substrate Specificity of Acetylcholinesterase. *J. Am. Chem. Soc.* **1996**, *118*, 2340–2346.
(5) Rosenberry, T. L.; Johnson, J. L.; Cusack, B.; Thomas, J. L.; Emani, S.; Venkatasubban, K. S. Interactions between the Peripheral Site and the Acylation Site in Acetylcholinesterase. *Chem. Biol. Interact.* **2005**, *157*−*158*, 181–189.
(6) Bourne, Y.; Radic, Z.; Sulzenbacher, G.; Kim, E.; Taylor, P.; Marchot, P. Substrate and Product Trafficking through the Active Center Gorge of Acetylcholinesterase Analyzed by Crystallography and Equilibrium Binding. *J. Biol. Chem.* **2006**, *281*, 29256–29267.
(7) Eddleston, M.; Juszczak, E.; Buckley, N. A.; Senarathna, L.; Mohamed, F.; Dissanayake, W.; Hittarage, A.; Azher, S.; Jeganathan, K.; Jayamanne, S.; Sheriff, M. R.; Warrell, D. A. Multiple-Dose Activated Charcoal in Acute Self-Poisoning: A Randomised Controlled Trial. *Lancet* **2008**, *371*, 579–587.
(8) *Report of the Specialists Appointed by the Secretary-General to Investigate Allegations by the Islamic Republic of Iran Concerning the Use of Chemical Weapons*; no. S/16433 ; United Nations Security Council: New York, Mar 26, **1984**.
(9) *Report of the Mission Dispatched by the Secretary-General to Investigate Allegations of the Use of Chemical Weapons in the Conflict between the Islamic Republic of Iran and Iraq*; no. S/17911 ; United Nations Security Council: New York, Mar 12, **1986**.
(10) *Report of the Mission Dispatched by the Secretary-General to Investigate Allegations of the Use of Chemical Weapons in the Conflict between the Islamic Republic of Iran and Iraq*; United Nations Security Council: New York, May 8, **1987**.
(11) Macilwain, C. Study Proves Iraq Used Nerve Gas. *Nature* **1993**, *363*, 3.
(12) Nagao, M.; Takatori, T.; Matsuda, Y.; Nakajima, M.; Iwase, H.; Iwadate, K. Definitive Evidence for the Acute Sarin Poisoning Diagnosis in the Tokyo Subway. *Toxicol. Appl. Pharmacol.* **1997**, *144*, 198–203.
(13) Viragh, C.; Akhmetshin, R.; Kovach, I. M.; Broomfield, C. Unique Push−Pull Mechanism of Dealkylation in Soman-Inhibited Cholinesterases. *Biochemistry* **1997**, *36*, 8243–8252.
(14) Michel, H. O.; Hackley, B. E., Jr.; Berkowitz, L.; List, G.; Hackley, E. B.; Gillilan, W.; Pankau, M. Ageing and Dealkylation of Soman (Pinacolylmethylphosphonofluoridate)-Inactivated Eel Cholinesterase. *Arch. Biochem. Biophys.* **1967**, *121*, 29–34.
(15) Segall, Y.; Waysbort, D.; Barak, D.; Ariel, N.; Doctor, B. P.; Grunwald, J.; Ashani, Y. Direct Observation and Elucidation of the Structures of Aged and Nonaged Phosphorylated Cholinesterases by $^{31}$P NMR Spectroscopy. *Biochemistry* **1993**, *32*, 13441–13450.
(16) Wins, P.; Wilson, I. B. The Inhibition of Acetylcholinesterase by Organophosphorus Compounds Containing a P−Cl Bond. *Biochim. Biophys. Acta* **1974**, *334*, 137–145.
(17) Saxena, A.; Doctor, B. P.; Maxwell, D. M.; Lenz, D. E.; Radic, Z.; Taylor, P. The Role of Glutamate-199 in the Aging of Cholinesterase. *Biochem. Biophys. Res. Commun.* **1993**, *197*, 343–349.
(18) Saxena, A.; Viragh, C.; Frazier, D. S.; Kovach, I. M.; Maxwell, D. M.; Lockridge, O.; Doctor, B. P. The pH Dependence of Dealkylation in Soman-Inhibited Cholinesterases and Their Mutants: Further Evidence for a Push−Pull Mechanism. *Biochemistry* **1998**, *37*, 15086–15096.
(19) Shafferman, A.; Ordentlich, A.; Barak, D.; Stein, D.; Ariel, N.; Velan, B. Aging of Phosphylated Human Acetylcholinesterase: Catalytic Processes Mediated by Aromatic and Polar Residues of the Active Centre. *Biochem. J.* **1996**, *318* (Pt 3), 833–840.
(20) Kovach, I. M. Stereochemistry and Secondary Reactions in the Irreversible Inhibition of Serine Hydrolases by Organophosphorus Compounds. *J. Phys. Org. Chem.* **2004**, *17*, 602–614.
(21) Ashani, Y.; Green, B. S. Are the Organophosphorus Inhibitors of AChE Transition State Analogs? In *Chemical Approaches to Understanding Enzyme Catalysis: Biometric Chemistry and Transition-State Analogs*; Green, B. S., Ashani, Y., Chipman, D., Eds.; Elsevier Scientific: Amsterdam, 1982; pp 169−188.
(22) Bencsura, A.; Enyedy, I.; Kovach, I. M. Origins and Diversity of the Aging Reaction in Phosphonate Adducts of Serine Hydrolase Enzymes: What Characteristics of the Active Site Do They Probe?. *Biochemistry* **1995**, *34*, 8989–8999.
(23) Millard, C. B.; Kryger, G.; Ordentlich, A.; Greenblatt, H. M.; Harel, M.; Raves, M. L.; Segall, Y.; Barak, D.; Shafferman, A.; Silman, I.; Sussman, J. L. Crystal Structures of Aged Phosphonylated Acetylcholinesterase: Nerve Agent Reaction Products at the Atomic Level. *Biochemistry* **1999**, *38*, 7032–7039.
(24) Benschop, H. P.; De Jong, L. P. A. Nerve Agent Stereoisomers: Analysis, Isolation and Toxicology. *Acc. Chem. Res.* **1988**, *21*, 368–374.
(25) Ordentlich, A.; Barak, D.; Kronman, C.; Benschop, H. P.; De Jong, L. P.; Ariel, N.; Barak, R.; Segall, Y.; Velan, B.; Shafferman, A. Exploring the Active Center of Human Acetylcholinesterase with Stereomers of an Organophosphorus Inhibitor with Two Chiral Centers. *Biochemistry* **1999**, *38*, 3055–3066.
(26) Berman, H. A.; Decker, M. M. Chiral Nature of Covalent Methylphosphonyl Conjugates of Acetylcholinesterase. *J. Biol. Chem.* **1989**, *264*, 3951–3956.
(27) Millard, C. B.; Koelnner, G.; Ordentlich, A.; Shafferman, A.; Silman, I.; Sussman, J. L. Reaction Products of Acetylcholinesterase and VX Reveal a Mobile Histidine in the Catalytic Triad. *J. Am. Chem. Soc.* **1999**, *121*, 9883–9884.
(28) Benschop, H. P.; Konings, C. A.; Van Genderen, J.; De Jong, L. P. Isolation, Anticholinesterase Properties, and Acute Toxicity in Mice of the Four Stereoisomers of the Nerve Agent Soman. *Toxicol. Appl. Pharmacol.* **1984**, *72*, 61–74.
(29) Millard, C. B.; Lockridge, O.; Broomfield, C. A. Organophosphorus Acid Anhydride Hydrolase Activity in Human Butyrylcholinesterase: Synergy Results in a Somanase. *Biochemistry* **1998**, *37*, 237–247.

(30) Wilson, I. B.; Ginsburg, S. Reactivation of Acetylcholinesterase Inhibited by Alkylphosphates. *Arch. Biochem.* **1955**, *54*, 569–571.
(31) Kewitz, H.; Wilson, I. B. A Specific Antidote against Lethal Alkylphosphate Intoxication. *Arch. Biochem. Biophys.* **1956**, *60*, 261–263.
(32) Wilson, I. B.; Froede, H. C. The Design of Reactivators for Irreversibly Blocked Acetylcholinesterase. In *Drug Design, Vol. II*; Ariens, E. J., Ed.; Academic Press: New York, 1971; pp 213−229.
(33) Worek, F.; Szinicz, L.; Thiermann, H. Estimation of Oxime Efficacy in Nerve Agent Poisoning: A Kinetic Approach. *Chem. Biol. Interact.* **2005**, *157−158*, 349–352.
(34) Marrs, T. C. Organophosphate Poisoning. *Pharmacol. Ther.* **1993**, *58*, 51–66.
(35) Antonijevic, B.; Stojiljkovic, M. P. Unequal Efficacy of Pyridinium Oximes in Acute Organophosphate Poisoning. *Clin. Med. Res.* **2007**, *5*, 71–82.
(36) de Jong, L. P.; Wolring, G. Z. Aging and Stereospecific Reactivation of Mouse Erythrocyte and Brain Acetylcholinesterases Inhibited by Soman. *Biochem. Pharmacol.* **1985**, *34*, 142–145.
(37) Yang, G. Y.; Oh, K. A.; Park, N. J.; Jung, Y. S. New Oxime Reactivators Connected with $CH_2O(CH_2)NOCH_2$ Linker and Their Reactivation Potency for Organophosphorus Agents-Inhibited Acetylcholinesterase. *Bioorg. Med. Chem.* **2007**, *15*, 7704–7710.
(38) Worek, F.; Thiermann, H.; Szinicz, L.; Eyer, P. Kinetic Analysis of Interactions between Human Acetylcholinesterase, Structurally Different Organophosphorus Compounds and Oximes. *Biochem. Pharmacol.* **2004**, *68*, 2237–2248.
(39) Ashani, Y.; Bhattacharjee, A. K.; Leader, H.; Saxena, A.; Doctor, B. P. Inhibition of Cholinesterases with Cationic Phosphonyl Oximes Highlights Distinctive Properties of the Charged Pyridine Groups of Quaternary Oxime Reactivators. *Biochem. Pharmacol.* **2003**, *66*, 191–202.
(40) Herkenhoff, S.; Szinicz, L.; Rastogi, V. K.; Cheng, T. C.; DeFrank, J. J.; Worek, F. Effect of Organophosphorus Hydrolysing Enzymes on Obidoxime-Induced Reactivation of Organophosphate-Inhibited Human Acetylcholinesterase. *Arch. Toxicol.* **2004**, *78*, 338–343.
(41) Ekstrom, F.; Akfur, C.; Tunemalm, A. K.; Lundberg, S. Structural Changes of Phenylalanine 338 and Histidine 447 Revealed by the Crystal Structures of Tabun-Inhibited Murine Acetylcholinesterase. *Biochemistry* **2006**, *45*, 74–81.
(42) Koellner, G.; Kryger, G.; Millard, C. B.; Silman, I.; Sussman, J. L.; Steiner, T. Active-Site Gorge and Buried Water Molecules in Crystal Structures of Acetylcholinesterase from *Torpedo californica*. *J. Mol. Biol.* **2000**, *296*, 713–735.
(43) Klebe, G. The Foundations of Protein−Ligand Interaction. In Crystallography and Drug Design, Erice, Italy, May 29−June 8, 2008.
(44) Petsko, G. A.; Ringe, D. *Protein Structure and Function*; New Science: London; Sinauer Associates: Sunderland, MA; Blackwell Publishing: Oxford, 2004; p xxii, 195 pp.
(45) Wang, E. I.; Braid, P. E. Oxime Reactivation of Diethylphosphoryl Human Serum Cholinesterase. *J. Biol. Chem.* **1967**, *242*, 2683–2687.
(46) Cygler, M.; Grochulski, P.; Kazlauskas, R. J.; Schrag, J. D.; Bouthillier, F.; Rubin, B.; Serreqi, A. N.; Gupta, A. K. A Structural Basis for the Chiral Preferences of Lipases. *J. Am. Chem. Soc.* **1994**, *116*, 3180–3186.
(47) Hornberg, A.; Tunemalm, A. K.; Ekstrom, F. Crystal Structures of Acetylcholinesterase in Complex with Organophosphorus Compounds Suggest That the Acyl Pocket Modulates the Aging Reaction by Precluding the Formation of the Trigonal Bipyramidal Transition State. *Biochemistry* **2007**, *46*, 4815–4825.
(48) Carletti, E.; Li, H.; Li, B.; Ekstrom, F.; Nicolet, Y.; Loiodice, M.; Gillon, E.; Froment, M. T.; Lockridge, O.; Schopfer, L. M.; Masson, P.; Nachon, F. Aging of Cholinesterases Phosphylated by Tabun Proceeds through O-Dealkylation. *J. Am. Chem. Soc.* **2008**, *130*, 16011–16020.
(49) Fleming, C. D.; Edwards, C. C.; Kirby, S. D.; Maxwell, D. M.; Potter, P. M.; Cerasoli, D. M.; Redinbo, M. R. Crystal Structures of Human Carboxylesterase 1 in Covalent Complexes with the Chemical Warfare Agents Soman and Tabun. *Biochemistry* **2007**, *46*, 5063–5071.
(50) Maxwell, D. M.; Brecht, K. M. Carboxylesterase: Specificity and Spontaneous Reactivation of an Endogenous Scavenger for Organophosphorus Compounds. *J Appl Toxicol.* **2001**, *21* (Suppl 1), S103–S107.
(51) Keijer, J. H.; Wolring, G. Z. Stereospecific Aging of Phosphonylated Cholinesterases. *Biochim. Biophys. Acta* **1969**, *185*, 465–468.
(52) Bourne, Y.; Taylor, P.; Marchot, P. Acetylcholinesterase Inhibition by Fasciculin: Crystal Structure of the Complex. *Cell* **1995**, *83*, 503–512.
(53) Kryger, G.; Harel, M.; Giles, K.; Toker, L.; Velan, B.; Lazar, A.; Kronman, C.; Barak, D.; Ariel, N.; Shafferman, A.; Silman, I.; Sussman, J. L. Structures of Recombinant Native and E202Q Mutant Human Acetylcholinesterase Complexed with the Snake-Venom Toxin Fasciculin-II. *Acta Crystallogr., Sect. D: Biol. Crystallogr.* **2000**, *56*, 1385–1394.
(54) Ordentlich, A.; Kronman, C.; Barak, D.; Stein, D.; Ariel, N.; Marcus, D.; Velan, B.; Shafferman, A. Engineering Resistance to "Aging" of Phosphylated Human Acetylcholinesterase. Role of Hydrogen Bond Network in the Active Center. *FEBS Lett.* **1993**, *334*, 215–220.
(55) Anslyn, E. V.; Dougherty, D. A. *Modern Physical Organic Chemistry*; University Science: Sausalito, CA, 2006; p xxviii, 1095.
(56) Cadogan, J. I. G.; Eastlick, D.; Hampson, F.; Mackie, R. K. Reactivity of Organophosphorus Compounds. Part XXIV. Acidic Hydrolysis of Dialkyl Methylphosphonates. *J. Chem. Soc. B* **1969**, 144–146.
(57) Kaplan, D.; Ordentlich, A.; Barak, D.; Ariel, N.; Kronman, C.; Velan, B.; Shafferman, A. Does "Butyrylization" Of Acetylcholinesterase through Substitution of the Six Divergent Aromatic Amino Acids in the Active Center Gorge Generate an Enzyme Mimic of Butyrylcholinesterase?. *Biochemistry* **2001**, *40*, 7433–7445.
(58) Gabel, F.; Masson, P.; Froment, M. T.; Doctor, B. P.; Saxena, A.; Silman, I.; Zaccai, G.; Weik, M. Direct Correlation between Molecular Dynamics and Enzymatic Stability: A Comparative Neutron Scattering Study of Native Human Butyrylcholinesterase and its "Aged" Soman Conjugate. *Biophys. J.* **2009**, *96*, 1489–1494.
(59) Masson, P.; Clery, C.; Guerra, P.; Redslob, A.; Albaret, C.; Fortier, P. L. Hydration Change During the Aging of Phosphorylated Human Butyrylcholinesterase: Importance of Residues Aspartate-70 and Glutamate-197 in the Water Network as Probed by Hydrostatic and Osmotic Pressures. *Biochem. J.* **1999**, *343*, 361–369.
(60) Masson, P.; Gouet, P.; Clery, C. Pressure and Propylene Carbonate Denaturation of Native And "Aged" Phosphorylated Cholinesterase. *J. Mol. Biol.* **1994**, *238*, 466–478.
(61) Felder, C. E.; Harel, M.; Silman, I.; Sussman, J. L. Structure of a Complex of the Potent and Specific Inhibitor BW284C51 with *Torpedo californica* Acetylcholinesterase. *Acta Crystallogr., Sect. D: Biol. Crystallogr.* **2002**, *58*, 1765–1771.
(62) Harel, M.; Schalk, I.; Ehret-Sabatier, L.; Bouet, F.; Goeldner, M.; Hirth, C.; Axelsen, P. H.; Silman, I.; Sussman, J. L. Quaternary Ligand Binding to Aromatic Residues in the Active-Site Gorge of Acetylcholinesterase. *Proc. Natl. Acad. Sci. U.S.A.* **1993**, *90*, 9031–9035.
(63) Colletier, J. P.; Sanson, B.; Nachon, F.; Gabellieri, E.; Fattorusso, C.; Campiani, G.; Weik, M. Conformational Flexibility in the Peripheral Site of *Torpedo californica* Acetylcholinesterase Revealed by the Complex Structure with a Bifunctional Inhibitor. *J. Am. Chem. Soc.* **2006**, *128*, 4526–4527.
(64) Rydberg, E. H.; Brumshtein, B.; Greenblatt, H. M.; Wong, D. M.; Shaya, D.; Williams, L. D.; Carlier, P. R.; Pang, Y. P.; Silman, I.; Sussman, J. L. Complexes of Alkylene-Linked Tacrine Dimers with *Torpedo californica* Acetylcholinesterase: Binding of Bis5-Tacrine Produces a Dramatic Rearrangement in the Active-Site Gorge. *J. Med. Chem.* **2006**, *49*, 5491–5500.
(65) Pang, Y. P.; Kollmeyer, T. M.; Hong, F.; Lee, J. C.; Hammond, P. I.; Haugabouk, S. P.; Brimijoin, S. Rational Design of Alkylene-Linked Bis-Pyridiniumaldoximes as Improved Acetylcholinesterase Reactivators. *Chem. Biol.* **2003**, *10*, 491–502.
(66) Ekstrom, F.; Pang, Y. P.; Boman, M.; Artursson, E.; Akfur, C.; Borjegren, S. Crystal Structures of Acetylcholinesterase in Complex with HI-6, Ortho-7 and Obidoxime: Structural Basis for Differences in the Ability to Reactivate Tabun Conjugates. *Biochem. Pharmacol.* **2006**, *72*, 597–607.
(67) Behrman, E. J.; Biallas, M. J.; Brass, H. J.; Edwards, J. O.; Isaks, M. Reactions of Phosphonic Acid Esters with Nucleophiles. I. Hydrolysis. *J. Org. Chem.* **1970**, *35*, 3063–3069.
(68) Behrman, E. J.; Biallas, M. J.; Brass, H. J.; Edwards, J. O.; Isaks, M. Reactions of Phosphonic Acid Esters with Nucleophiles. II. Survey of Nucleophiles Reacting with *p*-Nitrophenyl Methylphosphonate Anion. *J. Org. Chem.* **1970**, *35*, 3069–3075.
(69) Ekstrom, F. J.; Astot, C.; Pang, Y. P. Novel Nerve-Agent Antidote Design Based on Crystallographic and Mass Spectrometric Analyses of Tabun-Conjugated Acetylcholinesterase in Complex with Antidotes. *Clin. Pharmacol. Ther.* **2007**, *82*, 282–293.
(70) Luo, C.; Tong, M.; Chilukuri, N.; Brecht, K.; Maxwell, D. M.; Saxena, A. An in Vitro Comparative Study on the Reactivation of Nerve Agent-Inhibited Guinea Pig and Human Acetylcholinesterases by Oximes. *Biochemistry* **2007**, *46*, 11771–11779.

(71) Xu, Y.; Colletier, J. P.; Jiang, H.; Silman, I.; Sussman, J. L.; Weik, M. Induced-Fit or Preexisting Equilibrium Dynamics? Lessons from Protein Crystallography and MD Simulations on Acetylcholinesterase and Implications for Structure-Based Drug Design. *Protein Sci*. **2008**, *17*, 601–605.
(72) Xu, Y.; Colletier, J. P.; Weik, M.; Jiang, H.; Moult, J.; Silman, I.; Sussman, J. L. Flexibility of Aromatic Residues in the Active-Site Gorge of Acetylcholinesterase: X-Ray Versus Molecular Dynamics. *Biophys. J*. **2008**, *95*, 2500–2511.
(73) Kabsch, W. Automatic Processing of Rotation Diffraction Data from Crystals of Initially Unknown Symmetry and Cell Constants. *J. Appl. Crystallogr*. **1993**, *26*, 795–800.
(74) The CCP4 Suite: Programs for Protein Crystallography. *Acta Crystallogr., Sect. D: Biol. Crystallogr*. **1994**, *50*, 760-763.
(75) Emsley, P.; Cowtan, K. Coot: Model-Building Tools for Molecular Graphics. *Acta Crystallogr., Sect. D: Biol. Crystallogr*. **2004**, *60*, 2126–2132.
(76) Brunger, A. T. Version 1.2 of the Crystallography and NMR System. *Nat. Protoc*. **2007**, *2*, 2728–2733.
(77) DeLano, W. L. *The Pymol Molecular Graphics System*; DeLano Scientific: San Carlos, CA, 2002.
(78) Dundas, J.; Ouyang, Z.; Tseng, J.; Binkowski, A.; Turpaz, Y.; Liang, J. CASTp: Computed Atlas of Surface Topography of Proteins with Structural and Topographical Mapping of Functionally Annotated Residues. *Nucleic Acids Res*. **2006**, *34*, W116–W118.
(79) Theobald, D. L.; Wuttke, D. S. Theseus: Maximum Likelihood Superpositioning and Analysis of Macromolecular Structures. *Bioinformatics* **2006**, *22*, 2171–2172.
(80) Davis, I. W.; Leaver-Fay, A.; Chen, V. B.; Block, J. N.; Kapral, G. J.; Wang, X.; Murray, C L. W.; Arendall, W. B.III; Snoeyink, J.; Richardson, J. S.; Richardson, D. C. Molprobity: All-Atom Contacts and Structure Validation for Proteins and Nucleic Acids. *Nucleic Acids Res*. **2007**, *35*, W375–W383.
(81) Hooft, R. W.; Vriend, G.; Sander, C.; Abola, E. E. Errors in Protein Structures. *Nature* **1996**, *381*, 272.
(82) Schuttelkopf, A. W.; van Aalten, D. M.; PRODRG, A Tool for High-Throughput Crystallography of Protein−Ligand Complexes. *Acta Crystallogr., Sect. D: Biol. Crystallogr*. **2004**, *60*, 1355–1363.

# Reaction of Cresyl Saligenin Phosphate, the Organophosphorus Agent Implicated in Aerotoxic Syndrome, with Human Cholinesterases: Mechanistic Studies Employing Kinetics, Mass Spectrometry, and X-ray Structure Analysis

E. Carletti, L.M. Schopfer, J-P. Colletier, M-T. Froment, **F. Nachon**, M. Weik, O. Lockridge, P. Masson*

Chemical Research in Toxicology 24 (2011) 797-808

Chemical Research in Toxicology

ARTICLE

pubs.acs.org/crt

# Reaction of Cresyl Saligenin Phosphate, the Organophosphorus Agent Implicated in Aerotoxic Syndrome, with Human Cholinesterases: Mechanistic Studies Employing Kinetics, Mass Spectrometry, and X-ray Structure Analysis

Eugénie Carletti,[†] Lawrence M. Schopfer,[‡] Jacques-Philippe Colletier,[†] Marie-Thérèse Froment,[§] Florian Nachon,[§] Martin Weik,[†] Oksana Lockridge,[‡] and Patrick Masson*[,†,‡,§]

[†]Laboratoire de Biophysique Moléculaire, Institut de Biologie Structurale, 41 Rue Jules Horowitz, 38027 Grenoble, France

[‡]Eppley Institute and Department of Biochemistry and Molecular Biology, University of Nebraska Medical Center, Omaha, Nebraska 68198-5950, United States

[§]Département de Toxicologie, Institut de Recherche Biomédicale des Armées (IRBA)-Centre de Recherches du Service de Santé des Armées (CRSSA), 24 av des Marquis du Grésivaudan, 38702 La Tronche, France

**ABSTRACT:**

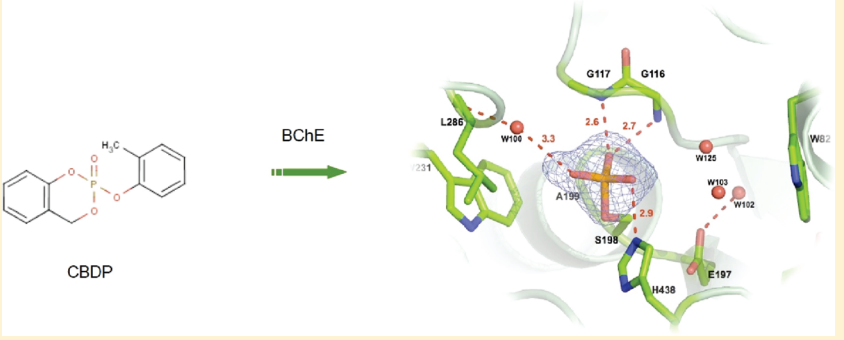


Aerotoxic syndrome is assumed to be caused by exposure to tricresyl phosphate (TCP), an antiwear additive in jet engine lubricants and hydraulic fluid. CBDP (2-(ortho-cresyl)-4*H*-1,2,3-benzodioxaphosphoran-2-one) is the toxic metabolite of triortho-cresylphosphate, a component of TCP. Human butyrylcholinesterase (BChE; EC 3.1.1.8) and human acetylcholinesterase (AChE; EC 3.1.1.7) are irreversibly inhibited by CBDP. The bimolecular rate constants of inhibition ($k_i$), determined under pseudo-first-order conditions, displayed a biphasic time course of inhibition with $k_i$ of $1.6 \times 10^8$ $M^{-1}$ $min^{-1}$ and $2.7 \times 10^7$ $M^{-1}$ $min^{-1}$ for E and E′ forms of BChE. The inhibition constants for AChE were 1 to 2 orders of magnitude slower than those for BChE. CBDP-phosphorylated cholinesterases are nonreactivatable due to ultra fast aging. Mass spectrometry analysis showed an initial BChE adduct with an added mass of 170 Da from cresylphosphate, followed by dealkylation to a structure with an added mass of 80 Da. Mass spectrometry in $^{18}$O-water showed that $^{18}$O was incorporated only during the final aging step to form phospho-serine as the final aged BChE adduct. The crystal structure of CBDP-inhibited BChE confirmed that the phosphate adduct is the ultimate aging product. CBDP is the first organophosphorus agent that leads to a fully dealkylated phospho-serine BChE adduct.

## INTRODUCTION

The cyclic organophosphorus agent 2-(*o*-cresyl)-4*H*-1,3,2-benzodioxaphosphoran-2-one (CBDP), also called cresyl saligenin phosphate, has been implicated in the development of organophosphate-induced delayed neuropathy (OPIDN).[1] OPIDN is a paralytic condition that is distinct from the toxicity associated with organophosphate inhibition of acetylcholinesterase (AChE).[2] Well known incidents of OPIDN have been attributed to the consumption of Jamaica ginger, a folk medicine, adulterated with tri-*o*-cresyl phosphate (TOCP),[3] and to the consumption of cooking oil adulterated with jet engine oil containing TOCP.[4] The toxicity of TOCP has been attributed to its conversion into CBDP, *in vivo*.[5,6] CBDP is formed *in vivo* by two consecutive reactions: (1) liver microsomal cytochrome P450-catalyzed oxidation[6] and (2) serum albumin-catalyzed cyclization of the oxidation product[7] (Scheme 1).

TOCP is a component of tricresyl phosphate (TCP) that is a combination of ten tricresyl phosphate isomers (triortho, tripara, trimeta, and mixtures of the three). TOCP is more toxic than the para and meta isomers.[8] TCP is used as an antiwear/extreme pressure agent and flame retardant in jet hydraulic fluids and

**Received:** December 21, 2010
**Published:** March 25, 2011

**Scheme 1. Metabolic Activation of TOCP to CBDP**

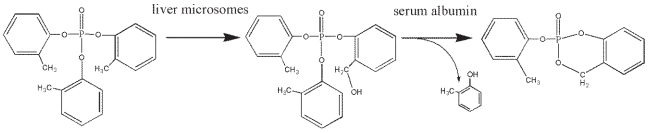


engine oils.[8,9] Because of its toxicity, the level of TOCP in commercial TCP mixtures has been reduced over time.[8] However, it is unclear whether this precaution has been sufficient to prevent toxic exposure to TOCP because safe levels of exposure are still in dispute.[10]

Over the past 30 years, an increasing number of reports have appeared documenting the occurrence of neurological signs associated with air travel, both commercial and military.[10] Short-term symptoms include blurred vision, dizziness, confusion, headache, tremors, nausea, vertigo, shortness of breath, increased heart rate, and irritation of the eyes and nose. Long-term symptoms include memory loss, numbness, lack of coordination, sleep disorders, severe headaches, nausea, diarrhea, susceptibility to upper respiratory infection, chest pain, skin blisters, signs of immunosuppression, muscle weakness, muscle pain, and fatigue.[10,11] The term aerotoxic syndrome has recently been coined to describe this condition.[10] Fumes escaping from the engine through leaky oil seals into the bleed air of the aircraft cabin are suspected to be the source of the toxicants that cause aerotoxic syndrome.[8,10]

Toxic components of these fumes include hexane, CO, $CO_2$, and TOCP. TOCP after bioactivation to CBDP is suspected of being responsible for the symptoms. A key gap in the evidence trail between fumes and syndrome is a quantitative biomarker for exposure to TOCP. CBDP has long been known as an inhibitor of carboxylesterases[12−14] and of neuropathy target esterase.[15] Animal studies have shown that CBDP is also an irreversible inhibitor of both AChE and BChE.[12,16] However, *in vitro* studies have indicated that CBDP reacts slowly with mammalian ChEs.[14,17] Modifications to the structure of CBDP have led to the development of insecticides, such as salioxon (2-methoxy-4*H*-1,3,2-benzodioxaphosphorin 2-oxide), that display strong anticholinesterase activity.[18−20] Recently, we established that human BChE reacts with CBDP. The organophosphorylated adduct undergoes two consecutive dealkylation reactions, i.e., aging, forming an ultimate phosphate adduct on the active site serine (Ser198).[1] This phosphorylated derivative is unique in the study of organophosphate (OP) reactions with BChE and therefore would be an ideal candidate for use as a biomarker of exposure to TOCP. Interest in BChE as a biomarker for exposure to TOCP has prompted us to investigate the mechanism and kinetics of the reaction of CBDP with BChE and AChE in more detail.

In the present article, we (1) investigated the kinetics of phosphorylation, inhibition, and aging of highly purified human AChE and human BChE by CBDP; (2) examined the chemistry for the formation of the postphosphorylation adducts, using mass spectrometry and $^{18}$O-water; and (3) determined the X-ray structure of the ultimate aged conjugate of CBDP-phosphorylated human BChE.

The kinetics for the reaction of CBDP with human BChE indicate that CBDP is one of the most potent OP inhibitors for BChE heretofore discovered and that postphosphorylation aging is extremely rapid. Because of this high reactivity, BChE very likely plays a role in protection against the toxicity of TOCP by scavenging CBDP from the human bloodstream. Both X-ray crystallography and mass spectrometry confirm that the ultimate product from the reaction of CBDP with BChE is a novel phosphorylated adduct of the catalytic serine, Ser198.

Kinetics for the reaction of CBDP with human AChE indicate that AChE is significantly sensitive to CBDP, although less than BChE by at least 1 order of magnitude.

## MATERIALS AND METHODS

**Caution:** *CBDP is a highly toxic organophosphorus compound. Handling requires suitable personal protection, training, and facilities. These requirements are the same as those for other poisonous organophosphorus compounds.*

**Chemicals.** CBDP was a gift from Dr. D. Lenz (USAMRICD, Aberdeen PG, MD, USA); this compound is 99.5% pure and was custom synthesized by Starks Associates Buffalo, NY, USA. A 0.1 M stock solution of CBDP was made in acetonitrile and stored at −70 °C. Working solutions of CBDP were made in anhydrous methanol, acetonitrile, or dimethylsulfoxide (DMSO) and stored at −70 °C. 2-PAM (pralidoxime methiodide, *N*-methyl-pyridin-1-ium 2-aldoxime methiodide) was Gold-label-grade from Ega-Chemie (Steinheim, Germany) and HI-6 (1-[[[4-(aminocarbonyl) pyridinio] methoxy] methyl]-2-[(hydroxyimino)-methyl] pyridinium dichloride monohydrate) was a gift from Dr. D. Genkin (Pharmsynthez, Saint Petersburg, Russia). Water-$^{18}$O (99 atom % $^{18}$O) was from Isotec (a member of the Sigma-Aldrich group St. Louis, MO; catalog number 487090). Sequencing grade modified trypsin was from Promega (Madison, WI, catalog number V5111). Alpha-cyano-2-hydroxy cinnamic acid (CHCA) was purchased from Fluka (a member of the Sigma-Aldrich group St. Louis, MO, catalog number 70990) and prepared as a saturating solution in 50% acetonitrile/water plus 0.3% trifluoroacetic acid. Acetonitrile used for mass spectrometry was of DNA sequencing grade from Fisher (Pittsburgh, PA, catalog number BP-1170), and trifluoroacetic acid used for mass spectrometry was of sequencing grade (>99.9%) from Beckman (Brea, CA, catalog number 290204). All other chemicals were of biochemical grade.

**Enzyme Sources.** Both native and recombinant human BChE (hBChE; accession number P06276) were used in this work. Native hBChE purified from plasma as described[21] was used for the kinetic studies and mass spectrometry. hBChE used for the kinetic studies consisted mostly of the tetrameric form. It was 61% pure with an activity of 41 units/mL, using BTC as the substrate at pH 8.0 and 25 °C (unit = 1 $\mu$mol of substrate hydrolyzed per min). The hBChE that was used for mass spectrometry had an activity of 73,400 units/mL (100 mg/mL) and was >50% pure. Both batches of enzyme were stored for months at +4 °C without activity loss in 30 mM Tris/HCl, pH 7.5, containing 0.1 M NaCl and 0.02% sodium azide. The recombinant hBChE was used for crystallization. It was a truncated monomer, containing residues 1−529 and 5 carbohydrate chains rather than the 9 in native hBChE. Recombinant human BChE was expressed in Chinese hamster ovary (CHO) cells and purified by affinity and ion exchange chromatographies, as described previously.[22] Its concentration was 6.47 mg/mL. Recombinant human AChE (hAChE; accession number P22303) was expressed in stably transfected Chinese hamster ovary cells (CHO) and purified as described previously.[23] Highly purified AChE (>90%) was 300-fold diluted into 0.1 M phosphate buffer at pH 8.0 supplemented with 0.1% bovine serum albumin (BSA) and 0.01% sodium azide for all kinetic studies.

**Enzyme Activity and Inhibition.** Cholinesterase activity was measured by the method of Ellman[24] at pH 8.0, at 25 °C in 50 mM phosphate buffer, using acetylthiocholine (ATC) iodide (1 mM) as the substrate for AChE and butyrylthiocholine (BTC) iodide (1 mM) as the substrate for BChE.

**Scheme 2. Reaction of OPs with Cholinesterases**

$$EH + I \supset \xleftrightarrow{K_I} EH.I \supset \xrightarrow{k_p} EHI$$

Progressive inhibition of enzymes by CBDP was performed in 50 mM sodium phosphate buffer at pH 8.0 at 25 °C, 10% methanol, or 5% acetonitrile. For inhibition studies of hBChE and hAChE, the final CBDP concentrations ranged from 0.5 nM to 10 nM and 0.1 to 5.5 $\mu$M, respectively. Ten percent MeOH has no denaturing effect on BChE and does not significantly alter its reactivity.[25,26] Despite the presence of 0.1% BSA, the addition of 10% methanol or 5% acetonitrile caused a decrease in AChE activity that stabilized in a few minutes at 75−80% residual activity. This solvent effect does not interfere with the inhibition mechanism of AChE during the time course of experiments.

Inhibition kinetics were performed under pseudofirst-order conditions ([E] ≪ [CBDP]). BChE active site concentration [E] in the inhibition medium was $6 \times 10^{-11}$ mol/L, and AChE active site concentration was $5 \times 10^{-11}$ mol/L. Enzyme active site concentrations were determined from the catalytic activity of diluted preparations at $V_{max}$, pH 8.0, and 25 °C, taking $k_{cat}$ = 45,500 min$^{-1}$ for BChE with BTC as the substrate[27] and $k_{cat}$ = 400,000 min$^{-1}$ for hAChE with ATC as the substrate.[28] The time course of enzyme inhibition was monitored by the Aldridge sampling method, i.e., samples were withdrawn at different incubation times (15 s to 20 min) after the addition of CBDP, and the remaining enzyme activity was determined. The pseudofirst-order rate constants for adduct formation ($k_{obs}$) were taken from the slopes of plots of log (residual activity) versus time.[29,30]

Previous work suggested that initial phosphorylation of the BChE active site serine would lead to a covalent, ring-opened CBDP-serine adduct.[1] Covalent adduct formation by CBDP may be described by the classical scheme for the reaction of OPs with ChEs (Scheme 2). In this scheme, EH stands for the free enzyme, I⊃ for the cyclic phosphotriester CBDP, EH.I⊃ for the noncovalent Michaelis complex between enzyme and CBDP, and EHI for the ring-opened CBDP phosphorylated enzyme. $K_I = k_{-1}/k_1$ is the dissociation constant of complex EH.I⊃, and $k_p$ is the enzyme phosphorylation rate constant. Assuming that rapid equilibrium conditions hold (i.e., $k_p \ll k_{-1}$), the observed rate for inhibition, $k_{obs}$, is as follows:

$$k_{obs} = \frac{k_p[\text{CBDP}]}{K_I + [\text{CBDP}]} \quad (1)$$

Analysis of kinetic data was performed using GOSA-fit, a fitting software based on a simulated annealing algorithm (BiogLog, Toulouse, France; http://www.bio-log.biz).

**Aging and Reactivation of CBDP-Inhibited Cholinesterases.** Reactivation and dealkylation rates for CBDP-phosphonylated ChEs were measured using standard procedure for the investigation of oxime-mediated reactivation and aging of ChEs.[31] Enzymes were inhibited with CBDP to 95% in less than 15 min, and aliquots were removed at various times (from 15 s to 10 min) following inhibition and immediately incubated with oxime reactivators in 0.1 M sodium phosphate buffer at pH 8.0 at 25 °C. Two different oxime reactivators were tested: 2-PAM (at 1 or 10 mM) and HI-6 (at 0.5 mM). ChE activity was measured as a function of incubation time in the presence of oxime, for up to 24 h.

**Mass Spectrometry of CBDP-Inhibited BChE.** hBChE was completely inhibited by excess CBDP in the presence and absence of $^{18}$O-water. For the reaction in the presence of $^{18}$O, 100 $\mu$L of $^{18}$O-water was combined with 1 $\mu$L of 1 M ammonium bicarbonate, 5 $\mu$L of BChE (73,400 units/mL), and 1 $\mu$L of CBDP (100 mM in acetonitrile). For the reaction in the absence of $^{18}$O, 100 $\mu$L of $^{16}$O-water was combined with 1 $\mu$L of 1 M ammonium bicarbonate, 5 $\mu$L of BChE (73,400 units/mL), and 1 $\mu$L of CBDP (100 mM). The final reaction mixtures contained 56 $\mu$M BChE and 930 $\mu$M CBDP in 10 mM ammonium bicarbonate. The reactions were incubated at room temperature for 30 min, after which time there was no measurable BChE activity remaining (1 $\mu$L from each sample was used for measuring activity). Parallel incubations of BChE were made without CBDP. All samples were prepared in siliconized, 1.7 mL microfuge tubes (Avant from Midwest Scientific, St. Louis, MO, cat# AVSC1510). After the incubations, all four samples were denatured by boiling for 10 min, then dried under vacuum in a Savant SpeedVac (Thermo Scientific, Waltham, MA). The purpose for drying was to remove the $^{18}$O-water. Removal of the $^{18}$O-water before trypsinolysis simplifies interpretation of the mass spectra because trypsin would introduce two $^{18}$O-oxygens into the C-terminus of every peptide during proteolysis if trypsinolysis were conducted in an $^{18}$O-medium.[33] The pellets were redissolved in 106 $\mu$L of 10 mM ammonium bicarbonate made with $^{16}$O-water. Four microliters of sequencing grade trypsin (0.4 $\mu$g/$\mu$L in 50 mM acetic acid, 200 nmol of acetic acid) was added to each preparation, followed by 2 $\mu$L of 0.1 M ammonium bicarbonate (200 nmol of bicarbonate) to neutralize the acetic acid. The preparations were incubated at 37 °C overnight.

Ten microliters of each digest was desalted using C18 ZipTips (Millipore, Billerica, MA catalog number ZTC18SO96). The ZipTip was wetted with 100% acetonitrile and activated with 0.1% trifluoroacetic acid. One microliter of 1% trifluoroacetic acid was added to each 10 $\mu$L aliquot of digest. Each acidified digest was loaded onto a separate activated ZipTip, washed with 0.1% trifluoroacetic acid, and eluted with 10 $\mu$L of 60% acetonitrile/water containing 0.1% trifluoroacetic acid. An aliquot of each eluant was diluted 10-fold with 50% acetonitrile/water plus 0.3% trifluoroacetic acid. Two microliters of each dilution was mixed with 2 $\mu$L of CHCA (alpha-cyano-4-hydroxycinnamic acid). One microliter aliquots of the mixture were spotted onto a MALDI target plate (384-well Opti-TOF plate, catalog number 1016491 from Applied Biosystems, Foster City, CA) and allowed to air dry.

Samples were analyzed in a MALDI TOFTOF 4800 mass spectrometer (Applied Biosystems, Foster City, CA) using both reflector positive and reflector negative modes with delayed extraction. Six 500 laser pulses were accumulated for each measurement, over a mass range of 2000 to 4000 amu, using a laser voltage of 3500 V in positive mode and 3600 V in negative mode. Data collection was controlled by 4000 Series Explorer software (version 3.5). Mass calibration was made with Cal Mix 5 (containing bradykinin, 2−9 clip; angiotensin I; Glu-fibrinopeptide B; adrenocorticotropic hormone [ACTH], 1−17 clip; ACTH, 18−39 clip; and ACTH, 7−38 clip, Applied Biosystems).

**Crystallization of Recombinant hBChE and Generation of the Ultimate Aged Conjugate of CBDP-Phosphorylated Human BChE.** Human BChE was crystallized as described previously.[22] The final conjugate of hBChE inhibited by CBDP was obtained by soaking crystals for 12 h in a mother liquor solution (0.1 M MES, pH 6.5, 2.1 M ammonium sulfate) containing 1 mM CBDP (at 4 °C). The CBDP stock solution was 10 mM in DMSO. Crystals were washed for 5 s in a cryoprotective solution (0.1 M MES buffer pH 6.5, 2.3 M ammonium sulfate, and 20% glycerol) before being flash-cooled in liquid nitrogen for data collection.

**X-ray Data Collection and Structure Solution of the Ultimate Aged Conjugate of CBDP-Phosphoryated Human BChE.** Diffraction data were collected at the European Synchrotron Radiation Facility (ESRF, Grenoble, France). Data for crystalline hBChE inhibited by CBDP were collected at 100 K, on the ID14-eh4 beamline using $\lambda$ = 0.9765 Å wavelength with an ADSC Quantum Q315r detector.[32] The data set was processed with XDS,[34] and the structure was solved with the CCP4 suite.[35] An initial model was determined by molecular replacement with MolRep,[36] starting from the recombinant hBChE structure (PDB entry 1P0I) from which all ligands and glycan chains were removed. The initial model was refined as follows: a rigid-body refinement, made with REFMAC5,[37] was followed by iterative cycles of model building with Coot[38] and then restrained, and TLS refinement

was carried out with REFMAC5.[37,39] TLS groups were defined with the help of the TLS Motion Determination server (http://skuld.bmsc.washington.edu/~tlsmd/index.html).[40] The bound ligand and its descriptions were built using the Dundee PRODRG2.5 server including energy minimization using GROMOS96.1 force field calculations.

## RESULTS AND DISCUSSION

**Kinetics for the Inhibition of Human Cholinesterases by CBDP.** Inhibition of BChE by CBDP did not follow simple first-order progressive kinetics. Plots of residual activity ($\ln(A/A_0)$) versus time were biphasic, despite the fact that the basic condition for a first-order reaction was maintained, i.e., the enzyme concentration in the reaction medium was much less than the CBDP concentrations, and that CBDP was stable during the course of inhibition. In addition, titration experiments with [CBDP] varying from 0.2 [$E_0$] to 0.9 [$E_0$] showed that there was no spontaneous reactivation of inhibited enzymes.

Thus, the biphasic progressive inhibition can be regarded as the sum of two first-order processes, a fast phase and a slow phase. It should be noted that the first-order lines for both phases extrapolated to ln50% activity at $t = 0$. Situations similar to this, where first-order lines do not pass through the origin, were described by Aldridge and Reiner.[30] In one case, they described partial inhibition at zero-time, i.e., rapid equilibrium formation of an inhibitory complex prior to phosphonylation. In another case, there was ongoing inhibition during the reaction with substrate.[41−43] These situations could be identified by the dilution of the enzyme prior to the measurement of residual activity or by increasing the substrate concentration during activity measurement. Neither dilution of the inhibited enzyme prior to the measurement of residual activity nor increasing the concentration of substrate ([BTC] from 0.25 mM to 10 mM) during the assay changed the extrapolated ln(% activity) of BChE. These observations indicate that neither ongoing inhibition nor rapid equilibrium binding of inhibitor is responsible for the biphasic inhibition behavior exhibited by CBDP. In addition, for the type of behavior described by Aldridge and Reiner[30] and Estevez and Vilanova,[41] the intercept on the activity axis depends on inhibitor concentration. In the case of the inhibition of BChE by CBDP, first-order lines for the slow phase extrapolated through the ordinate at [$E_0$] = 50 ± 10% regardless [CBDP]. After subtraction of the slow process contribution, the first-order lines for the fast phase also extrapolated through the ordinate at [$E'_0$] = 50 ± 10% whatever the [CBDP]. The sum of the two ordinate intercepts was always equal to 100%. Both fractional activities at $t_0$ may be regarded as the relative activities of two enzyme forms. Since both fractional activities are the same, the two enzyme forms are present in the preparation in similar amounts. Inhibition of AChE by CBDP is also biphasic. However, in this case, the extrapolated $y$-axis intercept for the fast phase is larger than the extrapolated intercept for the slow phase. Therefore, the fast phase form of AChE, [$E'_0$], is present in higher concentration than the slow phase form, [$E_0$].

The biphasic progressive inhibition indicates that CBDP reacts at different rates with two different active populations of butyrylcholinesterase (E and E′) that are in slow equilibrium.[44,45] The affinity of both forms for certain inhibitors can be different, and their reactivity can be different too. Such an inhibition pattern has also been observed for carbamylation of BChE with *N*-methyl-*N*-(2-nitrophenyl) carbamoyl chloride.[46] This situation is described in Scheme 3. Thus, the kinetics for inhibition of

**Scheme 3. Reaction of CBDP with Two Cholinesterase Forms in Slow Equilibrium**

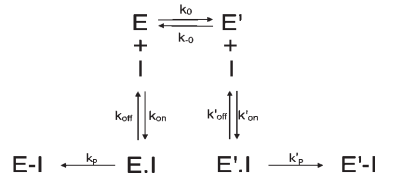


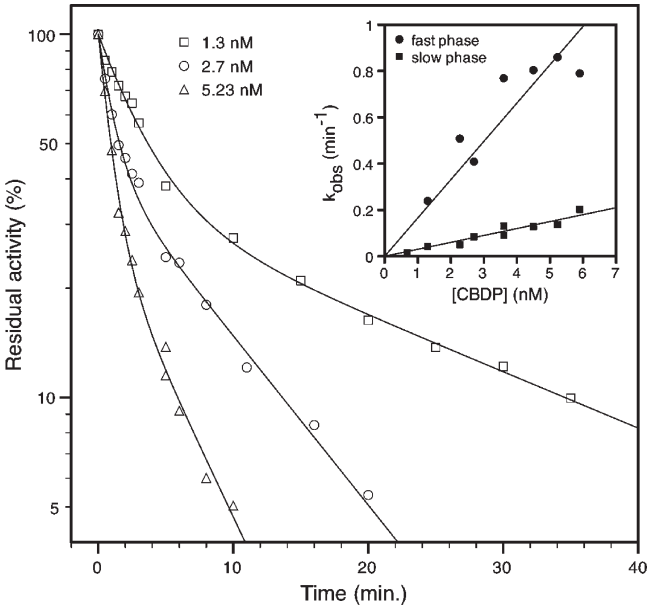


**Figure 1.** Time course of inhibition of hBChE by different concentrations of CBDP in 50 mM sodium phosphate at pH 8.0, containing 10% MeOH at 25 °C. The solid curve represents the nonlinear regression fit using eq 2. Insert: secondary plot used for the determination of the bimolecular rate constants of inhibition ($k_i$ and $k'_i$) for fast and slow phases, according to eq 4.

ChEs by CBDP, under pseudofirst-order conditions, can be described by the following equation:

$$[E]_t = [E]_0 e^{-k_{obs}\cdot t} + [E']_0 e^{-k'_{obs}\cdot t} \quad (2)$$

with $k_{obs} > k'_{obs}$, and

$$[E_{tot}]_0 = [E]_0 + [E']_0, k_{obs} = \frac{k_p \cdot [I]}{K_I + [I]},$$
$$k'_{obs} = \frac{k'_p \cdot [I]}{K'_I + [I]}, K_I = \frac{k_{off}}{k_{on}}, \text{and} K'_I = \frac{k'_{on}}{k'_{off}} \quad (3)$$

By convention, we refer to $k_{obs}$ for the fast phase and to $k'_{obs}$ for the slow phase. Figure 1 shows typical biphasic plots for the progressive inhibition of BChE by CBDP that fit with eq 2. Measured values for $k_{obs}$ and $k'_{obs}$ are calculated by nonlinear regression fit using eq 2.

For BChE, replots of $k_{obs}$ versus [CBDP] for both the fast and slow phases were linear, passing through the origin (Figure 1, insert). This indicates that for both the E and E′ forms of BChE, the highest CBDP concentration (10 nM) remained lower than

**Table 1. Bimolecular Rate Constants ($k_i$) for the Inhibition of Human AChE and BChE at pH 8.0 and 25 °C[a]**

| | AChE[b] | | BChE | |
|---|---|---|---|---|
| enzyme form | E | E′ | E | E′ |
| $k_i$ ($M^{-1}$ $min^{-1}$) 10% MeOH | >3.7 × $10^6$[c] | (1.06 ± 0.23) × $10^5$ | (1.5 ± 0.2) × $10^8$ | (2.5 ± 0.7) × $10^7$ |
| $k_i$ ($M^{-1}$ $min^{-1}$) 5% acetonitrile | ND | (0.33 ± 0.17) × $10^5$ | ND | ND |
| $k_i$ ($M^{-1}$ $min^{-1}$) 0.9% saline | ND | (0.73 ± 0.6) × $10^5$ | ND | ND |

[a] E, enzyme fast forms; E′ enzyme slow forms; ND, not determined. Experiments were performed in triplicate (mean values ± SE). [b] Experimental $k_i$ values for the E-form of AChE are not listed because the kinetics did not provide a second order rate constant in that instance. [c] Estimated minimum $k_i$ value using $k_p$= 0.37 $min^{-1}$ and $K_I \ll 0.1$ μM.

**Scheme 4. Reaction Pathway of CBDP with Cholinesterases**

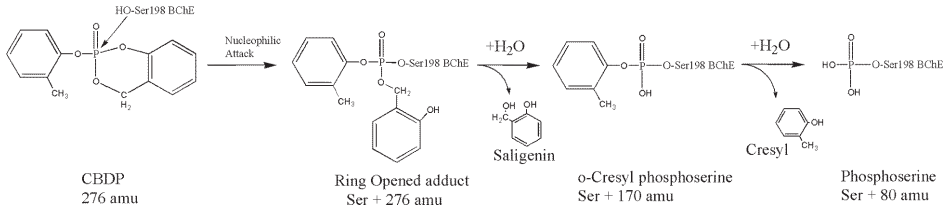


$K_I$ and $K'_I$. It follows that under our experimental conditions, $k_{obs}$ and $k'_{obs}$ reduce to

$$k_{obs} = \frac{k_p}{K_I}[I] = k_i \cdot [I] \quad \text{and} \quad k'_{obs} = \frac{k'_p}{K'_I}[I] = k'_i \cdot [I] \qquad (4)$$

with $k_i$ and $k'_i$ as the bimolecular rate constants of inhibition. Determined values of $k_i$ and $k'_i$ are given in Table 1.

The situation was somewhat different for AChE (data not shown). The inhibition kinetics were biphasic, and a replot of the slow phase $k'_{obs}$ versus [CBDP] was linear and passed through the origin. The linear dependence of $k'_{obs}$ on [CBDP] indicates that, as for BChE, the highest experimental CBDP concentration (5.5 μM) was far less than $K'_I$. However, the fast phase of inhibition was independent of the CBDP concentration, giving $k_{obs}$ = 0.37 ± 0.15 $min^{-1}$. Such a situation occurs if the CBDP concentration is very much larger than $K_I$ so that $k_{obs}$ reduces to $k_p$, i.e., the E form is saturated by CBDP even at the lowest concentration (0.1 μM).

Determined values of $k'_i$ for the inhibition of AChE form E′ under different solvent conditions are also given in Table 1. Experimental values remain in the same order of magnitude showing that the solvent effect is weak. The slight increase in $k'_i$ observed for the inhibition performed in 5% acetonitrile may reflect a specific effect of this solvent on AChE as has been reported by several investigators,[47] but did not reflect a change in the mechanism of inhibition.

The determined values of the bimolecular rate constants for the phosphonylation of both hBChE ($k_i$ = 1.5 ± 0.2 × $10^8$ and $k'_i$ = 2.5 ± 0.7 × $10^7$ $M^{-1}$ $min^{-1}$) and hAChE (>3.7 × $10^6$ and 1.06 ± 0.23 × $10^5$ $M^{-1}$ $min^{-1}$) by CBDP (Table 1) are much faster than values previously reported for the inhibition of cholinesterase by CBDP. Maxwell obtained a value of 1.1 × $10^3$ $M^{-1}$ $min^{-1}$ for rat brain AChE at pH 7.4 and 37 °C.[14] Cohen found a value of 2.1 × $10^3$ $M^{-1}$ $min^{-1}$ for recombinant human AChE and 2 × $10^4$ $M^{-1}$ $min^{-1}$ for human BChE at pH 8.0 and 27 °C.[20] The major difference between those experiments and ours is that those authors used CBDP stock solutions that were made in aqueous buffer. The problem with aqueous solutions of CBDP is that CBDP is unstable in water. We found that the hydrolysis rate of CBDP in 0.1 M sodium phosphate at pH 8.0 was 0.0126 $min^{-1}$ at 25 °C, i.e., $t_{1/2}$ = 55 min. This agrees with a previously reported $t_{1/2}$ value of 60 min in 36 mM barbiturate−8 mM potassium phosphate buffer at pH 8.0.[6] Saligenin-derived, six-membered cyclic phosphates (oxon) are even more sensitive to hydrolysis.[48] Instability of these compounds is reported to be due to a strain in the distorted benzodioxaphosphorin ring.[49,50]

Our results (Table 1, $k'_i$ in 10% MeOH) show that the slow phase reactivity of hBChE (form E′) with CBDP is 235 ± 110-fold faster than the reactivity of hAChE (form E′). Though it was not possible to determine $k_i$ for hAChE (form E) directly, an estimate could be made from the following. The $k_p$ for BChE (form E) can be estimated from its $k_i$, knowing from the experiments that $K_I$ for BChE must be much larger than 10 nM. Since $k_i$ for BChE is 1.5 × $10^8$ $M^{-1}$ $min^{-1}$ and $K_I \gg$ 10 nM, then $k_p = k_i \cdot K_I$ for BChE ≫ 1.5 $min^{-1}$ > 0.37 $min^{-1}$ = $k_p$ for AChE. Therefore, on the one hand we know that $k_p$ for BChE ≫ $k_p$ for AChE, and on the other hand, we do not expect that $K_I$ for AChE is smaller than that for BChE because the active site of AChE poorly accommodates large ligands like CBDP compared to the active site of BChE. It follows that $k_i$ for AChE (form E) ≪ $k_i$ for BChE, i.e., the reactivity of AChE (form E) is much lower than the reactivity for BChE (form E).

However, a lower limit value for $k_i$ for AChE (fast form, E) may be estimated from the experimental value of $k_p$ = 0.37 $min^{-1}$ and $K_I \ll 0.1$ μM, giving $k_i \gg$ 3.7 × $10^6$ $M^{-1}$ $min^{-1}$. Despite the reactivity of AChE with CBDP being lower than that of BChE, it appears to be larger than some nerve agents such as tabun (7.4 × $10^6$ $M^{-1}$ $min^{-1}$).[51]

**Aging and Nonreactivatibility of CBDP-Inhibited BChE.** Previous MALDI-TOF mass spectral studies suggested that two postinhibitory reactions occurred after the formation of the initial BChE covalent adduct, i.e., rapid hydrolysis of the ring-opened CBDP adduct into an *o*-cresyl-phospho-serine adduct with the release of saligenin, followed by conversion of this adduct into a phospho-serine adduct plus *o*-cresol[1] (Scheme 4). Both dealkylation steps can be considered aging steps.

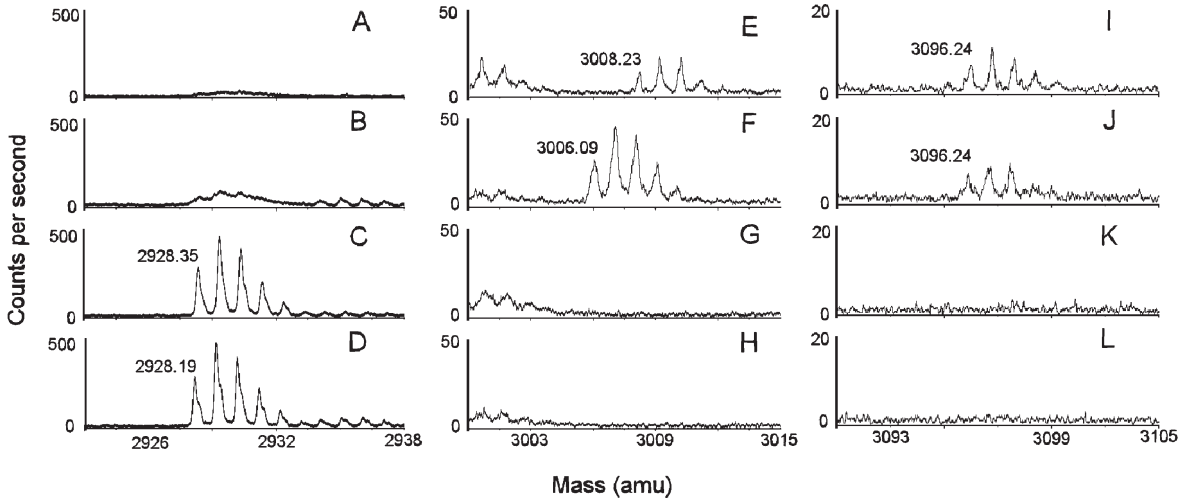


**Figure 2.** MALDI TOF mass spectra of the active site tryptic peptide from reactions of BChE with CBDP in the presence and absence of $^{18}$O-water. Reactions of BChE with CBDP were conducted as described in the Materials and Methods section. Masses of interest are shown: 2928 amu $[M + H]^{+1}$ for the unlabeled active site peptide SVTLFGESAGAASVSLHLLSPGSHSLFTR in positive mode; 3006 amu $[M - H]^{-1}$ for the phosphorylated active site peptide in the presence of $^{16}$O-water in negative mode; 3008 amu $[M - H]^{-1}$ for the phosphorylated active site peptide in the presence of $^{18}$O-water in negative mode; 3096 amu $[M - H]^{-1}$ for the *o*-cresyl-phosphorylated active site peptide in the presence of $^{18}$O-water and $^{16}$O-water in negative mode. Limited mass ranges around the masses of interest are shown to emphasize the isotopic splittings and peak resolution, to illustrate the relative intensities of the members of the isotopic families, and to avoid interference from other peptides with greater signal intensities. Panels A, E, and I are from the reaction of BChE with CBDP in the presence of $^{18}$O-water; panels B, F, and J are from the reaction of BChE with CBDP in the presence of $^{16}$O-water; panels C, G, and K are from an incubation of BChE in $^{18}$O-medium without CBDP; and panels D, H, and L are from an incubation of BChE in $^{16}$O-medium without CBDP. A mass shift of +2 from the incorporation of $^{18}$O-water is seen only in panel E for the phosphorylated active site peptide of mass 3008, which demonstrates that the P−O bond was broken when the cresylphosphate adduct aged to form phospho-serine. In contrast, $^{18}$O was not introduced during the formation of the cresylphosphate adduct (mass 3096 in panels I and J), which means this adduct resulted from cleavage of the O−C bond.

It is generally accepted that oximes can reactivate the initial, covalent adduct of organophosphate inhibited cholinesterases, but that after aging, oxime reactivation is ineffective. In order to determine how fast the CBDP aging reactions occur, we measured oxime-mediated reactivation of CBDP-inhibited BChE and AChE.

Attempts to reactivate both CBDP-phosphonylated AChE and BChE by oximes 2-PAM and HI-6 failed. Experiments were performed in triplicate. This strongly suggests that aging is very rapid after inhibition by CBDP. The kinetics indicated that loss of reactivatibility occurs in less than 15 s following inhibition. Aging of α-chymotrypsin[52] and fly AChE[19] inhibited by CBDP was also found to be very rapid. These enzymes were not reactivatable even with strong nucleophilic compounds. A previous mass spectrometry study of human albumin phosphonylated by CBDP indicated that a rapid, water-mediated loss of saligenin occurred after phosphonylation.[1] This reaction occurred despite the fact that albumin adducts of other organophosphates do not age at all.[53] A mass spectral study of the human BChE-CBDP adduct indicated that two consecutive postphosphorylation reactions occur: a rapid loss of saligenin was followed by a loss of the cresyl moiety, leading to a phospho-serine adduct.[1] Our kinetic results confirm the rapidity of the first postinhibitory reactions of CBDP-phosphonylated BChE and CBDP-phosphonylated AChE to form aged adducts, and illustrate the difficulties in reactivating such aged enzymes.

**Mass Spectrometry.** Following the formation of the initial reaction of CBDP with BChE, there are two adduct modifications (Scheme 4).[1] The initial ring opened adduct is not seen with BChE, but its presence can be inferred by analogy with the reactions of other OP with BChE and from a similar nucleophilic reaction between CBDP and tyrosine.[1] The dealkylation reactions that follow the initial adduct formation involve hydrolysis of the P−O−C linkage. The question to be addressed by the $^{18}$O-mass spectral experiments is whether the P−O bond or the O−C bond is cleaved during the course of these dealkylation reactions.

If the P−O bond is cleaved in a medium containing $^{18}$O-water, then an $^{18}$OH will be added to the phosphorus; but if the O−C bond is cleaved, then the $^{18}$OH will be added to the carbon, and the original $^{16}$O will remain on the phosphorus. Exchange of $^{18}$O for $^{16}$O can be discerned by a 2 amu increase in mass of the phospho(organophospho)-peptide adduct. MALDI TOF mass spectral analysis of tryptic digests from BChE reacted with CBDP in the presence $^{18}$O-water or in the presence of $^{16}$O-water is shown in Figure 2 (panels A, B, E, F, I, and J). The results are compared to tryptic digests of BChE incubated under the same conditions without CBDP (Figure 2; panels C, D, G, H, K, and L). Limited mass ranges are presented in order to illustrate the isotopic splitting for the masses of interest and to reduce interference from more intense signals. Spectra in panels A, B, C, and D show the mass of the unlabeled active site peptide from BChE, SVTLFGESAGAASVSLHLLSPGSHSLFTR, taken in positive reflector mode. The theoretical, protonated $[M + H]^{+1}$, monoisotopic mass of this peptide is 2928.52 amu (obtained with the assistance of the MS-Product algorithm from Protein Prospector at http://prospector.ucsf.edu/prospector). Spectra in panels E, F, G, and H show the mass of the phospho adduct of the active site peptide taken in negative reflector mode. The theoretical, deprotonated $[M - H]^{-1}$, monoisotopic mass of this peptide, is 3006.52 amu in negative mode. Spectra in panels I, J, K, and L show the mass of the cresyl-phospho adduct of the active site peptide taken in negative reflector mode. The

theoretical, deprotonated $[M - H]^{-1}$, monoisotopic mass of this peptide is 3096.52 amu. Negative mode spectra of the phospho-adducts showed better resolution and better signal-to-noise than spectra in the positive mode, despite the fact that the signal intensities were greater in the positive mode.

The unlabeled active site peptide produced by digestion in either $^{18}O$- or $^{16}O$-media gave identical spectra with a monoisotopic, $[M + H]^{+1}$ mass of 2928.27 ± 0.08 amu (Figure 2, panels C and D), indicating that spontaneous exchange of $^{18}O$ into the peptide did not occur. The 1 amu isotopic splitting and the isotopic pattern of this family of peaks are consistent with a mass of 2928 amu (the isotopic pattern was checked with the MS-Isotope algorithm from Protein Prospector at http://prospector.ucsf.edu/prospector). Weak, unresolved spectra in the vicinity of 2928 amu were seen in the digests from the CBDP-containing samples (Figure 2, panels A and B), despite the fact that CBDP had inhibited all of the BChE activity. The unresolved character of these spectra indicates that these masses arose in the MALDI TOF mass spectrometer from fragmentation in the flight path after the reflector.

The cresyl-phospho adducts from the CBDP reactions conducted in the presence of either $^{18}O$- or $^{16}O$-media gave identical spectra with a monoisotopic, $[M - H]^{-1}$ mass of 3096.15 ± 0.05 amu (Figure 2, panels I and J), indicating that oxygen from the medium was not added to the phosphorus during hydrolysis of saligenin. This in turn indicates that O−C bond fission accompanied this hydrolysis. This sort of dealkylation is characteristic of aging in BChE.[54] Aging is assisted by groups in the pi-cation binding pocket of the active site[55,56] and is specific for the ligand bound into this pocket.[23,24,57,58] This suggests that for the initial, ring-opened adduct, the saligenin moiety is bound to the pi-cation binding pocket. The 1 amu isotopic splitting and the isotopic pattern of this family of peaks support the argument that these signals are a genuine reflection of a monoisotopic 3096 amu mass. Absence of signal at 3096 amu from the digests of BChE incubated without CBDP (Figure 2, panels K and L) indicates that the 3096 signal is a characteristic of the CBDP reaction and is not an adventitious mass occurring in the BChE tryptic digest.

The phospho adduct from the reaction of BChE with CBDP in the presence $^{18}O$-water gave a mass of 3008.23 amu, whereas the same reaction in $^{16}O$-water resulted in a mass of 3006.09 (Figure 2, panels E and F). Since the theoretical mass for the phosphorylated active site peptide in negative mode is 3006.51 amu, the 3008.23 amu mass from the $^{18}O$-reaction indicates that one oxygen atom from the medium was added to the phosphorus during hydrolytic release of the cresyl. This in turn indicates that the P−O bond was broken during this hydrolysis. P−O bond breakage is consistent with the cresyl moiety being located in the acyl binding pocket where the classical aging type of assistance for fission of the O−C bond is unavailable. The 1 amu isotopic splittings and the isotopic patterns of these two families of peaks support the argument that these signals are genuine reflections of monoisotopic masses at 3006 and 3008 amu. The absence of signal in the 3006−3008 amu region from the digests from BChE incubated without CBDP (Figure 2, panels G and H) indicates that the 3006 and 3008 amu signals are characteristic of the CBDP reaction and are not adventitious masses occurring in the BChE tryptic digest.

**X-ray Structure of Phospho-hBChE.** The structure of CBDP-inhibited hBChE after 12 h of soaking was solved at 2.5 Å resolution. Data and refinement statistics are shown in Table 2. In the experimental $|F_o| - |F_c|$ electron density map, a strong positive peak is observed (above 15$\sigma$) at covalent bonding distance of the catalytic Ser198 confirming the presence of the phosphorus atom. The structure was unambiguously refined as a phospho-serine adduct, indicating the departure of both the *o*-cresyl and saligenin substituents after 12 h of incubation (Figure 3).

**Table 2. Data Collection and Refinement Statistics**

| Data Collection | |
|---|---|
| | phospho-hBChE |
| data | (PDB code 2y1k) |
| space group | *I*422 |
| unit cell axes, $a = b$, $c$ (Å) | 153.77, 127.60 |
| no. of reflections | 243 040 |
| unique reflections | 25 339 |
| resolution range (Å) | 40−2.5 (2.6−2.5)[a] |
| completeness (%) | 94.8 (97.4) |
| $R_{merge}$[b] (%) | 8.9 (49.0) |
| $I/\sigma$ (I) | 26.0 (4.8) |
| redundancy | 6.7 (7.0) |
| **Refinement Statistics** | |
| *R*-factor[c] (*R*-free[d]) | 18.3 (24.6) |
| no. of atoms | |
| protein | 4180 |
| solvent | 250 |
| others | 154 |
| mean *B*-factor (Å$^2$) | 36.0 |
| rms from ideality | |
| bond length (Å) | 0.018 |
| angles (deg) | 1.954 |
| chiral (Å$^3$) | 0.151 |

[a] Values in brackets refer to the highest resolution shell. [b] $R_{merge} = (\Sigma|I - \langle I\rangle|)/\Sigma I$, where $I$ is the observed intensity and $\langle I\rangle$ is the average intensity obtained from multiple observations of symmetry related reflections after rejections. [c] *R*-factor = $\Sigma\,||F_o| - |F_c||/\Sigma|F_o|$, $F_o$ and $F_c$ are observed and calculated structure factors, respectively. [d] The *R*-free set uses 5% of randomly chosen reflections.

In the structure of the BChE phosphoserine adduct, the phosphorus atom of the phosphate adduct is at 1.8 Å from Ser198O$\gamma$. The oxygen $O_2$ of the phosphate adduct is negatively charged and forms a salt bridge with the catalytic histidine His438N$\varepsilon$2 (2.9 Å). The oxygen O$\delta$ is stabilized by H-bonding with atoms from residues forming the oxyanion hole, Gly116N (2.7 Å), Gly117N (2.6 Å), and Ala199N (2.7 Å). $O_3$ is oriented toward the acyl-binding pocket and interacts with water molecule w100 (3.3 Å) stabilized by H-bond interaction with the main chain oxygen of the Leu286 (3.1 Å). The choline-binding pocket is occupied by water molecules (w125 and w103) at equal distance of the Trp82 and the oxygen $O_2$ of CBDP adduct (approximately 4 Å). This crystal structure confirmed the formation of a phospho-serine adduct resulting from two consecutive postphosphorylation reactions of the ring opened CBDP adduct in the hBChE active site.

This is the first time that a phosphoserine has been observed as the final conjugate from the reaction of BChE with an OP. A phosphoserine adduct resulting from dealkylation of human AChE inhibited by the phosphoramidate mipafox was already reported.[59] Evidence for this adduct was based on mass spectrometry and immuno-precipitation of trypsin digests with

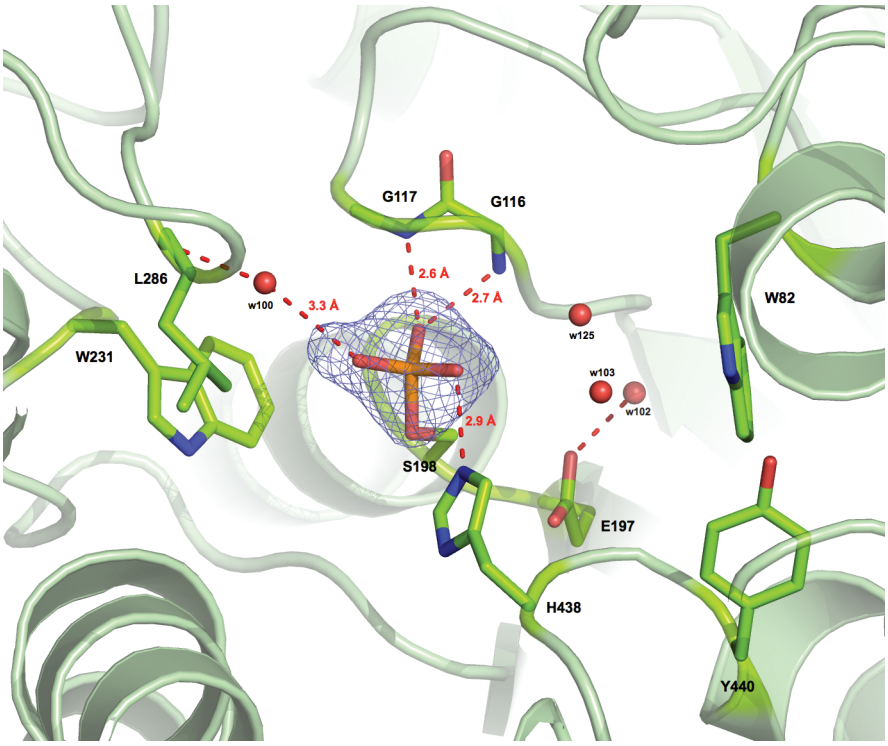


**Figure 3.** Active site view of the phospho-serine-hBChE conjugate. Key residues and the OP adduct are displayed as sticks, with carbon atoms in green, oxygen atoms in red, nitrogen atoms in blue, and the phosphorus atom in orange. Hydrogen bonds are represented as red dashed lines. The $F_o - F_c$ omit map is contoured at $3\sigma$.

monoclonal antibodies to phosphoserine. Our previous studies with phosphoramidates (tabun and tabun derivatives) showed that for phosphoramidates, displacement of isopropyl amine groups results from acid hydrolysis during sample preparation for mass spectrometry.[23] Thus, although mass spectrometry alone does not provide absolute evidence for nonartifactual formation of phosphoserine adduct, immuno-precipitation of trypsin digests rules out possible artifactual acid-induced formation of this adduct. In our study, X-ray analysis of the CBDP-aged BChE adduct provides direct and 3D evidence that the phosphoserine adduct does not result from sample preparation but results from postphosphorylation chemical events. Interestingly, both CBDP-phosphorylated human BChE and mouse AChE (Carletti et al., in preparation) lead to phosphoserine adducts, while only mipafox-inhibited AChE leads to phosphoserine adduct. With BChE, the mipafox-aged adduct is a monoisopropylphosphoroamido adduct.[60]

**Concluding Remarks.** *Kinetics and Mechanism.* With $k_i$ values of $10^7-10^8$ $M^{-1}$ $min^{-1}$, CBDP is one of the most potent OP inhibitors yet found for BChE. Comparable reactivities are seen with cyclosarin ($3.8 \times 10^8$ $M^{-1}$ $min^{-1}$),[61] FP-biotin ($1.6 \times 10^8$ $M^{-1}$ $min^{-1}$),[62] diazoxon ($7.7 \times 10^7$ $M^{-1}$ $min^{-1}$),[62] and soman ($5.1 \times 10^7$ $M^{-1}$ $min^{-1}$).[63] Only chlorpyrifos-oxon ($1.7 \times 10^9$ $M^{-1}$ $min^{-1}$)[64] and MEPQ ($6.3 \times 10^8$ $M^{-1}$ $min^{-1}$)[63] are appreciably more reactive. Thus, BChE should be a sensitive marker of low level exposure to CBDP.

The ultimate product of the reaction of CBDP with BChE is a unique phosphopeptide not previously reported for the reaction of OP with BChE. This phosphopeptide is the result of two consecutive, postphosphorylation reactions (aging), starting from the CBDP ring-opened adduct (see Scheme 4). The first reaction involves the hydrolysis of the O−C bond in the P−O−C linkage between the phosphorus and the saligenin moiety, which is indicated by the observation that oxygen from the medium is not added to the phosphorus.

Fission of the O−C bond is characteristic of enzyme assisted aging for phosphylated BChE adducts.[54] Aging involves phosphorus ligands located in the pi-cation binding site (i.e., near Trp82 in hBChE and Trp87 in hAChE).[23,57,58]

This argues that the saligenin moiety probably occupied the choline-binding site in the initial ring-opened form of the CBDP adduct, suggesting in turn that the *o*-cresyl substituent occupied the acyl-binding pocket of hBChE.

On the basis of chemical analyses, Toia and Casida[52] proposed a similar dealkylation process for chymotrypsin and trypsin inhibited by saligenin cyclic phosphonates and phosphates. In addition to the release of saligenin from phosphorus into the medium, they proposed that a portion of the saligenin released from phosphorus was trapped by the active site histidine. No evidence for a similar trapping of the released saligenin was seen for either AChE or BChE adducts of CBDP.

The second reaction involves hydrolysis of the P−O bond between the phosphorus and the cresyl moiety. Cleavage of the P−O bond is indicated because oxygen from the solvent is added to the phosphorus during this reaction. Fission of the P−O bond is consistent with either a dissociative ($S_N1$) hydrolysis of phosphoesters or a nucleophilic ($S_N2$) hydrolysis.[65] An $S_N2$ was earlier suggested as one of two alternative mechanisms for aging of diethylphosphoryl-BChE,[66] but it was later discarded in favor of a dealkylation-based mechanism because no incorporation of $^{18}$O-water to phosphorus was found by mass spectrometry analysis. However, structural analysis of the aging of some

**Scheme 5. Proposed Reaction Mechanism of CBDP with Cholinesterases, Leading to the Phospho Serine Adduct**

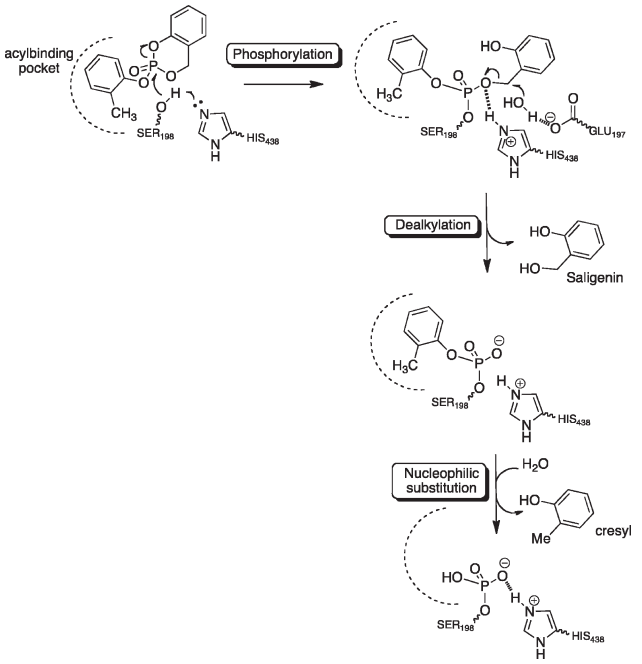


analogues of the nerve agent tabun suggested an $S_N2$ based mechanism.[67] An $S_N2$ mechanism requires that the nucleophile (in this case water) approach the phosphorus from the face of the tetrahedral phosphate structure that is opposite from the group to be displaced. This face is accessible to water after the departure of saligenin substituent in the previous step. The dissociative mechanism requires that the leaving group (in this case the cresyl) detach from the phosphorus and depart to make room for the replacing group (in this case water) to attach. At this point, the data do not allow one to discriminate between an $S_N1$ or $S_N2$ mechanism. The complete inhibition mechanism by CBDP up to the formation of the phosphoserine is summarized in Scheme 5.

*Aerotoxic Syndrome and Toxicity of CBDP.* Aerotoxic syndrome is speculated to be asociated with exposure to tri-*ortho*-cresylphosphate, but this association has not been proven. After exposure to TOCP, the CBDP generated *in vivo* can react with tissue enzymes such as liver carboxylesterase and neuropathy target esterase (NTE), and with blood bioscavengers such as albumin and BChE (note that CBDP does not react with paraoxonase 1, the naturally occurring plasma phosphotriesterase; Masson et al., unpublished results). Detection of low dose exposure to CBDP is critical to ongoing investigations into aerotoxic syndrome. It is suspected that aerotoxic syndrome is caused by internalization of an engine oil additive (TOCP) that gives rise to CBDP *in vivo*. Epidemiological studies into aerotoxic syndrome are currently ham-strung by the absence of a direct, quantitative, *in vivo* measure for exposure to TOCP. Phosphorylated BChE, as a biomarker for TOCP/CBDP exposure, is an appealing candidate to fill this vacancy. The unique nature of this adduct will reduce the incidence of false positive identifications when screening populations.

Use of a phosphorylated protein as a biomarker for aerotoxic syndrome entails the potential for conflict with other phosphorylated proteins, of which there are many. However, ongoing work in our laboratory has demonstrated that phosphorylated BChE (partially purified from serum by anion exchange and procainamide affinity chromatography to give 15−30% pure BChE) yields a phosphorylated peptic peptide that is specific for the active-site sequence of BChE (manuscript submitted for publication). This peptide is readily detectible by MALDI TOF TOF mass spectrometry, and its identity has been confirmed by mass spectral fragmentation analysis. It provides a unique biomarker for the reaction of CBDP with BChE. We have used this peptide marker to address the question of whether there is sufficient cresyl phosphate in aircraft cabin air to cause detectible adduct formation in passengers. This question is at the heart of the debate between expert bodies on the extent of potential exposure to and the toxic potency of cresyl phosphate. To date, we have found that about half of the passengers tested carried evidence for exposure to TOCP despite the fact that none of the subjects was exposed to high levels of engine gases (i.e., a fume event) and that none reported toxic symptoms. Since only a subgroup of passengers experience aerotoxic symptoms after a fume event, it can be concluded that some individuals are hyper-sensitive to the toxicants in the engine fumes. Evidence for TOCP toxicant in a substantial fraction of passengers exposed to normal cabin air provides ample reason to suspect that the level of TOCP in aircraft air (however small it may be) is a potential threat to sensitive passengers exposed to fume events.

The high reactivity of BChE toward CBDP also argues that it should play an important role in natural defenses against toxicity from low dose exposure to TOCP by scavenging CBDP from the bloodstream. Variation in the reactivity of BChE or cytochrome P450 enzymes due to naturally occurring mutations or diseases[68] may contribute to the explanation for why only selected passengers and aircraft workers fall victim to aerotoxic syndrome.

The initial neurological symptoms associated with aerotoxic syndrome are similar to symptoms associated with organophosphate inhibition of AChE. Though AChE is less reactive than BChE with CBDP, the reactivity of AChE with CBDP is similar to the reactivity with potent OPs such as paraoxon ($k_i \approx 10^6\ M^{-1}\ min^{-1}$) or (−)-tabun ($k_i \approx 2.7 \times 10^7\ M^{-1}\ min^{-1}$),[69] suggesting that human exposure to high doses of CBDP should cause the typical symptomatology of OP poisoning. Neurotoxicity that persists for years suggests targets in addition to AChE.

*Origin of Aerotoxic Syndrome and Organophosphate-Induced Delayed Neuropathy.* Aerotoxic syndrome is assumed to be caused by exposure to low doses of TOCP.[2] Organophosphate-induced delayed neuropathy (OPIDN) is known to be caused by exposure to high doses of TOCP.[10,70−72] High doses of TOCP result in paralysis of the legs, whereas low doses do not cause delayed paralysis. The processes leading to OPIDN and the long-term symptoms of aerotoxic syndrome are probably related. A long-standing candidate for the target of CBDP responsible for the induction of OPIDN is neuropathy target esterase (NTE), a membrane bound phospholipase that catalyzes the deacylation of membrane-phophatidylcholine to soluble glycerophosphocholine and fatty acids.[73−75] Low doses of TOCP inhibit neuropathy target esterase, though they do not cause neuropathy. A role for NTE in delayed neuropathy is supported by the finding that human genetic variants of NTE have motor neuron disease characterized by spastic paraplegia and distal muscle wasting.[76,77] Proposed noncholinergic mechanisms of OP neurotoxicity include activation of glutamatergic neurons and oxidative damage from reactive oxygen species and from peroxynitrite radicals.[78] The recent discovery that OP can covalently modify amino acid residues other than the traditionally accepted active site serines of serine esterases/proteases has fueled interest in nontraditional targets for OP. The covalent modification of tyrosine residues by

OP on nonenzymatic proteins such as serum albumin and tubulin, both *in vitro*[79] and *in vivo*,[80] and with lysine residues[81] opens the possibility for direct alteration of nonenzymatic, structural, and connective proteins in the neuron that could lead to degradation of function and the slow development of the long-term neurological symptoms associated with aerotoxic syndrome and organophosphate-induced delayed neuropathy.

## AUTHOR INFORMATION

### Corresponding Author

*E-mail: pmasson@unmc.edu.

### Funding Sources

This work was supported by U.S. Army Medical Research and Materiel Command [W81XWH-07-20034 to O.L.]; National Institutes of Health [U01 NS058056 to O.L. and P30CA36727 to Eppley Cancer Center]. Mass spectra were obtained with the support of the Mass Spectrometry and Proteomics core facility at the University of Nebraska Medical Center. We are grateful to the ESRF for beam-time under long-term projects MX498, MX609, and MX722 (IBS BAG) and MX551 and MX 666 (radiation-damage BAG), and the ESRF staff for providing efficient help during data collection. Financial support by the CEA, the CNRS, and the UJF is acknowledged, as well as a grant to M.W. and F.N. from the Agence Nationale de la Recherche (ANR; project number ANR-09-BLAN-0192-04) and to M.W. from the DGA (project number DGA-REI 2009-34-0023).

## ACKNOWLEDGMENT

We thank Dr. D. Lenz (USAMRICD, Aberdeen PG, MD, USA) for the gift of CBDP and Dr. D. Genkin (Pharmsynthez, Saint Petersburg, Russia) for the gift of HI-6 dichloride.

## ABBREVIATIONS

AChE, acetylcholinesterase (EC 3.1.1.7); ATC, acetylthiocholine; BChE, butyrylcholinesterase (EC. 3.1.1.8); BSA, bovine serum albumin; BTC, butyrylthiocholine; CBDP, 2-(*o*-cresyl)-4*H*-1,3,2-benzodioxaphosphoran-2-one; CSP, cresyl saligenin phosphate; ChE, cholinesterase; CHCA, alpha-cyano-4-hydroxycinnamic acid; CHO, Chinese hamster ovary; DMSO, dimethylsulfoxide; HI-6, 1-[[[4-(aminocarbonyl) pyridinio] methoxy] methyl]-2-[(hydroxyimino)methyl] pyridinium dichloride monohydrate; hAChE, human AChE; hBChE, human BChE; MALDI-TOF, matrix-assisted laser desorption/ionization-time-of-flight; NTE, neuropathy target esterase; OP, organophosphorus compound; OPIDN, organophosphate-induced delayed neuropathy; 2-PAM, pralidoxime methiodide, *N*-methyl-pyridin-1-ium 2-aldoxime methiodide; TCP, tricresyl phosphate; TOCP, triortho-cresyl phosphate.

## REFERENCES

(1) Schopfer, L. M., Furlong, C. E., and Lockridge, O. (2010) Development of diagnostics in the search for an explanation of aerotoxic syndrome. *Anal. Biochem. 404*, 64–74.

(2) Brown, M. A., and Brix, K. A. (1998) Review of health consequences from high-, intermediate- and low-level exposure to organophosphorus nerve agents. *J. Appl. Toxicol. 18*, 393–408.

(3) Kidd, J. G., and Langworthy, O. R. (1933) Jake paralysis: paralysis following the ingestion of Jamaica ginger extract adulterated with tri-ortho-cresyl phosphate. *Bull. Johns Hopkins Hosp. 52*, 39–65.

(4) Smith, H. V., and Spalding, J. M. K. (1959) Outbreak of paralysis in Morocco due to ortho-cresyl phosphate poisoning. *Lancet* 1019–1021.

(5) Casida, J. E., Eto, M., and Baron, R. L. (1961) Biological activity of a tri-o-cresyl phosphate metabolite. *Nature 191*, 1396–1397.

(6) Eto, M., Casida, J. E., and Eto, T. (1962) Hydroxylation and cyclization reactions envolved in the metabolism of tri-o-cresyl phosphate. *Biochem. Pharmacol. 11*, 337–352.

(7) Eto, M., Oshima, Y., and Casida, J. E. (1967) Plasma albumin as a catalyst in cyclization of diaryl o-(a-hydroxy)tolyl phosphate. *Biochem. Pharmacol. 16*, 295–308.

(8) De Nola, G., Kibby, J., and Mazurek, W. (2008) Determination of *ortho*-cresyl phosphate isomers of tricresyl phosphate used in aircraft turbina engine oils by gas chromatography and mass spectrometry. *J. Chromatogr., A 1200*, 211–216.

(9) Winder, C., and Balouet, J. C. (2002) The toxicity of commercial jet oils. *Environ. Res. 89*, 146–164.

(10) Winder, C. (2006) Hazardous chemicals on jet aircraft: case study- jet engine oils and aerotoxic syndrome. *Curr. Top. Toxicol. 3*, 65–88.

(11) Van Netten, C., and Leung, V. (2001) Hydraulic fluids and jet engine oil: pyrolysis and aircraft air quality. *Arch. Environ. Health 56*, 181–186.

(12) Clement, J. G. (1984) Importance of aliesterase as a detoxification mechanism for soman (pinacolylmethylphosphonofluoridate) in mice. *Biochem. Pharmacol. 33*, 3807–3811.

(13) Maxwell, D. M., Brecht, K. M., and O'Neill, B. L. (1987) The effect of carboxylesterase inhibition on interspecies differences in soman toxicity. *Toxicol. Lett. 39*, 35–42.

(14) Maxwell, D. M. (1992) The specificity of carboxylesterase protection against the toxicity of organophosphorus compounds. *Toxicol. Appl. Pharmacol. 114*, 306–312.

(15) Glynn, P. (1999) Neuropathy target esterase. *Biochem. J. 344*, 625–663.

(16) Boskovic, B. (1979) The influence of 2-/o-cresyl/-4 H-1:3:2-benzodioxa-phosphorin-2-oxide (CBDP) on organophosphate poisoning and its therapy. *Arch. Toxicol. 42*, 207–216.

(17) Cohen, O., Kronman, C., Raveh, L., Mazor, O., Ordentlich, A., and Shafferman, A. (2006) Comparison of polyethylene glycol-conjugated recombinant human acetylcholinesterase and serum human butyrylcholinesterase as bioscavengers of organophosphate compounds. *Mol. Pharmacol. 70*, 1121–1131.

(18) Eto, M. (1983) Development of insecticidal cyclic phosphoryl compounds through chemical and biochemical approaches. *J. Environ. Sci. Health B18*, 119–145.

(19) Shiotsuki, T., and Eto, M. (1987) Effect of salioxon and fenitroxon on altered acetylcholinesterase of organophosphate-resistant housefly. *J. Pestic. Sci. 12*, 17–21.

(20) Hirashima, A., Ishaaya, I., Ueno, R., Ichiyama, Y., Wu, S.-Y., and Eto, M. (1989) Biological activity of optically active salithion and salioxon. *Agric. Biol. Chem. 53*, 175–178.

(21) Lockridge, O., Schopfer, L. M., Winger, G., and Woods, G. H. (2005) Large scale purification of butyrylcholinesterase from human plasma suitable for injection into monkeys; a potential new therapeutic for protection against cocaine and nerve agent tocicity.*J. Med. Chem. Biol. Radiol. Def. 3*, on line.

(22) Nachon, F., Nicolet, Y., Viguié, N., Masson, P., Fontecilla-Camps, J. C., and Lockridge, O. (2002) Engineering of a monomeric and low-glycosylated form of human butyrylcholinesterase: expression, purification, characterization and crystallization. *Eur. J. Biochem. 269*, 630–637.

(23) Carletti, E., Li, H., Li, B., Ekström, F., Loiodice, M., Gillon, M., Froment, M. T., Lockridge, O., Schopfer, L. M., Masson, P., and Nachon, F. (2008) Aging of cholinesterases phosphylated by tabun proceeds through O-dealkylation. *J. Am. Chem. Soc. 130*, 16011–16020.

(24) Ellman, G. L., Courtney, K. D., Andres, V., and Featherstone, R. M. (1961) A new and rapid colorimetric determination of acetylcholinesterase activity. *Biochem. Pharmacol. 7*, 88–95.

(25) Whittaker, M. (1968) The pseudocholinesterase variants. Differentiation with n-butyl alcohol: recognition of new phenotypes. *Acta Genet. Stat. Med. 18*, 325–334.

(26) Ferro, A., and Masson, P. (1987) Kinetic evidence for thermally induced conformational change of butyrylcholinesterase. *Biochim. Biophys. Acta 916*, 193–199.

(27) Grunwald, J., Marcus, D., Papier, Y., Raveh, L., Pittel, Z., and Ashani, Y. (1997) Large-scale purification and long-term stability of human butyrylcholinesterase: a potential bioscavenger drug. *J. Biochem. Biophys. Methods 34*, 123–135.

(28) Ordentlich, A., Barak, D., Kronman, C., Ariel, N., Segall, Y., Velan, B., and Shafferman, A. (1995) Contribution of aromatic moieties of tyrosine 133 and of the anionic subsite tryptophan 86 to catalytic efficiency and allosteric modulation of acetylcholinesterase. *J. Biol. Chem. 270*, 2082–2091.

(29) Kitz, R., and Wilson, I. B. (1962) Esters of methanesulfonic acid as irreversible inhibitors of acetylcholinesterase. *J. Biol. Chem. 237*, 3245–3249.

(30) Aldridge, W. N., and Reiner, E. (1969) Acetylcholinesterase: two types of inhibition by an organophosphorus compound: one the formation of phosphorylated enzyme and the other analogous to the inhibition by substrate. *Biochem. J. 115*, 147–162.

(31) Masson, P., Fortier, P. L., Albaret, C., Froment, M.-T., Bartels, C. F., and Lockridge, O. (1997) Aging of di-isopropyl-phosphorylated human butyrylcholinesterase. *Biochem. J. 327*, 601–607.

(32) McCarthy, A. A., Brockhauser, S., Nurizzo, D., Theveneau, P., Mairs, T., Spruce, D., Guijarro, M., Lesourd, M., Ravelli, R. B., and McSweeney, S. (2009) A decade of user operation on the macromolecular crystallography MAD beamline ID 14−4 at the ESRF. *J. Synchrotron Radiat. 16*, 803–812.

(33) Yao, X., Freas, A., Ramirez, J., Demirev, P. A., and Fenselau, C. (2001) Proteolytic 18O labeling for comparative proteomics: model studies with two serotypes of adenovirus. *Anal. Chem. 73*, 2836–2842.

(34) Kabsch, W. (2010) XDS. *Acta Crystallogr., Sect. D 66*, 125–132.

(35) Collaborative-Computational-Project4. (1994) The CCP4 suite: programs for protein crystallography. *Acta Crystallogr., Sect. D 50* (Pt. 5), 760−763.

(36) Vagin, A., and Teplyakov, A. (1997) MOLREP: an automated program for molecular replacement. *J. Appl. Crystallogr. 30*, 1022–1025.

(37) Murshudov, G. N., Vagin, A. A., and Dodson, E. J. (1997) Refinement of macromolecular structures by the maximum-likelihood method. *Acta Crystallogr., Sect. D 53*, 240–255.

(38) Emsley, P., and Cowtan, K. (2004) Coot: model-building tools for molecular graphics. *Acta Crystallogr., Sect. D 60*, 2126–2132.

(39) Adams, P. D., Grosse-Kunstleve, R. W., Hung, L. W., Ioerger, T. R., McCoy, A. J., Moriarty, N. W., Read, R. J., Sacchettini, J. C., Sauter, N. K., and Terwilliger, T. C. (2002) PHENIX: building new software for automated crystallographic structure determination. *Acta Crystallogr., Sect. D 58*, 1948–1954.

(40) Painter, J., and Merritt, E. A. (2006) Optimal description of a protein structure in terms of multiple groups undergoing TLS motion. *Acta Crystallogr., Sect. D 62*, 439–450.

(41) Estevez, J., and Vilanova, E. (2009) Model equations for the kinetics of covalent irreversible enzyme inhibition and spontaneous reactivation: esterase and organophosphorus compounds. *Crit. Rev. Toxicol. 39*, 427–448.

(42) Estevez, J., Barril, J., and Vilanova, E. (2010) Inhibition with spontaneous reactivation and the "ongoing inhibition" effect of esterases by biotinylated organophosphorus compounds: S9B as a model. *Chem.-Biol. Interact. 187*, 397–402.

(43) Estevez, J., Garcia-Perez, A., Barril, J., and Vilanova, E. (2011) Inhibition with spontaneous reactivation of carboxyl esterases by organophosphorus compounds: paraoxon as a model. *Chem. Res. Toxicol. 24*, 135–143.

(44) Masson, P., Schopfer, L. M., Froment, M. T., Debouzy, J. C., Nachon, F., Gillon, E., Lockridge, O., Hrabovska, A., and Goldstein, B. N. (2005) Hysteresis of butyrylcholinesterase in the approach to steady-state kinetics. *Chem.-Biol. Interact. 157−158*, 143–152.

(45) Shenouda, J., Green, P., and Sultatos, L. (2009) An evaluation of the inhibition of human butyrylcholinesterase and acetylcholinesterase by the organophosphate chloryrifos oxon. *Toxicol. Appl. Pharmacol. 241*, 135–142.

(46) Loudwig, S., Nicolet, Y., Masson, P., Fontecilla-Camp, J. C., Bon, S., Nachon, F., and Goeldner, M. (2003) Photoreversible inhibition of cholinesterases: catalytic serine-labeled caged butyrylcholinesterase. *ChemBioChem. 4*, 762–767.

(47) Pietsch, M., Christian, L., Inhester, T., Petzold, S., and Gutschow, M. (2009) Kinetics of inhibition of acetylcholinesterase in the presence of acetonitrile. *FEBS J. 276*, 2292–2307.

(48) Eto, M. (1981) Studies on biologically active organophosphorus compounds. *J. Pestic. Sci. 6*, 365–375.

(49) Eto, M., Fukuhara, N., Kuwano, E., and Koyama, H. (1981) Molecular structure and conformation of 4H-1,3,2-benzodioxaphosphorins, including the insecticide salithion. *Agric. Biol. Chem. 45*, 915–923.

(50) Eto, M. (1997) Functions of phosphorus moiety in agrochemical molecules. *Biosci. Biotechnol., Biochem. 61*, 1–11.

(51) Worek, F., Thiermann, H., Szinicz, L., and Eyer, P. (2004) Kinetic analysis of interactions between human acetylcholinesterase, structurally different organophosphorus compounds and oximes. *Biochem. Pharmacol. 68*, 2237–2248.

(52) Toia, R. F., and Casida, J. E. (1979) Phosphorylation, "aging", and possible alkylation reactions of saligenin cyclic phosphorus esters with a-chymotrypsin. *Biochem. Pharmacol. 28*, 211–216.

(53) Li, B., Nachon, F., Froment, M.-T., Verdier, L., Debouzy, J.-C., Brasme, B., Gillon, E., Schopfer, L. M., Lockridge, O., and Masson, P. (2008) Binding and hydrolysis of soman by human serum albumin. *Chem. Res. Toxicol. 21*, 421–431.

(54) Li, H., Schopfer, L. M., Nachon, F., Froment, M.-T., Masson, P., and Lockridge, O. (2007) Aging pathways for organophosphate-inhibited human butyrylcholinesterase. *Toxicol. Sci. 100*, 136–145.

(55) Shafferman, A., Ordentlich, A., Barak, D., Stein, D., Ariel, N., and Velan, B. (1996) Aging of phosphylated human acetylcholinesterase: catalytic processes mediated by aromatic and polar residues of the active centre. *Biochem. J. 318*, 833–840.

(56) Viragh, C., Akhmetshin, R., Kovach, I. M., and Broomfield, C. (1997) Unique push-pull mechanism of dealkylation in soman-inhibited cholinesterases. *Biochemistry 36*, 8243–8252.

(57) Sanson, B., Nachon, F., Colletier, J. P., Froment, M.-T., Toker, L., Greenblatt, H. M., Sussman, J. L., Ashani, Y., Masson, P., Silman, I., and Weik, M. (2009) Crystallographic snapshots of nonaged and aged conjugates of soman with acetylcholinesterase, and a ternary complex of the aged conjugate with pralidoxime. *J. Med. Chem. 52*, 7593–7603.

(58) Kovach, I. M. (2004) Stereochemistry and secondary reactions in the irreversible inhibition of serine hydrolases by organophosphorus compounds. *J. Phys. Org. Chem. 17*, 602–604.

(59) Kropp, T. J., and Richardson, R. J. (2006) Aging of mipafox-inhibited human acetylcholinesterase proceeds by displacement of both isopropylamine groups to yield a phosphate adduct. *Chem. Res. Toxicol. 19*, 334–339.

(60) Kropp, T. J., and Richardson, R. J. (2007) mechanism of aging of mipafox-inhibited butyrylcholinesterase. *Chem. Res. Toxicol. 20*, 504–510.

(61) Worek, F., Eyer, P., and Szinicz, L. (1998) Inhibition, reactivation and aging kinetics of cyclohexylmethylphosphonofluoridate- inhibited human cholinesterases. *Arch. Toxicol. 72*, 580–587.

(62) Schopfer, L. M., Voelker, T., Bartels, C. F., Thompson, C. M., and Lockridge, O. (2005) Reaction kinetics of biotinylated organophosphorus toxicant, FP-biotin, with human acetylcholinesterase and human butyrylcholinesterase. *Chem. Res. Toxicol. 18*, 747–754.

(63) Raveh, L., Grunwald, J., Marcus, D., Papier, Y., Cohen, E., and Ashani, Y. (1993) Human butyrylcholinesterase as a general prophylactic antidotes for nerve agent toxicity. In vitro and in vivo quantitative characterization. *Biochem. Pharmacol. 45*, 2465–2474.

(64) Amitai, G., Moorad, D., Adani, R., and Doctor, B. P. (1998) Inhibition of acetylcholinesterase and butyrylcholinesterase by chlorpyrifos-oxon. *Biochem. Pharmacol. 56*, 293–299.

(65) Benkovic, S. J., and Schray, K. J. (1973) Chemical Basis of Biological Phosphoryl Transfer, in *The Enzymes* (Boyer, P. D. Ed.) 3rd ed., Vol. VIII, pp 2010−2238, Academic Press, New York.

(66) Nachon, F., Asojo, O. A., Borgstahl, G. E. O., Masson, P., and Lockridge, O. (2005) Role of water in aging of human butyrycholinesterase inhibited by echothiophate: the crystal stucture suggests two alternative mechanisms of aging. *Biochemistry 44*, 1154–1162.

(67) Nachon, F., Carletti, E., Worek, F., and Masson, P. (2010) Aging mechanism of butyrylcholinesterase inhibited by an N-methyl analogue of tabun: implications of the trigonal-bipyramidal transition state rearrangement for the phosphylation or reactivation of cholinesterases. *Chem.-Biol. Interact. 187*, 44–48.

(68) Whittaker, M. (1980) Plasma cholinesterase variants and the anaesthetist. *Anaesthesia 35*, 174–197.

(69) Tenberken, O., Thiermann, H., Worek, F., and Reiter, G. (2010) Chromatographic preparation and kinetic analysis of interactions between tabun enantiomers and acetylcholinesterase. *Toxicol. Lett. 195*, 142–146.

(70) Cavanagh, J. B. (1954) The toxic effect of triortho-cresyl phosphate on the nervous system; an experimental study in hens. *J. Neurol. Neurosurg. Psychiatr. 17*, 163–172.

(71) Abou-Donia, M. B. (1981) Organophosphorus ester-induced delayed neurotoxicity. *Annu. Rev. Pharmacol. Toxicol. 21*, 511–548.

(72) Lotti, M., and Moretto, A. (1999) Promotion of organophosphate induced delayed polyneuropathy by certain esterase inhibitors. *Chem.-Biol. Interact. 119−120*, 519–524.

(73) Kropp, T. J., Glynn, P., and Richardson, R. J. (2004) The mipafox-inhibited catalytic domain of human neuropathy target esterase ages by reversible proton loss. *Biochemistry 43*, 3716–3722.

(74) Glynn, P. (2006) A mechanism for organophosphate-induced delayed neuropathy. *Toxicol. Lett. 162*, 94–97.

(75) Wu, Y.-J., and Chang, P.-A. (2010) Molecular Toxicology of Neuropathy Target Esterase, in *Anticholinesterase Pesticides: Metabolism, Neurotoxicity, and Epidemiology* (Satoh, T. and Gupta, R. C., Eds.) pp 109−120. John Wiley & Sons, New York.

(76) Read, D. J., Li., Y., Chao, M. V., Cavanagh, J. B., and Glynn, P. (2010) Organophosphates induce distal axonal damage, but not brain oedema, by inactivating neuropathy target esterase. *Toxicol. Appl. Pharmacol. 245*, 108–115.

(77) Rainier, S., Bui, M., Mark, E., Thomas, D., Tokarz., D., Ming, L., Delaney, C., Richardson, R. J., Albers, J. W., Matsunami, N., Stevens, J., Coon, H., Leppert, M., and Fink, J. K. (2008) Neuropathy target esterase gene mutations cause motor neuron disease. *Am. J. Hum. Genet. 82*, 780–785.

(78) Zaja-Milatovic, S., Gupta, R. C., Aschner, M., and Milatovic, D. (2009) Protection of DFP-induced oxidative damage and neurodegeneration by antioxidants and NMDA receptor antagonist. *Toxicol. Appl. Pharmacol. 240*, 124–131.

(79) Schopfer, L. M., Grigoryan, H., Li, B., Nachon, F., Masson, P., and Lockridge, O. (2010) Mass spectral characterization of organophosphate-labeled, tyrosine-containing peptides: characteristic mass fragments and a new binding motif for organophosphates. *J. Chromatogr. B 878*, 1297–1311.

(80) Li, B., Ricordel, I., Schopfer, L. M., Baud, F., Megarbane, B., Nachon, F., Masson, P., and Lockridge, O. (2010) Detection of adduct on tyrosine 411 of albumin in humans poisoned by dichlorvos. *Toxicol. Sci. 116*, 23–31.

(81) Lockridge, O., and Schopfer, L. M. (2010) Review of tyrosine and lysine as new motifs for organophosphate binding to proteins that have no active site serine. *Chem.-Biol. Interact. 187*, 344–348.

# Inhibition Pathways of the Potent Organophosphate CBDP with Cholinesterases Revealed by X‑ray Crystallographic Snapshots and Mass Spectrometry

E. Carletti, J-P. Colletier, L.M. Schopfer, G. Santoni, P. Masson, O. Lockridge, **F. Nachon***, M. Weik*

Chemical Research in Toxicology 26 (2013) 280-289

Chemical Research in Toxicology

Article

pubs.acs.org/crt

# Inhibition Pathways of the Potent Organophosphate CBDP with Cholinesterases Revealed by X-ray Crystallographic Snapshots and Mass Spectrometry

Eugénie Carletti,[†,‡,§,∥] Jacques-Philippe Colletier,[†,‡,§] Lawrence M. Schopfer,[⊥] Gianluca Santoni,[†,‡,§,∥] Patrick Masson,[†,‡,§,∥,⊥] Oksana Lockridge,[⊥] Florian Nachon,*[,∥] and Martin Weik*[,†,‡,§,#]

[†]Institut de Biologie Structurale J.P. Ebel, Commissariat à l'Energie Atomique, 41, rue Jules Horowitz, F-38027 Grenoble, France

[‡]CNRS, UMR5075, F-38027 Grenoble, France

[§]Université Joseph Fourier, F-38000 Grenoble, France

[∥]Département de Toxicologie, Institut de Recherche Biomédicale des Armées, 24 avenue des Marquis du Grésivaudan, 38702 La Tronche, France

[⊥]Eppley Institute, University of Nebraska Medical Center, Omaha, Nebraska 68198-5950, United States

[#]ESRF, 6 rue Jules Horowitz, BP 220, 38043 Grenoble Cedex, France

Supporting Information

**ABSTRACT:** Tri-*o*-cresyl-phosphate (TOCP) is a common additive in jet engine lubricants and hydraulic fluids suspected to have a role in aerotoxic syndrome in humans. TOCP is metabolized to cresyl saligenin phosphate (CBDP), a potent irreversible inhibitor of butyrylcholinesterase (BChE), a natural bioscavenger present in the bloodstream, and acetylcholinesterase (AChE), the off-switch at cholinergic synapses. Mechanistic details of cholinesterase (ChE) inhibition have, however, remained elusive. Also, the inhibition of AChE by CBDP is unexpected, from a structural standpoint, i.e., considering the narrowness of AChE active site and the bulkiness of CBDP. In the following, we report on kinetic X-ray crystallography experiments that provided 2.7−3.3 Å snapshots of the reaction of CBDP with mouse AChE and human BChE. The series of crystallographic snapshots reveals that AChE and BChE react with the opposite enantiomers and that an induced-fit rearrangement of Phe297 enlarges the active site of AChE upon CBDP binding. Mass spectrometry analysis of aging in either $H_2{}^{16}O$ or $H_2{}^{18}O$ furthermore allowed us to identify the inhibition steps, in which water molecules are involved, thus providing insights into the mechanistic details of inhibition. X-ray crystallography and mass spectrometry show the formation of an aged end product formed in both AChE and BChE that cannot be reactivated by current oxime-based therapeutics. Our study thus shows that only prophylactic and symptomatic treatments are viable to counter the inhibition of AChE and BChE by CBDP.

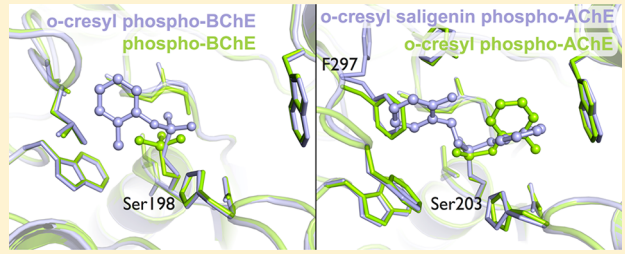


## INTRODUCTION

Tri-*o*-cresyl phosphate (TOCP), a toxic isomer of tricresyl phosphate (TCP), is suspected to play an important role in aerotoxic syndrome. TCP is added to commercial jet engine lubricants for its antiwear and flame-retardant properties.[1−3] When oil seals in jet-airplanes leak, the cabin bleed-air becomes contaminated with TOCP. TOCP is inhaled and metabolized by liver microsomal cytochrome P450 and serum albumin into 2-(*o*-cresyl)-4*H*-1,3,2-benzodioxaphosphoran-2-one (CBDP), also called cresyl saligenin phosphate.[4−6]

CBDP is a bicyclic organophosphorus compound (OP), which irreversibly inhibits both human acetylcholinesterase (hAChE; EC 3.1.1.7) and butyrylcholinesterase (hBChE; EC 3.1.1.8).[7] hAChE is the enzyme responsible for the termination of nerve-impulse transmission at cholinergic synapses, and as such, it is the primary target of chemically synthesized OPs. hBChE is a structurally and functionally homologous enzyme that is present in the bloodstream (50 nM, in humans) and acts as a stoichiometric bioscavenger of OPs.[8] Irreversible inhibition of hAChE and hBChE by OPs generally proceeds in two steps; phosphylation of the catalytic serine with concomitant release of a leaving group, followed by dealkylation of the OP-enzyme adduct, a process also called aging. It is noteworthy that medical countermeasures to reactivate cholinesterases are only efficient against nonaged enzymes:[9] aged ChEs can indeed no longer be reactivated by oximes used as antidotes against OP poisoning.

hAChE and hBChE differ mostly by the amino acid distribution in their active site gorges, the former containing more aromatic residues than the latter. In particular, the replacement of two phenylalanine residues in the acyl-binding

**Received:** November 9, 2012
**Published:** January 22, 2013

pocket of hAChE, by a leucine and a valine in BChE, results in an enlargement of the pocket, thereby allowing accommodation of bulkier substrates and inhibitors and expanding the substrate specificity of hBChE as compared to that of hAChE.[10] Accordingly, hAChE and hBChE have repeatedly been reported to preferentially react with different OP stereoisomers.[11]

The ensemble of neurological symptoms associated with aerotoxic syndrome includes memory impairment and uncontrollable shaking.[12,13] It has been shown that CBDP inhibits esterase enzymes, notably the neuropathy target esterase[14,15] but also hBChE and hAChE.[7,16−18] In addition, other serine esterases are likely inhibited by CBDP and tyrosine residues in several proteins have been shown to be reactive toward CBDP. Inhibition of such proteins may participate in the pathogenesis of aerotoxic syndrome.

We earlier investigated the inhibition mechanisms of hAChE and hBChE by CBDP using a combination of kinetic measurements, mass spectrometry, and X-ray crystallography.[7] As shown in Scheme 1, the inhibition of hBChE by CBDP occurs in three steps.

**Scheme 1. Reaction of CBDP with hBChE**

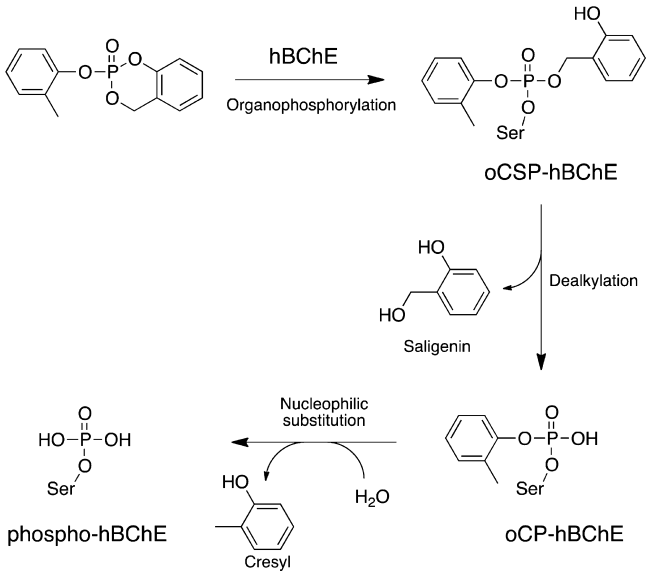


CBDP first forms a phosphorylserine conjugate of hBChE, with saligenin and *o*-cresyl as substituents (oCSP-hBChE). The first aging reaction corresponds to the release of the saligenin moiety, and results in the *o*-cresyl-phospho-BChE adduct (oCP-hBChE). A second aging reaction then occurs that allows the release of the *o*-cresyl moiety and yields phospho-hBChE, whose structure we reported already.[7] We also showed that the bimolecular rate constant of CBDP for hBChE is at least 10-fold higher than that for hAChE. CBDP is, in fact, one of the most potent BChE inhibitors reported to date ($1.5 \times 10^8$ $M^{-1}\cdot min^{-1}$), suggesting that hBChE efficiently scavenges CBDP in the bloodstream. The reactivity of CBDP toward hAChE is in the same range as that exhibited by paraoxon, tabun, or soman ($10^6$–$10^7$ $M^{-1}\cdot min^{-1}$). It remains unclear, however, if hAChE and hBChE inhibition by CBDP proceeds in the same fashion, and whether the same intermediate states form.

Here, we provide a detailed description of mouse (m) AChE and human (h) BChE inhibition by CBDP, based on crystallographic snapshots of inhibition intermediate states and on mass spectrometry analyses. We show that mAChE inhibition by CBDP occurs in two steps and involves a transient enlargement of the acyl-binding pocket to allow accommodation of the bulky CBDP adduct. The resulting *o*-cresyl-phospho-mAChE is a stable OP-aged adduct that does not evolve further. In contrast, the *o*-cresyl-phospho-hBChE adduct represents an unstable, strained conformer of hBChE that undergoes a second aging reaction yielding a phospho-serine-hBChE adduct. CBDP inhibition of mAChE and hBChE involves a different stereoisomer of CBDP, occurs through different pathways, and yields a different end-conjugate.

## EXPERIMENTAL PROCEDURES

**Caution:** *CBDP is a highly toxic organophosphorus compound. Handling requires suitable personal protection, training, and facilities. These requirements are the same as those for other poisonous organophosphorus compounds.*

**Chemicals.** CBDP was synthesized by Starks Associates Buffalo, NY, and provided by Dr. D. Lenz (USAMRICD, Aberdeen PG, MD) and Dr. Wolf Dettbarn (Vanderbilt University, Nashville, TN). A 0.1 M stock solution of CBDP in acetonitrile was stored at −20 °C and diluted in water on the day of the mass spectrometry or crystallography experiment. Pepsin (from porcine stomach mucosa) was purchased from Sigma (a member of the Sigma-Aldrich group, St. Louis, MO). $^{18}$O-Water (99% $^{18}$O) was purchased from ISOTEC (a member of the Sigma-Aldrich group). Chemical structures and reaction schemes were illustrated using the program ChemDraw (CambridgeSoft).

**Production of Recombinant ChEs.** Recombinant hBChE (L530stop) is a truncated monomer containing residues 1 to 529 but missing 45 C-terminal residues that include the tetramerization domain. Four of the nine carbohydrate attachment sites were deleted by site-directed mutagenesis. Mutagenesis of N486 resulted in glycosylation of N485, an asparagine that is not glycosylated in native hBChE so that the recombinant hBChE contains six N-linked glycans.[19] The recombinant hBChE gene was expressed in Chinese hamster ovary (CHO) cells, secreted into serum-free culture medium, and purified by affinity and ion-exchange chromatographies as described previously.[19]

The synthetic gene (GeneArt) coding for a truncated mutant of mAChE (L544Stop) was inserted into a pGS vector carrying the glutamine synthetase gene marker and expressed in Chinese hamster ovary (CHO)-K1 cells. The cells were maintained in serum-free Ultraculture Medium (BioWhittaker, Walkersville, MD) and transfected using DNA−calcium phosphate coprecipitation. Transfected clones were selected by incubation in media containing methionine sulfoximine. The mouse enzyme, secreted into the culture medium, was purified by affinity chromatography and ion-exchange chromatography using a protocol identical to that described for the recombinant human enzyme.[20] The enzyme was concentrated to 14 mg/mL using a Centricon-30 ultrafiltration microconcentrator (30000 MW cutoff, Amicon, Millipore, Billerica, MA) in 10 mM MES buffer at pH 6.5.

**Crystallization of hBChE and Generation of CBDP-hBChE Conjugates.** hBChE was concentrated to 9 mg/mL and crystallized using the hanging drop vapor-diffusion method as described previously.[19] Two different conjugates were obtained by soaking native crystals for either 2 min or 12 h at 4 °C in a mother liquor solution (0.1 M MES at pH 6.5 and 2.1 M ammonium sulfate) containing 1 mM CBDP. Crystals were then soaked for a few seconds in a cryoprotectant solution (0.1 M MES buffer at pH 6.5, 2.3 M ammonium sulfate, and 20% glycerol) before being flash-cooled in liquid nitrogen for data collection.

**Crystallization of mAChE and Generation of CBDP-mAChE Conjugates.** mAChE, concentrated to 14 mg/mL, was crystallized using the hanging drop vapor-diffusion method as described previously.[21] Two different conjugates were obtained by soaking native mAChE crystals for either 30 min or 12 h at 4 °C in a mother


dx.doi.org/10.1021/tx3004505 | *Chem. Res. Toxicol.* 2013, 26, 280−289

liquor solution (0.1 M Tris HCl buffer at pH 7.4 and 1.6 M ammonium sulfate) containing 1 mM CBDP. Crystals were soaked for a few seconds in a cryoprotective solution (0.1 M Tris HCl buffer at pH 7.4, 1.8 M ammonium sulfate, and 18% glycerol) and flash-cooled in liquid nitrogen.

**X-ray Data Collection and Processing, Structure Determination, and Refinement.** Diffraction data were collected on the ID14-eh4 beamline[22] at the European Synchrotron Radiation Facility (ESRF, Grenoble, France) with an ADSC Quantum Q315r detector. The beam was characterized by a wavelength of 0.9765 Å, and the crystals were held at 100 K during data collection. All data sets were processed with XDS,[23] intensities of integrated reflections were scaled using XSCALE, and structure factors were calculated using XDSCONV. The structures were solved by molecular replacement with the program MOLREP[24] of the CCP4 suite[25] using the recombinant hBChE structure (PDB entry 1P0I) and mAChE (PDB entry 4A16) as starting models. For all diffraction data sets, the initial models were refined as follows: a rigid-body refinement, carried out with REFMAC5,[26] was followed by iterative cycles of model building with Coot[27] and restrained TLS refinement was carried out with Phenix.[28] The bound ligands and their descriptions were built using the Dundee PRODRG2.5 server including energy minimization using GROMOS96.1 force field calculations. Successive alternation of refinement cycles and manual model building were performed until $R_{cryst}$ and $R_{free}$ did not decrease any further.

In addition, for mAChE, a refinement strategy involving TLS, Ramachandran, secondary structure restraints, and occupancy optimization was performed using Phenix. In the course of the refinement of oCSP-mAChE, it appeared that Phe297 adopts two alternative conformations and that occupancies of saligenin of oCSP-mAChE were partial. Therefore, the occupancies of Phe297 and saligenin in oCSP-mAChE were refined with Phenix as follows: *B*-factors and occupancy of Phe297 and saligenin were initially set to 30 Å$^2$ and 0.5, respectively. Then, coordinates and *B*-factors were refined resulting in a *B*-factor about 50 Å$^2$ for Ser198. To account for the higher disorder of oCSP, its *B*-factor was manually adjusted to the *B*-factor of Ser198 plus 20% (60 Å$^2$). Next, occupancies were refined, grouping the alternative conformation of Phe297 with saligenin. The resulting occupancies were rounded to the next digit, and a final refinement cycle of coordinate and *B*-factor was performed. Protein structures were illustrated using the program PyMOL (Schrödinger, LLC).

*Mass Spectrometry of CBDP-mAChE and CBDP-hBChE after Reaction in $H_2{}^{18}O$.* mAChE or hBChE (3.2 $\mu$M) was irreversibly inhibited by reaction with CBDP (93 $\mu$M) either in $H_2{}^{18}O$ (93% enriched) or $H_2{}^{16}O$ and 10 mM ammonium bicarbonate (pH 8) at 22 °C for 1 or 40 h. At the end of the inhibition period, there was no activity remaining for either mAChE or hBChE. Before proteolysis, water from both the $H_2{}^{18}O$ and $H_2{}^{16}O$ samples was removed by evaporation in a Savant SpeedVac (Thermo Fisher Scientific, Waltham, MA). The samples were then redissolved in $H_2{}^{16}O$ to a final concentration of 3.2 $\mu$M. Removal of the $^{18}O$ water simplified the mass spectra by preventing $^{18}O$ atoms from being incorporated into the carboxyl termini of the peptides during proteolysis. Proteolysis was performed by adding pepsin (5 mg/mL in 5% formic acid) to each tube to obtain a final cholinesterase to pepsin ratio of 1:2 (w/w) and a final pH of 2.5. Mixtures were incubated at 37 °C for 2 h. Aliquots of each digest were diluted 1 to 10 in 50% acetonitrile and 0.3% trifluoroacetic acid (TFA), spotted directly onto MALDI sample plates, and air-dried. Dried spots were overlaid with a 2,5-dihydroxy benzoic acid matrix (Acros Organics a part of the Thermo Fisher Scientific group, Geel, Belgium). Samples were analyzed in a MALDI TOF/TOF 4800 mass spectrometer (Applied Biosystems, Foster City, CA) in negative reflector mode with delayed extraction (625 ns) and a laser intensity of 5500 V.

*Molecular Dynamics Simulations of oCP-mAChE.* A monomer from the oCSP-mAChE X-ray structure was used as the initial model for molecular dynamics simulations. All crystallographic water molecules were conserved. Both alternate conformations of Phe297 being present in the experimental structure, we retained only the non-native one. The saligenin group located in the acyl-binding pocket was manually removed from the initial model in order to generate the oCP-mAChE conjugate. We developed a full force field (FF) for the o-CP serine. The modified serine was built using Chimera[29] with geometry optimization at the Molecular Mechanics level. RESP charges of the modified residue were calculated using the REDS server[30] following the recommended procedure, including a Quantum Mechanics optimization of the fragments achieved with the Gaussian09 package at the HF/6-31G* theoretical level. The new FF was included in the amber99sb FF.[31] When parameters (bond distances, angles, and dihedral) were not available in amber99sb, they were assigned from the General Amber Force Field[32] using Antechamber.[33] Molecular dynamics simulations were carried out using the GROMACS 4.5.4 package.[34] The protein system was immersed in a 10-Å layer truncated cubic periodic water box using the TIP3P solvation model.[35] Charge equilibration was made by adding 9 $Na^+$ ions. A 2-fs time step was used in all the simulations, and long-range electrostatic interactions were treated with the particle-mesh Ewald (PME) procedure[36] using a cubic B-spline interpolation and a $10^{-5}$ tolerance for the direct-space and with a 12-Å nonbonded cutoff. A 300 K temperature coupling scheme using a separated Berendsen thermostat for solvent and protein was applied. Pressure was kept constant at 1 bar by a Berendsen barostat considering a compressibility of $4.5 \times 10^{-5}$. Molecular dynamics was preceded by an energy minimization (500 cycles of Steepest Descent) and a 50 ps position-restrained MD-simulated soak. Six full MD simulations differing only by the seed used to generate initial velocities were performed for 10 ns at 300 K under these conditions. The resulting trajectories were visualized using VMD[37] and analyzed using the tools provided in the GROMACS package.

## RESULTS

**Crystallographic Structures of *o*-Cresyl-phospho-hBChE (oCP-hBChE) and Phospho-hBChE.** The oCP-hBChE adduct was generated by soaking a hBChE crystal for 2 min in a mother liquor solution containing 1 mM CBDP. The crystal was then flash-cooled to 100 K, and diffraction data were collected to a resolution of 2.7 Å (Table 1).

The initial Fourier-difference electron density map ($F_o - F_c$) featured a strong positive peak (10.4 $\sigma$) at covalent bonding distance from catalytic Ser198O$\gamma$ (not shown), allowing to assign the position of the phosphorus atom of the CBDP adduct. The saligenin substituent was not present despite the short soaking time. Rather, the ligand was modeled as an *o*-cresyl phosphate, with its *o*-cresyl moiety bound in the acyl-binding pocket (Figure 1A); this binding scenario implies that the P(R) enantiomer of CBDP initially bound to the enzyme. In the refined model, the covalent bonds oCP600P-Ser198O$\gamma$, Ser198O$\gamma$-Ser198C$\beta$, and Ser198C$\beta$-Ser198C$\alpha$ are elongated and characterized by distances of 2.0, 1.7, and 1.65 Å, respectively. These values can be compared to predicted values of 1.60, 1.45, and 1.55 Å (calculated *ab initio* using Gaussian09) and to observed values of 1.85, 1.45, and 1.55 Å, in the previously determined crystal structure of phospho-hBChE, the end product of the hBChE inhibition by CBDP (Figure 1B; pdb ID 2y1k). Restraining the length of these bonds to their ideal values led to the appearance, in the resulting Fourier-difference map, of a large negative peak (>5 $\sigma$) between the phosphorus atom and Ser198O$\gamma$, and of equivalent positive peaks on the opposite side of the phosphorus atom and Ser198O$\gamma$. We interpret this observation as an indication of strain in the 3 consecutive bonds between the phosphorus atom and the serine main chain, which we propose to stem from the steric exclusion of the *o*-cresyl group by Trp231 (closest distance between non-hydrogen atoms: 3.5 Å). The entire phosphoryl group is pushed-up the active site gorge by 1.3 Å


dx.doi.org/10.1021/tx3004505 | Chem. Res. Toxicol. 2013, 26, 280−289

**Table 1. Crystallographic and Refinement Statistics**

| | oCP-BChE | oCSP-AChE | oCP-AChE |
|---|---|---|---|
| PDB entry code | 4bbz | 4bc0 | 4bc1 |
| space group | *I*422 | $P2_12_12_1$ | $P2_12_12_1$ |
| unit cell (Å) | | | |
| a | 154.7 | 135.5 | 136.9 |
| b | 154.7 | 173.3 | 174.0 |
| c | 127.0 | 224.9 | 225.6 |
| resolution (Å) | 54.7−2.7 | 48.3−2.95 | 48.6−3.35 |
| completeness (%)[a] | 98.1 (99.0) | 99.7 (99.4) | 96.6 (98.6) |
| $R_{sym}$ (%)[a] | 7.1 (46.5) | 8.1 (52.8) | 7.5 (58.4) |
| $I/\sigma(I)$[a] | 28.1 (5.2) | 17.1 (3.1) | 16.2 (2.8) |
| unique reflections[a] | 21 049 | 111 473 | 75 488 |
| redundancy[a] | 10.1 (9.2) | 4.4 (4.5) | 3.6 (3.4) |
| Wilson *B* factor (Å$^2$) | 53.4 | 63.9 | 94.92 |
| $R_{fact}$ (%) | 16.6 | 18.6 | 16.2 |
| $R_{free}$ (%) | 22.5 | 23.8 | 20.7 |
| non-hydrogen atoms | 4547 | 17994 | 17432 |
| protein | 4222 | 16 899 | 16 806 |
| ligands | 186 | 260 | 215 |
| solvent | 139 | 835 | 411 |
| RMS bond length (Å) | 0.008 | 0.009 | 0.009 |
| RMS bond angles (deg) | 1.269 | 1.368 | 1.482 |
| Ramachandran | | | |
| favored (%) | 94 | 92 | 94 |
| allowed (%) | 6 | 7.8 | 5.7 |
| outliers (%) | 0 | 1.2 | 0.3 |
| average *B* factor (Å$^2$) | 41.3 | 46.8 | 47.2 |
| protein | 40 | 46.9 | 47.1 |
| ligands | 74.1 | 91.2 | 92.7 |
| solvent | 36.2 | 31.5 | 28.3 |

[a]Values in parentheses refer to the highest resolution shell.

and twisted counter-clockwise around the Ser198O$\gamma$-P bond when compared to its conformation in the phospho-BChE structure (Figure 2, panel A). This results in the absence of hydrogen-bonding interaction between the phosphoryl oxygen (O3P) of oCP600 and Ala199N in the oxyanion hole, again in contrast to what is observed in the phospho-hBChE structure (4.5 Å interatomic distance vs 2.7 Å in the oCP- and phospho-hBChE structures, respectively). Likewise, the hydrogen bond interaction between O1P of oCP and His438N$\varepsilon$2 and Ser198O$\gamma$ are both weakened (3.3 Å and 3.2 Å, respectively) relative to phospho-hBChE (2.9 Å and 3.0 Å; Figure 1B).

Altogether, these observations indicate that the oCP-hBChE adduct is not as stable as a canonical aged-BChE-OP conjugate, which the phospho-hBChE structure resembles more.

**Crystallographic Structure of *o*-Cresyl Saligenin Phospho-mAChE (oCSP-mAChE).** The oCSP-mAChE adduct was trapped by flash cooling a mAChE crystal that had been soaked for 30 min in a mother liquor solution containing 1 mM CBDP. The structure was solved at 2.95 Å resolution (Table 1). In this space group, the asymmetric unit contains two mAChE biological dimers that are related by noncrystallographic symmetry, and in each, monomers associate through a four helix-bundle.[38] In each dimer, one monomer features a solvent accessible peripheral site, while the peripheral site of the other is occupied by the Cys257-Cys272 loop from another monomer in the asymmetric unit tetramer. The *o*-cresyl and saligenin substituents are located in the choline- and acyl-binding pockets, respectively, indicating a preferential binding of the P(S) enantiomer of CBDP in mAChE (Figure 1C). This is in contrast with hBChE, in which it is the P(R) enantiomer that preferentially binds and where the *o*-cresyl substituent is located in the acyl-binding pocket (Figure 1A). In the acyl-binding pocket of oCSP-mAChE, Phe297 adopts an alternate conformation with a $\chi$1 rotation of about 145° (around the C$\alpha$-C$\beta$ bond), as required for the accommodation of saligenin (Figure 1C). We used the direct correlation between the alternate conformation of Phe297 and the presence of the saligenin moiety in the acyl-binding site to evaluate the partial occupancy of saligenin in the oCSP-mAChE structure (see the Experimental Procedures section for details). The fraction of bound CBDP retaining saligenin ranges from 0.4 to 0.5, depending on which of the four monomers is inspected. Overall, the geometry of catalytic-Ser203 in oCSP-mAChE is not distorted compared to catalytic-Ser198 in oCP-hBChE (Figure 2, compare the slate colored structures in panels A and B). The refined length of the covalent oCSP600P-Ser203O$\gamma$ bond is 1.7 Å in the mAChE structure, compared to a predicted value of 1.59 Å (as calculated *ab initio*). Finally, the catalytic His447N$\varepsilon$2 forms a H-bond with Ser203O$\gamma$ (2.8 Å) but does not interact with O2P of the cresyl substituent (Figure 1C).

**Crystallographic Structure of *o*-Cresyl-phospho-mAChE (oCP-mAChE).** The oCP-mAChE adduct was obtained by extending the soaking time to 12 h before flash cooling the crystal. The resolution of this structure is relatively low (3.35 Å) in comparison to that of the analogous oCP-hBChE structure (Table 1). It is unclear whether it is the relatively long soaking time or the effect of enzymatically produced saligenin that affected the crystal quality and the resolution of the diffraction data. Electron density maps were yet of good quality and thus allowed the unambiguous modeling of the *o*-cresyl moiety into a strong peak of positive $F_o - F_c$ electron density (10 $\sigma$) in the vicinity of the catalytic-serine hydroxyl group (Figure 1D). No electron density is observed in the acyl-binding pocket, indicating that the saligenin moiety has exited the active site (Figure 1D). Accordingly, Phe297 fully occupies its native position as indicated by the electron density maps and further confirmed by the occupancy refinement of its side chain. The *o*-cresyl moiety is stabilized in the choline-binding pocket by a perpendicular $\pi$-stacking interaction with the aromatic rings of Trp86. No H-bond interaction is noticeable between the *o*-cresyl O2 atom and His447N$\varepsilon$2, the later being hydrogen-bonded to Ser203O$\gamma$ (2.9 Å). With the *o*-cresyl substituent in the choline-binding pocket, the oCP-mAChE adduct appears to be the mirror image of the oCP-hBChE adduct in which the substituent is found in the acyl-binding pocket (Figure 1A and D). X-ray data collected after soaking periods ≥12 h repeatedly yielded an oCP-mAChE adduct and not a phosphoserine adduct as observed in hBChE.

**Mass Spectrometry Analysis.** The repeatedly unproductive attempts to obtain the structure of a phospho-mAChE adduct suggested that CBDP inhibition of mAChE occurs in two steps, i.e. phosphorylation of the enzyme and a canonical aging reaction. From our crystallographic data alone, however, we could not determine whether the observation of an *o*-cresyl phosphoserine adduct as the end-product of mAChE inhibition by CBDP was a crystallographic artifact or, rather, a sign for CBDP inhibition of AChE and BChE occurring through different pathways.

In order to ascertain the number of steps involved in the *in vitro* mAChE inhibition by CBDP, MALDI-TOF mass-spectrometry of proteolyzed, CBDP-inhibited mAChE was


dx.doi.org/10.1021/tx3004505 | *Chem. Res. Toxicol.* 2013, 26, 280−289

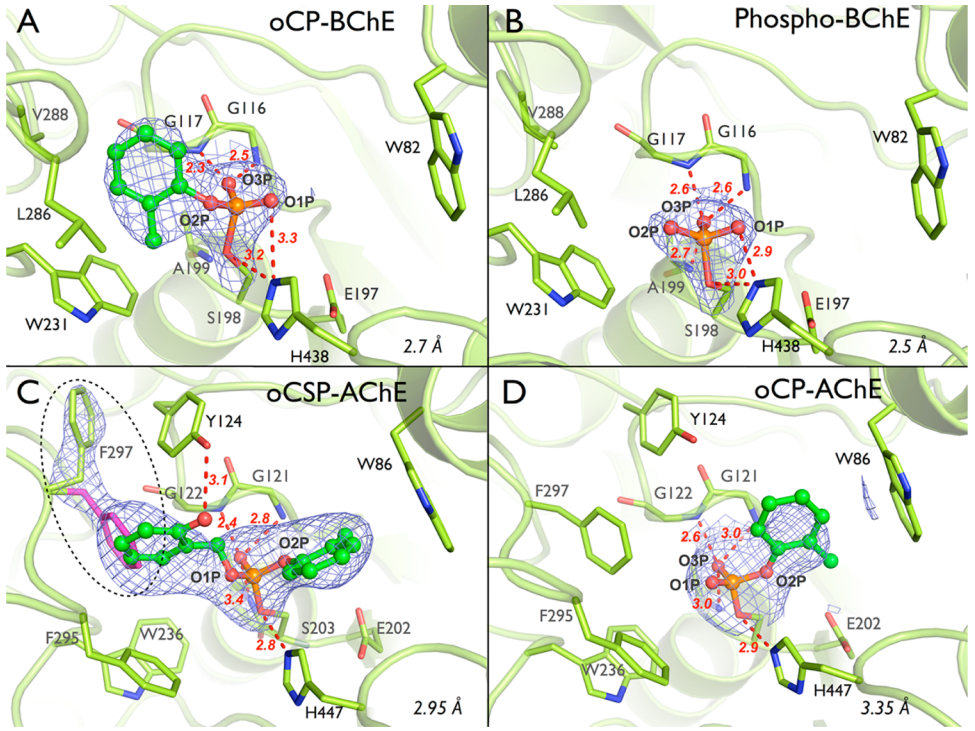


**Figure 1.** Sequential crystallographic snapshots of mAChE and BChE inhibition by CBDP. For BChE (upper panels), a soaking time of 2 min yielded an *o*-cresyl-phospho-BChE conjugate (A, current work). A soaking time of 12 h yielded the final phospho-BChE conjugate[7] (B). For mAChE (lower panels), soaking times of 30 min and 12 h yielded the *o*-cresyl saligenin phospho-AChE conjugate (C) and the *o*-cresyl-phospho-AChE conjugate (D), respectively. Key residues are represented as sticks with carbon atoms in green, nitrogen atoms in blue, phosphorus in orange, and oxygen atoms in red. Atoms and bonds of the adducts are represented as ball and sticks, respectively. Hydrogen bonds are represented by red dashes with distances in Å. A dashed ellipse in panel C highlights the native (magenta) and an alternate (green) position of Phe297. The electron density $2F_o - F_c$ is represented by a blue mesh contoured at 1.0 $\sigma$.

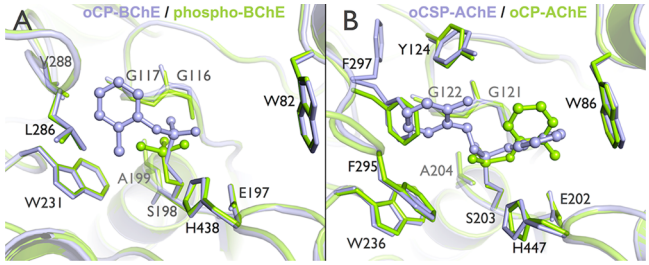


**Figure 2.** (A) Superimposition of oCP-BChE (slate) and phospho-BChE (green) structures. (B) Superimposition of oCSP-AChE (slate) and oCP-AChE (green) structures. Key residues are represented as sticks. Atoms and bonds of the adducts are represented as ball and sticks, respectively.

used, as previously described for hBChE.[7] We investigated the involvement of water molecules in the various steps of mAChE inhibition by CBDP by performing the inhibition in either $H_2{}^{16}O$ or in $H_2{}^{18}O$, which allowed us to characterize the step at which water is incorporated into the enzyme adducts. As a control, the same analyses were performed on CBDP-inhibited hBChE. Inhibition yields reached 100%, for both mAChE and hBChE, as evidenced by the absence of catalytic activity at the end of the reaction period and by the absence of unlabeled active-site peptides in the mass spectra.

From the hBChE-CBDP reaction, both *o*-cresyl phosphate (oCP) and phosphate adducts on the active-site peptic-peptide were detected.[18] Post source decay fragmentation confirmed that these adducts were on the active-site serine. Figure 3, panels A and B, show mass spectra (in negative mode) for *o*-cresyl phosphate adducts at 877 amu (for the peptic peptide FGESAGAA) and at 964 amu (for the miscleavage peptide FGESAGAAS). These adducts are formed following the release of saligenin from the initial CBDP-hBChE reaction product. The masses of these adducts are not affected by the presence of $H_2{}^{18}O$ indicating that no oxygen atoms from water are incorporated into the phosphorus moiety upon the release of saligenin. Figure 3, panels A and B, also show mass spectra (negative mode) for phosphate adducts. In $H_2{}^{16}O$, the phosphate adduct appears at 874 amu (for peptide FGESAGAAS). In $H_2{}^{18}O$, the 874 amu mass is shifted to 876 amu indicating the incorporation of an oxygen atom from water into the phosphate adduct upon the hydrolytic release of the *o*-cresyl moiety.

From the mAChE-CBDP reaction, only an *o*-cresyl-phosphate adduct was detected (Figure 3, panels C–D). No evidence for the phosphate adduct was obtained after the 1 h reaction period used for this experiment, nor was the phosphate adduct detected when the reaction was allowed to proceed for 40 h. Post-source decay fragmentation showed that the *o*-cresyl phosphate adduct was located on the active site serine. In mass spectra (negative mode) for both the $H_2{}^{16}O$ and $H_2{}^{18}O$ samples, masses for the oCP adducts appeared at 877 amu (for peptide FGESAGAA) and 964 amu (for peptide FGESAGAAS) indicating that no oxygen atom from water is incorporated into the adduct upon release of saligenin.

**Molecular Dynamics Simulations.** Phe297 is in an alternate conformation in the oCSP-mAChE adduct and moved back to its native position during aging as seen in the crystallographic structure of the oCP-mAChE adduct. We


dx.doi.org/10.1021/tx3004505 | *Chem. Res. Toxicol.* 2013, 26, 280–289

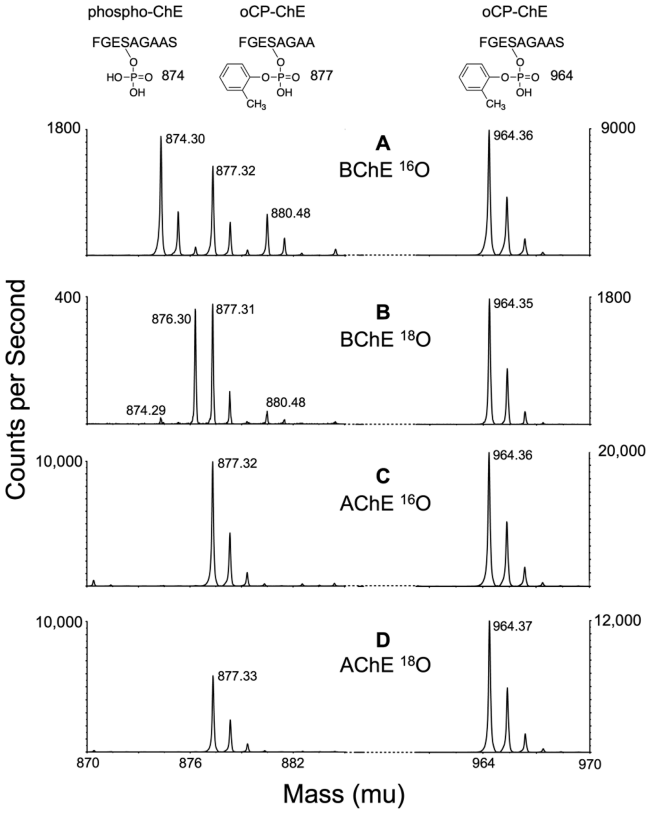


**Figure 3.** Reaction of hBChE and mAChE with CBDP in the presence of $O^{16}$-water (A and C) and $O^{18}$-water (B and D). The 874−877 amu region and 964 amu region of pepsin-digested 1-h CBDP-inhibited ChEs are shown. All spectra were taken in negative mode. The sequence of the phosphopeptide of mass 874 is FGES*AGAAS with $PO_4$ on serine. The sequences of the *o*-cresyl phosphate adducts of mass 877 and 964 are FGES*AGAA and FGES*AGAAS, where the asterisk indicates the labeled serine.

carried out molecular dynamics (MD) simulations in order to address whether the observed conformational change is part of equilibrium dynamics preexisting to ligand binding or a fit induced by ligand binding.[39] An initial model was created based on the oCSP-mAChE crystallographic structure, i.e., with the side chain of Phe297 in the alternate conformation but not with the saligenin substituent. In none of the six 10-ns MD simulations was a reversal of Phe297 to its native conformation observed.

## DISCUSSION

Previously, we showed that hBChE inhibition by CBDP proceeds through a three-step reaction mechanism.[18] First, the catalytic serine is organophosphorylated to form the ring-opened CBDP-hBChE adduct. A dealkylation step then occurs viz. the first aging reaction, which results in the loss of the saligenin moiety. Last, the oCP-hBChE adduct undergoes hydrolysis with the concomitant departure of the *o*-cresyl moiety yielding the final phosphoserine hBChE adduct (Scheme 1).[7] That the latter is the end product of hBChE inhibition by CBDP was known from its X-ray structure at 2.7 Å resolution as well as from previous mass spectrometry experiments. It remained unclear, however, how these steps proceed at the atomic level of resolution. Also, it was unknown if mAChE follows the same inhibition pathway as hBChE and/or displays the same enantiomer selectivity.

In the current study, a combination of X-ray crystallography and mass-spectrometry was used to specifically address the above-mentioned unresolved issues. Atomic-resolution crystallographic snapshots of hBChE and mAChE were taken at different time points during their reaction with CBDP. Together with adduct masses obtained from the mass spectra, they allow one to develop detailed mechanistic models for the CBDP inhibitions of mAChE and hBChE, respectively.

**Inhibition of mAChE by CBDP.** In this study, mAChE was employed instead of hAChE because our preparation of the latter only crystallizes in the presence of the gorge-capping peptide fasciculin. Such capping prevents inhibitors from entering the active site precluding the use of soaking techniques to introduce inhibitors. mAChE is yet a reliable model for hAChE in that nearly all of the residues lining the active site gorge of mAChE and hAChE are identical. Noteworthy, Cheung et al. very recently reported a truncated form of hAChE able to crystallize without fasciculin and suitable for soaking techniques.[40] Use of this new form of hAChE will be preferred for future crystallographic studies.

After soaking a crystal of mAChE for 30 min in a CBDP containing solution, the initial ring-opened oCSP-AChE adduct could be trapped by flash cooling (Figure 1C). The *o*-cresyl and saligenin moieties are located in the choline- and the acyl-binding pockets, respectively. This positioning indicates that crystalline mAChE preferentially binds and reacts with the P(S) enantiomer of CBDP.

Figure 1C also shows that the acyl-binding pocket is only partially occupied by saligenin. The partial occupancy (0.4−0.5) indicates that about half of the crystalline oCSP adducts have released saligenin after a 30 min soak (note that the *o*-cresyl site is fully occupied). Thus, the half-life for the first aging reaction is about 30 min *in crystallo*. Extending the soaking time to 12 h or more results in the complete elimination of saligenin and in the formation of an oCP-AChE conjugate (Figure 1D).

Mass spectral analysis after proteolysis, combined with the crystal structures, shows that mAChE inhibition by CBDP occurs in two steps, viz. organophosphorylation and dealkylation of saligenin in the acyl-binding pocket, yielding a final *o*-cresyl-phosphoserine adduct (Scheme 2). The fact that no water was incorporated in the *o*-cresyl-phosphoserine mAChE adduct indeed excludes the possibility that saligenin was released through its hydrolysis. Dealkylation is an unusual reaction for a substituent located in the acyl-binding pocket: the two residues known to catalyze dealkylation of OPs adducts, His447 and Glu202, are indeed part of the choline-binding pocket, on the opposite site of the active site gorge. No unusual strain is observed in the o-CSP adduct, which eliminates this source of enthalpy as the driving force for the dealkylation reaction. This implies that another driving force must be involved. A possibility is that the hydroxyl group of saligenin stabilizes a water molecule that could in turn react with the benzylic carbocation, thereby promoting the dealkylation reaction. The return to its native conformation of the Phe297 side chain, which was displaced from the acyl-binding pocket by the saligenin substituent, could constitute an additional driving force for the dealkylation.

Both the 40-h mass spectrometry and the 12-h crystallographic data indicate that the oCP adduct is the end product of mAChE inhibition by CBDP, in contrast to hBChE where the oCP adduct reacts further to yield a phosphoserine adduct (Figure 1B).[7] This difference is most likely to ascribe to the


dx.doi.org/10.1021/tx3004505 | *Chem. Res. Toxicol.* 2013, 26, 280−289

**Scheme 2. Detailed Chemical Mechanism for CBDP Inhibition of mAChE and hBChE**

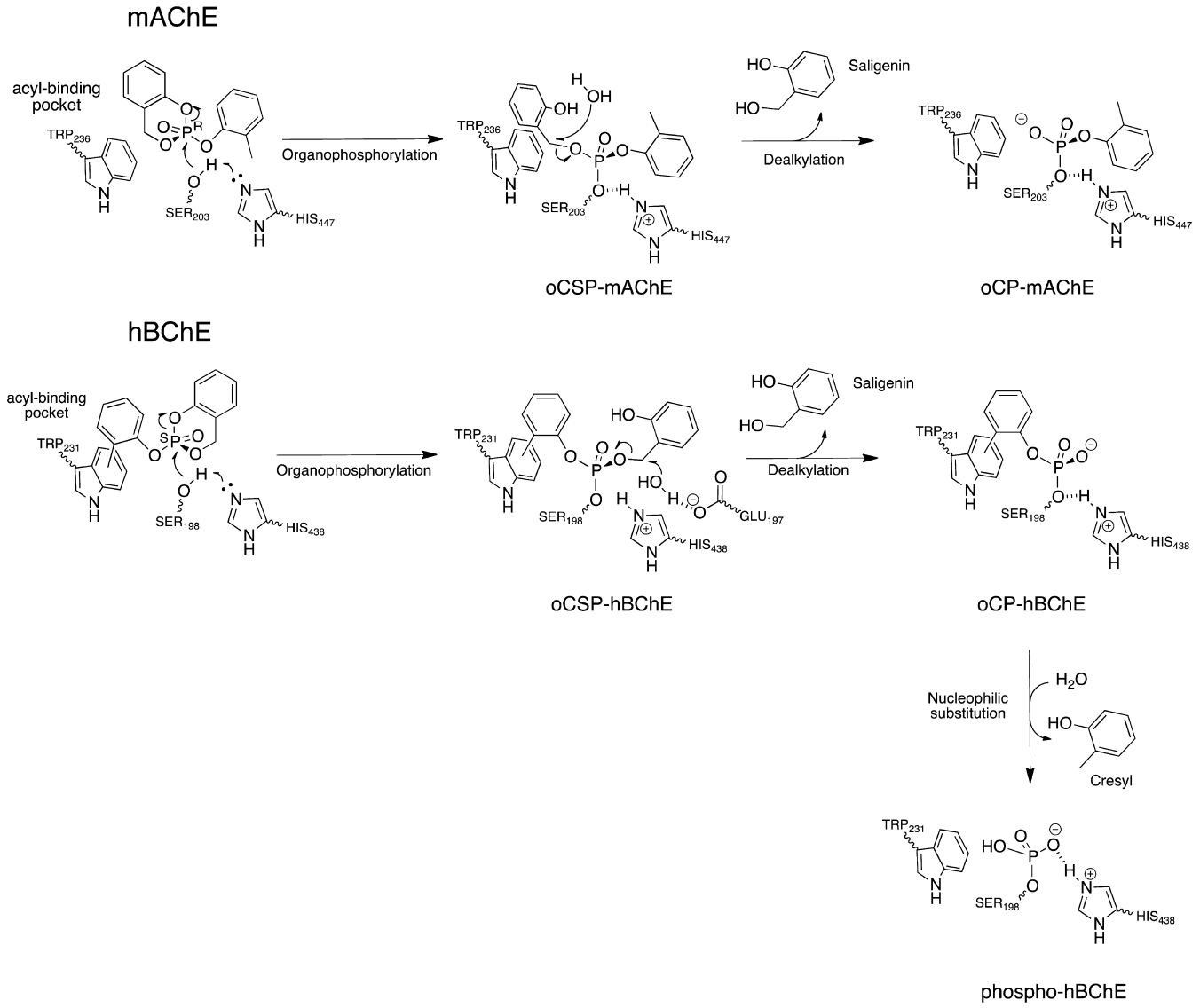


symmetric configuration of the *o*-cresyl substituent in mAChE and hBChE. In hBChE, the *o*-cresyl substituent is in the acyl-binding pocket; thus, the choline-binding pocket remains free for a water to approach the phosphorus atom, resulting in oCP adduct hydrolysis. Conversely in mAChE, hydrolysis does not occur because the *o*-cresyl substituent is located in the choline-binding pocket, meaning that the water would have to attack from the crowded acyl-binding pocket. While dearylation of the oCP-mAChE adduct could theoretically have occurred, considering that the *o*-cresyl substituent is located in proximity to His447/Glu202, our data unequivocally show that it does not. In this context, it is noteworthy mentioning that one of the strategies envisaged to counteract OP-intoxication is to realkykate aged phosphylconjugates;[41] by showing that dearylation does not occur on the time scale of our experiments (tens of hours), our data thus suggest that arylation may be more promising than realkylation.

In mAChE, organophosphorylation correlates with a rotation of the Phe297 side chain (Figure 1C), which enlarges the acyl-binding pocket and is thus required to accommodate the saligenin moiety. An identical conformational change was observed in the crystal structures of fenamiphos-inhibited mAChE in complex with the ortho-7 reactivator (pdb accession code 2wu4)[42] as well as in a *Tc*AChE/Bis(5)-tacrine complex (pdb accession code 2cmf).[43] In the ortho-7 complex, one pyridinium ring of ortho-7 pushes the isopropylamino substituent of fenamiphos toward the acyl-loop 285−298 and leads to its rearrangement. In the *Tc*AChE complex, non-covalent binding of the tacrine produces drastic rearrangements in the active site gorge, including a rotation of Phe290 (Phe297 in mAChE), that are induced by a tilt of Tyr121.[43] Since molecular dynamics simulations of native *Tc*AChE did not reveal alternate Phe290 conformations,[44] the rotation seen in the *Tc*AChE/Bis(5)-tacrine complex must be induced by the ligand rather than being selected by the ligand among preexisting native conformations. By extrapolation, the rotation of Phe297 observed in mAChE is also most likely the consequence of an induced fit mechanism, meaning that the conformational change is induced by ligand binding, rather than being part of preexisting equilibrium fluctuations. Although the acyl-loop determines the specificity of hAChE for the natural substrate acetylcholine,[45,46] the acyl-loop remains flexible enough to accommodate bulkier ligands at the cost of an induced fit rearrangement. This rearrangement is reversed once


dx.doi.org/10.1021/tx3004505 | *Chem. Res. Toxicol.* 2013, 26, 280−289

the acyl-binding pocket becomes unoccupied, as after the aging of oCSP-mAChE. The conformational change was not reproduced in six 10 ns molecular dynamics simulations, indicating that the crystallographically observed conformational change is not a simple side chain flip but rather requires a larger rearrangement of the acyl-loop region that is not observed on the time scale of the simulations. These larger rearrangements of the acyl-loop are probably part of the proposed induced-fit mechanism.

**Inhibition of hBChE by CBDP.** The first species observed in the reaction of CBDP with hBChE is oCP-hBChE (Figure 1A), which corresponds to the second intermediate in the reaction mechanism (see Scheme 1). oCP-hBChE is created by the loss of saligenin from the initial intermediate, the ring-opened CBDP adduct. The latter could not be trapped, even by reducing soaking times to as short as 30 s, indicating that this adduct decays faster than it forms.

The *o*-cresyl moiety is located in the acyl-binding pocket of the oCP-hBChE adduct, which indicates that the saligenin moiety was bound in the choline-binding pocket prior to the first aging step and suggests a preferential reaction of the P(R) enantiomer of CBDP with crystalline hBChE. MD and QM/MM studies of hBChE reacting with CBDP, as well as titration experiments, support the proposed stereoselectivity (Lushchekina et al., unpublished results). Mass spectrometry showed that no oxygen atom from water is incorporated into the oCP-adduct, inferring that the release of saligenin likely stems from a His438/Glu197-catalyzed dealkylation.[7] This conclusion is in agreement with the proposal that aging of OP-hBChE proceeds through O-dealkylation of substituents bound in the choline-binding pocket.[47] However, an oxygen atom from water is incorporated during the second aging reaction. This observation supports the hypothesis of a nucleophilic attack, by a water molecule, on the phosphorus atom of oCP, resulting in the release of the o-cresyl moiety and the formation of the phospho-BChE adduct.[7]

From a mechanistic point of view, the most probable scenario is that this water attacks from the open face opposite the cresyl−O-P bond, vicinal to Glu197 (refer to Figure 1A), leading to the formation of a bipyramidal transition state and its subsequent collapse, with the release of *o*-cresyl (Scheme 2). The other possibility is that water approaches from the side opposite to the Ser198O$\gamma$-P bond. However, we conjecture this scenario is unlikely considering the steric hindrance imposed by the presence of the *o*-cresyl moiety in the acyl-binding pocket. Also, a water attack from that side should lead to the scission of the Ser198O$\gamma$-P bond and, therefore, to the release of the entire *o*-cresyl phosphate group, not just the *o*-cresyl moiety. Yet, neither was a native active site peptide identified in our mass spectrometry study, nor was self-reactivation observed in our previous kinetics studies. Thus, the attack of water is proposed to occur from the open face opposite the cresyl−O-P bond, vicinal to Glu197. A similar mechanism was proposed for the aging reaction of an analogue of the nerve agent tabun.[48]

A structural comparison between the oCP- and the phospho-hBChE adducts shows a release of the strain imposed on the enzyme, when *o*-cresyl is released and the phospho-conjugate is formed (Figures 2A). We conjecture that the release of this strain contributes to the driving force responsible for the scission of the P−O bond linking the *o*-cresyl to the phosphorus. It should be noted that unlike in mAChE, no side chain undergoes major conformational changes upon the binding of CBDP in hBChE.

## CONCLUSIONS

The combination of crystallographic snapshots with mass spectrometric analysis shows that the inhibition of mAChE and hBChE by CBDP involves the binding of opposite enantiomers. Therefore, two different reaction pathways are undertaken by mAChE and hBChE for inhibition and aging. hBChE undergoes a three-step reaction process including (i) the organophosphorylation of the catalytic serine to form a CBDP ring-opened adduct, (ii) a dealkylation resulting in the loss of the saligenin substituent from the choline-binding pocket, and (iii) a nucleophilic hydrolysis of the *o*-cresyl substituent in the acyl-binding pocket, yielding a final phosphoserine-hBChE conjugate. In contrast, the inhibition of mAChE is a two-step reaction, resulting from of organophosphorylation and subsequent dealkylation, leading to the release of saligenin and the formation of the *o*-cresyl-phosphoserine mAChE adduct. Additionally, the crystallographic snapshots of the mAChE inhibition intermediates illustrate how a bulky inhibitor like CBDP is able to fit into the active site of mAChE through an induced fit rearrangement. It is worth noting that for both mAChE and hBChE, the final enzyme conjugate is aged, meaning that it cannot be reactivated by oximes.[47] In other words, there is currently no effective therapeutics to reactivate inhibited AChE in the case of severe TOCP intoxication.

## ASSOCIATED CONTENT

### Supporting Information

$2F_o - F_c$ and $F_o - F_c$ electron density maps. This material is available free of charge via the Internet at http://pubs.acs.org.

## AUTHOR INFORMATION

### Corresponding Author

*(F.N.) Tel: (+33) 476 636959. E-mail: florian@nachon.net. (M.W.) Tel: (+33) 438 789580. E-mail: martin.weik@ibs.fr.

### Funding

Financial support by the DGA (project number DGA-REI 2009-34-0023 to M.W. and DGA/DSP/STTC 08co501 to F.N.), CEA, the CNRS, and the UJF is acknowledged, as well as grants from the Agence Nationale de la Recherche (ANR; project number ANR-09-BLAN-0192-04 to M.W. and F.N.) and the DTRA (HDTRA1-11-C-0047 to M.W. and F.N.). J.P.C. is a recipient of the Young International Scientists fellowship from the Chinese Academy of Science.

### Notes

The authors declare no competing financial interest.

## ACKNOWLEDGMENTS

We are grateful to the ESRF for beam-time under long-term projects MX498, MX609, and MX722 (IBS BAG), and MX551 and MX 666 (radiation-damage BAG), and to the ESRF staff for providing efficient help during data collection. Mass spectra were obtained with the support of the Mass Spectrometry and Proteomics core facility at the University of Nebraska Medical Center.

## ABBREVIATIONS

TOCP, tri-*o*-cresyl-phosphate; TCP, tricresyl phosphate; CBDP, 2-(*ortho*-cresyl)-4*H*-1,2,3-benzodioxaphosphoran-2-one, cresyl saligenin phosphate; OP, organophosphorus compound; hBChE, human butyrylcholinesterase; hAChE, human acetylcholinesterase; mAChE, mouse acetylcholinester-

ase; ChE, cholinesterase; oCP-hBChE, *o*-cresyl phosphate human butyrylcholinesterase conjugate; oCP, *o*-cresyl phosphate; oCSP-mAChE, *o*-cresyl saligenin phosphate mouse acetylcholinesterase conjugate; oCSP, *o*-cresyl saligenin phosphate; oCP-mAChE, *o*-cresyl phosphate mouse acetylcholinesterase conjugate

## REFERENCES


(1) Winder, C. (2006) Air monitoring studies for aircraft cabin contamination. *Curr. Top. Toxicol. 3*, 33−48.

(2) Mackerer, C. R., Barth, M. L., Krueger, A. J., Chawla, B., and Roy, T. A. (1999) Comparison of neurotoxic effects and potential risks from oral administration or ingestion of tricresyl phosphate and jet engine oil containing tricresyl phosphate. *J. Toxicol. Environ. Health, Part A 57*, 293−328.

(3) Liyasova, M., Li, B., Schopfer, L. M., Nachon, F., Masson, P., Furlong, C. E., and Lockridge, O. (2011) Exposure to tri-o-cresyl phosphate detected in jet airplane passengers. *Toxicol. Appl. Pharmacol. 256*, 337−347.

(4) Casida, J. E., Eto, M., and Baron, R. L. (1961) Biological activity of a trio-cresyl phosphate metabolite. *Nature 191*, 1396−1397.

(5) Eto, M., Casida, J. E., and Eto, T. (1962) Hydroxylation and cyclization reactions involved in the metabolism of tri-o-cresyl phosphate. *Biochem. Pharmacol. 11*, 337−352.

(6) Eto, M., Oshima, Y., and Casida, J. E. (1967) Plasma albumin as a catalyst in cyclization of diaryl o-(alpha-hydroxy)tolyl phosphates. *Biochem. Pharmacol. 16*, 295−308.

(7) Carletti, E., Schopfer, L. M., Colletier, J. P., Froment, M. T., Nachon, F., Weik, M., Lockridge, O., and Masson, P. (2011) Reaction of cresyl saligenin phosphate, the organophosphorus agent implicated in aerotoxic syndrome, with human cholinesterases: mechanistic studies employing kinetics, mass spectrometry, and X-ray structure analysis. *Chem. Res. Toxicol. 24*, 797−808.

(8) Masson, P. (2011) Evolution of and perspectives on therapeutic approaches to nerve agent poisoning. *Toxicol. Lett. 206*, 5−13.

(9) Worek, F., Thiermann, H., Szinicz, L., and Eyer, P. (2004) Kinetic analysis of interactions between human acetylcholinesterase, structurally different organophosphorus compounds and oximes. *Biochem. Pharmacol. 68*, 2237−2248.

(10) Harel, M., Schalk, I., Ehret-Sabatier, L., Bouet, F., Goeldner, M., Hirth, C., Axelsen, P. H., Silman, I., and Sussman, J. L. (1993) Quaternary ligand binding to aromatic residues in the active-site gorge of acetylcholinesterase. *Proc. Natl. Acad. Sci. U.S.A. 90*, 9031−9035.

(11) Wandhammer, M., Carletti, E., Van der Schans, M., Gillon, E., Nicolet, Y., Masson, P., Goeldner, M., Noort, D., and Nachon, F. (2011) Structural study of the complex stereoselectivity of human butyrylcholinesterase for the neurotoxic V-agents. *J. Biol. Chem. 286*, 16783−16789.

(12) Winder, C., and Balouet, J. C. (2002) The toxicity of commercial jet oils. *Environ. Res. 89*, 146−164.

(13) van Netten, C. (2005) Aircraft air quality incidents: symptoms, exposures and possible solutions. *J. Occup. Health Saf. 21*, 460−468.

(14) Johnson, M. K. (1975) Structure-activity relationships for substrates and inhibitors of hen brain neurotoxic esterase. *Biochem. Pharmacol. 24*, 797−805.

(15) Glynn, P. (1999) Neuropathy target esterase. *Biochem. J. 344*, 625−631.

(16) Aldridge, W. N. (1954) Tricresyl phosphates and cholinesterase. *Biochem. J. 56*, 185−189.

(17) Earl, C. J., and Thompson, R. H. (1952) The inhibitory action of tri-ortho-cresyl phosphate on cholinesterases. *Br. J. Pharmacol. Chemother. 7*, 261−269.

(18) Schopfer, L. M., Furlong, C. E., and Lockridge, O. (2010) Development of diagnostics in the search for an explanation of aerotoxic syndrome. *Anal. Biochem. 404*, 64−74.

(19) Nachon, F., Nicolet, Y., Viguie, N., Masson, P., Fontecilla-Camps, J. C., and Lockridge, O. (2002) Engineering of a monomeric and low-glycosylated form of human butyrylcholinesterase: expression, purification, characterization and crystallization. *Eur. J. Biochem. 269*, 630−637.

(20) Carletti, E., Li, H., Li, B., Ekstrom, F., Nicolet, Y., Loiodice, M., Gillon, E., Froment, M. T., Lockridge, O., Schopfer, L. M., Masson, P., and Nachon, F. (2008) Aging of cholinesterases phosphylated by tabun proceeds through O-dealkylation. *J. Am. Chem. Soc. 130*, 16011−16020.

(21) Ronco, C., Carletti, E., Colletier, J. P., Weik, M., Nachon, F., Jean, L., and Renard, P. Y. (2011) Huprine derivatives as subnanomolar human acetylcholinesterase inhibitors: from rational design to validation by X-ray crystallography. *ChemMedChem 6*, 876−888.

(22) McCarthy, A. A., Brockhauser, S., Nurizzo, D., Theveneau, P., Mairs, T., Spruce, D., Guijarro, M., Lesourd, M., Ravelli, R. B., and McSweeney, S. (2009) A decade of user operation on the macromolecular crystallography MAD beamline ID14−4 at the ESRF. *J. Synchrotron Radiat. 16*, 803−812.

(23) Kabsch, W. (2010) XDS. *Acta Crystallogr., Sect. D 66*, 125−132.

(24) Vagin, A., and Teplyakov, A. (1997) MOLREP: an automated program for molecular replacement. *J. Appl. Crystallogr. 30*, 1022−1025.

(25) Collaborative-Computational-Project-4 (1994) The CCP4 suite: programs for protein crystallography. *Acta Crystallogr., Sect. D 50*, 760−763.

(26) Murshudov, G. N., Vagin, A. A., and Dodson, E. J. (1997) Refinement of macromolecular structures by the maximum-likelihood method. *Acta Crystallogr., Sect. D 53*, 240−255.

(27) Emsley, P., Lohkamp, B., Scott, W. G., and Cowtan, K. (2010) Features and development of Coot. *Acta Crystallogr., Sect. D 66*, 486−501.

(28) Adams, P. D., Afonine, P. V., Bunkoczi, G., Chen, V. B., Davis, I. W., Echols, N., Headd, J. J., Hung, L. W., Kapral, G. J., Grosse-Kunstleve, R. W., McCoy, A. J., Moriarty, N. W., Oeffner, R., Read, R. J., Richardson, D. C., Richardson, J. S., Terwilliger, T. C., and Zwart, P. H. (2010) PHENIX: a comprehensive Python-based system for macromolecular structure solution. *Acta Crystallogr., Sect. D 66*, 213−221.

(29) Pettersen, E. F., Goddard, T. D., Huang, C. C., Couch, G. S., Greenblatt, D. M., Meng, E. C., and Ferrin, T. E. (2004) UCSF Chimera: a visualization system for exploratory research and analysis. *J. Comput. Chem. 25*, 1605−1612.

(30) Vanquelef, E., Simon, S., Marquant, G., Garcia, E., Klimerak, G., Delepine, J. C., Cieplak, P., and Dupradeau, F. Y. (2011) R.E.D. Server: a web service for deriving RESP and ESP charges and building force field libraries for new molecules and molecular fragments. *Nucleic Acids Res. 39*, W511−517.

(31) Hornak, V., Abel, R., Okur, A., Strockbine, B., Roitberg, A., and Simmerling, C. (2006) Comparison of multiple Amber force fields and development of improved protein backbone parameters. *Proteins 65*, 712−725.

(32) Wang, J., Wolf, R. M., Caldwell, J. W., Kollman, P. A., and Case, D. A. (2004) Development and testing of a general amber force field. *J. Comput. Chem. 25*, 1157−1174.

(33) Wang, J., Wang, W., Kollman, P. A., and Case, D. A. (2006) Automatic atom type and bond type perception in molecular mechanical calculations. *J. Mol. Graphics Modell. 25*, 247−260.

(34) Hess, B., Kutzner, C., van der Spoel, D., and Lindahl, E. (2008) GROMACS 4: algorithms for highly efficient, load-balanced, and scalable molecular simulation. *J. Chem. Theory Comput. 4*, 435−447.

(35) Mahoney, M., and Jorgensen, W. (2000) A five-site model for liquid water and the reproduction of the density anomaly by rigid, nonpolarizable potential functions. *J. Chem. Phys. 112*, 8910−8922.

(36) Darden, T., York, D., and Pedersen, L. (1993) Particle mesh Ewald: an N.Log(N) method for Ewald sums in large systems. *J. Chem. Phys. 98*, 10089−10092.

(37) Humphrey, W., Dalke, A., and Schulten, K. (1996) VMD: visual molecular dynamics. *J. Mol. Graphics 14*, 33−38.

(38) Bourne, Y., Taylor, P., Bougis, P. E., and Marchot, P. (1999) Crystal structure of mouse acetylcholinesterase. A peripheral site-

occluding loop in a tetrameric assembly. *J. Biol. Chem. 274*, 2963−2970.
(39) Xu, Y., Colletier, J. P., Jiang, H., Silman, I., Sussman, J. L., and Weik, M. (2008) Induced-fit or preexisting equilibrium dynamics? Lessons from protein crystallography and MD simulations on acetylcholinesterase and implications for structure-based drug design. *Protein Sci. 17*, 601−605.
(40) Cheung, J., Rudolph, M. J., Burshteyn, F., Cassidy, M. S., Gary, E. N., Love, J., Franklin, M. C., and Height, J. J. (2012) Structures of human acetylcholinesterase in complex with pharmacologically important ligands. *J. Med. Chem. 55*, 10282−10286.
(41) Wandhammer, M., de Koning, M., van Grol, M., Loiodice, M., Saurel, L., Noort, D., Goeldner, M., and Nachon, F. (2012) A step toward the reactivation of aged cholinesterases - Crystal structure of ligands binding to aged human butyrylcholinesterase. *Chem.-Biol. Interact.*, DOI: 10.1016/j.cbi.2012.1008.1005.
(42) Hornberg, A., Artursson, E., Warme, R., Pang, Y. P., and Ekstrom, F. (2010) Crystal structures of oxime-bound fenamiphos-acetylcholinesterases: reactivation involving flipping of the His447 ring to form a reactive Glu334-His447-oxime triad. *Biochem. Pharmacol. 79*, 507−515.
(43) Rydberg, E. H., Brumshtein, B., Greenblatt, H. M., Wong, D. M., Shaya, D., Williams, L. D., Carlier, P. R., Pang, Y. P., Silman, I., and Sussman, J. L. (2006) Complexes of alkylene-linked tacrine dimers with Torpedo californica acetylcholinesterase: Binding of Bis5-tacrine produces a dramatic rearrangement in the active-site gorge. *J. Med. Chem. 49*, 5491−5500.
(44) Xu, Y., Colletier, J. P., Weik, M., Jiang, H., Moult, J., Silman, I., and Sussman, J. L. (2008) Flexibility of aromatic residues in the active-site gorge of acetylcholinesterase: X-ray versus molecular dynamics. *Biophys. J. 95*, 2500−2511.
(45) Harel, M., Sussman, J. L., Krejci, E., Bon, S., Chanal, P., Massoulie, J., and Silman, I. (1992) Conversion of acetylcholinesterase to butyrylcholinesterase: modeling and mutagenesis. *Proc. Natl. Acad. Sci. U.S.A. 89*, 10827−10831.
(46) Ordentlich, A., Barak, D., Kronman, C., Flashner, Y., Leitner, M., Segall, Y., Ariel, N., Cohen, S., Velan, B., and Shafferman, A. (1993) Dissection of the human acetylcholinesterase active center determinants of substrate specificity. Identification of residues constituting the anionic site, the hydrophobic site, and the acyl pocket. *J. Biol. Chem. 268*, 17083−17095.
(47) Masson, P., Nachon, F., and Lockridge, O. (2010) Structural approach to the aging of phosphylated cholinesterases. *Chem.-Biol. Interact. 187*, 157−162.
(48) Nachon, F., Carletti, E., Worek, F., and Masson, P. (2010) Aging mechanism of butyrylcholinesterase inhibited by an N-methyl analogue of tabun: implications of the trigonal-bipyramidal transition state rearrangement for the phosphylation or reactivation of cholinesterases. *Chem.-Biol. Interact. 187*, 44−48.

# Mutant of *Bungarus fasciatus* acetylcholinesterase with low affinity and low hydrolase activity toward organophosphorus esters

T. Poyot*, **F. Nachon**, M-T. Froment, M. Loiodice, S. wieseler, L.M. Schopfer, O. Lockridge, P. Masson

Biochimica et Biophysica Acta 1764 (2006) 1470-1478

Available online at www.sciencedirect.com
ScienceDirect
Biochimica et Biophysica Acta 1764 (2006) 1470–1478
BIOCHIMICA ET BIOPHYSICA ACTA
BBA
www.elsevier.com/locate/bbapap

# Mutant of *Bungarus fasciatus* acetylcholinesterase with low affinity and low hydrolase activity toward organophosphorus esters

Thomas Poyot [a,*,1], Florian Nachon [a,1], Marie-Thérèse Froment [a], Mélanie Loiodice [a], Stacy Wieseler [b], Lawrence M. Schopfer [b], Oksana Lockridge [b], Patrick Masson [a]

[a] *Département de Toxicologie, Centre de Recherches du Service de Santé des Armées, BP 87, 38702 La Tronche Cedex, France*
[b] *University of Nebraska Medical Center, Eppley Institute, 986805 Nebraska Medical Center, Omaha, NE 68198-6805, USA*

Received 30 March 2006; received in revised form 27 July 2006; accepted 27 July 2006
Available online 4 August 2006

**Abstract**

Enzymes hydrolysing highly toxic organophosphate esters (OPs) are promising alternatives to pharmacological countermeasures against OPs poisoning. *Bungarus fasciatus* acetylcholinesterase (BfAChE) was engineered to acquire organophosphate hydrolase (OPase) activity by reproducing the features of the human butyrylcholinesterase G117H mutant, the first mutant designed to hydrolyse OPs. The modification consisted of a triple mutation on the $_{122}$GFYS$_{125}$ peptide segment, resulting in $_{122}$HFQT$_{125}$. This substitution introduced a nucleophilic histidine above the oxyanion hole, and made space in that region. The mutant did not show inhibition by excess acetylthiocholine up to 80 mM. The $k_{cat}/K_m$ ratio with acetylthiocholine was 4 orders of magnitude lower than that of wild-type AChE. Interestingly, due to low affinity, the G122H/Y124Q/S125T mutant was resistant to sub-millimolar concentrations of OPs. Moreover, it had hydrolysing activity with paraoxon, echothiophate, and diisopropyl phosphofluoridate (DFP). DFP was characterised as a slow-binding substrate. This mutant is the first mutant of AChE capable of hydrolysing organophosphates. However, the overall OPase efficiency was greatly decreased compared to G117H butyrylcholinesterase.


*Keywords:* Acetylcholinesterase; Organophosphate hydrolase activity; Organophosphorus inhibitors; Molecular modelling; Site-directed mutagenesis; Slow-binding inhibition

## 1. Introduction

Organophosphorus anticholinesterases (OPs) are among the most toxic compounds synthesized by man. Originally, OPs were developed for use as insecticides, but their extreme toxicity toward vertebrates has led to malicious development of certain OPs as chemical warfare agents. Though the threat of the use of OPs in warfare is diminishing, the risk of chemical terrorist attacks has greatly increased in recent years. These toxic phosphoesters have a very high potency because they react rapidly with the active-site serine of cholinesterases (ChEs). Loss of acetylcholinesterase (AChE, EC. 3.1.1.7) physiological function leads to muscle paralysis, seizures and apnea followed by death [1].

Prophylaxis of OP poisoning is based on chemical protection of AChE by carbamylation. Current emergency therapy consists of counteracting the muscarinic effects of AChE inhibition, reactivating phosphylated AChE (i.e., phosphorylated or phosphonylated), and stopping seizures. Enzymes capable of degrading OPs are now emerging as a safe and efficient alternative to pharmacological approaches. Biological scavengers, either stoichiometric or catalytic, represent potential candidates for pre-treatment, treatment and decontamination of skin, mucosa and open wounds [2–4].

Given that slow spontaneous reactivation may occur for some OP-ChE conjugates, rational design of self-reactivating

*Abbreviations:* AChE, acetylcholinesterase; ATC, acetylthiocholine; BChE, butyrylcholinesterase; BTC, butyrylthiocholine; ChE, cholinesterase; DFP, diisopropyl phosphofluoridate; DTNB, dithio-bis-nitrobenzoic acid; OP, organophosphorus; OPase, organophosphorus hydrolase; TNB, 5-thio-2-nitrobenzoic acid

* Corresponding author. Tel.: +33 4 76 63 97 44; fax: +33 4 76 63 69 62.
*E-mail address:* tpoyot@crssa.net (T. Poyot).
[1] These authors contributed equally to this work.

1570-9639/$ - see front matter © 2006 Elsevier B.V. All rights reserved.
doi:10.1016/j.bbapap.2006.07.008

ChEs was proposed. An extensive work was made on human butyrylcholinesterase (hBChE, EC. 3.1.1.8) to design and express mutants with organophosphate hydrolase (OPase) activity [5–8]. hBChE was chosen first because it reacts with a broad range of OPs. Indeed, comparative substrate specificities [9,10], molecular models and later its 3D structure [11] showed that hBChE has a larger active site pocket than AChE. The mutants of hBChE were first designed with the aim of introducing a nucleophilic residue close to the adduct phosphorus atom. Mutating Gly117 of the oxyanion hole at position 117 into a histidine (G117H) or an aspartate (G117D) confers OP hydrolase activity to the enzyme [6,8]. Similarly, the natural mutation glycine to aspartate at the equivalent position was found to provide OP hydrolase activity to *Lucilia cuprina* carboxylesterase [12]. The OPase activity of G117H hBChE is the highest among these mutants, however it is too low for therapeutic use. The G117H mutant showed hydrolysing activity against paraoxon, sarin and VX, but not soman because of rapid dealkylation of the OP adduct (aging). Hydrolysis of soman was possible by introducing an additional mutation, E197Q, to slow down dealkylation of the adduct [7]. The molecular mechanism behind G117H hBChE OPase activity is not precisely determined. It has been suggested that histidine in position 117 acts as a hydrogen-bond acceptor to activate a water molecule, which subsequently hydrolyses the adduct [8]. However, molecular modelling suggests that the imidazole of His117 and the adduct phosphorus atom are in close contact, thus not allowing enough room for a water molecule. Therefore, transfer of the phosphyl moiety to His117 followed by hydrolysis of the phosphyl-histidine may be a more likely scenario.

In the present work, we followed the same approach, introducing the nucleophile histidine at the same position in *Bungarus fasciatus* AChE in order to convert it into an organophosphate hydrolase with high efficiency. Singly substituted AChE, containing only the His mutation at position 122 (equivalent to position 117 in hBChE), had no activity with ATC. Therefore, multiple mutations were introduced.

*Bungarus fasciatus* AChE (BfAChE) was chosen because it is easily expressed at high levels in mammalian cells as a monomer [13]. Analysis of the active site using molecular modelling tools suggested that if a histidine were introduced in place of Gly122, it would distort the active site due to steric hindrance. Thus, the replacement of Tyr124 by a smaller residue was expected to avoid active site distortion. This was finally achieved by mimicking G117H hBChE, i.e., substituting the complete peptide segment $_{122}$GFYS$_{125}$ by $_{122}$HFQT$_{125}$ in BfAChE. Residue F123 is present in both peptide segments, therefore we refer to this mutant as HQT. Energy minimized models of *Bungarus fasciatus* AChE G122H/Y124Q/S125T mutant (HQT) and of human BChE G117H mutant are shown in Fig. 1. The catalytic properties of HQT BfAChE mutant toward ATC and three OPs are described. Though the OPase activity is low, the engineered enzyme is the first AChE capable of hydrolysing OPs.

## 2. Experimental

### 2.1. Chemicals

Acetylthiocholine (ATC) iodide, demeton, dithio-bis-nitrobenzoic acid (DTNB), paraoxon and buffer components of biochemical grade were purchased from Sigma (St. Louis, MO, USA). Diisopropyl phosphofluoridate (DFP) was purchased from Acros (Geel, Belgium), chlorpyrifos-oxon from CIL Cluzeau (Puteaux-La Défense, France) and echothiophate from Biobasal (Basel, Switzerland).

### 2.2. Construction and expression of the mutants

The HQT mutants were made by PCR using Pfu polymerase and cloned into the mammalian expression plasmid pGS [5–8]. Stably transfected CHO-K1 cells (American Type Culture

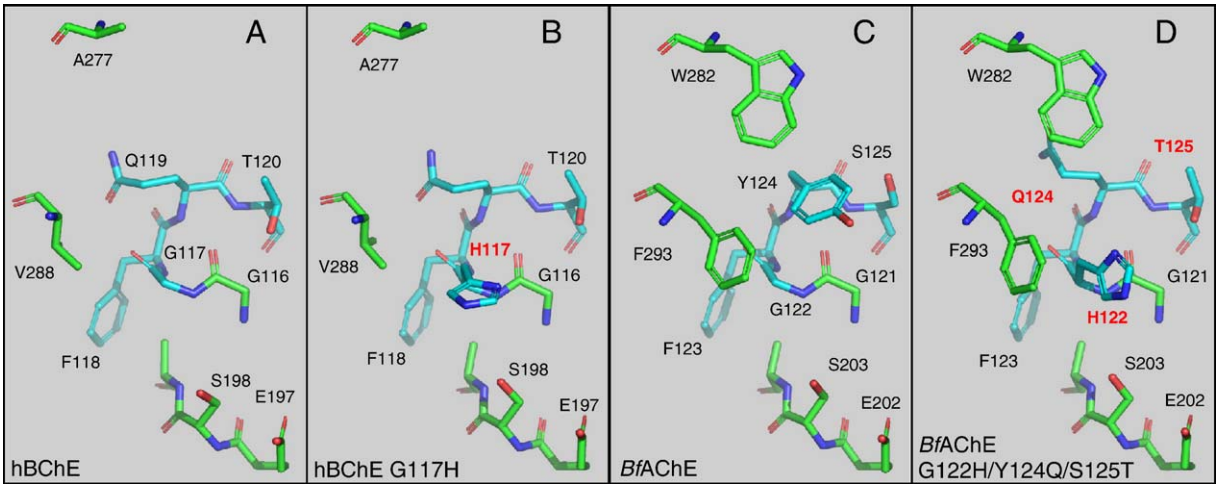


Fig. 1. Active site of hBChE (A), G117H hBChE (B), *Bungarus fasciatus* AChE (C) and G122H/Y124Q/S125T (HQT) *Bungarus fasciatus* AChE (D). Oxygen atoms are in red, nitrogen atoms are in blue and carbon atoms are in green. Ser198 (A and B) and Ser203 (C and D) are the active site serines. Ala277 and Trp282 mark the entrance to the active site gorge. The area occupied by G122H/Y124Q/S125T mutation is highlighted in blue. Mutated residues are labeled in red. (For interpretation of the references to colour in this figure legend, the reader is referred to the web version of this article.)

Collection, N° CCL61) were selected in 50 μM methionine sulfoximine. The G117H mutant of human butyrylcholinesterase was expressed in CHO cells [5,6].

### 2.3. Enzyme purification

The enzymes were purified in 2 steps. Six liters of culture medium were passed over a 200-mL sepharose-4B procainamide affinity gel column (GE Healthcare, UK). The enzymes were eluted with 300 mL 0.3 M NaCl/0.3 M tetramethylammonium bromide in 50 mM phosphate pH 7.0. The eluate was dialysed against 25 mM Tris/HCl pH 8.0 buffer to remove the salts. In a second step, 50 ml of the dialysate was chromatographed on a Mono Q ion exchange column (GE Healthcare, UK) and eluted with 0.35 M NaCl, 25 mM Tris/HCl pH 8.0.

The enzyme concentration, [E], was estimated for snake AChE from protein concentration as assayed with the bicinchoninic acid kit (Pierce) and comparison of activity and protein staining on non-denaturing gels [14]. The enzyme was estimated to be >95% pure and homogenous and it was assumed to be fully active.

The G117H mutant of human butyrylcholinesterase was purified on a procainamide affinity column, followed by ion exchange chromatography on a ProteinPak Waters Millipore HPLC column. A specific activity of 150 units/mg, as measured with 1 mM butyrylthiocholine, represented 100% pure enzyme [6].

### 2.4. Kinetics of substrate hydrolysis

Kinetic measurements were carried out using acetylthiocholine as substrate. All assays were carried out at pH 7.0, as a compromise between the optimal pH of enzyme activity and the stability of OPs in solution. All assays were made in triplicate. Hydrolysis of ATC was measured at 420 nm by the Ellman method [15] in 0.1 M sodium phosphate buffer pH 7.0 at 25 °C. Buffers were supplemented with 0.1% (w/v) bovine serum albumin as an enzyme stabilizer. The final concentration of Ellman's reagent, dithio-bis-nitrobenzoic acid (DTNB) in the cuvette was 0.35 mM.

Wild-type snake AChE displays inhibition by excess substrate with ATC [13]. This phenomenon is described by the mechanistic model of Radic [10] and its following rate equation:

$$v = \left(\frac{k_{cat}[E]}{1 + K_m/S}\right)\left(\frac{1 + b[S]/K_{ss}}{1 + [S]/K_{ss}}\right) \quad (1)$$

$K_m$ is the Michaelis constant, $k_{cat}$ the catalytic constant, [E] the enzyme active-site concentration and $K_{ss}$ the dissociation constant of the ternary SES complex. The parameter $b$ reflects the efficiency by which the ternary complex SES forms product. When $b>1$, there is substrate activation, when $b<1$, there is substrate inhibition; for an enzyme that obeys Michaelis–Menten model, $b=1$. Catalytic parameters $K_m$, $K_{ss}$ and $b$ values were calculated by nonlinear regression of Eq. (1): using the SIGMAPLOT 4.16 software (Jandel Scientific, San Rafael, CA, USA).

When the data corresponded to Michaelis–Menten behaviour, $K_m$ and $V_{max}$ were determined by simple weighted nonlinear regression of the Michaelis–Menten equation, i.e., the first part of Eq. (1) using the SIGMAPLOT 4.16 software.

For the HQT mutants, titration of active sites was not possible using a phosphorylating reagent. Therefore, enzyme concentration was estimated from protein concentration as described under enzyme purification, assuming that 100% of the catalytic sites of pure enzyme were active, $k_{cat}$ therefore represents the minimum theoretical $k_{cat}$.

### 2.5. Comparison of the hydrolysis of ATC by wild type and HQT BfAChE in presence of 100 μM organophosphate ester

Stock solution of echothiophate was 1 M in water. Stock solutions of paraoxon and DFP were respectively 1 M and 0.4 M in anhydrous MeOH. Stock solutions of demeton, and chlorpyrifos-oxon were 0.1 M in anhydrous MeOH. Hydrolysis of 1 mM ATC in 0.1 M phosphate buffer, pH 7.0 and 25 °C with 0.1% bovine serum albumin was followed at 420 nm using Ellman's method [15]. The initial rate for both wild type and HQT BfAChE was recorded for 2 min. Then 100 μM paraoxon, echothiophate, demeton, chlorpyrifos-oxon or DFP was added to the cuvette. The activity was recorded for an additional 10 min.

### 2.6. Hydrolysis of ATC by HQT BfAChE in presence of high concentration of paraoxon and echothiophate

Hydrolysis of 1 mM ATC by HQT BfAChE with 1–8 mM paraoxon or 10–200 mM echothiophate in 0.1 M phosphate buffer, pH 7.0 and 25 °C, was followed at 420 nm using Ellman's method [15]. As the product of hydrolysis of paraoxon and echothiophate could interfere with the Ellman's test, we controlled that in absence of ATC, no activity was detectable. Spontaneous hydrolysis rates of ATC were subtracted from enzyme-catalyzed rates. In a first set of experiments, the activity was monitored upon simultaneous mixing of the enzyme, substrate and organophosphate. In a second set of experiments, the enzyme was incubated for 15 min with the organophosphate prior to adding ATC and recording the activity.

### 2.7. Hydrolysis of organophosphate esters by HQT BfAChE and G117H hBChE

Hydrolysis of paraoxon, echothiophate and DFP by mutated BfAChE and G117H hBChE was carried out at 25 °C. Spontaneous hydrolysis rates of OPs were subtracted from enzyme-catalyzed rates.

Paraoxon hydrolysis was directly monitored in 0.1 M sodium phosphate buffer pH 7.0 at 400 nm, by measuring the release of its hydrolysis product, p-nitrophenol. Echothiophate iodide hydrolysis was followed in 0.1 M sodium phosphate buffer pH 7.0 in the presence of 0.35 mM DTNB, by recording the absorbance increase of 5-thio-2-benzoic acid (TNB) at 420 nm.

DFP hydrolysis was measured using an ionometer equipped with a fluoride-specific electrode (Radiometer analytical SAS, 69100 Villeurbanne, France), to follow the release of the fluoride product. In this case, 0.1 M phosphate buffer (with 0.1% bovine serum albumin) at pH 6.0 was used, in order to operate at the optimal pH of the electrode.

The concentration of stock solution of BfAChE was estimated using the bicinchoninic acid assay as described above. The concentration of G117H hBChE was calculated from its BTC activity and the $k_{cat}$ for BTC from the literature [6].

## 3. Results

### 3.1. Catalytic properties of snake mutated AChE

Table 1 shows the catalytic properties of wild-type BfAChE and HQT mutant, with acetylthiocholine as the substrate. Wild-type BfAChE showed excess substrate inhibition ($b=0.46$; $K_{ss}=36$ mM) as previously described [13,16]. By contrast, BfAChE HQT mutant displayed apparent Michaelis–Menten behaviour; no excess substrate inhibition was observed with ATC up to 80 mM. Its catalytic properties were dramatically altered. The $k_{cat}/K_m$ ratio for ATC ($0.52\times10^6$ $M^{-1}$ $min^{-1}$) was decreased by 4 orders of magnitude compared to the wild-type enzyme. This drop is mainly due to the decrease of affinity ($K_m=34\pm4$ mM instead of $0.052\pm0.003$ mM for the wild-type).

Noteworthy, when the same set of mutations was introduced into human AChE, the enzyme had also a drop of $K_m$ (8.6± 1.6 mM vs. 0.1 mM for the wild-type [17]) and lost inhibition by excess substrate. As the human AChE HQT mutant did not present better catalytic properties than BfAChE HQT mutant, it was not further studied.

### 3.2. Effects of echothiophate, paraoxon, chlorpyrifos-oxon and demeton on HQT BfAChE

We studied the effects of different classes of OPs on HQT BfAChE: insecticides (paraoxon, demeton, chlorpyrifos-oxon), glaucoma treatment (DFP, Echothiophate) (Fig. 2) Hydrolysis of 1 mM ATC by wild-type BfAChE was completely inhibited by 100 μM echothiophate, paraoxon, chlorpyrifos-oxon, DFP or demeton within seconds after mixing. On the other hand, the HQT BfAChE mutant was not inhibited under the same conditions for up to 10 min after the mixing, i.e., the mutant enzyme is resistant to OPs. It was important to further characterise the type of interaction of OPs with HQT BfAChE by increasing the concentration of OPs. We focused on 3 representative OPs: echothiophate, paraoxon and DFP.

In presence of echothiophate at concentrations in the millimolar range (10–200 mM), the rate of hydrolysis of 1 mM ATC was identical with or without 15-min preincubation of the enzyme, meaning there was no progressive inhibition. However, echothiophate behaved like an apparent competitive inhibitor with a calculated $K_i$ of $80\pm14$ mM. This result does not preclude the possibility that echothiophate is hydrolysed by HQT BfAChE mutant. Indeed, competitive inhibition is expected if echothiophate binds rapidly and reversibly to HQT BfAChE and if the hydrolysis rate of echothiophate is much slower than the hydrolysis rate of ATC.

We also investigated the effects of paraoxon on the hydrolysis of 1 mM ATC further. We observed a surprising, slight and reproducible activation of ATC hydrolysis for paraoxon in the millimolar range (Fig. 3). At 8 mM paraoxon, the rate of hydrolysis increased by 20% compared to the control. We could not investigate the effect of higher concentrations of paraoxon, because of its limited solubility in aqueous solutions (<10 mM).

### 3.3. Competition between DFP and ATC hydrolysis for BfAChE HQT mutant

To investigate the mechanism of interaction between HQT mutant and DFP, a series of measurements was initiated by adding the enzyme to mixtures of 1 mM ATC and 2–20 mM DFP. The concentration of ATC was well below the $K_m$ for HQT BfAChE (34 mM). The release of TNB was monitored at 420 nm for 20 min. Fig. 4A shows progress curves for hydrolysis of 1 mM ATC in the presence of increasing concentrations of DFP. Simple inspection of Fig. 4A revealed that the rate of ATC hydrolysis decreased slowly over the first 6 min of the time course, ultimately reaching steady state. The steady state rate decreased as DFP concentrations increased. The existence of a burst-like induction time in progress curves (from 180 s at 2 mM DFP to 50 s at 20 mM DFP) suggested that inhibition of HQT mutant by DFP obeys a slow-binding mechanism.

The induction rate constant $k$ was determined by fitting the progress curves to the following equation:

$$P = v_{ss}\cdot t + \frac{v_i - v_{ss}}{k}\cdot\left(1 - e^{-k\cdot t}\right) \quad (2)$$

Where P is the concentration of released product (thiocholine) at time $t$, $v_{ss}$ is the ultimate steady state rate at $t\rightarrow\infty$, $v_i$ is the initial rate, and $k$ is the apparent first order rate constant which describes the approach to steady state. We used GOSA, a simulated annealing based fitting software [18] (BioLog, Toulouse, France; http://www.bio-log.biz).

Table 1
Catalytic properties of wild-type and HQT mutant of *Bungarus fasciatus* AChE with acetylthiocholine as the substrate

| | $K_m$ (mM) | $k_{cat}$ ($min^{-1}$) | $\langle k_{cat}/K_m\rangle$ ($10^{-6}$ $M^{-1}$ .$min^{-1}$) | $b$ |
|---|---|---|---|---|
| Wild-type * | 0.052±0.003 | 265 000±39 700 | 5100 | 0.46 |
| HQT mutant | 34±4 | 17 600±1500 | 0.52 | 1 |

Kinetic measurements were carried out at 25 °C in 0.1 M phosphate buffer, pH 7.0.
* $k_{cat}$, $K_m$ and b values for WT BfAChE are from the literature [16].

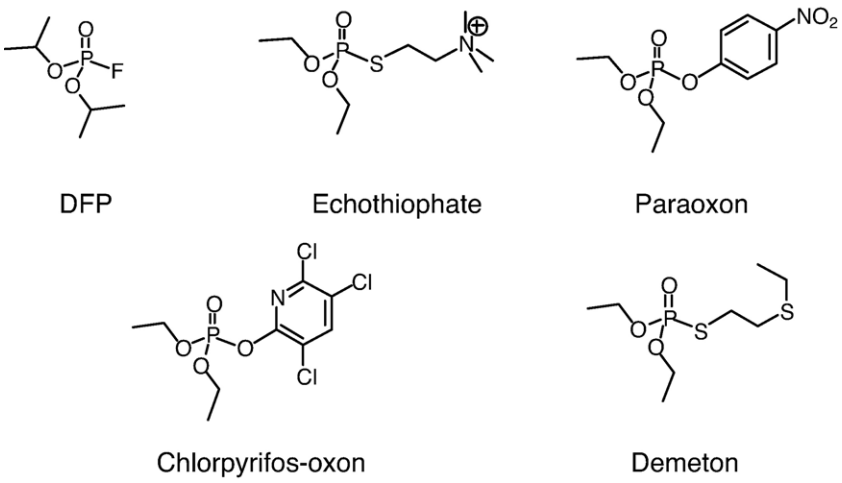


Fig. 2. Organophosphate compounds used in this study.

Three types of slow binding inhibition have been described which yield time courses of this type [19,20]. The time course for slow-binding inhibitors conforms to the general Eq. (2). The three mechanisms can be distinguished from the dependence of $k$ on inhibitor concentration. $k$ was obtained, for various concentrations of DFP, by nonlinear fitting of progress curves to Eq. (2). Fig. 4B shows an increasing hyperbolic dependence of $k$ on [DFP]. This indicates that binding of the inhibitor to the enzyme active site obeys mechanism B of slow binding inhibition (Scheme 1) [19,20].

In this mechanism, there is an initial rapid formation of an EY complex, which then undergoes a slow isomerization to EY*. Competition becomes progressively more pronounced as EY is slowly converted to EY*. Assuming that $[Y]$ and $[S] >> E_0$, then $v_i$, $v_{ss}$ and $k$ (from Eq. (2)) are given by:

$$v_i = \frac{k_2 \cdot E_0 \cdot [S]}{\left(K_m \cdot \left(1 + \frac{[Y]}{K_Y}\right) + [S]\right)} \quad (3)$$

$$v_{ss} = \frac{k_2 \cdot E_0 \cdot [S]}{\left(K_m \left(1 + [Y] \cdot \frac{K_{EY}+1}{K_Y \cdot K_{EY}}\right) + [S]\right)} = \frac{k_2 \cdot E_0 \cdot [S]}{\left(K_m \left(1 + \frac{[Y]}{K_Y + \frac{k_{-4}}{k_4 + k_{-4}}}\right) + [S]\right)} \quad (4)$$

$$k = k_4 \left(\frac{[Y]}{[Y] + K_Y\left(1 + \frac{[S]}{K_m}\right)} + K_{EY}\right) = \frac{k_4 \cdot [Y]}{[Y] + K_Y\left(1 + \frac{[S]}{K_m}\right)} + k_{-4} \quad (5)$$

With $E_0$ as the total enzyme concentration, $K_m = (k_{-1} + k_2)/k_1$, $K_Y = k_{-3}/k_3$ and $K_{EY} = k_{-4}/k_4$ (where $K_{EY} = [EY]/[EY^*]$ at the ultimate steady state). Non-linear fitting of $k$ versus [DFP] data from Fig 3A to Eq. (5) (where DFP = Y) did not yield accurate values for equilibrium constants $K_Y$ and $K_{EY}$. In order to improve the accuracy, it was necessary to use another relation linking $K_Y$ and $K_{EY}$ as a constraint to the non-linear fitting. Such relation was derived from the plot $1/v_{ss}$ versus [Y]. It should be noted that all concentrations of substrate, ATC, used in these experiments were very low relative to $K_m$ (where $K_m = 34$ mM from Table 1).

According to Eq. (4), when $1/v_{ss} = 0$ then $Y = -K_Y.K_{EY}/(1 + K_{EY})^*(1 + [S]/K_m)$, so that $K_Y.K_{EY}/(1 + K_{EY})^*(1 + [S]/K_m)$ is given by the intercept on the $x$-axis in the plot $1/v_{ss}$ versus Y. At times greater than 6 min, the reaction of HQT BfAChE, ATC and DFP reached the final steady state rate, allowing $v_{ss}$ to be measured. Simultaneous fitting of $1/v_{ss}$ versus [DFP] at 3 different ATC concentrations (1.5–3 mM) gave $K_Y.K_{EY}/(1 + K_{EY})^*(1 + [S]/K_m) = 0.44 \pm 0.02$ mM (Fig. 5). Since $[S] << K_m$, $K_Y.K_{EY}/(1 + K_{EY})^*(1 + [S]/K_m)$ reduces to $K_Y.K_{EY}/(1 + K_{EY})$. It is interesting to note that $K_Y.K_{EY}/(1 + K_{EY})$ is the apparent inhibition constant ($K_{i,app}$) for reversible inhibition of enzyme for HQT BfAChE by DFP.

A second set of experiments was performed for the purpose of obtaining a value for $K_Y.K_{EY}/(1 + K_{EY})$. The steady-state velocity, $v_{ss}$, was measured after 6-min incubation of the enzyme with various mixtures of (1.5, 2.0 and 3.0 mM) ATC and DFP (0.5, 1.0, 1.5, 2.0, 2.5 and 3.0 mM). The ATC

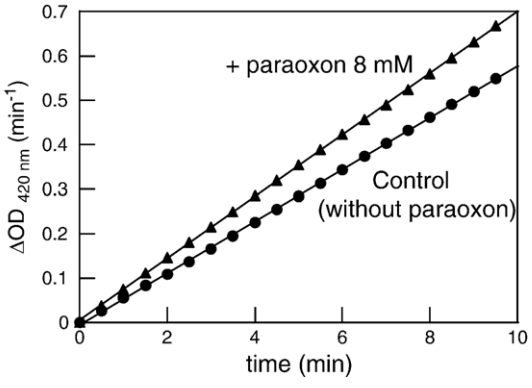


Fig. 3. Stimulatory effect of paraoxon on ATC hydrolysis by HQT BfAChE. Progress curves for the hydrolysis of 1 mM ATC in the absence and in presence of 8 mM paraoxon were monitored in 0.1 M phosphate buffer, pH 7.0, at 25 °C. Enzyme was pre-incubated with paraoxon for 15 min, and then the reaction was started by adding ATC. This assay, as other assays, was performed in triplicate; data presented here correspond to a representative assay.

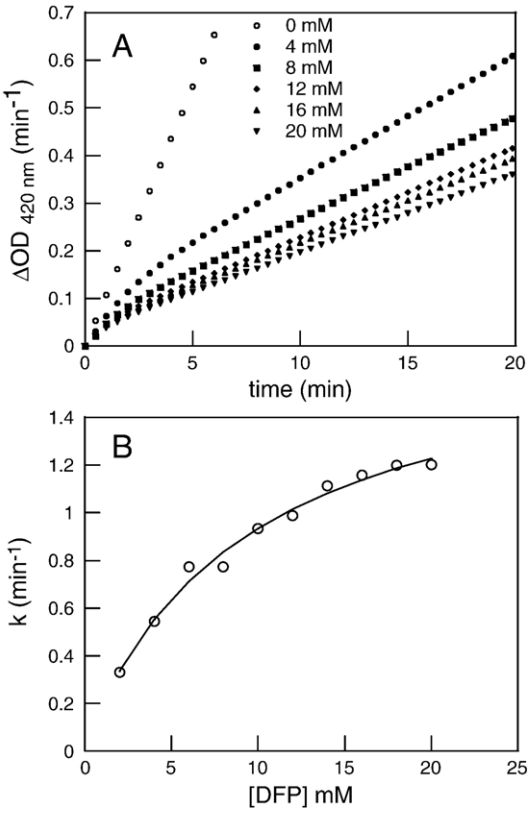


Fig. 4. Competition between DFP and ATC hydrolysis for BfAChE HQT mutant. (A) Progress curves for the hydrolysis of 1 mM ATC in the presence of various concentrations of DFP (4–20 mM), were monitored in 0.1 M phosphate buffer, pH 7.0, at 25 °C. For clarity of the figure, only a few points from the raw data are presented. (B) Apparent first order rate constant $k$ as a function of DFP concentration. The curve represents the fit of data using Eq. (5).

concentrations are low relative to $K_m$. $K_{i,app}=K_Y.K_{EY}/(1+K_{EY})$ was determined by simulated annealing fitting of the plots $1/v_{ss}$ versus [DFP] to Eq. (4). $k_4$, $K_Y$ and $K_{EY}$ were determined by simulated annealing fitting of $k$ versus [DFP] to Eq. (5) with the value of $K_Y.K_{EY}/(1+K_{EY})$ as a constraint, using GOSA.

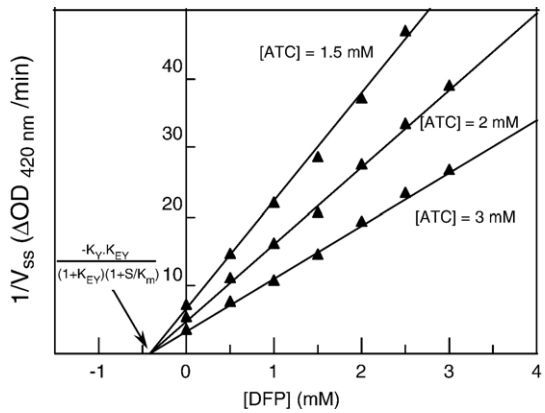


Fig. 5. Determination of $K_Y.K_{EY}/(1+K_{EY})$ from the plot $1/v_{ss}$ versus DFP. The plotted lines represent the reciprocal value of the $v_{ss}$ parameter obtained for 3 different ATC concentrations. $K_Y=k_{-3}/k_3$ is the equilibrium constant between E and EY, and $K_{EY}=k_{-4}/k_4$ is the ratio between EY and EY* at the final steady state (See Scheme 1).

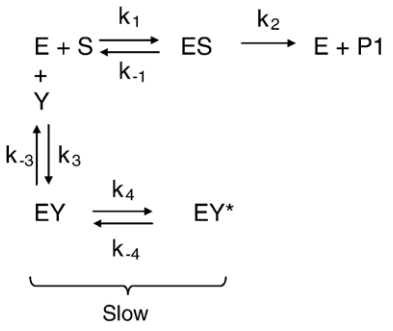


Scheme 1.

Using $K_Y.K_{EY}/(1+K_{EY})=0.44\pm0.02$ mM as a constraint, $k_4$, $K_Y$ and $K_{EY}$ were determined by non-linear fitting from Eq. (5). The values are $k_4=1.80\pm0.24$ min$^{-1}$, $K_Y=10.9\pm0.7$ mM and $K_{EY}=0.043\pm0.013$.

### 3.4. Hydrolysis of OPs by HQT Bungarus fasciatus AChE mutant

Echothiophate, paraoxon and DFP not only bind to HQT BfAChE but are slowly hydrolysed by the enzyme. However, the hydrolysis rate is so slow that the reversible binding of these compounds translates into apparent inhibition or activation. Large amounts of enzyme and long incubation times were required to study this slow hydrolysis.

We compared the catalytic efficiency of HQT BfAChE to G117H hBChE for hydrolysis of echothiophate, paraoxon and DFP. The rate of hydrolysis for each organophosphate was measured by monitoring product release, see Experimental. Table 2 presents the relative efficiency of the 2 enzymes for echothiophate, paraoxon and DFP at 1 mM. In analysing the data, the organophosphates were treated as substrates, and it was assumed that $[S]<<K_m$ for HQT BfAChE so that:

$$\frac{v}{E}=\frac{k_{cat}}{K_m}\cdot[S] \tag{6}$$

In contrast, based on values from various OPs like sarin (110 μM), VX (50 μM), paraoxon (70 μM) and echothiophate (74 μM) [6], the $K_m$ of G117H hBChE for DFP was reasonably assumed to be about 100 μM. Hence, it was assumed that $[S]>>K_m$ for G117H hBChE so that:

$$\frac{v}{E}=k_{cat} \tag{7}$$

values for $v/E$ for HQT BfAChE, together with the $[S]$ give $k_{cat}/K_m$ for HQT BfAChE. Values of $v/E$ for G117H hBChE together with the $K_m$ values for G117H, give access to $k_{cat}/K_m$ for G117H. The ratio $(k_{cat}/K_m)_{G117H}/(k_{cat}/K_m)_{HQT}$ reflects the relative efficiency of HQT BfAChE compared to the G117H mutant of hBChE. The efficiency of OP hydrolysis by G117H was higher than by HQT: 420 times for echothiophate, 90 times for paraoxon, and about 7 times for DFP. Reported $k_{cat}$ values for G117H with paraoxon and echothiophate are 0.75 min$^{-1}$, and $K_m$ values are 0.07 mM for paraoxon and 0.074 mM for echo-

Table 2
Comparison of $k_{cat}/K_m$ ratios for paraoxon, echothiophate and DFP with HQT BfAChE and G117H hBChE mutants

| | $\langle k_{cat}/K_m \rangle$ ($min^{-1}$ $M^{-1}$) | | Relative $\langle k_{cat}/K_m \rangle$ ratio $\frac{(k_{cat}/k_m)_{G117H}}{(k_{cat}/k_m)_{HQT}}$ |
|---|---|---|---|
| | G117H hBChE | HQT BfAChE | |
| Paraoxon | 5700 | 64 | 90 |
| Echothiophate | 10 100 | 24 | 420 |
| DFP | 5200 | 760 | 7 |

Kinetic measurements were carried out at 25 °C in 0.1 M phosphate buffer, pH 7.0 with paraoxon and echothiophate, and in 0.1 M phosphate buffer, pH 6.0 for DFP. Assays were performed in 3–5 times with standard deviations of 5–20%. For HQT BfAChE, it was assumed that $[S] << K_m$ so that $k_{cat}/K_m$ ratio was obtained using Eq. (6). For G117H hBChE, it was assumed that $[S] >> K_m$ so that $k_{cat}/K_m$ ratio was obtained using Eq. (7) and values taken from the literature.

thiophate [6], i.e., $k_{cat}/K_m = 10\,560$ $min^{-1}$ $M^{-1}$ for paraoxon and 10 130 $min^{-1}$ $M^{-1}$ for echothiophate. We obtained a similar value for echothiophate ($k_{cat}/K_m = 10\,100$ $min^{-1}$ $M^{-1}$). The difference between paraoxon values ($k_{cat}/K_m = 5700$ $min^{-1}$ $M^{-1}$ against 10 130 $min^{-1}$ $M^{-1}$) comes from the inaccuracy in our estimation of $k_{cat}$ (0.4 $min^{-1}$ instead of 0.75 $min^{-1}$).

## 4. Discussion

### 4.1. Catalytic properties with acetylthiocholine

The HQT BfAChE mutant's catalytic efficiency with ATC as the substrate is severely decreased compared to wild-type AChE (4 orders of magnitude for the $k_{cat}/K_m$ ratio). The magnitude of decrease is greater for its affinity (650-fold) than for its activity (15-fold). This was not the case for the G117H mutant of hBChE where the $K_m$ value for butyrylthiocholine (BTC) was only one order of magnitude lower compared to the wild-type [6]; $k_{cat}/K_m$ for BTC decreased by 11-fold for the G117H, and decreased by 110-fold for the G117H/E197Q [7]. So, the reorganized active site of the HQT BfAChE is far less efficient than the one in G117H hBChE. The decrease of $k_{cat}$ may be due to a change in the lining of the aromatic residues in the active site gorge. The aromatic residues have been described to control the optimal position of the catalytic histidine for hAChE [21]. These residues are conserved in BfAChE and the triple HQT mutation, notably Y124Q, is expected to disturb this lining.

HQT BfAChE mutant follows apparent Michaelis–Menten kinetics up to 80 mM ATC at pH 7.0. It is not inhibited by excess substrate. At physiological pH, excess cationic substrate usually causes inhibition of AChE, whereas it causes activation of BChE. Noteworthy, substrate inhibition is pH dependant [16]. The mechanistic model of Radic [10] and its rate Eq. (1) describe these particularities. At high substrate concentration a molecule of substrate binds to the peripheral site, slowing down the association and dissociation of substrate at the acylation site [22]. Rosenberry's group proposed that the changes in the binding of substrates at the acylation site is due to a steric blockade by substrate bound at the peripheral site. The crystal structure of *Torpedo californica* in presence of high concentration of acetylthiocholine recently confirmed this hypothesis [23]. No steric blockade can be achieved when substrate fully equilibrates with the active site. Given that the conformational integrity of the active site of BfAChE is affected by the triple HQT mutation resulting in low $k_{cat}/K_m$ for ATC, substrate would be expected to equilibrate and this is the reason that substrate inhibition is lost.

In contrast hBChE G117H displays the same level of activation by excess substrate ($b = 3$) as the wild-type enzyme [6]. This shows that the introduction of a histidine in hBChE's active site, does not significantly disturb association and dissociation of substrate.

### 4.2. Interaction with OPs

As a consequence of the likely disorganization of its active site architecture, HQT BfAChE binds the OPs we tested poorly and is therefore strongly resistant to inhibition by OPs. Interestingly, insect AChEs with natural mutations at the homologous glycine were reported to acquire resistance to carbamates. For example, G247S mutation in AChE (p-Ace) from *Culex pipiens* provides resistance to propoxur [24]. Because of the difference in the nature of carbamates and OPs, it is unlikely that the resistance mechanisms of HQT BfAChE and G247S *Culex pipiens* AChE are similar. In fact, our results show that HQT BfAChE is able to hydrolyse OPs. Therefore, the resistance we observed is a combination of both altered binding of the OPs and the ability to hydrolyse them.

There is a slight activation of ATC hydrolysis by HQT BfAChE at concentrations of paraoxon above 1 mM. A transient activation of human AChE with nanomolar concentration of paraoxon has also been observed by Rosenfeld and Sultatos (personal communication). The difference in effective concentration range for paraoxon could be explained by the decreased catalytic efficiency of the HQT mutant. It appears that interaction of some OPs with AChE is more complex than currently accepted. Indeed, it has been proposed that a peripheral binding site could be involved in the interactions between AChE and certain OPs such as paraoxon [25].

The HQT mutant of BfAChE is the first AChE mutant capable of hydrolysing OPs. However, its OP hydrolase activity is 1–2 orders of magnitude lower compared to G117H hBChE, depending on the OP tested. The lack of efficiency of HQT BfAChE is probably related to the alteration of the active site structure.

### 4.3. Slow-binding behaviour with DFP

Generally, equilibria between enzyme and reactants are set up rapidly, in the millisecond time scale. Kinetic measurements indicated that binding of DFP to HQT BfAChE involves a slow step. The behaviour of DFP was described by a mechanism, wherein there is an initial rapid interaction between the enzyme (E) and DFP (Y) to form an enzyme–DFP complex (EY), which then slowly isomerizes to EY*. Direct measurement of the hydrolysis of DFP using a specific fluoride electrode showed

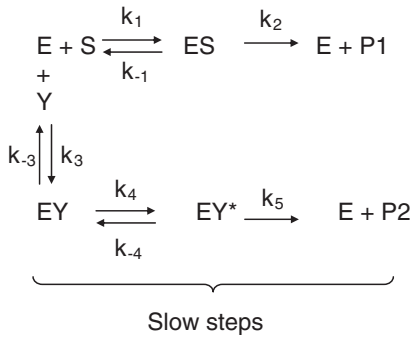


Scheme 2.

that EY* was further processed into E+P2, (P2=$F^-$). This leads to the following modification of the initial slow-binding model:

We used the assumptions ($k_1$, $k_{-1}$, $k_2$, $k_3$ and $k_{-3} >> k_4$, $k_{-4}$ and $k_5$) and the same derivation method to derive the rate equations for Scheme 2 that we used to derive the equations for Scheme 1. The resulting expression for the time dependence of product (P1) formation is actually identical to the one derived from Scheme 1 (Eq. (2)). $v_i$ is unchanged in the new model (Eq. (3)). $v_{ss}$ and $k$ are affected because the rate of disappearance of EY* becomes ($k_{-4}+k_5$) according to Scheme 2 while it was $k_{-4}$ according to Scheme 1. This makes $K_{EY}=(k_{-4}+k_5)/k_4$. However, $v_{ss}$ and $k$ remain unchanged when expressed as a function of $K_{EY}$ (Eqs. (4) and (5)).

Scheme 2 predicts that there should be a slow approach to the steady state of hydrolysis of DFP. However, due to slow equilibration of the fluoride electrode during the first 5 min of the assay, measurement of fluoride release does not allow detection of a lag in progress curve. Therefore, in Scheme 2, EY* corresponds to the phosphorylated enzyme. Phosphorylation of cholinesterases is generally considered to be irreversible, i.e. the phospho-enzyme does not return to organophosphate and enzyme. This corresponds to saying that $k_{-4}=0$. Then, it follows that the rate of disappearance of EY*, ($k_{-4}+k_5$), is reduced to $k_5$, the dephosphorylation rate constant. This change will not affect the values for $K_Y=10.9\pm2.7$ mM and $k_4=1.80\pm 0.24$ $min^{-1}$, however the product of $K_{EY}$ and $k_4$ becomes $k_5$ (instead of $k_{-4}$) the dephosphorylation rate ($k_5=0.080\pm 0.034$ $min^{-1}$).

## 5. Conclusion

This study describes the catalytic properties of a mutant of BfAChE with marginal OPase activity. This mutant was designed to reproduce the features of the first cholinesterase mutant with OPase activity, G117H hBChE. The HQT BfAChE mutant was resistant to OPs inhibition due to low affinity and presented an overall decreased catalytic and OP hydrolase efficiency compared to the G117H mutant of hBChE. Additionally, the G122H/Y124Q/S125T (HQT) mutant displayed Michaelis–Menten behaviour, i.e. it lost inhibition by excess substrate. To date, rational site-directed mutagenesis using molecular modelling of G117H-based mutants failed to generate an AChE mutant with sufficient OPase activity to be of therapeutic interest. However, a different rational approach using quantum mechanics/molecular mechanics may be more productive. This approach gave remarkable results when used to redesign hBChE to improve hydrolysis of (−)-cocaine [26]. Transition state simulations were used as the basis for the new mutant. In this study, the catalytic efficiency of hBChE for (−)-cocaine was increased by more than 400-fold, by introducing 4 mutations to stabilize the transition state of hydrolysis, as predicted by molecular dynamics. Starting from a sound mechanistic model for hydrolysis of OPs by G117H-based OPase, this approach could be used for the design of a future generation of ChE mutants. Directed evolution may also represent an alternative method for generating ChE mutants capable of hydrolysing OPs at higher rates. However, this method relies on expression of functional AChE and BChE in *E. coli*, which has yet to be achieved [27, 28].

## Acknowledgement

This work was supported by DGA/DSP/STTC contract PEA 010807 (03co010–05) to PM and OL.

## References

[1] B. Ballantyne, T.C. Marrs, Clinical and experimental toxicology of organophosphates and carbamates, Butterworth-Heinemann Publishers, Oxford, 1992.
[2] D.E. Lenz, D.M. Maxwell, I. Koplowitz, C.R. Clark, B.R. Capacio, D.M. Cerasoli, J.M. Federko, C. Luo, A. Saxena, B.P. Doctor, C. Olson, Protection against soman or VX poisoning by human butyrylcholinesterase in guinea pigs and cynomolgus monkeys, Chem. Biol. Interact. 157–158 (2005) 205–210.
[3] P. Masson, D. Josse, O. Lockridge, N. Viguié, C. Taupin, C. Buhler, Enzymes hydrolyzing organophosphates as potential scavengers against organophosphate poisoning, J. Physiol. (Paris) 92 (1998) 357–362.
[4] Y. Ashani, S. Pistinner, Estimation of the upper limit of human butyrylcholinesterase dose required for protection against organophosphate toxicity: a mathematical based toxicokinetic model, Toxicol. Sci. 77 (2004) 358–367.
[5] C.B. Millard, O. Lockridge, C.A. Broomfield, Design and expression of organophosphorus acid anhydride hydrolase activity in human butyrylcholinesterase, Biochemistry 34 (1995) 15925–15933.
[6] O. Lockridge, R.M. Blong, P. Masson, M.T. Froment, C.B. Millard, C.A. Broomfield, A single amino acid substitution, Gly117His, confers phosphotriesterase (organophosphorus acid anhydride hydrolase) activity on human butyrylcholinesterase, Biochemistry 36 (1997) 786–795.
[7] C.B. Millard, O. Lockridge, C.A. Broomfield, Organophosphorus acid anhydride hydrolase activity in human butyrylcholinesterase: synergy results in a somanase, Biochemistry 37 (1998) 237–247.
[8] L.M. Schopfer, A. Ticu Boeck, C.A. Broomfield, O. Lockridge, Mutants of human butyrylcholinesterase with organophosphate hydrolase activity; evidence that His117 is a general base catalyst for hydrolysis of echothiophate, J. Med. Chem. Def. 2 (2004) 1–21.
[9] M. Harel, J.L. Sussman, E. Krejci, S. Bon, P. Chanal, J. Massoulié, I. Silman, Conversion of acetylcholinesterase to butyrylcholinesterase: modeling and mutagenesis, Proc. Natl. Acad. Sci. U. S. A. 89 (1992) 10827–10831.
[10] Z. Radic, N.A. Pickering, D.C. Vellom, S. Camp, P. Taylor, Three distinct domains in the cholinesterase molecule confer selectivity for acetyl- and butyrylcholinesterases inhibitors, Biochemistry 34 (1993) 12074–12084.
[11] Y. Nicolet, O. Lockridge, P. Masson, J.C. Fontecilla-Camps, F. Nachon, Crystal structure of human butyrylcholinesterase and of its complexes with substrate and products, J. Biol. Chem. 278 (2003) 41141–41147.
[12] R.D. Newcomb, P.M. Campbell, D.L. Ollis, E. Cheah, R.J. Russell, J.G.

Oakeshott, A single amino acid substitution converts a carboxylesterase to an organophosphorus hydrolase and confers insecticide resistance on a blowfly, Proc. Natl. Acad. Sci. U. S. A. 94 (1997) 7464–7468.
[13] X. Cousin, S. Bon, N. Duval, J. Massoulié, C. Bon, Cloning and expression of acetylcholinesterase from *Bungarus fasciatus* venom, J. Biol. Chem. 271 (1996) 15099–15108.
[14] M.J. Karnovsky, L. Roots, A direct-coloring thiocholine method for cholinesterases, J. Histochem. Cytochem. 12 (1964) 219–221.
[15] G.L. Ellman, K.D. Courtney, V. Andres, R.M. Featherstone, A new and rapid colorimetric determination of acetylcholinesterase activity, Biochem. Pharmacol. 7 (1961) 88–95.
[16] P. Masson, L.M. Schopfer, C.F. Bartels, M.T. Froment, F. Ribes, F. Nachon, O. Lockridge, Substrate activation in acetylcholinesterase induced by low pH or mutation in the π-cation subsite, Biochim. Biophys. Acta 1594 (2002) 313–324.
[17] D. Kaplan, A. Ordentlich, D. Barak, N. Ariel, C. Kronman, B. Velan, A. Shafferman, Does "butyrylization" of acetylcholinesterase through substitution of the six divergent aromatic amino acids in the active site center generate an enzyme mimic of butyrylcholinesterase, Biochemistry 40 (2001) 7433–7445.
[18] S. Kirkpatrick, C.D. Gelatt Jr, M.P. Vecchi, Optimization by simulated annealing, Science 220 (1983) 671–680.
[19] R.G. Duggleby, P.V. Attwood, J.C. Wallace, D.B. Keech, Avidin is a slow-binding inhibitor of pyruvate carboxylase, Biochemistry 21 (1982) 3364–3370.
[20] J.F. Morrison, S.R. Stone, Approaches to the study and analysis of the inhibition of enzymes by slow- and tight-binding inhibitors, Comments Mol. Cell. Biophys. 2 (1985) 347–368.
[21] D. Kaplan, D. Barak, A. Ordentlich, C. Kronman, B. Velan, A. Shafferman, Is aromaticity essential for trapping the catalytic histidine 447 in human acetylcholinesterase, Biochemistry 43 (2004) 3129–3136.
[22] T. Szegletes, W.D. Mallender, P.J. Thomas, T.L. Rosenberry, Substrate binding to the peripheral site of acetylcholinesterase initiates enzymatic catalysis. Substrate inhibition arises as a secondary effect, Biochemistry 38 (1999) 122–133.
[23] J.-P. Colletier, D. Fournier, H.M. Greenblatt, J. Stojan, J.L. Sussman, G. Zaccai, I. Silman, M. Weik, Structural insights into substrate traffic and inhibition in acetylcholinesterase, EMBO J. 25 (2006) 2746–2756.
[24] M. Weill, G. Lutfalla, K. Mogensen, F. Chandre, A. Berthomieu, C. Berticat, N. Pasteur, A. Philips, P. Fort, M. Raymond, Insecticide resistance in mosquito vectors, Nature 423 (2003) 136–137.
[25] A.A. Kousba, L.G. Sultatos, T.S. Poet, C. Timchalk, Comparison of chlorpyrifos-oxon and paraoxon acetylcholinesterase inhibition dynamics: potential role of a peripheral binding site, Toxicol. Sci. 80 (2004) 239–248.
[26] Y. Pan, D. Gao, W. Yang, H. Cho, H.-H. Tai, C.-G. Zhan, Computational redesign of human butyrylcholinesterase for anticocaine medication, Proc. Natl. Acad. Sci. U. S. A. 102 (2005) 16656–16661.
[27] P. Masson, S. Adkins, P. Pham-Trong, O. Lockridge, Expression and refolding of functional human butyrylcholinesterase from *E. coli*, in: A. Shafferman, B. Velan (Eds.), Multidisciplinary Approaches to Cholinesterase Functions, Plenum Press, New York, 1992, pp. 49–52.
[28] M. Fischer, A. Ittah, M. Gorecki, M.M. Werber, Recombinant human acetylcholinesterase expressed in *Escherichia coli*: refolding, purification and characterization, Biotechnol. Appl. Biochem. 21 (1995) 295–311.

# X-ray crystallographic snapshots of reaction intermediates in the G117H mutant of human butyrylcholinesterase, a nerve agent target engineered into a catalytic bioscavenger

**F. Nachon***, E. Carletti, M. Wandhammer, Y. Nicolet, L.M. Schopfer, P. Masson, O. Lockridge

Biochemical Journal 434 (2011) 73-82

BJ www.biochemj.org



BJ Structure

Biochem. J. (2011) **434**, 73–82 (Printed in Great Britain) doi:10.1042/BJ20101648



# X-ray crystallographic snapshots of reaction intermediates in the G117H mutant of human butyrylcholinesterase, a nerve agent target engineered into a catalytic bioscavenger

Florian NACHON*[1], Eugenie CARLETTI*, Marielle WANDHAMMER*, Yvain NICOLET†, Lawrence M. SCHOPFER‡, Patrick MASSON*‡ and Oksana LOCKRIDGE‡

*Cellule Enzymologie, Département de Toxicologie, Institut de Recherche Biomédicale des Armées — CRSSA, 24 avenue des Maquis du Grésivaudan, 38700 La Tronche, France, †Laboratoire de Cristallogenèse et Cristallographie des Protéines, Institut de Biologie Structurale (CEA-CNRS-UJF), 41 rue Jules Horowitz, 38027 Grenoble, France, and ‡Eppley Institute and Department of Biochemistry and Molecular Biology, University of Nebraska Medical Center, Omaha, NE 68198-5950, U.S.A.

OPs (organophosphylates) exert their acute toxicity through inhibition of acetylcholinesterase, by phosphylation of the catalytic serine residue. Engineering of human butyrylcholinesterase, by substitution of a histidine residue for the glycine residue at position 117, led to the creation of OP hydrolase activity. However, the lack of structural information and poor understanding of the hydrolytic mechanism of the G117H mutant has hampered further improvements in the catalytic activity. We have solved the crystallographic structure of the G117H mutant with a variety of ligands in its active site. A sulfate anion bound to the active site suggested the positioning for an OP prior to phosphylation. A fluoride anion was found in the active site when NaF was added to the crystallization buffer. In the fluoride complex, the imidazole ring from the $His^{117}$ residue was substantially shifted, adopting a relaxed conformation probably close to that of the unliganded mutant enzyme. Additional X-ray structures were obtained from the transient covalent adducts formed upon reaction of the G117H mutant with the OPs echothiophate and VX [ethyl ({2-[bis-(propan-2-yl)amino]ethyl}sulfanyl](methyl)phosphinate]. The position of the $His^{117}$ residue shifted in response to the introduction of these adducts, overlaying the phosphylserine residue. These structural data suggest that the dephosphylation mechanism involves either a substantial conformational change of the $His^{117}$ residue or an adjacent nucleophilic substitution by water.

Key words: acetylcholinesterase, bioscavenger, butyrylcholinesterase, organophosphorus, protein engineering, spontaneous reactivation.

## INTRODUCTION

Recent progress in the understanding of enzyme catalysis, through the use of structural biology and molecular modelling, has opened a new era in protein engineering. It is now possible to develop rational strategies for modifying enzymes to confer upon them the ability to catalyse reactions for which they were not originally designed [1]. Human butyrylcholinesterase (BChE; EC 3.1.1.8) is an enzyme for which modifying its catalytic activity has been an ongoing subject of interest. This enzyme is related to acetylcholinesterase (AChE; EC 3.1.1.7), the enzyme that terminates the action of the neurotransmitter acetylcholine at postsynaptic membranes and neuromuscular junctions. BChE differs from AChE by its substrate specificity and inhibitor sensitivity [2,3]. Although BChE is present in numerous vertebrate tissues, its physiological role remains unclear [4].

Considerable interest has been shown in BChE because it hydrolyses a wide range of toxic esters, including heroin and cocaine, and because it scavenges toxic OP (organophosphylate) pesticides and nerve agents [5–7]. A lot of effort has been expended to improve its ability to hydrolyse these compounds. Redesign of its active site has improved its cocaine hydrolase activity 2000-fold, turning it into a very efficient cocaine detoxifying tool [8]. This redesign was based on hybrid QM/MM (quantum mechanical/molecular mechanical) studies aimed at finding ways to stabilize the acylation transition state of the cocaine hydrolysis reaction.

Reaction of cholinesterases with OP compounds is another area in which modification of the native cholinesterase activity has received considerable attention. This is a consequence of the irreversible inhibition of AChE (at the neuronal synapses and neuromuscular junctions) by OP compounds which leads to accumulation of acetylcholine and results in paralysis, seizures and other symptoms of cholinergic syndrome. Under extreme conditions, inhibition of AChE can lead to death [9]. Native plasma BChE works well as a stoichiometric bioscavenger because it reacts very efficiently with OP compounds, trapping them in a 1:1 complex in the bloodstream before they can reach synaptic AChE. Injection of wild-type BChE, intravenously or intramuscularly, protects animals against three to five $LD_{50}$ of the nerve agents soman [2-(fluoromethylphosphoryl)oxy-3,3-dimethylbutane], VX [ethyl ({2-[bis(propan-2-yl)amino]ethyl}-sulfanyl)(methyl)phosphinate] and tabun ethyl (*N*,*N*-dimethylphosphoramidocyanidate) [10]. BChE purified from human plasma (Baxter Healthcare) or produced in the milk of transgenic goats [11] has successfully completed clinical trials and is about to reach the market as a bioscavenger for pre-treatment against OP intoxication. A BChE dose up to 250 mg/70 kg of body weight is required to achieve efficient protection of humans following a challenge with one $LD_{50}$

Abbreviations used: AChE, acetylcholinesterase; BChE, butyrylcholinesterase; CHO, Chinese-hamster ovary; DEP, diethoxyphosphoryl; OP, organophosphylate; QM/MM, quantum mechanical/molecular mechanical; RMSD, root mean square deviation; TLS, translation libration screw-motion '.

[1] To whom correspondence should be addressed (email florian@nachon.net).

of OPs [12]. Thus a large amount of enzyme is necessary to achieve an efficient protection. This is due to the stoichiometric and irreversible nature of the reaction between the OP and BChE, and to the unfavourable OP/BChE mass ratio. Such large doses are expensive, and will prevent the widespread use of wild-type BChE as a pre-treatment. Research efforts are now devoted to circumventing this limitation by developing catalytic bioscavengers able to hydrolyse OPs [13].

Very early in the study of OP inhibition of cholinesterases, it was suggested that OP inhibitors could be considered as hemisubstrates of cholinesterases because formation of the enzyme–inhibitor complex was efficient but the dephosphylation was not. Slow dephosphylation was presumed to be a consequence of there being no amino acid groups at the appropriate positions to catalyse hydrolysis by in-line nucleophilic attack of water [14]. The idea of introducing a residue that was capable of catalysing the dephosphylation step into the active site came after. In principle, after such a modification, OPs would become full substrates for the modified cholinesterase, or, in other words, the added residue would turn the cholinesterase into an OP-hydrolase, i.e. a catalytic bioscavenger [15].

This approach proved to be qualitatively successful. BChE was shown to gain OP hydrolase activity when a histidine residue was substituted for the glycine residue at position 117 [16,17]. The G117H mutant is remarkably efficient at hydrolysing echothiophate, having a catalytic rate constant, $k_{cat}$ of 0.75 $min^{-1}$ in 0.1 M potassium phosphate, pH 7.0, at 25 °C. The G117H mutant can also hydrolyse the nerve agents sarin, VX and, additionally, soman if a second mutation (E197Q) is introduced to prevent fast aging of the conjugate [18]. Dephosphylation remains the rate-limiting step with $k_{cat}$ of $5.2 \times 10^{-3}$ $min^{-1}$ for sarin, $7.2 \times 10^{-3}$ $min^{-1}$ for VX and $77.0 \times 10^{-3}$ $min^{-1}$ for the most toxic isomer of soman ($P_SC_S$) (0.067 M phosphate buffer, pH 7.5, at 25 °C). Furthermore, it has been shown that transgenic mice expressing the G117H mutant are resistant to OP [19]. Although the G117H/E197Q mutant is generally considered to reactivate too slowly to be of general use as a catalytic bioscavenger for nerve agents, it provides an improvement over the native enzyme. Spontaneous reactivation of soman-, sarin- or VX-inhibited G117H/E197Q replenishes half of the affected enzyme in approx. 10 min [18]. This could be lifesaving in a scenario where successive exposures to these OPs occur.

To date, more than 60 BChE mutants have been made in an effort to improve the OP hydrolase activity of the original G117H mutant. It was found that G117D, G117E, L286H and several G117H-based double and triple mutants were capable of hydrolysing echothiophate [20]. However, the G117H mutant remains the most efficient by at least two orders of magnitude. One reason for this relative failure to find an improved mutant is that the dephosphylation mechanism is poorly understood. Knowledge of the structure of the active site of the G117H mutant now appears to be critical in order to understand the catalytic mechanism and to design more efficient G117H-based mutants. An indication of the pressing need for an experimentally determined structure of the active site of the G117H mutant is provided by two recent publications [21,22] in which the three-dimensional structure of the G117H BChE mutant was determined computationally. Although they are interesting, such models cannot replace an experimental structure.

In the present paper we provide the X-ray structure of the G117H mutant, the structures of the transient covalent adducts formed upon reaction of the G117H mutant with echothiophate and VX (Figure 1), and the structure of a fluoride complex that was the consequence of an attempt to create a transition-state phosphate analogue in the form of $MgF_3^-$. These crystal structures give a true picture of the active site of the G117H mutant under a variety of conditions and provide the essential information needed to perform QM/MM studies aimed at designing mutants with improved hydrolytic capabilities.

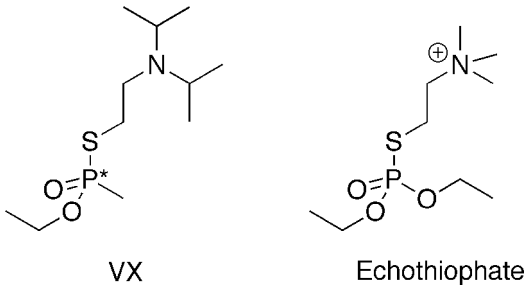


**Figure 1 Chemical structures of VX and echothiophate**

The asterisk (*) denotes a chiral centre.

## EXPERIMENTAL

### Materials

VX was obtained from the Centre DGA Maîtrise NRBC (Vert-le-Petit, France). VX is highly toxic. It belongs to schedule 1 chemicals as defined in the Chemical Weapons Convention. All work with VX is regulated by that Convention. Echothiophate [*O*-diethyl-*S*-(2-trimethylammonium ethyl)] phosphorothioate, was obtained from Biobasal. The handling of VX and echothiophate is dangerous and requires suitable personal protection, training and facilities.

### Production of the recombinant G117H mutant of human BChE, purification and crystallization

The crystallizable low-glycosylated monomeric form of human BChE was mutated into the G117H [16], produced in CHO (Chinese-hamster ovary) cells and purified under conditions similar to those described for the wild-type enzyme [23]. Crystals of the G117H mutant were prepared in five ways. First, crystals of the G117H mutant were grown in an ammonium sulfate containing mother liquor as previously reported, using the hanging-drop vapour-diffusion method, at room temperature [23]. Secondly, crystals were grown in the mother liquor plus 5 mM $MgCl_2$ and 10 mM NaF as additives. The purpose of this crystallization condition was to generate crystals wherein $MgF_3^-$ would appear as a mimic for $PO_3^-$ in the active site of the G117H mutant. Thirdly, crystals were grown in the presence of 5 mM $Al(NO_3)_3^-$ and 10 mM NaF with the purpose of generating crystals with $AlF_4^-$ in the active site, again as a mimic for $PO_3^-$. Fourthly and fifthly, crystals of the VX–G117H and echothiophate–G117H phosphylated enzyme transient adducts were prepared by flash-soaking the G117H mutant crystals for 2 min in 0.1 M Mes buffer, pH 6.5, 6 % glycerol and 2.1 M ammonium sulfate containing either 1 mM VX or 1 mM echothiophate. The crystals were then washed with a cryoprotectant solution (0.1 M Mes buffer, pH 6.5, with 2.1 M ammonium sulfate, containing 20 % glycerol) and flash-cooled in liquid nitrogen. At this stage, the VX–adduct in the crystals of VX–G117H BChE presents absolutely no danger.

### X-ray data collection and structure solution

Diffraction data for the G117H mutant (i) without additives, (ii) with $MgCl_2$ and NaF, (iii) with $Al(NO_3)_3^-$ and NaF, or (iv) after formation of the echothiophate–G117H adduct were

**Table 1 Data collection and refinement statistics**

*R*-factor = $\Sigma$ |$F_o$ − |$F_c$ / $\Sigma$ |$F_o$|, $F_o$ and $F_c$ are observed and calculated structure factors. The *R*-free set uses approx. 1000 randomly chosen reflections.

| Parameter | Value | | | |
|---|---|---|---|---|
| Ligand | Sulfate | Fluoride | Echothiophate | VX |
| PDB code | 2XMB | 2XMC | 2XMD | 2XMG |
| Data collection | | | | |
| ESRF beamline | ID14-2 | ID14-1 | ID14-2 | ID23-2 |
| Space group | *I*422 | *I*422 | *I*422 | *I*422 |
| Unit cell axes, $a = b$, $c$ (Å) | 154.8, 134.6 | 155.6, 128.0 | 154.9, 127.5 | 156.6, 128.4 |
| No. of measured reflections | 308251 | 154794 | 249541 | 166904 |
| Unique reflections | 47525 | 29897 | 33216 | 20940 |
| Resolution (Å) | 37.6−2.1 (2.4−2.1) | 41.1−2.4 (2.5−2.4) | 28.1−2.3 (2.4−2.3) | 55.5−2.7 (2.8−2.7) |
| Completeness (%) | 99.5 (99.0) | 96.7 (96.2) | 95.9 (85.4) | 94.3 (95.0) |
| $R_{sym}$ (%) | 6.1 (36.4) | 5.6 (51.0) | 4.9 (23.9) | 7.1 (56.0) |
| $I/\sigma$(I) | 21.3 (5.7) | 28.0 (3.6) | 28.9 (6.0) | 23.7 (3.8) |
| Redundancy | 6.4 (6.5) | 5.1 (4.9) | 7.5 (4.5) | 8.0 (7.4) |
| Refinement statistics | | | | |
| *R*-factor (*R*-free) | 16.8 (20.8) | 19.2 (25.2) | 17.0 (21.4) | 17.6 (25.0) |
| No. of atoms | | | | |
| Protein | 4209 | 4216 | 4226 | 4226 |
| Solvent | 380 | 229 | 285 | 151 |
| Others | 189 | 171 | 198 | 168 |
| *B*-factor (Å$^2$) | 41.7 | 46.08 | 40.08 | 56.14 |
| RMSD from ideality | | | | |
| Bond length (Å) | 0.024 | 0.021 | 0.023 | 0.018 |
| Angles (deg) | 2.182 | 2.009 | 2.090 | 1.933 |
| Chiral (Å$^3$) | 0.154 | 0.140 | 0.157 | 0.128 |

collected at the European Synchrotron Radiation Facility (ESRF, Grenoble, France), on the ID14-2 beamline using a wavelength of 0.933 Å (1 Å = 0.1 nm) and an ADSC Quantum 4 detector. Diffraction data for the VX−G117H adduct were collected at the ESRF on the ID23-2 beamline using a wavelength of 0.873 Å and a MAR-Research charge-coupled detector. All datasets were processed with XDS (http://xds.mpimf-heidelberg.mpg.de/) [24]. The structures were solved using the CCP4 suite (http://www.ccp4.ac.uk/) [25]. An initial model was determined by molecular replacement with MolRep [26], starting with the recombinant BChE structure (PDB code 1P0I) from which all ligands and glycan chains were removed. For all diffraction datasets, the model was refined as follows. An initial rigid-body refinement was made with REFMAC5 [27], which was followed by iterative cycles of model building with Coot [28]. Finally, restrained and TLS (translation libration screw-motion) refinements were carried out with REFMAC5. The bound ligands and their descriptions were built using the Dundee PRODRG2.5 server (http://davapc1.bioch.dundee.ac.uk/prodrg/), including energy minimization using GROMOS96.1 force field. Significant falls in *R*-factor and *R*-free occurred during the TLS refinement. TLS groups were defined with the help of the TLS Motion Determination server (http://skuld.bmsc.washington.edu/~tlsmd/index.html) [29]. The refined TLS parameters are included in the deposited PDB file for each entry. SA-composite omit maps were calculated using Phenix (http://www.phenix-online.org/) [30] in order to check for any bias in the model. Protein structures were displayed using the program PyMOL (DeLano Scientific; http://www.pymol.org).

## RESULTS

### Crystallographic structure of the G117H mutant without additives

Crystals were grown in the absence of any extra additives, using ammonium sulfate as a precipitant. Data were collected from tetragonal crystals of space group *I*422 and refined to 2.1 Å. The space group is identical with that formed by the wild-type enzyme. Data and refinement statistics are summarized in Table 1. The mutation does not induce any noticeable conformational change in the enzyme as shown by the marginal all-atoms RMSD (root mean square deviation) of 0.205 Å between G117H BChE and the wild-type BChE (PDB code 1P0I). In particular, the main-chain atoms of the Gly$^{117}$ residue in the wild-type enzyme and the His$^{117}$ residue in the mutant enzyme superimpose very well (RMSD = 0.225 Å).

Unexpectedly, there is a sulfate ion bound in the active site, opportunely mimicking an OP about to be attacked by the catalytic serine residue (Figure 2A). The sulfur atom of the sulfate ion is 2.8 Å from Ser$^{198}$−O$\gamma$; the O1 and S atoms of $SO_4^{2-}$ and the Ser$^{198}$−O$\gamma$ atom are colinear (175°); the distance between the O1 and Ser$^{198}$−O$\gamma$ atoms is 4.3 Å which favourably compares with the distance between the oxygens located at the apical vertices of a trigonal–bipyramidal phosphorus transition state (4.1 Å). However, the $2F_o$–$F_c$ map does not reveal any continuity of electron density between the S and Ser$^{198}$−O$\gamma$ atoms. Such continuity would have suggested a covalent bond between these atoms. The O4 atom of the $SO_4^{2-}$ is well stabilized in the oxyanion hole, being at hydrogen-bonding distance from the main-chain nitrogens of the Ala$^{199}$, Gly$^{116}$ and His$^{117}$ residues (2.9, 3.0 and 2.9 Å respectively). O3 is stabilized by a strong hydrogen bond with Ser$^{198}$−O$\gamma$ (2.6 Å) and a salt bridge with the His$^{117}$−N$\delta$1 atom (2.5 Å). A salt bridge between the O2 and the His$^{438}$−N$\varepsilon$2 atoms (2.6 Å) further stabilizes the sulfate ion. The His$^{117}$ residue adopts a conformation that is not standard (c1 = −116°, c2 = 44°) according to the penultimate rotamer library [31]. This adjustment probably results from the interaction of the His$^{117}$−N$\varepsilon$2 atom with the main-chain carbonyl oxygen of the Leu$^{286}$ residue (2.8 Å), and from a salt bridge between the His$^{117}$−N$\delta$1 atom and the O3 atom of the sulfate (2.5 Å). This conformation is probably not representative of that adopted by the His$^{117}$ residue in the absence of the sulfate ion, although it

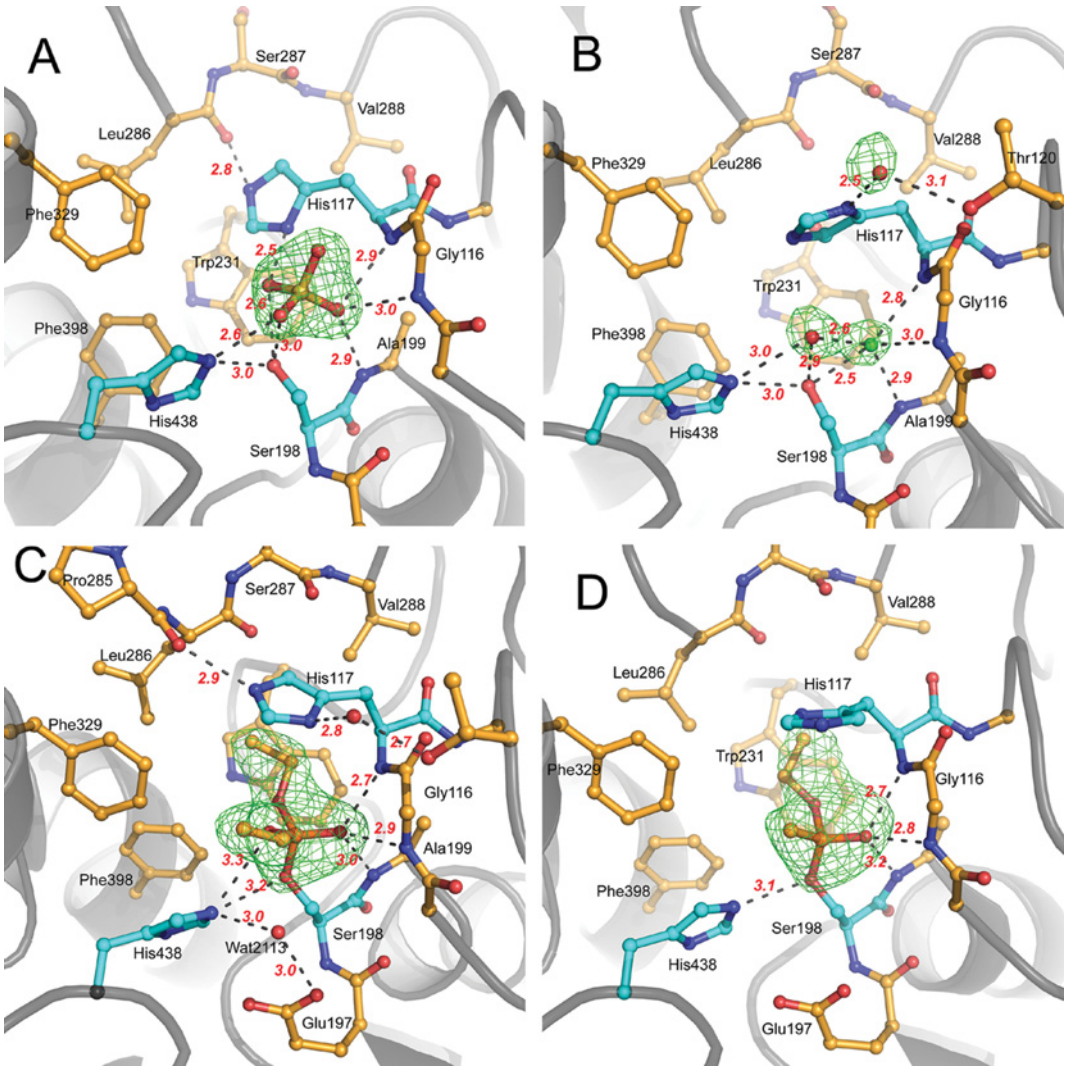


**Figure 2 The active site of G117H BChE**

(**A**) in the presence of sulfate, (**B**) in the presence of fluoride, (**C**) with diethylphosphate covalently attached to the Ser[198] residue, i.e. an echothiophate adduct and (**D**) with *O*-ethyl-methylphosphonate attached to the Ser[198] residue, i.e. a VX adduct. Active site residues are shown in the ball-and-sticks format. Carbon atoms are shown in bright orange (or cyan for key residues), nitrogen atoms in deep blue, the phosphorus atom in orange and oxygen atoms in red. Hydrogen bonds are represented by dashes. The electron density *Fo*-*Fc* omit map is represented by a green mesh contoured at 3$\sigma$.

could indicate the conformation in the OP complex just prior to phosphorylation of the Ser[198] residue.

As is often observed in the crystal structures of wild-type BChE [32–35], there is an unidentified ligand stacked against Trp[82] that we chose to model with dummy atoms. This ligand is at hydrogen-bonding distance from the O2 atom of $SO_4^{2-}$ (2.9 Å). In addition, the O1 atom is at hydrogen-bonding distance (2.5–3.0 Å) from another unidentified ligand, the electron density of which stretches between the Gln[119], His[117] and Thr[120] residues. This density was also modelled by dummy atoms.

## Crystallographic structure of the G117H mutant in complex with fluoride

Data were collected from tetragonal crystals grown in the presence of $MgCl_2$ and NaF. The original rationale for using these additives was to trap a transition-state analogue in which $MgF_3^-$ would mimic $PO_3^-$ [36]. This structure was refined to 2.4 Å resolution (see the details in Table 1).

There are two peaks of electron density in the $F_o$–$F_c$ omit maps (green mesh, 4.5 $\sigma$). Both are present at the heart of a dense hydrogen-bond network involving the oxyanion hole, the catalytic serine residue (Ser[198]) and the catalytic histidine residue (His[438]) (Figure 2B). One peak probably corresponds to a water molecule which forms one edge of a triangular hydrogen-bond network involving the Ser[198]–O$\gamma$ and His[438]–N$\varepsilon$2 atoms. The second peak corresponds to an atom that strongly interacts with both the water molecule (2.6 Å) and the Ser[198]–O$\gamma$ (2.5 Å) atom, and is at hydrogen-bonding distance from the three main-chain nitrogens of the oxyanion hole residues (Gly[116], 3.0 Å; His[117], 2.8 Å; and Ala[199], 2.9 Å). As the molecule represented by this density was able to displace the sulfate ion that was observed in the absence of NaF, and because there is a three-pronged interaction with the oxyanion hole as expected for a fluoride anion, we modelled this density as a putative fluoride ion.

This interpretation is supported by the fact that the fluoride anion is known to be a reversible inhibitor of BChE [37–39]. Although binding sites have not been identified yet, it has been reported that fluoride competes with OPs and it has been proposed that the binding involves two or more hydrogen donors necessary for enzyme catalysis [40]. Alternatively, a water molecule has been observed in a position similar to that of this putative fluoride ion for some BChE structures [41]. However, the interaction of that water with the oxyanion hole was clearly weaker, based on the distance of hydrogen donors, suggesting a two-pronged hydrogen-bond interaction.

Although the general conformation of the $His^{117}$ residue in this structure is well resolved, the orientation of the imidazole ring is not. This is because there are two peaks of electron density in the $F_o$–$F_c$ maps, one on each side of the imidazole ring, suggesting alternative interactions of the $His^{117}$–N$\delta$1 atom with two water molecules at relatively low occupancy. In the first option, the c1 and c2 angles of the $His^{117}$ residue are $-48°$ and $103°$ respectively (this is the structure shown in Figure 1B). The water molecule (peak at 4.1 $\sigma$) is at hydrogen-bonding distance from the backbone nitrogen of the $Thr^{120}$ residue (3.1 Å), and interacts strongly with the $His^{117}$–N$\delta$1 atom (2.5 Å). In the alternative refined model (position not shown in Figure 2B), the ring is simply flipped with c1 = $-46°$ and c2 = $-71°$. The water molecule (peak at 3.5 $\sigma$) is at hydrogen-bonding distance from the carbonyl oxygen of the $Leu^{286}$ residue (3.1 Å), and interacts very strongly with the $His^{117}$–N$\delta$1 atom (2.4 Å). This conformation is reasonably close to the m $-70°$ histidine conformation from the penultimate rotamer library (c1 = $-65°$ and c2 = $-70°$) [31]. We favoured the first option for the final model of the $His^{117}$ residue because it better modelled the strongest peak in the $F_o$–$F_c$ map and because it kept both water molecules in the structure. The conformation of the $His^{117}$ residue adopted in Figure 2(B) is probably representative of that found in the mutant structure in the absence of ligands.

Following the same logic we used for $MgCl_2$ and NaF as additives, we grew crystals in the presence of 5 mM $Al(NO_3)_3$ and 10 mM NaF. The idea was to trap an $AlF_4^-$-based transition-state analogue of $PO_3^-$ in the active site [42]. The crystal structure was refined to 2.4 Å resolution (results not shown). It yielded a crystal structure that was identical with that found when the crystals were grown in the presence of $MgCl_2$ and NaF. This confirmed that fluoride was the key additive leading to the observed complex.

### Crystallographic structure of echothiophate–G117H transient adduct

Data were collected from a crystal that was flash-soaked for 2 min in a solution containing 1 mM echothiophate. We chose to prepare the crystal in this way because dephosphorylation is partly rate-limiting for the hydrolysis of echothiophate (1.2 $min^{-1}$) [17]. Therefore we assumed that the phosphoryl intermediate would likely accumulate in the crystal in the presence of excess echothiophate. The structure was refined to 2.3 Å (see details in Table 1).

A strong peak of positive electronic density (11.8 $\sigma$), within covalent-bonding distance of the catalytic serine residue was seen in the initial $F_o$–$F_c$ map (Figure 1C). This is consistent with the presence of a bound DEP (diethoxyphosphoryl) moiety. The position of the DEP is similar to that which it adopts in wild-type BChE (PDB code 1XLW) [33]. The phosphorus atom is found at a covalent-bonding distance of 1.64 Å from the $Ser^{198}$–O$\gamma$ atom. The O3 atom, the phosphoryl oxygen, is at hydrogen-bonding distance from the main-chain amide nitrogens of the oxyanion hole residues with the shortest distance being to the $His^{117}$–N atom (2.7 Å). There is a very dense hydrogen-bond network involving the $His^{438}$–N$\varepsilon$2, $Ser^{198}$–O$\gamma$, DEP–O2, $Glu^{197}$–O$\varepsilon$1 atoms and water molecule 2113. Given the interatomic distances and angles, the strongest hydrogen bonds are between the $His^{438}$–N$\varepsilon$2 atom and water molecule 2113; and the $Glu^{197}$–O$\varepsilon$1 atom and water molecule 2113 (both 3.0 Å).

The water molecule 2113 is in the same position as the water molecule 101 described in the DEP conjugate with native BChE (PDB code 1XLW). This water molecule promotes 'aging', i.e. dealkylation of the nearby ethoxy group, by attacking the DEP–C3 atom [33,43]. Aging via dealkylation was proven by mass spectral analysis of the product after aging in the presence of $H_2{}^{18}O$ [33,43].

Comparing the DEP–G117H mutant with wild-type DEP–BChE, it appears that the $His^{117}$ residue side chain induces a concerted shift of DEP–C3 towards water molecule 2113 (by 1.2 Å) and water molecule 2113 towards the $Trp^{82}$ residue (by 0.7 Å). As a consequence, the distance between DEP–C3 and water molecule 2113 is only 2.9 Å in the DEP–G117H mutant compared with 3.8 Å in wild-type DEP–BChE. Thus the imidazole of the $His^{117}$ residue appears to be an obstacle to the formation of the phosphylated enzyme.

Given the preeminent role of water molecule 2113 in the dealkylation of DEP, it is expected that a shorter distance between DEP–C3 and water molecule 2113 would be more favourable for the aging reaction. This was experimentally verified. The dealkylation rate of the DEP–G117H mutant is about seven times higher than that for wild-type DEP–BChE under similar conditions [17].

The $His^{117}$ residue also induces a slight rearrangement of the second ethoxy group of DEP and its environment. The imidazole ring prevents DEP–C2 from pointing toward the $Val^{288}$ residue, and thus DEP–C2 is forced toward the $Leu^{286}$ residue. In response, the $Leu^{286}$–C$\delta$1 and $Leu^{286}$–C$\delta$2 atoms shift away by approx. 1 Å. A similar rearrangement of the $Leu^{286}$ residue was observed previously in an *N*-diethylphosphoramidyl conjugate of BChE [35].

The $His^{117}$ residue adopts a stable conformation (c1 = $-62°$; c2 = $-76°$) corresponding to m $-70°$ from the penultimate rotamer library. The imidazole ring is lying flat, above the DEP. This conformation is stabilized by a hydrogen bond between the $His^{117}$–N$\varepsilon$2 and the $Pro^{285}$–carbonyl–O atoms, and a hydrogen bond to a water molecule bridging the $His^{117}$–N$\delta$1, and $Thr^{120}$–O$\gamma$1 atoms.

The distances between the $His^{117}$ residue and the phosphorus of DEP provide some basis on which to address the mechanism of dephosphorylation for DEP–G117H. The $His^{117}$–N$\delta$1 atom is 4.6 Å from DEP–P and 3.9 Å from DEP–C3 (1.3 and 0.6 Å channel width respectively). These distances are too short to allow a water molecule to fit between the $His^{117}$ residue and the phosphorus as depicted on Scheme 1 (pathway B, 'attack is anti'). For this path to be active, a conformation change of the $His^{117}$ residue would have to occur. Alternatively, because the $His^{117}$–N$\delta$1, DEP–P and $Ser^{198}$–O$\gamma$ atoms are almost colinear (168°), a simple rotation of the imidazole ring by $-60°$ around the C$\beta$–C$\gamma$ atoms would place the N$\delta$1 atom of the $His^{117}$ residue 3.7 Å from DEP–P with the nitrogen lone pair pointing toward the phosphorus atom. This situation seems plausible for a nucleophilic attack of the $His^{117}$ residue on the phosphorus, i.e. the 'Nucleophile is $His^{117}$' path as depicted in Scheme 1 (pathway A).

### Crystallographic structure of VX–G117H transient adduct

Data were collected from a crystal that was flash-soaked for 2 min in a solution containing 1 mM VX. The reasons for preparing

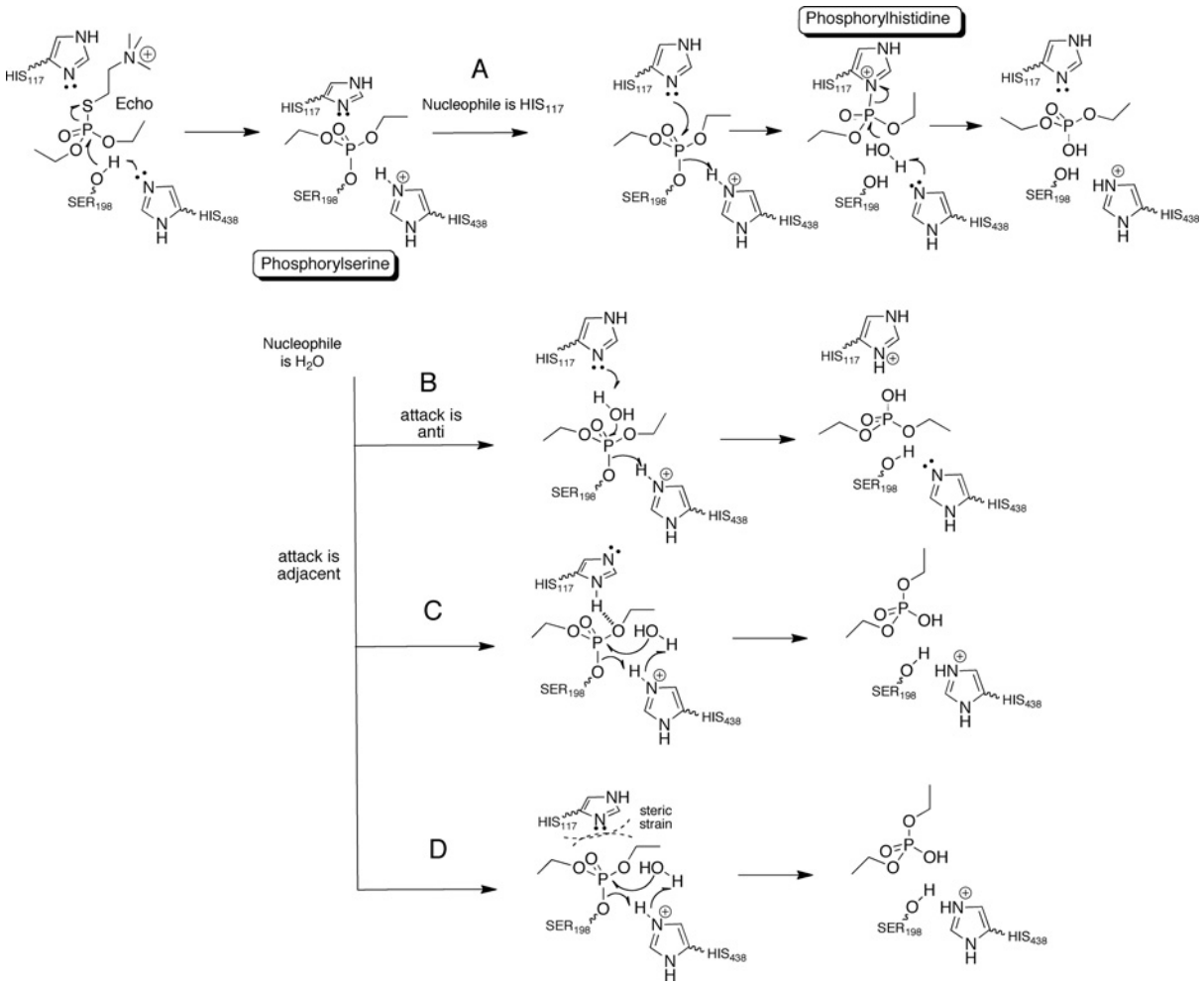


**Scheme 1 Potential mechanisms for the hydrolysis of echothiophate by the G117H mutant**

The upper pathway (**A**) involves the nucleophilic attack by the $His^{117}$ residue on the phosphorus of the adduct followed by the hydrolysis of the phosphylhistidine by a water molecule. The lower pathways involve a nucleophilic attack by a water molecule on the phosphorus of the adduct, either from a position anti (**B**) or adjacent (**C** and **D**) to the catalytic serine residue.

the crystal in this way are the same as those described in the 'Crystallographic structure of echothiophate–G117H transient adduct' section. As the dephosphonylation rate of VX–G117H is 200-fold lower than that of diethylphosphoryl–G117H, trapping the hydrolysis intermediate was expected to be less challenging. The structure was refined to 2.7 Å (see details in Table 1).

No water molecule equivalent to 2113 is present in the active site of the VX–adduct structure (Figure 2D). A peak of electron density more than 4 Å away from the $His^{438}$ and $Glu^{197}$ residues was modelled as an ammonium ion likely to be electrostatically interacting with the $Glu^{197}$ residue and the $\pi$ system of the $Trp^{82}$ residue (results not shown).

A peak in the initial $F_o$–$F_c$ map (3.7 $\sigma$) was found at a covalent-bonding distance from the $Ser^{198}$–O$\gamma$ atom (1.7 Å). The absolute configuration of the phosphorus atom is P(S). The methyl group is pointing towards the $His^{438}$ residue (Figure 2D). The ethoxy group is located in the acyl-binding pocket defined by the $Leu^{286}$, $Val^{288}$ and $Trp^{231}$ residues. This orientation is the mirror image of that observed in VX–*Tc*AChE [44], but identical with that observed in VX–BChE (results not shown).

The ethoxy group points towards the $Val^{288}$ residue and superimposes very well on the equivalent ethoxy in the wild-type DEP–BChE structure. However, this orientation is different from that just described for the DEP–G117H structure where the ethoxy group was pointing towards the $Leu^{286}$ residue. As a consequence, the shift of the $Leu^{286}$ residue that is observed in the DEP–G117H conjugate does not occur in the VX–G117H conjugate. Also, the carbonyl oxygen from the $Pro^{285}$ residue is not available for interaction with the $His^{117}$–N$\varepsilon$2 atom. This is reflected in two conformations for the $His^{117}$ residue that differ by the ring orientation, $c1 = -7°$ and $c2 = -124°$ or $c1 = -7°$ and $c2 = 57°$. These conformations are far from common histidine rotamers. This unusual conformational arrangement may be a consequence of the asymmetry of the adduct. That is, the $His^{117}$ residue imidazole ring is shifted over the methyl substituent and away from the bulkier ethoxy. In this position, it cannot be stabilized by hydrogen-bonding because it is too far from the acceptors in the acyl-binding pocket, and too close to the $Thr^{120}$ residue to let a bridging water molecule slip in. This translates into much higher residual *B*-factors for the imidazole ring atoms ($\approx$53 Å$^3$), in comparison with main-chain atoms ($\approx$38 Å$^3$). The corresponding *B*-factors are much smaller for the DEP–G117H adduct, where they are 16 Å$^3$ for the Ca atom and 10 Å$^3$ for the $His^{117}$–N$\varepsilon$2 atom. The large *B*-factors for the imidazole of

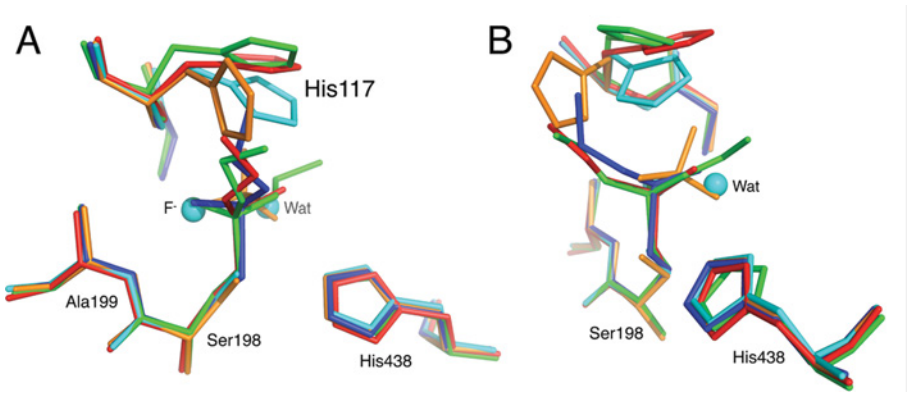


**Figure 3 Two views of the active site of butyryl-BChE**

The active site (blue; PDB code 1P0I) is superimposed on the G117H complex with sulfate (orange), fluoride (cyan), echothiophate (green) and VX (red). From the side (**A**) and front (**B**).

the $His^{117}$ residue in the VX–G117H adduct do not permit the orientation of the imidazole ring to be determined with confidence.

Much like in the DEP–G117H structure, the $His^{117}$–N$\delta$1 atom is at 4.5 Å from DEP–P and 3.8 Å from DEP–C3. These short distances would not allow a water molecule to get between the phosphorus and the $His^{117}$ residue in the absence of a large conformational change. The $His^{117}$–N$\delta$1, DEP–P and $Ser^{198}$–O$\gamma$ atoms are less colinear (157°) than in the DEP–G117H conjugate. C$\beta$ for the $His^{117}$ residue in the VX–G117H adduct is offset by 0.7 Å from its position in DEP–G117H adduct (Figure 3). Thus the maximum allowable side-chain rotation around C$\beta$–C$\gamma$ is −50°. That would partially orient the lone electron pair of the $His^{117}$–N$\delta$1 atom towards the adduct, but any further motion towards the phosphorus atom would lead to a clash between the $His^{117}$–N$\delta$1/C$\varepsilon$2 atoms and the methyl substituent of the VX. This situation is less favourable for a nucleophilic attack of the $His^{117}$ residue on the phosphorus than was the case in the DEP–G117H intermediate.

## DISCUSSION

### Impact of mutations at position 117 on the activity of BChE and related enzymes

When BChE is mutated at position 117 it loses catalytic efficiency for the hydrolysis of thio- and oxo-esters [15,16]. It was hypothesized that this loss in activity was related to a change in the orientation of the $His^{117}$ residue nitrogen proton donor of the oxyanion hole, leading to weaker transition state stabilization owing to suboptimal hydrogen-bonding [45]. We observe no such change in the X-ray structures of G117H presented in the present paper (Figure 3). Although there is some heterogeneity in the positions adopted by $His^{117}$, depending on the adduct, the positions of the critical oxyanion hole residues are unchanged.

Alternatively, loss of activity towards the normal thio- oxo-esters may be due to the imidazole ring of the $His^{117}$ residue blocking the approach of substrate and water. This suggestion is based on the fluoride–G117H structure, which we take to be representative of the unliganded resting enzyme. In this structure, the $His^{117}$ residue clutters access to the oxyanion hole (Figure 3B), and is very likely to be a steric obstruction to the formation of all substrate complexes, including the transition state. A change in the position of the $His^{117}$ residue would be necessary in order to properly orient a substrate in the oxyanion hole, but even then optimal orientation may not be achieved.

Such a conformational change is seen in the sulfate complex. If the $His^{117}$ residue were to maintain the position observed in the fluoride complex, it would collide with the sulfate oxygen that is opposite the serine. Consequently, the histidine residue is forced sideways in the sulfate complex.

Similarly, proper fitting of an OP into the active site of BChE requires a conformational change of the $His^{117}$ residue (compare Figure 2A with Figures 2C and 2D). Such steric hindrance from the $His^{117}$ residue could explain the two-to-four-orders of magnitude decrease in phosphylation rates observed for OPs reacting with G117H [46].

Loss of sensitivity to OP inhibitors in insects may be attributed to the same phenomenon. For example, a natural mutation in mosquito acetylcholinesterase G119S, a position equivalent of $Gly^{117}$ in BChE, is at the origin of their resistance to OP pesticides [47]. No OP-hydrolase activity was reported for this mutant, but resistance could arise from decreased affinity for OP. It is noteworthy of mention that no OP-hydrolase activity was observed for the equivalent BChE mutant, G117S [20]. A second example is the G137D mutant of carboxylesterase from sheep blowfly [48]. Position 137 is equivalent to position 117 in BChE and substitution an aspartate residue for the glycine residue at this position would be expected to hinder access to the oxyanion hole. The G137D mutation reduces sensitivity to OPs and confers OP-hydrolase activity on the carboxylesterase. OP-hydrolase activity was also found for the equivalent G117D mutation in BChE [20]. Finally, a triple mutation in *Bungarus fasciatus* AChE aimed at introducing a histidine into a position homologous with position 117 of BChE reduces sensitivity to OPs and turns this enzyme into an OP hydrolase [49].

### Candidate mechanisms for catalytic dephosphylation

Four different mechanisms have been proposed by previous investigators to explain why dephosphylation of G117H BChE is faster than dephosphylation of the native enzyme (Scheme 1).

#### Mechanism A

The first mechanism is based on a nucleophilic attack of the $His^{117}$ residue on the phosphorus, leading to a phosphylhistidine intermediate that is subsequently hydrolysed (Scheme 1, pathway A, the 'Nucleophile is $His^{117}$'). This mechanism was originally proposed by Fortier and colleagues on the basis of molecular mechanics calculations [50].

One argument against this mechanism is that phosphohistidines have a high-energy phosphoramidate bond and tend to transfer the phosphoryl group to other molecules [51,52]. Thus it would be expected that a phosphylhistidine would transfer its phosphyl moiety to the serine residue and not the other way around. Following this reasoning, early investigators proposed that the OP–serine adduct was formed via an intermediate OP–histidine donor rather than through a direct phosphylation by the OP [53].

Support for nucleophilic attack by the $His^{117}$ residue on the phosphorus comes from the colinearity of the $His^{117}-N\delta1$, the phosphorus and $Ser^{198}-O\gamma$ atoms in the DEP–G117H conjugate, and to a lesser extent in the VX–G117H conjugate. A 60° rotation of the imidazole ring around the $C\beta-C\gamma$ bond would orient the lone pair of electrons on the nitrogen toward the phosphorus for direct nucleophilic attack. Unfortunately, the phosphorus substituents are in close contact with the imidazole ring and these interactions would prevent a simple rotation around $C\beta-C\gamma$ bond. Rotation could occur only if the $His^{117}$ residue moved back from the phosphorus substantially. Even if the simple rotation were to occur, the imidazole would still be 3.7 Å from the phosphorus, too far for covalent interaction. Taken together, the crystal data and the thermodynamics argue that pathway A is unlikely. Proof for this mechanism would require trapping of the phosphylhistidine intermediate.

### Mechanism B

The second mechanism is a nucleophilic attack by water on the phosphorus atom, promoted by the $His^{117}$ residue. The oxygen of the attacking water would have to be positioned opposite the serine–phosphorus bond, i.e. in an apical or 'anti' position (Scheme 1, pathway B, 'attack is anti'). This mechanism formed the basis of the original rationale for the design of the G117H mutant [54]. Broomfield et al. [54] reasoned that "it might be possible to introduce a second nucleophilic centre into the active site in such a position that it could carry an activated water molecule to the face of the phosphorus moiety opposite the phosphorus–serine bond and thereby reactivate the enzyme". Newcomb et al. [48] extended this mechanism to the G137D mutant of the sheep blowfly carboxylesterase, the aspartate residue acting as a base to orient a water molecule in the appropriate position for hydrolysis. By analogy, this mechanism was also proposed for the G117D, G117E and L286H BChE mutants [20]. Finally, this mechanism was recently re-proposed by Amitay and Shurki [21] based on similarities with RNase A. The active site of RNase A contains two histidine residues, $His^{12}$ and $His^{119}$, in locations comparable with those of the $His^{117}$ and $His^{438}$ residues of BChE. The $His^{12}$ residue serves as a base to abstract a proton from the 2′-oxygen of the RNA substrate molecule, thereby activating it for attack on the phosphorus. The $His^{119}$ residue serves as an acid to protonate the oxygen of the leaving group [55].

The X-ray structures in Figures 2(C) and 2(D) show that the imidazole of the $His^{117}$ residue is in close contact with the phosphorus. In this position, the $His^{117}$ residue would not allow a water molecule to approach the phosphorus. A large conformational change of the $His^{117}$ residue would be required to make room. In addition, if one considers the sulfate–G117H complex to be a structural analogue of the dephosphylation transition state for mechanism B, then the formation of the transition state is obstructed by the ethoxy moiety in the acyl-binding pocket as seen by the superimposition of the sulfate, VX and DEP–G117H (Figure 3). Finally, the imidazole of the $His^{117}$ residue is an obstacle to the formation of the dephosphylation transition state, much like it is an obstacle to the formation of the phosphylation transition state in agreement with kinetic data [16]. These observations argue that a conformational change in the active centre would be necessary for mechanism B to occur. A partially rate-limiting conformational change in the course of forming the transition state for dephosphylation is consistent with the weak pH dependencies observed for dephosphylation [16,17]. QM/MM calculations based on the structures herein would be needed in order to determine if the change of conformation required corresponds to an energy barrier compatible with the measured dephosphylation rate.

### Mechanism C

The third mechanism, which was proposed by Millard et al. [16], derives from the suggestion of Kovach [56] that the dephosphylation rate is inversely proportional to the electron density on the phosphorus. Millard proposed that a hydrogen bond between the $His^{438}$ residue and an alkoxy ligand to the phosphorus stabilized the linkage between the phosphorus and the $Ser^{198}-O\gamma$ atom by making the $His^{438}$ residue unavailable to serve in its traditional role of transferring a proton to the $Ser^{198}$ residue. It was proposed that the $His^{117}$ residue would compete with the $His^{438}$ residue by forming a hydrogen bond with the one of the ethoxy groups, thus setting the $His^{438}$ residue free to form a hydrogen bond with a water molecule. Abstraction of a proton from that water molecule would promote attack of the water on the phosphorus atom. The structure of the VX–G117H adduct (Figure 2D) shows no hydrogen-bonding interactions for the imidazole of the $His^{117}$ residue with the ethoxy substituents. The structure of DEP–G117H (Figure 2C) shows the $His^{117}$ residue making hydrogen-bond contact with water molecules but not with the ethoxy substituent. In the DEP–G117H complex the $His^{438}$ residue is at an optimal position to transfer a proton between a water molecule and the serine residue while maintaining a hydrogen bond to an ethoxy group. These observations refute the idea that hydrogen-bonding of the $His^{438}$ residue to an ethoxy group is a critical feature of phosphylated G117H that would prevent it from acting as a base catalyst.

### Mechanism D

The structure in Figure 2(C) supports a mechanism in which a water molecule could be activated by the $His^{438}$ residue for attack on the phosphorus atom. The $His^{438}$ residue in DEP–G117H is hydrogen-bonded to a water located near the wide-open face of the DEP adduct, adjacent to the $Ser^{198}$ residue (Scheme 1, pathway C). If the $His^{438}$ residue is deprotonated then it could abstract a proton from the entering water molecule and subsequently transfer it to the serine. Alternatively, if it is protonated then it could serve as a relay in a concerted proton transfer from the water molecule to the catalytic serine residue as depicted in Scheme 1, pathway C. A similar adjacent nucleophilic substitution mechanism has been proposed in some phosphylation and aging reactions of cholinesterases [57,58].

Hydrogen-bonding of the water to the $Glu^{197}$ residue that is seen in Figure 2(C) can further stabilize the approaching water molecule. A role for the $Glu^{197}$ residue in dephosphylation is supported by the observation that there is 40-fold decrease in the dephosphorylation rate of the echothiophate–G117H/E197Q mutant [20], but a 10-fold increase in the dephosphonylation rate for VX– and sarin–G117H/E197Q mutants [18].

In mechanism D, the $His^{117}$ residue could accelerate dephosphylation by destabilizing the transient phosphylserine by

steric obstruction. Indeed, the conformation of the $His^{117}$ residue in the DEP− and methylethoxyphosphonyl−G117H transient conjugates, appears to be strained by comparison with the relaxed conformation observed in the fluoride−G117H complex (Figure 3). The imidazole ring puts a lot of strain on the phosphyl moiety and can be viewed as a molecular analogue of a loaded spring. This should result in a high-energy structure, destabilizing the adduct. The destabilizing role of the $His^{117}$ residue in the transition state would therefore be simply steric exclusion. Given this thesis, a diethylphosphoryl adduct is expected to be under greater strain than a methylethoxyphosphonyl adduct, thus explaining the higher hydrolysis rate for echothiophate than for VX. Additionally, if the $His^{117}$ residue is charged, it is expected to enhance the electrophily of the phosphorus atom by a local electrostatic effect. These effects would also be consistent with the modest pH dependence on the dephosphylation step [16,17]. All things considered, mechanism D appears to be most consistent with the X-ray data.

In summary, the structures reported in the present paper are not sufficient to definitively identify the molecular mechanism of G117H phosphyl hydrolysis; however, they do provide a basis on which to question the currently advanced possibilities. In addition, the X-ray structures of the echothiophate−G117H and VX−G117H adducts provide indispensable structural templates for future QM/MM calculations and valuable structural starting points for further explorations into the hydrolysis mechanism. The proposals provided in this discussion also may provide guidance for computational mutagenesis directed at improving the dephosphylation rates for the G117H mutant. A mutagenesis strategy based on computational design was successfully implemented to create a mutant of BChE with improved cocaine hydrolase activity [59]. Such a strategy could be applied to the design of new cholinesterases or other serine hydrolase mutants that can more efficiently reactivate from OP inhibition. Efficient catalytic bioscavengers would provide a great improvement in prophylaxis, decontamination and treatment of organophosphylate poisoning.

## AUTHOR CONTRIBUTION

Oksana Lockridge produced and purified the mutant enzyme. Florian Nachon, Eugenie Carletti and Marielle Wandhammer made the crystals, and collected and processed the diffraction data. Yvain Nicolet participated in the diffraction data collection. Florian Nachon analysed the structures. Patrick Masson, Lawrence Schopfer and Florian Nachon wrote the manuscript. Oksana Lockridge and Florian Nachon designed and planned the project.

## ACKNOWLEDGEMENT

We thank Dr S. Lushchekina (University of Lomonosov, Moscow, Russia) for fruitful discussions.

## FUNDING

This work was supported by the Agence Nationale de la Recherche [grant number ANR-06-BLAN-0163] and the Direction Generale de l' Armement [grant number DGA/PEA 08co501] to F.N.

## REFERENCES

1 Gerlt, J. A. and Babbitt, P. C. (2009) Enzyme (re)design: lessons from natural evolution and computation. Curr. Opin. Chem. Biol. **13**, 10–18
2 Harel, M., Sussman, J. L., Krejci, E., Bon, S., Chanal, P., Massoulie, J. and Silman, I. (1992) Conversion of acetylcholinesterase to butyrylcholinesterase: modeling and mutagenesis. Proc. Natl. Acad. Sci. U.S.A. **89**, 10827–10831
3 Kaplan, D., Ordentlich, A., Barak, D., Ariel, N., Kronman, C., Velan, B. and Shafferman, A. (2001) Does 'butyrylization' of acetylcholinesterase through substitution of the six divergent aromatic amino acids in the active center gorge generate an enzyme mimic of butyrylcholinesterase? Biochemistry **40**, 7433–7445
4 Li, B., Stribley, J. A., Ticu, A., Xie, W., Schopfer, L. M., Hammond, P., Brimijoin, S., Hinrichs, S. H. and Lockridge, O. (2000) Abundant tissue butyrylcholinesterase and its possible function in the acetylcholinesterase knockout mouse. J. Neurochem. **75**, 1320–1331
5 Schopfer, L. M., Furlong, C. E. and Lockridge, O. (2010) Development of diagnostics in the search for an explanation of toxic airline syndrome. Anal. Biochem. **404**, 64–74
6 Lockridge, O. and Masson, P. (2000) Pesticides and susceptible populations: people with butyrylcholinesterase genetic variants may be at risk. Neurotoxicology **21**, 113–126
7 Masson, P., Carletti, E. and Nachon, F. (2009) Structure, activities and biomedical applications of human butyrylcholinesterase. Protein Pept. Lett. **16**, 1215–1224
8 Zheng, F., Yang, W., Ko, M. C., Liu, J., Cho, H., Gao, D., Tong, M., Tai, H. H., Woods, J. H. and Zhan, C. G. (2008) Most efficient cocaine hydrolase designed by virtual screening of transition states. J. Am. Chem. Soc. **130**, 12148–12155
9 Heilbronn, E. (1993) Molecular biology of cholinesterases, a background and an introduction. In Cholinergic Function and Dysfunction. (Cuello, A. C., ed.). pp. 133−138, Elsevier, Amsterdam
10 Lenz, D. E., Broomfield, C. A., Yeung, D. T., Masson, P., Maxwell, D. M. and Cerasoli, D. M. (2007) Nerve agent bioscavengers: progress in development of a new mode of protection against organophosphorus exposure. In Chemical Warfare Agents: Chemistry, Pharmacology, Toxicology and Therapeutics (Romano, J. A., Luckey, B. J. and Salem, H., eds), pp. 145−173, CRC Press, Boca Raton
11 Huang, Y. J., Huang, Y., Baldassarre, H., Wang, B., Lazaris, A., Leduc, M., Bilodeau, A. S., Bellemare, A., Cote, M., Herskovits, P. et al. (2007) Recombinant human butyrylcholinesterase from milk of transgenic animals to protect against organophosphate poisoning. Proc. Natl. Acad. Sci. U.S.A. **104**, 13603–13608
12 Ashani, Y. and Pistinner, S. (2004) Estimation of the upper limit of human butyrylcholinesterase dose required for protection against organophosphates toxicity: a mathematically based toxicokinetic model. Toxicol. Sci. **77**, 358–367
13 Lenz, D. E., Yeung, D., Smith, J. R., Sweeney, R. E., Lumley, L. A. and Cerasoli, D. M. (2007) Stoichiometric and catalytic scavengers as protection against nerve agent toxicity: a mini review. Toxicology **233**, 31–39
14 Järv, J. (1984) Stereochemical aspects of cholinesterase catalysis. Bioorg. Chem. **12**, 259–278
15 Masson, P., Nachon, F., Broomfield, C. A., Lenz, D. E., Verdier, L., Schopfer, L. M. and Lockridge, O. (2008) A collaborative endeavor to design cholinesterase-based catalytic scavengers against toxic organophosphorus esters. Chem. Biol. Interact. **175**, 273–280
16 Millard, C. B., Lockridge, O. and Broomfield, C. A. (1995) Design and expression of organophosphorus acid anhydride hydrolase activity in human butyrylcholinesterase. Biochemistry **34**, 15925–15933
17 Lockridge, O., Blong, R. M., Masson, P., Froment, M. T., Millard, C. B. and Broomfield, C. A. (1997) A single amino acid substitution, Gly117His, confers phosphotriesterase (organophosphorus acid anhydride hydrolase) activity on human butyrylcholinesterase. Biochemistry **36**, 786–795
18 Millard, C. B., Lockridge, O. and Broomfield, C. A. (1998) Organophosphorus acid anhydride hydrolase activity in human butyrylcholinesterase: synergy results in a somanase. Biochemistry **37**, 237–247
19 Wang, Y., Boeck, A. T., Duysen, E. G., van Keuren, M., Saunders, T. L. and Lockridge, O. (2004) Resistance to organophosphorus agent toxicity in transgenic mice expressing the G117H mutant of human butyrylcholinesterase. Toxicol. Appl. Pharmacol. **196**, 356–366
20 Schopfer, L. M., Ticu-Boeck, A., Broomfield, C. A. and Lockridge, O. (2004) Mutants of human butyrylcholinesterase with organophosphate hydrolase activity; evidence that $His^{117}$ serves as a general base catalyst. J. Med. Chem. Def. **2**, 1–21
21 Amitay, M. and Shurki, A. (2009) The structure of G117H mutant of butyrylcholinesterase: nerve agents scavenger. Proteins **77**, 370–377
22 Vyas, S., Beck, J. M., Xia, S., Zhang, J. and Hadad, C. M. (2010) Butyrylcholinesterase and G116H, G116S, G117H, G117N, E197Q and G117H/E197Q mutants: a molecular dynamics study. Chem. Biol. Interact. **187**, 241–245
23 Nachon, F., Nicolet, Y., Viguie, N., Masson, P., Fontecilla-Camps, J. C. and Lockridge, O. (2002) Engineering of a monomeric and low-glycosylated form of human butyrylcholinesterase: expression, purification, characterization and crystallization. Eur. J. Biochem. **269**, 630–637
24 Kabsch, W. (2010) Xds. Acta Crystallogr. Sect. D Biol. Crystallogr. **66**, 125–132
25 Collaborative Computational Project, Number 4 (1994) The CCP4 suite: programs for protein crystallography. Acta. Crystallogr. Sect. D Biol. Crystallogr. **50**, 760–763
26 Vagin, A. and Teplyakov, A. (1997) MOLREP: an automated program for molecular replacement. J. Appl. Crystallogr. **30**, 1022–1025
27 Murshudov, G. N., Vagin, A. A. and Dodson, E. J. (1997) Refinement of macromolecular structures by the maximum-likelihood method. Acta Crystallogr. Sect. D Biol. Crystallogr. **53**, 240–255

28 Emsley, P. and Cowtan, K. (2004) Coot: model-building tools for molecular graphics. Acta Crystallogr. Sect. D Biol. Crystallogr. **60**, 2126–2132
29 Painter, J. and Merritt, E. A. (2006) Optimal description of a protein structure in terms of multiple groups undergoing TLS motion. Acta Crystallogr. Sect. D Biol. Crystallogr. **62**, 439–450
30 Adams, P. D., Afonine, P. V., Bunkoczi, G., Chen, V. B., Davis, I. W., Echols, N., Headd, J. J., Hung, L. W., Kapral, G. J., Grosse-Kunstleve, R. W. et al. (2010) PHENIX: a comprehensive Python-based system for macromolecular structure solution. Acta Crystallogr. Sect. D Biol. Crystallogr. **66**, 213–221
31 Lovell, S. C., Word, J. M., Richardson, J. S. and Richardson, D. C. (2000) The penultimate rotamer library. Proteins **40**, 389–408
32 Nicolet, Y., Lockridge, O., Masson, P., Fontecilla-Camps, J. C. and Nachon, F. (2003) Crystal structure of human butyrylcholinesterase and of its complexes with substrate and products. J. Biol. Chem. **278**, 41141–41147
33 Nachon, F., Asojo, O. A., Borgstahl, G. E., Masson, P. and Lockridge, O. (2005) Role of water in aging of human butyrylcholinesterase inhibited by echothiophate: the crystal structure suggests two alternative mechanisms of aging. Biochemistry **44**, 1154–1162
34 Carletti, E., Li, H., Li, B., Ekstrom, F., Nicolet, Y., Loiodice, M., Gillon, E., Froment, M. T., Lockridge, O., Schopfer, L.M et al. (2008) Aging of cholinesterases phosphylated by tabun proceeds through O-dealkylation. J. Am. Chem. Soc. **130**, 16011–16020
35 Carletti, E., Aurbek, N., Gillon, E., Loiodice, M., Nicolet, Y., Fontecilla-Camps, J. C., Masson, P., Thiermann, H., Nachon, F. and Worek, F. (2009) Structure-activity analysis of aging and reactivation of human butyrylcholinesterase inhibited by analogues of tabun. Biochem. J. **421**, 97–106
36 Baxter, N. J., Olguin, L. F., Golicnik, M., Feng, G., Hounslow, A. M., Bermel, W., Blackburn, G. M., Hollfelder, F., Waltho, J. P. and Williams, N. H. (2006) A Trojan horse transition state analogue generated by $MgF_3^-$ formation in an enzyme active site. Proc. Natl. Acad. Sci. U.S.A. **103**, 14732–14737
37 Cimasoni, G. (1966) Inhibition of cholinesterases by fluoride *in vitro*. Biochem. J. **99**, 133–137
38 Page, J. D., Wilson, I. B. and Silman, I. (1985) Butyrylcholinesterase: inhibition by arsenite, fluoride, and other ligands, cooperativity in binding. Mol. Pharmacol. **27**, 437–443
39 Masson, P., Adkins, S., Gouet, P. and Lockridge, O. (1993) Recombinant human butyrylcholinesterase G390V, the fluoride-2 variant, expressed in Chinese-hamster ovary cells, is a low affinity variant. J. Biol. Chem. **268**, 14329–14341
40 Ashani, Y., Segev, O. and Balan, A. (2004) The effect of fluoride on the scavenging of organophosphates by human butyrylcholinesterase in buffer solutions and human plasma. Toxicol. Appl. Pharmacol. **194**, 90–99
41 Ngamelue, M. N., Homma, K., Lockridge, O. and Asojo, O. A. (2007) Crystallization and X-ray structure of full-length recombinant human butyrylcholinesterase. Acta Crystallogr. Sect. F Struct. Biol. Cryst. Commun. **63**, 723–727
42 Xu, Y. W., Morera, S., Janin, J. and Cherfils, J. (1997) $AlF_3$ mimics the transition state of protein phosphorylation in the crystal structure of nucleoside diphosphate kinase and MgADP. Proc. Natl. Acad. Sci. U.S.A. **94**, 3579–3583
43 Li, H., Schopfer, L. M., Nachon, F., Froment, M. T., Masson, P. and Lockridge, O. (2007) Aging pathways for organophosphate-inhibited human butyrylcholinesterase, including novel pathways for isomalathion, resolved by mass spectrometry. Toxicol. Sci. **100**, 136–145
44 Millard, C. B., Koellner, G., Ordentlich, A., Shafferman, A., Silman, I. and Sussman, J. L. (1999) Reaction products of acetylcholinesterase and VX reveal a mobile histidine in the catalytic triad. J. Am. Chem. Soc. **121**, 9883–9884
45 Masson, P., Froment, M. T., Gillon, E., Nachon, F., Lockridge, O. and Schopfer, L. M. (2007) Hydrolysis of oxo- and thio-esters by human butyrylcholinesterase. Biochim. Biophys. Acta **1774**, 16–34
46 Broomfield, C. A., Lockridge, O. and Millard, C. B. (1999) Protein engineering of a human enzyme that hydrolyzes V and G nerve agents: design, construction and characterization. Chem. Biol. Interact. **119**–**120**, 413–418
47 Weill, M., Lutfalla, G., Mogensen, K., Chandre, F., Berthomieu, A., Berticat, C., Pasteur, N., Philips, A., Fort, P. and Raymond, M. (2003) Comparative genomics: insecticide resistance in mosquito vectors. Nature **423**, 136–137
48 Newcomb, R. D., Campbell, P. M., Ollis, D. L., Cheah, E., Russell, R. J. and Oakeshott, J. G. (1997) A single amino acid substitution converts a carboxylesterase to an organophosphorus hydrolase and confers insecticide resistance on a blowfly. Proc. Natl. Acad. Sci. U.S.A. **94**, 7464–7468
49 Poyot, T., Nachon, F., Froment, M. T., Loiodice, M., Wieseler, S., Schopfer, L. M., Lockridge, O. and Masson, P. (2006) Mutant of *Bungarus fasciatus* acetylcholinesterase with low affinity and low hydrolase activity toward organophosphorus esters. Biochim. Biophys. Acta **1764**, 1470–1478
50 Albaret, C., Masson, P., Broomfield, C. A., El Kaim, L. and Fortier, P. L. (1998) Mechanical aspects of the phosphotriesterase activity of human butyrylcholinesterase G117H mutant. In Structure and Function of Cholinesterases and Related Proteins (Doctor, B. P., ed.), pp. 399–405, Plenum Press, New York
51 Stock, J. B., Stock, A. M. and Mottonen, J. M. (1990) Signal transduction in bacteria. Nature **344**, 395–400
52 Attwood, P. V., Piggott, M. J., Zu, X. L. and Besant, P. G. (2007) Focus on phosphohistidine. Amino Acids **32**, 145–156
53 Hobbiger, F. (1955) Effect of nicotinhydroxamic acid methiodide on human plasma cholinesterase inhibited by organophosphates containing a dialkylphosphato group. Br. J. Pharmacol. Chemother. **10**, 356–362
54 Broomfield, C. A., Millard, C. B., Lockridge, O. and Caviston, T. L. (1995) Mutation of human butyryl cholinesterase glycine 117 to histidine preserves activity but confers resistance to organophosphorus inhibitors. In Enzymes of the Cholinesterase Family (Quinn, D. M., Balasubramanian, A. S., Doctor, B. P. and Taylor, P., eds), pp. 169–175, Plenum Press, New York
55 Raines, R. T. (1998) Ribonuclease A. Chem. Rev. **98**, 1045–1066
56 Kovach, I. M. (1988) Structure and dynamics of serine hydrolase–organophosphate adducts. J. Enzyme Inhib. **2**, 199–208
57 Kwasnieski, O., Verdier, L., Malacria, M. and Derat, E. (2009) Fixation of the two Tabun isomers in acetylcholinesterase: a QM/MM study. J. Phys. Chem. B **113**, 10001–10007
58 Nachon, F., Carletti, E., Worek, F. and Masson, P. (2010) Aging mechanism of butyrylcholinesterase inhibited by an *N*-methyl analogue of tabun: implications of the trigonal-bipyramidal transition state rearrangement for the phosphylation or reactivation of cholinesterases. Chem. Biol. Interact. **187**, 44–48
59 Zhan, C. G., Zheng, F. and Landry, D. W. (2003) Fundamental reaction mechanism for cocaine hydrolysis in human butyrylcholinesterase. J. Am. Chem. Soc. **125**, 2462–2474


Received 7 October 2010/15 November 2010; accepted 19 November 2010
Published as BJ Immediate Publication 19 November 2010, doi:10.1042/BJ20101648

# Применение суперкомпьютеров для установления механизмов биохимических реакций

## (Application des superordinateurs à l'étude des mécanismes biochimiques)

С.В. Лущекина, П. Массон, **Ф. Нашон**, Б.Л. Григоренко, А.В. Немухин, С.Д. Варфоломеев

Dans "Суперкомпьютерные технологии в науке, образовании и промышленности" Editeurs В.А. Садовничего et Г.И. Савина, Académie des Sciences de Russis (2010) 70-75

Московский государственный университет
имени М.В. Ломоносова
Суперкомпьютерный консорциум университетов России
Российская академия наук

# Суперкомпьютерные технологии в науке, образовании и промышленности

Под редакцией
академика В.А. Садовничего
академика Г.И. Савина
чл.-корр. РАН Вл.В. Воеводина

материалы серии
«Современные суперкомпьютерные технологии в фундаментальных и прикладных исследованиях»

книга издана в рамках проекта
«Создание системы подготовки высококвалифицированных кадров
в области суперкомпьютерных технологий и специализированного программного обеспечения»
комиссии Президента по модернизации и технологическому развитию экономики России


Издательство Московского университета

Москва
2010

# Применение суперкомпьютеров для установления механизмов биохимических реакций

# 10 Применение суперкомпьютеров для установления механизмов биохимических реакций

Развитие высокопроизводительных вычислений позволяет использовать методы квантовой химии для установления механизмов ферментативных реакций и исследования влияния на них направленных мутаций, что необходимо для создания лекарственных средств на основе ферментов с заданными каталитическими свойствами. В статье описывается проект по моделированию реакций гидролиза фосфорорганических соединений в активном сайте бутирилхолинэсетразы и ее модификаций.

## АВТОРЫ:

***С.В. Лущекина*** – мл. науч. сотрудник, Ин-т биохимической физики им. Н.М. Эмануэля РАН;
*e-mail: sofya.lushchekina@gmail.com*
***П. Массон*** – академик, профессор, Ин-т биомедицинских исследований МО, ЛаТронш–Гренобль, Франция, Ин-т структурной биологии, Гренобль, Франция, Медицинский центр Университета Небраски, г. Омаха, США (Patrick Masson — Département de Toxicologie, Institut de Recherche Biomédicale des Armées – CRSSA, La Tronche–Grenoble, France, Institut de Biologie Structurale, Grenoble, France, University of Nebraska Medical Center, Omaha, USA);
*e-mail: pmasson@unmc.edu*
***Ф. Нашон*** – Ph.D., Ин-т биомедицинских исследований МО, ЛаТронш–Гренобль, Франция (Florian Nachon — Département de Toxicologie, Institut de Recherche Biomédicale des Armées – CRSSA, La Tronche–Grenoble, France);
*e-mail: florian@nachon.net*
***Б.Л. Григоренко*** – докт. физ.-мат. наук, ст. науч. сотрудник, Химический ф-тет МГУ им. М.В. Ломоносова;
*e-mail: bell_grig@yahoo.com*
***А.В. Немухин*** – докт. хим. наук, профессор, зав. лаб., Химический ф-тет МГУ им. М.В. Ломоносова, Институт биохимической физики им. Н.М. Эмануэля РАН;
*e-mail: anemukhin@yahoo.com*
***С.Д. Варфоломеев*** – член.-кор., докт. хим. наук, профессор, директор Ин-та биохимической физики им. Н.М. Эмануэля РАН, зав. каф. химической энзимологии, Химический ф-тет МГУ им. М.В. Ломоносова;
*e-mail: sdvarf@sky.chph.ras.ru*

Для эффективного решения задач медицины, фармацевтики и биотехнологии необходимы представления о механизмах реакций ферментативного катализа, что предполагает знание элементарных стадий химических превращений в активных центрах белков. Экспериментальные приемы включают исследования структуры белков и их комплексов с аналогами субстратов с использованием методов рентгеноструктурного анализа и ядерно-магнитного резонанса. Закономерности протекания ферментативных реакций изучаются методами химической кинетики. Существенную поддержку этим исследованиям оказывают методы генной инженерии.

В настоящее время становится возможным проводить анализ элементарных стадий ферментативных реакций и обосновывать механизмы, предлагаемые в экспериментальных исследованиях, с привлечением методов квантовой механики. Ведущую роль в этом процессе играют суперкомпьютерные технологии, их последовательное развитие позволяет включать в расчет все большее число атомов, охватывая целиком макромолекулы, что является критичным для описания реакций ферментативного катализа.

Особо важным представляется применение суперкомпьютеров для моделирования реакций, механизм которых экспериментально недостаточно изучен, и для прогнозирования модификаций с желаемыми терапевтическими свойствами. Ярким примером такого рода задач является задача установления механизма реакций гидролиза в активном сайте холинэстераз и разработка на их основе детоксирующих агентов.

Ацетилхолинэстераза (АХЭ) является одним из ключевых ферментов центральной нервной системы. Его инактивация приводит к тяжелым последствиям, таким, как судороги, паралич и пр., вплоть до летального исхода. Основными агентами, блокирующими работу АХЭ, являются фосфорорганические соединения (ФОС), которые связываются с ней ковалентно и необратимо. Соединения этого типа широко используются в качестве пестицидов, также некоторые из них являются лекарственными и отравляющими веществами, и задача профилактики отравления ФОС стоит в настоящее время достаточно остро.

Бутирилхолинэстераза (БХЭ) является ферментом, близким по структуре к ацетилхолинэстеразе, ее физиологическая роль в организме до конца не ясна. БХЭ также необратимо связывается с ФОС (см. рис. 1), но поскольку это не приводит к заметным последствиям для организма, БХЭ выступает как стехиометрическая ловушка, ковалентно связывая в соотношении 1:1 часть ядовитых молекул ФОС в плазме крови до того, как они достигают нервной системы и находящейся в ней АХЭ.

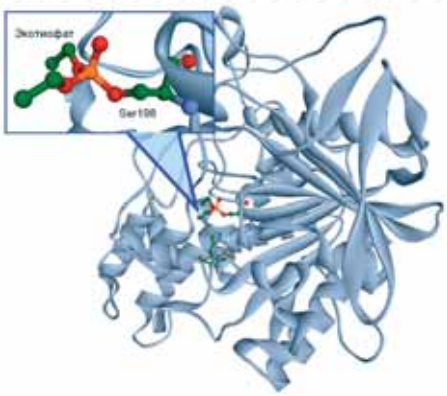


**Рис. 1.**
Структура бутирилхолинэстеразы, ковалентно связанной с молекулой экотиофата. Выделен конъюгат аминокислотного остатка каталитической триады Ser198 с ингибитором

В связи с этим начато использование нативной БХЭ для профилактики отравлений ФОС. Основной недостаток этого метода заключается в том, что для достижения терапевтического эффекта необходимо введение значительных доз БХЭ, что дорого и затрудняет его использование. Поэтому в настоящее время значительные усилия направлены на разработку каталитических ловушек, способных гидролизовать ФОС достаточно быстро, чтобы доза вводимого препарата была относительно невелика для практического применения.

Одним из направлений таких исследований является поиск модификаций БХЭ, способных к спонтанной реактивации комплекса с ФОС, сопровождающейся его гидролизом. Относительным успехом на этом пути явилось создание модификации Gly117His, способной гидролизовать ряд ФОС, но с довольно низкой скоростью, что не позволяет использовать его в клинической практике. Механизм гидролиза, который обеспечивает мутация Gly117His, до сих пор неизвестен. Объяснение роли этой мутации в гидролизе ФОС является необходимым шагом для создания более эффективных модификаций фермента, способных расщеплять ФОС с более высокой скоростью.

Основным подходом для решения задач такого типа является построение энергетического профиля на поверхности потенциальной энергии для всех этапов реакции гидролиза вдоль координаты реакции — от исходного состояния (в данном случае — ингибированного фермента) через интермедиаты и промежуточные состояния к продуктам реакции — свободному ферменту и фрагментам ФОС. Сравнение энергетических профилей для нативного и модифицированного фермента укажет на природу каталитической активности.

Отправной точкой молекулярного моделирования, во многом определяющей надежность его результатов, является исходная структура биологического объекта. В Институте биомедицинских исследований МО, ЛаТронш—Гренобль, Франция была получена кристаллографическая структура БХЭ с мутацией Gly117His ковалентно связанной с экотиофатом (рис. 1) — препаратом, исполь-

**Рис. 2.**
Наложение кристаллографических структур нативной (зеленый) и модифицированной (синий) бутирилхолинэстераз

зуемым в офтальмологии для лечения глаукомы [Nachon F. et al., 2011]. Трехмерные координаты атомов белка, введенного аминокислотного остатка His117 и ингибитора описывают структуру комплекса и служат для построения исходной системы для квантово-химических расчетов.

Анализ полученной структуры показывает, что данная мутация не сказывается на конформации белка в целом (рис. 2), поэтому ключевую роль в процессе гидролиза играют изменения в энергетических характеристиках элементарных стадий реакции гидролиза.

В ситуации, когда механизм моделируемой реакции неизвестен, необходимо рассматривать разнообразные варианты прохождения элементарных стадий и выбирать среди них наиболее энергетически выгодные. Помимо изучения различных координат реакций, крайне важно учитывать влияния строения активного центра, которое крайне редко бывает однозначным. В первую очередь, экспериментальные данные как правило не предоставляют информацию о зарядовом состоянии ионогенных аминокислот, таких как гистидин, который имеет два сайта протонирования. При моделировании реакций гидролиза решающее значение имеет аккуратное рассмотрение сети водородных связей и учет различных вариантов ориентации молекулы воды. Кроме того, известно, что в комплексах холинэстераз с ФОС протекают конкурирующие реакции, также требующие рассмотрения и сравнения с предлагаемым механизмом. Это вызывает значительные вычислительные трудности, поскольку установление механизма реакции требует построения многочисленных энергетических профилей, каждый из которых требует серьезных вычислительных затрат. Развитие высокопроизводительных вычислений позволяет рассматривать не только большие биологические системы, но исследовать влияние различных факторов на характеристики реакции. Решение данной конкретной задачи установления механизма гидролиза ФОС модифицированной бутирилхолинэстеразой и выявление факторов, стало возможно благодаря использованию суперкомпьютеров «Чебышев» и «Ломоносов» НИВЦ МГУ.

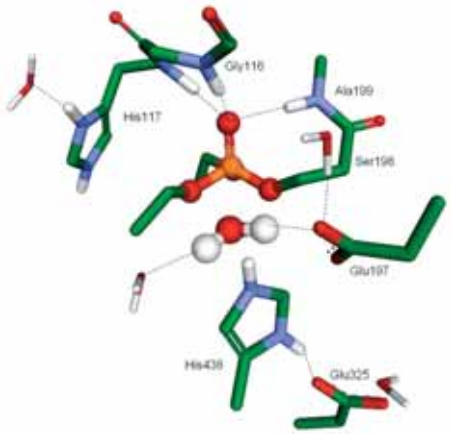


**Рис. 3.**
Активный сайт Gly117His БХЭ в комплексе с экотифатом. Показаны ключевые фрагменты аминокислотных остатков активного сайта. Пунктирными линиями показаны водородные связи

В ходе работы было установлено, что при протонировании введенного в ходе мутации остатка His117 образующийся положительный заряд на имидазольном кольце стабилизирует интермедиат и отрицательно заряженный продукт гидролиза (рис. 4), существенно снижая энергетический барьер реакции по сравнению с нативным ферментом, и делая возможным гидролиз ФОС. Полученные данные позволяют предложить методы ускорения этой реакции.

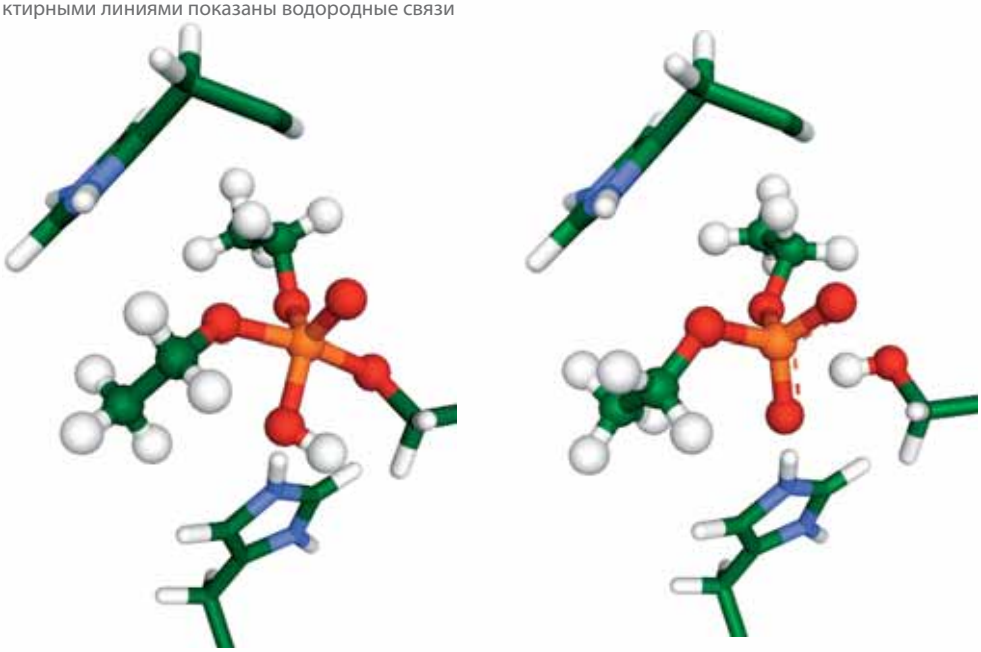

**Рис. 4.**
Интермедиат (слева) и продукты гидролиза (справа)

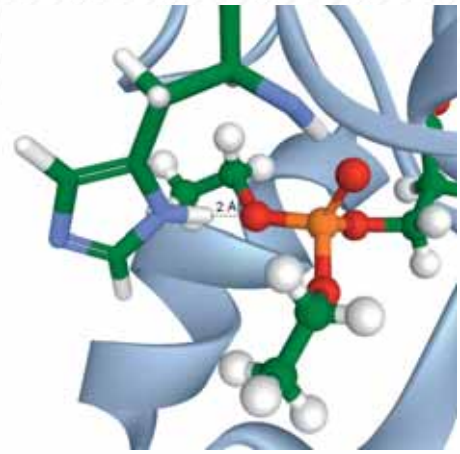


**Рис. 5.**
Конформация активного центра, благоприятствующая образованию водородной связи между His117 и атомом кислорода ингибитора

Предложенный механизм реакции может быть не единственным. Полученная кристаллографическая структура является лишь одной из возможных конформаций белка, в то время как основные группы активного центра могут принимать различные конформации. Методы молекулярной динамики позволяют проследить возможные изменения в конфигурации активного сайта и выделить наиболее вероятные варианты. Так, имидазольное кольцо His117 может менять свою ориентацию в пространстве, и образовывать водородную связь с атомом кислорода ингибитора (рис. 5). При этом основной принцип осуществления каталитического гидролиза ФОС в активном центре модифицированной БХЭ остается прежним, но это позволяет расширить ряд возможных направленных мутаций для ускорения гидролиза.

Работа выполняется при поддержке Российского фонда фундаментальных исследований (проект № 10-03-00085) и Российской академии наук (программа № 9 Отделения химии и наук о материалах РАН).

## СПИСОК ЛИТЕРАТУРЫ

1. *Nachon F. et al.* X-ray crystallographic snapshots of reaction intermediates in the G117H mutant of human butyrylcholinesterase, a nerve agent target engineered into a catalytic bioscavenger // Biochemical J. 2011 (в печати).

# Organophosphate hydrolases as catalytic bioscavengers of organophosphorus nerve agents

M. Trovaslet-Leroy, L. Musilova, F. Renault, X. Brazzolotto, J. Misik, L. Novotny, M-T. Froment, E. Gillon, M. Loiodice, L. Verdier, P. Masson, D. Rochu, D. Jun, **F. Nachon***

Toxicology Letters 206 (2011) 14-23

Toxicology Letters 206 (2011) 14–23

Contents lists available at ScienceDirect

Toxicology Letters

journal homepage: www.elsevier.com/locate/toxlet

# Organophosphate hydrolases as catalytic bioscavengers of organophosphorus nerve agents

Marie Trovaslet-Leroy[a], Lucie Musilova[b], Frédérique Renault[a], Xavier Brazzolotto[a], Jan Misik[c], Ladislav Novotny[d], Marie-Thérèse Froment[a], Emilie Gillon[a], Mélanie Loiodice[a], Laurent Verdier[e], Patrick Masson[a], Daniel Rochu[a], Daniel Jun[b,f,g], Florian Nachon[a,*]

[a] *Département de Toxicologie, Institut de Recherches Biomédicales des Armées, 38700 La Tronche, France*
[b] *Hospital Pharmacy, University Hospital Hradec Kralove, 500 05 Hradec Kralove, Czech Republic*
[c] *Department of Toxicology, Faculty of Military Health Sciences, University of Defence, 503 32 Hradec Kralove, Czech Republic*
[d] *Institute of Pathological Morphology, Faculty of Veterinary Medicine, University of Veterinary and Pharmaceutical Sciences Brno, Palackeho 1/3, 612 42 Brno, Czech Republic*
[e] *DGA Maîtrise NRBC, 91710 Vert le Petit, France*
[f] *Center of Advanced Studies, Faculty of Military Health Sciences, University of Defence, Trebesska 1575, 503 32 Hradec Kralove, Czech Republic*
[g] *Faculty of Environmental Sciences, Czech University of Life Sciences Prague, Kamýcká 129, Praha 6 – Suchdol, 165 21, Czech Republic*

ARTICLE INFO

*Article history:*
Available online 12 June 2011

*Keywords:*
Organophosphate poisoning
Prophylaxis
Bioscavenger
Acetylcholinesterase
Phosphotriesterase
Paraoxonase

ABSTRACT

Bioscavengers are molecules able to neutralize neurotoxic organophosphorus compounds (OP) before they can reach their biological target. Human butyrylcholinesterase (hBChE) is a natural bioscavenger each molecule of enzyme neutralizing one molecule of OP. The amount of natural enzyme is insufficient to achieve good protection. Thus, different strategies have been envisioned. The most straightforward consists in injecting a large dose of highly purified natural hBChE to increase the amount of bioscavenger in the bloodstream. This proved to be successful for protection against lethal doses of soman and VX but remains expensive. An improved strategy is to regenerate prophylactic cholinesterases (ChE) by administration of reactivators after exposure. But broad-spectrum efficient reactivators are still lacking, especially for inhibited hBChE. Cholinesterase mutants capable of reactivating spontaneously are another option. The G117H hBChE mutant has been a prototype. We present here the Y124H/Y72D mutant of human acetylcholinesterase; its spontaneous reactivation rate after V-agent inhibition is increased up to 110 fold. Catalytic bioscavengers, enzymes capable of hydrolyzing OP, present the best alternative. Mesophilic bacterial phosphotriesterase (PTE) is a candidate with good catalytic efficiency. Its enantioselectivity has been enhanced against the most potent OP isomers by rational design. We show that PEGylation of this enzyme improves its mean residence time in the rat blood stream 24-fold and its bioavailability 120-fold. Immunogenic issues remain to be solved. Human paraoxonase 1 (hPON1) is another promising candidate. However, its main drawback is that its phosphotriesterase activity is highly dependent on its environment. Recent progress has been made using a mammalian chimera of PON1, but we provide here additional data showing that this chimera is biochemically different from hPON1. Besides, the chimera is expected to suffer from immunogenic issues. Thus, we stress that interest for hPON1 must not fade away, and in particular, the 3D structure of the hPON1 eventually in complex with OP has to be solved.


*Abbreviations:* AUC, area under curve; hAChE, human acetylcholinesterase; hBChE, human butyrylcholinesterase; BSA, bovine serum albumin; CE, capillary electrophoresis; DSC, differential scanning calorimetry; DTNB, dithio-bis-nitrobenzoic acid; GA, tabun; GB, sarin; GD, soman; GF, cyclosarin; MRT, mean residence time; MPEG, methoxy polyethylene glycol; OP, neurotoxic organophosphorus compounds; PEG, polyethylene glycol; PON1, paraoxonase 1; PTE, phosphotriesterase; QM/MM, quantum mechanics/molecular mechanics; CVX, *O*-butyl-*S*-[2-(diethylamino) ethyl] methylphosphonothioate; VR, *O*-isobutyl-*S*-[2-(diethylamino) ethyl] methylphosphonothioate; VX, *O*-ethyl-*S*-[2-(diisopropylamino)ethyl] methylphosphonothioate.

* Corresponding author at: Département de Toxicologie, Institut de Recherche Biomédicale des Armées – CRSSA, 24 av. des Maquis du Grésivaudan, 38700 La Tronche, France.
*E-mail address:* florian@nachon.net (F. Nachon).

0378-4274/$ – see front matter © 2011 Elsevier Ireland Ltd. All rights reserved.
doi:10.1016/j.toxlet.2011.05.1041

## 1. Introduction

Irreversible inhibition of human acetylcholinesterase (hAChE) by neurotoxic organophosphorus compounds (OP) at cholinergic synapses and neuromuscular junctions is responsible for their acute toxicity (Maxwell et al., 2006). hAChE can be reactivated by powerful nucleophiles, all derivatives of pyridinium aldoximes. But these oximes are permanently charged and do not cross readily the blood–brain barrier (Lorke et al., 2008). As a consequence, central hAChE is poorly reactivated and acetylcholine accumulates in the central nervous system. The effects of this accumulation must be counteracted by antimuscarinic and anticonvulsant drugs, so that the current post-exposure treatments of OP poisoning are commonly based on a combination of a pyridinium aldoxime, atropine, and diazepam (Cannard, 2006). Several issues plague this treatment strategy, in particular, there is no universal oxime able to reactivate efficiently all OP-AChE conjugates (Worek et al., 2004), the treatment produces serious side-effects, and while it does prevent death, it does not prevent transient or permanent incapacitation, and irreversible brain damage (Maynard and Beswick, 1992). New generations of reactivators able to cross the blood–brain barrier would improve the post-exposure treatment, and some very promising candidates have being reported in the recent literature (de Koning et al., this issue; Kalisiak et al., 2011; Mercey et al., 2011).

Another strategy to avoid the adverse effects of OP poisoning is to rapidly neutralize the toxicants in the blood compartment before they can reach the physiological target hAChE. This is achieved by the administration of a bioscavenger, such as AChE itself (Wolfe et al., 1987). The most advanced bioscavenger, close to reach the market for pretreatment against OP intoxication is human butyrylcholinesterase (hBChE). hBChE traps OP into a one-to-one complex and an injection i.v. or i.m. protects animals against 3–5 LD50 doses of the nerve agents soman, VX, and tabun (Lenz et al., 2007). A hBChE dose up to 250 mg/70 kg is required to achieve efficient protection of humans following a challenge with 1 $LD_{50}$ OP (Ashani and Pistinner, 2004). The necessity of such a large dose of enzyme is owing to the stoichiometric and irreversible nature of the reaction between OP and hBChE, and to the unfavorable OP/BChE mass ratio. Large amounts of hBChE are available either purified from human plasma (Saxena et al., 2010) or produced in transgenic animals and plants (Geyer et al., 2010a; Huang et al., 2007). Plasma-derived hBChE has no adverse effect, is stable and displays circulating half-life over a week (Genovese et al., 2010; Saxena et al., 2011), but recombinant hBChE must be modified either by PEGylation (Huang et al., 2007) or fusion to human serum albumin (Huang et al., 2008) to extend its half-live over a few hours. All things considered, the large dose required remains very expensive and would prevent the widespread use of hBChE as a pretreatment. Research efforts now are devoted to circumventing this limitation.

One possible approach is to regenerate inhibited cholinesterase (ChE)-based stoichiometric bioscavengers by co-administration of reactivators, thus yielding a pseudo-catalytic bioscavenger. This approach could only be successful if the reactivation rate is fast enough to fully degrade the toxicant before it can reach synaptic AChE, which gives a time-window of only a couple of minutes (Heffron and Hobbiger, 1979). Unfortunately, this condition is not met with hBChE as the enzyme component (Aurbek et al., 2009; Kovarik et al., 2010). Using hAChE as the enzyme component seems to be more promising as oxime reactivation rates are significantly faster than for hBChE (Aurbek et al., 2009) and mutants with enhanced rates and reduced aging rate are identified (Kovarik et al., 2007; Kronman et al., 2010). Thus, the pseudo-catalytic approach is probably the most interesting short-term solution, but if reactivation rates cannot be improved, its interest will be limited for OP with slow distribution in the body (like percutaneous VX) or sufficiently time spaced multiple exposures to OP.

A much better solution consists in enzymes able to readily hydrolyze OP in the bloodstream also known as catalytic bioscavengers (Lenz et al., 2007). Indeed, if OP are substrates of these enzymes, the enzyme/OP ratio can be dramatically decreased without loss of protection efficiency, and thus, much smaller dose can be administered at reduced cost (Sweeney and Maxwell, 2003). In this paper, we will focus on the recent research efforts around three potential catalytic bioscavengers: cholinesterase mutants with enhanced spontaneous reactivation rates (Masson et al., 2008), human paraoxonase 1 (Rochu et al., 2007a), and bacterial phosphotriesterase.

## 2. Material and methods

### 2.1. Chemicals

Chemicals used in experiments were of analytical grade and were purchased from Sigma Aldrich (Prague, Czech Republic or L'Isle-d'Abeau France), Pliva-Lachema (Brno, Czech Republic), Acros Organics (Geel, Belgium), LaserBio Labs (Sophia-Antipolis Cedex, France) and PENTA (Prague, Czech Republic). Electroosmotic flow (EOF) marker (DMF) was from Pierce (Rockford, IL, USA). VX, VR and CVX were prepared by the French National Single Small-Scale Facility (DGA Maîtrise NRBC, Vert-le-Petit France). The VX, VR and CVX, in anhydrous isopropanol, used in these studies were >99% pure as determined by $^{31}P$ NMR.

### 2.2. Expression, purification and kinetic characterization of hAChE, Y124H and Y124H/Y72D mutants

Wild type human acetylcholinesterase was expressed in CHO-K1 cells (American Type Culture Collection, No. CCL61) and purified as previously described (Carletti et al., 2008). The Y124H and Y124H/Y72D mutants of human acetylcholinesterase were made by PCR using Pfu polymerase, cloned into the mammalian expression plasmid pGS, stably transfected into CHO-K1 cells, expressed and purified according to the protocol used for the wild type enzyme (Carletti et al., 2008).

Kinetic measurements were carried out at 25 °C, using ATC as the substrate, according to Ellman's method (Ellman et al., 1961). Buffer (0.1 M phosphate buffer pH 7.0) was supplemented with 0.1% (w/v) bovine serum albumin as an enzyme stabilizer. The final concentration of Ellman's reagent, dithio-bis-nitrobenzoic acid (DTNB) in the cuvette was 0.35 mM.

hAChE displays inhibition by excess substrate with ATC. This phenomenon is described by the following rate equation (Radic et al., 1993):

$$v = \frac{V_{max}[S]}{[S] + K_s}\left(\frac{1 + b[S]/K_{ss}}{1 + [S]/K_{ss}}\right)$$

$K_s$ is the Michaelis constant, $V_{max}$ is the maximal velocity and $K_{ss}$ the dissociation constant of the ternary SES complex. The parameter $b$ reflects the efficiency by which the ternary complex SES forms product. When $b > 1$, there is substrate activation, when $b < 1$, there is substrate inhibition; for an enzyme that obeys Michaelis–Menten model, $b = 1$. Catalytic parameters $K_s$, $K_{ss}$ and $b$ values were calculated by nonlinear regression using GOSA-fit (Bio-Log, Toulouse, France).

### 2.3. Spontaneous reactivation of hAChE, Y124H and Y124H/Y72D mutants inhibited by racemic VX, VR and CVX

Purified hAChE (≈3 nM) was incubated in phosphate buffer (0.1 M, pH 7.0, 0.1% BSA, 0.1% $NaN_3$), with 5 or 7 nM VX, 6 nM VR and 4 nM CVX at 25 °C. Purified Y124H-hAChE (≈2 nM) was incubated in phosphate buffer (0.1 M, pH 7.0, 0.1% BSA, 0.1% $NaN_3$), with 40 or 60 nM VX, 20 nM VR and 10 nM CVX at 25 °C. Purified Y124H/Y72D-hAChE (≈3 nM) was incubated in phosphate buffer (0.1 M, pH 7.0, 0.1% BSA, 0.1% $NaN_3$), with 43 nM VX, 44 nM VR and 43 nM CVX at 25 °C. The progressive inhibition and subsequent reactivation of these enzymes were followed during one week according to Ellman's method by measuring the absorbance at 412 nm of 50-μl aliquots, in 1 ml phosphate buffer (0.1 M, pH 7.0, 0.5 mM DTNB, 0.1% BSA, 1 mM ATC). Enzyme activities were referred to control activity (Eo) and are expressed as % of reactivation. The curves display two phases corresponding to inhibition by the most active isomer of V-agent, and reactivation of the conjugate up to a level depending on the aging rate. The following kinetic model applies:

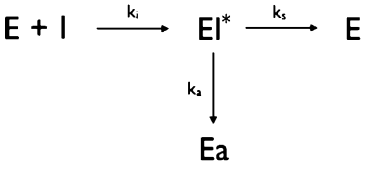


$E$ is the active enzyme, $I$ is the inhibitor, $k_i$ is the bimolecular inhibition rate constant, $EI^*$ is the conjugate, $k_s$ the spontaneous reactivation rate constant of $EI^*$,

and *Ea* the aged enzyme. Under the conditions retained, the inhibitor concentration varies with time so that a second-order treatment of this kinetic model must be adopted. In consequence, the kinetic model is described by the following system of coupled differential equations:

$$\frac{d[E]}{dt} = -k_i[I][E] - k_a[EI^*] + k_s[EI^*]$$
$$\frac{d[Ea]}{dt} = +k_a[EI^*]; \qquad \frac{d[I]}{dt} = -k_i[I][E]$$

Defining $R_E = [E]/[E]_0$, $R_{Ea} = [Ea]/[E]_0$ gives:

$$\frac{dR_E}{dt} = -k_i \bullet R_E[I] + k_s(1 - R_E - R_{Ea})$$
$$\frac{dR_{Ea}}{dt} = +k_a(1 - R_E - R_{Ea}); \qquad \frac{d[I]}{dt} = -k_i[I] \bullet P_E[E]_0$$

$k_i$, $k_s$ and $k_a$ are determined by fitting the experimental data against numerical solutions of this system of differential equation using pro Fit (QuantumSoft; www.quansoft.com).

### 2.4. Preparation of hPON1 and rPON1

Human PON1 was purified from pooled out-dated plasma (Établissement Français du Sang Rhône-Alpes, Beynost, France) as previously described (Renault et al., 2006). The mammalian recombinant PON1 dubbed G3C9, without or with a C-terminal-8Histidine tag (termed rPON1 and rPON1-8His, respectively), generated in *Escherichia coli* after a directed evolution process *via* gene shuffling of human, rabbit, rat and mouse PON1 genes was a gift from Dr. Dan S. Tawfik (The Weizmann Institute of Science, Rehovot, Israel). This evolved mammalian rPON1 was purified as previously described (Aharoni et al., 2004), and stored at 4 °C in 50 mM Tris, 50 mM NaCl, 1 mM $CaCl_2$, 0.1% Tergitol, at pH 8.0.

### 2.5. Oligomeric state analysis of hPON1 and rPON1 by capillary electrophoresis

Data collection and analysis were performed on a modified Beckman Coulter P/ACE 5510 system (Gagny, France), with P/ACE Station 1.21 software (Rochu et al., 1999). Protein migrations were carried out in a 250 mM borate buffer pH 9.0, at 30 °C, in a 50 μm i.d. × 67 cm fused-silica capillary, at constant voltage (16 kV). Detection was performed at 200 nm. Surfaces of overlapping peaks were fitted after deconvolution (using PeakFit v4 software; SPSS Science, Chicago, IL) with the Symmetric Double Gaussian Cumulative function. The sizes of oligomeric forms depicted by deconvolution were determined using the Offord model that correlates electrophoretic mobility with the charge-to-size parameter of the PON1s (Offord, 1966):

$$\mu_{ep} = \frac{A \bullet q}{M^{2/3}}$$

where $\mu_{ep}$ is the electrophoretic mobility, $q$ the charge, and $M$ the molar mass.

### 2.6. Temperature-induced inactivation of human and recombinant PON1 arylesterase activity

Enzyme samples were diluted 1000-fold in Tris/HCl buffer (25 mM, with 1 mM $CaCl_2$, pH 8) and incubated in a thermostated water bath at different fixed temperatures (between 30 and 75 °C) for 10 min. After temperature treatment, samples were cooled to 4 °C and residual activity was measured spectrophotometrically at 270 nm and 25 °C with phenylacetate (1 mM) in 50 mM Tris/HCl buffer pH 8.0 containing 1 mM $CaCl_2$. All experiments were performed in duplicate.

### 2.7. Human and recombinant PON1 thermal stabilities studied by differential scanning calorimetry (DSC)

DSC experiments were performed on a 6300 nano-DSC III high-sensitivity calorimeter (TA Instruments, Guyancourt, France). An overpressure (3 atm) was applied to prevent bubbling of the sample during heating. Protein samples (0.4 mg/ml) were dialysed extensively against the buffer used for the scanning experiment (50 mM Tris, 1 mM $CaCl_2$, 0.04% Triton, pH 8.0). The buffer and protein samples were degassed for 30 min before each calorimetric measurement. Each protein run (at 1 °C/min, between 20 and 90 °C) was preceded by a baseline with buffer-filled cells in the same conditions. Re-heating the protein after the first run checked irreversibility of the thermal transitions. Subtraction of the buffer–buffer baseline and conversion from power to molar heat capacity were performed with CpCalc, software provided with the calorimeter.

### 2.8. Modification of PTE

PTE from *Pseudomonas diminuta* was expressed in *E. coli* and purified as previously described (Rochu et al., 2002). MPEG polymers *O*-[2-(6-oxocaproylamino)ethyl]-*O′*-methylpolyethylene glycol aldehyde (MPEG 2 kDa; MW = 2 kDa) and *O*-[2-(6-oxocaproylamino)ethyl]-*O′*-methylpolyethylene glycol aldehyde (MPEG 5 kDa; MW = 5 kDa) were used for PTE modification. Polymers were dissolved in 0.2 M borate buffer (pH 8.5; 0.1 mM $CoCl_2$) together with reduction agent sodium cyanoborohydride ($NaBH_3CN$) and mixed with PTE solution. Different PTE/MPEG/$NaBH_3CN$ molar ratios were used for modification: 1:1 200:48 000 for MPEG 2 kDa and 1:800:40 000 for MPEG 5 kDa. Reaction time for conjugation of recombinant PTE with both MPEG 2 kDa and MPEG 5 kDa was 24 h to get fully modified PTE at given reactant ratios at 25 °C. Reaction was stopped after addition of 10% (w/v) glycine solution into the reaction mixture. The rest of the unreacted polymer was removed from modified PTE using ultrafiltration unit (cut-off 10 kDa; Vivascience AG, Germany). Modification process was monitored by measuring the enzyme activity and carrying out SDS-PAGE (7.5% separation gel). Electrophoresis was performed using Mini-PROTEAN 3 Cell system (Bio-Rad, Prague, Czech Republic). Proteins on gels were stained using EZBlue Gel Staining Reagent (colloidal Coomassie brilliant blue G-250; Sigma Aldrich, Prague, Czech Republic), Kaleidoscope Prestained Standard (Bio-Rad, Prague, Czech Republic) was used as an appropriate molecular marker.

### 2.9. Measurement of PTE activity after repeated in vivo administration of PTE

Female Wistar rats weighing 200–230 g from VELAZ Prague (Czech Republic) were kept in an air-conditioned room with light from 07:00 h to 19:00 h and allowed access to standard food and tap water ad libitum. The handling of the experimental animals was under the supervision of the Ethics Committee of the Faculty of Military Health Sciences, Czech Republic. All experiments were conducted in agreement with the Animal Protection Law of the Czech Republic (311/1997). The rats were divided into three groups of six animals each. All substances were administered intramuscularly (i.m.) in a total volume of 1 ml $kg^{-1}$. Enzyme was solubilized in sterile 50 mM borate buffer (pH 8.5; supplemented with 0.1 mM $CoCl_2$). The first group of animals was administered PTE conjugated to MPEG 5 kDa at a dose of 1.19 mg $kg^{-1}$ (corresponding to enzyme activity of 34.5 μkat $kg^{-1}$), second group of animals obtained native PTE at a dose 0.54 mg $kg^{-1}$ (corresponding activity was the same as for the first group) and the last group received buffer only (control group). Blood was withdrawn from tail vein at given time intervals (30 min, 1, 2, 3, 6, 12, 24 and 120 h) and the activity of PTE in sample was measured immediately: A 5-μl aliquot of fresh blood was hemolyzed in 980 μl of 50 mM borate buffer (pH 8.5; 0.1 mM $CoCl_2$) and the activity of enzyme was monitored at 25 °C using 1 mM paraoxon as the substrate. Activity measurements were performed using a spectrophotometer Helios Alfa (Thermo Fisher Scientific, Inc., Waltham, MA, USA) by monitoring the change in absorbance at 370 nm, corresponding to the released p-nitrophenol from paraoxon. Due to the strong absorption of hemoglobin around 400 nm, the reaction was monitored at 370 nm to avoid interference.

The curves representing activity versus time were fitted empirically using Pro Fit (Quantumsoft). $A_{max}$, the maximum activity, $T_{max}$, the time at which $A_{max}$ was reached, AUC, the area under curve and AUMC, the area under moment curve, were calculated from the fitted curve. The mean residence time (MRT) is AUMC/AUC.

The experiment was repeated one month later after first administration. Each group was treated again the same dose of enzyme (1.19 mg $kg^{-1}$ and 0.54 mg $kg^{-1}$, respectively) or sterile buffer.

## 3. Results and discussion

### 3.1. Engineered cholinesterases

OP are considered as hemisubstrates of cholinesterases, because the formation of the enzyme–OP conjugate is very efficient but the dephosphylation is very slow. It is hypothesized that the slow dephosphylation rate results from the absence of a nucleophilic residue able to activate a water molecule to attack the phosphyl adduct (Järv, 1984). Thus, it was thought that introducing a new nucleophilic residue in the active site by mutation at the proper location could promote hydrolysis. If the hydrolysis step is fast enough, then the enzyme becomes an anhydride organophosphate hydrolase, thus a catalytic bioscavenger (Masson et al., 2008). This hypothesis was successfully applied to human BChE, substituting a glycine at position 117 with a histidine (Lockridge et al., 1997; Millard et al., 1995). The G117H mutant could hydrolyze echothiophate, albeit at a modest rate ($k_{cat} = 0.75\ min^{-1}$). G117H can also hydrolyze the nerve agent sarin, VX, even soman provided an additional mutation (E197Q) aimed at reducing the aging rate is present (Millard et al., 1998), but at slower $k_{cat}$ than echothiophate ($5 \times 10^{-3}$ to $10^{-2}\ min^{-1}$). Transgenic mice expressing the G117H mutant are resistant to echothiophate poisoning (Wang et al., 2004). Due to slower phosphylation rates than the wild-type, i.v. injection of G117H/E197Q mutants fail to protect animals against GB, GD or VX challenge (Geyer et al., 2010b).

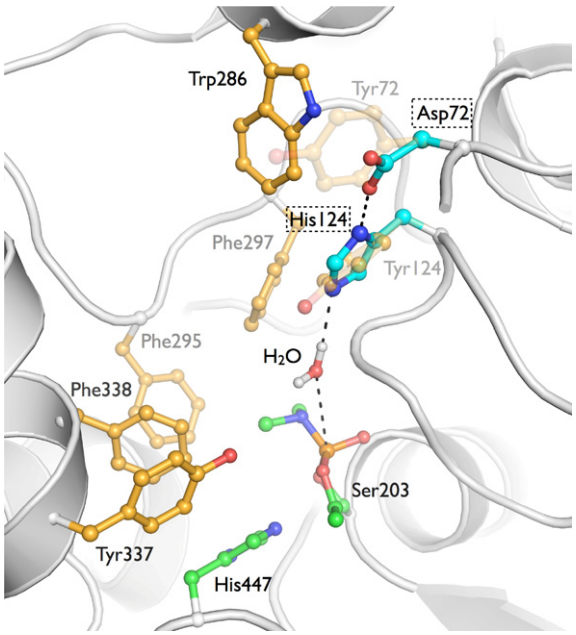


**Fig. 1.** Model of the Y124H-Y72D mutant of human AChE based on the X-ray structure of human AChE inhibited by tabun (pdb code 2X8B). Active site residues are shown in the ball-and-sticks format. Carbon atoms are shown in bright orange or cyan for mutated residues or green for the catalytic triad and tabun, nitrogen atoms in deep blue, phosphorus atom in orange, and oxygen atoms in red. Hydrogen bonds are represented by dashes.

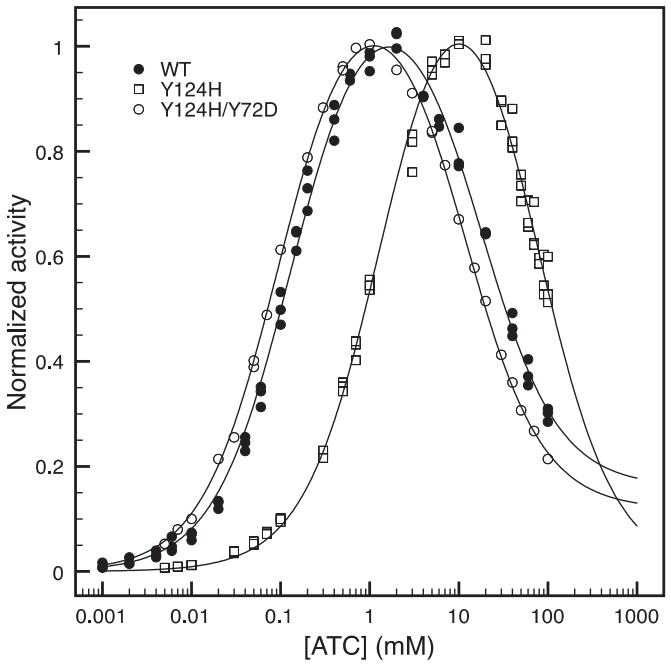


**Fig. 2.** Activity of wilt-type (WT) and mutated hAChE (Y124H and Y124H/Y72D) measured at different concentrations of acetylthiocholine (pS curves) in phosphate buffer (0.1 M, pH 7.0).

Some attempts to transpose the OP hydrolase activity of G117H-hChE to AChE have been made by simply substituting the conserved glycine by histidine, provided that some room was made in the active site of AChE by mutating a bulky aromatic residue to its equivalent in hBChE (Poyot et al., 2006). However, the resulting enzyme has dramatically altered catalytic properties, reactivates spontaneously but is actually strongly resistant to OP inhibition.

Recent structural study of the G117H mutant either suggests that a substantial conformational change is necessary if His117 is a general base catalyst, or His117 has a more passive role in a mechanism based on a water molecule nucleophilic attack from a position adjacent to the catalytic serine (Nachon et al., 2011). The latter hypothesis is supported by hybrid Quantum Mechanics/Molecular Mechanics simulations (QM/MM) (Lushchekina et al., 2011). Thus, the base catalyst role originally hypothesized for the mutant histidine is not achieved at position 117 in hBChE and most likely not in hAChE as well. With this hindsight, we examined the structure of hAChE to look for other residue positions in the active site gorge that could fulfill the conditions for a base catalyst role of a mutant histidine. According to molecular modelling, Tyr124, a component of the peripheral site of hAChE, is in an appropriate location (Fig. 1). The Y124H mutant can stabilize a water molecule at the right position for in-line displacement of the catalytic serine. Besides, further modelling shows that substituting Tyr72, another component of the peripheral site, by an aspartate residue, creates a synthetic diad that could enhance the base catalyst role designed for His124. Accordingly, we built the Y124H and Y124H/Y72D mutants of hAChE and examined its catalytic properties for acetylthiocholine and V-agents.

The effect of substrate concentration on acetylthiocholine hydrolysis for the wild-type (WT) and mutated hAChE is shown in Fig. 2. The data were fitted using Radic's equation that permits the description of substrate inhibition and determination of the kinetic parameters $K_m$ and $K_{ss}$ (Table 1; see Section 2) (Radic et al., 1993). The classical bell-shaped curved is markedly shifted to higher concentrations of acetylthiocholine for the Y124H mutant. This corresponds to an increase in $K_m$ of about 1 order of magnitude while $K_{ss}$ is increased more than 4 fold. These data indicate that the structure of the active site gorge was significantly altered, which is expected since Tyr124 is a key element of the peripheral site and is involved in the transient binding of the substrate on its route down to the gorge (Bourne et al., 2006; Colletier et al., 2006). Remarkably, the second mutation does better than restore the original activity as both $K_m$ and $K_{ss}$ are decreased about 30% compared to wild-type hAChE. The structural interpretation of this improvement is not straightforward, but among possible hypotheses, the presence of Asp72 may stabilize the histidine conformation and neutralize it as originally designed, and/or the aspartate negative charge may attract positively charged acetylthiocholine at the rim of the gorge. Thus, contrary to the mutants of AChE at the position equivalent to Gly117 of hBChE, the cholinesterase activity of Y124H/Y72D is not reduced.

We tested the activity of the Y124H and Y124H/Y72D against three V-agents whose chemical structures are represented in Fig. 3. We chose to carry out inhibition under conditions where inhibition, spontaneous reactivation and aging could all be observed in a single experiment. Aging is a secondary reaction leading to very stable adducts refractory to spontaneous or oxime-based reactivation (Masson et al., 2010). The progressive inhibition of hAChE and the two mutants by racemic VX, CVX, and VR and spontaneous reactivation are shown in Fig. 4. The curves display generally three phases: (1) an initial rapid inhibition followed by (2) a recovery of activity up to a plateau (3). The plateau indicates that full reactivation cannot be attained most likely due to the concurrent aging reaction. The data were fitted using the system of coupled differential equations that describe a kinetic model including inhibition, reacti-

**Table 1**
Kinetic parameters of hAChE catalyzed ATC hydrolysis at pH 7.0 and 25 °C.

| | $K_s$ (μM) | $K_{ss}$ (mM) | *b* factor |
|---|---|---|---|
| WT | 133 ± 10 | 17 ± 3 | 0.14 ± 0.04 |
| Y124H | 1400 ± 100 | 71 ± 5 | 0 |
| Y124H/Y72D | 97 ± 5 | 11.3 ± 1.0 | 0.10 ± 0.01 |

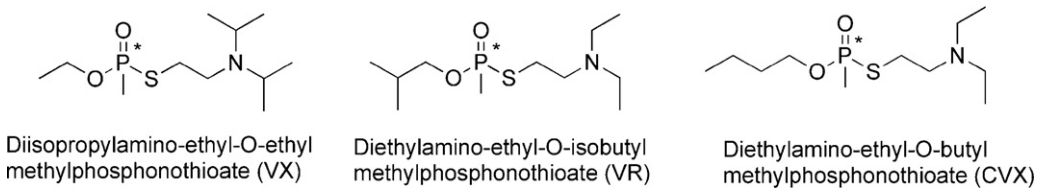


**Fig. 3.** Chemical structures of V-agents, VX, Russian VX (VR) and Chinese VX (CVX).

vation and aging (see Section 2.3). All the data were well fitted using the proposed model except for the wild type enzyme inhibited by CVX. For the latter the reactivation phase displays an additional elbow that was systematically present in 4 independent experiments performed with CVX concentrations ranging from 4 nM to 6.5 nM and that could not be explained by the model. This elbow suggests that the enzyme is inhibited by two different populations of inhibitor during this time range, and forms two conjugates spontaneously reactivating at different rates. One possible hypothesis is that these two inhibitors are the two enantiomers of CVX. The corresponding model introduces too many additional parameters to obtain reasonable restrain during the fit, so we adopted a conservative approach by limiting the fit to that data up to the elbow ($2 \times 10^3$ min).

The parameters corresponding to the fitted curves of Fig. 4 are found in Table 2. Bimolecular rate constants of inhibition ($k_i$) are altered for both mutants dropping from 10 fold (VX, wild-type *vs.* Y124H) up to 100 fold (CVX, wild-type *vs.* Y124H/Y72D) but still range in the order of $10^6$–$10^7$ $M^{-1}$ $min^{-1}$. Aging rates $k_a$ are relatively unaffected by the mutations, being all within 4 fold of that of the wild-type enzyme. Regarding spontaneous reactivation rates, large improvement is observed for VX conjugates of Y124H and Y124H/Y72D, with $k_s$ respectively up to 180 and 110 fold higher than wild-type hAChE. $k_s$ increases modestly about 10 fold for CVX,

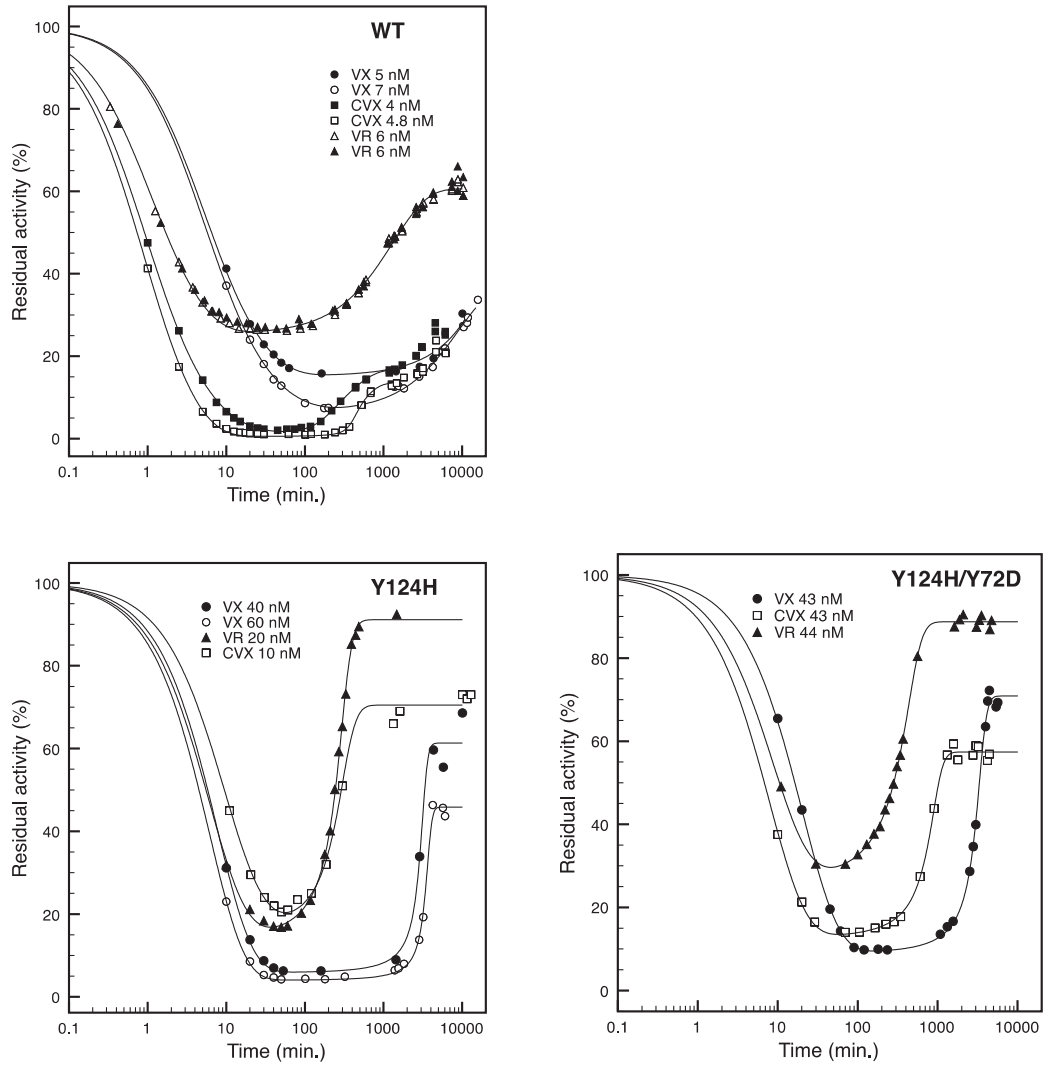


**Fig. 4.** Residual activity of wild-type (WT) and mutated hAChE (Y124H and Y124H/Y72D), inhibited by VX, VR and CVX. Activity was measured on aliquots over a period extending up to a week. The solid lines represent the numerical solution of the system of coupled differential equations presented in Section 2.3 using the fitted parameters of Table 2.

**Table 2**
Inhibition, spontaneous reactivation and aging rate constants of hAChE.

| | | $k_i$ ($\times 10^{-6}$ $M^{-1}$ $min^{-1}$) | $k_s$ ($\times 10^3$ $min^{-1}$) | $k_a$ ($\times 10^3$ $min^{-1}$) |
|---|---|---|---|---|
| WT | VX | 60 ± 8 | 0.038 ± 0.004 | 0.061 ± 0.002 |
| | CVX | 580 ± 90[a] | 1.1 ± 0.4[a] | 2.5 ± 0.6[a] |
| | VR | 240 ± 10 | 0.34 ± 0.03 | 0.34 ± 0.08 |
| Y124H | VX | 5.7 ± 0.5 | 6.8 ± 0.5 | 0.22 ± 0.03 |
| | CVX | 18 ± 1 | 17 ± 2 | 1.5 ± 0.1 |
| | VR | 14 ± 1 | 20 ± 1 | 0.45 ± 0.04 |
| Y124H | VX | 2.1 ± 0.1 | 4.1 ± 0.3 | 0.13 ± 0.02 |
| Y72D | CVX | 5.3 ± 0.2 | 15 ± 1 | 0.87 ± 0.009 |
| | VR | 3.8 ± 0.1 | 28 ± 1 | 0.48 ± 0.02 |

[a] Fitted parameters for data up to $2 \times 10^3$ min.

and respectively 60 and 80 fold for VR-conjugates. But in value, $k_s$ are higher for VR conjugates so that they are systematically faster to spontaneously reactivate whereas VX conjugates are slower. The fast reactivation of both mutants inhibited by VR leads to 90% of residual activity after 7 h despite at least 15 times excess of VR. CVX conjugates reactivate as readily as VR conjugates but reach lower residual activity level because aging is also faster. On the contrary, $k_s/k_a$ ratios are more favorable for VX-conjugates, and despite slower $k_s$ than CVX, the residual activity plateau is finally higher.

In summary, we designed new mutants aimed at improving the spontaneous reactivation rate of hAChE. *In vitro* experiments show that these mutants reactivate up to 2 orders of magnitude faster than wild-type hAChE without dramatic alteration of their catalytic activity. We emphasize that despite the important gain in reactivation rate, these rates remain too slow for considering these mutants of AChE as true catalytic bioscavengers. However, they can be perceived as self-regenerating stoichiometric bioscavengers, which we believe, constitute an improvement over native cholinesterases. Moreover these mutants provide an enzyme with minimal organophosphate anhydride hydrolase activity, which could be further improved by using a computational chemistry strategy based on QM/MM simulation of the dephosphylation reaction.

### 3.2. hPON1: natural catalytic scavenger

Human PON1, as the most promising catalytic bioscavenger for pre-treatment and therapy of OP poisoning, is the focus of intensive research to better understand its behavior and to improve its efficacy and functionalization (Clery-Barraud et al., 2009; Renault et al., 2010; Rochu et al., 2007b,c). Unfortunately, the 3D-structure and catalytic mechanism of hPON1 are not solved yet. Chimeric mammalian recombinant PON1 (rPON1) expressing in *E. coli* was made by directed evolution, and its X-ray structure was solved (Harel et al., 2004). Even if these chimeric enzymes are likely immunogenic in human, encouraging results have recently been obtained for evolved rPON1 showing *in vivo* prophylactic activity against G-type agents (Gupta et al., 2011). However, rPON1 differs from the human enzyme by at least 51 amino acid substitutions. The potential effects of these amino acid differences on the functional properties of the enzyme have to be cautiously considered. In fact, dramatic differences in OP-hydrolase activity between human and chimeric mammalian rPON1 enzymes have been described (Otto et al., 2009). Therefore, to further determine differences between hPON1 and rPON1 produced as tagged proteins, we have analyzed their oligomerization states in solution by capillary electrophoresis, their thermal denaturation and inactivation process.

Using capillary electrophoresis, multiple and variable oligomerization states of PON1s in solution were observed (Fig. 5). In all circumstances, electropherograms showed that PON1 peaks were non-Gaussian and thereby contained several oligomeric states. After deconvolution of these peaks, oligomer sizes were estimated using the Offord model (see Section 2.3). No monomers (even inactive) were observed but three oligomeric forms, corresponding to dimers, trimers, and tetramers, were discriminated for hPON1 (Fig. 5A) and rPON-8His (Fig. 5B). It is noteworthy that, within an identical environment, the proportion of dimers (42% *vs.* 7%), trimers (34% *vs.* 17%) and tetramers (24% *vs.* 76%) differs significantly between hPON1 and rPON1-8His.

Thermal stability of PON1s has been investigated using high-sensitivity DSC measurements. Fig. 6 shows typical DSC thermograms of hPON and rPON1-8His: endothermic transi-

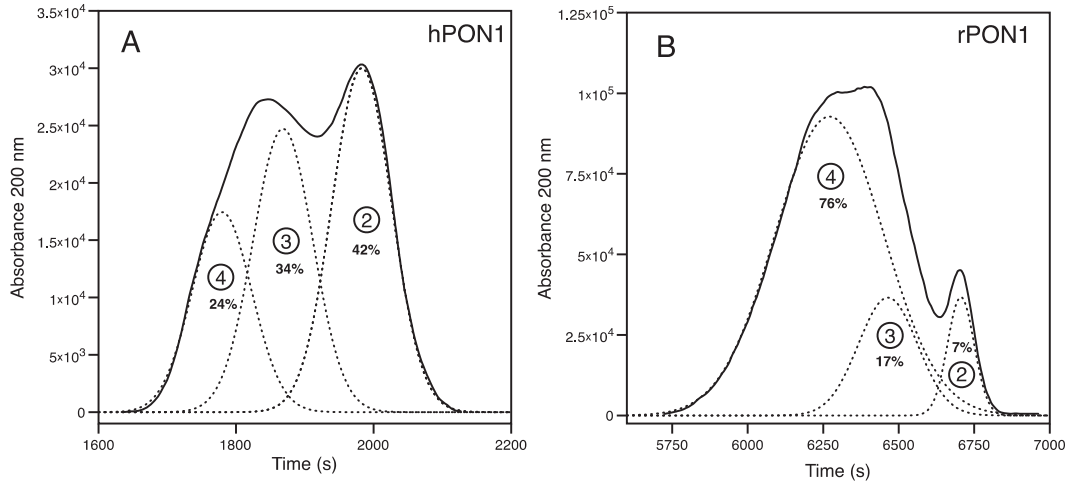


**Fig. 5.** Deconvolution of electropherograms for hPON1 and rPON1-8xHis. For both enzymes, deconvolutions showed three distinct molecular populations with different relative areas. Circled numbers 4, 3 and 2 indicate respectively tetramers, trimers and dimers.

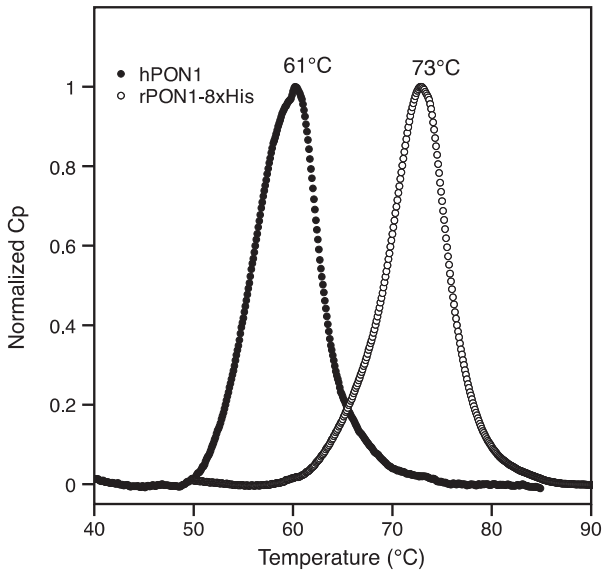


**Fig. 6.** Normalized DSC scans of hPON1 and rPON1-8xHis.

tions exhibiting $T_m$ differing by more than 12 °C were observed ($T_m$ = 61 °C for hPON1 *vs.* 73 °C for rPON1-8His). Because rPON1-8His contains mutations and a C-terminal tag, the respective impact of these two parameters on the higher thermostability of the recombinant enzyme was also investigated by studying the thermal inactivation of arylesterase activity of different PON1 formulations (Fig. 7). hPON1 alone is unstable. But it is stabilized by the presence of its most common partner protein, the human phosphate binding protein. Both rPON1s (with or without His tag) are more stable than human enzyme and were totally inactivated at similar temperature of about 75 °C. Unpredictably, the thermally induced inactivation of rPON1 was noticeably delayed compared to that of rPON1-8His, and retained 100% of the control activity at 68 °C. This strongly suggested that the higher stability of rPON1, achieved by mutations, is moderated by the presence of the 8xHis tag.

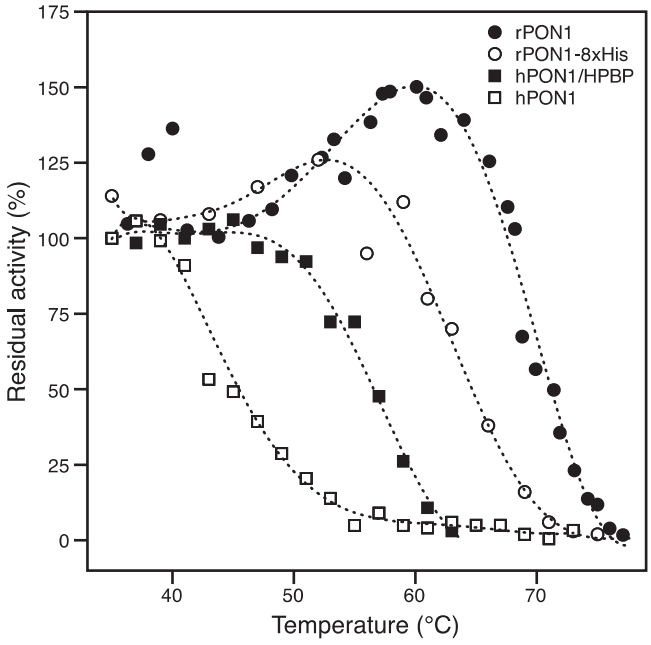


**Fig. 7.** Thermal inactivation of arylesterase activity of different PON1 formulations: hPON1 alone, hPON1 + HPBP, rPON1-8xHis and rPON1.

In summary, we showed that chimeric mammalian rPON1s produced with or without 8-His tag has a different oligomeric state and higher temperature stability than hPON1. These differences in biochemical properties, and the dramatic difference in catalytic properties observed earlier (Otto et al., 2009), strongly suggest that both enzymes must be considered as very different proteins, so that extrapolation of the behavior of one enzyme to the other is not possible. For example, mutations improving the catalytic activity of rPON1 are likely not systematically beneficial for hPON1. In that context, the determination of the 3D structure of hPON1 remains a priority to improve its catalytic efficiency toward nerve agents.

### 3.3. Bacterial phosphotriesterase

Bacterial phosphotriesterase (PTE) isolated from soil microbes like *P. diminuta* remains the most performant organophosphorus acid anhydrolase, able to hydrolyze the pesticide paraoxon with a catalytic efficiency ($k_{cat}/K_m$) approaching the diffusion-controlled limit of $10^8\ M^{-1}\ s^{-1}$ (Omburo et al., 1992). PTE can hydrolyze a wide variety of nerge agents, including GA, GB, GD, GF, VR, and VX (Chen-Goodspeed et al., 2001) but displays a stereoselectivity that is not systematically in favor of their most toxic enantiomers (Li et al., 2001). However, adopting a rational evolution approach, i.e., mutating specific residues in the active site can reverse the stereoselectivity (Tsai et al., 2010).

One possible drawback of phosphotriesterase is its relative instability related to the formation of its bimetallic catalytic center (Carletti et al., 2009; Rochu et al., 2004; Roodveldt and Tawfik, 2005). These stability issues can be resolved by turning to hyperthermophilic members of the phosphotriesterase enzyme family like the PTE isolated from *Sulfolobus solfataricus* (Merone et al., 2005). But the dramatic increase in thermal stability goes along with a decrease in activity at physiological temperature. Therefore, either rational design based on the 3D structure of this enzyme (Elias et al., 2008), or directed evolution is necessary to regain catalytic efficiency (Merone et al., 2010).

Conjugation with polyethylene glycol is an alternative approach to improve the stability of enzymes, in addition to increase circulating half-life and reduce immunogenicity (Harris and Chess, 2003). We successfully grafted methoxy-PEG molecules of different molecular weight on the 7 surface lysines of mesophilic PTE by mild reductive amination. Biochemical properties of the conjugates were determined (Jun et al., 2007; Jun et al., 2010). The catalytic properties of the enzyme conjugated to methoxy-PEG of molecular weight 5 kDa (MPEG 5 kDa) were not significantly modified compared to the native enzyme. For example, $K_m$ for paraoxon hydrolysis was conserved ($K_m$ native = 290 ± 100 μM; $K_m$ modified = 230 ± 50 μM) and a modest 2-fold decrease in $V_{max}$ was observed ($V_{max}$ native = 3.15 ± 0.40 μM min$^{-1}$; $V_{max}$ modified = 1.65 ± 0.10 μM min$^{-1}$). The conjugates displayed improved thermal stability, with a half-life at 37 °C and pH 7.4 increasing 48 fold from 0.256 h to 12.3 h for native PTE and PTE-MPEG 5 kDa, respectively. The improvement for the PTE-MPEG 3 kDa conjugate was only about 2-fold. As the stability in physiological conditions is crucial for long circulating half-life PTE-MPEG 5 kDa was the most suitable candidate for *in vivo* evaluation. Here, we report pharmacokinetic profiles of native PTE and PTE fully modified with MPEG 5 kDa injected i.m. in Wistar rats.

Two identical doses of unmodified and fully modified PTE (34.5 μkat kg$^{-1}$) were administered i.m. to rats at 4-week interval. Time courses of circulating PTE activity are shown in Fig. 8 and calculated pharmacokinetics parameters are shown in Table 3. Rats in which an initial dose of PTE-MPEG 5 kDa was administered, showed a rapid increase in PTE activity, which reached peak levels at $T_{max} \approx 47.5$ h. The activity level remained 50% higher than the maximum activity up to 80 h after administration. Mean residence

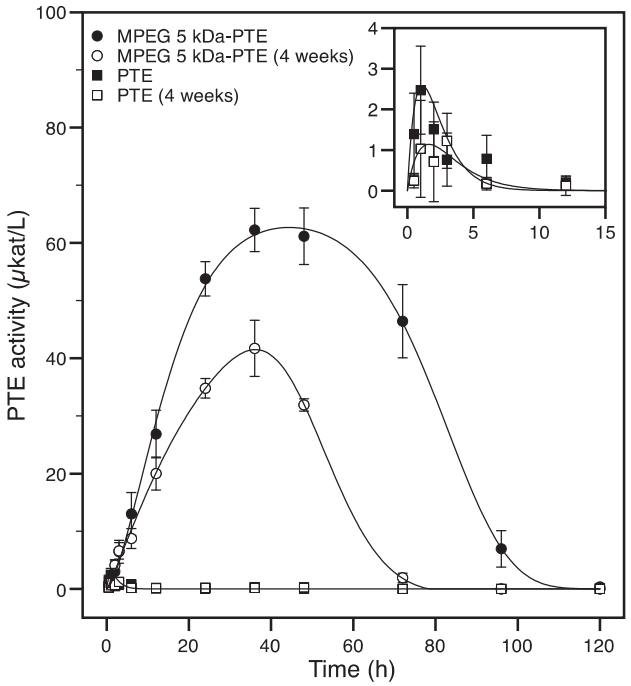


**Fig. 8.** Circulatory clearance profile of native PTE and PTE modified by MPEG 5 kDa. Female Wistar rats (3 groups, each 6 animals) received i.m. 1) control (isotonic borate buffer pH 8.5, 2) PTE and 3) PTE modified by MPEG 5 kDa; activity of PTE was measured directly in whole blood; applied dose (with the same total activity) of PTE and PTE-MPEG 5 kDa was 0.543 mg kg$^{-1}$ and 1.19 mg kg$^{-1}$, respectively. A second i.m. injection with the same amount of enzyme was repeated on the same animals 4 weeks later and whole blood activity was measured as for the first administration. Data are shown as mean ± SD.

**Table 3**
Pharmacokinetic parameters of PTE and PTE-MPEG 5 kDa in rats (i.m. injection; mean ± SD).

| | PTE | | PTE-MPEG 5 kDa | |
|---|---|---|---|---|
| No. of administration | 1st | 2nd | 1st | 2nd |
| $T_{max}$ (h) | 1.1 ± 0.2 | 1.6 ± 0.6 | 47.5 ± 2.0 | 37.0 ± 1.5 |
| $A_{max}$ (μkat.l$^{-1}$) | 2.6 ± 1.1 | 1.1 ± 0.7 | 62.7 ± 4.9 | 41 ± 4 |
| MRT (h) | 2.2 ± 0.7 | 3.2 ± 1.1 | 47.9 ± 1.0 | 34.5 ± 0.5 |

time was about 48 h. By comparison, unmodified PTE reached 24-fold lower peak levels at 1.1 h and MRT was only about 2.2 h, and the area under curve (AUC) of PTE-MPEG 5 kDa was about 525 fold higher than unmodified PTE. Animals did not display any sign of clinical toxicity and were administered the second dose injection by i.m. 4 weeks later. $T_{max}$, peak levels and MRT were decreased about 30% and AUC was decreased 2.4 fold for conjugated PTE compared to the first administration. This suggests that the enzyme was more rapidly eliminated, most likely due to the presence of antibodies targeting the enzyme. This hypothesis is supported by increased IgG levels after the second injection (data not shown). Though, the animals did not display any clinical signs of anaphylactic reaction.

In summary, MPEG conjugation allows to considerably extend the amount of circulating PTE as well as its circulating lifetime. However, the conjugation does not suppress immunogenicity. Branched PEG derivatives are under investigation to evaluate if they can provide a better reduction in immunogenicity.

## 4. Conclusion

In conclusion, the recent developments on catalytic bioscavengers of nerve agents focus on three enzyme types: engineered human cholinesterases, bacterial phosphotriesterase and PON1. Each enzyme has some drawbacks. Engineered cholinesterases display poor catalytic efficiencies, so that doses as large as those used for stoichiometric bioscavengers like plasma butyrylcholinesterase, are required to achieve good protection, provided that the phosphylation rates are not altered by the mutations. In that sense, they must be considered as self-regenerable stoichiometric bioscavengers rather than true catalytic bioscavengers. These cholinesterases could present an interest in the future for gene therapy approaches. Improvement of their catalytic efficiency cannot be based on directed evolution due to the lack of simple expression systems like bacterial ones. Multiple X-ray structures are available, so that the rational approach based on QM/MM simulations appears to be the method of choice for future research. Another issue is that engineered cholinesterases are produced in recombinant systems in which glycosylation and oligomerization are different from natural human enzymes. As a consequence, pharmacokinetic properties are degraded, and vectorization or PEGylation is required.

Human paraoxonase 1 is unstable, its catalytic efficiency is limited, a 3D structure is lacking for a rational design approach and expression in bacterial systems is not efficient enough for directed evolution methods. Recombinant PON1 has no drawbacks of the natural plasma enzyme but it is a non-human enzyme, whose chimeric and recombinant nature renders immunogenic with a short circulating half-life (Gupta et al., 2011). This enzyme cannot be used "as is" and chemical modification such as PEGylation is an absolute requirement for humanization and residence time extension.

Mesophilic PTE is the most efficient enzyme and stable if PEGylated. Thermophilic PTE is also a possible alternative. These enzymes present the same advantages and drawbacks as the recombinant chimeric PON1, e.g., optimization by directed evolution, both are immunogenic. So, all things considered, there is no reason to prefer recombinant chimeric PON1 to phosphotriesterase at this time, as no ideal candidate catalytic bioscavenger exists.

## Conflict of interest statement

The authors declare that there are no conflicts of interest.

## Acknowledgments

We are very thankful to Dr. Dan S. Tawfik and Dr. Leonid Gaidukov (The Weizmann Institute of Science, Rehovot, Israel) for providing mammalian rPON1 G3C9 and G3C9-8H plasmids. This work was funded by Direction Générale de l'Armement (DGA/SSA contract 08co501) and Agence Nationale de la Recherche (DetoxNeuro; ANR-06-BLAN-163). D.R. was under contract with the German Bundesministerium der Verteidigung (M/SABX/8A001).

## References

Aharoni, A., Gaidukov, L., Yagur, S., Toker, L., Silman, I., Tawfik, D.S., 2004. Directed evolution of mammalian paraoxonases PON1 and PON3 for bacterial expression and catalytic specialization. Proc. Natl Acad. Sci. U.S.A. 101, 482–487.

Ashani, Y., Pistinner, S., 2004. Estimation of the upper limit of human butyrylcholinesterase dose required for protection against organophosphates toxicity: a mathematically based toxicokinetic model. Toxicol. Sci. 77, 358–367.

Aurbek, N., Thiermann, H., Eyer, F., Eyer, P., Worek, F., 2009. Suitability of human butyrylcholinesterase as therapeutic marker and pseudo catalytic scavenger in organophosphate poisoning: a kinetic analysis. Toxicology 259, 133–139.

Bourne, Y., Radic, Z., Sulzenbacher, G., Kim, E., Taylor, P., Marchot, P., 2006. Substrate and product trafficking through the active center gorge of acetylcholinesterase analyzed by crystallography and equilibrium binding. J. Biol. Chem. 281, 29256–29267.

Cannard, K., 2006. The acute treatment of nerve agent exposure. J. Neurol. Sci. 249, 86–94.

Carletti, E., Jacquamet, L., Loiodice, M., Rochu, D., Masson, P., Nachon, F., 2009. Update on biochemical properties of recombinant *Pseudomonas diminuta* phosphotriesterase. J. Enzyme Inhib. Med. Chem. 24, 1045–1055.

Carletti, E., Li, H., Li, B., Ekstrom, F., Nicolet, Y., Loiodice, M., Gillon, E., Froment, M.T., Lockridge, O., Schopfer, L.M., Masson, P., Nachon, F., 2008. Aging of cholinesterases phosphylated by tabun proceeds through O-dealkylation. J. Am. Chem. Soc. 130, 16011–16020.

Chen-Goodspeed, M., Sogorb, M.A., Wu, F., Hong, S.B., Raushel, F.M., 2001. Structural determinants of the substrate and stereochemical specificity of phosphotriesterase. Biochemistry 40, 1325–1331.

Clery-Barraud, C., Renault, F., Leva, J., El Bakdouri, N., Masson, P., Rochu, D., 2009. Exploring the structural and functional stabilities of different paraoxonase-1 formulations through electrophoretic mobilities and enzyme activity parameters under hydrostatic pressure. Biochim. Biophys. Acta 1794, 680–688.

Colletier, J.P., Fournier, D., Greenblatt, H.M., Stojan, J., Sussman, J.L., Zaccai, G., Silman, I., Weik, M., 2006. Structural insights into substrate traffic and inhibition in acetylcholinesterase. EMBO J. 25, 2746–2756.

de Koning, M.C., van Grol, M., Noort, D., this issue. Peripheral site ligand conjugation to a non-quaternary oxime enhances reactivation of nerve agent-inhibited human acetylcholinesterase. Toxicol. Lett.

Elias, M., Dupuy, J., Merone, L., Mandrich, L., Porzio, E., Moniot, S., Rochu, D., Lecomte, C., Rossi, M., Masson, P., Manco, G., Chabriere, E., 2008. Structural basis for natural lactonase and promiscuous phosphotriesterase activities. J. Mol. Biol. 379, 1017–1028.

Ellman, G.L., Courtney, K.D., Andres Jr., V., Feather-Stone, R.M., 1961. A new and rapid colorimetric determination of acetylcholinesterase activity. Biochem. Pharmacol. 7, 88–95.

Genovese, R.F., Sun, W., Johnson, C.C., Ditargiani, R.C., Doctor, B.P., Saxena, A., 2010. Safety of administration of human butyrylcholinesterase and its conjugates with soman or VX in rats. Basic Clin. Pharmacol. Toxicol. 106, 428–434.

Geyer, B.C., Kannan, L., Cherni, I., Woods, R.R., Soreq, H., Mor, T.S., 2010a. Transgenic plants as a source for the bioscavenging enzyme, human butyrylcholinesterase. Plant Biotechnol. J. 8, 873–886.

Geyer, B.C., Kannan, L., Garnaud, P.E., Broomfield, C.A., Cadieux, C.L., Cherni, I., Hodgins, S.M., Kasten, S.A., Kelley, K., Kilbourne, J., Oliver, Z.P., Otto, T.C., Puffenberger, I., Reeves, T.E., Robbins, N., 2nd, Woods, R.R., Soreq, H., Lenz, D.E., Cerasoli, D.M., Mor, T.S., 2010b. Plant-derived human butyrylcholinesterase, but not an organophosphorous-compound hydrolyzing variant thereof, protects rodents against nerve agents. Proc. Natl. Acad. Sci. U.S.A. 107, 20251–20256.

Gupta, R.D., Goldsmith, M., Ashani, Y., Simo, Y., Mullokandov, G., Bar, H., Ben-David, M., Leader, H., Margalit, R., Silman, I., Sussman, J.L., Tawfik, D.S., 2011. Directed evolution of hydrolases for prevention of G-type nerve agent intoxication. Nat. Chem. Biol. 7, 120–125.

Harel, M., Aharoni, A., Gaidukov, L., Brumshtein, B., Khersonsky, O., Meged, R., Dvir, H., Ravelli, R.B., McCarthy, A., Toker, L., Silman, I., Sussman, J.L., Tawfik, D.S., 2004. Structure and evolution of the serum paraoxonase family of detoxifying and anti-atherosclerotic enzymes. Nat. Struct. Mol. Biol. 11, 412–419.

Harris, J.M., Chess, R.B., 2003. Effect of pegylation on pharmaceuticals. Nat. Rev. Drug Discov. 2, 214–221.

Heffron, P.F., Hobbiger, F., 1979. Relationship between inhibition of acetylcholinesterase and response of the rat phrenic nerve-diaphragm preparation to indirect stimulation at higher frequencies. Br. J. Pharmacol. 66, 323–329.

Huang, Y.J., Huang, Y., Baldassarre, H., Wang, B., Lazaris, A., Leduc, M., Bilodeau, A.S., Bellemare, A., Cote, M., Herskovits, P., Touati, M., Turcotte, C., Valeanu, L., Lemee, N., Wilgus, H., Begin, I., Bhatia, B., Rao, K., Neveu, N., Brochu, E., Pierson, J., Hockley, D.K., Cerasoli, D.M., Lenz, D.E., Karatzas, C.N., Langermann, S., 2007. Recombinant human butyrylcholinesterase from milk of transgenic animals to protect against organophosphate poisoning. Proc. Natl. Acad. Sci. U. S. A. 104, 13603–13608.

Huang, Y.J., Lundy, P.M., Lazaris, A., Huang, Y., Baldassarre, H., Wang, B., Turcotte, C., Cote, M., Bellemare, A., Bilodeau, A.S., Brouillard, S., Touati, M., Herskovits, P., Begin, I., Neveu, N., Brochu, E., Pierson, J., Hockley, D.K., Cerasoli, D.M., Lenz, D.E., Wilgus, H., Karatzas, C.N., Langermann, S., 2008. Substantially improved pharmacokinetics of recombinant human butyrylcholinesterase by fusion to human serum albumin. BMC Biotechnol. 8, 50.

Järv, J., 1984. Stereochemical aspects of cholinesterase catalysis. Bioorganic Chemistry 12, 259–278.

Jun, D., Kuca, K., Balgar, J., Hruby, M., Kucka, J., Renault, F., Masson, P., 2007. Phosphotriesterase modified by poly[N-(2-hydroxypropyl)methacrylamide]. Toxicology 233, 235.

Jun, D., Musilova, L., Link, M., Loiodice, M., Nachon, F., Rochu, D., Renault, F., Masson, P., 2010. Preparation and characterization of methoxy polyethylene glycol-conjugated phosphotriesterase as a potential catalytic bioscavenger against organophosphate poisoning. Chem. Biol. Interact. 187, 380–383.

Kalisiak, J., Ralph, E.C., Zhang, J., Cashman, J.R., 2011. Amidine-oximes: reactivators for organophosphate exposure. J. Med. Chem. 54, 3319–3330.

Kovarik, Z., Katalinic, M., Sinko, G., Binder, J., Holas, O., Jung, Y.S., Musilova, L., Jun, D., Kuca, K., 2010. Pseudo-catalytic scavenging: searching for a suitable reactivator of phosphorylated butyrylcholinesterase. Chem. Biol. Interact. 187, 167–171.

Kovarik, Z., Radic, Z., Berman, H.A., Taylor, P., 2007. Mutation of acetylcholinesterase to enhance oxime-assisted catalytic turnover of methylphosphonates. Toxicology 233, 79–84.

Kronman, C., Cohen, O., Mazor, O., Ordentlich, A., Raveh, L., Velan, B., Shafferman, A., 2010. Next generation OP-bioscavengers: a circulatory long-lived 4-PEG hypolysine mutant of F338A-HuAChE with optimal pharmacokinetics and pseudo-catalytic characteristics. Chem. Biol. Interact. 187, 253–258.

Lenz, D.E., Broomfield, C.A., Yeung, D.T., Masson, P., Maxwell, D.M., Cerasoli, D.M., 2007. Nerve agent bioscavengers: progress in development of a new mode of protection against organophosphorus exposure. In: Romano, J.A., Luckey, B.J., Salem, H. (Eds.), Chemical Warfare Agents: Chemistry, Pharmacology, Toxicology and Therapeutics. CRC Press, Boca Raton, FL, pp. 145–173.

Li, W.S., Lum, K.T., Chen-Goodspeed, M., Sogorb, M.A., Raushel, F.M., 2001. Stereoselective detoxification of chiral sarin and soman analogues by phosphotriesterase. Bioorg. Med. Chem. 9, 2083–2091.

Lockridge, O., Blong, R.M., Masson, P., Froment, M.T., Millard, C.B., Broomfield, C.A., 1997. A single amino acid substitution, Gly117His, confers phosphotriesterase (organophosphorus acid anhydride hydrolase) activity on human butyrylcholinesterase. Biochemistry 36, 786–795.

Lorke, D.E., Kalasz, H., Petroianu, G.A., Tekes, K., 2008. Entry of oximes into the brain: a review. Curr. Med. Chem. 15, 743–753.

Lushchekina, S., Masson, P., Nachon, F., Nemukhin, A.V., Varfolomeev, S.D., 2011. QM/MM modeling of the G117H butyrylcholinesterase catalyzed echothiophate hydrolysis reaction mechanism. Poster at the 13th Medical Chemical Defence Conference, Munich, 13–14th April 2011.

Masson, P., Nachon, F., Broomfield, C.A., Lenz, D.E., Verdier, L., Schopfer, L.M., Lockridge, O., 2008. A collaborative endeavor to design cholinesterase-based catalytic scavengers against toxic organophosphorus esters. Chem. Biol. Interact. 175, 273–280.

Masson, P., Nachon, F., Lockridge, O., 2010. Structural approach to the aging of phosphylated cholinesterases. Chem. Biol. Interact. 187, 157–162.

Maxwell, D.M., Brecht, K.M., Koplovitz, I., Sweeney, R.E., 2006. Acetylcholinesterase inhibition: does it explain the toxicity of organophosphorus compounds? Arch. Toxicol. 80, 756–760.

Maynard, R.L., Beswick, F.W., 1992. Organophosphorus compounds as chemical warfare agents. In: Ballantyne, B., Marrs, T.C. (Eds.), Clinical and Experimental Toxicology of Organophosphates and Carbamates. Butterworth, Oxford, pp. 373–385.

Mercey, G., Verdelet, T., Saint-Andre, G., Gillon, E., Wagner, A., Baati, R., Jean, L., Nachon, F., Renard, P.Y., 2011. First efficient uncharged reactivators for the dephosphylation of poisoned human acetylcholinesterase. Chem. Commun. (Camb.) 47, 5295–5297.

Merone, L., Mandrich, L., Porzio, E., Rossi, M., Muller, S., Reiter, G., Worek, F., Manco, G., 2010. Improving the promiscuous nerve agent hydrolase activity of a thermostable archaeal lactonase. Bioresour. Technol. 101, 9204–9212.

Merone, L., Mandrich, L., Rossi, M., Manco, G., 2005. A thermostable phosphotriesterase from the archaeon *Sulfolobus solfataricus*: cloning, overexpression and properties. Extremophiles 9, 297–305.

Millard, C.B., Lockridge, O., Broomfield, C.A., 1995. Design and expression of organophosphorus acid anhydride hydrolase activity in human butyrylcholinesterase. Biochemistry 34, 15925–15933.

Millard, C.B., Lockridge, O., Broomfield, C.A., 1998. Organophosphorus acid anhydride hydrolase activity in human butyrylcholinesterase: synergy results in a somanase. Biochemistry 37, 237–247.

Nachon, F., Carletti, E., Wandhammer, M., Nicolet, Y., Schopfer, L.M., Masson, P., Lockridge, O., 2011. X-ray crystallographic snapshots of reaction intermediates in the G117H mutant of human butyrylcholinesterase, a nerve agent target engineered into a catalytic bioscavenger. Biochem. J. 434, 73–82.

Offord, R.E., 1966. Electrophoretic mobilities of peptides on paper and their use in the determination of amide groups. Nature 211, 591–593.

Omburo, G.A., Kuo, J.M., Mullins, L.S., Raushel, F.M., 1992. Characterization of the zinc binding site of bacterial phosphotriesterase. J. Biol. Chem. 267, 13278–13283.

Otto, T.C., Harsch, C.K., Yeung, D.T., Magliery, T.J., Cerasoli, D.M., Lenz, D.E., 2009. Dramatic differences in organophosphorus hydrolase activity between human and chimeric recombinant mammalian paraoxonase-1 enzymes. Biochemistry 48, 10416–10422.

Poyot, T., Nachon, F., Froment, M.T., Loiodice, M., Wieseler, S., Schopfer, L.M., Lockridge, O., Masson, P., 2006. Mutant of Bungarus fasciatus acetylcholinesterase with low affinity and low hydrolase activity toward organophosphorus esters. Biochim. Biophys. Acta 1764, 1470–1478.

Radic, Z., Pickering, N.A., Vellom, D.C., Camp, S., Taylor, P., 1993. Three distinct domains in the cholinesterase molecule confer selectivity for acetyl- and butyrylcholinesterase inhibitors. Biochemistry 32, 12074–12084.

Renault, F., Carus, T., Clery-Barraud, C., Elias, M., Chabriere, E., Masson, P., Rochu, D., 2010. Integrative analytical approach by capillary electrophoresis and kinetics under high pressure optimized for deciphering intrinsic and extrinsic cofactors that modulate activity and stability of human paraoxonase (PON1). J. Chromatogr. B: Analyt. Technol. Biomed. Life. Sci. 878, 1346–1355.

Renault, F., Chabriere, E., Andrieu, J.P., Dublet, B., Masson, P., Rochu, D., 2006. Tandem purification of two HDL-associated partner proteins in human plasma, paraoxonase (PON1) and phosphate binding protein (HPBP) using hydroxyapatite chromatography. J. Chromatogr. B Analyt. Technol. Biomed. Life. Sci. 836, 15–21.

Rochu, D., Beaufet, N., Renault, F., Viguie, N., Masson, P., 2002. The wild type bacterial Co(2+)/Co(2+)-phosphotriesterase shows a middle-range thermostability. Biochim. Biophys. Acta 1594, 207–218.

Rochu, D., Chabriere, E., Masson, P., 2007a. Human paraoxonase: a promising approach for pre-treatment and therapy of organophosphorus poisoning. Toxicology 233, 47–59.

Rochu, D., Chabriere, E., Renault, F., Elias, M., Clery-Barraud, C., Masson, P., 2007b. Stabilization of the active form(s) of human paraoxonase by human phosphate-binding protein. Biochem. Soc. Trans. 35, 1616–1620.

Rochu, D., Ducret, G., Masson, P., 1999. Measuring conformational stability of proteins using an optimized temperature-controlled capillary electrophoresis approach. J. Chromatogr. A 838, 157–165.

Rochu, D., Renault, F., Clery-Barraud, C., Chabriere, E., Masson, P., 2007c. Stability of highly purified human paraoxonase (PON1): association with human phosphate binding protein (HPBP) is essential for preserving its active conformation(s). Biochim. Biophys. Acta 1774, 874–883.

Rochu, D., Viguie, N., Renault, F., Crouzier, D., Froment, M.T., Masson, P., 2004. Contribution of the active-site metal cation to the catalytic activity and to the conformational stability of phosphotriesterase: temperature- and pH-dependence. Biochem. J. 380, 627–633.

Roodveldt, C., Tawfik, D.S., 2005. Directed evolution of phosphotriesterase from *Pseudomonas diminuta* for heterologous expression in *Escherichia coli* results in stabilization of the metal-free state. Protein Eng. Des. Sel. 18, 51–58.

Saxena, A., Sun, W., Fedorko, J.M., Koplovitz, I., Doctor, B.P., 2011. Prophylaxis with human serum butyrylcholinesterase protects guinea pigs exposed to multiple lethal doses of soman or VX. Biochem. Pharmacol. 81, 164–169.

Saxena, A., Tipparaju, P., Luo, C., Doctor, B.P., 2010. Pilot-scale production of human serum butyrylcholinesterase suitable for use as a bioscavenger against nerve agent toxicity. Process Biochemistry 45, 1313–1318.

Sweeney, R.E., Maxwell, D.M., 2003. A theoretical expression for the protection associated with stoichiometric and catalytic scavengers in a single compartment model of organophosphorus poisoning. Math. Biosci. 181, 133–143.

Tsai, P.C., Bigley, A., Li, Y., Ghanem, E., Cadieux, C.L., Kasten, S.A., Reeves, T.E., Cerasoli, D.M., Raushel, F.M., 2010. Stereoselective hydrolysis of organophosphate nerve agents by the bacterial phosphotriesterase. Biochemistry 49, 7978–7987.

Wang, Y., Boeck, A.T., Duysen, E.G., Van Keuren, M., Saunders, T.L., Lockridge, O., 2004. Resistance to organophosphorus agent toxicity in transgenic mice expressing the G117H mutant of human butyrylcholinesterase. Toxicol. Appl. Pharmacol. 196, 356–366.

Wolfe, A.D., Rush, R.S., Doctor, B.P., Koplovitz, I., Jones, D., 1987. Acetylcholinesterase prophylaxis against organophosphate toxicity. Fundam. Appl. Toxicol. 9, 266–270.

Worek, F., Thiermann, H., Szinicz, L., Eyer, P., 2004. Kinetic analysis of interactions between human acetylcholinesterase, structurally different organophosphorus compounds and oximes. Biochem. Pharmacol. 68, 2237–2248.